Don Torrieri

Principles of Spread-Spectrum Communication Systems, Second Edition

Springer

Principles of Spread-Spectrum Communication Systems

Don Torrieri

Principles of Spread-Spectrum Communication Systems

Second Edition

Springer

Don Torrieri
US Army Research Laboratory
Adelphi, MD, USA

ISBN 978-1-4419-9594-0 e-ISBN 978-1-4419-9595-7
DOI 10.1007/978-1-4419-9595-7
Springer New York Dordrecht Heidelberg London

Library of Congress Control Number: 2011932168

Printed on acid-free paper

Springer is part of Springer Science+Business Media (www.springer.com)

To My Family

Preface

Spread-spectrum communication is a core area within the field of digital communication. Originally used in military networks as countermeasures against the threats of jamming and interception, spread-spectrum systems are now widely used in commercial applications and are part of several wireless and mobile communication standards. Although spread-spectrum communication is a staple topic in textbooks on digital communication, its treatment is usually cursory. This book is designed to provide a more intensive examination of the subject that is suitable for graduate students and practicing engineers with a solid background in the theory of digital communication. As the title indicates, this book stresses principles rather than specific current or planned systems, which are described in many other books. My goal in this book is to provide a concise but lucid explanation of the fundamentals of spread-spectrum systems with an emphasis on theoretical principles. The choice of specific topics to include was tempered by my judgment of their practical significance and interest to both researchers and system designers. Throughout the book, learning is facilitated by many new or streamlined derivations of the classical theory. Problems at the end of each chapter are intended to assist readers in consolidating their knowledge and to provide practice in analytical techniques. The listed references are ones that I recommend for further study and as sources of additional references.

A *spread-spectrum signal* is one with an extra modulation that expands the signal bandwidth greatly beyond what is required by the underlying coded-data modulation. Spread-spectrum communication systems are useful for suppressing interference, making secure communications difficult to detect and process, accommodating fading and multipath channels, and providing a multiple-access capability. Spread-spectrum signals cause relatively minor interference to other systems operating in the same spectral band. The most practical and dominant spread-spectrum systems are *direct-sequence* and *frequency hopping* systems.

There is no fundamental theoretical barrier to the effectiveness of spread-spectrum communications. That remarkable fact is not immediately apparent since the increased bandwidth of a spread-spectrum signal might require a receive filter

that passes more noise power than necessary to the demodulator. However, when any signal and white Gaussian noise are applied to a filter matched to the signal, the sampled filter output has a signal-to-noise ratio that depends solely on the energy-to-noise-density ratio. Thus, the bandwidth of the input signal is irrelevant, and spread-spectrum signals have no inherent limitations.

Chapter 1 reviews fundamental results of coding and modulation theory that are essential to a full understanding of spread-spectrum systems. *Channel codes*, which are also called *error-correction* or *error-control* codes, are vital in fully exploiting the potential capabilities of spread-spectrum systems. Although direct-sequence systems can greatly suppress interference, practical systems require channel codes to deal with the residual interference and channel impairments such as fading. Frequency-hopping systems are designed to avoid interference, but the possibility of hopping into an unfavorable spectral region usually requires a channel code to maintain adequate performance. In this chapter, coding and modulation theory are used to derive the required receiver computations and the error probabilities of the decoded information bits. The emphasis is on the types of codes and modulation that have proved most useful in spread-spectrum systems.

Chapter 2 presents the fundamentals of direct-sequence systems. *Direct-sequence modulation* entails the direct addition of a high-rate spreading sequence with a lower-rate data sequence, resulting in a transmitted signal with a relatively wide bandwidth. The removal of the spreading sequence in the receiver causes a contraction of the bandwidth that can be exploited by appropriate filtering to remove a large portion of the interference. This chapter begins with a discussion of spreading sequences and waveforms and then provides a detailed analysis of how the direct-sequence receiver suppresses various forms of interference. Several methods that supplement the inherent ability of a direct-sequence system to reject narrowband interference are explained.

Chapter 3 presents the fundamentals of frequency-hopping systems. *Frequency hopping* is the periodic changing of the carrier frequency of a transmitted signal. This time-varying characteristic potentially endows a communication system with great strength against interference. Whereas a direct-sequence system relies on spectral spreading, spectral despreading, and filtering to suppress interference. the basic mechanism of interference suppression in a frequency-hopping system is that of avoidance. When the avoidance fails, it is only temporary because of the periodic changing of the carrier frequency. The impact of the interference is further mitigated by the pervasive use of channel codes, which are more essential for frequency-hopping than for direct-sequence systems. The basic concepts, spectral and performance aspects, and coding and modulation issues are presented in the first five sections of this chapter. The effects of partial-band interference and jamming are examined, and the most important issues in the design of frequency synthesizers are described.

Chapter 4 focuses on synchronization. A spread-spectrum receiver must generate a spreading sequence or frequency-hopping pattern that is synchronized with the received sequence or pattern; that is, the corresponding chips or dwell intervals

must precisely or nearly coincide. Any misalignment causes the signal amplitude at the demodulator output to fall in accordance with the autocorrelation or partial autocorrelation function. Although the use of precision clocks in both the transmitter and the receiver limit the timing uncertainty in the receiver, clock drifts, range uncertainty, and the Doppler shift may cause synchronization problems. *Code synchronization*, which is either sequence or pattern synchronization, might be obtained from separately transmitted pilot or timing signals. It may be aided or enabled by feedback signals from the receiver to the transmitter. However, to reduce the cost in power and overhead, most spread-spectrum receivers achieve code synchronization by processing the received signal. Both acquisition, which provides coarse synchronization, and tracking, which provides fine synchronization, are described in this chapter. The emphasis is on the acquisition system because this system is almost always the dominant design issue and most expensive component of a complete spread-spectrum system.

Chapter 5 provides a general description of the most important aspects of fading and the role of diversity methods in counteracting it. *Fading* is the variation in received signal strength due to a time-varying communications channel. It is primarily caused by the interaction of multipath components of the transmitted signal that are generated and altered by changing physical characteristics of the propagation medium. The principal means of counteracting fading are *diversity methods*, which are based on the exploitation of the latent redundancy in two or more independently fading copies of the same signal. The rake demodulator, which is of central importance in most direct-sequence systems, is shown to be capable of exploiting undesired multipath signals rather than simply attempting to reject them. The multicarrier direct-sequence system is shown to be a viable alternative method of exploiting multipath signals that has practical advantages.

Chapter 6 presents the general characteristics of spreading sequences and frequency-hopping patterns that are suitable for *code-division multiple access* (CDMA) systems. *Multiple access* is the ability of many users to communicate with each other while sharing a common transmission medium. Wireless multiple-access communications are facilitated if the transmitted signals are orthogonal or separable in some sense. Signals may be separated in time, frequency, or code. CDMA is realized by using spread-spectrum modulation while transmitting signals from multiple users in the same frequency band at the same time. All signals use the entire allocated spectrum, but the spreading sequences or frequency-hopping patterns differ. CDMA is advantageous for cellular networks because it eliminates the need for frequency and time-slot coordination among cells, allows carrier-frequency reuse in adjacent cells, and imposes no sharp upper bound on the number of users. Another major CDMA advantage is the ease with which it can be combined with multibeamed antenna arrays that are either adaptive or have fixed patterns covering cell sectors. Inactive systems in a network reduce the interference received by an active CDMA system. These general advantages and its resistance to interference, interception, and frequency-selective fading make spread-spectrum CDMA an attractive choice for many mobile communication networks. The impact

of multiple-access interference in spread-spectrum CDMA systems and networks and the role of power control are analyzed. Multiuser detectors, which have great potential usefulness but are fraught with practical difficulties, are derived and explained.

The ability to detect the presence of spread-spectrum signals is often required by cognitive radio, ultra-wideband, and military systems. Chapter 7 presents an analysis of the detection of spread-spectrum signals when the spreading sequence or the frequency-hopping pattern is unknown and cannot be accurately estimated by the detector. Thus, the detector cannot mimic the intended receiver, and alternative procedures are required. The goal is limited in that only detection is sought, not demodulation or decoding. Nevertheless, detection theory leads to impractical devices for the detection of spread-spectrum signals. An alternative procedure is to use a radiometer or energy detector, which relies solely on energy measurements to determine the presence of unknown signals. The radiometer has applications not only as a detector of spread-spectrum signals, but also as a sensing method in cognitive radio and ultra-wideband systems.

Chapter 8 examines the role of iterative channel estimation in the design of advanced spread-spectrum systems. The estimation of channel parameters, such as the fading amplitude and the power spectral density of the interference plus noise, is essential to the effective use of soft-decision decoding. Channel estimation may be implemented by the transmission of pilot signals that are processed by the receiver, but pilot signals entail overhead costs, such as the loss of data throughput. Deriving maximum-likelihood channel estimates directly from the received data symbols is often prohibitively difficult. There is an effective alternative when turbo or low-density parity-check codes are used. The expectation-maximization algorithm provides an iterative approximate solution to the maximum-likelihood equations and is inherently compatible with iterative demodulation and decoding. Two examples of advanced spread-spectrum systems that apply the expectation-maximization algorithm for channel estimation are described and analyzed in this chapter. These systems provide good illustrations of the calculations required in the design of advanced systems.

Three appendices contain mathematical details about bandpass processes, basic probability distributions, and the convergence of important adaptive algorithms.

The evolution of spread spectrum communication systems and the prominence of new mathematical methods in their design provided the motivation to undertake this new edition of the book. This edition is intended to enable readers to understand the current state-of-the-art in this field. More than twenty percent of the material in this edition is new, including a chapter on systems with iterative channel estimation, and the remainder of the material has been thoroughly revised.

In writing this book, I have relied heavily on notes and documents prepared and the perspectives gained during my work at the US Army Research Laboratory. I am thankful to my colleagues Matthew Valenti, Hyuck Kwon, and John Shea for their trenchant and excellent reviews of selected chapters of the original manuscript. I am grateful to my wife, Nancy, who provided me not only with her usual unwavering support but also with extensive editorial assistance.

Contents

Chapter 1
Channel Codes and Modulation

This chapter reviews fundamental results of coding and modulation theory that are essential to a full understanding of spread-spectrum systems. *Channel codes*, which are also called *error-correction* or *error-control* codes, are vital in fully exploiting the potential capabilities of spread-spectrum communication systems. Although direct-sequence systems greatly suppress interference, practical systems require channel codes to deal with the residual interference and channel impairments such as fading. Frequency-hopping systems are designed to avoid interference, but the possibility of hopping into an unfavorable spectral region usually requires a channel code to maintain adequate performance. In this chapter, coding and modulation theory [1–5] are used to derive the required receiver computations and the error probabilities of the decoded information bits. The emphasis is on the types of codes and modulation that have proved most useful in spread-spectrum systems.

1.1 Block Codes

A *channel code* for forward error control or error correction is a set of *codewords* that are used to improve communication reliability. An (n, k) *block code* uses a codeword of n code symbols to represent k information symbols. Each symbol is selected from an alphabet of q symbols, and there are q^k codewords. If $q = 2^m$, then an (n, k) code of q-ary symbols is equivalent to an (mn, mk) binary code. A block encoder can be implemented by using logic elements or memory to map a k-symbol information word into an n-symbol codeword. After the waveform representing a codeword is received and demodulated, the decoder uses the demodulator output to determine the information symbols corresponding to the codeword. If the demodulator produces a sequence of discrete symbols and the decoding is based on these symbols, the demodulator is said to make *hard decisions*. Conversely, if the demodulator produces analog or multilevel quantized samples of the waveform, the demodulator is said to make *soft decisions*. The advantage of soft decisions is

D. Torrieri, *Principles of Spread-Spectrum Communication Systems*,
DOI 10.1007/978-1-4419-9595-7_1, © Springer Science+Business Media, LLC 2011

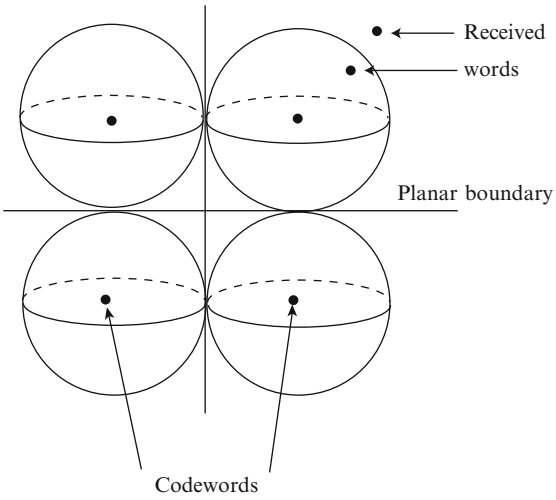

Fig. 1.1 Conceptual representation of n-dimensional vector space of sequences

that reliability or quality information is provided to the decoder, which can use this information to improve its performance.

The number of symbol positions in which the symbol of one sequence differs from the corresponding symbol of another equal-length sequence is called the *Hamming distance* between the sequences. The minimum Hamming distance between any two codewords is called the *minimum distance* of the code. When hard decisions are made, the demodulator output sequence is called the *received sequence* or the *received word*. Hard decisions imply that the overall channel between the output and the decoder input is the classical binary symmetric channel. If the channel symbol error probability is less than one-half, then the maximum-likelihood criterion implies that the correct codeword is the one that is the smallest Hamming distance from the received word. A *complete decoder* is a device that implements the maximum-likelihood criterion. An *incomplete decoder* does not attempt to correct all received words.

The n-dimensional vector space of sequences is conceptually represented as a three-dimensional space in Fig. 1.1. Each codeword occupies the center of a *decoding sphere* with radius t in Hamming distance, where t is a positive integer. A complete decoder has decision regions defined by planar boundaries surrounding each codeword. A received word is assumed to be a corrupted version of the codeword enclosed by the boundaries. A *bounded-distance decoder* is an incomplete decoder that attempts to correct symbol errors in a received word if it lies within one of the decoding spheres. Since unambiguous decoding requires that none of the spheres may intersect, the maximum number of random errors that can be corrected by a bounded-distance decoder is

$$t = \lfloor (d_m - 1)/2 \rfloor \tag{1.1}$$

where d_m is the minimum Hamming distance between codewords and $\lfloor x \rfloor$ denotes the largest integer less than or equal to x. When more than t errors occur, the received word may lie within a decoding sphere surrounding an incorrect codeword or it may lie in the interstices (regions) outside the decoding spheres. If the received word lies within a decoding sphere, the decoder selects the incorrect codeword at the center of the sphere and produces an output word of information symbols with undetected errors. If the received word lies in the interstices, the decoder cannot correct the errors, but recognizes their existence. Thus, the decoder fails to decode the received word.

Since there are $\binom{n}{i}(q-1)^i$ words at exactly distance i from the center of the sphere, the number of words in a decoding sphere of radius t is determined from elementary combinatorics to be

$$V = \sum_{i=0}^{t} \binom{n}{i} (q-1)^i. \tag{1.2}$$

Since a block code has q^k codewords, $q^k V$ words are enclosed in some sphere. The number of possible received words is $q^n \geq q^k V$, which yields

$$q^{n-k} \geq \sum_{i=0}^{t} \binom{n}{i} (q-1)^i. \tag{1.3}$$

This inequality implies an upper bound on t and, hence, d_m. The upper bound on d_m is called the *Hamming bound*.

The *Galois field* of two elements, which is denoted by $GF(2)$, consists of the symbols 0 and 1 and the operations of modulo-2 addition and modulo-2 multiplication. These binary operations are defined by

$$\begin{array}{cccc} 0 \oplus 0 = 0, & 0 \oplus 1 = 1, & 1 \oplus 0 = 1, & 1 \oplus 1 = 0 \\ 0 \cdot 0 = 0, & 0 \cdot 1 = 0, & 1 \cdot 0 = 0, & 1 \cdot 1 = 1 \end{array}$$

where $\oplus$ denotes modulo-2 addition. From these equations, it is easy to verify that the field is closed under both modulo-2 addition and modulo-2 multiplication and that both operations are *associative* and *commutative*. Since -1 is defined as that element which when added to 1 yields 0, we have $-1 = 1$, and subtraction is the same as addition. The equations imply that the additive identity element is 0, the multiplicative identity is 1, and the multiplicative inverse of 1 is $1^{-1} = 1$. The substitutions of all possible symbol combinations verify the *distributive laws*:

$$a(b \oplus c) = ab \oplus ac, \quad (b \oplus c)a = ba \oplus ca$$

where a, b, and c can each equal 0 or 1. The equality of subtraction and addition implies that if $a \oplus b = c$, then $a = b \oplus c$.

A block code is called a *linear block code* if its codewords form a k-dimensional subspace of the vector space of sequences with n symbols. Thus, the vector sum of two codewords or the vector difference between them is a codeword. If $q = 2^m$, then a q-ary symbol may be represented by m bits, and a nonbinary codeword of n_1 symbols may be mapped into a binary codeword of length $n = mn_1$. If a binary block code, which uses an alphabet of symbols 0 and 1, is linear, the symbols of a codeword are modulo-2 sums of information bits. Since a linear block code is a subspace of a vector space, it must contain the additive identity. Thus, the all-zero sequence is always a codeword in any linear block code. Since nearly all practical block codes are linear, henceforth block codes are assumed to be linear.

Let $\mathbf{m}$ denote a row vector of k message bits and $\mathbf{c}$ denote a row vector of n binary codeword symbols. Let $\mathbf{G}$ denote a $k \times n$ *generator matrix*, each row of which is a basis vector of the subspace of codewords. The definitions imply that

$$\mathbf{c} = \mathbf{mG} \tag{1.4}$$

where modulo-2 additions are used in the matrix multiplication. The orthogonal complement of the row space of $\mathbf{G}$ is an $(n - k)$-dimensional subspace of the n-dimensional binary space such that each of its vectors is orthogonal to the row space, and hence to the codewords. An $(n - k) \times n$ *parity-check matrix* $\mathbf{H}$ has row vectors that span the orthogonal complement. Therefore,

$$\mathbf{GH}^T = \mathbf{0}. \tag{1.5}$$

A *cyclic code* is a linear block code in which a cyclic shift of the symbols of a codeword produces another codeword. This characteristic allows the implementation of encoders and decoders that use linear feedback shift registers. Relatively simple encoding and hard-decision decoding techniques are known for cyclic codes belonging to the class of *Bose-Chaudhuri-Hocquenghem* (BCH) *codes*, which may be binary or nonbinary. A BCH code has a length that is a divisor of $q^m - 1$, where $m \geq 2$, and is designed to have an error-correction capability of $t = \lfloor (\delta - 1)/2 \rfloor$, where δ is the *design distance*. Although the minimum distance may exceed the design distance, the standard BCH decoding algorithms cannot correct more than t errors. The parameters (n, k, t) for binary BCH codes with $7 \leq n \leq 127$ are listed in Table 1.1.

A *perfect code* is a block code such that every n-symbol sequence is at a distance of at most t from some n-symbol codeword, and the sets of all sequences at distance t or less from each codeword are disjoint. Thus, the Hamming bound is satisfied with equality, and a complete decoder is also a bounded-distance decoder. The only perfect codes are the binary repetition codes of odd length, the Hamming codes, the binary (23, 12) Golay code, and the ternary (11, 6) Golay code. *Repetition codes* represent each information bit by n binary code symbols. When n is odd, the $(n, 1)$ repetition code is a perfect code with $d_m = n$ and $t = (n - 1)/2$. A hard-decision decoder makes a decision based on the state of the majority of the demodulated symbols. Although repetition codes are not efficient for the additive-white-Gaussian-noise (AWGN) channel, they can improve the system performance

Table 1.1 Binary BCH codes

n	k	t	D_p	n	k	t	D_p	n	k	t	D_p
7	4	1	1	63	45	3	0.1592	127	92	5	0.0077
7	1	3	1	63	39	4	0.0380	127	85	6	0.0012
15	11	1	1	63	36	5	0.0571	127	78	7	$1.68 \cdot 10^{-4}$
15	7	2	0.4727	63	30	6	0.0088	127	71	9	$2.66 \cdot 10^{-4}$
15	5	3	0.5625	63	24	7	0.0011	127	64	10	$2.48 \cdot 10^{-5}$
15	1	7	1	63	18	10	0.0044	127	57	11	$2.08 \cdot 10^{-6}$
31	26	1	1	63	16	11	0.0055	127	50	13	$1.42 \cdot 10^{-6}$
31	21	2	0.4854	63	10	13	0.0015	127	43	14	$9.11 \cdot 10^{-8}$
31	16	3	0.1523	63	7	15	0.0024	127	36	15	$5.42 \cdot 10^{-9}$
31	11	5	0.1968	63	1	31	1	127	29	21	$2.01 \cdot 10^{-6}$
31	6	7	0.1065	127	120	1	1	127	22	23	$3.56 \cdot 10^{-7}$
31	1	15	1	127	113	2	0.4962	127	15	27	$7.75 \cdot 10^{-7}$
63	57	1	1	127	106	3	0.1628	127	8	31	$8.10 \cdot 10^{-7}$
63	51	2	0.4924	127	99	4	0.0398	127	1	63	1

Table 1.2 Code words of Hamming (7,4) code

0000000	0001011	0010110	0011101
0100111	0101100	0110001	0111010
1000101	1001110	1010011	1011000
1100010	1101001	1110100	1111111

for fading channels if the number of repetitions is properly chosen. An (n, k) *Hamming code* is a perfect BCH code with $d_m = 3$ and

$$n = \frac{q^{n-k} - 1}{q - 1}. \tag{1.6}$$

Since $t = 1$, a Hamming code is capable of correcting all single errors. Binary Hamming codes with $n \leq 127$ are found in Table 1.1. The 16 codewords of a $(7, 4)$ Hamming code are listed in Table 1.2. The first four bits of each codeword are the information bits. The perfect *(23, 12) Golay code* is a binary cyclic code with $d_m = 7$ and $t = 3$. The perfect *(11, 6) Golay code* is a ternary cyclic code with $d_m = 5$ and $t = 2$.

Any (n, k) linear block code with an odd value of d_m can be converted into an $(n + 1, k)$ *extended code* by adding a parity symbol. The advantage of the extended code stems from the fact that the minimum distance of the block code is increased by one, which improves the performance, but the decoding complexity and code rate are usually changed insignificantly. The (24, 12) *extended Golay code* is formed by adding an overall parity symbol to the (23, 12) Golay code, thereby increasing the minimum distance to $d_m = 8$. As a result, some received sequences with four errors can be corrected with a complete decoder. The (24, 12) code is often preferable to the (23, 12) code because the *code rate*, which is defined as the ratio k/n, is exactly one-half, which simplifies the system timing.

The *Hamming weight* of a codeword is the number of nonzero symbols in a codeword. For a linear block code, the vector difference between two codewords is another codeword with weight equal to the distance between the two original codewords. By subtracting the codeword **c** to all the codewords, we find that the set of Hamming distances from any codeword **c** is the same as the set of codeword weights. Consequently, in evaluating decoding error probabilities, one can assume without loss of generality that the all-zero codeword was transmitted, and the minimum Hamming distance is equal to the minimum weight of the nonzero codewords. For binary block codes, the Hamming weight is the number of ones in a codeword.

A *systematic block code* is a code in which the information symbols appear unchanged in the codeword, which also has additional parity symbols. Thus, a systematic codeword can be expressed in the form $\mathbf{c} = [\mathbf{m}\ \mathbf{p}]$, where $\mathbf{p}$ is the row vector of $n-k$ parity bits, and the generator matrix has the form

$$\mathbf{G} = [\mathbf{I}_k\ \ \mathbf{P}] \tag{1.7}$$

where $\mathbf{I}_k$ is the $k \times k$ identity matrix and $\mathbf{P}$ is a $k \times (n-k)$ matrix. This equation and (1.5) indicate that the parity check matrix for a binary code is

$$\mathbf{H} = \left[\mathbf{P}^T\ \ \mathbf{I}_{n-k}\right]. \tag{1.8}$$

In terms of the word error probability for hard-decision decoding, every linear code is equivalent to a systematic linear code. Therefore, systematic block codes are the standard choice and are assumed henceforth. Some systematic codewords have only one nonzero information symbol. Since there are at most $n-k$ parity symbols, these codewords have Hamming weights that cannot exceed $n-k+1$. Since the minimum distance of the code is equal to the minimum codeword weight,

$$d_m \leq n-k+1. \tag{1.9}$$

This upper bound is called the *Singleton bound*. A linear block code with a minimum distance equal to the Singleton bound is called a *maximum-distance separable code.*

Nonbinary block codes can accommodate high data rates efficiently because decoding operations are performed at the symbol rate rather than the higher information-bit rate. *Reed–Solomon codes* are nonbinary BCH codes with $n = q-1$ and are maximum-distance separable codes with $d_m = n-k+1$. For convenience in implementation, q is usually chosen so that $q = 2^m$, where m is the number of bits per symbol. Thus, $n = 2^m - 1$ and the code provides correction of 2^m-ary symbols. Most Reed–Solomon decoders are bounded-distance decoders with $t = \lfloor (d_m - 1)/2 \rfloor$.

The most important single determinant of the code performance is its *weight distribution,* which is a list or function that gives the number of codewords with each possible weight. The weight distributions of the Golay codes are listed in Table 1.3.

Table 1.3 Weight distributions of Golay codes

	Number of codewords	
Weight	(23,12)	(24,12)
0	1	1
7	253	0
8	506	759
11	1,288	0
12	1,288	2,576
15	506	0
16	253	759
23	1	0
24	0	1

Analytical expressions for the weight distribution are known in a few cases. Let A_l denote the number of codewords with weight l. For a binary Hamming code, each A_l can be determined from the weight-enumerator polynomial

$$A(x) = \sum_{l=0}^{n} A_l x^l = \frac{1}{n+1}\left[(1+x)^n + n(1+x)^{(n-1)/2}(1-x)^{(n+1)/2}\right]. \quad (1.10)$$

For example, the (7,4) Hamming code gives $A(x) = \frac{1}{8}[(1+x)^7 + 7(1+x)^3 (1-x)^4] = 1 + 7x^3 + 7x^4 + x^7$, which yields $A_0 = 1$, $A_3 = 7$, $A_4 = 7$, $A_7 = 1$, and $A_l = 0$, otherwise. For a maximum-distance separable code, $A_0 = 1$ and

$$A_l = \binom{n}{l}(q-1)\sum_{i=0}^{l-d_m}(-1)^i \binom{l-1}{i} q^{l-i-d_m}, \quad d_m \le l \le n. \quad (1.11)$$

The weight distribution of other codes can be determined by examining all valid codewords if the number of codewords is not too large for a computation.

1.1.1 Error Probabilities for Hard-Decision Decoding

There are two types of bounded-distance decoders: erasing decoders and reproducing decoders. They differ only in their actions following the detection of uncorrectable errors in a received word. An *erasing decoder* discards the received word and may initiate an automatic retransmission request. For a systematic block code, a *reproducing decoder* reproduces the information symbols of the received word as its output.

Let P_s denote the *channel-symbol error probability*, which is the probability of error in a demodulated code symbol. It is assumed that the channel-symbol errors are statistically independent and identically distributed, which is usually an

accurate model for systems with appropriate symbol interleaving (Sect. 1.3). Let P_w denote the *word error probability*, which is the probability that a received word is not decoded correctly due to both undetected errors and decoding failures. There are $\binom{n}{i}$ distinct ways in which i errors may occur among n symbols. Since a received sequence may have more than t errors but no information-symbol errors, a reproducing decoder that corrects t or few errors has

$$P_w \leq \sum_{i=t+1}^{n} \binom{n}{i} P_s^i (1-P_s)^{n-i}. \tag{1.12}$$

For an erasing decoder, (1.12) becomes an equality. For reproducing decoders, t is given by (1.1) because it is pointless to make the decoding spheres smaller than the maximum allowed by the code. However, if a block code is used for both error correction and error detection, an erasing decoder is often designed with t less than the maximum. If a block code is used exclusively for error detection, then $t = 0$.

Conceptually, a complete decoder correctly decodes even if the number of symbol errors exceeds t provided that the received sequence lies within the planar boundaries associated with the correct codeword, as depicted in Fig. 1.1. When a received sequence is equidistant from two or more codewords, a complete decoder selects one of them according to some arbitrary rule. Thus, the word error probability for a complete decoder satisfies (1.12). If $P_s \leq 1/2$, a complete decoder is a maximum-likelihood decoder.

Let P_{ud} denote the probability of an *undetected error*, and let P_{df} denote the probability of a *decoding failure*. For a bounded-distance decoder

$$P_w = P_{ud} + P_{df} = \sum_{i=t+1}^{n} \binom{n}{i} P_s^i (1-P_s)^{n-i}. \tag{1.13}$$

Thus, it is easy to calculate P_{df} once P_{ud} is determined. Since the set of Hamming distances from a given codeword to the other codewords is the same for all given codewords of a linear block code, it is legitimate to assume for convenience in evaluating P_{ud} that the all-zero codeword was transmitted. This assumption is always made in the subsequent analysis. If channel-symbol errors in a received word are statistically independent and occur with the same probability P_s, then the probability of an error in a specific set of i positions that results in a specific set of i erroneous symbols is

$$P_e(i) = \left(\frac{P_s}{q-1}\right)^i (1-P_s)^{n-i}. \tag{1.14}$$

For an undetected error to occur at the output of a bounded-distance decoder, the number of erroneous symbols must exceed t and the received word must lie within an incorrect decoding sphere of radius t. Let $N(l, i)$ is the number of sequences of

Hamming weight i that lie within a decoding sphere of radius t associated with a particular codeword of weight l. Then

$$P_{ud} = \sum_{i=t+1}^{n} P_e(i) \sum_{l=\max(i-t,d_m)}^{\min(i+t,n)} A_l N(l,i)$$

$$= \sum_{i=t+1}^{n} \left(\frac{P_s}{q-1}\right)^i (1-P_s)^{n-i} \sum_{l=\max(i-t,d_m)}^{\min(i+t,n)} A_l N(l,i). \tag{1.15}$$

Consider sequences of weight i that are at distance s from a particular codeword of weight l, where $|l-i| \le s \le t$ so that the sequences are within the decoding sphere of the codeword. By counting these sequences and then summing over the allowed values of s, we can determine $N(l,i)$. The counting is done by considering changes in the components of this codeword that can produce one of these sequences. Let ν denote the number of nonzero codeword symbols that are changed to zeros, α the number of codeword zeros that are changed to any of the $(q-1)$ nonzero symbols in the alphabet, and β the number of nonzero codeword symbols that are changed to any of the other $(q-2)$ nonzero symbols. For a sequence at distance s to result, it is necessary that $0 \le \nu \le s$. The number of sequences that can be obtained by changing any ν of the l nonzero symbols to zeros is $\binom{l}{\nu}$, where $\binom{b}{a} = 0$ if $a > b$. For a specified value of ν, it is necessary that $\alpha = \nu + i - l$ to ensure a sequence of weight i. The number of sequences that result from changing any α of the $n-l$ zeros to nonzero symbols is $\binom{n-l}{\alpha}(q-1)^\alpha$. For a specified value of ν and hence α, it is necessary that $\beta = s - \nu - \alpha = s + l - i - 2\nu$ to ensure a sequence at distance s. The number of sequences that result from changing β of the $l-\nu$ remaining nonzero components is $\binom{l-\nu}{\beta}(q-2)^\beta$, where $0^x = 0$ if $x \ne 0$ and $0^0 = 1$. Summing over the allowed values of s and ν, we obtain

$$N(l,i) = \sum_{s=|l-i|}^{t} \sum_{\nu=0}^{s} \binom{l}{\nu}\binom{n-l}{\nu+i-l}\binom{l-\nu}{s+l-i-2\nu}$$

$$\times (q-1)^{\nu+i-l}(q-2)^{s+l-i-2\nu}. \tag{1.16}$$

Equations (1.15) and (1.16) allow the exact calculation of P_{ud}.

When $q = 2$, the only term in the inner summation of (1.16) that is nonzero has the index $\nu = (s+l-i)/2$ provided that this index is an integer and $0 \le (s+l-i)/2 \le s$. Using this result, we find that for binary codes,

$$N(l,i) = \sum_{s=|l-i|}^{t} \binom{n-l}{\frac{s+i-l}{2}}\binom{l}{\frac{s+l-i}{2}}, \quad q = 2 \tag{1.17}$$

where $\binom{m}{1/2} = 0$ for any nonnegative integer m. Thus, $N(l,l) = 1$ and $N(l,i) = 0$ for $|l-i| \ge t+1$.

The word error probability is a performance measure that is important primarily in applications for which only a decoded word completely without symbol errors is acceptable. When the utility of a decoded word degrades in proportion to the number of information bits that are in error, the *information-bit error probability* is frequently used as a performance measure. To evaluate it for block codes that may be nonbinary, we first examine the information-symbol error probability.

Let $P_{is}(\nu)$ denote the probability of an error in information symbol ν at the decoder output. In general, it cannot be assumed that $P_{is}(\nu)$ is independent of ν. The *information-symbol error probability*, which is defined as the unconditional error probability without regard to the symbol position, is

$$P_{is} = \frac{1}{k} \sum_{\nu=1}^{k} P_{is}(\nu). \tag{1.18}$$

The random variables Z_ν, $\nu = 1, 2, \ldots, k$, are defined so that $Z_\nu = 1$ if information symbol ν is in error and $Z_\nu = 0$ if it is correct. The expected number of information-symbol errors is

$$E[I] = E\left[\sum_{\nu=1}^{k} Z_\nu\right] = \sum_{\nu=1}^{k} E[Z_\nu] = \sum_{\nu=1}^{k} P_{is}(\nu) \tag{1.19}$$

where $E[\,]$ denotes the expected value. The *information-symbol error rate* is defined as $E[I]/k$. Equations (1.18) and (1.19) imply that

$$P_{is} = \frac{E[I]}{k} \tag{1.20}$$

which indicates that *the information-symbol error probability is equal to the information-symbol error rate*.

Let $P_{ds}(\nu)$ denote the probability of an error in symbol j of the codeword chosen by the decoder or symbol j of the received sequence if a decoding failure occurs. The decoded-symbol error probability is

$$P_{ds} = \frac{1}{n} \sum_{\nu=1}^{n} P_{ds}(\nu). \tag{1.21}$$

If $E[D]$ is the expected number of decoded-symbol errors, a derivation similar to the preceding one yields

$$P_{ds} = \frac{E[D]}{n} \tag{1.22}$$

which indicates that *the decoded-symbol error probability is equal to the decoded-symbol error rate*. It can be shown [6] that for cyclic codes, the error rate among the information symbols in the output of a bounded-distance decoder is equal to the error rate among all the decoded symbols; that is,

$$P_{is} = P_{ds}. \tag{1.23}$$

This equation, which is at least approximately valid for linear block codes, significantly simplifies the calculation of P_{is} because P_{ds} can be expressed in terms of the code weight distribution, whereas an exact calculation of P_{is} requires additional information. For binary codes, the information-bit error probability is $P_b = P_{is} = P_{ds}$.

An erasing decoder makes an error only if it fails to detect one. If the received word lies within a decoding sphere associated with a codeword of weight l, then the probability of an information-symbol error is l/n. Therefore, (1.15) implies that the *information-symbol error rate for an erasing decoder* is

$$P_{is} = \sum_{i=t+1}^{n} \left(\frac{P_s}{q-1}\right)^i (1-P_s)^{n-i} \sum_{l=\max(i-t,d_m)}^{\min(i+t,n)} A_l N(l,i) \frac{l}{n}. \tag{1.24}$$

The number of sequences of weight i that lie in the interstices outside the decoding spheres is

$$L(i) = (q-1)^i \binom{n}{i} - \sum_{l=\max(i-t,d_m)}^{\min(i+t,n)} A_l N(l,i), \quad i \geq t+1 \tag{1.25}$$

where the first term is the total number of sequences of weight i, and the second term is the number of sequences of weight i that lie within incorrect decoding spheres. When i symbol errors in the received word cause a decoding failure, the decoded symbols in the output of a reproducing decoder contain i errors. Therefore, (1.19) implies that the *information-symbol error rate for a reproducing decoder* is

$$P_{is} = \sum_{i=t+1}^{n} \left(\frac{P_s}{q-1}\right)^i (1-P_s)^{n-i} \left[\sum_{l=\max(i-t,d_m)}^{\min(i+t,n)} A_l N(l,i) \frac{l}{n} + L(i)\frac{i}{n}\right]. \tag{1.26}$$

Two major problems still arise in calculating P_{is} from (1.24) or (1.26). The computational complexity may be prohibitive when n and q are large, and the weight distribution is unknown for many linear or cyclic block codes.

The *packing density* is defined as the ratio of the number of words in the q^k decoding spheres to the total number of sequences of length n. From (2), it follows that the packing density is

$$D_p = \frac{q^k}{q^n} \sum_{i=0}^{t} \binom{n}{i} (q-1)^i. \tag{1.27}$$

For perfect codes, $D_p = 1$. If $D_p > 0.5$, undetected errors tend to occur more often then decoding failures, and the code is considered *tightly packed*. If $D_p < 0.1$, decoding failures predominate, and the code is considered *loosely packed*. The packing densities of binary BCH codes are listed in Table 1.1. The codes are tightly packed if $n = 7$ or 15. For $k > 1$ and $n = 31, 63$, or 127, the codes are tightly packed only if $t = 1$ or 2.

To approximate P_{is} for tightly packed codes, let $A(i)$ denote the event that i errors occur in a received sequence of n symbols at the decoder input. If the symbol errors are independent, the probability of this event is

$$P[A(i)] = \binom{n}{i} P_s^i (1 - P_s)^{n-i}. \tag{1.28}$$

Given event $A(i)$ for i such that $d_m \leq i \leq n$, it is plausible to assume that a reproducing bounded-distance decoder usually chooses a codeword with approximately i symbol errors. For i such that $t + 1 \leq i \leq d_m$, it is plausible to assume that the decoder usually selects a codeword at the minimum distance d_m. These approximations, (1.23), (1.28), and the identity $\binom{n}{i}\frac{i}{n} = \binom{n-1}{i-1}$ indicate that P_{is} for reproducing decoders of systematic codes is approximated by

$$P_{is} \approx \sum_{i=t+1}^{d_m} \frac{d_m}{n}\binom{n}{i} P_s^i (1 - P_s)^{n-i} + \sum_{i=d_m+1}^{n} \binom{n-1}{i-1} P_s^i (1 - P_s)^{n-i}. \tag{1.29}$$

The virtues of this approximation are its lack of dependence on the code weight distribution and its generality. Computations for specific codes indicate that the accuracy of this approximation tends to increase with P_{ud}/P_{df}. The right-hand side of (1.29) gives an approximate upper bound on P_{is} for erasing bounded-distance decoders, for loosely packed codes with bounded-distance decoders, and for complete decoders because some received sequences with $t + 1$ or more errors can be corrected and, hence, produce no information-symbol errors. When a symbol is modified by the decoder, the bit error probability tends to be near 1/2. Thus, $P_b \approx 0.5P_{is}$ for a tightly packed code and a reproducing bounded-distance decoder.

For a loosely packed code, it is plausible that P_{is} for a reproducing bounded-distance decoder might be accurately estimated by ignoring undetected errors. Dropping the terms involving $N(l, i)$ in (1.25) and (1.26) and using (1.23) gives

$$P_{is} \geq \sum_{i=t+1}^{n} \binom{n-1}{i-1} P_s^i (1 - P_s)^{n-i}. \tag{1.30}$$

The virtue of this lower bound as an approximation is its independence of the code weight distribution. The bound is tight when decoding failures are the predominant error mechanism. For cyclic Reed–Solomon codes, numerical examples [6] indicate that the exact P_{is} and the approximate bound are quite close for all values of P_s when $t \geq 3$, a result that is not surprising in view of the paucity of sequences in the decoding spheres for a Reed–Solomon code with $t \geq 3$. A comparison of (1.30) with (1.29) indicates that the latter overestimates P_{is} by a factor of less than $d_m/(t + 1)$.

Since at least one of the information bits is incorrect when an information-symbol error occurs,

$$\frac{P_{is}}{m} \leq P_b. \tag{1.31}$$

This lower bound approximates P_b when there tends to be a single bit error per code-symbol error before decoding and the reproducing decoder is unlikely to change an information symbol. A *constellation labeling* or *labeling map* is the mapping of a bit pattern or group of m bits into each of the 2^m symbols or points in a signal-set constellation. A *Gray labeling* or *Gray mapping* is a labeling in which nearest neighbors in the constellation are assigned bit patterns that differ by only one bit. Thus, the bound in (1.31) closely approximates P_b when a Gray mapping is used and the signal-to-noise ratio is high.

A *q-ary symmetric channel* or *uniform discrete channel* is one in which an incorrectly decoded information symbol is equally likely to be any of the remaining $q-1$ symbols in the alphabet. Consider a linear (n,k) block code and a q-ary symmetric channel such that q is a power of 2. Among the $q-1$ incorrect symbols, a given bit is incorrect in $q/2$ instances. Therefore, the information-bit error probability is

$$P_b = \frac{q}{2(q-1)} P_{is}. \tag{1.32}$$

The uniform discrete channel is a suitable model and (1.32) is applicable when the code symbols are transmitted as orthogonal signals and the reproducing decoder is unlikely to change an information symbol.

Let r denote the ratio of information bits to transmitted channel symbols. For binary codes, r is the code rate. For block codes with $m = \log_2 q$ information bits per symbol, $r = mk/n$. When coding is used but the information rate is preserved, the duration of a channel symbol is changed relative to that of an information bit. Thus, the energy per received channel symbol is

$$\mathcal{E}_s = r\mathcal{E}_b = \frac{mk}{n}\mathcal{E}_b \tag{1.33}$$

where $\mathcal{E}_b$ is the energy per information bit. When $r < 1$, a code is potentially beneficial if its error-control capability is sufficient to overcome the degradation due to the reduction in the energy per received symbol.

For the AWGN channel and coherent binary phase-shift keying (BPSK), it is shown subsequently in a more general setting that the symbol error probability at the demodulator output is

$$P_s = Q\left(\sqrt{\frac{2r\mathcal{E}_b}{N_0}}\right) \tag{1.34}$$

where the Q-function is defined as

$$Q(x) = \frac{1}{\sqrt{2\pi}} \int_x^\infty \exp\left(-\frac{y^2}{2}\right) dy = \frac{1}{2}\text{erf}\, c\left(\frac{x}{\sqrt{2}}\right) \tag{1.35}$$

and $erfc(\cdot)$ is the complementary error function.

If the alphabets of the code symbols and the transmitted channel symbols are the same, then the channel-symbol error probability P_{cs} equals the code-symbol

error probability P_s. If not, then the q-ary code symbols may be mapped into q_1-ary channel symbols. If $q = 2^m$ and $q_1 = 2^{m_1}$, then choosing m/m_1 to be an integer is strongly preferred for implementation simplicity. Since any of the channel-symbol errors can cause an error in the corresponding code symbol, the independence of channel-symbol errors implies that

$$P_s = 1 - (1 - P_{cs})^{m/m_1}. \tag{1.36}$$

A common application is to map nonbinary code symbols into binary channel symbols ($m_1 = 1$). For coherent BPSK, (1.34) and (1.36) imply that

$$P_s = 1 - \left[1 - Q\left(\sqrt{\frac{2r\mathcal{E}_b}{N_0}}\right)\right]^m. \tag{1.37}$$

1.1.2 *Soft-Decision Decoding and Code Metrics for Pulse Amplitude Modulation*

A symbol is said to be erased when the demodulator, after deciding that a symbol is unreliable, instructs the decoder to ignore that symbol during the decoding. The simplest practical soft-decision decoding uses *erasures* to supplement hard-decision decoding. If a code has a minimum distance d_m and a received word is assigned ϵ erasures, then all codewords differ in at least $d_m - \epsilon$ of the unerased symbols. Hence, ν errors can be corrected if $2\nu + 1 \leq d_m - \epsilon$. If d_m or more erasures are assigned, a decoding failure occurs. Let P_e denote the probability of an erasure. For independent symbol errors and erasures, the probability that a received sequence has i errors and ϵ erasures is $P_s^i P_e^\epsilon (1 - P_s - P_e)^{n-i-\epsilon}$. Therefore, for a bounded-distance decoder,

$$P_w \leq \sum_{\epsilon=0}^{n} \sum_{i=i_0}^{n-\epsilon} \binom{n}{\epsilon} \binom{n-\epsilon}{i} P_s^i P_e^\epsilon (1 - P_s - P_e)^{n-i-\epsilon},$$

$$i_0 = \max(0, \lceil (d_m - \epsilon)/2 \rceil) \tag{1.38}$$

where $\lceil x \rceil$ denotes the smallest integer greater than or equal to x. This inequality becomes an equality for an erasing decoder. For the AWGN channel, decoding with optimal erasures provides an insignificant performance improvement relative to hard-decision decoding, but erasures are often effective against fading or sporadic interference. Codes for which *errors-and-erasures decoding* is most attractive are those with relatively large minimum distances such as Reed–Solomon codes.

Traditional decoders (excluding turbo and low-density parity-check decoders) are maximum-likelihood sequence detectors that seek to minimize the word error probability assuming that the *a priori* word probabilities are equal. Soft decisions

are used to associate a number called the *metric* with each possible codeword. The metric is a function of both the codeword and the demodulator output samples. A soft-decision decoder selects the codeword with the largest metric and then produces the corresponding information bits as its output. Let $\mathbf{y}$ denote the n-dimensional vector of noisy output samples $y_i, i = 1, 2, \ldots, n$, produced by a demodulator that receives a sequence of n symbols. Let $\mathbf{x}_m$ denote the mth codeword vector with symbols $x_{mi}, i = 1, 2, \ldots, n$. Let $f(\mathbf{y}|\mathbf{x}_l)$ denote the *likelihood function*, which is the conditional probability density function of $\mathbf{y}$ given that $\mathbf{x}_m$ was transmitted. The maximum-likelihood decoder finds the value of m, $1 \leq m \leq q^k$, for which the likelihood function is largest. If this value is m_0, the decoder decides that codeword m_0 was transmitted. Any monotonically increasing function of $f(\mathbf{y}|\mathbf{x}_m)$ may serve as the metric of a maximum-likelihood decoder. A convenient choice is often proportional to the logarithm of $f(\mathbf{y}|\mathbf{x}_m)$, which is called the *log-likelihood function*. For statistically independent demodulator outputs, the log-likelihood function for each of the q^k possible codewords is

$$\ln f(\mathbf{y}|\mathbf{x}_l) = \sum_{i=1}^{n} \ln f(y_i|x_{mi}), \qquad m = 1, 2, \ldots, q^k \tag{1.39}$$

where $f(y_i|x_{mi})$ is the conditional probability density function of y_i given the value of x_{mi}.

Consider *pulse amplitude modulation*, which includes q-ary *quadrature amplitude modulation* (QAM) and *phase-shift keying (PSK)*. If symbol i of codeword m is transmitted over the AWGN channel, then the received signal is

$$r_i(t) = \mathrm{Re}\left[\sqrt{2\mathcal{E}_s}x_{mi}\psi(t)e^{j2\pi f_c t+\theta_i}\right]+n(t), \quad (i-1)T_s \leq t \leq iT_s, \quad i = 1, 2, \ldots, n \tag{1.40}$$

where $j = \sqrt{-1}$, $\mathcal{E}_s$ is the symbol energy, T_s is the symbol duration, f_c is the carrier frequency, x_{mi} is a complex number representing a point in the signal constellation, $\psi(t)$ is the real-valued symbol waveform, θ_i is the carrier phase, and $n(t)$ is zero-mean, Gaussian noise. The complex numbers representing constellation points are normalized so that they have unity average power. It is assumed that $\psi(t)$ has unit energy in a symbol interval:

$$\int_{(i-1)T_s}^{iT_s} \psi^2(t)dt = 1. \tag{1.41}$$

It is assumed that the spectrum of $\psi(t)$ is negligible unless $|f| < f_c$. Therefore, the symbol energy is

$$\mathcal{E}_{si} = \int_{(i-1)T_s}^{iT_s} s_{mi}^2(t)dt \tag{1.42}$$

where $s_{mi}(t) = \mathrm{Re}[\sqrt{2\mathcal{E}_s}x_{mi}\psi(t)e^{j2\pi f_c t+\theta_i}]$. This result is verified by the latter equation into the right-hand side of (1.42) expanding the result in terms of

integrals, and then using the spectral assumption to eliminate negligible integrals. For coherent demodulation, the receiver is synchronized with the carrier phase, which is removed. A frequency translation to baseband is provided by multiplying $r_i(t)$ by $\sqrt{2}\psi(t)\exp(-2\pi f_c t + \theta_i)$. After discarding a negligible integral, we find that the matched-filter demodulator, which is matched to $\psi(t)$, produces the output samples

$$y_i = \sqrt{\mathcal{E}_{si}}x_{mi} + n_i, \quad i = 1, 2, \ldots, n \tag{1.43}$$

where

$$n_i = \sqrt{2}\int_{(i-1)T_s}^{iT_s} n(t)\psi(t)\exp\left(-2\pi f_c t + \theta_i\right) dt. \tag{1.44}$$

These outputs provide sufficient statistics because $\psi(t)\cos(2\pi f_c t + \theta_i)$ and $\psi(t)\sin(2\pi f_c t + \theta_i)$ are the basis functions for the signal space.

The autocorrelation of the zero-mean Gaussian noise is

$$E[n(t)n(t+\tau)] = \frac{N_{0i}}{2}\delta(\tau), \quad (i-1)T_s \le t \le iT_s, \quad i = 1, 2, \ldots, n \tag{1.45}$$

where $N_{0i}/2$ is the two-sided power spectral density of $n(t)$ in the interval $(i-1)T_s \le t \le iT_s$, and $\delta(\tau)$ is the Dirac delta function. Straightforward calculations using (1.45) and the confined spectrum of $\psi(t)$ indicate that n_i is zero-mean and that $E[n_i n_k] = 0$. Because of the latter two properties, the random variables $n_i, i = 1, 2, \ldots, n$ are said to have *circular symmetry*. Similar calculations indicate that $E[|n_i|^2] = N_{0i}$ and that $E[n_i n_k^*] = 0$, $i \ne k$, where the asterisk denotes the complex conjugate. Since the real and imaginary components of each n_i are jointly Gaussian, n_i is a circularly symmetric, *complex-valued Gaussian random variable*. Expansions of $E[n_i n_k] = 0$, $E[|n_i|^2] = N_{0i}$, and $E[n_i n_k^*] = 0$, $i \ne k$, in terms of the real and are imaginary components of n_i and n_k imply that these components are uncorrelated, and hence statistically independent, and that the components of n_i have the same variance $N_{0i}/2$. Therefore, the $\{y_i\}$ are statistically independent. Since the density of a complex-valued random variable is defined to be the joint density of its real and imaginary parts, the conditional probability density function of y_i given x_{mi} is

$$f\left(y_i \mid x_{mi}\right) = \frac{1}{\pi N_{0i}}\exp\left(-\frac{\left|y_i - \sqrt{\mathcal{E}_{si}}x_{mi}\right|^2}{N_{0i}}\right), \; i = 1, 2, \ldots, n \tag{1.46}$$

and the log-likelihood function is

$$\log f(\mathbf{y}|\mathbf{x}_l) = -\frac{1}{2}\sum_{i=1}^{n}\log\left(\pi N_{0i}\right) - \sum_{i=1}^{n}\frac{\left|y_i - \sqrt{\mathcal{E}_{si}}x_{mi}\right|^2}{N_{0i}}. \tag{1.47}$$

Since the first sum is independent of the codeword m, it may be discarded in the metric derived from the log-likelihood function. Therefore, the *maximum-likelihood metric* for pulse amplitude modulation is

$$U(m) = -\sum_{i=1}^{n} \frac{\left| y_i - \sqrt{\mathcal{E}_{si}} x_{mi} \right|^2}{N_{0i}}, \quad m = 1, 2, \ldots, 2^k \tag{1.48}$$

which requires knowledge of N_{0i}, $i = 1, 2, \ldots, n$. If the $\{N_{0i}\}$ are all equal, then these factors are irrelevant to the decision making and may be discarded. As a result, the maximum-likelihood metric is the negative of the sum of *Euclidean distances* between the received sequence and the sequence of codeword symbols.

Consider BPSK in which $x_{mi} = +1$ when binary symbol i is a 1 and $x_{mi} = -1$ when binary symbol i is a 0. Then $\mathcal{E}_{si} = \mathcal{E}_s$ for each symbol. If each $N_{0i} = N_0$, then these factors are irrelevant. After discarding irrelevant terms and factors that are identical for all codewords, we obtain the maximum-likelihood metric

$$U(m) = \sum_{i=1}^{n} x_{mi} y_{ri}, \quad m = 1, 2, \ldots, 2^k \tag{1.49}$$

where $y_{ri} = \mathrm{Re}(y_i)$. Equation (1.46) implies that

$$f\left(y_{ri} \mid x_{mi}\right) = \frac{1}{\sqrt{\pi N_{0i}}} \exp\left[-\frac{\left(y_{ri} - \sqrt{\mathcal{E}_s} x_{mi}\right)^2}{N_{0i}} \right], \; i = 1, 2, \ldots, n. \tag{1.50}$$

Let $P_2(l)$ denote the probability that the metric for an incorrect codeword at Hamming distance l from the correct codeword exceeds the metric for the correct codeword. After reordering the samples $\{y_{ri}\}$, the difference between the metrics for the correct codeword and the incorrect one may be expressed as

$$D(l) = \sum_{i=1}^{l} (x_{1i} - x_{2i}) y_{ri} = 2 \sum_{i=1}^{l} x_{1i} y_{ri} \tag{1.51}$$

where the sum includes only the l terms that differ, x_{1i} refers to the correct codeword, x_{2i} refers to the incorrect codeword, and $x_{2i} = -x_{1i}$. Then $P_2(l)$ is the probability that $D(l) < 0$. Since each of its terms is independent and each y_{ri} has a Gaussian distribution, $D(l)$ has a Gaussian distribution with mean $l\sqrt{\mathcal{E}_s}$ and variance $lN_{0i}/2$. Since $\mathcal{E}_s = r\mathcal{E}_b$, a straightforward calculation yields

$$P_2(l) = Q\left(\sqrt{\frac{2lr\mathcal{E}_b}{N_0}} \right) \tag{1.52}$$

which reduces to (1.34) when a single symbol is considered and $l = 1$.

Consider the detection of a single QPSK data symbols so that $n = 1$ and $k = 2$. The constellation symbols are $x_m = (\pm 1 \pm j)/\sqrt{2}$, and the maximum-likelihood metric of (1.48) becomes

$$U(m) = -\left| y - \sqrt{\mathcal{E}_s} x_m \right|^2, \quad m = 1, 2, 3, 4. \tag{1.53}$$

Without loss of generality because of the constellation symmetry, we assume the transmitted symbol is $x_m = (1 + j)/\sqrt{2}$. A symbol error occurs if y does not lie in the first quadrant. The symbol error probability is

$$P_s = 1 - P\left[\mathrm{Re}\,(y) > 0\right] P\left[\mathrm{Im}\,(y) > 0\right] \tag{1.54}$$

and a straightforward calculation using $\mathcal{E}_s = 2r\mathcal{E}_b$yields

$$\begin{aligned} P_s &= 2Q\left[\sqrt{\frac{2r\mathcal{E}_b}{N_0}}\right] - Q^2\left[\sqrt{\frac{2r\mathcal{E}_b}{N_0}}\right] \\ &\cong 2Q\left[\sqrt{\frac{2r\mathcal{E}_b}{N_0}}\right], \quad \frac{2r\mathcal{E}_b}{N_0} \gg 1. \end{aligned} \tag{1.55}$$

A fundamental property of a probability, called *countable subadditivity*, is that the probability of a finite or countable union of events B_n, $n = 1, 2, \ldots$, satisfies

$$P\left[\cup_n B_n\right] \leq \sum_n P\left[B_n\right]. \tag{1.56}$$

In communication theory, a bound obtained from this inequality is called a *union bound*. To determine P_w for linear block codes, it suffices to assume that the all-zero codeword was transmitted. The union bound and the relation between weights and distances imply that P_w for soft-decision decoding satisfies

$$P_w \leq \sum_{l=d_m}^{n} A_l P_2(l). \tag{1.57}$$

Let β_l denote the total information-symbol weight of the codewords of weight l. The union bound and (1.20) imply that

$$P_{is} \leq \sum_{l=d_m}^{n} \frac{\beta_l}{k} P_2(l). \tag{1.58}$$

To determine β_l for any cyclic (n, k) code, consider the set S_l of A_l codewords of weight l. The total weight of all the codewords in S_l is $A_T = lA_l$. Let α and β denote any two fixed positions in the codewords. By definition, any cyclic shift of

a codeword produces another codeword of the same weight. Therefore, for every codeword in S_l that has a zero in α, there is some codeword in S_l that results from a cyclic shift of that codeword and has a zero in β. Thus, among the codewords of S_l, the total weight of all the symbols in a fixed position is the same regardless of the position and is equal to A_T/n. The total weight of all the information symbols in S_l is $\beta_l = kA_T/n = klA_l/n$. Therefore,

$$P_{is} \leq \sum_{l=d_m}^{n} \frac{l}{n} A_l P_2(l). \tag{1.59}$$

Optimal soft-decision decoding cannot be efficiently implemented except for very short block codes, primarily because the number of codewords for which the metrics must be computed is prohibitively large, but approximate maximum-likelihood decoding algorithms are available. The *Chase algorithm* generates a small set of candidate codewords that will almost always include the codeword with the largest metric. Test patterns are generated by first making hard decisions on each of the received symbols and then altering the least reliable symbols, which are determined from the demodulator outputs given by (1.43). Hard-decision decoding of each test pattern and the discarding of decoding failures generate the candidate codewords. The decoder selects the candidate codeword with the largest metric.

The quantization of soft-decision information to more than two levels requires analog-to-digital conversion of the demodulator output samples. Since the optimal location of the levels is a function of the signal, thermal noise, and interference powers, automatic gain control is often necessary. For the AWGN channel, it is found that an eight-level quantization represented by three bits and a uniform spacing between threshold levels cause no more than a few tenths of a decibel loss relative to what could theoretically be achieved with unquantized analog voltages or infinitely fine quantization.

The *coding gain* of one code compared with another one is the reduction in the signal power or value of E_b/N_0 required to produce a specified information-bit or information-symbol error probability. Calculations for specific communication systems and codes operating over the AWGN channel have shown that an optimal soft-decision decoder provides a coding gain of approximately 2 dB relative to a hard-decision decoder. However, soft-decision decoders are much more complex to implement and may be too slow for the processing of high information rates. For a given level of implementation complexity, hard-decision decoders can accommodate much longer block codes, thereby at least partially overcoming the inherent advantage of soft-decision decoders. In practice, soft-decision decoding other than erasures is seldom used with block codes of length greater than 50.

1.1.3 Code Metrics for Orthogonal Signals

For q-ary orthogonal complex-valued symbol waveforms, $s_1(t)$, $s_2(t)$, ..., $s_q(t)$, q matched filters, each implemented as a pair of baseband matched filters, are needed.

The observation vector is $\mathbf{y} = [\mathbf{y}_1\ \mathbf{y}_2 \ldots\ \mathbf{y}_q]$, where each $\mathbf{y}_k$ is an n-dimensional row vector of matched-filter output samples for filter k with components $y_{ki}, i = 1, 2, \ldots, n$. Suppose that symbol i of codeword m uses unit-energy waveform $s_{v_{mi}}(t)$, where v_{mi} is an integer that denotes which waveform was transmitted and $1 \leq v_{mi} \leq q$. If codeword m is transmitted over the AWGN channel, the received signal for symbol i can be expressed as

$$r_i(t) = \mathrm{Re}\left[\sqrt{2\mathcal{E}_s} s_{v_{mi}}(t) e^{j2\pi f_c t + \theta_i}\right] + n(t), \quad (i-1)T_s \leq t \leq iT_s, \quad i = 1, 2, \ldots, n \tag{1.60}$$

where $n(t)$ is zero-mean Gaussian noise with autocorrelation given by (1.45), f_c is the carrier frequency, and θ_i is the phase. Since the symbol energy for all the waveforms is unity,

$$\int_{(i-1)T_s}^{iT_s} |s_k(t)|^2 dt = 1, \quad k = 1, 2, \ldots, q. \tag{1.61}$$

The orthogonality of symbol waveforms implies that

$$\int_{(i-1)T_s}^{iT_s} s_k(t) s_l^*(t) dt = 0, \quad k \neq l. \tag{1.62}$$

It is assumed that each of the $\{s_k(t)\}$ has a spectrum confined to $|f| < f_c$. Therefore, the symbol energy is

$$\mathcal{E}_s = \int_{(i-1)T_s}^{iT_s} x_{mi}^2(t) dt \tag{1.63}$$

where $x_{mi}(t) = \mathrm{Re}[\sqrt{2\mathcal{E}_s} s_{v_{mi}}(t) e^{j2\pi f_c t + \theta_i}]$. This result is verified by substituting the latter equation into the right-hand side of (1.63), expanding the result in terms of integrals, and then using the spectral assumption to eliminate negligible integrals. A frequency translation or *downconversion* to baseband is followed by matched filtering. Matched-filter k, which is matched to $s_k(t)$, produces the output samples

$$y_{ki} = \sqrt{2} \int_{(i-1)T_s}^{iT_s} r_i(t) e^{-j2\pi f_c t} s_k^*(t) dt, \quad i = 1, 2, \ldots, n \quad k = 1, 2, \ldots, q. \tag{1.64}$$

where the factor $\sqrt{2}$ has been inserted for mathematical convenience. The substitution of (1.60) into (1.64), (1.62), and the assumption that each of the $\{s_k(t)\}$ has a spectrum confined to $|f| < f_c$ yields

$$y_{ki} = \sqrt{\mathcal{E}_s} e^{j\theta_i} \delta_{k v_{mi}} + n_{ki} \tag{1.65}$$

where $\delta_{k\nu_{mi}} = 1$ if $k = \nu_{mi}$ and $\delta_{k\nu_{mi}} = 0$ otherwise, and

$$n_{ki} = \sqrt{2} \int_{(i-1)T_s}^{iT_s} n(t) e^{-j2\pi f_c t} s_k^*(t) dt. \tag{1.66}$$

Since the real and imaginary components of n_{ki} are jointly Gaussian, this random process is a *complex-valued Gaussian random variable*. Straightforward calculations using (1.45) and the confined spectra of the $\{s_k(t)\}$ indicate that n_{ki} is zero-mean and that $E[n_{ki}n_{lm}] = 0$. Thus, the random variables n_{ki}, $k = 1, 2, \ldots, q$, $i = 1, 2, \ldots, n$, are *circularly symmetric.* Similar calculations and the orthogonality condition (1.62) indicate that $E[|n_{ki}|^2] = N_{0i}$, $k = 1, 2, \ldots, q$, and that $E[n_{ki}n_{lm}^*] = 0$, $l \neq k$ or $i \neq m$. Since the real and imaginary components of each n_{ki} are jointly Gaussian, n_{ki} is a circularly symmetric, *complex-valued Gaussian random variable*. Expansions of the three preceding equations in terms of the real and are imaginary components of n_{ki} and n_{lm} imply that these components are uncorrelated, and hence statistically independent, and that the components of n_{ki}, $k = 1, 2, \ldots, q$, have the same variance $N_{0i}/2$. Therefore, the $\{y_{ki}\}$ are statistically independent. Since the density of a complex-valued random variable is defined to be the joint density of its real and imaginary parts, the conditional probability density function of y_{ki} given θ_i and ν_{mi} is

$$f(y_{ki} \mid \nu_{mi}, \theta_i) = \frac{1}{\pi N_{0i}} \exp\left(-\frac{\left| y_{ki} - \sqrt{\mathcal{E}_s} e^{j\theta_i} \delta_{k\nu_{mi}} \right|^2}{N_{0i}} \right),$$
$$i = 1, 2, \ldots, n, \quad k = 1, 2, \ldots, q. \tag{1.67}$$

Thus, the likelihood function of the qn-dimensional observation vector $\mathbf{y}$, which has components equal to the $\{y_{ki}\}$, is the product of the qn densities specified by (1.67):

$$f(\mathbf{y} \mid \boldsymbol{\nu}_m, \boldsymbol{\theta}) = \prod_{i=1}^{n} \left[\left(\frac{1}{\pi N_{0i}} \right)^q \exp\left(-\frac{\left| y_{\nu_{li}} - \sqrt{\mathcal{E}_s} e^{j\theta_i} \right|^2}{N_{0i}} - \sum_{k=1, k\neq\nu_{mi}}^{q} \frac{|y_{ki}|^2}{N_{0i}} \right) \right] \tag{1.68}$$

where $\boldsymbol{\theta}$ and $\boldsymbol{\nu}_m$ are the n-dimensional vectors that have the $\{\theta_i\}$ and $\{\nu_{mi}\}$ as components, respectively.

For *coherent* signals, the $\{\theta_i\}$ are tracked by the phase synchronization system and, thus, ideally may be set to zero. Forming the log-likelihood function with the $\{\theta_i\}$ set to zero, eliminating irrelevant terms that are independent of m, we obtain the maximum-likelihood metric

$$U(m) = \sum_{i=1}^{n} \frac{\mathrm{Re}(V_{mi})}{N_{0i}} \tag{1.69}$$

where $V_{mi} = y_{v_{mi}}$ is the sampled output i of the filter matched to $s_{v_{mi}}(t)$, the signal representing symbol i of codeword m. The maximum-likelihood decoder finds the value of m for which $U(m)$ is largest. If this value is m_0, the decoder decides that codeword m_0 was transmitted. A problem with this metric is that each N_{0i} value must be known or estimated. However, If it is known that each $N_{0i} = N_0$, then N_0 is common to the metrics of all codewords. Thus, the *maximum-likelihood metric for coherent orthogonal signals* is

$$U(m) = \sum_{i=1}^{n} \mathrm{Re}\,(V_{mi}) \tag{1.70}$$

and the common value N_0 does not need to be known to apply this metric.

The modified Bessel function of the first kind and order zero may be defined as

$$I_0(x) = \sum_{i=0}^{\infty} \frac{1}{i!i!}\left(\frac{x}{2}\right)^{2i}. \tag{1.71}$$

A substitution of the series expansion of the exponential function and a term-by-term integration gives the representation

$$I_0(x) = \frac{1}{2\pi}\int_0^{2\pi} \exp(x\cos u)du. \tag{1.72}$$

Since the cosine is a periodic function and the integration is over the same period, we may replace $\cos u$ with $\cos(u+\theta)$ for any θ in (1.72). A trigonometric expansion with $x_1 = |x|\cos\theta$ and $x_2 = |x|\sin\theta$ then yields

$$\begin{aligned} I_0(|x|) &= \frac{1}{2\pi}\int_0^{2\pi} \exp\{\mathrm{Re}[|x|\,e^{j(u+\theta)}]\}du \\ &= \frac{1}{2\pi}\int_0^{2\pi} \exp\left(x_1\cos u - x_2\sin u\right)du, \quad |x| = \sqrt{x_1^2 + x_2^2}. \end{aligned} \tag{1.73}$$

For *noncoherent* signals, it is assumed that each θ_i is independent and uniformly distributed over $[0, 2\pi)$, which preserves the independence of the $\{y_{ki}\}$. Expanding the argument of the exponential function in (1.59), expressing y_{ki} in polar form, and using (1.73) to integrate over each θ_i, we obtain the likelihood function of the observation vector $\mathbf{y}$:

$$f(\mathbf{y} \mid \boldsymbol{v}_m) = \prod_{i=1}^{n}\left[\begin{array}{l} \left(\frac{1}{\pi N_{0i}}\right)^q \exp\left(-\frac{|y_{v_{mi}}|^2+\mathcal{E}_s}{N_{0i}} - \sum\limits_{k=1,k\neq v_{mi}}^{q} \frac{|y_{ki}|^2}{N_{0i}}\right) \\ \qquad \times I_0\left(\frac{2\sqrt{\mathcal{E}_s}|y_{v_{mi}}|}{N_{0i}}\right) \end{array}\right]. \tag{1.74}$$

Let $R_{mi} = |y_{v_{mi}}|$ denote the sampled envelope produced by the filter matched to $s_{v_{mi}}(t)$, the signal representing symbol i of codeword m. We form the log-likelihood function and eliminate terms and factors that do not depend on the codeword, thereby obtaining the *maximum-likelihood metric for noncoherent orthogonal signals*:

$$U(m) = \sum_{i=1}^{n} \log I_0\left(\frac{2\sqrt{\mathcal{E}_s}R_{mi}}{N_{0i}}\right) \tag{1.75}$$

which requires that each N_{0i} value must be known or estimated. If each $N_{0i} = N_0$, then the maximum-likelihood metric is

$$U(m) = \sum_{i=1}^{n} \log I_0\left(\frac{2\sqrt{\mathcal{E}_s}R_{mi}}{N_0}\right) \tag{1.76}$$

and $\sqrt{\mathcal{E}_s}/N_0$ must be known to apply this metric.

It is highly desirable to have an approximation of (1.76) to reduce the computational requirements. From the series representation of $I_0(x)$, it follows that

$$I_0(x) \leq \exp\left(\frac{x^2}{4}\right). \tag{1.77}$$

From the integral representation, we obtain

$$I_0(x) \leq \exp(|\ x\ |). \tag{1.78}$$

The upper bound in (1.77) is tighter for $0 \leq x < 4$, while the upper bound in (1.78) is tighter for $4 < x < \infty$. If we assume that $\sqrt{\mathcal{E}_s}R_{mi}/N_{0i}$ is often less than 2, then the approximation of $I_0(x)$ by $\exp(x^2/4)$ is reasonable. Substitution into (1.75) and dropping an irrelevant constant gives the metric

$$U(m) = \sum_{i=1}^{n} \frac{R_{mi}^2}{N_{0i}^2}. \tag{1.79}$$

If each $N_{0i} = N_0$, then the value of N_0 is irrelevant, and we obtain the *Rayleigh metric*

$$U(m) = \sum_{i=1}^{n} R_{mi}^2 \tag{1.80}$$

which is suboptimal for the AWGN channel but is the maximum-likelihood metric for the Rayleigh fading channel with identical statistics for each of the symbols (Sect. 5.6). Similarly, (1.78) can be used to obtain suboptimal metrics suitable for large values of $\sqrt{\mathcal{E}_s}R_{mi}/N_{0i}$.

To determine the maximum-likelihood metric for making a hard decision on each symbol, we set $n = 1$ and drop the subscript i in (1.69) and (1.75). We find that the maximum-likelihood symbol metric is $Re(V_m)$ for coherent orthogonal signals

and $\log [I_0(\sqrt{8\mathcal{E}_s}R_m/N_0)]$ for noncoherent orthogonal signals, where the index m ranges over the symbol alphabet. Since the latter function increases monotonically and $\sqrt{8\mathcal{E}_s}/N_0$ is a constant, optimal symbol metrics or decision variables for noncoherent orthogonal signals are R_m or R_m^2 for $m = 1, 2, \ldots, q$.

1.1.4 Metrics and Error Probabilities for Uncoded FSK Symbols

For noncoherent orthogonal frequency-shift keying (FSK), a pair of baseband matched-filter are matched to each unit-energy waveform $s_l(t) = \exp(j2\pi f_l t)/\sqrt{T_s}$, $0 \le t \le T_s$, $l = 1, 2, \ldots, q$. If $r(t)$ is the received signal, a downconversion to baseband and a parallel set of pairs of matched filters and envelope detectors provide the decision variables

$$R_l^2 = \left| \int_0^{T_s} r(t) e^{-j2\pi f_c t} e^{-j2\pi f_l t} dt \right|^2 \tag{1.81}$$

where an irrelevant constant have been omitted. The orthogonality condition (1.62) is satisfied if the adjacent frequencies are separated by k/T_s, where k is a nonzero integer. Expanding (1.81), we obtain

$$R_l^2 = R_{lc}^2 + R_{ls}^2 \tag{1.82}$$

$$R_{lc} = \int_0^{T_s} r(t) \cos [2\pi (f_c + f_l)t] \, dt \tag{1.83}$$

$$R_{ls} = \int_0^{T_s} r(t) \sin [2\pi (f_c + f_l)t] \, dt. \tag{1.84}$$

These equations imply the correlator structure depicted in Fig. 1.2. The comparator decides what symbol was transmitted by observing which comparator input is the largest.

To derive an alternative implementation, we observe that when the waveform is $s_l(t) = A \cos 2\pi (f_c + f_l)t$, $0 \le t \le T_s$, the impulse response of a filter matched to it is $A \cos 2\pi (f_c + f_l)(T_s - t)$, $0 \le t \le T_s$. Therefore, the matched-filter output at time t is

$$\begin{aligned} y_l(t) &= \int_0^t r(\tau) \cos [2\pi (f_c + f_l)(\tau - t + T_s)] \, d\tau \\ &= \left\{ \int_0^t r(\tau) \cos [2\pi (f_c + f_l)\tau] \, d\tau \right\} \cos [2\pi (f_c + f_l)(t - T_s)] \\ &\quad + \left\{ \int_0^t r(\tau) \sin [2\pi (f_c + f_l)\tau] \, d\tau \right\} \sin [2\pi (f_c + f_l)(t - T_s)] \\ &= R_l(t) \cos [2\pi (f_c + f_l)(t - T_s) + \phi(t)], \quad 0 \le t \le T_s \end{aligned} \tag{1.85}$$

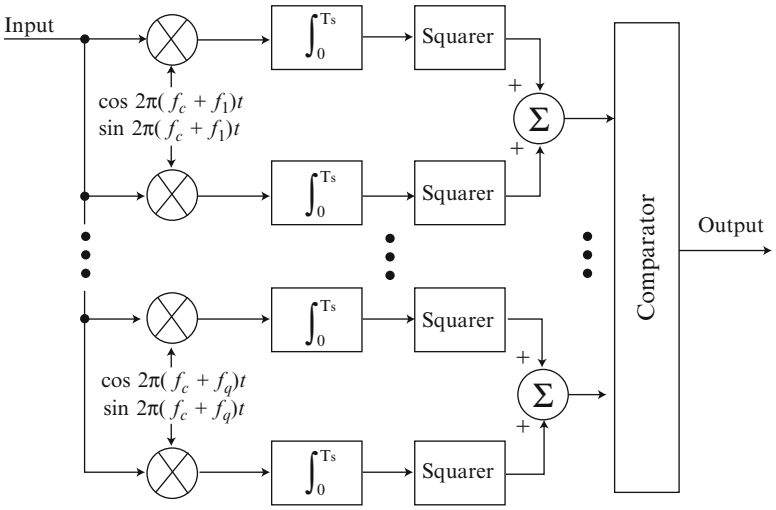

Fig. 1.2 Noncoherent FSK receiver using correlators

where the envelope is

$$R_l(t) = \left\{ \left[\int_0^t r(\tau) \cos\left[2\pi(f_c + f_l)\tau\right] d\tau \right]^2 + \left[\int_0^t r(\tau) \sin\left[2\pi\left(f_c + f_l\right)\tau\right] d\tau \right]^2 \right\}^{1/2}. \tag{1.86}$$

Since $R_l(T_s) = R_l$ given by (1.82), we obtain the receiver structure depicted in Fig. 1.3. A practical envelope detector consists of a peak detector followed by a lowpass filter.

To derive the symbol error probability for equally likely FSK symbols, we assume that the signal $s_1(t)$ was transmitted over the AWGN channel. The received signal has the form $r(t) = \sqrt{2\mathcal{E}_s/T_s}\cos\left[2\pi\left(f_c + f_1\right)t + \theta\right] + n(t)$, $0 \le t \le T_s$. Since $n(t)$ is white,

$$E[n(t)n(t+\tau)] = \frac{N_0}{2}\delta(\tau). \tag{1.87}$$

Using the orthogonality of the symbol waveforms and (1.87) and assuming that $f_c + f_l \gg 1/T_s$ in (1.83) and (1.84), we obtain

$$E[R_{1c}] = \sqrt{\mathcal{E}_s T_s/2}\cos\theta, \quad E[R_{1s}] = \sqrt{\mathcal{E}_s T_s/2}\sin\theta \tag{1.88}$$

$$E[R_{lc}] = E[R_{ls}] = 0, \quad l = 2, \ldots, q \tag{1.89}$$

$$\text{var}(R_{lc}) = \text{var}(R_{ls}) = N_0 T_s/4, \quad l = 1, 2, \ldots, q. \tag{1.90}$$

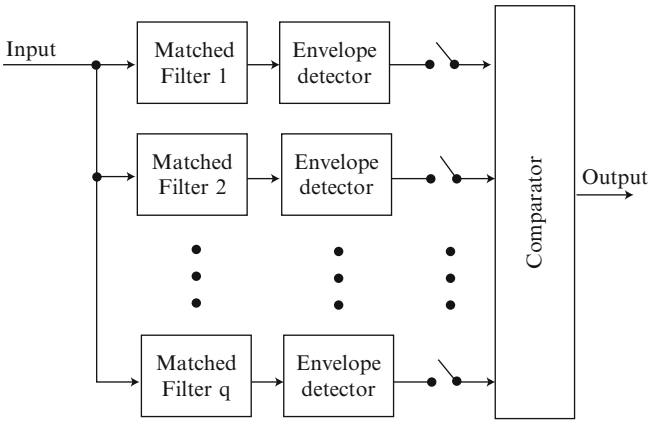

Fig. 1.3 Noncoherent FSK receiver with passband matched filters

Since $n(t)$ is Gaussian, R_{lc} and R_{ls} are jointly Gaussian. Since the covariance of R_{lc} and R_{ls} is zero, they are mutually statistically independent. Therefore, the joint probability density function of R_{lc} and R_{ls} is

$$g_1(r_{lc}, r_{ls}) = \frac{1}{\pi V} \exp\left[-\frac{(r_{lc} - m_{lc})^2 + (r_{ls} - m_{ls})^2}{V}\right] \tag{1.91}$$

where $m_{lc} = E[R_{lc}]$, $m_{ls} = E[R_{ls}]$, and $V = N_0 T_s/2$.

Let R_l and Θ_l be implicitly defined by $R_{lc} = R_l \cos\Theta_l$ and $R_{ls} = R_l \sin\Theta_l$. Since the Jacobian of the transformation is r, we find that the joint density of R_l and Θ_l is

$$g_2(r, \theta) = \frac{r}{\pi V} \exp\left[-\frac{r^2 - 2rm_{lc}\cos\theta - 2rm_{ls}\sin\theta + m_{lc}^2 + m_{ls}^2}{V}\right],$$
$$r \geq 0, \quad |\theta| \leq \pi. \tag{1.92}$$

The density of the envelope R_l is obtained by integration of (1.92) over θ. Using trigonometry and the integral representation of the Bessel function in 1.73, we obtain the density

$$g_3(r) = \frac{2r}{V} \exp\left(-\frac{r^2 + m_{lc}^2 + m_{ls}^2}{V}\right) I_0\left(4r\sqrt{m_{lc}^2 + m_{ls}^2}\right) u(r) \tag{1.93}$$

where $u(r) = 1$ if $r \geq 0$, and $u(r) = 0$ if $r < 0$. Substituting (1.88), we obtain the densities for the R_l, $l = 1, 2, \ldots, q$:

$$f_1(r) = \frac{4r}{N_0 T_s} \exp\left(-\frac{r^2 + \mathcal{E}_s T_s/2}{N_0 T_s/2}\right) I_0\left(\frac{\sqrt{8\mathcal{E}_s T_s}\, r}{N_0 T_s}\right) u(r) \tag{1.94}$$

$$f_l(r) = \frac{4r}{N_0 T_s} \exp\left(-\frac{r^2}{N_0 T_s/2}\right) u(r), \quad l = 2, \ldots, q \tag{1.95}$$

where $u(r) = 1$ if $r \geq 0$, and $u(r) = 0$ if $r < 0$. The orthogonality of the symbol waveforms and the white noise imply that the random variables $\{R_l\}$ are independent. A symbol error occurs when $s_1(t)$ was transmitted if R_1 is not the largest of the $\{R_l\}$. Since the $\{R_l\}$ are identically distributed for $l = 2, \ldots, q$, the probability of a symbol error when $s_1(t)$ was transmitted is

$$P_s = 1 - \int_0^\infty \left[\int_0^r f_2(y)dy\right]^{q-1} f_1(r)dr. \tag{1.96}$$

Substituting (1.95) into the inner integral gives

$$\int_0^r f_2(y)dy = 1 - \exp\left(-\frac{r^2}{N_0 T_s/2}\right). \tag{1.97}$$

Expressing the $(q-1)$th power of this result as a binomial expansion and then substituting into (1.96), the remaining integration may be done by using the fact that for $\lambda > 0$,

$$\int_0^\infty r \exp\left(-\frac{r^2}{2b^2}\right) I_0\left(\frac{r\sqrt{\lambda}}{b^2}\right) dr = b^2 \exp\left(\frac{\lambda}{2b^2}\right) \tag{1.98}$$

which follows from the fact that the density in (1.94) must integrate to unity. The final result is the symbol error probability for noncoherent q-ary FSK over the AWGN channel:

$$P_s = \sum_{i=1}^{q-1} \frac{(-1)^{i+1}}{i+1} \binom{q-1}{i} \exp\left[-\frac{i\mathcal{E}_s}{(i+1)N_0}\right]. \tag{1.99}$$

When $q = 2$, this equation reduces to the classical formula for binary FSK (BFSK):

$$P_s = \frac{1}{2} \exp\left(-\frac{\mathcal{E}_s}{2N_0}\right). \tag{1.100}$$

1.1.5 Performance Examples

Figure 1.4 depicts the information-bit error probability $P_b = P_{is}$ versus $\mathcal{E}_b/N_0$ for various binary block codes with coherent BPSK over the AWGN channel. Equation (1.29) is used to compute P_b for the (23, 12) Golay code with hard decisions. Since the packing density D_p is small for these codes, (1.30) is used for the (63, 36) BCH

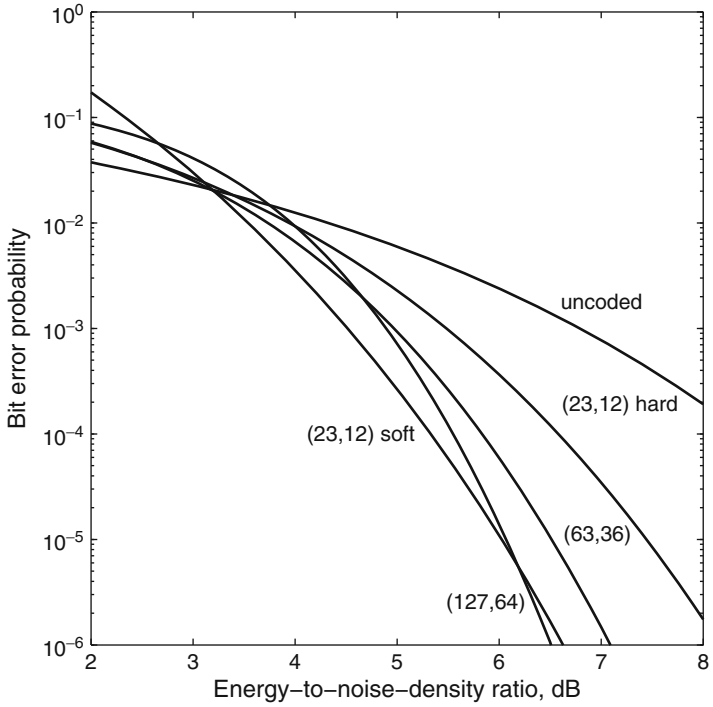

Fig. 1.4 Information-bit error probability for binary block (n, k) codes and coherent BPSK

code, which corrects $t = 5$ errors, and the (127, 64) BCH code, which corrects $t = 10$ errors. Equation (1.34) is used for P_s. Inequality (1.59) and Table 1.2 are used to compute the upper bound on $P_b = P_{is}$ for the (23, 12) Golay code with optimal soft decisions. The graphs illustrate the power of the soft-decision decoding. For the (23, 12) Golay code, soft-decision decoding provides an approximately 2 dB coding gain for $P_b = 10^{-5}$ relative to hard-decision decoding. Only when $P_b < 10^{-5}$ does the (127, 64) BCH code begin to outperform the (23, 12) Golay code with soft decisions. If $\mathcal{E}_b/N_0 \leq 3$ dB, an uncoded system with coherent BPSK provides a lower P_b than a similar system that uses one of the block codes of the figure.

Figure 1.5 illustrates the performance of loosely packed Reed–Solomon codes with hard-decision decoding over the AWGN channel as a function of $\mathcal{E}_b/N_0$. The lower bound in (1.30) is used to compute the approximate information-bit error probabilities for binary channel symbols with coherent BPSK and for nonbinary channel symbols with noncoherent orthogonal FSK. For the nonbinary channel symbols, (1.99) is applicable and the orthogonality of the signals ensures that the channel is q-ary symmetric, and, hence, (1.32) is at least approximately correct. For the binary channel symbols, (1.36) with $m_1 = 1$, 1.34, and the lower bound in (1.31) are used. For the chosen values of n, the best performance at $P_b = 10^{-5}$ is obtained if the code rate is $k/n \approx 3/4$. Further gains result from increasing

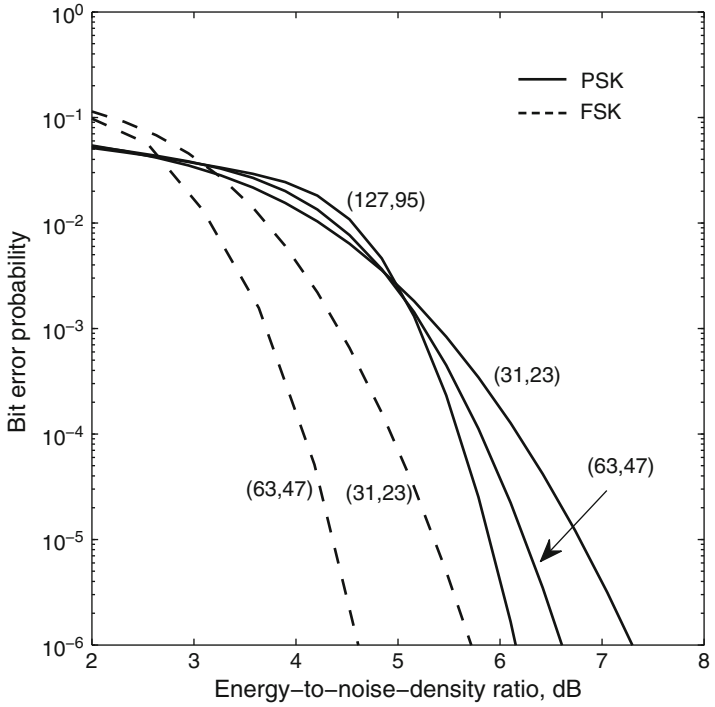

Fig. 1.5 Information-bit error probability for Reed–Solomon (n, k) codes. Modulation is coherent BPSK or noncoherent FSK

n and hence the implementation complexity. Although the figure indicates the performance advantage of Reed–Solomon codes with orthogonal FSK, there is a major bandwidth penalty. Let B denote the bandwidth required for an uncoded BPSK signal. If the same data rate is accommodated by using uncoded BFSK, the required bandwidth for demodulation with envelope detectors is approximately $2B$. For uncoded orthogonal FSK using $q = 2^m$ frequencies, the required bandwidth is $2^m B/m$ because each symbol represents m bits. If a Reed–Solomon (n, k) code is used with FSK, the required bandwidth becomes $2^m nB/mk$.

1.2 Convolutional Codes and Trellis Codes

In contrast to a block codeword, a convolutional codeword represents an entire message of indefinite length. A *convolutional encoder* converts an input of k information bits into an output of n code bits that are Boolean functions of both the current k input bits and the preceding information bits. After k bits are shifted into a shift register and k bits are shifted out, n code bits are read out. Each code bit

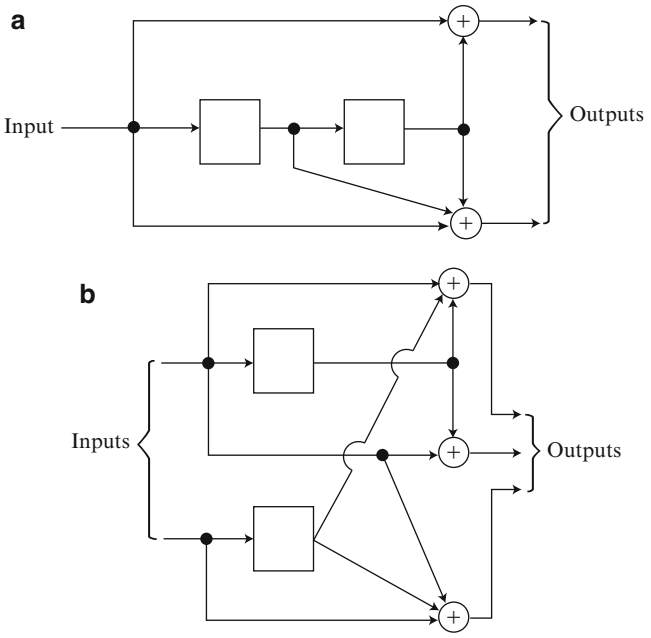

Fig. 1.6 Encoders of nonsystematic convolutional codes with (**a**) $K = 3$ and rate $= 1/2$ and (**b**) $K = 2$ and rate $= 2/3$

is a Boolean function of the outputs of selected shift-register stages. A convolutional code is *linear* if each Boolean function is a modulo-2 sum because the superposition property applies to the input-output relations and the all-zero codeword is a member of the code. For a linear convolutional code, the minimum Hamming distance between codewords is equal to the minimum Hamming weight of a codeword. The *constraint length* K of a convolutional code is the maximum number of sets of n output bits that can be affected by an input bit. A convolutional code is *systematic* if the information bits appear unaltered in each codeword.

A nonsystematic linear convolutional encoder with $k = 1$, $n = 2$, and $K = 3$ is shown in Fig. 1.6a. The shift register consists of 2 memory stages, each of which is implemented as a bistable memory element. Information bits enter the shift register in response to clock pulses. After each clock pulse, the most recent information bit becomes the content and output of the first memory stage, the previous contents of stages are shifted to the right, and the previous content of the final stage is shifted out of the register. The outputs of the modulo-2 adders (exclusive-OR gates) provide two code bits. The *generators* of the output bits are the vectors $\mathbf{g}_1 = [1\,0\,1]$ and $\mathbf{g}_2 = [1\,1\,1]$, which indicate the impulse responses at the two outputs and the stages that are connected to the adders, starting from the left-hand side. In octal form, the three bits of the two generator vectors are represented by (5, 7). The encoder of a nonsystematic convolutional code with $k = 2$, $n = 3$, and $K = 2$ is shown in Fig. 1.6b. Its generators are $\mathbf{g}_1 = [1\,1\,0\,1]$, $\mathbf{g}_2 = [1\,1\,0\,0]$, and $\mathbf{g}_3 = [1\,0\,1\,1]$.

In octal form, (e.g., $1101 \rightarrow 15$, where groups of three bits are octally represented starting from the right-hand side and zeros are understood when fewer than three bits remain), its generators are (15, 14, 13).

Polynomials allow a compact description of the input and output sequences of an encoder. A *polynomial* over the binary field $GF(2)$ has the form

$$f(x) = f_0 + f_1 x + f_2 x^2 + \cdots + f_n x^n$$

where the coefficients $f_0, f_1, \cdots, f_n$ are elements of $GF(2)$ and the symbol x is an indeterminate introduced for convenience in calculations. The *degree* of a polynomial is the largest power of x with a nonzero coefficient. The *sum* of a polynomial $f(x)$ of degree n_1 and a polynomial $g(x)$ of degree n_2 is another polynomial over $GF(2)$ defined as

$$f(x) + g(x) = \sum_{i=0}^{\max(n_1, n_2)} (f_i \oplus g_i)\, x^i$$

where $\max(n_1, n_2)$ denotes the larger of n_1 and n_2. An example is

$$(1 + x^2 + x^3) + (1 + x^2 + x^4) = x^3 + x^4.$$

The *product* of two polynomials over $GF(2)$ is another polynomial over $GF(2)$ defined as

$$f(x)g(x) = \sum_{i=0}^{n_1+n_2} \left(\sum_{k=0}^{i} f_k g_{i-k} \right) x^i$$

where the inner addition is modulo 2. For example,

$$(1 + x^2 + x^3)(1 + x^2 + x^4) = 1 + x^3 + x^5 + x^6 + x^7.$$

It is easily verified that associative, commutative, and distributive laws apply to polynomial addition and multiplication.

The input sequence $m_0, m_1, m_2, \ldots$ is represented by the input polynomial $m(x) = m_0 + m_1 x + m_2 x^2 + \ldots$, and similarly the output polynomial $c(x) = c_0 + c_1 x + c_2 x^2 + \ldots$ represents an output stream. The *generator polynomial* $g(x) = g_0 + g_1 x + \ldots + g_n x^{K-1}$ represents the K or fewer elements of a generator or impulse response. In Fig. 1.6a, encoder output sequences $\mathbf{c}_1$ and $\mathbf{c}_2$ are the convolutions of the input sequence $\mathbf{m}$ and the impulse responses $\mathbf{g}_1$ and $\mathbf{g}_2$, respectively. Since a convolution in the time domain is equivalent to a multiplication in the transform domain, the output vector $\mathbf{c}(x) = [c_1(x)\ c_2(x)]$ is given by

$$\mathbf{c}(x) = m(x)\,\mathbf{G}(x) \tag{1.101}$$

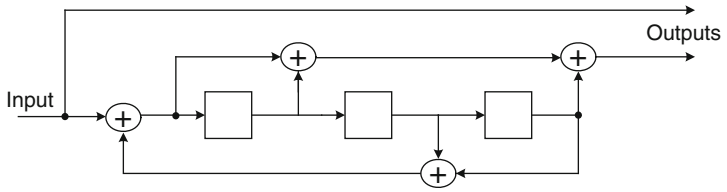

Fig. 1.7 Encoder of recursive systematic convolutional code with $K = 4$ and rate $= 1/2$

where $\mathbf{G}(x) = [g_1(x)\ g_2(x)]$ is the *generator matrix* with transfer functions $g_1(x) = 1 + x^2$ and $g_2(x) = 1 + x + x^2$. In Fig. 1.6b, $\mathbf{c}(x) = [c_1(x)\ c_2(x)\ c_3(x)]$ and $\mathbf{G}(x) = [g_1(x)\ g_2(x)\ g_3(x)]$ with $g_1(x) = 1 + x + x^3$, $g_2(x) = 1 + x$, and $g_3(x) = 1 + x^2 + x^3$.

A *recursive systematic convolutional code* uses feedback and has a generator matrix with at least one rational function. A recursive systematic convolutional code with $K = 4$ and rate $= 1/2$ is generated by the encoder diagrammed in Fig. 1.7. Let $m(i)$ and $m_1(i)$ denote the message and the output of the first adder at discrete-time i, respectively. Then

$$m_1(i) = m(i) \oplus m_1(i-2) \oplus m_1(i-3) \tag{1.102}$$

which implies that $m_1(x)\left(1 + x^2 + x^3\right) = m(x)$. Therefore, the output vector $\mathbf{c}(x) = [c_1(x)\ c_2(x)]$ is given by (1.96) with $\mathbf{G}(x) = [1\ \ G_2(x)]$ and

$$G_2(x) = \frac{\left(1 + x + x^3\right)}{(1 + x^2 + x^3)}. \tag{1.103}$$

The output polynomials are $c_1(x) = m(x)$ and $c_2(x) = m(x)\,G_2(x)$, which is determined by long division. The generators for Fig. 1.7 are $\mathbf{g}_1 = [1\,1\,0\,1]$, which describes the feedforward connections, and $\mathbf{g}_2 = [1\,0\,1\,1]$, which describes the feedback connections. To bring the encoder back to the all-zero state after a codeword transmission, three consecutive feedback bits are inserted as input bits to the leftmost adder. As a result, the encoder will return to the all-zero state after three clock pulses.

Since k bits exit from the shift register as k new bits enter it, only the contents of the $(K-1)k$ memory stages prior to the arrival of new bits affect the subsequent output bits of a convolutional encoder. Therefore, the contents of these $(K-1)k$ stages define the *state* of the encoder. The initial state of a feedforward encoder, which has no feedback connections, is generally the all-zero state. After the message sequence has been encoded $(K-1)k$ zeros must be inserted into the feedforward encoder to complete and terminate the codeword. If the number of message bits is much greater than $(K-1)k$, these terminal zeros have a negligible effect and the *code rate* is well approximated by $r = k/n$. However, the need for the terminal

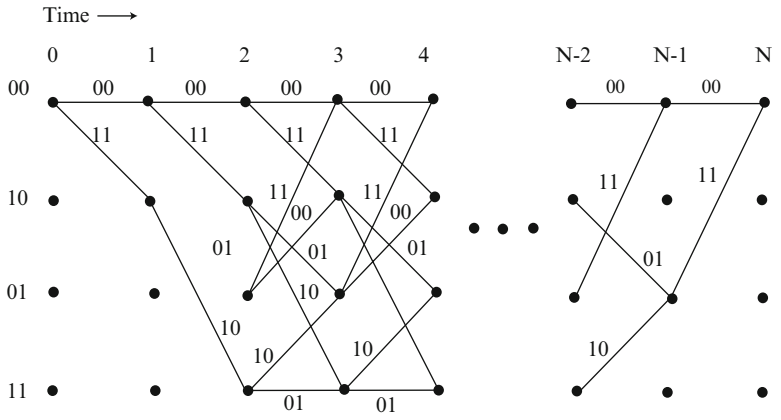

Fig. 1.8 Trellis diagram corresponding to encoder of Fig. 1.6a

zeros renders the convolutional codes unsuitable for short messages. For example, if 12 information bits are to be transmitted, the Golay (23, 12) code provides a better performance than the same convolutional codes that are much more effective when 1,000 or more bits are to be transmitted.

A *trellis diagram* corresponding to the encoder of Fig. 1.6a is shown in Fig. 1.8. Each of the nodes in a column of a trellis diagram represents the state of the encoder at a specific time prior to a clock pulse. The first bit of a state represents the content of the first memory stage, while the second bit represents the content of the second memory stage. Branches connecting nodes represent possible changes of state. Each branch is labeled with the output bits or symbols produced following a clock pulse and the formation of a new encoder state. In this example, the first bit of a branch label refers to the upper output of the encoder. The upper branch leaving a node corresponds to a 0 input bit, while the lower branch corresponds to a 1. Every path from left to right through the trellis represents a possible codeword. If the encoder begins in the all-zero state, not all of the other states can be reached until the initial contents have been shifted out. The trellis diagram then becomes identical from column to column until the final $(K-1)k$ input bits force the encoder back to the zero state.

Each branch of the trellis is associated with a branch metric, and the metric of a codeword is defined as the sum of the branch metrics for the path associated with the codeword. A maximum-likelihood decoder selects the codeword with the largest metric (or smallest metric, depending on how branch metrics are defined). The *Viterbi decoder* implements maximum-likelihood decoding efficiently by sequentially eliminating many of the possible paths. At any node, only the partial path reaching that node with the largest partial metric is retained, for any partial path stemming from the node will add the same branch metrics to all paths that merge at that node.

Since the decoding complexity grows exponentially with constraint length, Viterbi decoders are limited to use with convolutional codes of short constraint

lengths. A Viterbi decoder for a rate-1/2, $K = 7$ convolutional code has approximately the same complexity as a Reed–Solomon (31, 15) decoder. If the constraint length is increased to $K = 9$, the complexity of the Viterbi decoder increases by a factor of approximately 4.

The suboptimal *sequential decoding* of convolutional codes does not invariably provide maximum-likelihood decisions, but its implementation complexity only weakly depends on the constraint length. Thus, very low error probabilities can be attained by using long constraint lengths. The number of computations needed to decode a frame of data is fixed for the Viterbi decoder, but is a random variable for the sequential decoder. When strong interference is present, the excessive computational demands and consequent memory overflows of sequential decoding usually result in a higher bit error probability than for Viterbi decoding and a much longer decoding delay. Thus, Viterbi decoding predominates in communication systems.

To bound bit error probability for the Viterbi decoder of a linear convolutional code, we use the fact that the distribution of either Hamming or Euclidean distances is invariant to the choice of a reference sequence. Consequently, whether the demodulator makes hard or soft decisions, the assumption that the all-zero sequence is transmitted entails no loss of generality in the derivation of the error probability. Let $a(l, i)$ denote the number of paths diverging at a node from the correct path, each having Hamming weight l and i incorrect information symbols over the unmerged segment of the path before it merges with the correct path. Thus, the unmerged segment is at Hamming distance l from the correct all-zero segment. Let d_f denote the *minimum free distance*, which is the minimum distance between any two codewords. Although the encoder follows the all-zero path through the trellis, the decoder in the receiver essentially observes successive columns in the trellis, eliminating paths and thereby sometimes introducing errors at each node. The decoder may select an incorrect path that diverges at node j and introduces errors over its unmerged segment. Let $E[N_e(v)]$ denote the expected value of the number of errors introduced at node v. It is known from (1.20) that the bit error probability P_b equals the *information-bit error rate*, which is defined as the ratio of the expected number of information-bit errors to the number of information bits applied to the convolutional encoder. Therefore, if there are N branches in a complete path,

$$P_b = \frac{1}{kN} \sum_{v=1}^{N} E[N_e(v)]. \tag{1.104}$$

Let $B_v(l, i)$ denote the event that the path with the largest metric diverges at node v and has Hamming weight l and i incorrect information bits over its unmerged segment. Then,

$$E\left[N_e(v)\right] = \sum_{i=1}^{I_v} \sum_{l=d_f}^{D_v} E\left[N_e(v)|B_v(l,i)\right] P\left[B_v(l,i)\right] \tag{1.105}$$

when $E[N_e(v)|B_v(l,i)]$ is the conditional expectation of $N_e(v)$ given event $B_v(l,i)$, $P[B_v(l,i)]$ is the probability of this event, and I_v and D_v are the maximum values of i and l, respectively, that are consistent with the position of node v in the trellis. When $B_v(l,i)$ occurs, i bit errors are introduced into the decoded bits; thus,

$$E[N_e(v)|B_v(l,i)] = i. \tag{1.106}$$

Since the decoder may already have departed from the correct path before node v, the union bound gives

$$P\,[B_v(l,i)] \le a(l,i)P_2(l) \tag{1.107}$$

where $P_2(l)$ is the probability that the correct path segment has a smaller metric than an unmerged path segment that differs in l code symbols. Substituting (1.105) to (1.107) into (1.104) and extending the two summations to ∞, we obtain

$$P_b \le \frac{1}{k}\sum_{i=1}^{\infty}\sum_{l=d_f}^{\infty} i\,a(l,i)P_2(l). \tag{1.108}$$

The *information-weight spectrum* or *distribution* is defined as

$$B(l) = \sum_{i=1}^{\infty} i\,a(l,i), \quad l \ge d_f. \tag{1.109}$$

In terms of this distribution, (1.108) becomes

$$P_b \le \frac{1}{k}\sum_{l=d_f}^{\infty} B(l)P_2(l). \tag{1.110}$$

For coherent BPSK signals over an AWGN channel and soft decisions, (1.52) indicates that

$$P_2(l) = Q\left(\sqrt{\frac{2lr\mathcal{E}_b}{N_0}}\right). \tag{1.111}$$

When the demodulator makes hard decisions and a correct path segment is compared with an incorrect one, correct decoding results if the number of symbol errors in the demodulator output is less than half the number of symbols in which the two segments differ. If the number of symbol errors is exactly half the number of differing symbols, then either of the two segments is chosen with equal probability.

Table 1.4 Parameter values of rate-1/2 convolutional codes with favorable distance properties

			$B(d_f + i)$ for $i = 0, 1, \ldots, 6$						
K	d_f	Generators	0	1	2	3	4	5	6
3	5	5, 7	1	4	12	32	80	192	448
4	6	15, 17	2	7	18	49	130	333	836
5	7	23, 35	4	12	20	72	225	500	1,324
6	8	53, 75	2	36	32	62	332	701	2,342
7	10	133, 171	36	0	211	0	1,404	0	11,633
8	10	247, 371	2	22	60	148	340	1,008	2,642
9	12	561, 763	33	0	281	0	2,179	0	15,035
10	12	1131, 1537	2	21	100	186	474	1,419	3,542
11	14	2473, 3217	56	0	656	0	3,708	0	27,518
12	15	4325, 6747	66	98	220	788	2,083	5,424	13,771

Assuming the independence of symbol errors, it follows that for hard-decision decoding

$$P_2(l) = \begin{cases} \displaystyle\sum_{i=(l+1)/2}^{l} \binom{l}{i} P_s^i \, (1 - P_s)^{l-i} \,, & l \text{ is odd} \\ \displaystyle\sum_{i=l/2+1}^{l} \binom{l}{i} P_s^i \, (1 - P_s)^{l-i} + \frac{1}{2} \binom{l}{l/2} [P_s \, (1 - P_s)]^{l/2} \,, & l \text{ is even.} \end{cases} \tag{1.112}$$

Soft-decision decoding typically provides a 2 dB power savings at $P_b = 10^{-5}$ compared to hard-decision decoding for communications over the AWGN channel. Since the loss due to even three-bit quantization usually is 0.2 to 0.3 dB, soft-decision decoding is highly preferable.

Among the convolutional codes of a given code rate and constraint length, the one giving the smallest upper bound in (1.110) can sometimes be determined by a complete computer search. The codes with the largest value of d_f are selected, and the *catastrophic codes*, for which a finite number of demodulated symbol errors can cause an infinite number of decoded information-bit errors, are eliminated. All remaining codes that do not have the minimum value of $B(d_f)$ are eliminated. If more than one code remains, codes are eliminated on the basis of the minimal values of $B(d_f + 1)$, $B(d_f + 2)$, ..., until one code remains. For binary codes of rates 1/2, 1/3, and 1/4, codes with these favorable distance properties have been determined [7]. For these codes and constraint lengths up to 12, Tables 1.4–1.6 list the corresponding values of d_f and $B(d_f + i)$, $i = 0, 1, \ldots, 7$. Also listed in octal form are the generator sequences that determine which shift-register stages feed the modulo-2 adders associated with each code bit. For example, the best $K = 3$, rate-1/2 code in Table 1.4 has generator sequences 5 and 7, which specify the connections illustrated in Fig. 1.6a.

Approximate upper bounds on P_b for rate-1/2, rate-1/3, and rate-1/4 convolutional codes with coherent BPSK, soft-decision decoding, and infinitely fine

Table 1.5 Parameter values of rate-1/3 convolutional codes with favorable distance properties

			$B(d_f + i)$ for $i = 0, 1, \ldots, 6$						
K	d_f	Generators	0	1	2	3	4	5	6
3	8	5, 7, 7	3	0	15	0	58	0	201
4	10	13, 15, 17	6	0	6	0	58	0	118
5	12	25, 33, 37	12	0	12	0	56	0	320
6	13	47, 53, 75	1	8	26	20	19	62	86
7	15	117, 127, 155	7	8	22	44	22	94	219
8	16	225, 331, 367	1	0	24	0	113	0	287
9	18	575, 673, 727	2	10	50	37	92	92	274
10	20	1167, 1375, 1545	6	16	72	68	170	162	340
11	22	2325, 2731, 3747	17	0	122	0	345	0	1,102
12	24	5745, 6471, 7553	43	0	162	0	507	0	1,420

Table 1.6 Parameter values of rate-1/4 convolutional codes with favorable distance properties

			$B(d_f + i)$ for $i = 0, 1, \ldots, 6$						
K	d_f	Generators	0	1	2	3	4	5	6
3	10	5, 5, 7, 7	1	0	4	0	12	0	32
4	13	13, 13, 15, 17	4	2	0	10	3	16	34
5	16	25, 27, 33, 37	8	0	7	0	17	0	60
6	18	45, 53, 67, 77	5	0	19	0	14	0	70
7	20	117, 127, 155, 171	3	0	17	0	32	0	66
8	22	257, 311, 337, 355	2	4	4	24	22	33	44
9	24	533, 575, 647, 711	1	0	15	0	56	0	69
10	27	1173, 1325, 1467, 1751	7	10	0	28	54	58	54

quantization are depicted in Figs. 1.9–1.11. The graphs are computed by using (1.111), $k = 1$, and Tables 1.4–1.6 in (1.110) and then truncating the series after seven terms. This truncation gives a tight upper bound in P_b for $P_b \leq 10^{-2}$. However, the truncation may exclude significant contributions to the upper bound when $P_b > 10^{-2}$, and the bound itself becomes looser as P_b increases. The figures indicate that the code performance improves with increases in the constraint length and as the code rate decreases if $K \geq 4$. The decoder complexity is almost exclusively dependent on K because there are 2^{K-1} encoder states. However, as the code rate decreases, more bandwidth is required and bit synchronization becomes more challenging due to a reduced energy per symbol.

For convolutional codes of rate $1/n$, two trellis branches enter each state. For higher-rate codes with k information bits per branch, 2^k trellis branches enter each state and the computational complexity may be large. This complexity can be avoided by using *punctured convolutional codes*. These codes are generated by periodically deleting bits from one or more output streams of an encoder for an unpunctured rate-$1/n$ code. For a period-p punctured code, p sets of n bits are

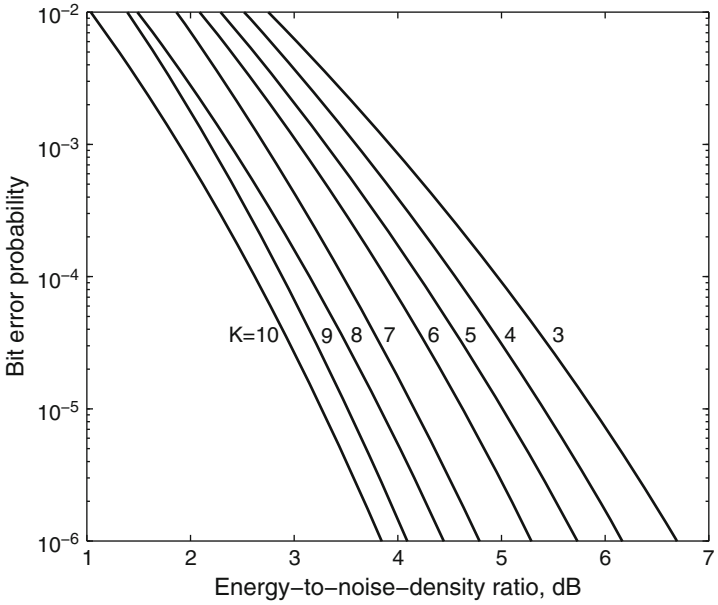

Fig. 1.9 Information-bit error probability for rate = 1/2 convolutional codes with different constraint lengths and coherent BPSK

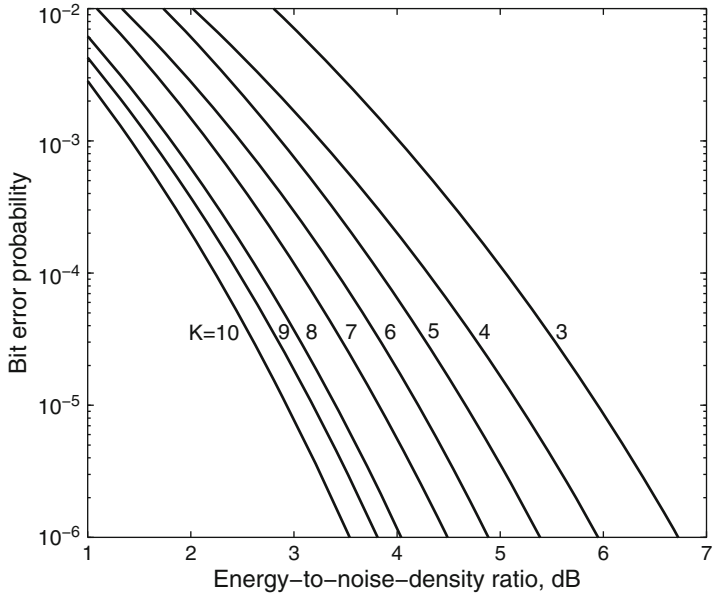

Fig. 1.10 Information-bit error probability for rate = 1/3 convolutional codes with different constraint lengths and coherent BPSK

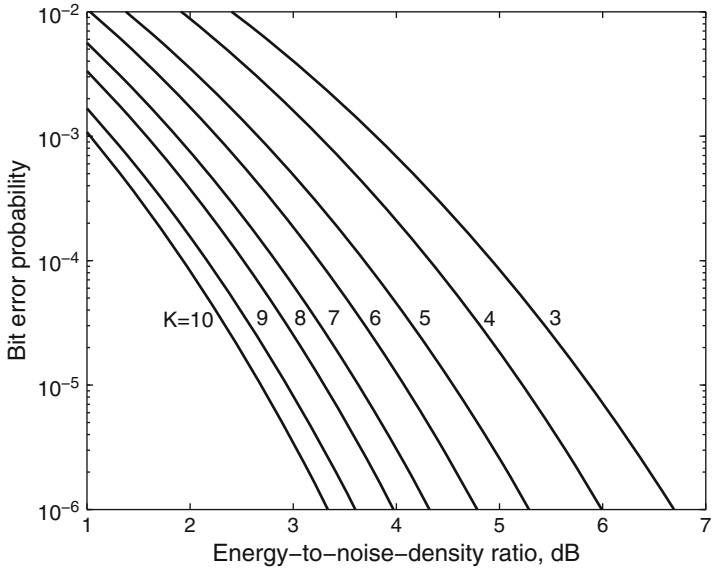

Fig. 1.11 Information-bit error probability for rate = 1/4 convolutional codes with different constraint lengths and coherent BPSK

written into a buffer from which $p + \nu$ bits are read out, where $1 \leq \nu \leq (n-1)p$. Thus, a punctured convolutional code has a rate of the form

$$r = \frac{p}{p+\nu}, \quad 1 \leq \nu \leq (n-1)p. \tag{1.113}$$

The decoder of a punctured code may use the same decoder and trellis as the parent code, but uses only the metrics of the unpunctured bits as it proceeds through the trellis. The pattern of puncturing is concisely described by an $n \times p$ puncturing matrix $\mathbf{P}$ in which each column specifies the output bits produced by the encoder due to an input bit. Matrix element P_{ij} is set equal to 1 if code-bit i is transmitted during epoch j of the puncturing period p; otherwise, $P_{ij} = 0$. For most code rates, there are punctured codes with the largest minimum free distance of any convolutional code with that code rate. Punctured convolutional codes enable the efficient implementation of a variable-rate error-control system with a single encoder and decoder. However, the periodic character of the trellis of a punctured code requires that the decoder acquire frame synchronization.

Coded nonbinary sequences can be produced by converting the outputs of a binary convolutional encoder into a single nonbinary symbol, but this procedure does not optimize the nonbinary code's Hamming distance properties. Better nonbinary codes, such as the dual-k codes, are possible but do not provide as good a performance as the nonbinary Reed–Solomon codes with the same transmission bandwidth.

In principle, $B(l)$ can be determined from the *generating function*, $T(D, I)$, which can be derived for some convolutional codes by treating the state diagram as a signal flow graph. The generating function is a polynomial in D and I of the form

$$T(D, I) = \sum_{i=1}^{\infty} \sum_{l=d_f}^{\infty} a(l, i) D^l I^i \tag{1.114}$$

where $a(l, i)$ represents the number of distinct unmerged segments characterized by l and i. The derivative at $I = 1$ is

$$\left.\frac{\partial T(D, I)}{\partial I}\right|_{I=1} = \sum_{i=1}^{\infty} \sum_{l=d_f}^{\infty} i a(l, i) D^l = \sum_{l=d_f}^{\infty} B(l) D^l. \tag{1.115}$$

Thus, the bound on P_b given by (1.110) is determined by substituting $P_2(l)$ in place of D^l in the polynomial expansion of the derivative of $T(D, I)$ and multiplying the result by $1/k$. In many applications, it is possible to establish an inequality of the form

$$P_2(l) \le \alpha Z^l \tag{1.116}$$

where α and Z are independent of l. It then follows from (1.110), (1.115), and (1.116) that

$$P_b \le \frac{\alpha}{k} \left.\frac{\partial T(D, I)}{\partial I}\right|_{I=1, D=Z}. \tag{1.117}$$

For soft-decision decoding and coherent BPSK, $P_2(l)$ is given by (1.111). Using the definition of $Q(x)$ given by (1.35), changing variables, and comparing the two sides of the following inequality, we verify that

$$\begin{aligned} Q\left(\sqrt{\nu + \beta}\right) &= \frac{1}{\sqrt{2\pi}} \int_0^{\infty} \exp\left[-\frac{1}{2}\left(y + \sqrt{\nu + \beta}\right)^2\right] dy \\ &\le \frac{1}{\sqrt{2\pi}} \exp\left(-\frac{\beta}{2}\right) \int_0^{\infty} \exp\left[-\frac{1}{2}(y + \sqrt{\nu})^2\right] dy, \quad \nu \ge 0, \ \beta \ge 0. \end{aligned} \tag{1.118}$$

A change of variables yields

$$Q(\sqrt{\nu + \beta}) \le \exp\left(-\frac{\beta}{2}\right) Q(\sqrt{\nu}), \quad \nu \ge 0, \ \beta \ge 0. \tag{1.119}$$

Substituting this inequality into (1.111) with the appropriate choices for ν and β gives

$$P_2(l) \le Q\left(\frac{\sqrt{2 d_f r \mathcal{E}_b}}{N_0}\right) \exp\left[-(l - d_f) r \mathcal{E}_b / N_0\right]. \tag{1.120}$$

Thus, the upper bound on $P_2(l)$ may be expressed in the form given by (1.116) with

$$\alpha = Q\left(\frac{\sqrt{2d_f r\mathcal{E}_b}}{N_0}\right)\exp(d_f r\mathcal{E}_b/N_0) \tag{1.121}$$

$$Z = \exp(-r\mathcal{E}_b/N_0). \tag{1.122}$$

For other channels, codes, and modulations, an upper bound on $P_2(l)$ in the form given by (1.116) can often be derived from the Chernoff bound.

1.2.1 Chernoff Bound

The Chernoff bound is an upper bound on the probability that a random variable equals or exceeds a constant. The usefulness of the Chernoff bound stems from the fact that it is often much more easily evaluated than the probability it bounds. The *moment generating function* of the random variable X with distribution function $F(x)$ is defined as

$$M(s) = E\left[e^{sX}\right] = \int_{-\infty}^{\infty}\exp(sx)dF(x) \tag{1.123}$$

for all real-valued s for which the integral is finite. For all nonnegative s, the probability that $X \geq 0$ is

$$P[X \geq 0] = \int_0^{\infty} dF(x) \leq \int_0^{\infty}\exp(sx)dF(x). \tag{1.124}$$

Thus,

$$P[X \geq 0] \leq M(s), \quad 0 \leq s < s_1 \tag{1.125}$$

where s_1 is the upper limit of an open interval in which $M(s)$ is defined. To make this bound as tight as possible, we choose the value of s that minimizes $M(s)$. Therefore,

$$P[X \geq 0] \leq \min_{0\leq s<s_1} M(s) \tag{1.126}$$

which indicates the upper bound called the *Chernoff bound*. From (1.126) and (1.123), we obtain the generalization

$$P[X \geq b] \leq \min_{0\leq s<s_1} M(s)\exp(-sb). \tag{1.127}$$

Since the moment generating function is finite in some neighborhood of $s = 0$, we may differentiate under the integral sign in (1.123) to obtain the derivative of $M(s)$. The result is

$$M'(s) = \int_{-\infty}^{\infty} x \exp(sx) dF(x) \tag{1.128}$$

which implies that $M'(0) = E[X]$. Differentiating (1.128) gives the second derivative

$$M''(s) = \int_{-\infty}^{\infty} x^2 \exp(sx) dF(x) \tag{1.129}$$

which implies that $M''(s) \geq 0$. Consequently, $M(s)$ is convex in its interval of definition. Consider a random variable is such that

$$E(X) < 0, \quad P[X > 0] > 0. \tag{1.130}$$

The first inequality implies that $M'(0) < 0$, and the second inequality implies that $M(s) \to \infty$ as $s \to \infty$. Thus, since $M(0) = 1$, the convex function $M(s)$ has a minimum value that is less than unity at some positive $s = s_0$. We conclude that (1.130) is sufficient to ensure that the Chernoff bound is less than unity and $s_0 > 0$.

The Chernoff bound can be tightened if X has a density function $f(x)$ such that

$$f(-x) \geq f(x), \quad x \geq 0. \tag{1.131}$$

For $s \in A$, where $A = (s_0, s_1)$ is the open interval over which $M(s)$ is defined, (1.123) implies that

$$\begin{aligned} M(s) &= \int_0^{\infty} \exp(sx) f(x) dx + \int_{-\infty}^{0} \exp(sx) f(x) dx \\ &\geq \int_0^{\infty} [\exp(sx) + \exp(-sx)] f(x) dx = \int_0^{\infty} 2\cosh(sx) f(x) dx \\ &\geq 2 \int_0^{\infty} f(x) dx = 2P[X \geq 0]. \end{aligned} \tag{1.132}$$

Thus, we obtain the following version of the Chernoff bound:

$$P[X \geq 0] \leq \frac{1}{2} \min_{s \in A} M(s) \tag{1.133}$$

where the minimum value s_0 is not required to be nonnegative. However, if (1.130) holds, then the bound is less than 1/2, $s_0 > 0$, and

$$P[X \geq 0] \leq \frac{1}{2} \min_{0 < s < s_1} M(s). \tag{1.134}$$

In soft-decision decoding, the encoded sequence or codeword with the largest associated metric is converted into the decoded output. Let $U(\nu)$ denote the value of the metric associated with sequence ν of length L. Consider additive metrics having the form

$$U(\nu) = \sum_{i=1}^{L} m(\nu, i) \tag{1.135}$$

where $m(\nu, i)$ is the *symbol metric* associated with symbol i of the encoded sequence. Let $\nu = 1$ label the correct sequence and $\nu = 2$ label an incorrect one. Let $P_2(l)$ denote the probability that the metric for an incorrect codeword at distance l from the correct codeword exceeds the metric for the correct codeword. By suitably relabeling the l symbol metrics that may differ for the two sequences, we obtain

$$\begin{aligned} P_2(l) &\leq P\left[U(2) \geq U(1)\right] \\ &= P\left[\sum_{i=1}^{l} [m(2,i) - m(1,i)] \geq 0\right] \end{aligned} \tag{1.136}$$

where the inequality results because $U(2) = U(1)$ does not necessarily cause an error if it occurs. In all practical cases, (1.130) is satisfied for the random variable $X = U(2) - U(1)$. Therefore, the Chernoff bound implies that

$$P_2(l) \leq \alpha \min_{0<s<s_1} E\left[\exp\left\{s \sum_{i=1}^{l} [m(2,i) - m(1,i)]\right\}\right] \tag{1.137}$$

where s_1 is the upper limit of the interval over which the expected value is defined. Depending on which version of the Chernoff bound is valid, either $\alpha = 1$ or $\alpha = 1/2$. If $m(2,i) - m(1,i)$, $i = 1, 2, \ldots, l$, are independent, identically distributed random variables and we define

$$Z = \min_{0<s<s_1} E\left[\exp\left\{s\left[m(2,i) - m(1,i)\right]\right\}\right] \tag{1.138}$$

then

$$P_2(l) \leq \alpha Z^l. \tag{1.139}$$

This bound is often much simpler to compute than the exact $P_2(l)$. As l increases, the central-limit theorem implies that the distribution of $X = U(2) - U(1)$ approximates the Gaussian distribution. Thus, for large enough l, (1.131) is satisfied when $E[X] < 0$, and we can set $\alpha = 1/2$ in (1.139). For small l, (1.131) may be difficult to establish mathematically, but is often intuitively clear; if not, setting $\alpha = 1$ in (1.139) is always valid.

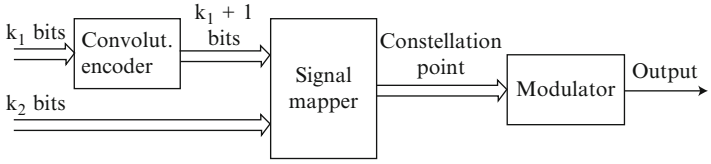

Fig. 1.12 Encoder for trellis-coded modulation

1.2.2 Trellis-Coded Modulation

To add a channel code to a communication system while avoiding a bandwidth expansion, one may increase the number of signal constellation points. For example, if a rate-2/3 code is added to a system using quadriphase-shift keying (QPSK), then the bandwidth is preserved if the modulation is changed to eight-phase PSK (8-PSK). Since each symbol of the latter modulation represents 3/2 as many bits as a QPSK symbol, the channel-symbol rate is unchanged. The problem is that the change from QPSK to the more compact 8-PSK constellation causes an increase in the channel-symbol error probability that cancels most of the decrease due to the encoding. This problem is avoided integrating coding into a *trellis-coded modulation* system.

A *coded modulation system* is one that integrates the modulation and coding processes. *Trellis-coded modulation* is coded modulation produced by a system with the form shown in Fig. 1.12. For $k > 1$, each input of k information bits is divided into two groups. One group of k_1 bits is applied to a convolutional encoder while the other group of $k_2 = k - k_1$ bits remains uncoded. The $k_1 + 1$ output bits of the convolutional encoder select one of 2^{k_1+1} possible subsets of the points in the constellation of the modulator. The k_2 uncoded bits select one of 2^{k_2} points in the chosen subset. If $k_2 = 0$, there are no uncoded bits and the convolutional encoder output bits select the constellation point. Each constellation point is a complex number representing an amplitude and phase. The process of using code bits and uncoded bits to select or label constellation points is called *set partitioning*.

For example, suppose that $k_1 = k_2 = 1$ and $n = 2$ in the encoder of Fig. 1.12, and an 8-PSK modulator produces an output from a constellation of eight points. Each of the four subsets that may be selected by the two convolutional-code bits comprises two antipodal points in the 8-PSK constellation, as shown in Fig. 1.13. If the convolutional encoder has the form of Fig. 1.6a, then the trellis of Fig. 1.8 illustrates the state transitions of both the underlying convolutional code and the trellis code. The presence of the single uncoded bit implies that each transition between states in the trellis corresponds to two different transitions and two different phases of the transmitted 8-PSK waveform.

In general, there are 2^{k_2} parallel transitions between every pair of states in the trellis. Often, the dominant error events consist of mistaking one of these parallel transitions for the correct one. If the symbols corresponding to parallel

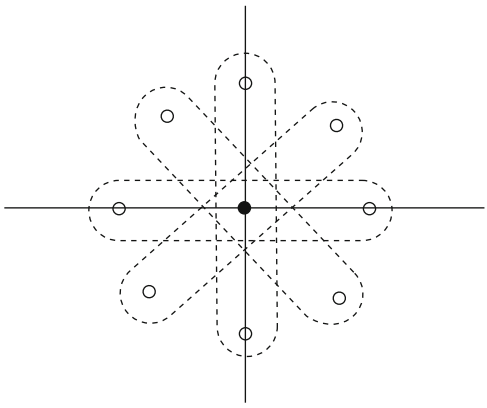

Fig. 1.13 The constellation of 8-PSK symbols partitioned into four subsets

transitions are separated by large Euclidean distances, and the constellation subsets associated with transitions are suitably chosen, then the trellis-coded modulation with soft-decision Viterbi decoding can yield a substantial coding gain. This gain usually ranges from 4 to 6 dB, depending on the number of states and, hence, the implementation complexity. The minimum Euclidean distance between a correct trellis-code path and an incorrect one is called the *free Euclidean distance* and is denoted by $d_{fe}\sqrt{\mathcal{E}_s}$. Let B_{fe} denote the total number of information bit errors associated with erroneous paths that are at the free Euclidian distance from the correct path. The latter paths dominate the error events when $\mathcal{E}_b/N_0$ is high. An analysis similar to the one for convolutional codes indicates that for the AWGN channel and a high $\mathcal{E}_b/N_0$, the information-bit error probability is

$$P_b \approx \frac{B_{fe}}{k} Q\left(\sqrt{\frac{d_{fe}^2 r \mathcal{E}_b}{2N_0}}\right). \tag{1.140}$$

1.3 Interleavers

An *interleaver* is a device that permutes the order of a sequence of symbols. A *deinterleaver* is the corresponding device that restores the original order of the sequence. A major application is the interleaving of modulated symbols transmitted over a communication channel. After deinterleaving at the receiver, a burst of channel-symbol errors or corrupted symbols is dispersed over a number of codewords or constraint lengths, thereby facilitating the removal of the errors by the decoding. Ideally, the interleaving and deinterleaving ensures that the decoder encounters statistically independent symbol decisions or metrics, as it would if the channel were memoryless. Interleaving of channel symbols is useful when error bursts are caused by fast fading, interference, or even decision- directed equalization.

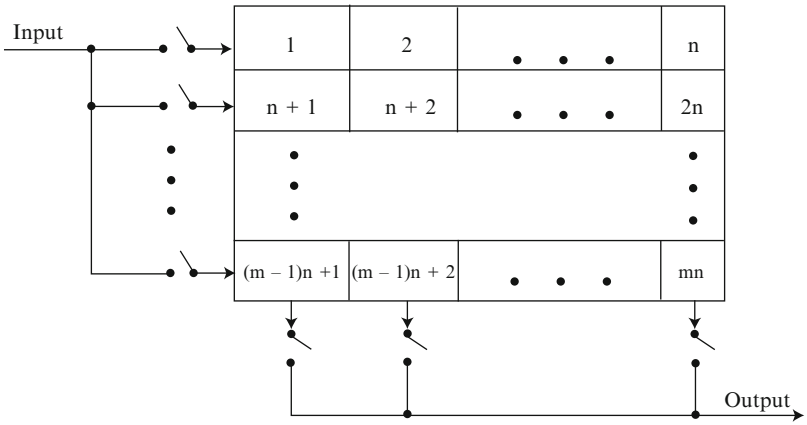

Fig. 1.14 Block interleaver

A *block interleaver* performs identical permutations on successive blocks of symbols. As illustrated in Fig. 1.14, mn successive input symbols are stored in a random-access memory (RAM) as a matrix of m rows and n columns. The input sequence is written into the interleaver in successive rows, but successive columns are read to produce the interleaved sequence. Thus, if the input sequence is numbered $1, 2, \ldots, n, n+1, \ldots, mn$, the interleaved sequence is $1, n+1, 2n+1, \ldots, 2, n+2, \ldots, mn$. For continuous interleaving, two RAMs are needed. Symbols are written into one RAM matrix while previous symbols are read from the other. In the deinterleaver, symbols are stored by column in one matrix, while previous symbols are read by rows from another. Consequently, a delay of $2mnT_s$ must be accommodated and synchronization is required at the deinterleaver.

When channel symbols are interleaved, the parameter n equals or exceeds the block codeword length or a few constraint lengths of a convolutional code. Consequently, if a burst of m or fewer consecutive symbol errors occurs and there are no other errors, then each block codeword or constraint length, after deinterleaving, has at most one error, which can be eliminated by the error-correcting code. Similarly, a block code that can correct t errors is capable of correcting a single burst of errors spanning as many as mt symbols. Since fading can cause correlated errors, it is necessary that mT_s exceed the channel coherence time. Interleaving effectiveness can be thwarted by slow fading that cannot be accommodated without large buffers that cause an unacceptable delay.

Other types of interleavers that are closely related to the block interleaver include the *convolutional interleaver* and the *helical interleaver*. A convolutional interleaver consists of a bank of interleavers of successively increasing length. A helical interleaver reads symbols from its matrix diagonally instead of by column in such a way that consecutive interleaved symbols are never read from the same row or column. Both helical and convolutional interleavers and their corresponding

deinterleavers confer advantages in certain applications, but do not possess the inherent simplicity and compatibility with block structures that block interleavers have.

A *pseudorandom interleaver* permutes each block of symbols pseudorandomly. Pseudorandom interleavers may be applied to channel symbols, but their main application is as critical elements in turbo encoders and encoders of serially concatenated codes that use iterative decoding (Sect. 1.4). The desired permutation may be stored in a read-only memory (ROM) as a sequence of addresses or permutation indices. Each block of symbols is written sequentially into a RAM matrix and then interleaved by reading them in the order dictated by the contents of the ROM.

If the interleaver is large, it is often preferable to generate the permutation indices by an algorithm rather than storing them in a ROM. If the interleaver size is $N = mn = 2^{\nu} - 1$, then a linear feedback shift register with ν stages that produces a maximal-length sequence can be used. The binary outputs of the shift-register stages constitute the *state* of the register. The state specifies the index from 1 to N that defines a specific interleaved symbol. The shift register generates all N states and indices periodically.

An *S-random interleaver* is a pseudorandom interleaver that constrains the minimum interleaving distance. A tentative permutation index is compared with the S previously selected indices, where $1 \leq S < N$. If the tentative index does not differ in absolute value from the S previous ones by at least S, then it is discarded and replaced by a new tentative index. If it does, then the tentative index becomes the next selected index. This procedure continues until all N pseudorandom indices are selected. The S-random interleaver is frequently used in turbo or serially concatenated encoders.

1.4 Classical Concatenated Codes

Classical concatenated codes are serially concatenated codes with the encoder and decoder forms shown in Fig. 1.15. In the most common configuration for classical concatenated codes, an *inner code* uses binary symbols and a Reed– Solomon *outer code* uses nonbinary symbols. The outer-encoder output symbols are interleaved, and then these nonbinary symbols are converted into binary symbols that are encoded by the inner encoder. In the receiver, a grouping of the binary inner-decoder output symbols into nonbinary outer-code symbols is followed by symbol deinterleaving that disperses the outer-code symbol errors. Consequently, the outer decoder is able to correct most symbol errors originating in the inner-decoder output. The concatenated code has rate

$$r = r_1 r_0 \tag{1.141}$$

where r_1 is the inner-code rate and r_0 is the outer-code rate.

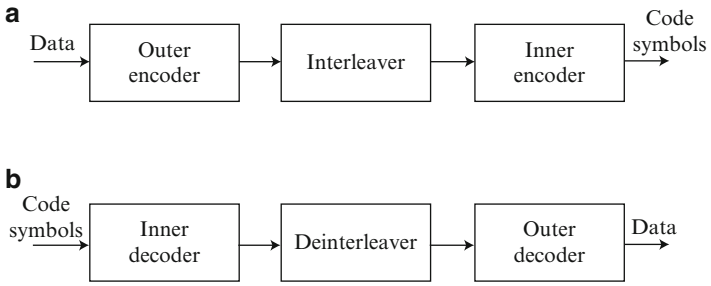

Fig. 1.15 Structure of serially concatenated code: (**a**) encoder and (**b**) classical decoder

A variety of inner codes have been proposed. The dominant and most powerful concatenated code of this type comprises a binary convolutional inner code and a Reed–Solomon outer code. At the output of a convolutional inner decoder using the Viterbi algorithm, the bit errors occur over spans with an average length that depends on the $\mathcal{E}_b/N_0$. The deinterleaver is designed to ensure that Reed–Solomon symbols formed from bits in the same typical error span do not belong to the same Reed–Solomon codeword. Let $m = \log_2 q$ denote the number of bits in a Reed–Solomon code symbol. In the worst case, the inner decoder produces bit errors that are separated enough that each one causes a separate symbol error at the input to the Reed–Solomon decoder. Since there are m times as many bits as symbols, the symbol error probability P_{s1} is upper-bounded by m times the bit error probability at the inner-decoder output. Since P_{s1} is no smaller than it would be if each set of m bit errors caused a single symbol error, P_{s1} is lower-bounded by this bit error probability. Thus, for binary convolutional inner codes,

$$\frac{1}{k}\sum_{l=d_f}^{\infty} B(l)P_2(l) \le P_{s1} \le \frac{\log_2 q}{k}\sum_{l=d_f}^{\infty} B(l)P_2(l) \tag{1.142}$$

where $P_2(l)$ is given by (1.139) and (1.138). Assuming that the deinterleaving ensures independent symbol errors at the outer-decoder input, and that the Reed–Solomon code is loosely packed, (1.30) and (1.32) imply that

$$P_b \approx \frac{q}{2(q-1)}\sum_{i=t+1}^{n}\binom{n-1}{i-1}P_{s1}^{i}(1-P_{s1})^{n-1}. \tag{1.143}$$

For coherent BPSK modulation with soft decisions, $P_2(l)$ is given by (1.111); if hard decisions are made, (1.112) applies.

Figure 1.16 depicts examples of the approximate upper bound on the performance in white Gaussian noise of concatenated codes with coherent BPSK, soft demodulator decisions, an inner binary convolutional code with $k = 1$, $K = 7$, and rate $= 1/2$, and various Reed–Solomon outer codes. Equation (1.143) and the upper

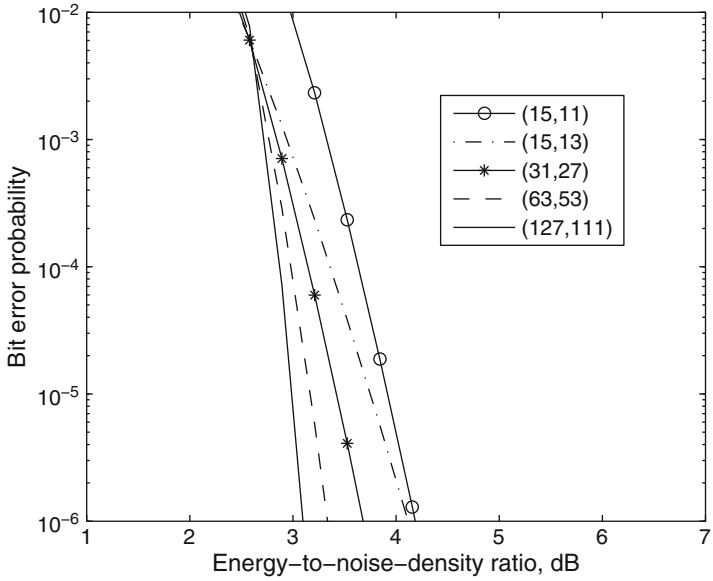

Fig. 1.16 Information-bit error probability for concatenated codes with inner convolutional code ($K = 7$, rate $= 1/2$), various Reed–Solomon (n, k) outer codes, and coherent PSK

bound in (1.142) are used. The bandwidth required by a concatenated code is B/r, where B is the uncoded BPSK bandwidth. Since (1.141) gives $r < 1/3$, the codes of the figure require more bandwidth than rate-1/3 convolutional codes.

1.5 Turbo Codes

Turbo codes are concatenated codes that use iterative decoding. There are two principal types: turbo codes with parallel concatenated codes, which are the original turbo codes, and serially concatenated turbo codes, which are related to the classical concatenated codes. The iterative decoding requires that both component codes be systematic and of the same type, that is, both convolutional or both block. Each component decoder uses a version of the *maximum a posteriori* (MAP) or *BCJR algorithm* (proposed by Bahl, Cocke, Jelinek, and Raviv).

1.5.1 MAP Decoding Algorithm

The MAP or BCJR algorithm minimizes the decoded BER for each information bit of a code, whereas the Viterbi algorithm minimizes the probability of error in

a sequence of message bits. Both algorithms process soft input information. They differ in that the MAP algorithm produces soft output information derived from estimates of the *a posteriori* probabilities of the bit states, whereas the Viterbi algorithm makes hard bit decisions. The provision of soft output information for each information bit is what makes the MAP algorithm essential for the iterative decoding of turbo codes. The MAP algorithm exploits the Markov properties of a convolutional code or other code that can be described in terms of a trellis structure.

For each information bit b_k of a systematic code, the MAP algorithm computes estimates of the log-likelihood ratio (LLR) of the probabilities that this bit is 1 or 0 given the received vector $\mathbf{y}$:

$$\Lambda_k = \ln\left[\frac{P(b_k = 1|\mathbf{y})}{P(b_k = 0|\mathbf{y})}\right]. \tag{1.144}$$

Since the *a posteriori* probabilities are related by $P(b_k = 1|\mathbf{y}) = 1 - P(b_k = 0|\mathbf{y})$, Λ_k completely characterizes the *a posteriori* probabilities.

Let ψ_k denote the state of the encoder at discrete-time k. The transmission of b_k is associated with a state transition from state s' to state s. Applying Bayes' rule and the mutual exclusive nature of state transitions to (1.144) yields

$$\Lambda_k = \log\left[\frac{\sum\limits_{s',s:b_k=1} f\left(\psi_k = s', \psi_{k+1} = s, \mathbf{y}\right)}{\sum\limits_{s',s:b_k=0} f\left(\psi_k = s', \psi_{k+1} = s, \mathbf{y}\right)}\right] \tag{1.145}$$

where $f(\cdot)$ is a probability density function, and the summations are over all states consistent with $b_k = 1$ and $b_k = 0$, respectively.

The vector $\mathbf{y}$ is decomposed into three separate sets of observations: $\mathbf{y}_k^- = \{y_l, l < k\}$ represents the observations prior to time k, y_k is the current observation, and $\mathbf{y}_k^+ = \{y_l, l > k\}$ represents the observations that occur after time k. We define

$$\alpha_k\left(s'\right) = f\left(\psi_k = s', \mathbf{y}_k^-\right) \tag{1.146}$$

$$\gamma_k\left(s', s\right) = f\left(\psi_{k+1} = s, y_k \mid \psi_k = s'\right) \tag{1.147}$$

$$\beta_{k+1}(s) = f\left(\mathbf{y}_k^+ \mid \psi_{k+1} = s\right). \tag{1.148}$$

After conditioning on the event $\psi_{k+1} = s$, $\mathbf{y}_k^+$ is independent of y_k, $\mathbf{y}_k^-$, and the event that $\psi_k = s'$. Therefore,

$$\begin{aligned} f\left(\psi_k = s', \psi_{k+1} = s, \mathbf{y}\right) &= \beta_{k+1}(s)\, f\left(\psi_k = s', \psi_{k+1} = s, y_k, \mathbf{y}_k^-\right) \\ &= \alpha_k\left(s'\right)\gamma_k\left(s', s\right)\beta_{k+1}(s). \end{aligned} \tag{1.149}$$

Substitution of this equation into (1.145) yields the LLR

$$\Lambda_k = \log\left[\frac{\sum\limits_{s',s:b_k=1} \alpha_k\left(s'\right)\gamma_k\left(s',s\right)\beta_{k+1}\left(s\right)}{\sum\limits_{s',s:b_k=0} \alpha_k\left(s'\right)\gamma_k\left(s',s\right)\beta_{k+1}\left(s\right)}\right]. \tag{1.150}$$

The MAP algorithm requires a *forward recursion* to compute $\alpha_k\left(a\right)$ and a backward recursion to compute $\beta_{k+1}\left(s\right)$. The forward recursion for $\alpha_k\left(s'\right)$ may be derived from its definition. If $\{0, 1, \ldots, Q-1\}$ denotes the set of Q states, then the theorem of total probability implies that

$$\begin{aligned}\alpha_{k+1}\left(s\right) &= \sum_{s'=0}^{Q-1} f\left(\psi_{k+1}=s, y_k, \mathbf{y}_k^-, \psi_k=s'\right)\\ &= \sum_{s'=0}^{Q-1} f\left(\psi_{k+1}=s, y_k \mid \mathbf{y}_k^-, \psi_k=s'\right)\alpha_k\left(s'\right).\end{aligned} \tag{1.151}$$

Given that $\psi_k = s'$, the value of $\mathbf{y}_k^-$ is irrelevant; therefore,

$$\alpha_{k+1}\left(s\right) = \sum_{s'=0}^{Q-1} \alpha_k\left(s'\right)\gamma_k\left(s',s\right). \tag{1.152}$$

The *backward recursion* for $\beta_{k+1}\left(s\right)$ may be derived similarly. We have

$$\begin{aligned}\beta_k\left(s'\right) &= \sum_{s=0}^{Q-1} f\left(\mathbf{y}_k^+, y_k, \psi_{k+1}=s \mid \psi_k=s'\right)\\ &= \sum_{s=0}^{Q-1} f\left(\mathbf{y}_k^+ \mid y_k, \psi_{k+1}=s, \psi_k=s'\right)\gamma_k\left(s',s\right).\end{aligned} \tag{1.153}$$

Given that $\psi_{k+1} = s$, the event $\psi_k = s'$ and the value of y_k are irrelevant; therefore,

$$\beta_k\left(s'\right) = \sum_{s=0}^{Q-1} \gamma_k\left(s',s\right)\beta_{k+1}\left(s\right). \tag{1.154}$$

Assuming that the encoder begins in the zero state and ends in the zero state at the time $k = L$, recursions for $\alpha_{k+1}\left(s\right)$ and $\beta_k\left(s'\right)$ are initialized according to

$$\alpha_0\left(x\right) = \delta\left(x\right),\ \beta_L\left(x\right) = \delta\left(x\right) \tag{1.155}$$

where $\delta\left(x\right) = 1$ if $x = 0$, and $\delta\left(x\right) = 0$ otherwise.

If state s' changes to state s when bit k is $u(s', s)$, then $P(\psi_{k+1} = s \mid \psi_k = s') = P(u(s', s))$, which is the *a priori* probability that bit k is $u(s', s)$, and $f(y_k \mid \psi_{k+1} = s, \psi_k = s') = f(y_k \mid u(s', s))$, the conditional probability density given that bit k is $u(s', s)$. Therefore, the *branch metric* is

$$\gamma_k(s', s) = f\left(y_k \mid u\left(s', s\right)\right) P\left(u\left(s', s\right)\right) \tag{1.156}$$

which shows how the *a priori* information is used by the MAP algorithm. The conditional density $f(y_k \mid u(s', s))$ is determined by the communication channel. An LLR Λ_k is produced for transmitted bit b_k. When a decision is desired, it is provided as $\widehat{b}_k = 1$, $\Lambda_k > 0$, and $\widehat{b}_k = 0$, $\Lambda_k < 0$.

The generic name for a version of the MAP algorithm or an approximation of it is *soft-in soft-out (SISO) algorithm*. The *log-MAP algorithm* is an SISO algorithm that transforms the MAP algorithm into the logarithmic domain, thereby simplifying operations and reducing numerical problems while causing no performance degradation. The log-MAP algorithm requires both a forward and a backward recursion through the code trellis. Since the log-MAP algorithm also requires additional memory and calculations, it is roughly four times as complex as the standard Viterbi algorithm.

The log-MAP algorithms expedites computations by using the *max-star function*, which is defined as

$$\max_i{}^*\{x_i\} = \log\left(\sum_i e^{x_i}\right). \tag{1.157}$$

By separately considering $x > y$ and $x < y$, we verify that for two variables

$$\max{}^*(x.y) = \max(x, y) + \log\left(1 + e^{|x-y|}\right) \tag{1.158}$$

whereas for more than two variables, the calculation can be done recursively. For example, for three variables,

$$\max{}^*(x, y, z) = \max{}^*[x, \max{}^*(y, z)]. \tag{1.159}$$

The second term on the right-hand side of (1.158) may be stored in a table accessed by the log-MAP algorithm.

The log-MAP algorithm computes $\overline{\alpha}_k(s') = \log(\alpha_k(s'))$, $\overline{\gamma}_k(s', s) = \log(\gamma_k(s', s))$, and $\overline{\beta}_{k+1}(s) = \log(\beta_{k+1}(s))$. The forward and backward recursions are

$$\overline{\alpha}_{k+1}(s) = \max_{s'}{}^*\{\overline{\alpha}_k\left(s'\right) + \overline{\gamma}_k\left(s', s\right)\} \tag{1.160}$$

$$\overline{\beta}_k\left(s'\right) = \max_s{}^*\{\overline{\beta}_{k+1}(s) + \overline{\gamma}_k\left(s', s\right)\} \tag{1.161}$$

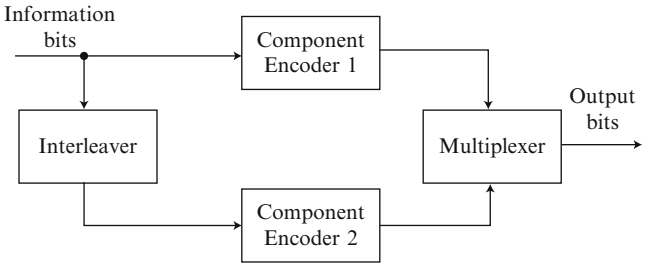

Fig. 1.17 Encoder of turbo code

respectively, while the LLR is

$$\Lambda_k = \max_{s',s:b_k=1}{}^{*}\{\overline{\alpha}_k\left(s'\right) + \overline{\gamma}_k\left(s',s\right) + \overline{\beta}_{k+1}\left(s\right)\} - \max_{s',s:b_k=0}{}^{*}\{\overline{\alpha}_k\left(s'\right) + \overline{\gamma}_k\left(s',s\right) + \overline{\beta}_{k+1}\left(s\right)\}. \tag{1.162}$$

Straightforward calculations verify the equivalence of (1.160), (1.161), and (1.162) with (1.150), (1.152), and (1.154). If the encoder begins and terminates in the zero state, then the recursions are initialized by $\overline{\alpha}_0(s) = \overline{\beta}_L(s) = 0$ if $s = 0$; $\overline{\alpha}_0(s) = \overline{\beta}_L(s) = -\infty$, otherwise.

The *max-log-MAP algorithm* and the *soft-output Viterbi algorithm (SOVA)* are SISO algorithms that reduce the complexity of the log-MAP algorithm at the cost of some performance degradation. The max-log-MAP algorithm uses the approximation $\max^{*}(x.y) \simeq \max(x, y)$ to reduce its complexity to roughly 2/3 the complexity of the log-MAP algorithm. The SOVA algorithm is roughly 1/3 as complex as the log-MAP algorithm. The MAP, log-MAP, max-log-MAP, and SOVA algorithms have complexities that increase linearly with the number of states of the component codes.

1.5.2 Turbo Codes with Parallel Concatenated Codes

As shown in Fig. 1.17, the encoder of a turbo code may use two parallel component encoders, one of which directly encodes the information bits while the other encodes interleaved bits. Within this architecture, the component codes might be convolutional codes, block codes, or trellis-coded modulation. More than two component codes have been found to be unnecessary.

A *convolutional turbo code* uses two convolutional codes as its component codes. The multiplexer output of the turbo encoder in Fig. 1.17 comprises both the information and parity bits produced by component encoder 1 but only the parity bits produced by component encoder 2. Usually, identical component codes are used.

If the multiplexer punctures the parity streams, higher-rate codes can be generated. Although it requires frame synchronization in the decoder, the puncturing may serve as a convenient means of adapting the code rate to the channel conditions.

The purpose of the interleaver, which may be a block or pseudorandom interleaver, is to permute the input bits of encoder 2 so that it is unlikely that both component codewords will have a low weight even if the input word has a low weight. *Recursive systematic convolutional encoders* are used in the component encoders because they map most low-weight information sequences into higher-weight coded sequences. Although the number of low weight codewords is greatly reduced, some remain, and there is little or no change in the minimum free distance. Thus, a turbo code has very few low-weight codewords, whether or not its minimum distance is large. When large interleavers are used, the weight distribution of a turbo code resembles that of a random code. The interleavers and deinterleavers in the turbo decoder weaken the correlations among the LLRs associated with different bits.

Terminating tail bits are inserted into both component convolutional codes so that the turbo trellis terminates in the all-zero state and the turbo code can be treated as a block code. Recursive encoders require nonzero tail bits that are functions of the preceding nonsystematic output bits and, hence, the information bits.

To produce a rate-1/2 turbo code from rate-1/2 convolutional component codes, alternate puncturing of the even parity bits of encoder 1 and the odd parity bits of encoder 2 is done. Consequently, an odd information bit has its associated parity bit of code 1 transmitted. However, because of the interleaving that precedes encoder 2, an even information bit may have neither its associated parity bit of code 1 nor that of code 2 transmitted. Instead, some odd information bits may have both associated parity bits transmitted, although not successively because of the interleaving. Since some information bits have no associated parity bits transmitted, the decoder is less likely to be able to correct errors in those information bits. A convenient means of avoiding this problem, and ensuring that exactly one associated parity bit is transmitted for each information bit, is to use a block interleaver with an odd number of rows and an odd number of columns. If bits are written into the interleaver matrix in successive rows, but successive columns are read, then odd and even information bits alternate at the input of encoder 2, thereby ensuring that all information bits have an associated parity bit that is transmitted. This procedure, or any other that separates the odd and even information bits, is called *odd-even separation*. Simulation results confirm that odd-even separation improves the system performance when puncturing and block interleavers are used, but odd-even separation is not beneficial in the absence of puncturing. In a system with a small interleaver size, block interleavers with odd-even separation usually give a better system performance than pseudorandom interleavers, but the latter are usually superior when the interleaver size is large.

The interleaver size is equal to the block length or frame length of the codes. The number of low-weight or minimum-distance codewords tends to be inversely proportional to the interleaver size. With a large interleaver and a sufficient number of decoder iterations, the performance of the convolutional turbo code can approach

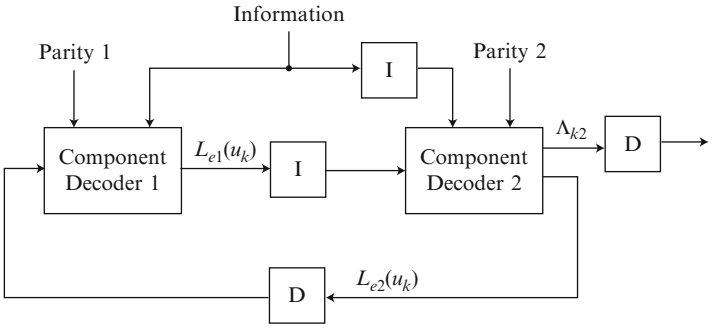

Fig. 1.18 Decoder of turbo code. I = interleaver; D = deinterleaver

within less than 1 dB of the information-theoretic limit. However, as the block length increases, so does the *system latency*, which is the delay between the input and final output. As the symbol energy increases, the bit error rate of a turbo code decreases until it eventually falls to an *error floor* or bit error rate that continues to decrease very slowly. The potentially large system latency, the system complexity, and sometimes the error floor are the primary disadvantages of turbo codes.

A maximum-likelihood decoder such as the Viterbi decoder minimizes the probability that a received codeword or an entire received sequence is in error. A turbo decoder is designed to minimize the error probability of each information bit. Under either criterion, an optimal decoder would use the sampled demodulator output streams for the information bits and the parity bits of both component codes. A turbo decoder comprises separate component decoders for each component code, which is theoretically suboptimal but crucial in reducing the decoder complexity. Each component decoder uses a version of the *MAP algorithm.* As shown in Fig. 1.18, component decoder 1 of a turbo decoder is fed by demodulator outputs denoted by the vector $\mathbf{y}_1 = [\mathbf{x}_0\ \mathbf{x}_1]$, where the components of sequence $\mathbf{x}_0$ are the information bits and the components of sequence $\mathbf{x}_1$ are the parity bits of encoder 1. Similarly, component decoder 2 is fed by outputs denoted by $\mathbf{y}_2 = [\mathbf{x}_0\ \mathbf{x}_2]$, where the components of sequence $\mathbf{x}_2$ are the parity bits of encoder 2. For each information bit b_k, the MAP algorithm of decoder i computes estimates of the log-likelihood ratio (LLR) of the probabilities that this bit is 1 or 0 given the vector $\mathbf{y}_i$:

$$\Lambda_{ki} = \log\left[\frac{P(b_k = 1|\mathbf{y}_i)}{P(b_k = 0|\mathbf{y}_i)}\right], \quad i = 1, 2. \tag{1.163}$$

Since the *a posteriori* probabilities are related by $P(b_k = 1 \mid \mathbf{y}_i) = 1 - P(b_k = 0 \mid \mathbf{y}_i)$, Λ_{ki} completely characterizes the *a posteriori* probabilities. The LLRs of the information bits are iteratively updated in the two component decoders by passing information between them. Since it is interleaved or deinterleaved, arriving information is largely decorrelated from any other information in a decoder and thereby enables the decoder to improve its estimate of the LLR.

From the definition of a conditional probability, (1.163) may be expressed in terms of probability density functions as

$$\Lambda_{ki} = \log\left[\frac{f(b_k = 1, y_{sk}, \overline{\mathbf{y}}_i)}{f(b_k = 0, y_{sk}, \overline{\mathbf{y}}_i)}\right], \quad i = 1, 2 \tag{1.164}$$

where y_{sk} is the demodulator output corresponding to the systematic or information bit b_k and $\overline{\mathbf{y}}_i$ is the sequence $\mathbf{y}_i$ excluding y_{sk}. Given b_k, y_{sk} is independent of $\mathbf{y}_i$. Therefore,

$$f(b_k = l, y_{sk}, \overline{\mathbf{y}}_i) = f(y_{sk} \mid b_k = l) f(\overline{\mathbf{y}}_i \mid b_k = l) P(b_k = l), \quad l = 1, 2. \tag{1.165}$$

Substitution of this equation into (1.164) and decomposing the results, we obtain

$$\Lambda_{ki} = L(b_k) + L(y_{sk}|b_k) + L_{ei}(b_k), \quad i = 1, 2 \tag{1.166}$$

where the *a priori* LLR is initially

$$L(b_k) = \log\left[\frac{P(b_k = 1)}{P(b_k = 0)}\right] \tag{1.167}$$

and the *extrinsic information*

$$L_{ei}(b_k) = \log\left[\frac{f(\overline{\mathbf{y}}_i \mid b_k = 1)}{f(\overline{\mathbf{y}}_i \mid b_k = 0)}\right], \quad i = 1, 2 \tag{1.168}$$

is a function of the parity bits processed by the component decoder i. The term $L(y_{sk}|b_k)$, which represents information about b_k provided by y_{sk}, is defined as

$$L(y_{sk}|b_k) = \log\left[\frac{f(y_{sk}|b_k = 1)}{f(y_{sk}|b_k = 0)}\right] \tag{1.169}$$

where $f(y_{sk}|b_k = b)$ is the conditional density of y_{sk} given that $b_k = b$.

Let u_k denote an information bit after the antipodal mapping $\{0 \to +1, 1 \to -1\}$ so that $u_k = 1 - 2b_k$. Let N_{0k} denote the noise-power spectral density associated with u_k. For coherent BPSK, a derivation similar to that of (1.50) gives the conditional density

$$f(y_{sk}|b_k = b) = \frac{1}{\sqrt{\pi N_{0k}}} \exp\left[-\frac{(y_{sk} - (1 - 2b)\sqrt{\mathcal{E}_s}\alpha)^2}{N_{0k}}\right] \tag{1.170}$$

where α accounts for the fading attenuation. Substitution into (1.169) yields

$$L(y_{sk}|b_k) = L_c y_{sk}, \quad L_c = 4\alpha\frac{\sqrt{2\mathcal{E}_s}}{N_{0k}}. \tag{1.171}$$

The *channel reliability factor* L_c must be known or estimated to compute Λ_{ki}.

Since almost always no *a priori* knowledge of the likely value of the bit u_k is available, $P(b_k) = 0.5$ is assumed, and $L(b_k)$ is set to zero for the first iteration of component decoder 1. However, for subsequent iterations of either component decoder, $L(b_k)$ for one decoder is set equal to the extrinsic information calculated by the other decoder at the end of its previous iteration. As indicated by (1.166), $L_{ei}(b_k)$ can be calculated by subtracting $L(b_k)$ and $L_c y_{sk}$ from Λ_{ki}, which is computed by the MAP algorithm. Since the extrinsic information depends primarily on the constraints imposed by the code used, it provides additional information to the decoder to which it is transferred. As indicated in Fig. 1.18, appropriate interleaving or deinterleaving is required to ensure that the extrinsic information $L_{e1}(b_k)$ or $L_{e2}(b_k)$ is applied to each component decoder in the correct sequence. Let $B\{\ \}$ denote the function calculated by the MAP algorithm during a single iteration, $I[\ ]$ denote the interleave operation, $D[\ ]$ denote the deinterleave operation, and a numerical superscript (n) denote the nth iteration. The turbo decoder calculates the following functions for $n \geq 1$:

$$\Lambda_{k1}^{(n)} = B\{\mathbf{x}_0, \mathbf{x}_1, D[L_{e2}^{(n-1)}(b_k)]\} \tag{1.172}$$

$$L_{e1}^{(n)}(b_k) = \Lambda_{k1}^{(n)} - L_c y_{sk} - D[L_{e2}^{(n-1)}(b_k)] \tag{1.173}$$

$$\Lambda_{k2}^{(n)} = B\{I[\mathbf{x}_0], \mathbf{x}_2, I[L_{e1}^{(n)}(b_k)]\} \tag{1.174}$$

$$L_{e2}^{(n)}(b_k) = \Lambda_{k2}^{(n)} - L_c y_{sk} - I[L_{e1}^{(n)}(b_k)] \tag{1.175}$$

where $D[L_{e2}^{(0)}] = L(b_k)$. When the iterative process terminates after N iterations, the LLR $\Lambda_{k2}^{(N)}$ from component decoder 2 is deinterleaved and then applied to a device that makes a hard decision. Thus, the decision for bit k is

$$\widehat{u_k} = sgn\{D[\Lambda_{k2}^{(N)}(b_k)]\}, \quad \widehat{b_k} = (1 - \widehat{u_k})/2. \tag{1.176}$$

Performance improves with the number of iterations, but simulation results indicate that typically little is gained beyond roughly 4 to 12 iterations.

For identical component decoders and typically 8 algorithm iterations, the overall complexity of a turbo decoder is roughly 64 times that of a Viterbi decoder for one of the component codes. The complexity of the decoder increases while the performance improves as the constraint length K of each component code increases. The complexity of a turbo decoder using 8 iterations and component convolutional codes with $K = 3$ is approximately the same as that of a Viterbi decoder for a convolutional code with $K = 9$. The max-log-MAP algorithm is roughly 2/3 as complex as the log-MAP algorithm and typically degrades the performance by 0.1 dB to 0.2 dB at $P_b = 10^{-4}$. The SOVA algorithm is roughly 1/3 as complex as the log-MAP algorithm and typically degrades the performance by 0.5 dB to 1.0 dB at $P_b = 10^{-4}$.

A *block turbo code* uses two linear block codes as its component codes. To limit the decoding complexity, high-rate binary BCH codes are generally used as

the component codes, and the turbo code is called a *turbo BCH code*. The encoder of a block turbo code has the form of Fig. 1.17. Puncturing is generally not used as it causes a significant performance degradation. Suppose that the component block codes are binary systematic (n_1, k_1) and (n_2, k_2) codes, respectively. Encoder 1 converts k_1 information bits into n_1 codeword bits. Each block of $k_1 k_2$ information bits are written successively into the interleaver as k_1 columns and k_2 rows. Encoder 2 converts each column of k_2 interleaver bits into a codeword of n_2 bits. The multiplexer passes the n_1 bits of each of k_2 encoder-1 codewords, but only the $n_2 - k_2$ parity bits of each of k_1 encoder-2 codewords so that information bits are transmitted only once. Consequently, the code rate of the block turbo code is

$$r = \frac{k_1 k_2}{k_2 n_1 + (n_2 - k_2) k_1}. \tag{1.177}$$

If the two block codes are identical, then $r = k/(2n-k)$. If the minimum Hamming distances of the component codes are d_{m1} and d_{m2}, respectively, then the minimum distance of the concatenated code is

$$d_m = d_{m1}(d_{m2} - 1). \tag{1.178}$$

The decoder of a block turbo code has the form of Fig. 1.18, and only slight modifications of the SISO decoding algorithms are required. Long, high-rate turbo BCH codes approach the Shannon limit in performance, but their complexities are higher then those of convolutional turbo codes of comparable performance.

Approximate upper bounds on the bit error probability for turbo codes have been derived. Since these bounds are difficult to evaluate except for short codewords, simulation results are generally used to predict the performance of a turbo code.

Turbo trellis-coded modulation (TTCM), which produces a nonbinary bandwidth-efficient modulation, is obtained by using identical trellis codes as the component codes in a turbo code. The encoder has the form illustrated in Fig. 1.19. The code rate and, hence, the required bandwidth of the component trellis code is preserved by the TTCM encoder because it alternately selects constellation points or complex symbols generated by the two parallel component encoders. To ensure that all information bits, which constitute the encoder input, are transmitted only once and that the parity bits are provided alternately by the two component encoders, the symbol interleaver transfers symbols in odd positions to odd positions and symbols in even positions to even positions, where each symbol is a group of bits. After the complex symbols are produced by signal mapper 2, the symbol deinterleaver restores the original ordering. The selector passes the odd-numbered complex symbols from mapper 1 and the even-numbered complex symbols from mapper 2. The channel interleaver permutes the selected complex symbols prior to the modulation. The TTCM decoder uses a symbol-based SISO algorithm analogous to the SISO algorithm used by turbo-code decoders. TTCM can provide a performance close to the theoretical limit for the AWGN channel, but its implementation complexity is much greater than that of conventional trellis-coded modulation.

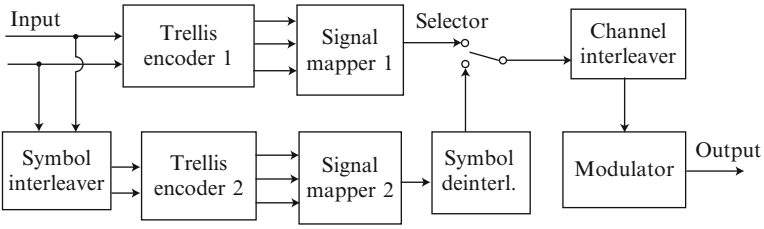

Fig. 1.19 Encoder for turbo trellis-coded modulation

Fig. 1.20 Iterative decoder for serially concatenated code. *D* deinterleaver; *I* interleaver

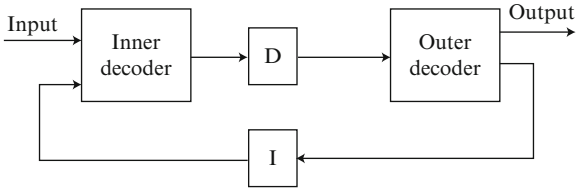

1.5.3 Serially Concatenated Turbo Codes

Serially concatenated turbo codes differ from classical concatenated codes in their use of large interleavers and iterative decoding. The interchange of information between the inner and outer decoders gives the serially concatenated codes a major performance advantage. Both the inner and outer codes must be amenable to efficient decoding by an SISO algorithm and, hence, are either binary systematic block codes or binary systematic convolutional codes. The encoder for a serially concatenated turbo code has the form of Fig. 1.16a. The outer encoder generates n_1 bits for every k_1 information bits. After the interleaving, each set of n_1 bits is converted by the inner encoder into n_2 bits. Thus, the overall code rate of the serially concatenated code is k_1/n_2. If the component codes are block codes, then an outer (n_1, k_1) code and an inner (n_2, n_1) code are used. A functional block diagram of an iterative decoder for a serially concatenated code is illustrated in Fig. 1.20. For each inner codeword, the input comprises the demodulator outputs corresponding to the n_2 bits. For each iteration, the inner decoder computes the LLRs for the n_1 systematic bits. After a deinterleaving, these LLRs provide extrinsic information about the n_1 code bits of the outer code. The outer decoder then computes the LLRs for all its code bits. After an interleaving, these LLRs provide extrinsic information about the n_1 systematic bits of the inner code. The final output of the iterative decoder comprises the k_1 information bits of the concatenated code.

A *product code* is a serially concatenated code that is constructed from a particular type of multidimensional array and linear block codes. A *turbo product code* is a product code that uses iterative decoding. An encoder for a two-dimensional turbo product code has the form of Fig. 1.16a. The outer encoder produces codewords of an (n_1, k_1) code. For an inner (n_2, k_2) code, k_2 codewords are placed in a $k_2 \times n_1$ interleaver array of k_2 rows and n_1 columns. The block interleaver columns are read

by the inner encoder to produce n_1 codewords of length n_2 that are transmitted. The resulting product code has $n = n_1 n_2$ code symbols, $k = k_1 k_2$ information symbols, and code rate

$$r = \frac{k_1 k_2}{n_1 n_2}. \tag{1.179}$$

The code may be represented by an $n_2 \times n_1$ matrix. Let d_{m1} and d_{m2} denote the minimum Hamming distances of the outer and inner codes, respectively. For a nonzero product codeword, every nonzero row in the matrix must have a weight of at least d_{m1}, and there must be at least d_{m2} nonzero rows. Thus, the minimum Hamming distance of the product code, which is equal to the minimum Hamming weight of a nonzero codeword, is at least $d_{m1} d_{m2}$. Let $\mathbf{c}_1$ and $\mathbf{c}_2$ denote outer and inner minimum-weight codewords, respectively. A valid product codeword is defined by a matrix in which all columns corresponding to zeros in $\mathbf{c}_1$ are zeros and all columns corresponding to ones in $\mathbf{c}_1$ are the same as $\mathbf{c}_2$. Therefore, a product codeword of weight $d_{m1} d_{m2}$ exists, and the product code has a minimum distance

$$d_m = d_{m1} d_{m2}. \tag{1.180}$$

Hard-decision decoding is done sequentially on an $n_2 \times n_1$ array of received code symbols. The inner codewords are decoded and code-symbol errors are corrected. Any residual errors are then corrected during the decoding of the outer codewords. Let t_1 and t_2 denote the error-correcting capability of the outer and inner codes, respectively. Incorrect decoding of the inner codewords requires that there are at least $t_2 + 1$ errors in at least one inner codeword or array column. For the outer decoder to fail to correct the residual errors, there must be at least $t_1 + 1$ inner codewords that have $t_2 + 1$ or more errors, and the errors must occur in certain array positions. Thus, the number of errors that is always correctable is

$$t = (t_1 + 1)(t_2 + 1) - 1 \tag{1.181}$$

which is roughly half of what (1.1) guarantees for classical block codes. However, although not all patterns with more than t errors are correctable, most of them are.

When iterative decoding is used, a product code is called a *turbo product code*. A comparison of (1.180) with (1.178) indicates that d_m for a turbo product code is generally larger than d_m for a block turbo code with the same component codes. The decoder for a turbo product code has the form shown in Fig. 1.21. The demodulator outputs are applied to both the inner decoder, and after deinterleaving, the outer decoder. The LLRs of both the information and parity bits of the corresponding code are computed by each decoder. These LLRs are then exchanged between the decoders after the appropriate deinterleaving or interleaving converts the LLRs into extrinsic information. A large reduction in the complexity of a turbo product code in exchange for a relatively small performance loss is obtained by using the Chase algorithm (Sect. 1.1) in the SISO algorithm of the component decoders. For a given complexity, the performance of turbo product codes and block turbo codes are similar.

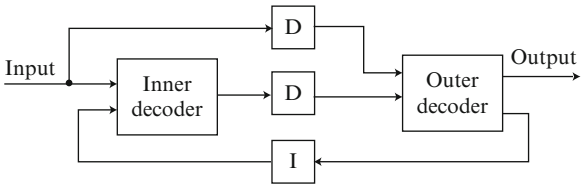

Fig. 1.21 Decoder of turbo product code. D = deinterleaver; I = interleaver

1.6 Low-Density Parity-Check Codes

Low-density parity-check (LDPC) *codes* are linear block codes specified by a parity-check matrix that is sparsely populated with nonzero elements, which are ones for binary codes, as is henceforth assumed because of their predominance. Since (1.4) and (1.5) imply that $\mathbf{cH}^T = \mathbf{0}$ or, equivalently that $\mathbf{Hc}^T = \mathbf{0}$, each of the $m = n - k$ rows of $\mathbf{H}$ specifies a constraint among the codeword symbols. Thus, one may solve for the parity-check bits sequentially by proceeding downward from the top row of $\mathbf{H}$. A *regular* LDPC code has the same number of ones in each column and the same number of ones in each row; otherwise, the LDPC code is *irregular*. Irregular LDPC codes are competitive with turbo codes in terms of the performance obtained for a given level of implementation complexity.

A *Tanner graph* is a bipartite graph that represents the parity-check matrix. One set of nodes, called the *variable nodes* , represent the codeword symbols. Another set of nodes, called the *check nodes*, represents the m constraints among the symbols. An edge connects variable-node i to check-node l if component $H_{il} = 0$. The (7,4) Hamming code has the parity-check matrix

$$\mathbf{H} = \begin{bmatrix} 1 & 1 & 1 & 0 & 1 & 0 & 0 \\ 0 & 1 & 1 & 1 & 0 & 1 & 0 \\ 1 & 1 & 0 & 1 & 1 & 0 & 1 \end{bmatrix} \tag{1.182}$$

and the associated Tanner graph is shown in Fig. 1.22.

A *cycle* of a graph is a sequence of distinct edges that start and terminate at the same node. The length of the shortest cycle in a graph is called its *girth*. The Tanner graph of the $(7, 4)$ Hamming code has a girth equal to 4, which is the minimum length of a cycle. The most effective LDPC codes have girths exceeding 4 because a low girth corresponds to a limited amount of independent information exchange among some variable and check nodes.

The soft-decision decoding algorithm for LDPC codes is called the *sum-product*, *message-passing*, or *belief-propagation* algorithm. The first name refers to the main computations required. The second name refers to the iterative passing of information messages between variable and check nodes, each of which is regarded as a processor. The third name emphasizes that the messages are measures of the credibility of the most recent computations. The sparseness of the parity-check matrix facilitates LDPC decoding.

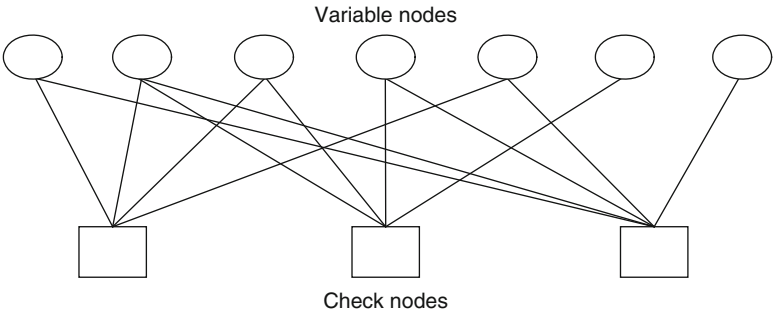

Fig. 1.22 Tanner graph for (7, 4) Hamming code

The basis of the sum-product algorithm is an LLR associated with the likelihood that a parity-check equation is satisfied. Let $b_1, b_2, \ldots, b_n$ denote n statistically independent bits with LLRs defined as $\lambda_i = \log[P(b_i = 1)/P(b_i = 0)]$. Let $\lambda_s = \log[P(s = 1)/P(s = 0)]$ denote the LLR associated with the parity modulo-2 sum $s = \sum_{i=1}^{n} b_i$, which is equal to zero when the parity-check equation is satisfied. It may be verified by considering an even number of ones among the n bits and then an odd number of ones that

$$s = \frac{1}{2}\left[1 - \prod_{i=1}^{n}(1 - 2b_i)\right]. \tag{1.183}$$

The independence of the bits and the easily verified facts that $P(s = 1) = E[s]$ and $E[b_i] = \exp(\lambda_i) / [1 + \exp(\lambda_i)]$ imply that

$$P(s = 1) = \frac{1}{2}\left[1 - \prod_{i=1}^{n}\left(1 - \frac{2e^{\lambda_i}}{1 + e^{\lambda_i}}\right)\right]. \tag{1.184}$$

Using algebra and the definition $tanh(x) = (e^x - e^{-x}) / (e^x + e^{-x})$, we obtain

$$P(s = 1) = \frac{1}{2}\left[1 - \prod_{i=1}^{n}\tanh\left(-\frac{\lambda_i}{2}\right)\right]. \tag{1.185}$$

Since $P(b_i = 1) + P(b_i = 0) = 1$, the definition of λ_s and a direct calculation give $tanh(-\lambda_s/2) = 1 - 2P(s = 1)$. The substitution of (1.185) into this equation and its inversion yields

$$\lambda_s = -2\tanh^{-1}\left[\prod_{i=1}^{n}\tanh\left(-\frac{\lambda_i}{2}\right)\right]. \tag{1.186}$$

In the first iteration of the sum-product algorithm, variable-node i uses the matched-filter output y_i associated with code-symbol b_i to compute

$$\lambda_i^{(0)} = \log\left[\frac{P(b_i = 1|y_i)}{P(b_i = 0|y_i)}\right]. \tag{1.187}$$

This LLR is the message sent to each adjacent check node. Each check node receives LLRs from variable nodes corresponding to bits that have a modulo-2 sum equal to zero. During iteration ν, check-node l combines its input LLRs $\lambda_i^{(\nu)}, i = 1, 2, ..., N_l$, each of which is assumed to be independent of the others, to produce output LLRs that constitute the messages sent to each of its adjacent variable nodes in subsequent iterations. Let $\mu_{li}^{(0)} = 0$ for all i and l. After receiving message $\nu - 1$, $\nu = 1, 2 \ldots, \nu_{\max}$, check- node l updates the LLR that will subsequently be sent to variable-node i by slightly modifying (1.186):

$$\mu_{li}^{(\nu)} = -2\tanh^{-1}\left[\prod_{m=N_l/i}\tanh\left(-\frac{\lambda_m^{(\nu-1)} - \mu_{lm}^{(\nu-1)}}{2}\right)\right] \tag{1.188}$$

where N_l/i is the set of variable nodes adjacent to check-node l but excluding variable-node i. The exclusion is to prevent redundant information originating in node i from recycling back to it, thereby causing an instability. The value passed to variable-node m in the preceding iteration is subtracted from $\lambda_m^{(\nu-1)}$ to reduce the correlation with previous iterations.

After receiving message ν, variable-node i updates its LLR as

$$\lambda_i^{(l)} = \lambda_i^{(0)} + \sum_{l \in M_i} \mu_{li}^{(\nu)} \tag{1.189}$$

where M_i is the set of check nodes adjacent to variable-node i. The algorithm can terminate when all of the parity-check equations specified by $\mathbf{H}$ are satisfied. If the algorithm terminates after ν_0 iterations, then the LDPC decoder sets $u = 1$ if $\lambda_i^{(\nu_0)} > 0$ and $u = -1$ otherwise.

LDPC codes are often characterized by the degree distributions of the nodes in their Tanner graphs. The *degree* of a node is defined as the number of edges emanating from it. The *degree distribution of the variable nodes* is defined as the polynomial

$$v(x) = \sum_{i=2}^{d_v} n_i x^{i-1} \tag{1.190}$$

where n_i denotes the fraction of variable nodes with degree i, and d_v denotes the maximum degree or number of edges connected to a variable node. The *degree distribution of the check nodes* is defined as the polynomial

$$\chi(x) = \sum_{i=2}^{d_c} \chi_i x^{i-1} \tag{1.191}$$

where χ_i denotes the fraction of check nodes with degree i, and d_c denotes the maximum degree or number of edges connected to a check node. Theoretically optimal degree distributions for infinitely long codes can be used as a starting point in the design of finite LDPC codes.

A well-designed LDPC code does not require an interleaver in the encoder because interleaving is equivalent to the permutation of the columns of the parity-check matrix H. If the ones in a large H are approximately randomly distributed, then any bit that is subjected to a deep fade is likely to be applied to a check node that also receives more reliable information from other bits. Since a deinterleaver is not required in its decoder, an LDPC code has less latency than a turbo code.

1.6.1 Irregular Repeat-Accumulate Codes

The sparse parity-check matrix of LDPC codes enables decoding with a complexity that increases linearly with the codeword or block length. However, the corresponding generator matrix is usually not sparse. Since the encoding requires the matrix multiplication indicated in (1.4), the encoding complexity increases quadratically with the codeword length. To reduce this complexity, preprocessing prior to encoding may be used. An alternative is to use LDPC codes, such as repeat-accumulate codes, with additional structure that limits the encoding complexity.

The *repeat-accumulate code* is a serially concatenated code that may be decoded as either an LDPC code or a turbo code. It has an outer repetition code, which is followed by an interleaver. Its inner code is a rate-1 recursive convolutional code with an encoder that functions as an accumulator, producing an output that is a modulo-2 sum of an input and a previous output. A limitation of the repeat-accumulate code, whether it is systematic or not, is that its code rate cannot exceed 1/2.

The repeat-accumulate code can be generalized to an *irregular repeat-accumulate* (IRA) *code* that retains linear complexity of encoding and decoding, but is not limited in its code rate, is more flexible in design options, and can provide a much better performance. The systematic IRA code, which is a special type of an irregular LDPC code, repeats each information bit a variable number of times. The repeated bits are interleaved, and then a variable number of them are combined and applied as successive inputs to an accumulator. A systematic IRA encoder generates the codeword $\mathbf{c} = [\mathbf{m}\ \mathbf{p}]$, where $\mathbf{m}$ is the row vector of k information bits, and $\mathbf{p}$ is the row vector of m accumulator outputs.

The parity-check matrix for a systematic IRA code has the form

$$\mathbf{H} = [\mathbf{H}_1\ \ \mathbf{H}_2] \tag{1.192}$$

where $\mathbf{H}_1$ is an $m \times k$ sparse matrix, and $\mathbf{H}_2$ is the sparse $m \times m$ matrix with the dual-diagonal form

$$\mathbf{H}_2 = \begin{bmatrix} 1 & 0 & 0 & & & & & \\ 1 & 1 & 0 & & & & & \\ 0 & 1 & 1 & & & & & \\ & & & \cdot & & & & \\ & & & & \cdot & & & \\ & & & & & 1 & 1 & 0 \\ & & & & & 0 & 1 & 1 \end{bmatrix}. \tag{1.193}$$

The generator matrix corresponding to $\mathbf{H}$ is

$$\mathbf{G} = \left[\mathbf{I} \;\; \mathbf{H}_1^T \mathbf{H}_2^{-T}\right] \tag{1.194}$$

which satisfies (1.5). A matrix inversion of (1.193) yields the upper triangular matrix of ones:

$$\mathbf{H}_2^{-T} = \begin{bmatrix} 1 & 1 & 1 & & & & \\ 0 & 1 & 1 & & & & \\ 0 & 0 & 1 & & & & \\ & & & \cdot & & & \\ & & & & \cdot & & \\ & & & & & 1 & 1 \\ & & & & & 0 & 1 \end{bmatrix}. \tag{1.195}$$

The encoder produces the codeword

$$\mathbf{c} = \left[\mathbf{m} \;\; \mathbf{m}\mathbf{H}_1^T \mathbf{H}_2^{-T}\right] \tag{1.196}$$

and the form of $\mathbf{H}_2^{-T}$ indicates that its premultiplication by the row vector $\mathbf{m}\mathbf{H}_1^T$ may be implemented as an accumulator.

1.7 Iterative Demodulation and Decoding

The idea of doing iterative computations using two decoders can be extended to a demodulator and decoder by designing the demodulator to exploit information provided by the decoder. The major components of a communication system with iterative decoding and demodulation are diagrammed in Fig. 1.23. In the transmitter, message bits are encoded, bit-interleaved or symbol-interleaved, and then applied to the modulator. A *constellation labeling* or *labeling map* is the mapping of a bit pattern to each symbol or point in a signal-set constellation. Each set of $m = \log_2 q$ consecutive bits in the input $\mathbf{b} = \{b_0, ..., b_{m-1}\} \in [0, 1]^m$ is mapped into a q-ary symbol $\mathbf{s} = \mu(\mathbf{b})$, where $\mu(\mathbf{b})$ is the labeling map, and the set of constellation

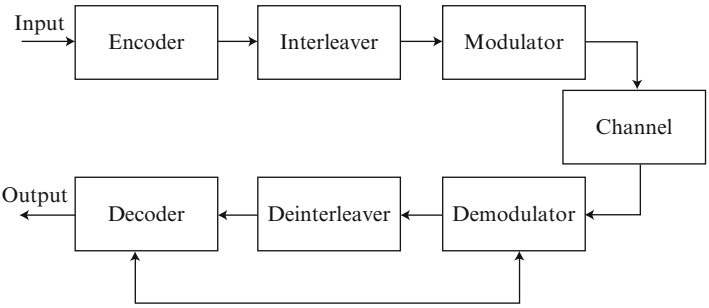

Fig. 1.23 Iterative demodulation and decoding with transmitter and receiver

symbols has cardinality q. In the receiver, the demodulator converts the received signal into a sequence of received symbols. A demapper within the demodulator processes each received symbol to produce a vector of bit metrics. This vector provides extrinsic information that is deinterleaved and passed to the decoder. The demapper and decoder exchange extrinsic information until bit decisions are made by the decoder after a specified number of iterations.

The demodulator computes a LLR for each of the m code bits constituting each received symbol. The LLR for bit k produced by the demodulator is

$$\Lambda_k = \log\left[\frac{P(b_k = 1|\mathbf{y})}{P(b_k = 0|\mathbf{y})}\right] \tag{1.197}$$

where $\mathbf{y}$ is the received vector when a q-ary symbol $\mathbf{s}$ representing m bits is transmitted. From the theorem of total probability and Bayes' rule,

$$\begin{aligned} P(b_k = b|\mathbf{y}) &= \sum_{\mathbf{s}_i} P(b_k = b, \mathbf{s} = \mathbf{s}_i|\mathbf{y}) \\ &= \sum_{\mathbf{s}_i} f(\mathbf{y}\,|b_k = b, \mathbf{s} = \mathbf{s}_i) P(b_k{=}b, \mathbf{s} = \mathbf{s}_i)/f\,(\mathbf{y}) \end{aligned} \tag{1.198}$$

where $b = 1$ or 0, and the summation is over all possible symbols $\mathbf{s}_i$, $i = 1, 2, \ldots, q$. Let D_k^b denote the set of all symbols such that $b_k = b$. If $\mathbf{s}_i \notin D_k^b$, then $P(b_k = b, \mathbf{s} = \mathbf{s}_i) = 0$. If $\mathbf{s}_i \in D_k^b$, then $P(b_k = b, \mathbf{s} = \mathbf{s}_i) = P\,(\mathbf{s} = \mathbf{s}_i)$, and $f(\mathbf{y}\,|b_k = b, \mathbf{s} = \mathbf{s}_i) = f(\mathbf{y} \mid \mathbf{s}_i)$. Using these results in (1.198) before substituting it into (1.197) yields

$$\Lambda_k = \log\left[\frac{\sum\limits_{\mathbf{s}_i \in D_k^1} f(\mathbf{y} \mid \mathbf{s}_i) P\,(\mathbf{s} = \mathbf{s}_i)}{\sum\limits_{\mathbf{s}_i \in D_k^0} f(\mathbf{y} \mid \mathbf{s}_i) P\,(\mathbf{s} = \mathbf{s}_i)}\right]. \tag{1.199}$$

The *a priori* probability $P(\mathbf{s} = \mathbf{s}_i)$ is assumed to be uniformly distributed during the first iteration. After the demodulator output is passed to the decoder, the decoder feeds back *a posteriori* probabilities that become the *a priori* probabilities of the demodulator. During the second and subsequent iterations, the assumption of statistically independent code bits leads to the estimator

$$P(\mathbf{s} = \mathbf{s}_i) = \prod_{l=1}^{m} P_e(b_l = b_l(\mathbf{s}_i)) \tag{1.200}$$

where $b_l(\mathbf{s}_i)$ is the value of bit l of symbol i, and $P_e(b_l = b_l(\mathbf{s}_i))$ is an estimated probability supplied by the decoder. Since $b_k(\mathbf{s}_i) = b$ when $\mathbf{s}_i \in D_k^b$, a factor $P_e(b_k = b)$ appears in (1.200). Therefore, when (1.200) is substituted into (1.199), the latter can be decomposed as

$$\Lambda_k = \Lambda_k^e + \log\left[\frac{P_e(b_k = 1)}{P_e(b_k = 0)}\right]. \tag{1.201}$$

The second term is calculated by the decoder using information supplied by the demodulator. Thus, only the first term is included in the extrinsic LLR passed to the decoder during the second and subsequent iterations. From the decomposition, we obtain

$$\Lambda_k^e = \log\left[\frac{\sum_{\mathbf{s}_i \in D_k^1} f(\mathbf{y} \mid \mathbf{s}_i) \prod_{l=1, l\neq k}^{m} P_e(b_l = b_l(\mathbf{s}_i))}{\sum_{\mathbf{s}_i \in D_k^0} f(\mathbf{y} \mid \mathbf{s}_i) \prod_{l=1, l\neq k}^{m} P_e(b_l = b_l(\mathbf{s}_i))}\right] \tag{1.202}$$

where the products are omitted if the symbols are binary.

The decoder computes the bit LLR

$$v_l = \log\left(\frac{P_e(b_l = 1)}{P_e(b_l = 0)}\right). \tag{1.203}$$

Since $P_e(b_l = 1) + P_e(b_l = 0) = 1$, it can be verified by substituting $b_l(\mathbf{s}_i) = 1$ and then $b_l(\mathbf{s}_i) = 0$ that

$$P_e(b_l = b_l(\mathbf{s}_i)) = \frac{\exp[b_l(\mathbf{s}_i)\, v_l]}{1 + \exp(v_l)}. \tag{1.204}$$

The substitution of (1.204) into (1.202) and a cancellation yields

$$\Lambda_k^e = \log\left[\frac{\sum_{\mathbf{s}_i \in D_k^1} f(\mathbf{y} \mid \mathbf{s}_i) \prod_{l=1, l\neq k}^{m} \exp[b_l(\mathbf{s}_i)\, v_l]}{\sum_{\mathbf{s}_i \in D_k^0} f(\mathbf{y} \mid \mathbf{s}_i) \prod_{l=1, l\neq k}^{m} \exp[b_l(\mathbf{s}_i)\, v_l]}\right] \tag{1.205}$$

where the products are omitted if the symbols are binary. Only Λ_k^e needs to be calculated by the demodulator. After the final iteration, the final decoded outputs are the hard decisions based on the decoder LLRs.

For *orthogonal* signals, a derivation that closely follows that of (1.67), but models the reception of a single symbol, yields the conditional probability density of the sampled matched-filter output y_k given that symbol s_i is transmitted and the phase is θ_i:

$$f\left(y_k \mid s_i, \theta_i\right) = \frac{1}{\pi N_0} \exp\left(-\frac{\left|y_k - \sqrt{\mathcal{E}_s} e^{j\theta_i} \delta_{ki}\right|^2}{N_0}\right), \quad k, i = 1, 2, \ldots, q \tag{1.206}$$

and hence the conditional density of $\mathbf{y}$, the vector with y_k as component k, is

$$f\left(\mathbf{y} \mid s_i, \theta_i\right) = \left(\frac{1}{\pi N_0}\right)^q \exp\left(-\frac{\left|y_i - \sqrt{\mathcal{E}_s} e^{j\theta_i}\right|^2}{N_0} - \sum_{k=1, k\neq i} \frac{|y_k|^2}{N_0}\right),$$
$$i = 1, 2, \ldots, q. \tag{1.207}$$

For *coherent* orthogonal signals, the $\{\theta_i\}$ are tracked by the phase synchronization system and, thus, ideally may be set to zero in (1.207). Discarding irrelevant terms that are common to all q symbols, we obtain the normalized density that can be used in (1.205):

$$f\left(\mathbf{y} \mid s_i\right) = \exp\left(-\frac{2\sqrt{\mathcal{E}_s}\,\mathrm{Re}\left(y_i\right)}{N_0}\right). \tag{1.208}$$

For *noncoherent* orthogonal signals, it is assumed that each θ_i is independent and uniformly distributed over $[0, 2\pi)$. Expanding the argument of the exponential function in (1.207), expressing y_i in polar form, integrating over each θ_i, and discarding irrelevant terms that are common to all q symbols, we obtain the normalized density:

$$f\left(\mathbf{y} \mid s_i\right) = I_0\left(\frac{2\sqrt{\mathcal{E}_s}\,|y_i|}{N_0}\right). \tag{1.209}$$

Similarly, for coherent q-ary QAM or PSK, (1.207) implies that the normalized density is

$$f\left(\mathbf{y} \mid s_i\right) = \exp\left(-\frac{2\sqrt{\mathcal{E}_s}\,\mathrm{Re}\left(s_i^* y_i\right) + \mathcal{E}_s\,|s_i|^2}{N_0}\right). \tag{1.210}$$

1.7.1 Bit-Interleaved Coded Modulation

Modulation and coding could be combined into a single operation, termed *coded modulation* (CM), but a more pragmatic approach is to use a *binary* encoder

followed by a bitwise interleaver prior to performing q-ary modulation. Such an approach is known as *bit-interleaved coded modulation* (BICM) [8–11]. In addition to easing implementation and analysis, BICM has diversity advantages over CM when used to mitigate fading. BICM increases time diversity by replacing symbol interleaving (depth exceeding the channel coherence time) with bit interleaving, thereby providing improved performance over a fading channel (Chap. 8). Although true maximum-likelihood decoding of BICM requires joint demodulation and decoding, in a practical receiver the demodulator separately generates bit metrics that are applied to the decoder. BICM has become a standard method for signaling over fading channels, forming the basis of most cellular, satellite, and wireless networking systems. However, a reduced minimum Euclidean distance degrades the performance of BICM over the AWGN channel.

Many communication systems include iterative decoding and demodulation in which soft-decision information is exchanged between the demodulator and the decoder, which itself may be internally iterative. The method of combining BICM with iterative decoding and demodulation is called *bit-interleaved coded modulation with iterative decoding* (BICM-ID). In BICM-ID, independent bit interleaving disperses bits throughout code sequences so that bit information fed back to the demodulator is independent of the bit for which the bit metric is calculated. When used with a convolutional code and a two-dimensional signal set, such as QAM or q-ary PSK, BICM-ID can offer superior bit-error-rate performance relative to BICM with any symbol labeling. If, however, the same signal set is used with a capacity-approaching code, such as a turbo or LDPC code, then the BICM capacity can be approached without needing feedback from the decoder, and hence there is very little to gain by using BICM-ID.

A *Gray labeling map* labels adjacent symbols the same except for one bit. When a Gray labeling or even a quasi-Gray labeling exists, BICM usually provides better performance than CM. With nonbinary orthogonal modulation, Gray labeling does not exist since all neighbors are equidistant, and there is a loss in capacity when BICM is used instead of CM. The use of BICM-ID can offer significant performance gains over BICM, even when a capacity-approaching code is used, and minimizes any performance degradation experienced by BICM over the AWGN channel. For binary modulations, BICM-ID and BICM are identical.

Plots of the bit error probability for systems with iterative decoding and demodulation generally exhibit a *waterfall* region, which is characterized by a rapid decrease in the bit error rate as $\mathcal{E}_b/N_0$ increases, and an *error-floor* region, in which the bit error rate decreases much more slowly. A hypothetical plot illustrating these regions is shown in Fig. 1.24. A low error floor may be important for radio-relay communication, space-ground communication, compressed-data transfer, optical transmission, or when an automatic-repeat request is not feasible because of the variable delays.

A *Gray labeling map* minimizes the number of bit errors that occur if an adjacent symbol of a received symbol is assigned the highest likelihood or largest metric by the decoder. Thus, a Gray labeling map will provide an early onset of the waterfall region, but produces a relatively high error floor primarily determined by

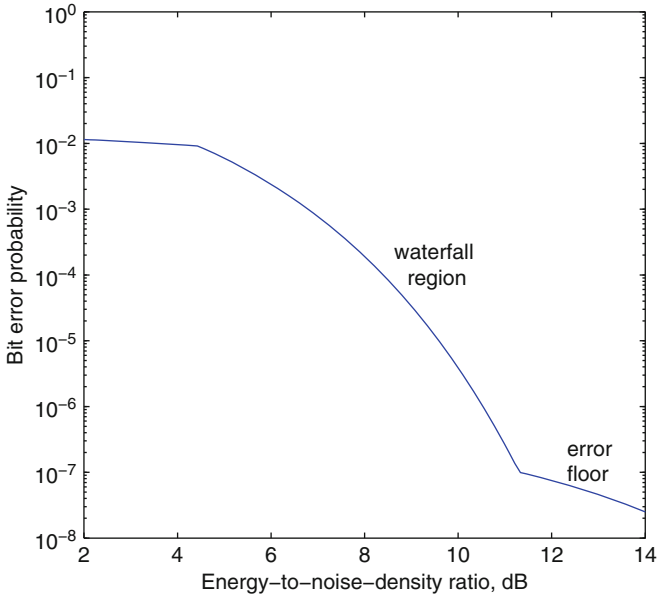

Fig. 1.24 Illustration of regions of bit error probability plot

the minimum Euclidean distance of the symbol set. In this book, a Gray labeling will always be assumed when a non-orthogonal modulation is used unless otherwise stated. Methods exist for constructing labeling maps that produce low error floors for an arbitrary constellation at the cost of an adversely shifted waterfall region [12]. LDPC codes often provide lower error floors than turbo codes of similar complexity.

1.7.2 Simulation Examples

The performance examples in this section, which are plots of the bit error probability as a function of $\mathcal{E}_b/N_0$, are generated by Monte Carlo simulations. It is assumed here and elsewhere in this book that the front-end and lowpass filters of both the transmitter and receiver are perfect.

CDMA2000 is a family of communication standards for the wireless transmission of data. Figures 1.25–1.29 illustrate the performance of a CDMA2000 system [13] that uses a rate-1/2 turbo code with parallel concatenated codes. The turbo encoder has the form shown in Fig. 1.17. Each component code is a recursive systematic convolutional code that has the configuration shown in Fig. 1.7. The puncturing matrix is

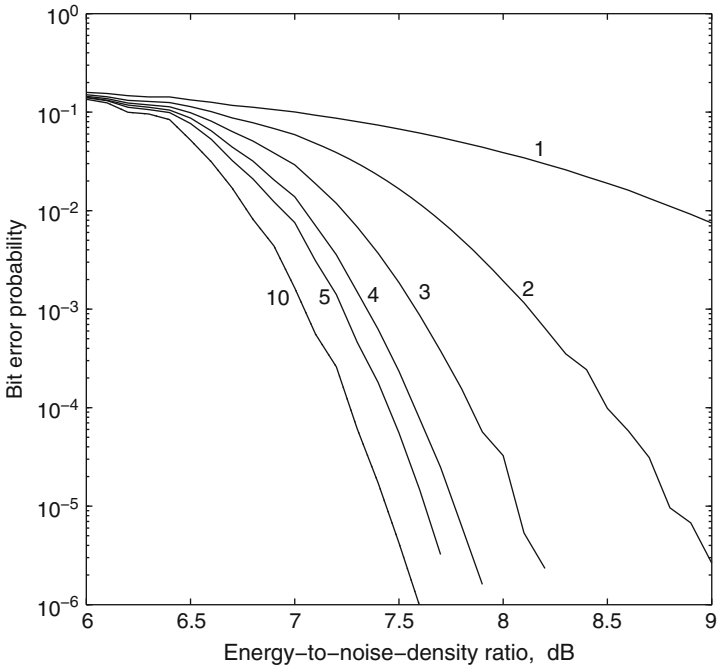

Fig. 1.25 Performance of turbo code with 4-FSK and BICM-ID over Rayleigh channel as number of decoding iterations varies

$$\mathbf{P} = \begin{bmatrix} 1 & 1 \\ 1 & 0 \\ 0 & 0 \\ 0 & 1 \end{bmatrix}. \tag{1.211}$$

The modulation is noncoherent q-ary FSK (q-FSK), and channel state information is assumed to be available in the receiver. The codeword size is $k = 1,530$ information bits, and the AWGN or Rayleigh fading (cf. Chap. 5 for details) channel is assumed. Ideal bit interleaving is assumed for binary symbols when BICM is used. When BICM is not used, symbol-interleaved coded modulation (SICM), which interleaves q-ary channel symbols, is assumed. Ideal interleaving is implemented in the simulation for the Rayleigh channel by having each modulated symbol multiplied by an independent fading coefficient. The actual size of a practical interleaver preceding the labeling mapping in the modulator of Fig. 1.23 is $3,060/\log_2 m$ q-ary symbols.

Figure 1.25 illustrates the improvement in the bit error probability of a system that uses 4-FSK and BICM-ID over the Rayleigh channel as the number of decoding iterations increases. The improvement exhibits diminishing returns and is insignificant beyond 10 iterations. Figure 1.26 compares the bit error probabilities

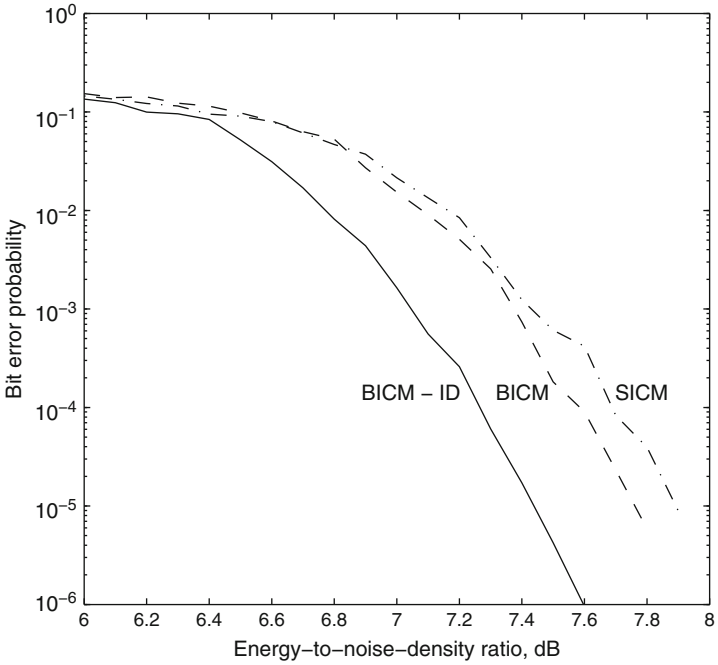

Fig. 1.26 Performance of turbo code with 4-FSK over Rayleigh channel for SICM, BICM, and BICM-ID

of systems using SICM, BICM, and BICM-ID with 4-FSK over the Rayleigh channel, whereas Fig. 1.27 makes the same comparisons for communications over the AWGN channel. In both figures, it is observed that BICM provides a small improvement relative to SICM, but BICM-ID provides a more substantial improvement. Figure 1.28 illustrates the degradation that occurs when the turbo decoder of the system with BICM-ID uses the max-log-MAP algorithm instead of the log-MAP algorithm for communications over the Rayleigh channel. The degradation for the AWGN channel is similar.

If larger alphabets are used, the performance improves at the cost of a larger signal bandwidth. For example, a system that use 4-FSK is compared with a system that uses 16-FSK in Fig. 1.29. Both systems use BICM-ID over the Rayleigh channel. It is observed that the 16-FSK system provides an improvement of roughly 1.5 dB at a bit error probability of 10^{-5}, but the bandwidth requirement is increased by a factor of 4. A code-rate reduction also provides an improved performance but an increased signal bandwidth.

WiMAX is a telecommunications protocol that provides internet access [14]. Figure 1.30 illustrates the performance over the Rayleigh channel of a WiMAX system with coherent 16-QAM, a rate-1/2 LDPC code, and channel state information. The codeword length is 2,304, 4,608, or 9,216 bits. The bit error probability decreases rapidly with increases in the codeword length.

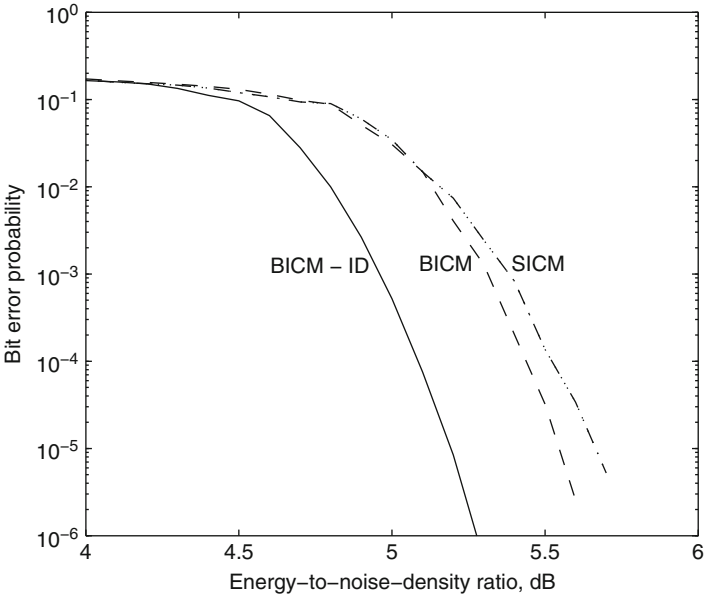

Fig. 1.27 Performance of turbo code with 4-FSK over AWGN channel for SICM, BICM, and BICM-ID

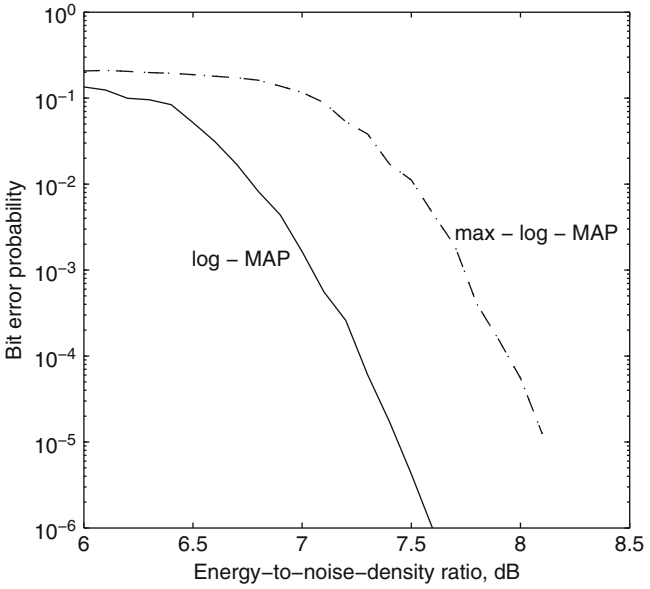

Fig. 1.28 Performance of turbo code with 4-FSK and BICM-ID over Rayleigh channel for log-MAP and max-log-MAP algorithms

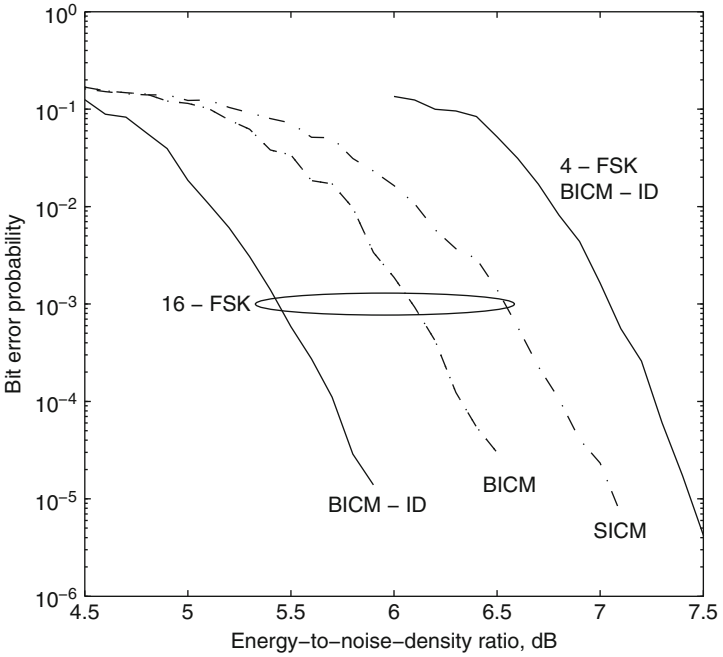

Fig. 1.29 Performance of turbo code with 16-FSK over Rayleigh channel for SICM, BICM, and BICM-ID and comparison with 4-FSK and BICM-ID

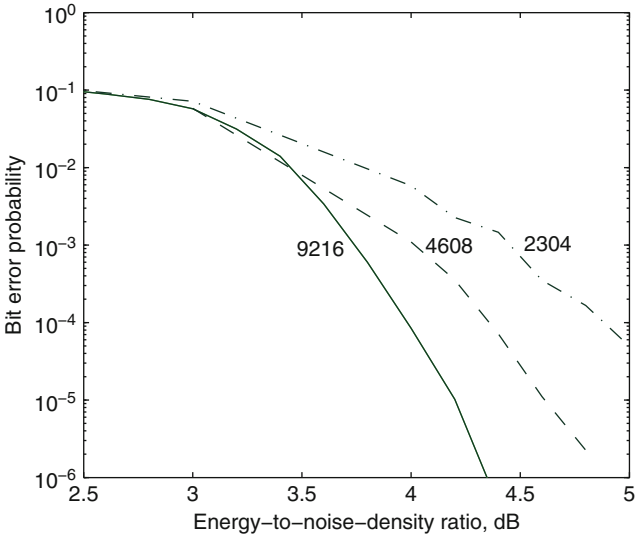

Fig. 1.30 Performance of LDPC code with 16-QAM over Rayleigh channel for codewords of length 2,304, 4,608, and 9,216

Problems

1.1. Verify that both Golay perfect codes satisfy the Hamming bound with equality.

1.2. (a) Use (1.16) to show that $N(d_m, d_m - t) = \binom{d_m}{t}$. Can the same result be derived directly? (b) Use (1.17) to derive $N(l, i)$ for Hamming codes. Consider the cases $l = i, i + 1, i - 1$, and $i - 2$ separately.

1.3. (a) Use (1.25) with $d_m = 2t + 1$ to derive an upper bound on A_{d_m}. (b) Explain why this upper bound becomes an equality for perfect codes. (c) Show that $A_3 = \frac{n(n-1)}{6}$ for Hamming codes. (d) Show that for perfect codes as $P_s \to 0$, both the exact equation (1.26) and the approximation (1.29) give the same expression for P_b.

1.4. Evaluate P_b for the (7,4) Hamming code using both the exact equation and the approximate one. Use the result of problem 2(b) and the weight distribution given in the text. Compare the two results.

1.5. Use erasures to show that a Reed–Solomon codeword can be recovered from any k correct symbols.

1.6. Suppose that a binary (7,4) Hamming code is used for coherent BPSK communications with a constant noise-power spectral density. A codeword has $x_{vi} = +1$ if symbol i in candidate codeword v is a 1, and $x_{vi} = -1$ if it is a 0. The received output samples are −0.4, 1.0, 1.0, 1.0, 1.0, 1.0, 0.4. Use the table of (7,4) Hamming codewords to find the decision made when the maximum-likelihood metric is used.

1.7. Prove that the word error probability for a block code with soft-decision decoding satisfies $P_w \leq (q^k - 1)Q(d)$.

1.8. Use (1.59) and (1.52) to show that the coding gain of a block code is roughly $d_m r$ relative to no code when P_{is} is low.

1.9. (a) Show that $P[X \geq b] \geq 1 - \min_{0 \leq s \leq s_1} [M(-s)e^{sb}]$. (b) Derive the Chernoff bound for a Gaussian random variable with mean μ and variance σ^2.

1.10. The Chernoff bound can be applied to hard-decision decoding, which can be regarded as a special case of soft-decision decoding with the following symbol metric. If symbol i of a candidate binary sequence v agrees with the corresponding detected symbol at the demodulator output, then $m(v, i) = 1$; otherwise $m(v, i) = 0$. Apply (1.138) and (1.139) with $\alpha = 1$ to obtain

$$P_2(l) \leq [4P_s(1 - P_s)]^{l/2}.$$

This upper bound is not always tight but has great generality since no specific assumptions have been made about the modulation or coding.

1.11. Consider a system that uses coherent BPSK and a convolutional code in the presence of white Gaussian noise. (a) What is the coding gain of a binary system

with soft decisions, $K = 7$, and $r = 1/2$ relative to an uncoded system for large E_b/N_0? (b) Use the approximation

$$Q(x) \approx \frac{1}{\sqrt{2\pi}x} \exp\left(-\frac{x^2}{2}\right), \quad x > 0$$

to show that as $E_b/N_0 \to \infty$, soft-decision decoding of a binary convolutional code has a 3 dB coding gain relative to hard-decision decoding.

1.12. A concatenated code comprises an inner binary $(2^m, m)$ block code, which is called a *Hadamard code*, and an outer (n, k) Reed–Solomon code. The outer encoder maps every m bits into one Reed–Solomon symbol, and every k symbols are encoded as an n-symbol codeword. After the symbol interleaving, the inner encoder maps every Reed–Solomon symbol into 2^m bits. After the interleaving of these bits, they are transmitted using a binary modulation. (a) Describe the removal of the encoding by the inner and outer decoders. (b) What is the value of n as a function of m? (c) What are the block length and code rate of the concatenated code?

1.13. For the binary symmetric channel with bit error probability p, the densities in (1.169) are replaced by probabilities. Show that

$$L(y_{sk}|b_k) = (-1)^{y_{sk}} \log\left(\frac{p}{1-p}\right).$$

1.14. If N_{0k} is unknown and may be significantly different from symbol to symbol, a standard procedure is to replace the LLR of (1.169) with the *generalized log-likelihood ratio*

$$L(y_{sk}|u_k) = \log\left[\frac{f(y_{sk}|u_k = +1, N_1)}{f(y_{sk}|u_k = -1, N_2)}\right] \tag{1.143}$$

where N_1 and N_2 are maximum-likelihood estimates of N_{0k} obtained from (1.170) with $u_k = +1$ and $u_k = -1$, respectively. Derive the estimators for N_1 and N_2 and then and then the corresponding $L(y_{sk}|u_k)$ in terms of y_{sk}, α, and $\mathcal{E}_s$. What practical difficulty is encountered if one attempts to use this LLR?

1.15. Use (1.205) to show that BICM-ID and BICM are identical for binary modulations.

References

1. W. E. Ryan and S. Lin, *Channel Codes: Classical and Modern*. Cambridge, UK: Cambridge University Press, 2009.
2. J. G. Proakis and M. Salehi, *Digital Communications, 5th ed.* New York: McGraw-Hill, 2008.
3. T. K. Moon, *Error Correction Coding*. Hoboken, NJ: Wiley, 2005.
4. D. R. Barry, E. A. Lee, and D. G. Messerschmitt, *Digital Communication, 3rd ed.* Boston: Kluwer Academic, 2004.

5. L. Hanzo, T. H. Liew, and B. L. Yeap, *Turbo Coding, Turbo Equalisation and Space-Time Coding*. Chichester, UK: Wiley, 2002.
6. D. Torrieri, "Information-Bit, Information-Symbol, and Decoded-Symbol Error Rates for Linear Block Codes," *IEEE Trans. Commun.*, vol. 36, pp. 613-617, May 1988.
7. J.-J. Chang, D.-J. Hwang, and M.-C. Lin, "Some Extended Results on the Search for Good Convolutional Codes," *IEEE Trans. Inform. Theory*, vol. 43, pp. 1682–1697, Sept. 1997.
8. A. Chindapol and J. A. Ritcey, "Design, Analysis and Performance Evaluation for BICM-ID with Square QAM Constellations in Rayleigh Fading Channels," *IEEE J. Select. Areas Commun.*, vol. 19, pp. 944-957, May 2001.
9. X. Li, A. Chindapol, and J. A. Ritcey, "Bit-interleaved Coded Modulation with Iterative Decoding and 8PSK Modulation," *IEEE Trans. Commun.*, vol. 50, pp. 1250-1257, Aug. 2002.
10. M. C. Valenti and S. Cheng, "Iterative Demodulation and Decoding of Turbo Coded M-ary Noncoherent Orthogonal Modulation," *IEEE J. Select. Areas Commun.*, vol. 23, pp. 1738–1747, Sept. 2005.
11. G. Caire, G. Taricco, and E. Biglieri, "Bit-interleaved Coded Modulation," *IEEE Trans. Inform. Theory*, vol. 44, pp. 927–946, May 1998.
12. D. Torrieri and M. C. Valenti, "Constellation Labeling Maps for Low Error Floors," *IEEE Trans. Wireless Commun.*, vol. 7, pp. 5401-5407, Dec. 2008.
13. M.C. Valenti and J. Sun, "Turbo codes," Chapter 12 of *Handbook of RF and Wireless Technologies*, F. Dowla, ed. New York: Elsevier, Newnes Press, 2004.
14. IEEE Computer society, "Part 16: Air Interface for Broadband Wireless Access Systems," *IEEE Std. 802.16-2009*, http://standards.ieee.org/getieee802/download/802.16-2009.pdf, 2009.

Chapter 2
Direct-Sequence Systems

A *spread-spectrum signal* is one with an extra modulation that expands the signal bandwidth greatly beyond what is required by the underlying coded-data modulation. Spread-spectrum communication systems are useful for suppressing interference, making secure communications difficult to detect and process, accommodating fading and multipath channels, and providing a multiple-access capability. Spread-spectrum signals cause relatively minor interference to other systems operating in the same spectral band. The most practical and dominant spread-spectrum systems are *direct-sequence* and *frequency hopping* systems.

There is no fundamental theoretical barrier to the effectiveness of spread-spectrum communications. That remarkable fact is not immediately apparent since the increased bandwidth of a spread-spectrum signal might require a receive filter that passes more noise power than necessary to the demodulator. However, when any signal and white Gaussian noise are applied to a filter matched to the signal, the sampled filter output has a signal-to-noise ratio that depends solely on the energy-to-noise-density ratio. Thus, the bandwidth of the input signal is irrelevant, and spread-spectrum signals have no inherent limitations.

Direct-sequence modulation entails the direct addition of a high-rate spreading sequence with a lower-rate data sequence, resulting in a transmitted signal with a relatively wide bandwidth. The removal of the spreading sequence in the receiver causes a contraction of the bandwidth that can be exploited by appropriate filtering to remove a large portion of the interference. This chapter begins with a discussion of spreading sequences and waveforms and then provides a detailed analysis of how the direct-sequence receiver suppresses various forms of interference. The final section presents several methods that supplement the inherent ability of a direct-sequence system to reject narrowband interference.

D. Torrieri, *Principles of Spread-Spectrum Communication Systems*,
DOI 10.1007/978-1-4419-9595-7_2, © Springer Science+Business Media, LLC 2011

2.1 Definitions and Concepts

A *direct-sequence signal* is a spread-spectrum signal generated by the direct mixing of the data with a spreading waveform before the final carrier modulation. Ideally, a direct-sequence signal with BPSK or differential PSK (DPSK) data modulation can be represented by

$$s(t) = Ad(t)p(t)\cos(2\pi f_c t + \theta) \tag{2.1}$$

where A is the signal amplitude, $d(t)$ is the data modulation, $p(t)$ is the spreading waveform, f_c is the carrier frequency, and θ is the phase at $t = 0$. The data modulation is a sequence of nonoverlapping rectangular pulses of duration T_s, each of which has an amplitude $d_i = +1$ if the associated data symbol is a 1 and $d_i = -1$ if it is a 0 (alternatively, the mapping could be $1 \rightarrow -1$ and $0 \rightarrow +1$). The *spreading waveform* has the form

$$p(t) = \sum_{i=-\infty}^{\infty} p_i \psi(t - iT_c) \tag{2.2}$$

where each p_i equals $+1$ or -1 and represents one *chip* of the *spreading sequence*. The *chip waveform* $\psi(t)$ is ideally designed to prevent interchip interference in the receiver. A *rectangular chip waveform* has $\psi(t) = w(t, T_c)$, where

$$w(t, T) = \begin{cases} 1, & 0 \le t < T \\ 0, & \text{otherwise.} \end{cases} \tag{2.3}$$

Figure 2.1 depicts an example of $d(t)$ and $p(t)$ for a rectangular chip waveform.

Message privacy is provided by a direct-sequence system if a transmitted message cannot be recovered without knowledge of the spreading sequence. To ensure message privacy, which is assumed henceforth, the data-symbol transitions must coincide with the chip transitions. Since the transitions coincide, the *processing gain* $G = T_s/T_c$ is an integer equal to the number of chips in a symbol interval. If W is the bandwidth of $p(t)$ and B is the bandwidth of $d(t)$, the spreading due to $p(t)$ ensures that $s(t)$ has a bandwidth $W \gg B$.

Figure 2.2 is a functional or conceptual block diagram of the basic operation of a direct-sequence system with BPSK. To provide message privacy, data symbols and chips, which are represented by digital sequences of 0's and 1's, are synchronized by the same clock and then modulo-2 added in the transmitter. The adder output is converted according to $0 \rightarrow -1$ and $1 \rightarrow +1$ before the chip and carrier modulations. Assuming that chip and symbol synchronization has been established, the received signal passes through the wideband filter and is multiplied by a synchronized local replica of $p(t)$. In this conceptual analysis, the effects of the propagation channel and the filtering are assumed to be negligible. If $\psi(t)$ is rectangular with unit amplitude, then $p(t) = \pm 1$ and $p^2(t) = 1$. Therefore, if the filtered signal is given by (2.1), the multiplication yields the *despread signal*

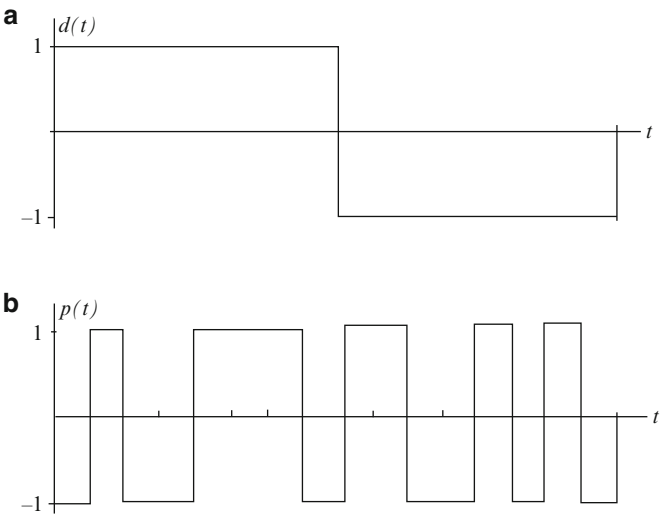

Fig. 2.1 Examples of (**a**) data modulation and (**b**) spreading waveform

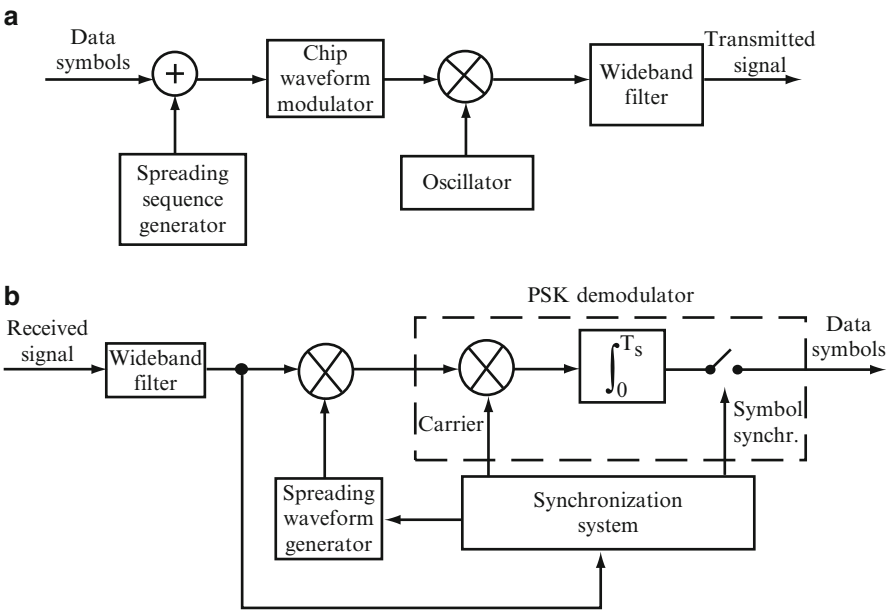

Fig. 2.2 Functional block diagram of direct-sequence system with BPSK or DPSK: (**a**) transmitter and (**b**) receiver

$$s_1(t) = p(t)s(t) = Ad(t)\cos(2\pi f_c t + \theta) \tag{2.4}$$

at the input of the PSK demodulator. Since the despread signal is a PSK signal, a standard coherent demodulator extracts the data symbols.

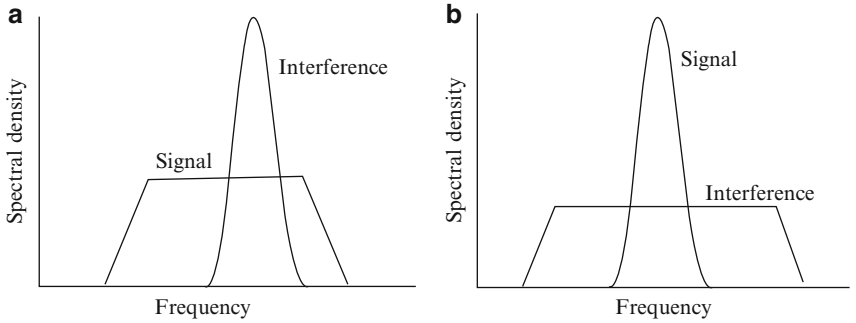

Fig. 2.3 Spectra of desired signal and interference: (**a**) wideband-filter output and (**b**) demodulator input

Figure 2.3a is a qualitative depiction of the relative spectra of the desired signal and narrowband interference at the output of the wideband filter. Multiplication of the received signal by the spreading waveform, which is called *despreading*, produces the spectra of Fig. 2.3b at the demodulator input. The signal bandwidth is reduced to B, while the interference energy is spread over a bandwidth exceeding W. Since the filtering action of the demodulator then removes most of the interference spectrum that does not overlap the signal spectrum, most of the original interference energy is eliminated. An approximate measure of the interference suppression capability is given by the ratio W/B. Whatever the precise definition of a bandwidth, W and B are proportional to $1/T_c$ and $1/T_s$, respectively, with the same proportionality constant. Therefore,

$$G = \frac{T_s}{T_c} = \frac{W}{B} \tag{2.5}$$

which links the processing gain with the interference suppression illustrated in the figure. Since its spectrum is unchanged by the despreading, white Gaussian noise is not suppressed by a direct-sequence system.

In practical systems, the wideband filter in the transmitter is used to limit the out-of-band radiation. This filter and the propagation channel disperse the chip waveform so that it is no longer confined to $[0, T_c]$. To prevent significant *interchip interference* in the receiver, the filtered chip waveform must be designed so that the Nyquist criterion for no interchip interference is approximately satisfied. A convenient representation of a direct-sequence signal when the chip waveform may extend beyond $[0, T_c]$ is

$$s(t) = A \sum_{i=-\infty}^{\infty} d_{\lfloor i/G \rfloor} p_i \psi\left(t - iT_c\right) \cos\left(2\pi f_c t + \theta\right) \tag{2.6}$$

where $\lfloor x \rfloor$ denotes the integer part of x. When the chip waveform is assumed to be confined to $[0, T_c]$, then (2.6) can be expressed by (2.1) and (2.2).

2.2 Spreading Sequences and Waveforms

2.2.1 Random Binary Sequence

A *random binary sequence* $x(t)$ is a stochastic process that consists of independent, identically distributed symbols, each of duration T. Each symbol takes the value $+1$ with probability $1/2$ or the value -1 with probability $1/2$. Therefore, $E[x(t)] = 0$ for all t, and

$$P\left[x\left(t\right) = i\right] = 1/2, \quad i = +1, -1. \tag{2.7}$$

A sample function of a *random binary sequence* $x(t)$ is illustrated in Fig. 2.4.

The *autocorrelation* of a stochastic process $x(t)$ is defined as

$$R_x(t, \tau) = E\left[x(t)x(t + \tau)\right]. \tag{2.8}$$

A stochastic process is wide-sense stationary if its mean is constant and $R_x\left(t, \tau\right)$ is a function of τ alone so that the autocorrelation may be denoted by $R_x(\tau)$. As shown subsequently, a random binary sequence is wide-sense stationary if the location of the first symbol transition or start of a new symbol after $t = 0$ is a random variable uniformly distributed over the half-open interval $(0, T]$. From (2.7) and the definitions of an expected value and a conditional probability, it follows that the autocorrelation of a random binary sequence is

$$\begin{aligned} R_x(t, \tau) = {} & \frac{1}{2}P[x(t + \tau) = 1 | x(t) = 1] - \frac{1}{2}P[x(t + \tau) = -1 | x(t) = 1] \\ & + \frac{1}{2}P[x(t + \tau) = -1 | x(t) = -1] - \frac{1}{2}P[x(t + \tau) = 1 | x(t) = -1] \end{aligned} \tag{2.9}$$

where $P[A|B]$ denotes the conditional probability of event A given the occurrence of event B. From the theorem of total probability, it follows that

$$\begin{aligned} & P[x(t + \tau) = i | x(t) = i] + P[x(t + \tau) = -i | x(t) = i] = 1, \\ & \qquad i = +1, -1. \end{aligned} \tag{2.10}$$

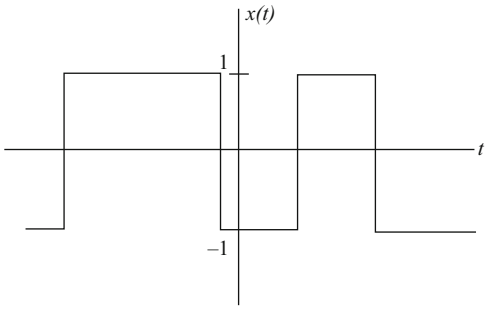

Fig. 2.4 Sample function of a random binary sequence

Since both of the following probabilities are equal to the probability that $x(t)$ and $x(t+\tau)$ differ,

$$P[x(t+\tau)=1|x(t)=-1]=P[x(t+\tau)=-1|x(t)=1]. \tag{2.11}$$

Substitution of (2.10) and (2.11) into (2.9) yields

$$R_x(t,\tau)=1-2P[x(t+\tau)=1|x(t)=-1]. \tag{2.12}$$

If $|\tau|\geq T$, then $x(t)$ and $x(t+\tau)$ are independent random variables because t and $t+\tau$ are in different symbol intervals. Therefore,

$$P[x(t+\tau)=1|x(t)=-1]=P[x(t+\tau)=1]=\tfrac{1}{2} \tag{2.13}$$

and (2.6) implies that $R_x(t,\tau)=0$ for $|\tau|\geq T$. If $|\tau|<T$, then $x(t)$ and $x(t+\tau)$ are independent only if a symbol transition occurs in the half-open interval $I_0=(t,t+\tau]$. Consider any half-open interval I_1 of length T that includes I_0. Exactly one transition occurs in I_1. Since the first transition for $t>0$ is assumed to be uniformly distributed over $(0,T]$, the probability that a transition in I_1 occurs in I_0 is $|\tau|/T$. If a transition occurs in I_0, then $x(t)$ and $x(t+\tau)$ are independent and differ with probability $\frac{1}{2}$; otherwise, $x(t)=x(t+\tau)$. Consequently, $P[x(t+\tau)=1|x(t)=-1]=|\tau|/2T$ if $|\tau|<T$. Substitution of the preceding results into (2.12) confirms the wide-sense stationarity of $x(t)$ and gives the *autocorrelation of the random binary sequence*:

$$R_x(t,\tau)=R_x(\tau)=\Lambda\left(\frac{\tau}{T}\right) \tag{2.14}$$

where the *triangular function* is defined by

$$\Lambda(t)=\begin{cases}1-|t|, & |t|\leq 1\\ 0, & |t|>1.\end{cases} \tag{2.15}$$

The *power spectral density of the random binary sequence* is the Fourier transform of the autocorrelation. A straightforward calculation gives the power spectral density

$$\begin{aligned}\mathcal{S}_x(f)&=\int_{-\infty}^{\infty}\Lambda\left(\frac{t}{T}\right)\exp(-j2\pi ft)\,dt\\ &=T\,\mathrm{sinc}^2 fT\end{aligned} \tag{2.16}$$

where $j=\sqrt{-1}$ and $\mathrm{sinc}\,x=(\sin\pi x)/\pi x$.

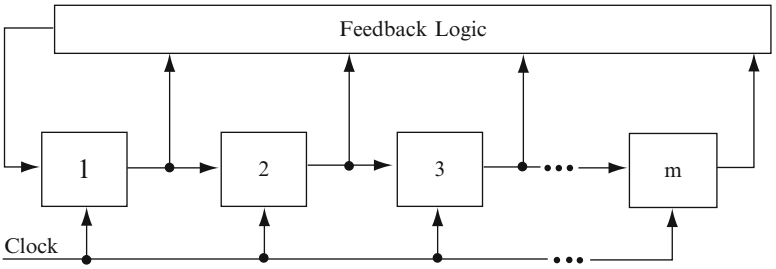

Fig. 2.5 General feedback shift register with m stages

2.2.2 Shift-Register Sequences

Ideally, one would prefer a random binary sequence as the spreading sequence. However, practical synchronization requirements in the receiver force one to use periodic binary sequences. A *shift-register sequence* is a periodic binary sequence generated by combining the outputs of feedback shift registers. A *feedback shift register*, which is diagrammed in Fig. 2.5, consists of consecutive two-state memory or storage stages and feedback logic. Binary sequences drawn from the alphabet {0,1} are shifted through the shift register in response to clock pulses. The *contents* of the stages, which are identical to their outputs, are logically combined to produce the input to the first stage. The initial contents of the stages and the feedback logic determine the successive contents of the stages. If the feedback logic consists entirely of modulo-2 adders (exclusive-OR gates), a feedback shift register and its generated sequence are called *linear*.

Figure 2.6a illustrates a linear feedback shift register with three stages and an output sequence extracted from the final stage. The input to the first stage is the modulo-2 sum of the contents of the second and third stages. After each clock pulse, the contents of the first two stages are shifted to the right, and the input to the first stage becomes its content. If the initial contents of the shift-register stages are 0 0 1, the subsequent contents after successive shifts are listed in Fig. 2.6b. Since the shift register returns to its initial state after seven shifts, the periodic output sequence extracted from the final stage has a period of seven bits.

The *state* of the shift register after clock pulse i is the vector

$$\mathbf{S}(i) = [s_1(i)\, s_2(i) \ldots s_m(i)], \quad i \geq 0 \tag{2.17}$$

where $s_l(i)$ denotes the content of stage l after clock pulse i and $\mathbf{S}(0)$ is the initial state. The definition of a shift register implies that

$$s_l(i) = s_{l-k}(i-k), \quad i \geq k \geq 0, \quad k \leq l \leq m \tag{2.18}$$

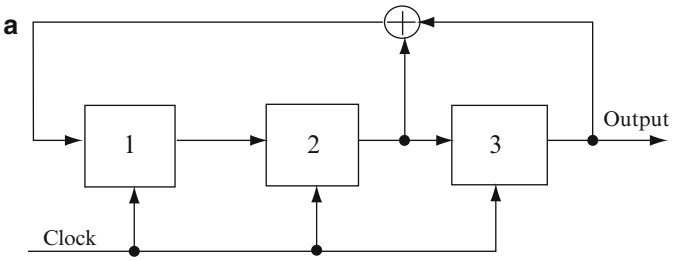

b

Shift	Contents		
	Stage 1	Stage 2	Stage 3
Initial	0	0	1
1	1	0	0
2	0	1	0
3	1	0	1
4	1	1	0
5	1	1	1
6	0	1	1
7	0	0	1

Fig. 2.6 (**a**) Three-stage linear feedback shift register and (**b**) contents after successive shifts

where $s_0(i)$ denotes the input to stage 1 after clock pulse i. If a_i denotes the state of bit i of the output sequence, then $a_i = s_m(i)$. The state of a feedback shift register uniquely determines the subsequent sequence of states and the shift-register sequence. The period N of a periodic sequence $\{a_i\}$ is defined as the smallest positive integer for which $a_{i+N} = a_i, i \geq 0$. Since the number of distinct states of an m-stage nonlinear feedback shift register is 2^m, the sequence of states and the shift-register sequence have period $N \leq 2^m$.

The input to stage 1 of a linear feedback shift register is

$$s_0(i) = \sum_{k=1}^{m} c_k s_k(i), \quad i \geq 0 \tag{2.19}$$

where the operations are modulo-2 and the feedback coefficient c_k equals either 0 or 1, depending on whether the output of stage k feeds a modulo-2 adder. An m-stage shift register is defined to have $c_m = 1$; otherwise, the final state would not contribute to the generation of the output sequence, but would only provide a one-shift delay. For example, Fig. 2.6 gives $c_1 = 0, c_2 = c_3 = 1$, and $s_0(i) = s_2(i) \oplus s_3(i)$. A general representation of a linear feedback shift register is shown in Fig. 2.7a. If $c_k = 1$, the corresponding switch is closed; if $c_k = 0$, it is open.

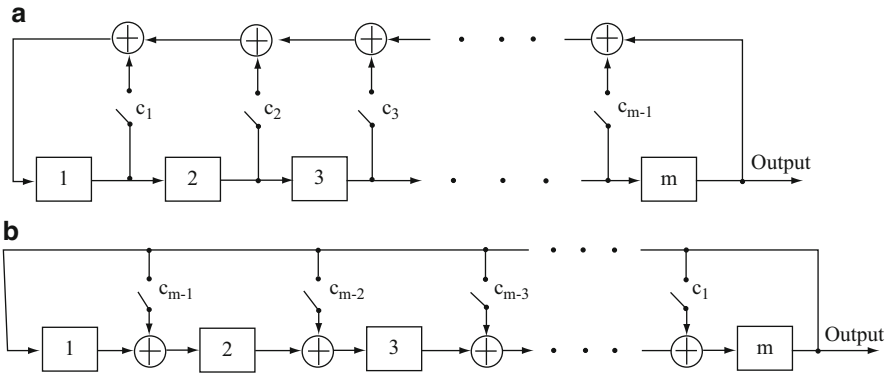

Fig. 2.7 Linear feedback shift register: (**a**) standard representation and (**b**) high-speed form

Since the output bit $a_i = s_m(i)$, (2.18) and (2.19) imply that for $i \geq m$,

$$a_i = s_0(i-m) = \sum_{k=1}^{m} c_k s_k(i-m) = \sum_{k=1}^{m} c_k s_m(i-k) \tag{2.20}$$

which indicates that each output bit satisfies the *linear recurrence relation*:

$$a_i = \sum_{k=1}^{m} c_k a_{i-k}, \quad i \geq m. \tag{2.21}$$

The first m output bits are determined solely by the initial state:

$$a_i = s_{m-i}(0), \quad 0 \leq i \leq m-1. \tag{2.22}$$

Figure 2.7a is not necessarily the best way to generate a particular shift-register sequence. Figure 2.7b illustrates an implementation that allows higher-speed operation. From this diagram, it follows that

$$s_l(i) = s_{l-1}(i-1) \oplus c_{m-l+1} s_m(i-1), \quad i \geq 1, \quad 2 \leq l \leq m \tag{2.23}$$

$$s_1(i) = s_m(i-1) \qquad i \geq 1. \tag{2.24}$$

Repeated application of (2.23) implies that

$$\begin{aligned} s_m(i) &= s_{m-1}(i-1) \oplus c_1 s_m(i-1), && i \geq 1 \\ s_{m-1}(i-1) &= s_{m-2}(i-2) \oplus c_2 s_m(i-2), && i \geq 2 \\ &\vdots \\ s_2(i-m+2) &= s_1(i-m+1) \oplus c_{m-1} s_m(i-m+1), && i \geq m-1. \end{aligned} \tag{2.25}$$

Addition of these m equations yields

$$s_m(i) = s_1(i-m+1) \oplus \sum_{k=1}^{m-1} c_k s_m(i-k), \quad i \geq m-1. \tag{2.26}$$

Substituting (2.24 and then $a_i = s_m(i)$ into (2.26), we obtain

$$a_i = a_{i-m} \oplus \sum_{k=1}^{m-1} c_k a_{i-k}, \quad i \geq m. \tag{2.27}$$

Since $c_m = 1$, (2.27) is the same as (2.20). Thus, the two implementations can produce the same output sequence indefinitely if the first m output bits coincide. However, they require different initial states and have different sequences of states. Successive substitutions into the first equation of sequence (2.25) yields

$$s_m(i) = s_{m-i}(0) \oplus \sum_{k=1}^{i} c_k s_m(i-k), \qquad 1 \leq i \leq m-1. \tag{2.28}$$

Substituting $a_i = s_m(i)$, $a_{i-k} = s_m(i-k)$, and $j = m-i$ into (2.28) and then using binary arithmetic, we obtain

$$s_l(0) = a_{m-l} \oplus \sum_{k=1}^{m-l} c_k a_{m-l-k}, \qquad 1 \leq l \leq m. \tag{2.29}$$

If $a_0, a_1, \ldots a_{m-1}$ are specified, then (2.29) gives the corresponding initial state of the high-speed shift register.

The sum of binary sequence $\mathbf{a} = (a_0, a_1, \cdots)$ and binary sequence $\mathbf{b} = (b_0, b_1, \cdots)$ is defined to be the binary sequence $\mathbf{a} \oplus \mathbf{b}$, each bit of which is the modulo-2 sum of the corresponding bits of $\mathbf{a}$ and $\mathbf{b}$. Thus, if $\mathbf{d} = \mathbf{a} \oplus \mathbf{b}$, we can write

$$d_i = a_i \oplus b_i, \quad i \geq 0. \tag{2.30}$$

Consider sequences $\mathbf{a}$ and $\mathbf{b}$ that are generated by the same linear feedback shift register but may differ because the initial states may be different. For the sequence $\mathbf{d} = \mathbf{a} \oplus \mathbf{b}$, (2.30) and the associative and distributive laws of binary fields imply that

$$\begin{aligned} d_i &= \sum_{k=1}^{m} c_k a_{i-k} \oplus \sum_{k=1}^{m} c_k b_{i-k} = \sum_{k=1}^{m} (c_k a_{i-k} \oplus c_k b_{i-k}) \\ &= \sum_{k=1}^{m} c_k (a_{i-k} \oplus b_{i-k}) = \sum_{k=1}^{m} c_k d_{i-k}. \end{aligned} \tag{2.31}$$

Since the linear recurrence relation is identical, **d** can be generated by the same linear feedback logic as **a** and **b**. Thus, if **a** and **b** are two output sequences of a linear feedback shift register, then $\mathbf{a} \oplus \mathbf{b}$ is also. If $\mathbf{a} = \mathbf{b}$, then $\mathbf{a} \oplus \mathbf{b}$ is the sequence of all 0's, which can be generated by any linear feedback shift register.

2.2.3 Maximal Sequences

If a linear feedback shift register reached the zero state with all its contents equal to 0 at some time, it would always remain in the zero state, and the output sequence would subsequently be all 0's. Since a linear m-stage feedback shift register has exactly $2^m - 1$ nonzero states, the period of its output sequence cannot exceed $2^m - 1$. A sequence of period $2^m - 1$ generated by a linear feedback shift register is called a *maximal* or *maximal-length sequence*. If a linear feedback shift register generates a maximal sequence, then all of its nonzero output sequences are maximal, regardless of the initial states.

Out of 2^m possible states, the content of the last stage, which is the same as the output bit, is a 0 in 2^{m-1} states. Among the nonzero states, the output bit is a 0 in $2^{m-1} - 1$ states. Therefore, in one period of a maximal sequence, the number of 0's is exactly $2^{m-1} - 1$, while the number of 1's is exactly 2^{m-1}.

Given the binary sequence **a**, let $\mathbf{a}(l) = (a_l, a_{l+1}, \ldots)$ denote a shifted binary sequence. If **a** is a maximal sequence and $l \neq 0$, modulo $2^m - 1$, then $\mathbf{a} \oplus \mathbf{a}(l)$ is not the sequence of all 0's. Since $\mathbf{a} \oplus \mathbf{a}(l)$ is generated by the same shift register as **a**, it must be a maximal sequence and, hence, some cyclic shift of **a**. We conclude that the modulo-2 sum of a maximal sequence and a cyclic shift of itself by l digits, where $l \neq 0$, modulo $2^m - 1$, produces another cyclic shift of the original sequence; that is,

$$\mathbf{a} \oplus \mathbf{a}(l) = \mathbf{a}(k), \quad l \neq 0 \text{ (modulo } 2^m - 1). \tag{2.32}$$

In contrast, a non-maximal linear sequence $\mathbf{a} \oplus \mathbf{a}(l)$ is not necessarily a cyclic shift of **a** and may not even have the same period. As an example, consider the linear feedback shift register depicted in Fig. 2.8. The possible state transitions depend on the initial state. Thus, if the initial state is 0 1 0, then the second state diagram indicates that there are two possible states, and, hence, the output sequence has a period of two. The output sequence is $\mathbf{a} = (0, 1, 0, 1, 0, 1, \ldots)$, which implies that $\mathbf{a}(1) = (1, 0, 1, 0, 1, 0, \ldots)$ and $\mathbf{a} \oplus \mathbf{a}(1) = (1, 1, 1, 1, 1, 1, \ldots)$; this result indicates that there is no value of k for which (2.32) is satisfied.

Maximal sequences have many properties that make them difficult to distinguish from random sequences. Suppose that one observes i bits within a maximal sequence of period $2^n - 1$ bits, and $i \leq n$. The i bits are part of a sequence of n bits that constitute a state of the shift register that generated the maximal sequence. If not all of the i bits are 0's, the $n - i$ unobserved bits in the n-bit sequence may be any of 2^{n-i} possible sequences. Since there are $2^n - 1$ possible n-bit sequences, the relative frequency of a particular sequence of i observed bits is $2^{n-i}/(2^n - 1)$ if the

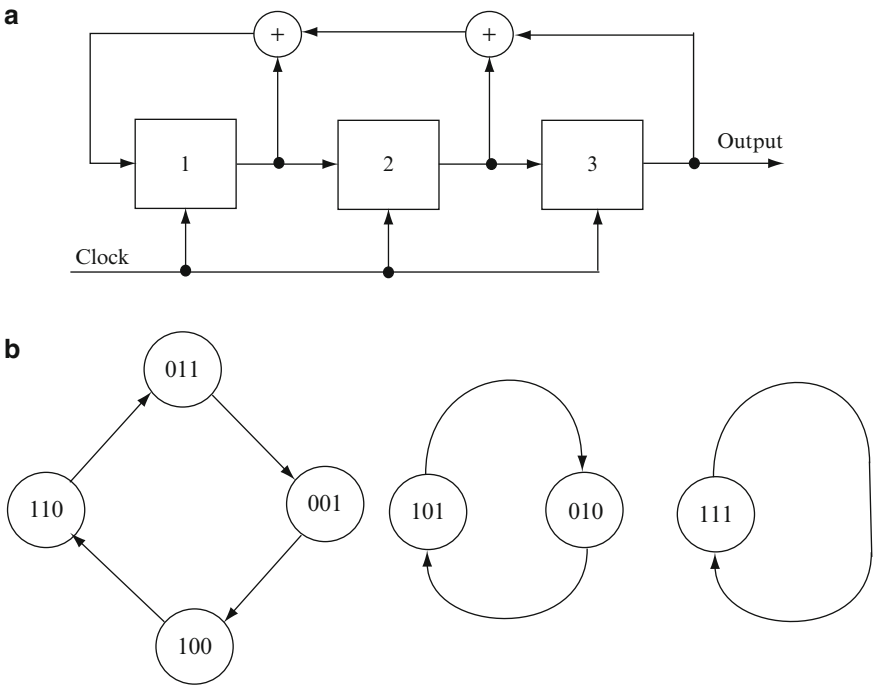

Fig. 2.8 (**a**) Nonmaximal linear feedback shift register and (**b**) state diagrams

bits are not all 0's. If one observes i 0's, then the unobserved bits cannot be all 0's because the n-bit sequence constitutes a state of the maximal-sequence generator. Thus, the relative frequency of i observed 0's is $(2^{n-i}-1)\,/\,(2^n-1)$. Both of these ratios approach 2^{-i} as $n \to \infty$, which is what would happen if the n-bit sequence were random.

2.2.4 Autocorrelations and Power Spectrums

A binary sequence **a** with components $a_i \in GF(2)$, can be mapped into a binary antipodal sequence **p** with components $p_i \in \{-1, +1\}$ by means of the transformation

$$p_i = (-1)^{a_i+1}, \quad i \geq 0 \tag{2.33}$$

or, alternatively, $p_i = (-1)^{a_i}$. The *periodic autocorrelation* of a periodic binary sequence **a** with period N is defined as the periodic autocorrelation of the corresponding binary antipodal sequence **p**:

$$\theta_p(k) = \frac{1}{N}\sum_{i=n}^{n+N} p_i\, p_{i+k}, \quad n = 0, 1, \ldots \tag{2.34}$$

$$= \frac{1}{N}\sum_{i=0}^{N} p_i\, p_{i+k} \tag{2.35}$$

which has period N because $\theta_p(k+N) = \theta_p(k)$. Substitution of (2.33) into (2.34) yields

$$\theta_p(k) = \frac{1}{N}\sum_{i=0}^{N-1}(-1)^{a_i + a_{i+k}} = \frac{1}{N}\sum_{i=0}^{N-1}(-1)^{a_i \oplus a_{i+k}} = \frac{A_k - D_k}{N} \tag{2.36}$$

where A_k denotes the number of agreements in the corresponding bits of $\mathbf{a}$ and $\mathbf{a}$(k), and D_k denotes the number of disagreements. Equivalently, A_k is the number of 0's in one period of $\mathbf{a} \oplus \mathbf{a}$(k), and $Dk = N - A_k$ is the number of 1's.

Consider a maximal sequence. From (2.32), it follows that A_k equals the number of 0's in a maximal sequence if $k \neq 0$, modulo N. Thus, $A_k = (N-1)/2$ and, similarly, $D_k = (N+1)/2$ if $k \neq 0$, modulo N. Therefore,

$$\theta_p(k) = \begin{cases} 1, & k = 0 (\text{mod } N) \\ -\frac{1}{N}, & k \neq 0 (\text{mod } N). \end{cases} \tag{2.37}$$

The *periodic autocorrelation* of a periodic function $x(t)$ with period T is defined as

$$R_x(\tau) = \frac{1}{T}\int_c^{c+T} x(t)x(t+\tau)dt \tag{2.38}$$

where τ is the relative delay variable and c is an arbitrary constant. It follows that $R_x(\tau)$ has period T. We derive the average autocorrelation of the spreading waveform $p(t)$ assuming an ideal periodic spreading waveform of infinite extent and a rectangular chip waveform. If the spreading sequence has period N, then $p(t)$ has period $T = NT_c$. Equations (2.2) and (2.38) with $c = 0$ yield the autocorrelation of $p(t)$:

$$R_p(\tau) = \frac{1}{NT_c}\sum_{i=0}^{N-1} p_i \sum_{l=0}^{N-1} p_l \int_0^{NT_c} \psi(t - iT_c)\psi(t - lT_c + \tau)\, dt. \tag{2.39}$$

If $\tau = kT_c$, where k is an integer, then $\psi(t) = w(t, T_c)$, (2.3), and (2.39) yield

$$R_p(kT_c) = \frac{1}{N}\sum_{i=0}^{N-1} p_i\, p_{i+k} = \theta_p(k). \tag{2.40}$$

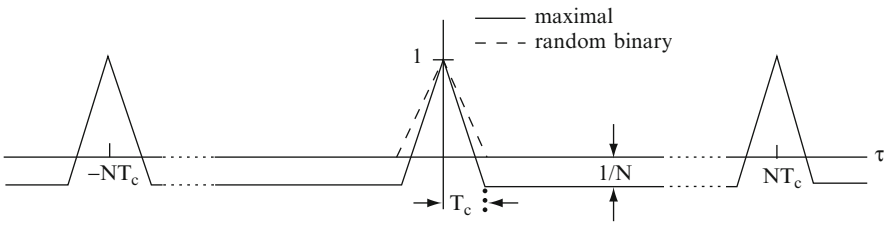

Fig. 2.9 Autocorrelations of maximal sequence and random binary sequence

Any delay can be expressed in the form $\tau = kT_c + \epsilon$, where k is an integer and $0 \le \epsilon < T_c$. Therefore, (2.39) and $\psi(t) = w(t, T_c)$ give

$$R_p(kT_c + \epsilon) = \frac{1}{NT_c} \sum_{i=0}^{N-1} p_i p_{i+k} \int_0^{NT_c} w(t - iT_c, T_c) w(t - iT_c + \epsilon, T_c)\, dt$$
$$+ \frac{1}{NT_c} \sum_{i=0}^{N-1} p_i p_{i+k+1} \int_0^{NT_c} w(t - iT_c, T_c)$$
$$\times w(t - iT_c + \epsilon - T_c, T_c)\, dt. \tag{2.41}$$

Using (2.40) and (2.3) in (2.41), we obtain

$$R_p(kT_c + \epsilon) = \left(1 - \frac{\epsilon}{T_c}\right) \theta_p(k) + \frac{\epsilon}{T_c} \theta_p(k+1). \tag{2.42}$$

For a maximal sequence, the substitution of (2.37) into (2.42) yields $R_p(\tau)$ over one period:

$$R_p(\tau) = \frac{N+1}{N} \Lambda\left(\frac{\tau}{T_c}\right) - \frac{1}{N}, \quad |\tau| \le NT_c/2 \tag{2.43}$$

where $\Lambda(\,)$ is the triangular function defined by (2.15). Since it has period NT_c, the autocorrelation can be compactly expressed as

$$R_p(\tau) = -\frac{1}{N} + \frac{N+1}{N} \sum_{i=-\infty}^{\infty} \Lambda\left(\frac{\tau - iNT_c}{T_c}\right). \tag{2.44}$$

Over one period, this autocorrelation resembles that of a random binary sequence, which is given by (2.14) with $T = T_c$. Both autocorrelations are shown in Fig. 2.9.

Since the infinite series in (2.44) is a periodic function of τ, it can be expressed as a complex exponential Fourier series. From (2.16) and the fact that the Fourier transform of a complex exponential is a delta function, we obtain the Fourier transform of the series:

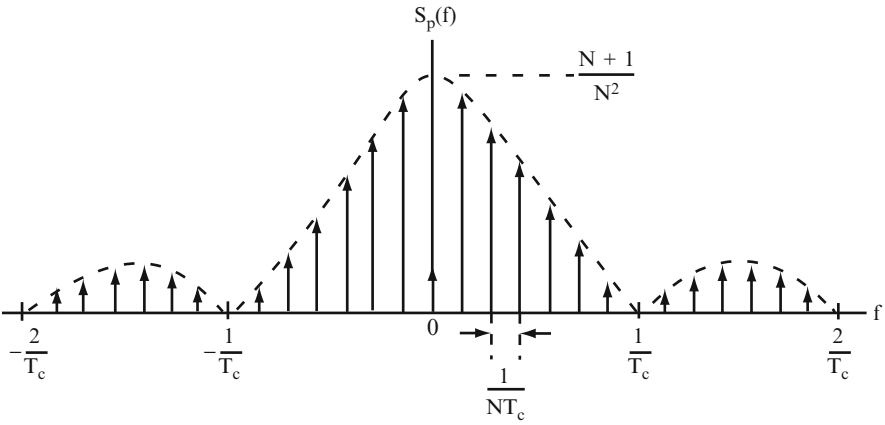

Fig. 2.10 Power spectral density of maximal sequence

$$\mathcal{F}\left\{\sum_{i=-\infty}^{\infty}\Lambda\left(\frac{t-iNT_c}{T_c}\right)\right\}=\frac{1}{N}\sum_{i=-\infty}^{\infty}\operatorname{sinc}^2\left(\frac{i}{N}\right)\delta\left(f-\frac{i}{NT_c}\right) \tag{2.45}$$

where $\delta(\,)$ is the Dirac delta function and $\operatorname{sinc} x = (\sin \pi x)/\pi x$. Applying this identity to (2.44), we determine $S_p(f)$, the *power spectral density of the spreading waveform* $p(t)$, which is defined as the Fourier transform of $R_p(\tau)$:

$$S_p(f)=\frac{N+1}{N^2}\sum_{\substack{i=-\infty\\ i\neq 0}}^{\infty}\operatorname{sinc}^2\left(\frac{i}{N}\right)\delta\left(f-\frac{i}{NT_c}\right)+\frac{1}{N^2}\delta(f). \tag{2.46}$$

This function, which consists of an infinite series of delta functions, is depicted in Fig. 2.10.

A *pseudonoise* or *pseudorandom sequence* is a periodic binary sequence with a nearly even balance of 0's and 1's and an autocorrelation that roughly resembles, over one period, the autocorrelation of a random binary sequence. Pseudonoise sequences, which include the maximal sequences, provide practical spreading sequences because their autocorrelations facilitate code synchronization in the receiver (Chap. 4). Other sequences have peaks that hinder synchronization.

The *average autocorrelation* of a stochastic process $x(t)$ is

$$\bar{R}_x(\tau)=\lim_{T\to\infty}\frac{1}{2T}\int_{-T}^{T}R_x(t,\tau)dt. \tag{2.47}$$

The limit exists and may be nonzero if $x(t)$ has finite power and infinite duration. If $x(t)$ is stationary, $\bar{R}_x(\tau) = R_x(\tau)$. The *average power spectral density* $\bar{S}_x(f)$ is defined as the Fourier transform of the average autocorrelation.

For the direct-sequence signal of (2.1), $d(t)$ is modeled as a random binary sequence with autocorrelation given by (2.14), and θ is modeled as a random variable uniformly distributed over $[0, 2\pi)$ and statistically independent of $d(t)$. Neglecting the constraint that the bit transitions must coincide with chip transitions, we obtain the autocorrelation of the direct-sequence signal $s(t)$:

$$R_s(t,\tau) = \frac{A^2}{2} p(t)p(t+\tau)\Lambda\left(\frac{\tau}{T_s}\right)\cos 2\pi f_c \tau \tag{2.48}$$

where $p(t)$ is the periodic spreading waveform. A *cyclostationary process* is one that has a mean and autocorrelation with the same period. Since its mean is zero and $R_s(t+T_s,\tau) = R_s(t,\tau)$, $s(t)$ is a cyclostationary process with period T_s. However, $s(t)$ is not wide-sense stationary. Substituting (2.48) into (2.47) and using (2.38), we obtain

$$\bar{R}_s(\tau) = \frac{A^2}{2} R_p(\tau)\,\Lambda\left(\frac{\tau}{T_s}\right)\cos 2\pi f_c \tau \tag{2.49}$$

where $R_p(\tau)$ is the average autocorrelation of $p(t)$. For a maximal spreading sequence, the convolution theorem, (2.49), (2.16), and (2.46) provide the *average power spectral density of the direct-sequence signal* $s(t)$:

$$\bar{S}_s(f) = \frac{A^2}{4}\left[S_{s1}(f-f_c) + S_{s1}(f+f_c)\right] \tag{2.50}$$

where the lowpass equivalent density is

$$S_{s1}(f) = \frac{T_s}{N^2}\text{sinc}^2 f T_s + \frac{N+1}{N^2} T_s \sum_{\substack{i=-\infty \\ i\neq 0}}^{\infty} \text{sinc}^2\left(\frac{i}{N}\right)\text{sinc}^2\left(f T_s - \frac{i T_s}{N T_c}\right). \tag{2.51}$$

For a random binary sequence, $S_s(f) = \bar{S}_s(f)$ is given by (2.50) with $S_{s1}(f) = T_c \text{sinc}^2 f T_c$.

2.2.5 Characteristic Polynomials

Polynomials over the binary field $GF(2)$ allow a compact description of the dependence of the output sequence of a linear feedback shift register on its feedback coefficients and initial state. The *characteristic polynomial* associated with a linear feedback shift register of m stages is defined as

$$f(x) = 1 + \sum_{i=1}^{m} c_i x^i \tag{2.52}$$

where $c_m = 1$ assuming that stage m contributes to the generation of the output sequence. The *generating function* associated with the output sequence is defined as

$$G(x) = \sum_{i=0}^{\infty} a_i x^i. \tag{2.53}$$

Substitution of (2.21) into this equation yields

$$\begin{aligned} G(x) &= \sum_{i=0}^{m-1} a_i x^i + \sum_{i=m}^{\infty} \sum_{k=1}^{m} c_k a_{i-k} x^i \\ &= \sum_{i=0}^{m-1} a_i x^i + \sum_{k=1}^{m} c_k x^k \sum_{i=m}^{\infty} a_{i-k} x^{i-k} \\ &= \sum_{i=0}^{m-1} a_i x^i + \sum_{k=1}^{m} c_k x^k \left[G(x) + \sum_{i=0}^{m-k-1} a_i x^i \right]. \end{aligned} \tag{2.54}$$

Combining this equation with (2.52), and defining $c_0 = 1$, we obtain

$$\begin{aligned} G(x) f(x) &= \sum_{i=0}^{m-1} a_i x^i + \sum_{k=1}^{m} c_k x^k \left(\sum_{i=0}^{m-k-1} a_i x^i \right) \\ &= \sum_{k=0}^{m-1} c_k x^k \left(\sum_{i=0}^{m-k-1} a_i x^i \right) = \sum_{k=0}^{m-1} \sum_{i=0}^{m-k-1} c_k a_i x^{k+i} \\ &= \sum_{k=0}^{m-1} \sum_{l=k}^{m-1} c_k a_{l-k} x^l = \sum_{l=0}^{m-1} \sum_{k=0}^{l} c_k a_{l-k} x^l \end{aligned} \tag{2.55}$$

which implies that

$$G(x) = \frac{\sum_{i=0}^{m-1} x^i \left(\sum_{k=0}^{i} c_k a_{i-k} \right)}{f(x)}, \qquad c_0 = 1. \tag{2.56}$$

Thus, the generating function of the output sequence generated by a linear feedback shift register with characteristic polynomial $f(x)$ may be expressed in the form $G(x) = \phi(x)/f(x)$, where the degree of $\phi(x)$ is less than the degree of $f(x)$. The output sequence is said to be *generated* by $f(x)$. Equation (2.56) explicitly shows that the output sequence is completely determined by the feedback coefficients $c_k, k = 1, 2, \ldots, m$, and the initial state $a_i = s_{m-i}(0), i = 0, 1, \ldots, m-1$.

In Fig. 2.6, the feedback coefficients are $c_1 = 0, c_2 = 1$, and $c_3 = 1$, and the initial state gives $a_0 = 1, a_1 = 0$, and $a_2 = 0$. Therefore,

$$G(x) = \frac{1 + x^2}{1 + x^2 + x^3}. \tag{2.57}$$

Performing the long polynomial division according to the rules of binary arithmetic yields $1 + x^3 + x^5 + x^6 + x^7 + x^{10} + \ldots$, which implies the output sequence listed in the figure.

The polynomial $p(x)$ is said to *divide* the polynomial $b(x)$ if there is a polynomial $h(x)$ such that $b(x) = h(x)p(x)$. A polynomial $p(x)$ over $GF(2)$ of degree m is called *irreducible* if $p(x)$ is not divisible by any polynomial over $GF(2)$ of degree less than m but greater than zero. If $p(x)$ is irreducible over $GF(2)$, then $p(0) \neq 0$, for otherwise x would divide $p(x)$. If $p(x)$ has an even number of terms, then $p(1) = 0$ and the fundamental theorem of algebra implies that $x + 1$ divides $p(x)$. Therefore, an irreducible polynomial over $GF(2)$ must have an odd number of terms, but this condition is not sufficient for irreducibility. For example, $1+x+x^2$ is irreducible, but $1 + x + x^5 = (1 + x^2 + x^3)(1 + x + x^2)$ is not.

If a shift-register sequence $\{a_i\}$ is periodic with period n, then its generating function $G(x) = \phi(x)/f(x)$ may be expressed as

$$\begin{aligned} G(x) &= g(x) + x^n g(x) + x^{2n} g(x) + \cdots \\ &= g(x) \sum_{i=0}^{\infty} x^{in} \\ &= \frac{g(x)}{1 + x^n} \end{aligned} \tag{2.58}$$

where $g(x)$ is a polynomial of degree $n - 1$. Therefore,

$$g(x) = \frac{\phi(x)(1 + x^n)}{f(x)}. \tag{2.59}$$

Suppose that $f(x)$ and $\phi(x)$ have no common factors, which is true if $f(x)$ is irreducible since $\phi(x)$ is of lower degree than $f(x)$. Then $f(x)$ must divide $1 + x^n$. Conversely, if the characteristic polynomial $f(x)$ divides $1 + x^n$, then $f(x)h(x) = 1 + x^n$ for some polynomial $h(x)$, and

$$G(x) = \frac{\phi(x)}{f(x)} = \frac{\phi(x)h(x)}{1 + x^n} \tag{2.60}$$

which has the form of (2.58). Thus, $f(x)$ generates a sequence of period n for all $\phi(x)$ and, hence, all initial states.

A polynomial over $GF(2)$ of degree m is called *primitive* if the smallest positive integer n for which the polynomial divides $1 + x^n$ is $n = 2^m - 1$. Thus, a primitive characteristic polynomial of degree m can generate a sequence of period $2^m - 1$, which is the period of a maximal sequence generated by a characteristic polynomial of degree m. Suppose that a primitive characteristic polynomial of positive degree

m could be factored so that $f(x) = f_1(x)f_2(x)$, where $f_1(x)$ is of positive degree m_1 and $f_2(x)$ is of positive degree $m - m_1$. A partial-fraction expansion yields

$$\frac{1}{f(x)} = \frac{a(x)}{f_1(x)} + \frac{b(x)}{f_2(x)}. \tag{2.61}$$

Since $f_1(x)$ and $f_2(x)$ can serve as characteristic polynomials, the period of the first term in the expansion cannot exceed $2^{m_1} - 1$ while the period of the second term cannot exceed $2^{m-m_1} - 1$. Therefore, the period of $1/f(x)$ cannot exceed $(2^{m_1} - 1)(2^{m-m_1} - 1) \leq 2^m - 3$, which contradicts the assumption that $f(x)$ is primitive. Thus, a *primitive characteristic polynomial must be irreducible*.

Theorem. *A characteristic polynomial of degree m generates a maximal sequence of period* $2^m - 1$ *if and only if it is a primitive polynomial.*

Proof. To prove sufficiency, we observe that if $f(x)$ is a primitive characteristic polynomial, it divides $1 + x^n$ for $n = 2^m - 1$ so a maximal sequence of period $2^m - 1$ is generated. If a sequence of smaller period could be generated, then the irreducible $f(x)$ would have to divide $1 + x^{n_1}$ for $n_1 < n$, which contradicts the assumption of a primitive polynomial. To prove necessity, we observe that if the characteristic polynomial $f(x)$ generates a maximal sequence with period $n = 2^m - 1$, then $f(x)$ cannot divide $1 + x^{n_1}, n_1 < n$, because a sequence with a smaller period would result, and such a sequence cannot be generated by a maximal sequence generator. Since $f(x)$ does divide $1 + x^n$, it must be a primitive polynomial. □

Primitive polynomials have been tabulated and may be generated [1] by recursively producing polynomials and evaluating whether they are primitive by using them as characteristic polynomials. Those which generate maximal sequences are primitive. Primitive polynomials for which $m \leq 7$ and one of those of minimal coefficient weight for $8 \leq m \leq 25$ are listed in Table 2.1 as octal numbers in increasing order (e.g., $51 \leftrightarrow 1\ 0\ 1\ 1\ 0\ 0 \leftrightarrow 1 + x^2 + x^3$). For any positive integer m, the number of different primitive polynomials of degree m over $GF(2)$ is

$$\lambda(m) = \frac{\phi_e(2^m - 1)}{m} \tag{2.62}$$

where the *Euler function* $\phi_e(n)$ is the number of positive integers that are less than and relatively prime to the positive integer n. If n is a prime number, $\phi_e(n) = n - 1$. In general,

$$\phi_e(n) = n \prod_{i=1}^{k} \frac{\nu_i - 1}{\nu_i} \leq n - 1 \tag{2.63}$$

where $\nu_1, \nu_2, \ldots, \nu_k$ are the prime integers that divide n. Thus, $\lambda(6) = \phi_e(63)/6 = 6$ and $\lambda(13) = \phi_e(8191)/13 = 630$.

Other short spreading sequences, notably the Gold and Kasami sequences, are covered in Chap. 6.

Table 2.1 Primitive polynomials

Degree	Primitive	Degree	Primitive	Degree	Primitive
2	7	7	103	8	534
3	51		122	9	1201
	31		163	10	1102
4	13		112	11	5004
	32		172	12	32101
5	15		543	13	33002
	54		523	14	30214
	57		532	15	300001
	37		573	16	310012
	76		302	17	110004
	75		323	18	1020001
6	141		313	19	7400002
	551		352	20	1100004
	301		742	21	50000001
	361		763	22	30000002
	331		712	23	14000004
	741		753	24	702000001
			772	25	110000002

2.2.6 *Long Nonlinear Sequences*

A *long sequence* or *long code* is a spreading sequence with a period that is much longer than the data-symbol duration and may even exceed the message duration. A *short sequence* or *short code* is a spreading sequence with a period that is equal to or less than the data-symbol duration. Since short sequences are susceptible to interception and linear sequences are inherently susceptible to mathematical cryptanalysis [2], long nonlinear pseudonoise sequences and programmable code generators are needed for communications with a high level of security. However, if a modest level of security is acceptable, short or moderate-length pseudonoise sequences are preferable for rapid acquisition, burst communications, and multiuser detection.

The algebraic structure of linear feedback shift registers makes them susceptible to cryptanalysis. Let

$$\mathbf{c} = [c_1\ c_2 \ldots c_m]^T \tag{2.64}$$

denote the column vector of the m feedback coefficients of an m-stage linear feedback shift register, where T denotes the transpose of a matrix or vector. The column vector of m successive sequence bits produced by the shift register starting at bit i is

$$\mathbf{a}_i = [a_i\ a_{i+1}\ \ldots a_{i+m-1}]^T\ . \tag{2.65}$$

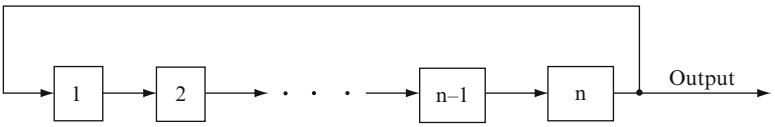

Fig. 2.11 Linear generator of binary sequence with period n

Let $\mathbf{A}(i)$ denote the $m \times m$ matrix with columns consisting of the $\mathbf{a}_k$ vectors for $i \le k \le i + m - 1$:

$$\mathbf{A}(i) = \begin{bmatrix} a_{i+m-1} & a_{i+m-2} & \cdots a_i \\ a_{i+m} & a_{i-m-1} & \cdots a_{i+1} \\ \vdots & \vdots & \vdots \\ a_{i+2m-2} & a_{i+2m-3} & \cdots a_{i+m-1} \end{bmatrix}. \tag{2.66}$$

The linear recurrence relation (2.15) indicates that the output sequence and feedback coefficients are related by

$$\mathbf{a}_{i+m} = \mathbf{A}(i)\mathbf{c}, \quad i \ge 0. \tag{2.67}$$

If $2m$ consecutive sequence bits are known, then $\mathbf{A}(i)$ and $\mathbf{a}_{i+m}$ are completely known for some i. If $\mathbf{A}(i)$ is invertible, then the feedback coefficients can be computed from

$$\mathbf{c} = \mathbf{A}^{-1}(i)\mathbf{a}_{i+m}, \quad i \ge 0. \tag{2.68}$$

A shift-register sequence is completely determined by the feedback coefficients and any state vector. Since any m successive sequence bits determine a state vector, $2m$ successive bits provide enough information to reproduce the output sequence unless $\mathbf{A}(i)$ is not invertible. In that case, one or more additional bits are required.

If a binary sequence has period n, it can always be generated by a n-stage linear feedback shift register by connecting the output of the last stage to the input of the first stage and inserting n consecutive bits of the sequence into the output sequence, as illustrated in Fig. 2.11. The polynomial associated with one period of the binary sequence is

$$g(x) = \sum_{i=0}^{n-1} a_i x^i. \tag{2.69}$$

Let $gcd(g(x), 1 + x^n)$ denote the greatest common polynomial divisor of the polynomials $g(x)$ and $1 + x^n$. Then (2.58) implies that the generating function of the sequence may be expressed as

$$G(x) = \frac{g(x)/gcd\,(g(x), 1 + x^n)}{(1 + x^n)\,/gcd\,(g(x), 1 + x^n)}. \tag{2.70}$$

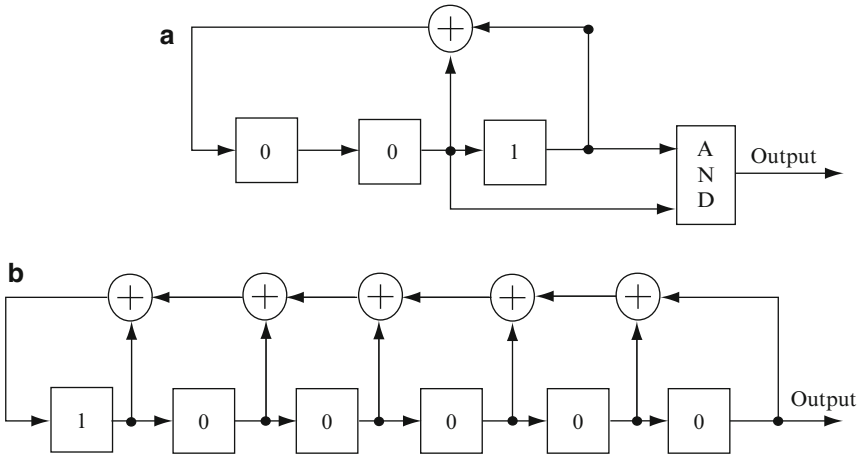

Fig. 2.12 (**a**) Nonlinear generator and (**b**) its linear equivalent

If $gcd(g(x), 1 + x^n) \neq 1$, the degree of the denominator of $G(x)$ is less than n. Therefore, the sequence represented by $G(x)$ can be generated by a linear feedback shift register with fewer stages than n and with the characteristic function given by the denominator. The appropriate initial state can be determined from the coefficients of the numerator.

The *linear equivalent* of the generator of a sequence is the linear shift register with the fewest stages that produces the sequence. The number of stages in the linear equivalent is called the *linear complexity* of the sequence. If the linear complexity is equal to m, then (2.68) determines the linear equivalent after the observation of $2m$ consecutive sequence bits. Security improves as the period of a sequence increases, but there are practical limits to the number of shift-register stages. To produce sequences with a long enough period for high security, the feedback logic in Fig. 2.5 must be nonlinear. Alternatively, one or more shift-register sequences or several outputs of shift-register stages may be applied to a nonlinear device to produce the sequence [5]. Nonlinear generators with relatively few shift-register stages can produce sequences of enormous linear complexity. As an example, Fig. 2.12a depicts a nonlinear generator in which two stages of a linear feedback shift register have their outputs applied to an AND gate to produce the output sequence. The initial contents of the shift-register stages are indicated by the enclosed binary numbers. Since the linear generator produces a maximal sequence of length 7, the output sequence has period 7. The first period of the sequence is (0 0 0 0 0 1 1), from which the linear equivalent with the initial contents shown in Fig. 2.12b is derived by evaluating (2.70).

While a large linear complexity is necessary for the cryptographic integrity of a sequence, it is not necessarily sufficient because other statistical characteristics, such as a nearly even distribution of 1's and 0's, are required. For example, a long

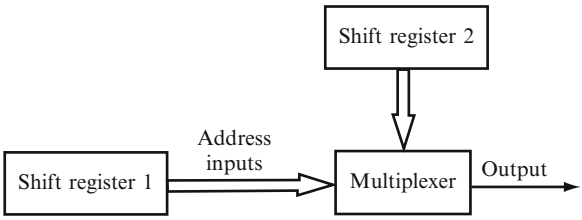

Fig. 2.13 Nonlinear generator that uses a multiplexer

sequence of many 0's followed by a single 1 has a linear complexity equal to the length of the sequence, but the sequence is very weak. The generator of Fig. 2.12a produces a relatively large number of 0's because the AND gate produces a 1 only if both of its inputs are 1's.

As another example, a nonlinear generator that uses a multiplexer is shown in Fig. 2.13. The outputs of various stages of feedback shift register 1 are applied to the multiplexer, which interprets the binary number determined by these outputs as an address. The multiplexer uses this address to select one of the stages of feedback shift register 2. The selected stage provides the multiplexer output and, hence, one bit of the output sequence. Suppose that register 1 has m stages and register 2 has n stages. If h stages of register 1, where $h < m$, are applied to the multiplexer, then the address is one of the numbers $0, 1, ..., 2^h - 1$. Therefore, if $n \geq 2^h$, each address specifies a distinct stage of register 2. The initial states of the two registers, the feedback connections, and which stages are used for addressing may be parts of a variable *key* that provides security. The security of the nonlinear generator is further enhanced if nonlinear feedback is used in both shift registers.

2.2.7 *Chip Waveforms*

The spectrum of the spreading waveform $p(t)$ is largely determined by the chip waveform $\psi(t)$, which is designed to cause negligible *interchip interference* among the matched-filter output samples in the receiver. If the bandwidth of $\psi(t)$ is sufficiently large, then the energy in $\psi(t)$ can be largely concentrated within a chip interval of duration T_c, and the Nyquist criterion can be satisfied at the output of a matched filter sampled at the rate $1/T_c$ except possibly for the effects of the channel. As the bandwidth of $\psi(t)$ increases, the duration of a matched-filter response becomes shorter and approaches a duration slightly larger than that of the channel impulse response. Narrow matched-filter output pulses ensure negligible *intersymbol interference* if the delay spread of the multipath signals is slightly less than the symbol duration. A rectangular chip waveform is ideal in the sense that it causes no interchip interference and has a minimal peak-to-average power ratio (PAPR), but filtering in the channel and receiver will alter its shape and tend to introduce some interchip interference.

2.3 Systems with BPSK Modulation

A received direct-sequence signal with coherent BPSK modulation and ideal carrier synchronization can be represented by (2.1) or (2.6) with $\theta = 0$ to reflect the absence of phase uncertainty. the received signal is

$$s(t) = \sqrt{2\mathcal{E}_s}d(t)p(t)\cos 2\pi f_c t \tag{2.71}$$

where $\sqrt{2\mathcal{E}_s}$ is the signal amplitude, $d(t)$ is the data modulation, $p(t)$ is the spreading waveform, and f_c is the carrier frequency. The data modulation is a sequence of nonoverlapping rectangular pulses, each of which has an amplitude equal to $+1$ or -1. Each pulse of $d(t)$ represents a data symbol and has a duration of T_s. The spreading waveform has the form

$$p(t) = \sum_{i=-\infty}^{\infty} p_i \psi(t - iT_c) \tag{2.72}$$

where p_i is equal to $+1$ or -1 and represents one chip of a spreading sequence $\{p_i\}$. Assuming that the chip waveform $\psi(t)$ is well approximated by a waveform of duration T_c, it is convenient, and entails no loss of generality, to normalize the energy content of the chip waveform according to

$$\int_0^{T_c} \psi^2(t)dt = \frac{T_c}{T_s}. \tag{2.73}$$

With this normalization, a straightforward integration over a symbol interval indicates that $\mathcal{E}_s$ is the energy per symbol assuming that $f_c \gg 1/T_c$ so that the integral over a double-frequency term is negligible. Because the transitions of a data symbol and the chips coincide on both sides of a symbol, the *processing gain*, defined as

$$G = \frac{T_s}{T_c} \tag{2.74}$$

is an integer equal to the number of chips in a symbol interval.

A practical direct-sequence system differs from the functional diagram of Fig. 2.2. The transmitter needs practical devices, such as a power amplifier and a filter, to limit out-of-band radiation. In the receiver, the radio-frequency front end includes devices for wideband filtering and automatic gain control. These devices are assumed to have a negligible effect on the operation of the demodulator in the subsequent analysis. Thus, the front-end circuitry is omitted from Fig. 2.14, which shows the optimum demodulator in the form of a correlator for the detection of a single symbol in the presence of white Gaussian noise. This correlator is more practical and flexible for digital processing than the alternative one shown in Fig. 2.2. It is a suboptimal but reasonable approach against non-Gaussian interference. An equivalent matched-filter demodulator is implemented with a transversal filter or tapped delay

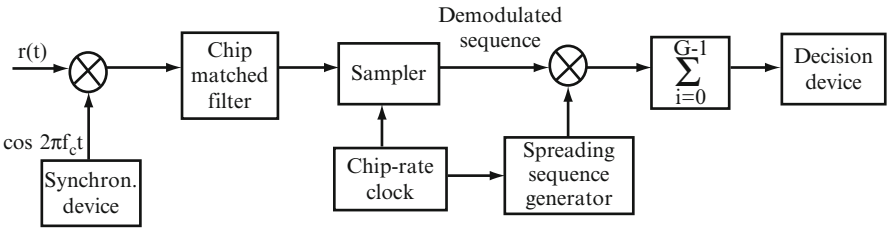

Fig. 2.14 Basic elements of correlator for direct-sequence signal with coherent BPSK

line and a stored spreading sequence. However, the matched-filter implementation is not practical for a long sequence that extends over many data symbols. If the chip-rate synchronization in Fig. 2.14 is accurate, then the demodulated sequence and the receiver-generated spreading sequence are multiplied together, and G successive products are added in an accumulator to produce the decision variable. The effective sampling rate of the decision variable is the symbol rate.

The sequence generator, multiplier, and adder function as a discrete-time matched filter that is matched to each G-bit sequence of the spreading sequence. The matched filter has a fixed impulse response for short spreading sequences and has a time-varying impulse response for long spreading sequences. Since the direct-sequence signal has a large bandwidth and the chip waveform has a short duration, the response of this matched filter to a G-bit sequence is insignificantly affected by previous G-bit sequences. Thus, if the multipath delay spread (Chap. 5) is slightly less than the data-symbol duration T_s and the processing gain G is sufficiently large, then the *intersymbol interference* is negligible. The lack of significant intersymbol interference is an important advantage of direct-sequence communications and will always be assumed in this chapter.

In the subsequent analysis, perfect phase, sequence, and symbol synchronization are assumed. The received signal is

$$r(t) = s(t) + i(t) + n(t) \tag{2.75}$$

where $i(t)$ is the interference, and $n(t)$ denotes the zero-mean white Gaussian noise. The chip matched filter has impulse response $\psi(-t)$. Its output is sampled at the chip rate to provide G samples per data symbol. It is assumed that the Nyquist criterion for the desired signal after the matched filter is approximately satisfied so that the interchip interference is negligible, and that there is negligible error in the phase and frequency synchronization at the receiver. If $d(t) = d_0$ over $[0, T_s]$ and $f_c \gg 1/T_c$, then (2.71) to (2.75) indicate that the demodulated sequence corresponding to this data symbol is

$$Z_i = \sqrt{2}\int_{iT_c}^{(i+1)T_c} r(t)\psi\,(t - iT_c)\cos 2\pi f_c t\; dt = S_i + J_i + N_{si}, \qquad 0 \le i \le G-1 \tag{2.76}$$

where the $\sqrt{2}$ is introduced for mathematical convenience and

$$S_i = \sqrt{2}\int_{iT_c}^{(i+1)T_c} s(t)\psi(t - iT_c)\cos 2\pi f_c t\, dt = p_i d_0 \sqrt{\mathcal{E}_s}\frac{T_c}{T_s} \tag{2.77}$$

$$J_i = \sqrt{2}\int_{iT_c}^{(i+1)T_c} i(t)\psi(t - iT_c)\cos 2\pi f_c t\, dt \tag{2.78}$$

$$N_{si} = \sqrt{2}\int_{iT_c}^{(i+1)T_c} n(t)\psi\,(t - iT_c)\cos 2\pi f_c t\, dt. \tag{2.79}$$

The input to the decision device is

$$V = \sum_{i=0}^{G-1} p_i Z_i = d_0\sqrt{\mathcal{E}_s} + V_1 + V_2 \tag{2.80}$$

where

$$V_1 = \sum_{\nu=0}^{G-1} p_i J_i \tag{2.81}$$

$$V_2 = \sum_{\nu=0}^{G-1} p_i N_{si}. \tag{2.82}$$

The white Gaussian noise has autocorrelation

$$R_n(\tau) = \frac{N_0}{2}\delta(t - \tau) \tag{2.83}$$

where $N_0/2$ is the two-sided noise-power spectral density. Since $E[n(t)] = 0$, (2.88) implies that $E[V_2] = 0$. A straightforward calculation using (2.79), (2.82), (2.83), the limited duration of $\psi(t)$, and $f_c \gg 1/T_c$ yields

$$var\,(V_2) = \frac{N_0}{2}. \tag{2.84}$$

It is natural and analytically desirable to model a long spreading sequence as a random binary sequence. The random-binary-sequence model does not seem to obscure important exploitable characteristics of long sequences and is a reasonable approximation even for short sequences in networks with asynchronous communications. A random binary sequence consists of statistically independent symbols, each of which takes the value +1 with probability 1/2 or the value −1 with probability 1/2. Thus, $E[p_i] = E[p(t)] = 0$. It then follows from (2.81) that $E[V_1] = 0$, and the mean value of the decision variable is

$$E[V] = d_0\sqrt{\mathcal{E}_s} \tag{2.85}$$

for the direct-sequence system with coherent PSK. Since p_i and p_k are independent for $i \neq k$;

$$E\left[p_i p_k\right] = 0, \quad i \neq k. \tag{2.86}$$

Therefore, the independence of p_i and J_k for all i and k implies that $E[p_i J_i p_k J_k] = 0, i \neq k$, and hence

$$var\left(V_1\right) = \sum_{i=0}^{G-1} E\left[J_i^2\right]. \tag{2.87}$$

If $d_0 = +1$ represents the logic symbol 1 and $d_0 = -1$ represents the logic symbol 0, then the decision device produces the symbol 1 if $V > 0$ and the symbol 0 if $V < 0$. An error occurs if $V < 0$ when $d_0 = +1$ or if $V > 0$ when $d_0 = -1$. The probability that $V = 0$ is zero.

2.3.1 *Tone Interference at Carrier Frequency*

For tone interference with the same carrier frequency as the desired signal, a nearly exact, closed-form equation for the symbol error probability can be derived. The tone interference has the form

$$i\left(t\right) = \sqrt{2I}\cos\left(2\pi f_c t + \phi\right) \tag{2.88}$$

where I is the average power and ϕ is the phase relative to the desired signal. Assuming that $f_c \gg 1/T_c$, (2.78), (2.81), (2.88) and a change of variables give

$$V_1 = \sqrt{I}\cos\phi \sum_{i=0}^{G-1} p_i \int_0^{T_c} \psi\left(t\right) dt. \tag{2.89}$$

A normalized rectangular chip waveform has $\psi(t) = w(t, T_c)/\sqrt{T_s}$, where $w(t, T)$ is given by (2.3). For sinusoidal chips in the spreading waveform, $\psi(t) = \psi_s(t, T_c)$, where

$$\psi_s(t, T) = \begin{cases} \sqrt{\frac{2}{T}}\sin\left(\frac{\pi}{T}t\right), & 0 \leq t \leq T \\ 0, & \text{otherwise.} \end{cases} \tag{2.90}$$

Let k_1 denote the number of chips in $[0, T_s]$ for which $p_i = +1$; the number for which $p_i = -1$ is $G - k_1$. Equations (2.89), (2.3), and (2.90) yield

$$V_1 = \sqrt{\frac{I\kappa}{T_s}} T_c \left(2k_1 - G\right)\cos\phi \tag{2.91}$$

where κ depends on the chip waveform, and

$$\kappa = \begin{cases} 1, & \textit{rectangular chip} \\ \frac{8}{\pi^2}, & \textit{sinusoidal chip}. \end{cases} \tag{2.92}$$

These equations indicate that the use of sinusoidal chip waveforms instead of rectangular ones effectively reduces the interference power by a factor $8/\pi^2$ if $V_1 \neq 0$. Thus, the advantage of sinusoidal chip waveforms is 0.91 dB against tone interference at the carrier frequency. Equation (2.91) indicates that tone interference at the carrier frequency would be completely rejected if $k_1 = G/2$ in every symbol interval.

In the random-binary-sequence model, p_i is equally likely to be $+1$ or -1. Therefore, the conditional symbol error probability given the value of ϕ is

$$P_s(\phi) = \sum_{k_1=0}^{G} \binom{G}{k_1} \left(\frac{1}{2}\right)^G \left[\frac{1}{2} P_s(\phi, k_1, +1) + \frac{1}{2} P_s(\phi, k_1, -1)\right] \tag{2.93}$$

where $P_s(\phi, k_1, d_0)$ is the conditional symbol error probability given the values of ϕ, k_1 and d_0. Under these conditions, V_1 is a constant, and V has a Gaussian distribution. Equations (2.80) and (2.91) imply that the conditional expected value of V is

$$E[V|\phi, k_1, d_0] = d_0\sqrt{\mathcal{E}_s} + \sqrt{\frac{I\kappa}{T_s}}\, T_c (2k_1 - G)\cos\phi. \tag{2.94}$$

The conditional variance of V is equal to the variance of V_2, which is given by (2.84). Using the Gaussian density to evaluate $P_s(\phi, k_1, +1)$ and $P_s(\phi, k_1, -1)$ separately and then consolidating the results yields

$$P_s(\phi, k_1, d_0) = Q\left[\sqrt{\frac{2\mathcal{E}_s}{N_0}} + d_0\sqrt{\frac{2I T_c \kappa}{G N_0}}\,(2k_1 - G)\cos\phi\right] \tag{2.95}$$

where $Q(x)$ is defined by (1.35). Assuming that ϕ is uniformly distributed over $[0, 2\pi)$ during each symbol interval and exploiting the periodicity of $\cos\phi$, we obtain the symbol error probability

$$P_s = \frac{1}{\pi}\int_0^{\pi} P_s(\phi)\, d\phi \tag{2.96}$$

where $P_s(\phi)$ is given by (2.93) and (2.95).

2.3.2 General Tone Interference

To simplify the preceding equations for P_s and to examine the effects of tone interference with a carrier frequency different from the desired frequency, a

Gaussian approximation is used. Consider interference due to a single tone of the form

$$i\,(t) = \sqrt{2I}\cos\left(2\pi f_1 t + \theta_1\right) \tag{2.97}$$

where I, f_1, and θ_1 are the average power, frequency, and phase angle of the interference signal at the receiver. The frequency f_1 is assumed to be close enough to the desired frequency f_c that the tone is undisturbed by the initial wideband filtering that precedes the correlator. If $f_1 + f_c \gg f_d = f_1 - f_c$ so that a term involving $f_1 + f_c$ is negligible, (2.97) and (2.78) and a change of variable yield

$$J_i = \sqrt{I}\int_0^{T_c} \psi\,(t)\cos\left(2\pi f_d t + \theta_1 + i\,2\pi f_d T_c\right)dt. \tag{2.98}$$

For a rectangular chip waveform, evaluation of the integral and trigonometry yield

$$J_i = \sqrt{\frac{I}{T_s}}T_c\,\mathrm{sinc}\left(f_d T_c\right)\cos\left(i\,2\pi f_d T_c + \theta_2\right) \tag{2.99}$$

where

$$\theta_2 = \theta_1 + \pi f_d T_c. \tag{2.100}$$

Substituting (2.99) into (2.87) and expanding the squared cosine, we obtain

$$var\left(V_1\right) = \frac{1}{2G}I\,T_c\mathrm{sinc}^2\left(f_d T_c\right)\left[G + \sum_{i=0}^{G-1}\cos\left(i\,4\pi f_d T_c + 2\theta_2\right)\right]. \tag{2.101}$$

To evaluate the inner summation, we use the identity

$$\sum_{v=0}^{n-1}\cos\left(a + vb\right) = \cos\left(a + \frac{n-1}{2}b\right)\frac{\sin\left(nb/2\right)}{\sin\left(b/2\right)} \tag{2.102}$$

which is proved by using mathematical induction and trigonometric identities. Evaluation and simplification yield

$$var(V_1) = \frac{1}{2}I\,T_c\mathrm{sinc}^2\left(f_d T_c\right)\left[1 + \frac{\mathrm{sinc}\left(2f_d T_s\right)}{\mathrm{sinc}\left(2f_d T_c\right)}\cos 2\phi\right] \tag{2.103}$$

where

$$\phi = \theta_2 + \pi f_d\left(T_s - T_c\right) = \theta_1 + \pi f_d T_s. \tag{2.104}$$

Given the value of ϕ, the J_i in (2.99) are uniformly bounded constants, and, hence, the terms of V_1 in (2.81) are independent and uniformly bounded. Since $var(V_1) \to \infty$ as $G \to \infty$, the central limit theorem [3] implies that when G is large, the conditional distribution of V_1 is approximately Gaussian. Thus, V is nearly Gaussian with mean given by (2.85) and $var(V) = var(V_1) + var(V_2)$. Because of the symmetry of the model, the conditional symbol error probability

may be calculated by assuming $d_0 = 1$ and evaluating the probability that $V < 0$. A straightforward derivation using (2.103) indicates that the conditional symbol error probability is well approximated by

$$P_s(\phi) = Q\left[\sqrt{\frac{2\mathcal{E}_s}{N_{0e}(\phi)}}\right] \tag{2.105}$$

where

$$N_{0e}(\phi) = N_0 + IT_c \text{sinc}^2(f_d T_c)\left[1 + \frac{\text{sinc}(2f_d T_s)}{\text{sinc}(2f_d T_c)}\cos 2\phi\right] \tag{2.106}$$

and $N_{0e}(\phi)/2$ can be interpreted as the *equivalent two-sided power spectral density* of the interference plus noise, given the value of ϕ. For sinusoidal chip waveforms, a similar derivation yields (2.105) with

$$N_{0e}(\phi) = N_0 + IT_c\left(\frac{8}{\pi^2}\right)\left(\frac{\cos \pi f_d T_c}{1 - 4f_d^2 T_c^2}\right)^2\left[1 + \frac{\text{sinc}(2f_d T_s)}{\text{sinc}(2f_d T_c)}\cos 2\phi\right]. \tag{2.107}$$

To explicitly exhibit the reduction of the interference power by the factor G, we may substitute $T_c = T_s/G$ in (2.106) or (2.107). A comparison of these two equations confirms that sinusoidal chip waveforms provide a $\pi^2/8 = 0.91$ dB advantage when $f_d = 0$, but this advantage decreases as $|f_d|$ increases and ultimately disappears. The preceding analysis can easily be extended to multiple tones, but the resulting equations are complicated.

If θ_1 in (2.104) is modeled as a random variable that is uniformly distributed over $[0, 2\pi)$ during each symbol interval, then the modulo-2π character of $\cos 2\phi$ in (2.106) implies that its distribution is the same as it would be if ϕ were uniformly distributed over $[0, 2\pi)$. Therefore, we can henceforth assign a uniform distribution for ϕ. The symbol error probability, which is obtained by averaging $P_s(\phi)$ over the range of ϕ, is

$$P_s = \frac{2}{\pi}\int_0^{\pi/2} Q\left[\sqrt{\frac{2\mathcal{E}_s}{N_{0e}(\phi)}}\right] d\phi \tag{2.108}$$

where the fact that $\cos 2\phi$ takes all its possible values over $[0, \pi/2]$ has been used to shorten the integration interval.

Figure 2.15 depicts the symbol error probability as a function of the *despread signal-to-interference ratio*, $G\mathcal{E}_s/IT_s$, for one tone-interference signal, rectangular chip waveforms, $f_d = 0, G = 50 = 17$ dB, and $\mathcal{E}_s/N_0 = 14$ dB and 20 dB. One pair of graphs are computed using the approximate model of (2.106) and (2.108), while the other pair are derived from the nearly exact model of (2.93), (2.95), and (2.96) with $\kappa = 1$. For the nearly exact model, P_s depends not only on $G\mathcal{E}_s/IT_s$, but also on G. A comparison of the two graphs indicates that the error introduced by the Gaussian approximation is on the order of or less than 0.1 dB

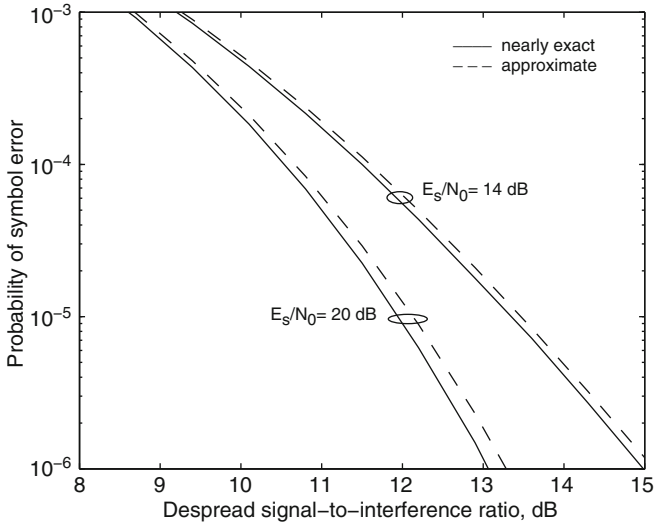

Fig. 2.15 Symbol error probability of binary direct-sequence system with tone interference at carrier frequency and $G = 17\,\text{dB}$

when $P_s \geq 10^{-6}$. This example and others provide evidence that the Gaussian approximation introduces insignificant error if $G \geq 50$ and practical values for the other parameters are assumed.

Figure 2.16 uses the approximate model to plot P_s versus the normalized frequency offset $f_d T_c$ for rectangular and sinusoidal chip waveforms, $G = 17\,\text{dB}$, $\mathcal{E}_s/N_0 = 14\,\text{dB}$, and $G\mathcal{E}_s/IT_s = 10\,\text{dB}$. The performance advantage of sinusoidal chip waveforms is apparent, but their realization or that of Nyquist chip waveforms in a transmitted PSK waveform is difficult because of the distortion introduced by a nonlinear power amplifier in the transmitter when the signal does not have a constant envelope.

2.3.3 Gaussian Interference

Gaussian interference is interference that approximates a zero-mean, stationary Gaussian process. If $i(t)$ is modeled as Gaussian interference and $f_c \gg 1/T_c$, then (2.78), a trigonometric expansion, the dropping of a negligible double integral, and a change of variables give

$$E\left[J_i^2\right] = \int_0^{T_c} \int_0^{T_c} R_j\left(t_1 - t_2\right) \psi\left(t_1\right) \psi\left(t_2\right) \cos\left[2\pi f_c\left(t_1 - t_2\right)\right] dt_1 dt_2 \quad (2.109)$$

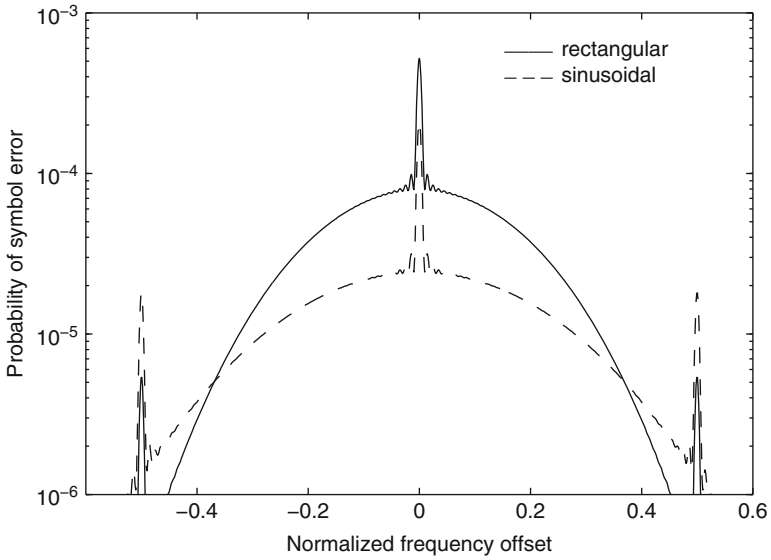

Fig. 2.16 Symbol error probability for direct-sequence system with PSK, rectangular and sinusoidal chip waveforms, $G = 17\,\text{dB}$, $\mathcal{E}_s/N_0 = 14\,\text{dB}$, and $GS/I = 10\,\text{dB}$ in the presence of tone interference

where $R_j(t)$ is the autocorrelation of $i(t)$. Since $E[J_i^2]$ does not depend on the index i, (2.87) gives

$$var(V_1) = GE\left[J_i^2\right]. \tag{2.110}$$

Assuming that $\psi(t)$ is rectangular, we change variables in (2.109) by using $\tau = t_1 - t_2$ and $s = t_1 + t_2$. The Jacobian of this transformation is 2. Evaluating one of the resulting integrals and substituting the result into (2.110) yields

$$var(V_1) = \int_{-T_c}^{T_c} R_j(\tau)\Lambda\left(\frac{\tau}{T_c}\right)\cos 2\pi f_c\tau\, d\tau. \tag{2.111}$$

The limits in this equation can be extended to $\pm\infty$ because the integrand is truncated. Since $R_j(\tau)\Lambda\left(\frac{\tau}{T_c}\right)$ is an even function, the cosine function may be replaced by a complex exponential. Then the convolution theorem and the known Fourier transform of $\Lambda(t)$ yield the alternative form

$$var(V_1) = T_c\int_{-\infty}^{\infty} S_j(f)\,\text{sinc}^2\left[(f - f_c)\,T_c\right]df \tag{2.112}$$

where $S_j(f)$ is the power spectral density of the interference after passage through the initial wideband filter of the receiver.

Since $i(t)$ is a zero-mean Gaussian process, the $\{J_i\}$ are zero-mean and jointly Gaussian. Therefore, if the $\{p_i\}$ are given, then (V_1) is conditionally zero-mean and Gaussian. Since $var(V_1)$ does not depend on the $\{p_i\}$, V_1 without conditioning is a zero-mean Gaussian random variable. The independence of the thermal noise and the interference imply that the decision variable V defined by (2.80) has a mean given by (2.85) and a variance equal to $var\,(V_1) + var\,(V_2)$, where $var\,(V_1)$ is given by (2.112) and $var\,(V_2)$ is given by (2.84). Thus, a standard derivation yields the symbol error probability:

$$P_s = Q\left(\sqrt{\frac{2\mathcal{E}_s}{N_{0e}}}\right) \tag{2.113}$$

where

$$N_{0e} = N_0 + 2T_c \int_{-\infty}^{\infty} S_j\,(f)\,\mathrm{sinc}^2\,[(f - f_c)\,T_c]\,df. \tag{2.114}$$

If $S_j'(f)$ is the interference power spectral density at the input and $H(f)$ is the transfer function of the initial wideband filter, then $S_j(f) = S_j'(f)|H(f)|^2$. Suppose that the interference has a flat spectrum over a band within the passband of the wideband filter so that

$$S_j\,(f) = \begin{cases} \frac{I}{2W_1}, & [f - f_1| \le \frac{W_1}{2}, \quad |f + f_1| \le \frac{W_1}{2} \\ 0, & \text{otherwise.} \end{cases} . \tag{2.115}$$

If $f_c \gg 1/T_c$, the integration over negative frequencies in (2.114) is negligible and

$$N_{0e} = N_0 + \frac{IT_c}{W_1} \int_{f_1 - W_1/2}^{f_1 + W_1/2} \mathrm{sinc}^2\,[(f - f_c)\,T_c]\,df. \tag{2.116}$$

This equation shows that $f_1 = f_c$ or $f_d = 0$ coupled with a narrow bandwidth increases the impact of the interference power. Since the integrand is upper-bounded by unity, $N_{0e} \le N_0 + IT_c$. This upper bound is intuitively reasonable because $IT_c \approx I/B = I_0$, where $B \approx 1/T_c$ is the bandwidth of narrowband interference after the despreading, and I_0 is its power spectral density. Equation (2.113) yields

$$P_s \le Q\left(\sqrt{\frac{2\mathcal{E}_s}{N_0 + IT_c}}\right). \tag{2.117}$$

This upper bound is tight if $f_d \approx 0$ and the Gaussian interference is narrowband. A plot of (2.117) with the parameter values of Fig. 2.15 indicates that roughly 2 dB more interference power is required for worst-case Gaussian interference to degrade P_s as much as tone interference at the carrier frequency.

2.4 Quaternary Systems

A received *quaternary direct-sequence signal* with ideal carrier synchronization and a chip waveform of duration T_c can be represented by

$$s(t) = \sqrt{\mathcal{E}_s} d_1(t) p_1(t) \cos 2\pi f_c t + \sqrt{\mathcal{E}_s} d_2(t + t_0) p_2(t + t_0) \sin 2\pi f_c t \quad (2.118)$$

where two spreading waveforms, $p_1(t)$ and $p_2(t)$, and two data signals, $d_1(t)$ and $d_2(t)$, are used with two quadrature carriers, and t_0 is the relative delay between the in-phase and quadrature components of the signal. For a *quadriphase direct-sequence system*, which uses QPSK, $t_0 = 0$. For a direct-sequence system with offset QPSK (OQPSK) or minimum-shift keying (MSK), $t_0 = T_c/2$. For OQPSK, the chip waveforms are rectangular; for MSK, they are sinusoidal. One might use MSK to limit the spectral sidelobes of the direct-sequence signal, which may interfere with other signals. Let T_s denote the duration of the data symbols before the generation of (2.118), and let $T_{s1} = 2T_s$ denote the duration of each of the binary channel-symbol components, which are transmitted in pairs. Of the available desired-signal power, half is in each of the two components of (2.118). Since $T_{s1} = 2T_s$, the energy per binary channel-symbol component is $\mathcal{E}_s$, the same as for a direct-sequence system with PSK.

Consider the *classical* or *dual* quaternary system in which $d_1(t)$ and $d_2(t)$ are independent. Let T_c denote the common chip duration of $p_1(t)$ and $p_2(t)$. The number of chips per channel symbol is $2G$, where $G = T_s/T_c$. It is assumed that the synchronization is perfect in the receiver, which is shown in Fig. 2.17. It is assumed that the Nyquist criterion is approximately satisfied so that the interchip interference is negligible. Consequently, if the received signal is given by (2.118), then the upper decision variable applied to the decision device at the end of a symbol interval during which $d_1(t) = d_{10}$ is

$$V = d_{10}\sqrt{2\mathcal{E}_s} + \sum_{i=0}^{2G-1} p_{1i} J_i + \sum_{i=0}^{2G-1} p_{1i} N_{si} \quad (2.119)$$

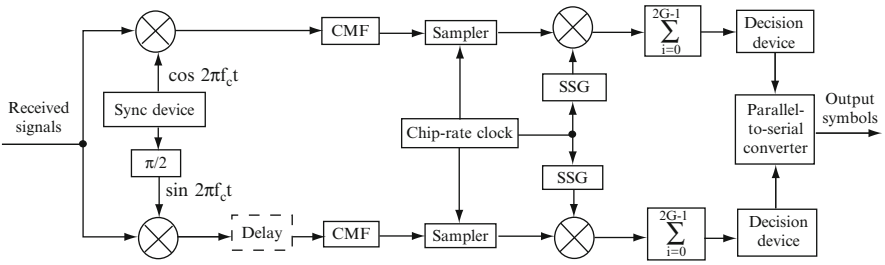

Fig. 2.17 Receiver for direct-sequence signal with dual quaternary modulation; *CMF* chip-matched filter; *SSG* spreading sequence generator. Delay = 0 for QPSK; delay = $T_c/2$ for OQPSK and MSK

where J_i and N_{si} are given by (2.78) and (2.79), respectively. The term representing crosstalk,

$$V_c = \sum_{i=0}^{2G-1} p_{1i} \sqrt{\frac{\mathcal{E}_s}{2}} \int_{iT_c}^{(i+1)T_c} d_2\,(t+t_0)\, p_2\,(t+t_0)\, \psi\,(t-iT_c) \sin 4\pi f_c t\; dt \tag{2.120}$$

is negligible if $f_c \gg 1/T_c$ so that the sinusoid in (2.120) varies much more rapidly than the other factors. Similarly, the lower decision variable at the end of a channel-symbol interval during which $d_2(t) = d_{20}$ is

$$U = d_{20}\sqrt{2\mathcal{E}_s} + \sum_{i=0}^{2G-1} p_{2i} J_i' + \sum_{i=0}^{2G-1} p_{2i} N_i' \tag{2.121}$$

where

$$J_i' = \int_{iT_c}^{(i+1)T_c} i(t)\psi\,(t-iT_c) \sin 2\pi f_c t \;\; dt \tag{2.122}$$

$$N_i' = \int_{iT_c}^{(i+1)T_c} n(t)\psi\,(t-iT_c) \sin 2\pi f_c t \;\; dt. \tag{2.123}$$

Of the available desired-signal power S, half is in each of the two components of (2.118). Since $T_{s1} = 2T_s$, the energy per channel-symbol component is $\mathcal{E}_s = ST_s$, the same as for a direct-sequence system with PSK, and

$$E[V] = d_{10}\sqrt{2\mathcal{E}_s}, \quad E(U) = d_{20}\sqrt{2\mathcal{E}_s}. \tag{2.124}$$

A derivation similar to the one leading to (2.90) gives the variances of the noise terms V_2 and U_2 in (2.119) and (2.121):

$$var\,(V_2) = var\,(U_2) = N_0. \tag{2.125}$$

Using the tone-interference model of Sect. 2.3, and averaging the error probabilities for the two parallel symbol streams, we obtain the conditional symbol error probability:

$$P_s\,(\phi) = \frac{1}{2} Q\left[\sqrt{\frac{2\mathcal{E}_s}{N_{0e}^{(0)}(\phi)}}\right] + \frac{1}{2} Q\left[\sqrt{\frac{2\mathcal{E}_s}{N_{0e}^{(1)}(\phi)}}\right] \tag{2.126}$$

where $N_{0e}^{(0)}(\phi)$ and $N_{0e}^{(1)}(\phi)$ arise from the upper and lower branches of Fig. 2.17, respectively. A derivation similar to that of (2.106) and (2.107) but using $T_{s1} = 2T_s$ indicates that for rectangular chip waveforms (QPSK and OQPSK signals),

$$N_{0e}^{(l)}(\phi) = N_0 + IT_c \mathrm{sinc}^2\,(f_d T_c)\left[1 + \frac{\mathrm{sinc}\,(4f_d T_s)}{\mathrm{sinc}\,(2f_d T_c)} \cos(2\phi + l\pi)\right] \tag{2.127}$$

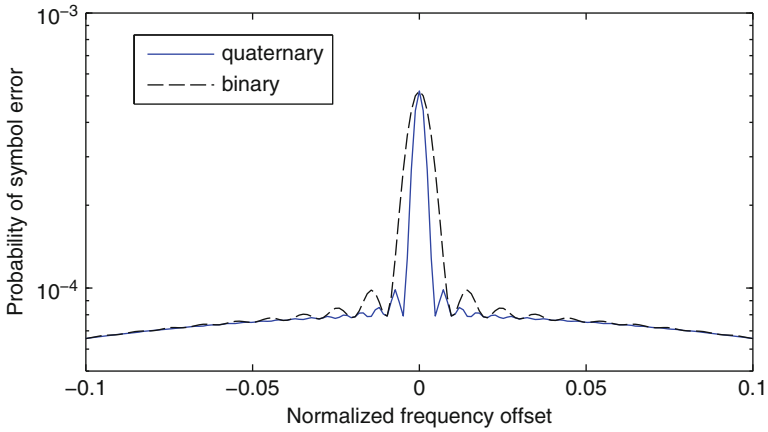

Fig. 2.18 Symbol error probability for quaternary and binary direct-sequence systems with $G = 17\,\text{dB}$, $\mathcal{E}_s/N_0 = 14\,\text{dB}$, and $GS/I = 10\,\text{dB}$ in the presence of tone interference

and for sinusoidal chip waveforms,

$$N_{0e}^{(l)}(\phi) = N_0 + IT_c\left(\frac{8}{\pi^2}\right)\left(\frac{\cos\pi f_d T_c}{1-4f_d^2T_c^2}\right)^2\left[1+\frac{\text{sinc}\,(4f_dT_s)}{\text{sinc}\,(2f_dT_c)}\cos(2\phi+l\pi)\right] \tag{2.128}$$

where $l = 0, 1$, and

$$\phi = \theta_1 + 2\pi f_d T_s. \tag{2.129}$$

These equations indicate that $P_s(\phi)$ for a quaternary direct-sequence system and the worst value of ϕ is usually lower than $P_s(\phi)$ for a binary direct-sequence system with the same chip waveform and the worst value of ϕ. The symbol error probability is determined by integrating $P_s(\phi)$ over the distribution of ϕ during a symbol interval. For a uniform distribution, the two integrals are equal. Using the periodicity of $\cos 2\phi$ to shorten the integration interval, we obtain

$$P_s = \frac{2}{\pi}\int_0^{\pi/2} Q\left[\sqrt{\frac{2\mathcal{E}_s}{N_{0e}^{(0)}(\phi)}}\right]d\phi. \tag{2.130}$$

The quaternary system provides a slight advantage relative to the binary system against tone interference. Both systems provide the same P_s when $f_d = 0$ and nearly the same P_s when $f_d > 1/T_s$. Figure 2.18 illustrates P_s versus the normalized frequency offset f_dT_c for quaternary and binary systems, $G = 17\,\text{dB}$, $\mathcal{E}_s/N_0 = 14\,\text{dB}$, and $G\mathcal{E}_s/IT_s = 10\,\text{dB}$.

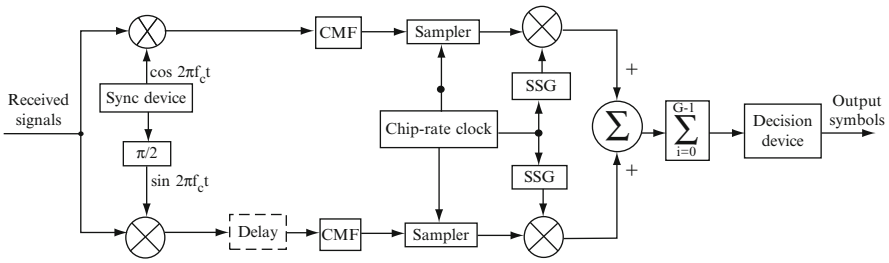

Fig. 2.19 Receiver for direct-sequence signal with balanced quaternary modulation (delay = 0 for QPSK and delay = $T_c/2$ for OQPSK and MSK); *CMF* chip-matched filter; *SSG* spreading sequence generator

In a *balanced quaternary system,* the same data symbols are carried by both the in-phase and quadrature components, which implies that the received direct-sequence signal has the form given by (2.118) with $d_1(t) = d_2(t) = d(t)$. Thus, although the spreading is done by quadrature carriers, the data modulation may be regarded as BPSK. A receiver for this system is shown in Fig. 2.19. The synchronization system is assumed to operate perfectly in the subsequent analysis. If $f_c \gg 1/T_c$, the crosstalk terms similar to (2.120) are negligible. The duration of both a data symbol and a channel symbol is T_s. If the transmitted symbol is $d_{10} = d_{20} = d_0$, then the input to the decision device is

$$V = d_0\sqrt{2\mathcal{E}_s} + \sum_{i=0}^{G-1} p_{1i}J_i + \sum_{i=0}^{G-1} p_{2i}J_i' + \sum_{i=0}^{G-1} p_{1i}N_i + \sum_{i=0}^{G-1} p_{2i}N_i'. \tag{2.131}$$

If $p_1(t)$ and $p_2(t)$, are approximated by independent random binary sequences, then the last four terms of (2.131) are zero-mean uncorrelated random variables. Therefore, the variance of V is equal to the sum of the variances of these four random variables, and

$$E[V] = d_0\sqrt{2\mathcal{E}_s}. \tag{2.132}$$

Straightforward evaluations verify that both types of quaternary signals provide the same performance against Gaussian interference as direct-sequence signals with PSK.

Consider a *balanced QPSK system*, for which $t_0 = 0$. If $i(t)$ is a tone, then a straightforward extension of the preceding analysis for general tone interference (Sect. 2.3) yields a $P_s(\phi)$ that is independent of ϕ. Therefore,

$$P_s = P_s(\phi) = Q\left(\sqrt{\frac{2\mathcal{E}_s}{N_{0e}}}\right) \tag{2.133}$$

where for rectangular chip waveforms,

$$N_{0e} = N_0 + I T_c \text{sinc}^2 (f_d T_c) \tag{2.134}$$

and for sinusoidal chip waveforms,

$$N_{0e} = N_0 + I T_c \left(\frac{8}{\pi^2}\right) \left(\frac{\cos \pi f_d T_c}{1 - 4 f_d^2 T_c^2}\right)^2. \tag{2.135}$$

If $f_d = 0$, a nearly exact model similar to the one in Sect. 2.3 implies that the conditional symbol error probability is

$$P_s(\phi) = \sum_{k_1=0}^{G} \sum_{k_2=0}^{G} \binom{G}{k_1} \binom{G}{k_2} \left(\frac{1}{2}\right)^{2G} \left[\frac{1}{2} P_s(\phi, k_1, k_2, +1) + \frac{1}{2} P_s(\phi, k_1, k_2, -1)\right] \tag{2.136}$$

where k_1 and k_2 are the number of chips in a symbol for which $p_1(t) = +1$ and $p_2(t) = +1$, respectively, and $P_s(\phi, k_1, k_2, d_0)$ is the conditional symbol error probability given the values of ϕ, k_1, and k_2 and that $d(t) = d_0$. A derivation analogous to that of (2.95) yields

$$P_s(\phi, k_1, k_2, d_0) = Q\left\{\sqrt{\frac{2\mathcal{E}_s}{N_0}} + d_0 \sqrt{\frac{I T_c \kappa}{G N_0}} [(2k_1 - G)\cos\phi - (2k_2 - G)\sin\phi]\right\}. \tag{2.137}$$

If ϕ is uniformly distributed over $[0, 2\pi)$ during a symbol interval, then

$$P_s = \frac{1}{2\pi} \int_0^{2\pi} P_s(\phi) d\phi. \tag{2.138}$$

Numerical comparisons of the nearly exact model with the approximate results given by (2.133) for $f_d = 0$ indicate that the approximate results typically introduce an insignificant error if $G \geq 50$.

Figure 2.20 illustrates the performance advantage of the balanced QPSK system of Fig. 2.19 against tone interference when $f_d < 1/T_s$. Equations (2.126) to (2.130) and (2.133) to (2.135) are used for the dual quaternary and the balanced QPSK systems, respectively, and $G = 17\,\text{dB}$, $\mathcal{E}_s/N_0 = 14\,\text{dB}$, and $G\mathcal{E}_s/I T_s = 10\,\text{dB}$. The normalized frequency offset is $f_d T_c$. The advantage of the balanced QPSK system when f_d is small exists because a tone at the carrier frequency cannot have a phase that causes desired-signal cancellation simultaneously in both receiver branches.

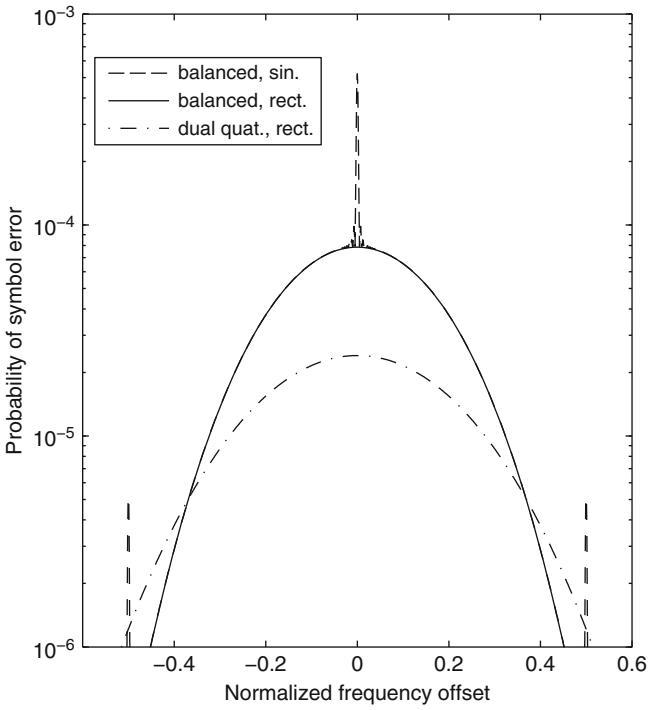

Fig. 2.20 Symbol error probability for direct-sequence systems with balanced QPSK and dual quaternary modulations, rectangular and sinusoidal chip waveforms, $G = 17\,\text{dB}$, $\mathcal{E}_s/N_0 = 14\,\text{dB}$, and $GS/I = 10\,\text{dB}$ in the presence of tone interference

2.4.1 Systems with Channel Codes

When channel codes are used, the calculation of the bit error probability for direct-sequence systems affected by tone or Gaussian interference is difficult or intractable, and thus is usually evaluated by a simulation. However, a simple approximation makes it possible to adapt the analytical or simulation results for systems using channel codes over the AWGN channel. The approximation is based on the assumption that the interference is whitened by the despreading. Thus, the effect of the interference and noise is similar to that of white Gaussian noise with the equivalent two-sided power spectral density N_{0e} or $N_{0e}(\phi)$. Let P_{b0} and P_{b1} denote the bit error probabilities when no channel code is used and interference is absent or present, respectively. Both probabilities are functions of $\mathcal{E}_b/N_0$, where the energy per bit is $\mathcal{E}_b = \mathcal{E}_s/r$ and r is the code rate. When interference is present, $\mathcal{E}_b/N_0$ must be increased by the factor Δ to maintain P_{b1} equal to some specified P_{b0}. Let P_{b2} and P_{b3} denote the bit error probabilities when a channel code is used and interference is absent or present, respectively. According to the approximation,

when interference is present, $\mathcal{E}_b/N_0$ must be increased by the same factor Δ to maintain P_{b3} equal to some specified P_{b2}. Thus, if a simulation or an analysis generates a plot of P_{b2}, then a plot of P_{b3} is obtained by shifting the plot of P_{b2} by $10 \log \Delta$ dB.

As an example, consider a direct-sequence system with balanced QPSK. For the AWGN channel, (2.133) indicates that the shift is $10 \log \Delta = 10 \log(N_{0e}/N_0)$ dB, where N_{0e} is given by (2.134) or (2.135).

2.5 Pulsed Interference

Pulsed interference is interference that occurs periodically or sporadically for brief durations. Whether it is generated unintentionally or by an opponent, pulsed interference can cause a substantial increase in the bit error rate of a communication system relative to the rate caused by continuous interference with the same average power. Pulsed interference may be produced in a receiver by a signal with a variable center frequency that sweeps over a frequency range that intersects or includes the receiver passband.

Consider a direct-sequence system with BPSK that operates in the presence of pulsed interference. Let μ denote either the pulse duty cycle, which is the ratio of the pulse duration to the repetition period, or the probability of pulse occurrence if the pulses occur randomly. During a pulse, the interference is modeled as Gaussian interference with power I/μ, where I is the average interference power. According to (2.116), the equivalent noise-power spectral density may be decomposed as

$$N_{0e} = N_0 + I_0 \tag{2.139}$$

where the power spectral density of continuous interference ($\mu = 1$) is

$$I_0 = \frac{I T_c}{W_1} \int_{f_1 - W_1/2}^{f_1 + W_1/2} \text{sinc}^2[(f - f_c) T_c] \, df. \tag{2.140}$$

In the absence of a pulse, $N_{0e} = N_0$, whereas $N_{0e} = N_0 + I_0/\mu$ in the presence of a pulse. If the interference pulse duration approximately equals or exceeds the channel-symbol duration, then (2.113) implies that

$$P_s \cong \mu Q\left(\sqrt{\frac{2\mathcal{E}_s}{N_0 + I_0/\mu}}\right) + (1 - \mu) Q\left(\sqrt{\frac{2\mathcal{E}_s}{N_0}}\right), \quad 0 \le \mu \le 1. \tag{2.141}$$

If μ is treated as a continuous variable over $[0, 1]$ and $I_0 \gg N_0$, calculus gives the value of μ that maximizes P_s:

$$\mu_0 \cong \begin{cases} 0.7\left(\frac{\mathcal{E}_s}{I_0}\right)^{-1} & \frac{\mathcal{E}_s}{I_0} > 0.7 \\ 1 & \frac{\mathcal{E}_s}{I_0} \le 0.7. \end{cases} \tag{2.142}$$

Thus, worst-case pulsed interference is more damaging than continuous interference if $\mathcal{E}_s/I_0 > 0.7$.

By substituting $\mu = \mu_0$ into (2.141), we obtain an approximate expression for the worst-case P_s when $I_0 \gg N_0$:

$$P_s \cong \begin{cases} 0.083\left(\frac{\mathcal{E}_s}{I_0}\right)^{-1}, & \frac{\mathcal{E}_s}{I_0} > 0.7 \\ Q\left(\sqrt{\frac{2\mathcal{E}_s}{I_0}}\right), & \frac{\mathcal{E}_s}{I_0} \leq 0.7. \end{cases} \tag{2.143}$$

This equation indicates that the worst-case P_s varies inversely, rather than exponentially, with $\mathcal{E}_s/I_0$ if this ratio is sufficiently large. To restore a nearly exponential dependence on $\mathcal{E}_s/I_0$, a channel code and symbol interleaving are necessary.

Decoding metrics that are effective against white Gaussian noise are not necessarily effective against worst-case pulsed interference. We examine the performance of five different metrics against pulsed interference when the direct-sequence system uses PSK, ideal symbol interleaving, a binary convolutional code, and Viterbi decoding [4]. The results are the same when either dual or balanced QPSK is the modulation.

Let $B(l)$ denote the total information weight of the paths at Hamming distance l from the correct path over an unmerged segment in the trellis diagram of the convolutional code. Let $P_2(l)$ denote the pairwise probability of an error in comparing the correct path segment with a particular path segment that differs in l symbols. According to (1.110) with $k = 1$, the information-bit error rate is upper-bounded by

$$P_b \leq \sum_{l=d_f}^{\infty} B(l)P_2(l) \tag{2.144}$$

where d_f is the minimum free distance. If r is the code rate, $\mathcal{E}_b$ is the energy per information bit, T_b is the bit duration, and G_u is the processing gain of the uncoded system, then

$$\mathcal{E}_s = r\mathcal{E}_b, \quad T_s = rT_b, \quad G = rG_u. \tag{2.145}$$

The decrease in the processing gain is compensated by the coding gain. An upper bound on P_b for worst-case pulsed interference is obtained by maximizing the right-hand side of (2.144) with respect to μ, where $0 \leq \mu \leq 1$. The maximizing value of μ, which depends on the decoding metric, is not necessarily equal to the actual worst-case μ because a bound rather than an equality is maximized. However, the discrepancy is small when the bound is tight.

The simplest practical metric to implement is provided by hard-decision decoding. Assuming that the deinterleaving ensures the independence of symbol errors, (1.112) indicates that

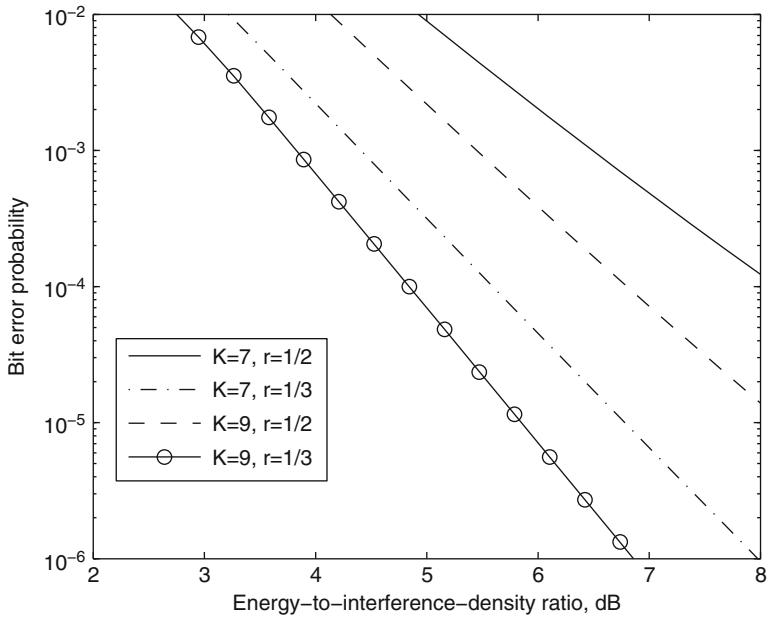

Fig. 2.21 Worst-case performance against pulsed interference for convolutional codes of constraint length K, rate r, $\mathcal{E}_b/N_0 = 20\,\text{dB}$, and hard decisions

$$P_2(l) = \begin{cases} \displaystyle\sum_{i=(l+1)/2}^{l} \binom{l}{i} P_s^i (1-P_s)^{l-i}, & l \text{ is odd} \\ \displaystyle\sum_{i=l/2+1}^{l} \binom{l}{i} P_s^i (1-P_s)^{l-i} + \frac{1}{2}\binom{l}{l/2}[P_s(1-P_s)]^{l/2}, & l \text{ is even.} \end{cases} \tag{2.146}$$

Since $\mu = \mu_0$ approximately maximizes P_s, it also approximately maximizes the upper bound on P_b for hard-decision decoding given by (2.153) to (2.155).

Figure 2.21 depicts the upper bound on P_b as a function of $\mathcal{E}_b/I_0$ for worst-case pulsed interference, $\mathcal{E}_b/N_0 = 20\,\text{dB}$, and binary convolutional codes with several constraint lengths and rates. Tables 1.4 and 1.5 for $B(l)$ are used, and the series in (2.144) is truncated after the first seven terms. This truncation gives reliable results only if $P_b \leq 10^{-3}$ because the series converges very slowly. However, the truncation error is partially offset by the error incurred by the use of the union bound because the latter error is in the opposite direction. Figure 2.21 indicates the significant advantage of raising the constraint length K and reducing r at the cost of increased implementation complexity and synchronization requirements, respectively.

Let $N_{0i}/2$ denote the equivalent noise-power spectral density due to noise and interference in output sample y_i of a coherent PSK demodulator. For convenience, y_i is assumed to have the form of the right-hand side of (2.80) normalized by multiplying the latter by $\sqrt{2/T_s}$. Thus, y_i has variance $N_{0i}/2$. Given that code

symbol i of sequence k has value x_{ki}, the conditional probability density function of y_i is determined from the Gaussian character of the interference and noise. For a sequence of L code symbols, the density is

$$f\,(y_i|x_{ki}) = \frac{1}{\sqrt{\pi N_{0i}}} \exp\left[-\frac{(y_i - x_{ki})^2}{N_{0i}}\right], \quad i = 1, 2, \ldots, L. \tag{2.147}$$

From the log-likelihood function and the statistical independence of the samples, it follows that when the values of $N_{01}, N_{02}, \ldots, N_{0L}$ are known, the *maximum-likelihood metric* for optimal soft-decision decoding of the sequence of L code symbols is

$$U(k) = \sum_{i=1}^{L} \frac{x_{ki}\, y_i}{N_{0i}}. \tag{2.148}$$

This metric weights each output sample y_i according to the level of the equivalent noise. Since each y_i is assumed to be an independent Gaussian random variable, $U(k)$ is a Gaussian random variable.

Without loss of generality, let $k = 1$ label the correct sequence and $k = 2$ label an incorrect one at distance l. We assume that there is no quantization of the sample values or that the quantization is infinitely fine. Therefore, the probability that $U(2) = U(1)$ is zero, and the probability of an error in comparing a correct sequence with an incorrect one that differs in l symbols, $P_2(l)$, is equal to probability that $M_0 = U(2) - U(1) > 0$. The symbols that are the same in both sequences are irrelevant to the calculation of $P_2(l)$ and are ignored subsequently. Let $P_2(l|\nu)$ denote the conditional probability that $M_0 > 0$ given that an interference pulse occurs during ν out of l differing symbols and does not occur during $l - \nu$ symbols. Because of the interleaving, the probability that a symbol is interfered is statistically independent of the rest of the sequence and equals μ. Thus, (2.144) yields

$$P_b \leq \sum_{l=d_f}^{\infty} B(l) \sum_{\nu=0}^{l} \binom{l}{\nu} \mu^{\nu} (1-\mu)^{l-\nu} P_2(l/\nu). \tag{2.149}$$

Since M_0 is a Gaussian random variable, $P_2(l|\nu)$ is determined from the conditional mean and variance. A straightforward calculation gives

$$P_2(l|\nu) = Q\left(\frac{-E\,[M_0|\nu]}{\sqrt{var\,[M_0|\nu]}}\right) \tag{2.150}$$

where $E[M_0|\nu]$ is the conditional mean and $var[M_0|\nu]$ is the conditional variance. When an interference pulse occurs, $N_{0i} = N_0 + I_0$; otherwise, $N_{0i} = N_0$. Reordering the symbols for calculative simplicity and observing that $x_{2i} = -x_{1i}$, $x_{1i}^2 = \mathcal{E}_s$, and $E[y_i] = x_{1i}$, we obtain

$$E[M_0|\nu] = \sum_{i=1}^{\nu} \frac{(x_{2i} - x_{1i})\, E[y_i]}{N_0 + I_0/\mu} + \sum_{i=\nu+1}^{l} \frac{(x_{2i} - x_{1i})\, E[y_i]}{N_0}$$

$$= \sum_{i=1}^{\nu} \frac{-2\mathcal{E}_s}{N_0 + I_0/\mu} + \sum_{i=\nu+1}^{l} \frac{-2\mathcal{E}_s}{N_0}$$

$$= -2\mathcal{E}_s \left[\frac{\nu}{N_0 + I_0/\mu} + \frac{l-\nu}{N_0} \right]. \tag{2.151}$$

Using the statistical independence of the samples and observing that $var[y_i] = N_{0i}/2$, we find similarly that

$$var[M_0|\nu] = 2\mathcal{E}_s \left[\frac{\nu}{N_0 + I_0/\mu} + \frac{l-\nu}{N_0} \right]. \tag{2.152}$$

Substituting (2.151) and (2.152) into (2.150), we obtain

$$P_2[l|\nu] = Q\left\{ \sqrt{\frac{2\mathcal{E}_s}{N_0}} \left[l - \nu \left(1 + \frac{\mu N_0}{I_0} \right)^{-1} \right]^{1/2} \right\}. \tag{2.153}$$

The substitution of this equation into (2.149) gives the upper bound on P_b for the maximum-likelihood metric.

The upper bound on P_b versus $\mathcal{E}_b/I_0$ for worst-case pulsed interference, $\mathcal{E}_b/N_0 = 20$ dB, and several binary convolutional codes is shown in Fig. 2.22. Although the worst value of μ varies with $\mathcal{E}_b/I_0$, it is found that worst-case pulsed interference causes very little degradation relative to continuous interference. When $K = 9$ and $r = 1/2$, the *maximum-likelihood metric* provides a performance that is more than 4 dB superior at $P_b = 10^{-5}$ to that provided by hard-decision decoding; when $K = 9$ and $r = 1/3$, the advantage is approximately 2.5 dB. However, the implementation of the maximum-likelihood metric entails knowledge of not only the presence of interference, but also its density level. Estimates of the N_{0i} might be based on power measurements in adjacent frequency bands only if the interference-power spectral density is fairly uniform over the desired-signal and adjacent bands. Any measurement of the power within the desired-signal band is contaminated by the presence of the desired signal, the average power of which is usually unknown *a priori* because of the fading. Since iterative estimation of the N_{0i} and decoding is costly in terms of system latency and complexity, we examine another approach.

Consider an *automatic gain control* (AGC) device that measures the average power at the demodulator output before sampling and then weights the sampled demodulator output y_i in proportion to the inverse of the measured power to form the *AGC metric*. The average power during channel-symbol i is $N_{0i}B + \mathcal{E}_s/T_s$, where B is the equivalent bandwidth of the demodulator and T_s is the channel-symbol duration. If the power measurement is perfect and $BT_s \approx 1$, then the AGC metric is

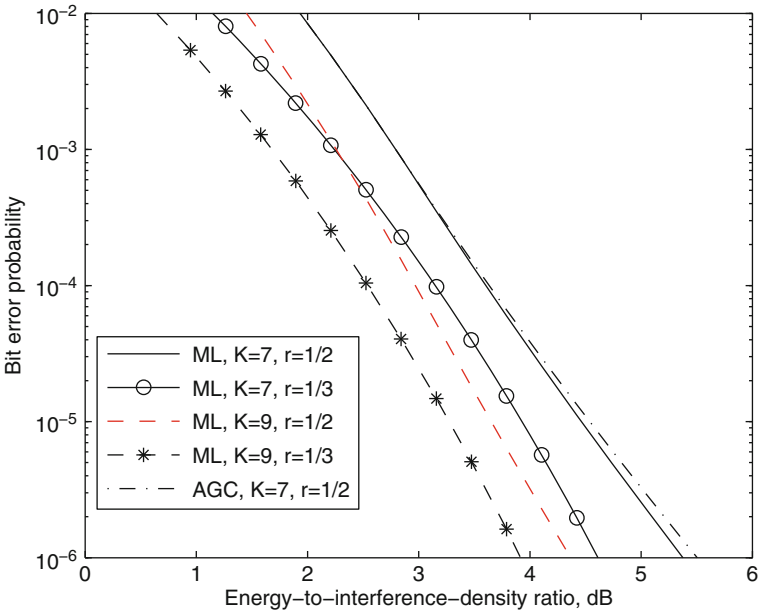

Fig. 2.22 Worst-case performance against pulsed interference for convolutional codes of constraint length K, rate r, $\mathcal{E}_b/N_0 = 20\,\text{dB}$ and maximum-likelihood (ML) and AGC metrics

$$U(k) = \sum_{i=1}^{L} \frac{x_{ki}\, y_i}{N_{0i} + \mathcal{E}_s} \tag{2.154}$$

which is a Gaussian random variable. This metric and (2.150) yield

$$P_2(l/\nu) = Q\left\{ \sqrt{\frac{2\mathcal{E}_s}{N_0}} \frac{l\,(N_0 + \mathcal{E}_s + I_0/\mu) - \nu I_0/\mu}{\left[l\,(N_0 + \mathcal{E}_s + I_0/\mu)^2 - \nu\left(N_0 + I_0/\mu - \mathcal{E}_s^2/N_0\right) I_0/\mu\right]^{1/2}} \right\}. \tag{2.155}$$

This equation and (2.149) give the upper bound on P_b for the AGC metric.

The upper bound on P_b versus $\mathcal{E}_b/I_0$ for worst-case pulsed interference, the AGC metric, the rate-1/2 binary convolutional code with $K = 7$, and $\mathcal{E}_b/N_0 = 20\,\text{dB}$ is plotted in Fig. 2.22. The figure indicates that the potential performance of the AGC metric is nearly as good as that of the maximum-likelihood metric.

The measurement of $N_{0i}BT_s + \mathcal{E}_s$ may be performed by a *radiometer*, which is a device that measures the energy at its input. An ideal radiometer (Chap. 7) provides an unbiased estimate of the energy received during a symbol interval. The radiometer outputs are accurate estimates only if the standard deviation of the output is much less than its expected value. This criterion and theoretical

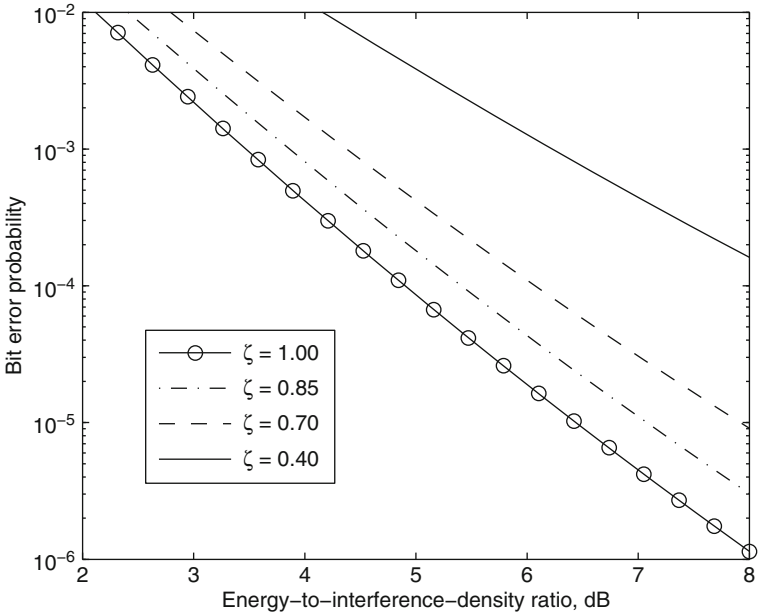

Fig. 2.23 Performance against pulsed interference for convolutional code with white-noise metric, $K = 7$, $r = 1/2$, and $\mathcal{E}_b/N_0 = 20$ dB

results for $BT_s = 1$ indicate that the energy measurements over a symbol interval will be unreliable if $\mathcal{E}_s/N_{0i} \leq 10$ during interference pulses. Thus, the potential performance of the AGC metric is expected to be significantly degraded in practice unless each interference pulse extends over many channel symbols and its energy is measured over the corresponding interval.

The maximum-likelihood metric for continuous interference (N_{0i} is constant for all i) is the *white-noise metric*:

$$U(k) = \sum_{i=1}^{L} x_{ki}\, y_i \tag{2.156}$$

which is much simpler to implement than the AGC metric. For the white-noise metric, calculations similar to the preceding ones yield

$$P_2(l|\nu) = Q\left\{ \sqrt{\frac{2\mathcal{E}_s}{N_0}}\, l \left(l + \nu \frac{I_0}{\mu N_0} \right)^{-1/2} \right\}. \tag{2.157}$$

This equation and (2.149) give the upper bound on P_b for the white-noise metric. Figure 2.23 illustrates the upper bound on P_b versus $\mathcal{E}_b/I_0$ for $K = 7$, $r = 1/2$, $\mathcal{E}_b/N_0 = 20$ dB, and several values of $\zeta = \mu/\mu_0$. The figure demonstrates the vulnerability of soft-decision decoding with the white-noise metric to short

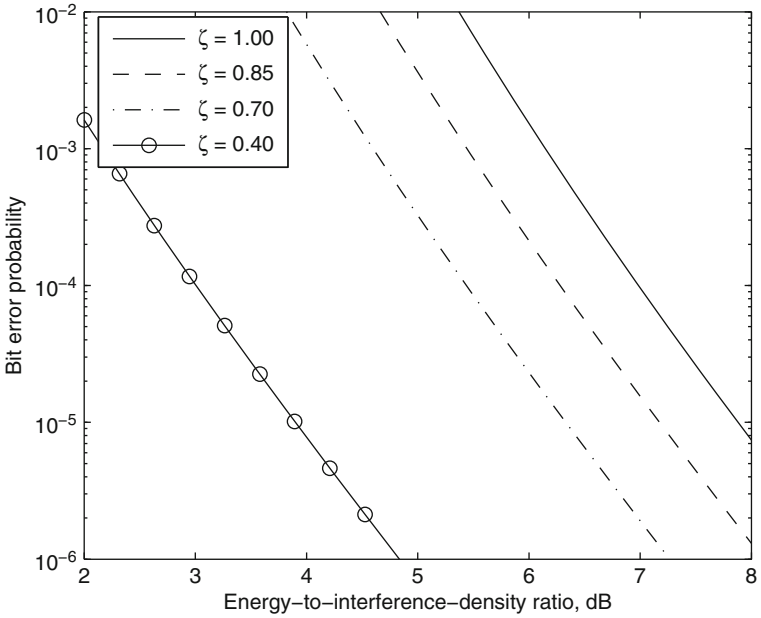

Fig. 2.24 Performance against pulsed interference for convolutional code with erasures, $K = 7$, $r = 1/2$, and $\mathcal{E}_b/N_0 = 20\,\text{dB}$

high-power pulses if interference power is conserved. The high values of P_b for $\zeta < 1$ are due to the domination of the metric by a few degraded symbol metrics.

Consider a coherent PSK demodulator that erases its output and, hence, a received symbol whenever an interference pulse occurs. The presence of the pulse might be detected by examining a sequence of the demodulator outputs and determining which ones have inordinately large magnitudes compared to the others. Alternatively, the demodulator might decide that a pulse has occurred if an output has a magnitude that exceeds a known upper bound for the desired signal. Consider an ideal demodulator that unerringly detects the pulses and erases the corresponding received symbols. Following the deinterleaving of the demodulated symbols, the decoder processes symbols that have a probability of being erased equal to μ. The unerased symbols are decoded by using the white-noise metric. The erasing of ν symbols causes two sequences that differ in l symbols to be compared on the basis of $l - \nu$ symbols where $0 \le \nu \le l$. As a result,

$$P_2(l|\nu) = Q\left[\sqrt{\frac{2\mathcal{E}_s}{N_0}(l-\nu)}\right]. \tag{2.158}$$

The substitution of this equation into (2.149) give the upper bound on P_b for errors-and-erasures decoding.

The upper bound on P_b is illustrated in Fig. 2.24 for $K = 7$, $r = 1/2$, $\mathcal{E}_b/N_0 = 20\,\text{dB}$, and several values of $\zeta = \mu/\mu_0$. In this example, erasures provide no

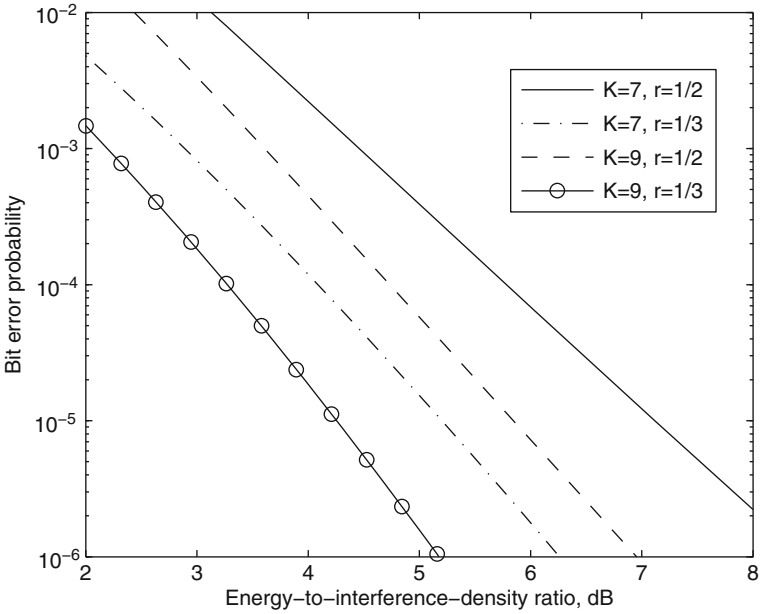

Fig. 2.25 Worst-case performance against pulsed interference for convolutional codes with ideal erasure decoding, constraint length K, rate r, and $\mathcal{E}_b/N_0 = 20\,\text{dB}$

advantage over the white-noise metric in reducing the required $\mathcal{E}_b/I_0$ for $P_b = 10^{-5}$ if $\zeta > 0.85$, but are increasingly useful as ζ decreases. Consider an ideal demodulator that activates erasures only when μ is small enough that the erasures are more effective than the white-noise metric. When this condition does not occur, the white-noise metric is used. The upper bound on P_b for this *ideal erasure decoding*, worst-case pulsed interference, $\mathcal{E}_b/N_0 = 20\,\text{dB}$, and several binary convolutional codes is illustrated in Fig. 2.25. The required $\mathcal{E}_b/I_0$ at $P_b = 10^{-5}$ is roughly 2 dB less than for worst-case hard-decision decoding. However, a practical demodulator will sometimes erroneously make erasures or fail to erase, and its performance advantage may be much more modest.

2.6 Despreading with Bandpass Matched Filters

A matched filter can be implemented at baseband as a digital transversal filter. Alternatively, bandpass matched filtering can be implemented by analog devices. Despreading short spreading sequences with bandpass matched filters provides inherent code synchronization and is the basis for simple direct-sequence receivers, which are described in this section.

The spreading waveform for a short spreading sequence may be expressed as

$$p(t) = \sum_{i=-\infty}^{\infty} p_1(t - iT) \tag{2.159}$$

where $p_1(t)$ is one period of the spreading waveform and T is its period. If the short spreading sequence has length N, then

$$p_1(t) = \begin{cases} \sum_{i=0}^{N-1} p_i \psi\left(t - iT_c\right), & 0 \le t \le T \\ 0, & \text{otherwise.} \end{cases} \tag{2.160}$$

where $p_i = \pm 1$, and $T = NT_c$.

Consider a signal $x(t)$ that is zero outside the interval $[0, T]$. A filter is said to be *matched* to this signal if the impulse response of the filter is $h(t) = x(T - t)$. When $x(t)$ is applied to a filter matched to it, the filter output is

$$\begin{aligned} y(t) &= \int_{-\infty}^{\infty} x(u)h(t-u)du = \int_{-\infty}^{\infty} x(u)x(u+T-t)du \\ &= \int_{\max(t-T,0)}^{\min(t,T)} x(u)x(u+T-t)du. \end{aligned} \tag{2.161}$$

The *aperiodic autocorrelation* of a deterministic signal with finite energy is defined as

$$R_x(\tau) = \int_{-\infty}^{\infty} x(u)x(u+\tau)du = \int_{-\infty}^{\infty} x(u)x(u-\tau)du. \tag{2.162}$$

Therefore, the response of a matched filter to the matched signal is

$$y(t) = R_x(t - T). \tag{2.163}$$

If this output is sampled at $t = T$, then $y(T) = R_x(0)$, the signal energy.

Consider a *bandpass matched filter* that is matched to

$$x(t) = \begin{cases} p_1(t)\cos\left(2\pi f_c t + \theta_1\right), & 0 \le t \le T \\ 0, & \text{otherwise} \end{cases} \tag{2.164}$$

where $p_1(t)$ is one period of a spreading waveform and f_c is the desired carrier frequency. We evaluate the filter response to the received signal corresponding to a single data symbol:

$$s(t) = \begin{cases} 2Ap_1(t - t_0)\cos\left(2\pi f_1 t + \theta\right), & t_0 \le t \le t_0 + T \\ 0, & \text{otherwise} \end{cases} \tag{2.165}$$

where t_0 is a measure of the unknown arrival time, the polarity of A is determined by the data symbol, and f_1 is the received carrier frequency, which differs from f_c because of oscillator instabilities and the Doppler shift. The matched-filter output is

$$y_s(t) = \int_{t-T}^{t} s(u)\, p_1(u+T-t) \cos\left[2\pi f_c(u+T-t)+\theta_1\right] du. \tag{2.166}$$

If $f_c \gg 1/T$, then substituting (2.168) into (2.169) yields

$$y_s(t) = A \int_{\max(t-T,t_0)}^{\min(t,t_0+T)} p_1\,(u-t_0)\; p_1(u-t+T) \cos\left(2\pi f_d u + 2\pi f_c t + \theta_2\right) du \tag{2.167}$$

where $\theta_2 = \theta - \theta_1 - 2\pi f_c T$ is the phase mismatch and $f_d = f_1 - f_c$. If $f_d \ll 1/T$, the carrier-frequency error is inconsequential, and

$$y_s(t) \approx A_s(t) \cos\left(2\pi f_c t + \theta_3\right), \quad t_0 \le t \le t_0 + 2T \tag{2.168}$$

where $\theta_3 = \theta_2 + 2\pi f_d t_0$ and

$$A_s(t) = A \int_{\max(t-T,t_0)}^{\min(t,t_0+T)} p_1\,(u-t_0)\; p_1(u-t+T) du. \tag{2.169}$$

In the absence of noise, the matched-filter output $y_s(t)$ is a sinusoidal spike with a polarity determined by A. Equation (2.169) indicates that the peak magnitude, which occurs at the ideal sampling time $t = t_0 + T$, equals $|A|T$. However, if $f_d > 0.1/T$, then (2.167) is not well-approximated by (2.168), and the matched-filter output is significantly degraded.

The response of the matched filter to the interference plus noise, denoted by $N(t) = i(t) + n(t)$, may be expressed as

$$\begin{aligned} y_n(t) &= \int_{t-T}^{t} N(u)\, p_1(u+T-t) \cos\left[2\pi f_c(u+T-t)+\theta_1\right] du \\ &= N_1(t) \cos\left(2\pi f_c t + \theta_2\right) + N_2(t) \sin\left(2\pi f_c t + \theta_2\right) \end{aligned} \tag{2.170}$$

where

$$N_1(t) = \int_{t-T}^{t} N(u)\, p_1(u+T-t) \cos\left(2\pi f_c u + \theta\right) du \tag{2.171}$$

$$N_2(t) = \int_{t-T}^{t} N(u)\, p_1(u+T-t) \sin\left(2\pi f_c u + \theta\right) du. \tag{2.172}$$

These equations exhibit the spreading and filtering of the interference spectrum.

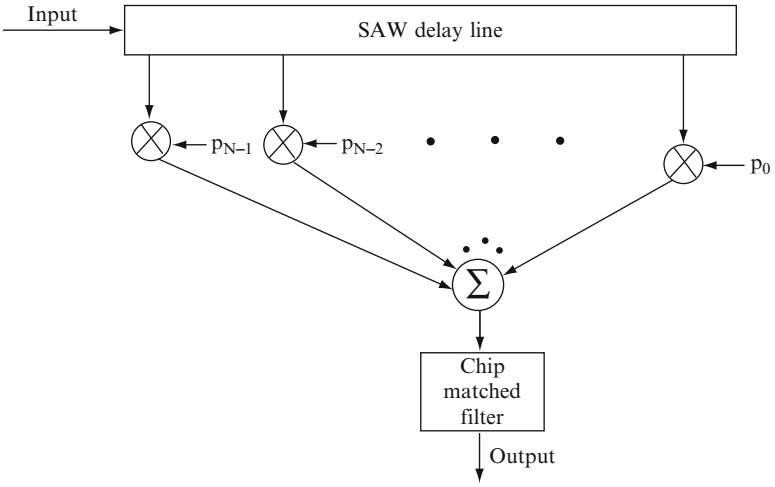

Fig. 2.26 Matched filter that uses a SAW transversal filter. Output is $y_s(t) + y_n(t)$

The envelope of the matched-filter output $y(t) = y_s(t) + y_n(t)$ is

$$E(t) = \left\{[A_s(t) + N_1(t)]^2 + N_2^2(t)\right\}^{1/2}. \tag{2.173}$$

If

$$|AT + N_1(t_0 + T)| \gg |N_2(t_0 + T)| \tag{2.174}$$

then (2.173) implies that

$$E(t_0 + T) \approx |AT + N_1(t_0 + T)| \tag{2.175}$$

at the ideal sampling time. Equations (2.168), (2.170), and (2.174) imply that if $y(t)$ is sampled at $t = t_0 + T$,

$$\begin{aligned} y(t_0 + T) &\le |A_s(t_0 + T) + N_1(t_0 + T)| + |N_2(t_0 + T)| \\ &\approx |AT + N_1(t_0 + T)| \end{aligned} \tag{2.176}$$

where $A_s(t_0 + T) = AT$. A comparison of this approximate upper bound with (2.175) indicates that there is relatively little degradation in using an envelope detector after the matched filter rather than directly detecting the peak magnitude of the matched-filter output, which is much more difficult.

Figure 2.26 illustrates the basic form of a *surface-acoustic-wave* (SAW) *transversal filter*, which is a passive matched filter that essentially stores a replica of the underlying spreading sequence and waits for the received sequence to align itself with the replica. The SAW delay line consists primarily of a piezoelectric substrate, which serves as the acoustic propagation medium, and interdigital transducers, which serve as the taps and the input transducer. The transversal filter is matched

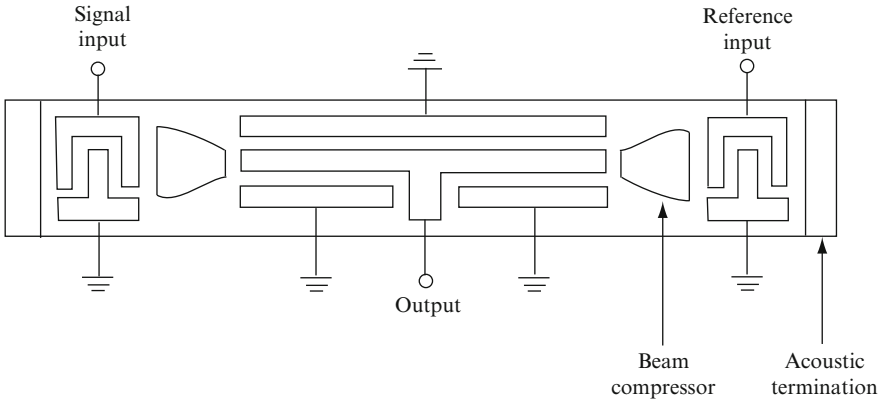

Fig. 2.27 SAW elastic convolver

to one period of the spreading waveform, the propagation delay between taps is T_c, and $f_c T_c$ is an integer. The chip matched filter following the summer is matched to $\psi(t)\cos(2\pi f_c t + \theta)$. It is easily verified that the impulse response of the transversal filter is that of a filter matched to $p_1(t)\cos(2\pi f_c t + \theta)$.

A *convolver* is an *active matched filter* that produces the convolution of the received signal with a local reference [5]. When used as a direct-sequence matched filter, a convolver uses a recirculating, time-reversed replica of the spreading waveform as a reference waveform. In a *SAW elastic convolver*, which is depicted in Fig. 2.27, the received signal and the reference are applied to interdigital transducers that generate acoustic waves at opposite ends of the substrate. The acoustic waves travel in opposite directions with speed υ, and the acoustic terminations suppress reflections. The signal wave is launched at position $x = 0$ and the reference wave at $x = L$. The signal wave travels to the right in the substrate and has the form

$$F(t,x) = f\left(t - \frac{x}{\upsilon}\right)\cos\left[2\pi f_c\left(t - \frac{x}{\upsilon}\right) + \theta\right] \tag{2.177}$$

where $f(t)$ is the modulation at position $x = 0$. The reference wave travels to the left and has the form

$$G(t,x) = g\left(t + \frac{x}{\upsilon} - \frac{L}{\upsilon}\right)\cos\left[2\pi f_c\left(t + \frac{x}{\upsilon} - \frac{L}{\upsilon}\right) + \theta_1\right] \tag{2.178}$$

where $g(t)$ is the modulation at position $x = L$. Both $f(t)$ and $g(t)$ are assumed to have bandwidths much smaller than f_c. The beam compressors, which consist of thin metallic strips, focus the acoustic energy to increase the convolver's efficiency. When the acoustic waves overlap beneath the central electrode, a nonlinear piezoelectric effect causes a surface charge distribution that is spatially integrated by the electrode. The primary component of the convolver output is proportional to

$$y(t) = \int_0^L [F(t,x) + G(t,x)]^2 dx. \tag{2.179}$$

Substituting (2.177) and (2.178) into (2.179) and using trigonometry, we find that $y(t)$ is the sum of a number of terms, some of which are negligible if $f_c L/v \gg 1$. Others are slowly varying and are easily blocked by a filter. The most useful component of the convolver output is

$$y_s(t) = \left[\int_0^L f\left(t - \frac{x}{\upsilon}\right) g\left(t + \frac{x}{\upsilon} - \frac{L}{\upsilon}\right) dx\right] \cos(4\pi f_c t + \theta_2) \tag{2.180}$$

where $\theta_2 = \theta + \theta_1 - 2\pi f_c L/v$. Changing variables, we find that the amplitude of the output is

$$A_s(t) = \int_{t-L/\upsilon}^{t} f(y) g(2t - y - L/\upsilon) dy \tag{2.181}$$

where the factor $2t$ results from the counterpropagation of the two acoustic waves.

Suppose that an acquisition pulse is a single period of the spreading waveform. Then $f(t) = Ap_1(t - t_0)$ and $g(t) = p(T - t)$, where t_0 is the uncertainty in the arrival time of an acquisition pulse relative to the launching of the reference signal at $x = L$. The periodicity of $g(t)$ allows the time origin to be selected so that $0 \le t_0 \le T$. Equations (2.181) and (2.159) and a change of variables yield

$$A_s(t) = A \sum_{i=-\infty}^{\infty} \int_{t-t_0-L/\upsilon}^{t-t_0} p_1(y) p_1(y + iT + t_0 - 2t + L/\upsilon)\, dy. \tag{2.182}$$

Since $p_1(t) = 0$ unless $0 \le t < T$, $A_s(t) = 0$ unless $t_0 < t < t_0 + T + L/\upsilon$. For every positive integer k, let

$$\tau_k = \frac{kT + t_0 + L/\upsilon}{2}, \qquad k = 1, 2, \ldots \tag{2.183}$$

Only one term in (2.179) can be nonzero when $t = \tau_k$, and

$$A_s(\tau_k) = A \int_{\tau_k - t_0 - L/\upsilon}^{\tau_k - t_0} p_1^2(y) dy. \tag{2.184}$$

The maximum possible magnitude of $A_s(\tau_k)$ is produced if $\tau_k - t_0 \ge T$ and $\tau_k - t_0 - L/\upsilon \le 0$; that is, if

$$t_0 + T \le \tau_k \le t_0 + \frac{L}{\upsilon}. \tag{2.185}$$

Since (2.183) indicates that $\tau_{k+1} - \tau_k = T/2$, there is some τ_k that satisfies (2.185) if

$$L \ge \frac{3}{2}\upsilon T. \tag{2.186}$$

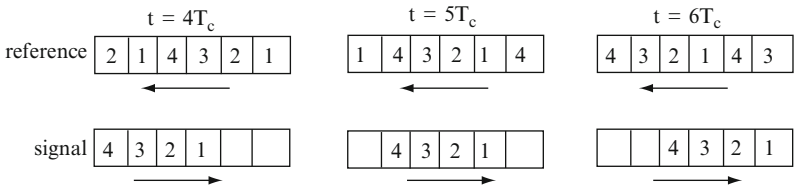

Fig. 2.28 Chip configurations within convolver at time instants $t = 4T_c$, $5T_c$, and $6T_c$ when $t_0 = 0$, $L/\upsilon = T_c$, and $T = 4T_c$

Thus, if L is large enough, then there is some k such that $A_s(\tau_k) = AT$, and the envelope of the convolver output at $t = \tau_k$ has the maximum possible magnitude $|A|T$. If $L = 3\upsilon T/2$ and $t_0 \neq T/2$, only one peak value occurs in response to the single received pulse.

As an example, let $t_0 = 0$, $L/\upsilon = 6T_c$, and $T = 4T_c$. The chips propagating in the convolver for three separate time instants $t = 4T_c$, $5T_c$, and $6T_c$ are illustrated in Fig. 2.28. The top diagrams refer to the counterpropagating periodic reference signal, whereas the bottom diagrams refer to the single received pulse of four chips. The chips are numbered consecutively. The received pulse is completely contained within the convolver during $4T_c \leq t \leq 6T_c$. The maximum magnitude of the output occurs at time $t = 5T_c$, which is the instant of perfect alignment of the reference signal and the received chips.

2.6.1 Noncoherent Systems

In a noncoherent direct-sequence system with binary *code-shift keying* (CSK), one of two orthogonal spreading sequences is transmitted, as shown in Fig. 2.29a. One sequence represents the symbol 1, and the other represents the symbol 0. The receiver uses two matched filters, each matched to a different sequence and followed by an envelope detector, as shown in Fig. 2.29b. In the absence of noise and interference, each sequence causes only one envelope detector to produce a significant output. The data is recovered by comparing the two detector outputs every symbol period.

Since each of the two orthogonal sequences has a period equal to the symbol duration, symbol or bit synchronization is identical to code synchronization. The *symbol synchronizer*, which provides timing pulses to the comparator or decision device, must lock onto the autocorrelation spikes appearing in the envelope-detector outputs. Ideally, these spikes have a triangular shape. The symbol synchronizer must be impervious to the autocorrelation sidelobe peaks and any cross-correlation peaks. A simple implementation with a single threshold detector would result in an unacceptable number of false alarms, premature detections, or missed detections when the received signal amplitude is unknown and has a wide dynamic range.

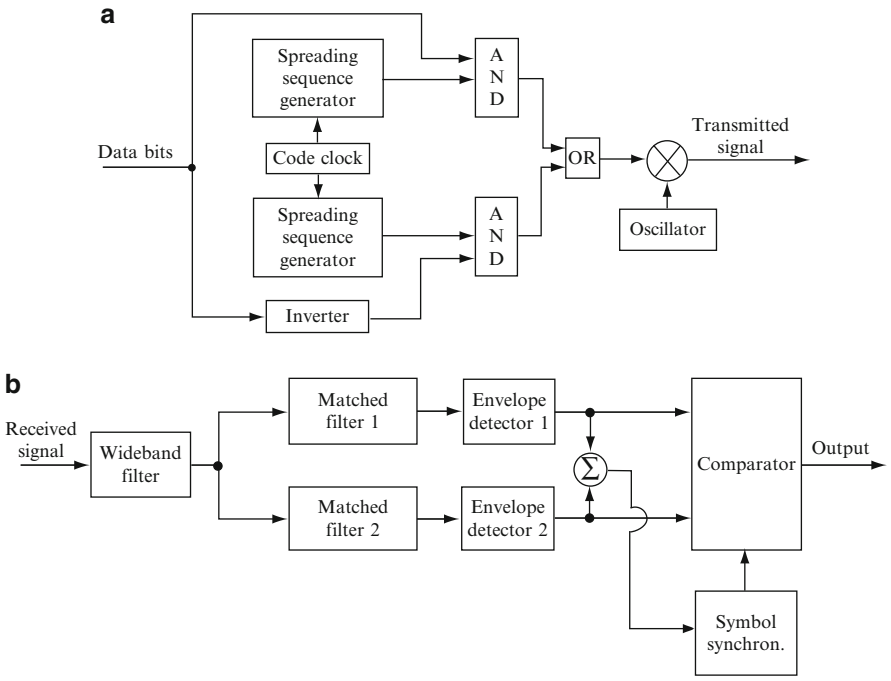

Fig. 2.29 Direct-sequence system with binary code-shift keying: (**a**) transmitter and (**b**) receiver

Limiting or automatic gain control only exacerbates the problem when the signal power level is below that of the interference plus noise. More than one threshold detector with precedence given to the highest threshold crossed will improve the accuracy of the decision timing or sampling instants produced by the symbol synchronizer. Another approach is to use peak detection based on a differentiator and a zero-crossing detector. Finally, a phase-locked or feedback loop of some type could be used in the symbol synchronizer. A preamble may be transmitted to initiate accurate synchronization so that symbols are not incorrectly detected while synchronization is being established.

Consider the detection of a symbol represented by (2.165), where $p_1(t)$ is the CSK waveform to which filter 1 is matched. Assuming perfect symbol synchronization, the channel symbol is received during the interval $0 \leq t \leq T_s$. From (2.168) to (2.172) with $T = T_s$ and $t_0 = 0$, we find that the output of envelope detector 1 at $t = T_s$ is

$$R_1 = \left(Z_1^2 + Z_2^2\right)^{1/2} \tag{2.187}$$

where

$$Z_1 = AT_s + \int_0^{T_s} N(u)\, p_1(u) \cos\left(2\pi f_c u + \theta\right) du \tag{2.188}$$

$$Z_2 = \int_0^{T_s} N(u)\, p_1(u) \sin(2\pi f_c u + \theta) du. \tag{2.189}$$

Similarly, if filter 2 is matched to sequence $p_2(t)$, then the output of envelope detector 2 at $t = T_s$ is

$$R_2 = \left(Z_3^2 + Z_4^2\right)^{1/2} \tag{2.190}$$

where

$$Z_3 = \int_0^{T_s} N(u)\, p_2(u) \cos(2\pi f_c u + \theta)\, du \tag{2.191}$$

$$Z_4 = \int_0^{T_s} N(u)\, p_2(u) \sin(2\pi f_c u + \theta)\, du \tag{2.192}$$

and the response to the transmitted symbol at $t = T_s$ is zero because of the orthogonality of the sequences.

Suppose that the interference plus noise $N(t)$ is modeled as zero-mean, Gaussian interference, and the spreading sequences are modeled as deterministic and orthogonal. Then $E[Z_1] = AT_s$ and $E[Z_i] = 0, i = 2, 3, 4$. If $N(t)$ is assumed to be wideband enough that its autocorrelation is approximated by (2.83), then straightforward calculations using $f_c T_s \gg 1$ and the orthogonality of $p_1(t)$ and $p_2(t)$ indicate that Z_1, Z_2, Z_3, and Z_4 are all uncorrelated with each other. The jointly Gaussian character of the random variables then implies that they are statistically independent of each other, and hence R_1 and R_2 are independent. Analogous results can be obtained when the transmitted symbol is represented by CSK waveform $p_2(t)$. A straightforward derivation similar to the classical one for orthogonal signals, but allowing for the spreading and filtering of the Gaussian interference, then yields the symbol error probability

$$P_s = \frac{1}{2} \exp\left(-\frac{\mathcal{E}_s}{2N_{0e}}\right) \tag{2.193}$$

where N_{0e} is given by (2.116). A comparison of (2.193) with (2.113) indicates that the performance of the direct-sequence system with noncoherent binary CSK in the presence of wideband Gaussian interference is approximately 4 dB worse than that of a direct-sequence system with coherent BPSK. This difference arises because binary CSK uses orthogonal rather than antipodal signaling. A much more complicated coherent version of Fig. 2.29 would only recover roughly 1 dB of the disparity.

A direct-sequence system with q-ary CSK encodes each group of m binary symbols as one of $q = 2^m$ sequences chosen to be orthogonal or have negligible cross correlations and nearly ideal autocorrelations. For mutual orthogonality, the sequences must have length $L \geq q$. Suppose that bandwidth constraints limit the chip rate of a binary CSK system to G chips per data bit. For a fixed data-bit rate, the q-ary CSK system produces $L = mG$ chips to represent each group of m bits, which may be regarded as a single q-ary symbol. Thus, the processing gain is

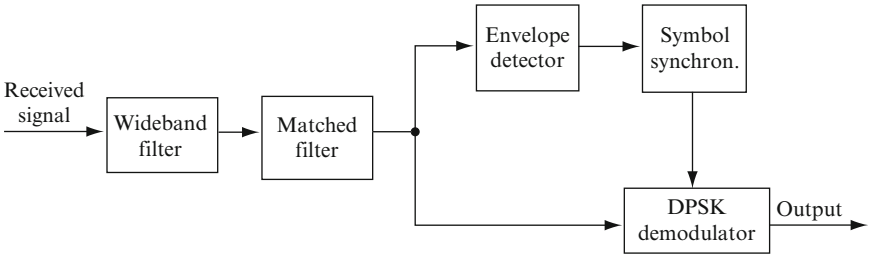

Fig. 2.30 Receiver for direct-sequence system with DPSK

$G \geq q/\log_2 q$. In the presence of wideband Gaussian interference, the performance improvement of quaternary CSK is more than 2 dB relative to binary CSK, but four filters matched to four sequences are required. Further gains and implementation costs occur as q increases.

Elimination of the lower branch in Fig. 2.29b leaves a system that uses a single CSK sequence and a minimum amount of hardware. The symbol 1 is signified by the transmission of the sequence, whereas the symbol 0 is signified by the absence of a transmission. Decisions are made after comparing the envelope-detector output with a threshold. One problem with this system is that the optimal threshold is a function of the amplitude of the received signal, which must somehow be estimated. Another problem is the degraded performance of the symbol synchronizer when many consecutive zeros are transmitted. Thus, a system with binary CSK is much more practical.

A direct-sequence system with DPSK signifies the symbol 1 by the transmission of a spreading sequence without any change in the carrier phase; the symbol 0 is signified by the transmission of the same sequence after a phase shift of π radians in the carrier phase or multiplication of the signal by -1. A matched filter despreads the received direct-sequence signal, as illustrated in Fig. 2.30. The filter output is applied to a standard DPSK demodulator that makes symbol decisions. An analysis of this system in the presence of wideband Gaussian interference indicates that it is more than 2 dB superior to the system with binary CSK. However, the system with DPSK is more sensitive to Doppler shifts and is more than 1 dB inferior to a system with coherent BPSK.

2.6.2 Multipath-Resistant Coherent System

Carrier synchronization is essential for the coherent demodulation of a direct-sequence signal. Prior to despreading, the signal-to-interference-plus-noise ratio (SINR) may be too low for the received signal to serve as the input to a phase-locked loop that produces a phase-coherent carrier. Although the despread matched-filter output has a large SINR near the autocorrelation peak, the average SINR may be

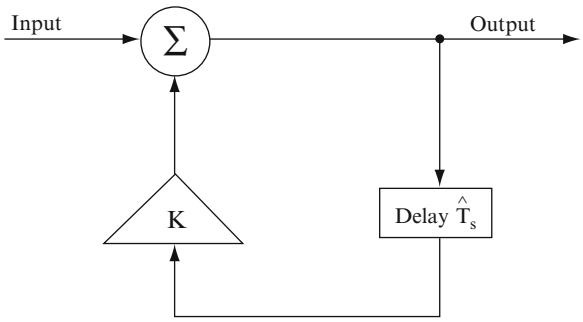

Fig. 2.31 Recirculation loop

insufficient for a phase-locked loop. An alternative approach is to use a recirculation loop to produce a synchronized carrier during the main lobe of the matched-filter output.

A *recirculation loop* is designed to reinforce a periodic input signal by positive feedback. As illustrated in Fig. 2.31, the feedback elements are an attenuator of gain K and a delay line with delay $\widehat{T}_s$ approximating a symbol duration T_s. The basic concept behind this architecture is that successive signal pulses are coherently added while the interference and noise are noncoherently added, thereby producing an output pulse with an improved SINR. The periodic input consists of N symbol pulses such that

$$s_0(t) = \sum_{i=0}^{N} g\left(t - iT_s\right) \tag{2.194}$$

where $g(t) = 0$ for $t < 0$ or $t \geq T_s$. The figure indicates that the loop output is

$$s_1(t) = s_0(t) + Ks_1\left(t - \widehat{T}_s\right). \tag{2.195}$$

Substitution of this equation into itself yields

$$s_1(t) = s_0(t) + Ks_0\left(t - \widehat{T}_s\right) + K^2 s_1\left(t - 2\widehat{T}_s\right). \tag{2.196}$$

Repeating this substitution process n times leads to

$$s_1(t) = \sum_{m=0}^{n} K^m s_0\left(t - m\widehat{T}_s\right) + K^{n+1} s_1\left[t - (n+1)\widehat{T}_s\right] \tag{2.197}$$

which indicates that $s_1(t)$ increases with n if $K \geq 1$ and enough input pulses are available. To prevent an eventual loop malfunction, $K < 1$ is a design requirement that is assumed henceforth.

During the interval $[n\widehat{T}_s, (n+1)\widehat{T}_s]$, n or fewer recirculations of the symbols have occurred. Since $s_1(t) = 0$ for $t < 0$, the substitution of (2.194) into (2.197) yields

$$s_1(t) = \sum_{m=0}^{n} \sum_{i=0}^{N} K^m g\left(t - m\widehat{T}_s - iT_s\right), \qquad n\widehat{T}_s \le t < (n+1)\widehat{T}_s. \tag{2.198}$$

This equation indicates that if $\widehat{T}_s$ is not exactly equal to T_s, then the pulses do not add coherently, and may combine destructively. However, since $K < 1$, the effect of a particular pulse decreases as m increases and will eventually be negligible. The delay $\widehat{T}_s$ is designed to match T_s. Suppose that the design error is small enough that

$$N\left|\widehat{T}_s - T_s\right| \ll \widehat{T}_s. \tag{2.199}$$

Since $t - m\widehat{T}_s - iT_s = t - (m+i)T_s - m(\widehat{T}_s - T_s)$ and $g(t)$ is time-limited, (2.199) and $n \le N$ imply that only the term in (2.198) with $i = n - m$ contributes appreciably to the output. Therefore,

$$s_1(t) \approx \sum_{m=0}^{n} K^m g\left[t - nT_s - m\left(\widehat{T}_s - T_s\right)\right], \qquad nT_s \le t < (n+1)T_s. \tag{2.200}$$

Let ν denote a positive integer such that K^m is negligible if $m > \nu$. Consider an input pulse of the form

$$g(t) = A(t)\cos 2\pi f_c t, \qquad 0 \le t < \min\left(T_s, \widehat{T}_s\right) \tag{2.201}$$

which implies that each of the N pulses in (2.194) has the same initial phase. Assume that the amplitude $A(t)$ varies slowly enough that

$$A\left[t - nT_s - m\left(\widehat{T}_s - T_s\right)\right] \approx A\left(t - nT_s\right), \qquad 0 \le m \le \nu \tag{2.202}$$

and that the design error is small enough that

$$\nu f_c\left|\widehat{T}_s - T_s\right| \ll 1. \tag{2.203}$$

Then (2.200) to (2.203) yield

$$\begin{aligned} s_1(t) &\approx g\left(t - nT_s\right) \sum_{m=0}^{n} K^m \\ &= g\left(t - nT_s\right)\left(\frac{1 - K^{n+1}}{1 - K}\right), \qquad nT_s \le t \le (n+1)T_s. \end{aligned} \tag{2.204}$$

If S is the average power in an input pulse, then (2.204) indicates that the average power in an output pulse during the interval $nT_s \leq t < (n+1)T_s$ is approximately

$$S_n = \left(\frac{1-K^{n+1}}{1-K}\right)^2 S, \qquad K < 1. \tag{2.205}$$

If $\widehat{T}_s$ is large enough that the recirculated noise is uncorrelated with the input noise, which has average power σ^2, then the output noise power after n recirculations is

$$\begin{aligned}\sigma_n^2 &= \sigma^2 \sum_{m=0}^{n} \left(K^2\right)^m \\ &= \sigma^2 \left(\frac{1-K^{2n+2}}{1-K^2}\right), \qquad K < 1.\end{aligned} \tag{2.206}$$

The improvement in the signal-to-noise ratio (SNR) due to the presence of the recirculation loop is

$$\begin{aligned}I(n,K) = \frac{S_n/\sigma_n^2}{S/\sigma^2} &= \frac{\left(1-K^{n+1}\right)(1+K)}{(1+K^{n+1})\quad(1-K)} \\ &\leq \frac{1+K}{1-K}, \qquad K < 1.\end{aligned} \tag{2.207}$$

Since it was assumed that K^m is negligibly small when $m > \nu$, the maximum improvement is nearly attained when $n \geq \nu$. However, the upper bound on ν for the validity of (2.203) decreases as the loop phase error $2\pi f_c|\widehat{T}_s - T_s|$ increases. Thus, K must be decreased as the phase error increases. The phase error of a practical SAW recirculation loop may be caused by a temperature fluctuation, a Doppler shift, oscillator instability, or an imprecise delay-line length. Various other loop imperfections limit the achievable value of K and, hence, the improvement that the loop can provide [6].

Figure 2.32 illustrates a *coherent decision-directed demodulator* for a direct-sequence signal with BPSK and the same carrier phase at the beginning of each symbol. The bandpass matched filter removes the spreading waveform and produces compressed sinusoidal pulses, as indicated by (2.168) and (2.169) when A is bipolar. A compressed pulse due to a direct-path signal may be followed by one or more compressed pulses due to multipath signals, as illustrated conceptually in Fig. 2.33a for pulses corresponding to the transmitted symbols 101. Each compressed pulse is delayed by one symbol and then mixed with the demodulator's output symbol. If this symbol is correct, it coincides with the same data symbol that is modulated onto the compressed pulse. Consequently, the mixer removes the data modulation and produces a phase-coherent reference pulse that is independent of the data symbol, as illustrated in Fig. 2.33b, where the middle pulses are inverted in phase relative to the corresponding pulses in Fig. 2.33a. The reference pulses are amplified by

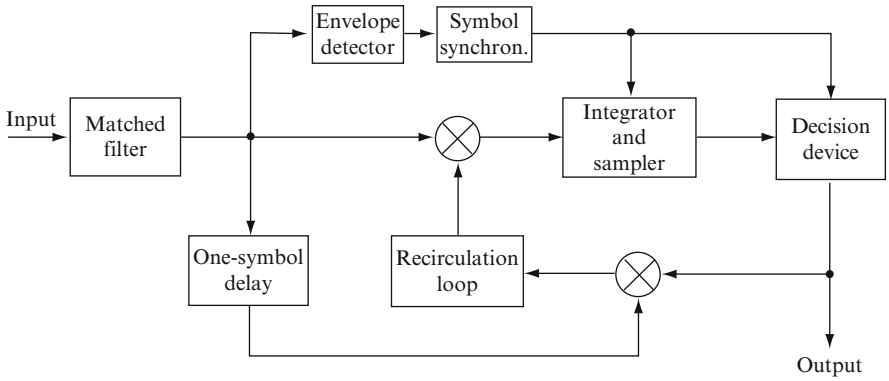

Fig. 2.32 Coherent decision-directed demodulator

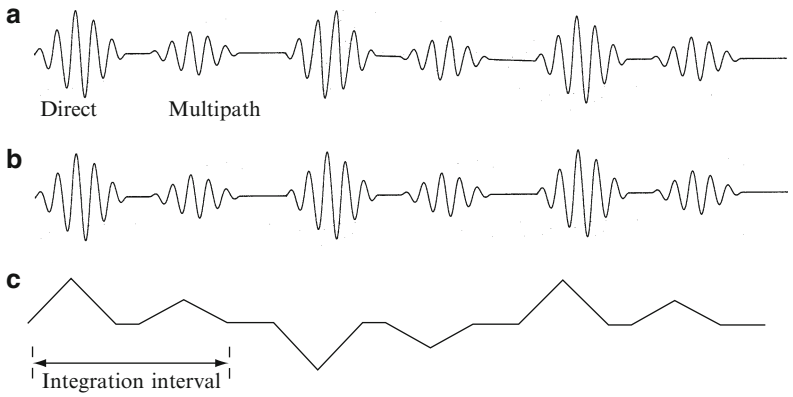

Fig. 2.33 Conceptual waveforms of demodulator: (**a**) matched-filter output, (**b**) recirculation loop input or output, and (**c**) baseband integrator input

a recirculation loop. The loop output and the matched-filter output are applied to a mixer that produces the baseband integrator input illustrated in Fig. 2.33c. The length of the integration interval is equal to a symbol duration. The integrator output is sampled and applied to a decision device that produces the data output. Since multipath components are coherently integrated, the demodulator provides an improved performance in a fading environment.

Even if the desired-signal multipath components are absent, the coherent decision-directed receiver potentially suppresses interference approximately as much as the correlator of Fig. 2.14. The decision-directed receiver is much simpler to implement because code acquisition and tracking systems are unnecessary, but it requires a short spreading sequence and an accurate recirculation loop. More efficient exploitation of multipath components is possible with rake combining (Chap. 5).

2.7 Rejection of Narrowband Interference

Narrowband interference presents a crucial problem for *spread-spectrum overlay systems*, which are systems that have been assigned a spectral band already occupied by narrowband communication systems. Jamming against tactical spread-spectrum communications is another instance of narrowband interference that may exceed the natural resistance of a practical spread-spectrum system, which has a limited processing gain. There are a wide variety of techniques that supplement the inherent ability of a direct-sequence system to reject narrowband interference [7, 8]. All of the techniques directly or indirectly exploit the spectral disparity between the narrowband interference and the wideband direct-sequence signal. The most useful methods can be classified as time-domain adaptive filtering, transform-domain processing, nonlinear filtering, or code-aided techniques. The general form of a receiver that rejects narrowband interference and demodulates a direct-sequence signal with BPSK is shown in Fig. 2.34. The processor, which follows the chip-rate sampling of the baseband signal, implements one of the rejection methods. Since the narrowband interference is rarely known with any precision, adaptive filters are an essential part of transform-domain processing and nonlinear filtering.

2.7.1 Adaptive Filters

2.7.1.1 Complex Gradients

A complex function $f(z)$ defined in a neighborhood of the point z_0 has a *derivative* at z_0 defined by

$$f'(z_0) = \lim_{\Delta z \to 0} \frac{f(z_0 + \Delta z) - f(z_0)}{\Delta z} \tag{2.208}$$

if the limit exists and is the same when z approaches z_0 along any path in the complex plane. The complex function $f(z)$ is *analytic* in a domain if $f(z)$ is differentiable at all points of the domain. Similar proofs establish the same differentiation rules as the standard ones in the calculus of real variables. Thus, the derivatives of sums, products, and quotients of differentiable functions are the same. The chain rule, the

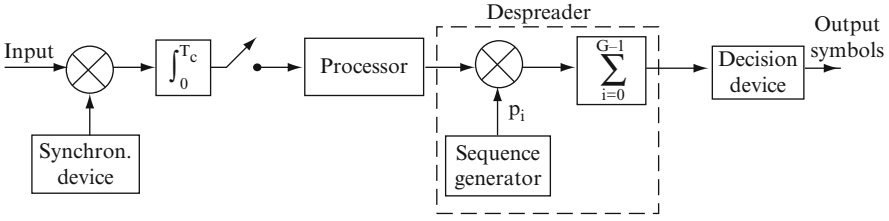

Fig. 2.34 Direct-sequence receiver with processor for rejecting narrowband interference

derivative of an exponential function, and the derivative of a variable raised to a power are the same.

The complex variable z may be expressed in terms of its real and imaginary parts as $z = x + jy$, where $j = \sqrt{-1}$. Similarly, $f(z)$ may be expressed as

$$f(z) = u(x, y) + j\,v(x, y). \tag{2.209}$$

If $f(z)$ is analytic in a domain, then the first partial derivatives of $u(x, y)$ and $v(x, y)$ exist and satisfy the *Cauchy–Riemann* conditions:

$$\frac{\partial u}{\partial x} = \frac{\partial v}{\partial y}, \quad \frac{\partial u}{\partial y} = -\frac{\partial v}{\partial x}. \tag{2.210}$$

Conversely, if the real-valued functions $u(x, y)$ and $v(x, y)$ have continuous first partial derivatives that satisfy the Cauchy–Riemann equations in a domain, then $f(z) = u(x, y) + j\,v(x, y)$ is analytic in that domain.

Let z_i, x_i and $y_i, i = 1, 2, \ldots, N$, denote the components of the $N \times 1$ column vectors $\mathbf{z}, \mathbf{x}$, and $\mathbf{y}$, respectively, where $\mathbf{z} = \mathbf{x} + j\mathbf{y}$. The *gradient* of f with respect to the N-dimensional, complex vector $\mathbf{z}$ is defined as the column vector $\nabla_{\mathbf{z}} f$ with components $\partial f/\partial z_i, i = 1, 2, \ldots, N$. Similarly, $\nabla_x f$ and $\nabla_y f$ are the $N \times 1$ gradient vectors with respect to the real-valued vectors $\mathbf{x}$ and $\mathbf{y}$, respectively. The *complex gradient* with respect to the N-dimensional, complex-valued vector $\mathbf{z} = \mathbf{x} + j\mathbf{y}$ is defined as

$$\bar{\nabla}_{\mathbf{z}} = \nabla_{\mathbf{x}} + j\,\nabla_{\mathbf{y}}. \tag{2.211}$$

Let $g(\mathbf{z}, \mathbf{z}^*)$ denote a real-valued function of $\mathbf{z}$ and its complex conjugate $\mathbf{z}^*$. The function $g(\mathbf{z}, \mathbf{z}^*)$ is an analytic function of $\mathbf{z}$ and $\mathbf{z}^*$ if $g(\mathbf{z}, \mathbf{z}^*)$ is an analytic function of each z_i when $\mathbf{z}^*$ is held constant and an analytic function of each z_i^* when $\mathbf{z}$ is held constant. Thus, if $\mathbf{z}$ and $\mathbf{z}^*$ are regarded as independent vectors, then $g(\mathbf{z}, \mathbf{z}^*)$ is an analytic function of both of these vectors. We define $\nabla_{z^*} f$ as the gradient of f with respect to $\mathbf{z}^*$. Since $z_i = x_i + jy_i$,

$$\frac{\partial z_i}{\partial x_i} = 1, \quad \frac{\partial z_i}{\partial y_i} = j, \quad \frac{\partial z_i^*}{\partial x_i} = 1, \quad \frac{\partial z_i^*}{\partial y_i} = -j. \tag{2.212}$$

The chain rule then implies that

$$\frac{\partial g}{\partial x_i} = \frac{\partial g}{\partial z_i} + \frac{\partial g}{\partial z_i^*}, \quad \frac{\partial g}{\partial y_i} = j\,\frac{\partial g}{\partial z_i} - j\,\frac{\partial g}{\partial z_i^*} \tag{2.213}$$

which yields

$$\begin{aligned} \bar{\nabla}_z g\left(\mathbf{z}, \mathbf{z}^*\right) &= \nabla_x g + j\,\nabla_y g \\ &= \nabla_z g + \nabla_{z^*} g + j\,\left(j\,\nabla_z g - j\,\nabla_{z^*} g\right). \end{aligned} \tag{2.214}$$

Thus,

$$\bar{\nabla}_z g\left(\mathbf{z}, \mathbf{z}^*\right) = 2\nabla_{z^*} g\left(\mathbf{z}, \mathbf{z}^*\right). \tag{2.215}$$

This result allows a major simplification in calculations.

As a one-dimensional example, consider the real-valued function $f(z) = |z|^2 = x^2 + y^2$. The Cauchy–Riemann equations are not satisfied so $f(z)$ is not an analytic function of z. However, the function $g(z, z^*) = zz^*$is an analytic function of z and z^*. Therefore, $\bar{\nabla}_z g(z, z^*) = 2\nabla_{z^*} g(z, z^*) = 2z = 2x + 2y = \bar{\nabla}_z f(z)$.

2.7.1.2 Optimal Weight Vector

The input and weight vectors of an adaptive filter are

$$\mathbf{x} = [x_1\ x_2 \ldots x_N]^T, \quad \mathbf{W} = [W_1\ W_2 \ldots W_N]^T \tag{2.216}$$

where the components of the vectors may be real or complex. The filter output is the scalar

$$y = \mathbf{W}^H \mathbf{x}. \tag{2.217}$$

The derivation of the optimal filter weights depends on the specification of a performance criterion or estimation procedure. A number of different estimators of the desired signal can be implemented by linear filters that produce (2.217). Unconstrained estimators that depend only on the second-order moments of $\mathbf{x}$ can be derived by using performance criteria based on the mean square error or the SNR of the filter output. Similar estimators result from using the maximum-*a-posteriori* or the maximum-likelihood criteria, but the standard application of these criteria includes the restrictive assumption that any interference in $\mathbf{x}$ has a Gaussian distribution.

The difference between the desired response d and the filter output is the *error signal*:

$$\epsilon = d - \mathbf{W}^H \mathbf{x}. \tag{2.218}$$

The most widely used method of estimating the desired signal is based on the minimization of the expected value of the squared error magnitude, which is proportional to the mean power in the error signal. Let H denote the conjugate transpose and an asterisk denote the complex conjugate of a matrix, vector, or scalar. We obtain

$$\begin{aligned} E[|\epsilon|^2] &= E\left[\epsilon\epsilon^*\right] = \mathrm{E}\left[\left(d - \mathbf{W}^H\mathbf{x}\right)\left(d^* - \mathbf{x}^H\mathbf{W}\right)\right] \\ &= E[|d|^2] - \mathbf{W}^H\mathbf{R}_{xd} - \mathbf{R}_{xd}^H\mathbf{W} + \mathbf{W}^H\mathbf{R}_{xx}\mathbf{W} \end{aligned} \tag{2.219}$$

where

$$\mathbf{R}_{xx} = E\left[\mathbf{x}\mathbf{x}^H\right] \tag{2.220}$$

is the $N \times N$ Hermitian *correlation matrix* of $\mathbf{x}$ and

$$\mathbf{R}_{xd} = E\left[\mathbf{x}d^*\right] \tag{2.221}$$

is the $N \times 1$ *cross-correlation* vector. If we assume that $y \neq \mathbf{0}$ when $\mathbf{W} \neq \mathbf{0}$, then $\mathbf{R}_{xx}$ must be positive definite.

In terms of its real part $\mathbf{W}_R$, and its imaginary part $\mathbf{W}_I$, a complex weight vector is defined as

$$\mathbf{W} = \mathbf{W}_R + j\,\mathbf{W}_I\,. \tag{2.222}$$

We define ∇_{w*}, ∇_{wr}, and ∇_{wi} as the gradients with respect to $\mathbf{W}^*$, $\mathbf{W}_R$, and $\mathbf{W}_I$, respectively. The *complex gradient* with respect to $\mathbf{W}$ is defined as

$$\bar{\nabla}_w = \nabla_{wr} + j\,\nabla_{wi}\,. \tag{2.223}$$

Straightforward calculations verify that $\nabla_{\mathbf{x}}\left(\mathbf{x}^{\mathbf{T}}\mathbf{y}\right) = \nabla_{\mathbf{x}}\left(\mathbf{y}^{\mathbf{T}}\mathbf{x}\right) = \mathbf{y}$. Since $E\left[|\epsilon|^2\right]$ is an analytic function of $\mathbf{W}$ and $\mathbf{W}^*$, (2.219) and (2.215) yield

$$\bar{\nabla}_w E\left[|\epsilon|^2\right] = 2\mathbf{R}_{xx}\mathbf{W} - 2\mathbf{R}_{xd}\,. \tag{2.224}$$

Since $\nabla_{wr} g = 0$ and $\nabla_{wi} g = 0$ imply that $\bar{\nabla}_w g = 0$, a necessary condition for the optimal weight is obtained by setting $\bar{\nabla}_w E[|\epsilon|^2] = \mathbf{0}$. Thus, if $\mathbf{R}_{xx}$ is positive definite and hence nonsingular, the necessary condition provides the *Wiener–Hopf equation* for the optimal weight vector:

$$\mathbf{W}_0 = \mathbf{R}_{xx}^{-1}\mathbf{R}_{xd}\,. \tag{2.225}$$

To prove the optimality, we substitute $\mathbf{W} = \mathbf{W}_0$ into (2.219) to obtain the corresponding mean square error

$$\epsilon_m^2 = E[|d|^2] - \mathbf{R}_{xd}^H\mathbf{R}_{xx}^{-1}\mathbf{R}_{xd}\,. \tag{2.226}$$

Equations (2.219), (2.225), and (2.226) imply that

$$E[|\epsilon|^2] = \epsilon_m^2 + (\mathbf{W} - \mathbf{W}_0)^H\,\mathbf{R}_{xx}\,(\mathbf{W} - \mathbf{W}_0)\,. \tag{2.227}$$

Since $\mathbf{R}_{xx}$ is positive definite, this equation shows that the Wiener–Hopf equation provides a unique optimal weight vector and that (2.226) gives the minimum mean square error (MMSE).

2.7.1.3 LMS Algorithm

Since the computational difficulty of inverting the correlation matrix is considerable when the number of weights is large, and insofar as time-varying signal statistics may require frequent computations, adaptive algorithms not entailing matrix

inversion have been developed. Suppose that a performance measure, $P(\mathbf{W})$, is defined so that it has a minimum value when the weight vector has its optimal value. In the *method of steepest descent*, the weight vector at discrete-time $n+1$ is changed along the direction of the negative gradient of the performance measure at discrete-time n. This direction gives the largest decrease in $P(\mathbf{W})$. If the signals and weights are complex, separate steepest-descent equations can be written for the real and imaginary parts of the weight vector. Combining these equations, we obtain

$$\mathbf{W}(n+1) = \mathbf{W}(n) - \mu \bar{\nabla}_w P(\mathbf{W}(n)) \tag{2.228}$$

where the *adaptation constant* μ controls the rate of convergence and the stability. For complex signals and weights, a suitable performance measure is $P(\mathbf{W}) = E[|\epsilon|^2]$. The application of (2.224) and (2.228) leads to the *steepest-descent algorithm*:

$$\mathbf{W}(n+1) = \mathbf{W}(n) - 2\mu \left[\mathbf{R}_{xx}\mathbf{W}(n) - \mathbf{R}_{xd}\right]. \tag{2.229}$$

This ideal algorithm produces a deterministic sequence of weights and does not require a matrix inversion, but it requires the knowledge of $\mathbf{R}_{xx}$ and $\mathbf{R}_{xd}$. However, the possible presence of interference means that $\mathbf{R}_{xx}$ is unknown. In the absence of information about the direction of the desired signal, $\mathbf{R}_{xd}$ is also unknown.

Let $\mathbf{x}(n)$ and $d(n)$ denote the input vector and the desired response, respectively, at discrete-time n. The *least-mean-square (LMS) algorithm* is obtained when $\mathbf{R}_{xx}$ is estimated by $\mathbf{x}(n)\mathbf{x}^H(n)$, $\mathbf{R}_{xd}$ is estimated by $\mathbf{x}(n)d^*(n)$, and (2.218) is applied in (2.229). The LMS algorithm is

$$\mathbf{W}(n+1) = \mathbf{W}(n) + 2\mu\epsilon^*(n)\mathbf{x}(n) \tag{2.230}$$

where

$$\epsilon(n) = d(n) - \mathbf{W}^H(n)\mathbf{x}(n). \tag{2.231}$$

For a fixed value of $\mathbf{W}(n)$, the product $\epsilon^*(n)\mathbf{x}(n)$ is an unbiased estimate of the gradient vector. According to this algorithm, the next weight vector is obtained by adding to the present weight vector the input vector scaled by the amount of error. It is shown in Appendix C that, for an appropriate value of μ, the mean of the weight vector converges to the optimal value given by the Wiener–Hopf equation.

2.7.2 Time-Domain Adaptive Filtering

A time-domain *adaptive filter* [9] for interference suppression processes the baseband sample values of a received signal to adaptively estimate the interference. This estimate is subtracted from the sample values, thereby canceling the interference. The adaptive filter is primarily a predictive system that exploits the inherent predictability of a narrowband signal to form an accurate replica of it for the

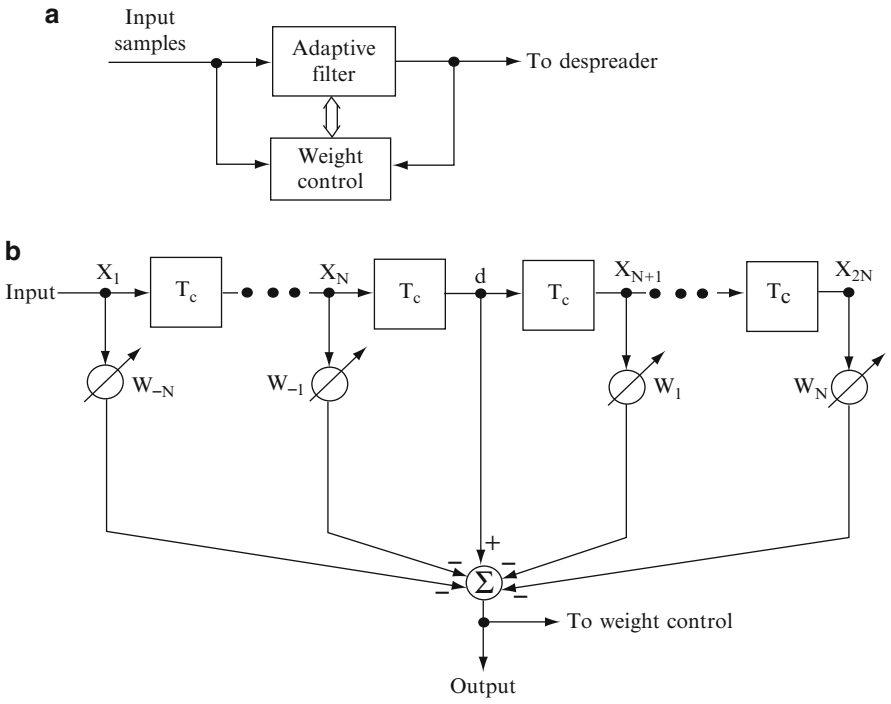

Fig. 2.35 (**a**) Processor using adaptive filter and (**b**) two-sided adaptive transversal filter

subtraction. Since the wideband desired signal is largely unpredictable, it does not significantly impede the prediction of a narrowband signal. When adaptive filtering is used, the processor in Fig. 2.34 has the form of Fig. 2.35a. The adaptive filter may be a one-sided or two-sided transversal filter.

The *two-sided adaptive transversal filter* multiplies each tap output by a weight except for the central tap output, as diagrammed in Fig. 2.35b. This filter is an *interpolator* in that it uses *both* past and future samples to estimate the value to be subtracted. The two-sided filter provides a better performance than the one-sided filter, which is a *predictor*. The adaptive algorithm of the weight-control mechanism is designed to adjust the weights so that the power in the filter output is minimized. The direct-sequence components of the tap outputs, which are delayed by integer multiples of a chip duration, are largely uncorrelated with each other, but the narrowband interference components are strongly correlated. As a result, the adaptive algorithm causes the interference cancellation in the filter output, but the direct-sequence signal is largely unaffected.

An adaptive filter with $2N + 1$ taps and $2N$ weights, as shown in Fig. 2.35b, has input vector at iteration n given by

$$\mathbf{x}(n) = [x_1(n)\ x_2(n) \ldots x_{2N}(n)]^T \tag{2.232}$$

and weight vector

$$\mathbf{W}(n) = [W_{-N}(n)\ W_{-N+1}(n) \ldots W_{-1}(n)\ W_1(n) \ldots W_N(n)]^T \tag{2.233}$$

where the central tap output, which is denoted by $d(n)$ and serves as an approximation of the desired response, has been excluded from $\mathbf{x}(n)$. Since coherent demodulation produces real-valued inputs to the adaptive filter, $\mathbf{x}(n)$ and $\mathbf{W}(n)$ are assumed to have real-valued components. The optimal weight vector is given by (2.225), but the symmetric *correlation matrix* of $\mathbf{x}(n)$ is defined as $\mathbf{R}_{xx} = E[\mathbf{x}(n)\mathbf{x}^T(n)]$, and the *cross-correlation vector* is defined as $\mathbf{R}_{xd} = E[\mathbf{x}(n)d(n)]$.

The least-mean-square (LMS) algorithm computes the weight vector as

$$\mathbf{W}(n+1) = \mathbf{W}(n) + 2\mu\epsilon(n)\mathbf{x}(n) \tag{2.234}$$

where $\epsilon(n) = d(n) - y(n)$ is the estimation error, $y(n) = \mathbf{W}^T(n)\mathbf{x}(n)$ is the filter output, and μ is the adaptation constant, which controls the rate of convergence of the algorithm. The output of the adaptive filter is $\epsilon(n)$, which is applied to the despreader. Under certain conditions, the mean weight vector converges to $\mathbf{W}_0$ after a number of iterations of the adaptive algorithm. If it is assumed that $\mathbf{W} = \mathbf{W}_0$, then a straightforward analysis indicates that the adaptive transversal filter provides a substantial suppression of narrowband interference [7]. Although the interference suppression increases with the number of taps, it is always incomplete if the interference has a nonzero bandwidth because a finite-impulse-response filter can only place a finite number of zeros in the frequency domain.

The adaptive transversal filter is inhibited by the presence of direct-sequence components in the filter input vector $\mathbf{x}(n)$. These components can be suppressed by using decision-directed feedback, as shown in Fig. 2.36. Previously detected symbols remodulate the spreading sequence delayed by G chips (long sequence) or one period of the spreading sequence (short sequence). After an amplitude compensation by a factor η, the resulting sequence provides estimates of the direct-sequence components of previous input samples. A subtraction then provides estimated sample values of the interference plus noise that are largely free of direct-sequence contamination. These samples are then applied to an adaptive transversal filter that has the form of Fig. 2.35 except that it has no central tap. The transversal filter output consists of refined interference estimates that are subtracted from the input samples to produce samples that have relatively small interference components. An erroneous symbol from the decision device causes an enhanced direct-sequence component in samples applied to the transversal filter, and error propagation is possible. However, for moderate values of the signal-to-interference ratio at the input, the performance is not degraded significantly.

Adaptive filtering is only effective after the convergence of the adaptive algorithm, which may not be able to track time-varying interference. In contrast, transform-domain processing suppresses interference almost instantaneously.

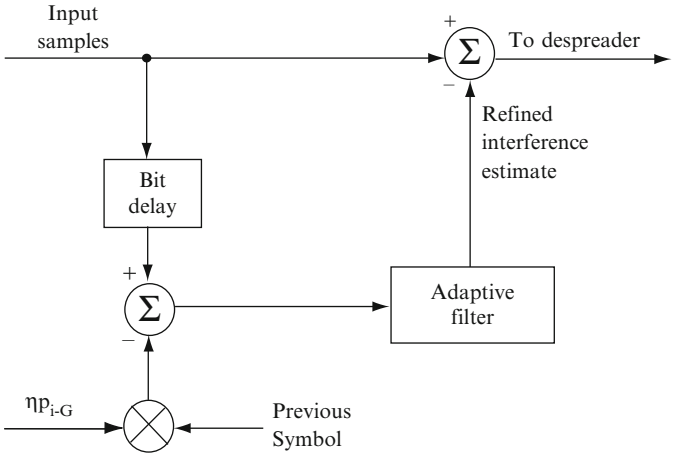

Fig. 2.36 Processor with decision-directed adaptive filter

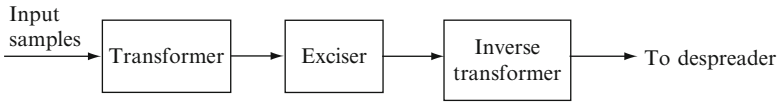

Fig. 2.37 Transform-domain processor

2.7.3 Transform-Domain Processing

The input of a *transform-domain processor* could be a continuous-time received signal that feeds a real-time Fourier transformer implemented as a chirp transform processor [2]. In a more versatile implementation, which is depicted in Fig. 2.37 and assumed henceforth, the input consists of the output samples of a chip-matched filter. Blocks of these samples feed a discrete-time Fourier or wavelet transformer. The transform is selected so that the transform-domain forms of the desired signal and interference are easily distinguished. Ideally, the transform produces interference components that are largely confined to a few transform bins while the desired-signal components have nearly the same magnitude in all the transform bins. A simple exciser can then suppress the interference with little impact on the desired signal by setting to zero the spectral weights corresponding to components in bins containing strong interference while setting to one all remaining spectral weights. The decision as to which bins contain interference can be based on the comparison of each component to a threshold or by selecting those transform bins with the largest average magnitudes. After the excision operation, the desired signal is largely restored by the inverse transformer.

Much better performance against stationary narrowband interference may be obtained by using a transform-domain adaptive filter as the exciser [10]. This

filter adjusts a single nonbinary weight at each transform-bin output. The adaptive algorithm is designed to minimize the difference between the weighted transform and a desired signal that is the transform of the spreading sequence used by the input block of the processor. If the direct-sequence signal uses the same short spreading sequence for each data symbol and each processor input block includes the chips for a single data symbol, then the desired-signal transform may be stored in a read-only memory. However, if a long spreading sequence is used, then the desired-signal transform may have to be continuously produced from the output of the receiver's code generator. The main disadvantage of the adaptive filter is that its convergence rate may be insufficient to track rapidly time-varying interference.

A transform that operates on disjoint blocks of N input samples may be defined in terms of N orthonormal, N-component basis vectors:

$$\boldsymbol{\phi}_i = [\phi_{i1}\ \phi_{i2} \ldots \phi_{iN}]^T, \qquad i = 1, 2, \ldots, N \tag{2.235}$$

which span a linear vector space of dimension N. Since the components may be complex numbers, the orthonormality implies that

$$\boldsymbol{\phi}_i^H \boldsymbol{\phi}_k = \begin{cases} 0, & i \neq k \\ 1, & i = k \end{cases} \tag{2.236}$$

The input block

$$\mathbf{x} = [x_1\ x_2 \ldots x_N]^T \tag{2.237}$$

may be expressed in terms of the basis as

$$\mathbf{x} = \sum_{i=1}^{N} c_i \boldsymbol{\phi}_i \tag{2.238}$$

where

$$c_i = \boldsymbol{\phi}_i^H \mathbf{x}, \quad i = 1, 2, \ldots N. \tag{2.239}$$

If the discrete Fourier transform is used, then $\phi_{ik} = \exp(j2\pi ik/N)$, where $j = \sqrt{-1}$.

The transformer extracts the vector

$$\mathbf{c} = [c_1\ c_2\ \ldots\ c_N]^T \tag{2.240}$$

by computing

$$\mathbf{c} = \mathbf{B}^H \mathbf{x} \tag{2.241}$$

where $\mathbf{B}$ is the unitary matrix of basis vectors:

$$\mathbf{B} = [\boldsymbol{\phi}_1\ \boldsymbol{\phi}_2\ \ldots\ \boldsymbol{\phi}_N]. \tag{2.242}$$

The exciser weights each component of the transform $\mathbf{c}$ by computing

$$\mathbf{e} = \mathbf{W}_d \mathbf{c} \tag{2.243}$$

where $\mathbf{W}_d$ is the $N \times N$ diagonal weight matrix with diagonal elements W_1, W_2, ..., W_N. The inverse transformer then produces the excised block that is applied to the despreader:

$$\mathbf{z} = [z_1 \; z_2 \ldots z_N]^T = \mathbf{B}\,\mathbf{e} = \mathbf{B}\,\mathbf{W}_d \mathbf{c} = \mathbf{B}\,\mathbf{W}_d \mathbf{B}^H \mathbf{x}. \tag{2.244}$$

If there were no weighting, then $\mathbf{W}_d = \mathbf{I}$. Since $\mathbf{B}\mathbf{B}^H = \mathbf{I}$, $\mathbf{z} = \mathbf{x}$ would result, as expected when the transformer and inverse transformer are in tandem. In general, the diagonal elements of $\mathbf{W}_d$ are either set by a threshold device fed by $\mathbf{c}$ or they are the outputs of the weight-control mechanism of an adaptive filter. When N equals the processing gain G and the input comprises the unmodulated spreading sequence, the despreader correlates its input block with the appropriate segment of the spreading sequence to form the decision variable:

$$V = \sum_{i=1}^{G} p_i z_i. \tag{2.245}$$

The filtering and despreading can be simultaneously performed in the transform domain. Let

$$\mathbf{p} = [p_1 \; p_2 \; \ldots \; p_G]^T \tag{2.246}$$

denote a synchronous replica of the spreading sequence, which is generated by the receiver code generator. Then (2.244) to (2.246) give

$$V = \mathbf{p}^T \mathbf{z} = \mathbf{p}^T \mathbf{B} \mathbf{W}_d \mathbf{c}. \tag{2.247}$$

Thus, if the spreading sequence is used to produce the matrix $\mathbf{p}^T \mathbf{B} \mathbf{W}_d$, then the product of this matrix and the transform $\mathbf{c}$ gives V without the need for a separate inverse transformer and despreader.

2.7.4 Nonlinear Filtering

By modeling the narrowband interference as part of a dynamic linear system, one can use the Kalman–Bucy filter [9] to extract an optimal linear estimate of the interference. A subtraction of this estimate from the filter input then removes a large part of the interference from the despreader input. However, a superior nonlinear filter can be designed by approximating an extension of the Kalman–Bucy filter.

Consider the estimation of an $n \times 1$ state vector $\mathbf{x}_k$ of a dynamic system based on the $r \times 1$ observation vector $\mathbf{z}_k$. Let $\boldsymbol{\phi}_k$ denote the $n \times n$ state transition matrix, $\mathbf{H}_k$

an $r \times n$ observation matrix, and $\mathbf{u}_k$ and $\mathbf{v}_k$ disturbance vectors of dimensions $n \times 1$ and $r \times 1$, respectively. According to the linear dynamic system model, the state and observation vectors satisfy

$$\mathbf{x}_{k+1} = \boldsymbol{\phi}_k \mathbf{x}_k + \mathbf{u}_k, \qquad 0 \le k < \infty \tag{2.248}$$

$$\mathbf{z}_k = \mathbf{H}_k \mathbf{x}_k + \mathbf{v}_k, \qquad 0 \le k < \infty. \tag{2.249}$$

It is assumed that the sequences $\{\mathbf{u}_k\}, \{\mathbf{v}_k\}$ are independent sequences of independent, zero-mean random vectors that are also independent of the initial state $\mathbf{x}_0$. The covariance of $\mathbf{u}_k$ is $E\left[\mathbf{u}_k \mathbf{u}_k^T\right] = \mathbf{Q}_k$. Let $Z^k = (\mathbf{z}_1, \mathbf{z}_2, \ldots \mathbf{z}_k)$ denote the first k observation vectors. Let $f(\mathbf{z}_k | Z^{k-1})$ and $f(\mathbf{x}_k | Z^{k-1})$ denote the probability density functions of $\mathbf{z}_k$ and $\mathbf{x}_k$, respectively, conditioned on Z^{k-1}. A fundamental result of estimation theory is that the estimate $\hat{\mathbf{x}}_k$ that minimizes the mean-norm-squared error $E\left[\|\mathbf{x}_k - \hat{\mathbf{x}}_k\|^2\right]$ is the expectation conditioned on Z^k:

$$\hat{\mathbf{x}}_k = E\left[\mathbf{x}_k \,\middle|\, Z^k\right]. \tag{2.250}$$

The corresponding conditional covariance is denoted by

$$\mathbf{P}_k = E\left[(\mathbf{x}_k - \hat{\mathbf{x}}_k)(\mathbf{x}_k - \hat{\mathbf{x}}_k)^T \,\middle|\, Z^k\right]. \tag{2.251}$$

From (2.248), it follows that the expectation of $\mathbf{x}_k$ conditioned on Z^{k-1} is

$$\bar{\mathbf{x}}_k = E\left[\mathbf{x}_k \,\middle|\, Z^{k-1}\right] = \boldsymbol{\phi}_{k-1} \hat{\mathbf{x}}_{k-1}. \tag{2.252}$$

The covariance of $\mathbf{x}_k$ conditioned on Z^{k-1} is defined as

$$\mathbf{M}_k = E\left[(\mathbf{x}_k - \bar{\mathbf{x}}_k)(\mathbf{x}_k - \bar{\mathbf{x}}_k)^T \,\middle|\, Z^{k-1}\right]. \tag{2.253}$$

The following theorem due to Masreliez extends the Kalman–Bucy filter.

Theorem. *Assume that $f(\mathbf{x}_k | Z^{k-1})$ is a Gaussian density with mean $\bar{\mathbf{x}}_k$ and $n \times n$ covariance matrix $\mathbf{M}_k$, and that $f(\mathbf{z}_k | Z^{k-1})$ is twice differentiable with respect to the components of $\mathbf{z}_k$. Then the conditional expectation $\hat{\mathbf{x}}_k$ and the conditional covariance $\mathbf{P}_k$ satisfy*

$$\hat{\mathbf{x}}_k = \bar{\mathbf{x}}_k + \mathbf{M}_k \mathbf{H}_k^T \mathbf{g}_k(\mathbf{z}_k) \tag{2.254}$$

$$\mathbf{P}_k = \mathbf{M}_k - \mathbf{M}_k \mathbf{H}_k^T \mathbf{G}_k(\mathbf{z}_k) \mathbf{H}_k \mathbf{M}_k \tag{2.255}$$

$$\mathbf{M}_{k+1} = \boldsymbol{\phi}_k \mathbf{P}_k \boldsymbol{\phi}_k^T + \mathbf{Q}_k \tag{2.256}$$

$$\bar{\mathbf{x}}_{k+1} = \boldsymbol{\phi}_k \hat{\mathbf{x}}_k \tag{2.257}$$

where $\mathbf{g}_k(\mathbf{z}_k)$ *is an* $r \times 1$ *vector with components*

$$\{\mathbf{g}_k(\mathbf{z}_k)\}_i = -\frac{1}{f\left(\mathbf{z}_k \left| Z^{k-1}\right.\right)} \frac{\partial f\left(\mathbf{z}_k \left| Z^{k-1}\right.\right)}{\partial z_{ki}} \tag{2.258}$$

$\mathbf{G}_k(\mathbf{z}_k)$ *is an* $r \times r$ *matrix with elements*

$$\{\mathbf{G}_k(\mathbf{z}_k)\}_{il} = \frac{\partial \{\mathbf{g}_k(\mathbf{z}_k)\}_i}{\partial z_{kl}} \tag{2.259}$$

and z_{kl} *is the* l*th component of* $\mathbf{z}_k$.

Proof. When $\mathbf{x}_k$ is given, (2.252) indicates that $\mathbf{z}_k$ is independent of Z^{k-1}. Therefore, Bayes' rule gives

$$f\left(\mathbf{x}_k \left| Z^k\right.\right) = \frac{f\left(\mathbf{x}_k \left| Z^{k-1}\right.\right) f\left(\mathbf{z}_k \left| \mathbf{x}_k\right.\right)}{f\left(\mathbf{z}_k \left| Z^{k-1}\right.\right)}. \tag{2.260}$$

With the concise notation $b = [f(\mathbf{z}_k|Z^{k-1})]^{-1}$, (2.250) and the fact that a density is a scalar function yield

$$\begin{aligned}\hat{\mathbf{x}}_k - \bar{\mathbf{x}}_k &= b\int_{R^n} (\mathbf{x}_k - \bar{\mathbf{x}}_k)\, f\left(\mathbf{z}_k \left| \mathbf{x}_k\right.\right) f\left(\mathbf{x}_k \left| Z^{k-1}\right.\right) d\mathbf{x}_k \\ &= b\mathbf{M}_k \int_{R^n} f\left(\mathbf{z}_k \left| \mathbf{x}_k\right.\right) \mathbf{M}_k^{-1} (\mathbf{x}_k - \bar{\mathbf{x}}_k)\, f\left(\mathbf{x}_k \left| Z^{k-1}\right.\right) d\mathbf{x}_k. \end{aligned} \tag{2.261}$$

Using the Gaussian density $f(\mathbf{x}_k|Z^{k-1})$, (2.252), and (2.253), and then integrating by parts and observing that the Gaussian density $f\left(\mathbf{x}_k \left| Z^{k-1}\right.\right)$ is zero at its extreme points, we obtain

$$\begin{aligned}\hat{\mathbf{x}}_k - \bar{\mathbf{x}}_k &= -b\mathbf{M}_k \int_{R^n} f\left(\mathbf{z}_k \left| \mathbf{x}_k\right.\right) \frac{\partial}{\partial \mathbf{x}_k} f\left(\mathbf{x}_k \left| Z^{k-1}\right.\right) d\mathbf{x}_k \\ &= b\mathbf{M}_k \int_{R^n} f\left(\mathbf{x}_k \left| Z^{k-1}\right.\right) \frac{\partial}{\partial \mathbf{x}_k} f\left(\mathbf{z}_k \left| \mathbf{x}_k\right.\right) d\mathbf{x}_k \end{aligned} \tag{2.262}$$

where the $n \times 1$ gradient vector $\partial/\partial\mathbf{x}_k$ has $\partial/\partial x_{ki}$ as its ith component. Equation (2.249) implies that

$$\begin{aligned}\frac{\partial}{\partial \mathbf{x}_k} f\left(\mathbf{z}_k \left| \mathbf{x}_k\right.\right) &= \frac{\partial}{\partial \mathbf{x}_k} f_v(\mathbf{z}_k - \mathbf{H}_k\mathbf{x}_k) = -\mathbf{H}_k^T \frac{\partial}{\partial \mathbf{z}_k} f_v(\mathbf{z}_k - \mathbf{H}_k\mathbf{x}_k) \\ &= -\mathbf{H}_k^T \frac{\partial}{\partial \mathbf{z}_k} f\left(\mathbf{z}_k \left| \mathbf{x}_k\right.\right) \end{aligned} \tag{2.263}$$

where $f_v(\ )$ is the density of $\mathbf{v}_k$. Substitution of this equation into the preceding one gives

$$\begin{aligned}\hat{\mathbf{x}}_k - \bar{\mathbf{x}}_k &= -b\mathbf{M}_k\mathbf{H}_k^T \int_{R^n} f\left(\mathbf{x}_k \left| Z^{k-1}\right.\right) \frac{\partial}{\partial \mathbf{z}_k} f\left(\mathbf{z}_k \left| \mathbf{x}_k\right.\right) d\mathbf{x}_k \\ &= -b\mathbf{M}_k\mathbf{H}_k^T \frac{\partial}{\partial \mathbf{z}_k} \int_{R^n} f\left(\mathbf{x}_k \left| Z^{k-1}\right.\right) f\left(\mathbf{z}_k \left| \mathbf{x}_k\right.\right) d\mathbf{x}_k \end{aligned} \tag{2.264}$$

where the second equality results because $f(\mathbf{x}_k|Z^{k-1})$ is not a function of $\mathbf{z}_k$. Substituting (2.250) into this equation and evaluating the integral, we obtain (2.254).

To derive (2.255), we add and subtract $\bar{\mathbf{x}}_k$ in (2.251) and simplify, which gives

$$\mathbf{P}_k = E\left[\left(\mathbf{x}_k - \bar{\mathbf{x}}_k\right)\left(\mathbf{x}_k - \bar{\mathbf{x}}_k\right)^T \left| Z^k \right.\right] - \left(\hat{\mathbf{x}}_k - \bar{\mathbf{x}}_k\right)\left(\hat{\mathbf{x}}_k - \bar{\mathbf{x}}_k\right)^T. \tag{2.265}$$

The second term of this equation may be evaluated by substituting (2.254). The first term may be evaluated in a similar manner as the derivation of (2.254) except that an integration by parts must be done twice. After a tedious calculation, we obtain (2.255). Equation (2.256) is derived by using the definition of $\mathbf{M}_{k+1}$ given by (2.253) and then substituting (2.248), (2.252), and (2.251). Equation (2.257) follows from (2.252). □

The filter defined by this theorem is the Kalman–Bucy filter if $f(\mathbf{z}_k|Z^{k-1})$ is a Gaussian density. Since (2.252) and (2.256) indicate that the covariance of $\mathbf{z}_k$ conditioned on Z^{k-1} is $\mathbf{H}_k\mathbf{M}_k\mathbf{H}_k^T + \mathbf{R}_k$, where $\mathbf{R}_k = E\left[\mathbf{v}_k\mathbf{v}_k^T\right]$, a Gaussian density implies that

$$\mathbf{g}_k\left(\mathbf{z}_k\right) = \left(\mathbf{H}_k\mathbf{M}_k\mathbf{H}_k^T + \mathbf{R}_k\right)^{-1}\left(\mathbf{z}_k - \mathbf{H}_k\bar{\mathbf{x}}_k\right) \tag{2.266}$$

$$\mathbf{G}_k\left(\mathbf{z}_k\right) = \left(\mathbf{H}_k\mathbf{M}_k\mathbf{H}_k^T + \mathbf{R}_k\right)^{-1}. \tag{2.267}$$

Substitution of these two equations into (2.254) and (2.255) yields the usual Kalman–Bucy equations.

To apply this theorem to the interference suppression problem, the narrowband interference sequence $\{i_k\}$ at the filter input is modeled as an autoregressive process that satisfies

$$i_k = \sum_{l=1}^{q} \phi_l i_{k-l} + e_k \tag{2.268}$$

where e_k is a white Gaussian process with variance σ_i^2 and the $\{\phi_l\}$ are known to the receiver. The state-space representation of the system is

$$\mathbf{x}_k = \boldsymbol{\phi}\mathbf{x}_{k-1} + \mathbf{u}_k \tag{2.269}$$

$$z_k = \mathbf{H}\mathbf{x}_k + v_k \tag{2.270}$$

where

$$\mathbf{x}_k = \begin{bmatrix} i_k & i_{k-1} & \ldots & i_{k-q+1} \end{bmatrix}^T \tag{2.271}$$

$$\boldsymbol{\phi} = \begin{bmatrix} \phi_1 & \phi_2 & \dots & \phi_{q-1} & \phi_q \\ 1 & 0 & \dots & 0 & 0 \\ 0 & 1 & \dots & 0 & 0 \\ \vdots & \vdots & \dots & \vdots & \vdots \\ 0 & 0 & \dots & 1 & 0 \end{bmatrix} \tag{2.272}$$

$$\mathbf{u}_k = [e_k \quad 0 \quad \dots \quad 0]^T \tag{2.273}$$

$$\mathbf{H} = [1 \quad 0 \quad \dots \quad 0]\,. \tag{2.274}$$

The observation noise v_k is the sum of the direct-sequence signal s_k and the white Gaussian noise n_k:

$$v_k = s_k + n_k\,. \tag{2.275}$$

Since the first component of the state vector $\mathbf{x}_k$ is the interference i_k, the state estimate $\mathbf{H}\hat{\mathbf{x}}_k$ provides an interference estimate that can be subtracted from the received signal to cancel the interference.

For a random spreading sequence, $s_k = +c$ or $-c$ with equal probability. If n_k is zero-mean and Gaussian with variance σ_n^2, then v_k has the density

$$f_v(v) = \frac{1}{2} N_{\sigma_n^2}(v - c) + \frac{1}{2} N_{\sigma_n^2}(v + c) \tag{2.276}$$

where

$$N_{\sigma^2}(x) = \frac{1}{\sqrt{2\pi}\sigma} \exp\left(-\frac{x^2}{2\sigma^2}\right). \tag{2.277}$$

For this non-Gaussian density, the optimal filter that computes the exact conditional mean given by (2.253) is nonlinear with exponentially increasing complexity and, thus, is impractical. The density $f(\mathbf{x}_k|Z^{k-1})$ is not Gaussian as required by Masreliez's theorem. However, by assuming that this density is approximately Gaussian, we can use results of the theorem to derive the *approximate conditional mean* (ACM) filter [11].

Conditioned on Z^{k-1} and s_k, the expected value of z_k is $\mathbf{H}\bar{\mathbf{x}}_k + s_k$ since $\mathbf{x}_k$ and n_k are independent of s_k. From the definition of $\mathbf{M}_k$ and (2.272), it follows that the conditional variance of z_k is

$$\sigma_z^2 = \mathbf{H}\,\mathbf{M}_k\,\mathbf{H}^T + \sigma_n^2. \tag{2.278}$$

Since $f(\mathbf{x}_k|Z^{k-1})$ is approximated by a Gaussian density, we obtain

$$f\left(z_k \,|Z^{k-1}\right) = \frac{1}{2} N_{\sigma_z^2}(z_k - \mathbf{H}\bar{\mathbf{x}}_k - c) + \frac{1}{2} N_{\sigma_z^2}(z_k - \mathbf{H}\bar{\mathbf{x}}_k + c)\,. \tag{2.279}$$

Substitution of this equation into (2.258) and (2.259) yields

$$g_k(z_k) = \frac{1}{\sigma_z^2}\left[\epsilon_k - c\tanh\left(\frac{c\epsilon_k}{\sigma_z^2}\right)\right] \tag{2.280}$$

$$G_k(z_k) = \frac{1}{\sigma_z^2}\left[1 - \frac{c^2}{\sigma_z^2}\operatorname{sech}^2\left(\frac{c\epsilon_k}{\sigma_z^2}\right)\right] \tag{2.281}$$

where the *innovation* or prediction residual is $\widehat{z}$

$$\epsilon_k = z_k - \mathbf{H}\bar{\mathbf{x}}_k = z_k - \widehat{z}_k \tag{2.282}$$

and

$$\widehat{z}_k = \mathbf{H}\bar{\mathbf{x}}_k \tag{2.283}$$

is the predicted observation based on Z^{k-1}. The update equations of the ACM filter are given by (2.254) to (2.259) and (2.280) to (2.283). The difference between the ACM filter and the Kalman–Bucy filter is the presence of the nonlinear *tanh* and *sech* functions in (2.280) and (2.281).

2.7.5 Adaptive ACM Filter

In practical applications, the elements of the matrix $\boldsymbol{\phi}$ in (2.275) are unknown and may vary with time. To cope with these problems, an adaptive algorithm that can track the interference is desirable. The *adaptive ACM filter* receives $z_k = i_k + s_k + n_k$ and produces the interference estimate denoted by $\bar{z}_k$. The output of the filter is denoted by $\epsilon_k = z_k - \bar{z}_k$ and ideally is $s_k + n_k$ plus a small residual of i_k. An adaptive transversal filter is embedded in the adaptive ACM filter. To use the structure of the nonlinear ACM filter, we observe that the second term inside the brackets in (2.280) would be absent if s_k were absent. Therefore, $c\tanh(c\epsilon_k/\sigma_z^2)$ may be interpreted as a soft decision on the direct-sequence signal s_k. The input to the adaptive transversal filter at time k is taken to be the difference between the observation z_k and the soft decision:

$$\widetilde{z}_k = z_k - c\tanh\left(\frac{c\epsilon_k}{\sigma_z^2}\right) = \widehat{z}_k + \rho(\epsilon_k) \tag{2.284}$$

where

$$\rho(\epsilon_k) = \epsilon_k - c\tanh\left(\frac{c\epsilon_k}{\sigma_z^2}\right). \tag{2.285}$$

The input $\widetilde{z}_k$ is a reasonable estimate of the interference that is made more accurate by the adaptive filter. The architecture of the one-sided adaptive ACM filter [11] is shown in Fig. 2.38. The output of the N-tap transversal filter provides the interference estimate

$$\widehat{z}_k = \mathbf{W}^T(k)\widetilde{\mathbf{z}}_k \tag{2.286}$$

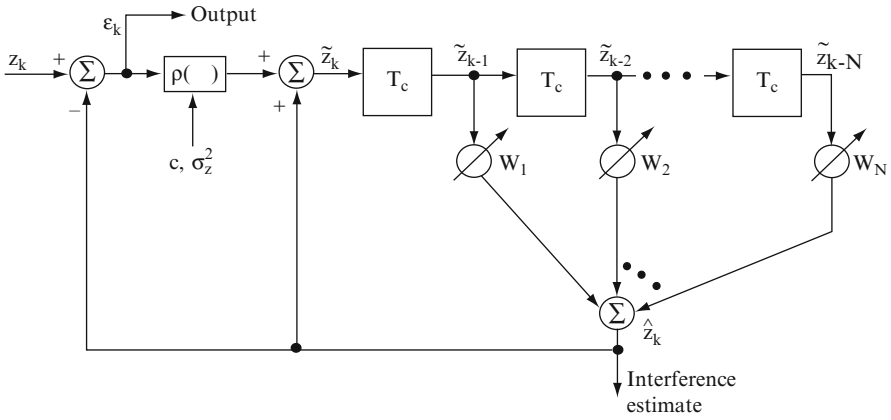

Fig. 2.38 Adaptive ACM filter

where $\mathbf{W}(k)$ is the weight vector and

$$\widetilde{\mathbf{z}}_k = [\widetilde{z}_{k-1}\, \widetilde{z}_{k-2} \ldots \widetilde{z}_{k-N}]^T \tag{2.287}$$

which is extracted from the filter taps. When $\tilde{z}_k$ has only a small component due to s_k, the filter can effectively track the interference, and $\bar{z}_k$ is a good estimate of this interference.

A normalized version of the LMS algorithm for the adaptive ACM filter is given by the weight-update equation:

$$\mathbf{W}(k) = \mathbf{W}(k-1) + \frac{\mu_0}{r_k}\,(\widetilde{z}_k - \widehat{z}_k)\,\widetilde{\mathbf{z}}_k \tag{2.288}$$

where μ_0 is the adaptation constant and r_k is an estimate of the input power iteratively determined by

$$r_k = r_{k-1} + \mu_0 \left[||\widetilde{\mathbf{z}}_k||^2 - r_{k-1} \right]. \tag{2.289}$$

The division by r_k in (2.288) normalizes the algorithm by making the choice of an appropriate μ_0 for fast convergence and good performance much less dependent on the input power level.

The calculation of $\rho(\epsilon_k)$ requires the estimation of σ_z^2. If the $\widehat{z}_k$ produced by the adaptive filter approximates the prediction residual of (2.283), then (2.282), (2.280), (2.275), and (2.253) imply that $var(\epsilon_k^2) \approx \sigma_z^2 + c^2$. Therefore, if $var(\epsilon_k^2)$ is estimated by computing the sample variance of the filter output, then the subtraction of c^2 from the sample variance gives an estimate of σ_z^2.

A figure of merit for filters is the *SINR improvement*, which is the ratio of the output SINR to the input SINR. Since the filters of concern do not change the signal power, the SINR improvement is

$$R = \frac{E\left\{|z_k - s_k|^2\right\}}{E\left\{|\epsilon_k - s_k|^2\right\}}. \tag{2.290}$$

In terms of this performance measure, the nonlinear adaptive ACM filter has been found to provide much better suppression of narrowband interference than the linear Kalman–Bucy filter if the noise power in n_k is less than the direct-sequence signal power in s_k. If the latter condition is not satisfied, the advantage is small or absent. Disadvantages apparent from (2.285) are the requirements to estimate the parameters c and σ_z^2 and to compute or store the *tanh* function.

The preceding linear and nonlinear methods are primarily predictive methods that exploit the inherent predictability of narrowband interference. Further improvements in interference suppression are theoretically possible by using *code-aided methods*, which exploit the predictability of the spread-spectrum signal itself [11]. Most of these methods are based on methods that were originally developed for multiuser detection (Chap. 6). Some of them can potentially be used to simultaneously suppress both narrowband interference and multiple-access interference. However, code-aided methods require even more computation and parameter estimation than the ACM filter, and the most powerful of the adaptive methods are practical only for short spreading sequences.

Problems

2.1. Consider a linear feedback shift register with characteristic polynomial $f(x) = 1 + x^3$. Find all possible state sequences.

2.2. Derive (2.45) using the steps specified in the text.

2.3. The characteristic polynomial associated with a linear feedback shift register is $f(x) = 1 + x^2 + x^3 + x^5 + x^6$. The initial state is $a_0 = a_1 = 0, a_2 = a_3 = a_4 = a_5 = 1$. Use polynomial long division to determine the first nine bits of the output sequence.

2.4. If the characteristic polynomial associated with a linear feedback shift register is $1 + x^m$, what is the linear recurrence relation? Write the generating function associated with the output sequence. What is the period of the output sequence? Derive it by polynomial long division.

2.5. Prove by exhaustive search that the polynomial $f(x) = 1 + x^2 + x^3$ is primitive.

2.6. Derive the characteristic function of the linear equivalent of Fig. 2.12a. Verify the structure of Fig. 2.12b and derive the initial contents indicated in the figure.

2.7. This problem illustrates the limitations of an approximate model in an extreme case. Suppose that tone interference at the carrier frequency is coherent with a BPSK direct-sequence signal so that $\phi = 0$ in (2.88). Assume that $N_0 \to 0$ and $\mathcal{E}_s > \kappa I T_c$. Show that $P_s = 0$. Show that the general tone-interference model of Sect. 2.3 leads to a nonzero approximate expression for P_s.

2.8. Derive (2.111) using the steps specified in the text.

2.9. To assess the effect of wideband filtering on the thermal noise, we may substitute bN_0 in place of N_0, where b is the factor that accounts for the presence of the filter. Show that for an ideal rectangular bandpass filter of bandwidth W_1,

$$b = 2\int_0^{W_1 T_c/2} sinc^2(x)dx$$

If $W_1 T_c \geq 2$, then $0.9 \leq b \leq 1.0$, and the impact of the wideband filtering is modest or small.

2.10. Derive (2.126)–(2.128) using the results of Sect. 2.2.

2.11. Derive (2.133)–(2.135) using the results of Sect. 2.2.

2.12. Derive the expression for $E[V \mid \phi, k_1, k_2, d_0]$ that leads to (2.137).

2.13. Use the general interference model to plot P_s versus $G\mathcal{E}_s/IT_s$ for dual and balanced quadriphase direct-sequence systems with tone interference at the carrier frequency and $\mathcal{E}_s/N_0 = 20\,\text{dB}$. Observe that the balanced system has more than a 2 dB advantage at $P_s = 10^{-6}$.

2.14. Consider a direct-sequence system with BPSK, a required $P_s = 10^{-5}$, and $N_0 = 0$. How much additional power is required against worst-case pulsed interference beyond that required against continuous interference. Use $Q(\sqrt{20}) = 10^{-5}$.

2.15. For a direct-sequence system with binary DPSK, $P_s = \frac{1}{2}\exp(-\mathcal{E}_s/N_0)$ in the presence of white Gaussian noise. Derive the worst-case duty cycle and P_s for strong pulsed interference when the power spectral density of continuous interference is I_0. Show that DPSK has a more than 3 dB disadvantage relative to PSK against worst-case pulsed interference when $\mathcal{E}_s/I_0$ is large.

2.16. What are the values of $E[M_0|\nu]$and $var[M_0|\nu]$ for the white noise metric and for the AGC metric?

2.17. Expand (2.167) to determine the degradation in $A_s(t_0 + T)$ when $f_d \neq 0$ and the chip waveform is rectangular.

2.18. Evaluate the impulse response of a transversal filter with the form of Fig. 2.26. Show that this impulse response is equal to that of a filter matched to $p_1(t)cos(2\pi f_c t + \theta)$.

2.19. Consider an elastic convolver for which $L/v = nT$ for some positive integer n and $g(t) = p(T-t)$, where p(t) is the periodic spreading waveform. The received signal is $f(t) = Ap(t - t_0)$, where A is a positive constant. Express $A_s(t)$ as a function of $R_p(\ )$, the periodic autocorrelation of the spreading waveform. How might this result be applied to acquisition?

2.20. Consider the soft-decision term in (2.284). What are its values as $\sigma_z \to \infty$ and as $\sigma_z \to 0$? Give an engineering interpretation of these results.

References

1. T. K. Moon, *Error Correction Coding*. Hoboken, NJ: Wiley, 2005.
2. D. Torrieri, *Principles of Secure Communication Systems*, 2nd ed. Boston: Artech House, 1992.
3. R. B. Ash and C. A. Doleans-Dade, *Probability and Measure Theory, 2nd ed.* San Diego: Academic Press, 2000.
4. D. J. Torrieri, "The Performance of Five Different Metrics Against Pulsed Jamming," *IEEE Trans. Commun.*, vol. 34, pp. 200–207, Feb. 1986.
5. C. Campbell, *Surface Acoustic Wave Devices for Mobile and Wireless Communications*. New York: Academic Press, 1998.
6. D. P. Morgan and J. M. Hannah, "Surface Wave Recirculation Loops for Signal Processing," *IEEE Trans. Sonics and Ultrason.*, vol. 25, pp. 30–38, Jan. 1978.
7. L. B. Milstein, "Interference Rejection Techniques in Spread Spectrum Communications," *Proc. IEEE*, vol. 76, pp. 657–671, June 1988.
8. H. V. Poor, "Active Interference Suppression in CDMA Overlay Systems," *IEEE J. Select. Areas Commun.*, vol. 19, pp. 4–20, Jan. 2001.
9. A. H. Sayed, *Adaptive Filters*. Hoboken, NJ: Wiley, 2008.
10. M. Medley, G. Saulnier, and P. Das, "The Application of Wavelet-Domain Adaptive Filtering to Spread-Spectrum Communications," *Proc. SPIE Wavelet Applications for Dual-Use*, vol. 2491, pp. 233–247, April 1995.
11. X. Wang and H. V. Poor, *Wireless Communication Systems*, Upper Saddle River, NJ: Prentice-Hall, 2004.

Chapter 3
Frequency-Hopping Systems

Frequency hopping is the periodic changing of the carrier frequency of a transmitted signal. This time-varying characteristic potentially endows a communication system with great strength against interference. Whereas a direct-sequence system relies on spectral spreading, spectral despreading, and filtering to suppress interference. the basic mechanism of interference suppression in a frequency-hopping system is that of avoidance. When the avoidance fails, it is only temporary because of the periodic changing of the carrier frequency. The impact of the interference is further mitigated by the pervasive use of channel codes, which are more essential for frequency-hopping than for direct-sequence systems. The basic concepts, spectral and performance aspects, and coding and modulation issues are presented in the first five sections of this chapter. The effects of partial-band interference and jamming are examined, whereas the impact of multiple-access interference is presented in Chap. 6. The most important issues in the design of frequency synthesizers are described in the final section.

3.1 Concepts and Characteristics

The sequence of carrier frequencies transmitted by a frequency-hopping system is called the *frequency-hopping pattern*. The set of M possible carrier frequencies $\{f_1, f_2, \ldots, f_M\}$ is called the *hopset*. The rate at which the carrier frequency changes is called the *hop rate*. Hopping occurs over a frequency band called the *hopping band* that includes M *frequency channels*. Each frequency channel is defined as a spectral region that includes a single carrier frequency of the hopset as its center frequency and has a bandwidth B large enough to include most of the power in a signal pulse with a specific carrier frequency. Figure 3.1 illustrates the frequency channels associated with a particular frequency-hopping pattern. The time interval between hops is called the *hop interval*. Its duration is called the *hop duration* and is denoted by T_h. The hopping band has bandwidth $W \geq MB$.

D. Torrieri, *Principles of Spread-Spectrum Communication Systems*,
DOI 10.1007/978-1-4419-9595-7_3, © Springer Science+Business Media, LLC 2011

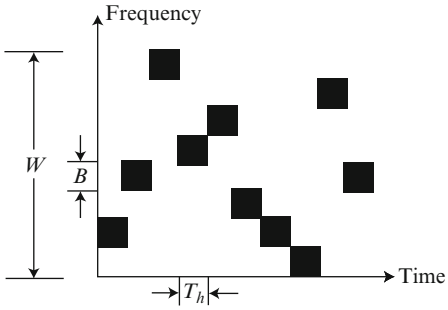

Fig. 3.1 Frequency-hopping patterns

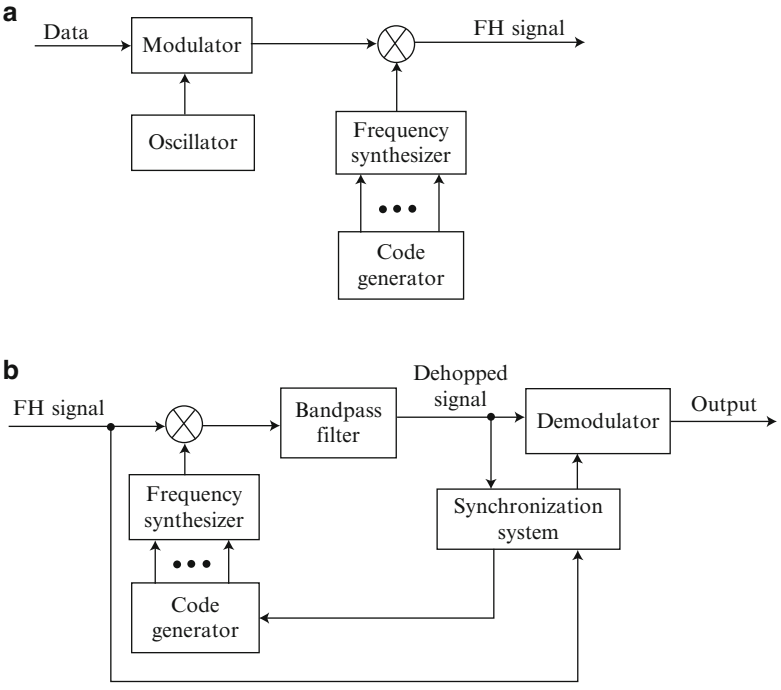

Fig. 3.2 General form of frequency-hopping system: (**a**) transmitter and (**b**) receiver

Figure 3.2 depicts the general form of a frequency-hopping system. The frequency synthesizers (Sect. 3.4) produce frequency-hopping patterns determined by the time-varying multilevel sequence specified by the output bits of the code generators. In the transmitter, the data-modulated signal is mixed with the synthesizer output pattern to produce the frequency-hopping signal. If the data modulation is some form of angle modulation $\phi(t)$, then the received signal for the ith hop is

$$s(t) = \sqrt{2S}\cos\left[2\pi f_{ci}t + \phi(t) + \phi_i\right], \quad (i-1)T_h \le t \le iT_h \tag{3.1}$$

where S is the average power, f_{ci} is the carrier frequency for the ith hop, and ϕ_i is a random phase angle for the ith hop. The frequency-hopping pattern produced by the receiver synthesizer is synchronized with the pattern produced by the transmitter, but is offset by fixed intermediate frequency (IF), which may be zero. The mixing operation removes the frequency-hopping pattern from the received signal and, hence, is called *dehopping*. The mixer output is applied to a bandpass filter that excludes double-frequency components and power that originated outside the appropriate frequency channel and produces the data-modulated *dehopped signal*, which has the form of (3.1) with f_{ci} replaced by the IF.

Although it provides no advantage against white noise, frequency hopping enables signals to hop out of frequency channels with interference or slow frequency-selective fading. To fully exploit this capability against narrowband interference signals, disjoint frequency channels are necessary. The disjoint channels may be contiguous or have unused spectral regions between them. Some spectral regions with steady interference or a susceptibility to fading may be omitted from the hopset, a process called *spectral notching*. Frequency-shift keying (FSK) differs fundamentally from frequency hopping in that all the FSK subchannels affect each receiver decision. No escape from or avoidance of a subchannel with interference is possible.

To ensure the secrecy and unpredictably of the frequency-hopping pattern, the pattern should be a pseudorandom with a large period and an approximately uniform distribution over the frequency channels. For military and some other applications, the pattern should be difficult to reproduce or dehop by an opponent. The pattern of frequencies can be generated by a nonlinear sequence generator (Sect. 2.2) with a large linear span. The *linear span* is the length of the shortest linear feedback shift register that can generate the sequence. A large linear span inhibits the reconstruction of the pattern from a short segment of it. A frequency-hopping pattern is obtained by associating a frequency with each generator state, the bits of which constitute a symbol drawn from a finite field with the necessary properties. More is required of frequency-hopping patterns to alleviate multiple-access interference when similar frequency-hopping systems are part of a network (Chap. 6).

An architecture that enhances the *transmission security* by encrypting the control bits, which determine the carrier frequency in the hopset that is selected, is shown in Fig. 3.3. The specific algorithm for generating the control bits is determined by the key and the time-of-day (TOD). The *key,* which is the ultimate source of security, is a set of bits that are changed infrequently and must be kept secret. The TOD is a set of bits that are derived from the stages of the TOD counter and change with every transition of the TOD clock. For example, the key might change daily while the TOD might change every second. The purpose of the TOD is to vary the generator algorithm without constantly changing the key. In effect, the generator algorithm is controlled by a time-varying key. The code clock, which regulates the changes of state in the code generator and thereby controls the hop rate, operates at a much higher rate than the TOD clock. In a receiver, the code clock is produced by the synchronization system. In both the transmitter and the receiver, the TOD clock may be derived from the code clock.

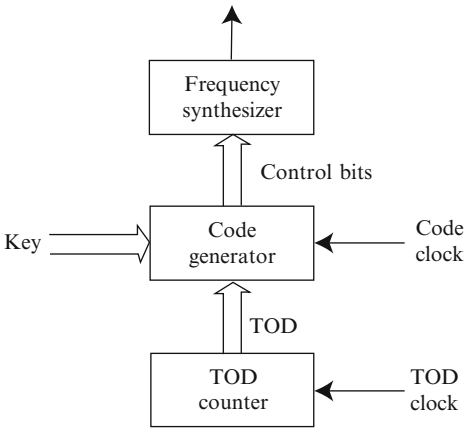

Fig. 3.3 Secure method of synthesizer control

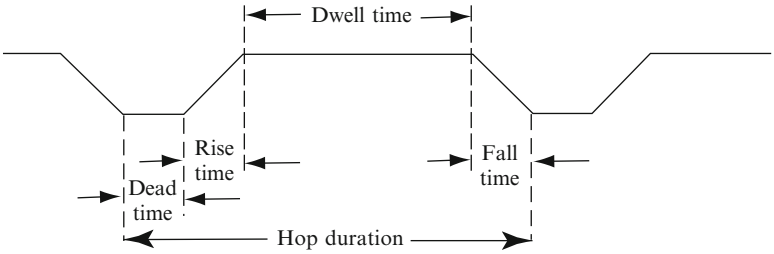

Fig. 3.4 Time durations of a frequency-hopping pulse

A frequency-hopping pulse with a fixed carrier frequency occurs during a portion of the hop interval called the *dwell interval*. As illustrated in Fig. 3.4, the *dwell time* is the duration of the dwell interval during which the channel symbols are transmitted. The hop duration T_h is equal to the sum of the dwell time T_d and the switching time T_{sw}. The *switching time* is equal to the *dead time*, which is the duration of the interval when no signal is present, plus the rise and fall times of a pulse. Even if the switching time is absent in the transmitted signal, it will be present in the dehopped signal in the receiver because of the imperfect synchronization of received and receiver-generated waveforms. The nonzero switching time, which may include an intentional *guard time*, decreases the transmitted symbol duration T_s. If T_{so} is the symbol duration in the absence of frequency hopping, then $T_s = T_{so}(T_d / T_h)$. The reduction in symbol duration expands the transmitted spectrum and thereby reduces the number of frequency channels within a fixed hopping band. Since the receiver filtering will ensure that rise and fall times of pulses have durations on the order of a symbol duration, $T_{sw} > T_s$ in practical systems. Implementing a short switching time becomes an obstacle as the hop rate decreases.

Frequency hopping may be classified as fast or slow. *Fast frequency hopping* occurs if there is more than one hop for each information symbol. *Slow frequency*

hopping occurs if one or more information symbols are transmitted in the time interval between frequency hops. Although these definitions do not refer to the absolute hop rate, fast frequency hopping is an option only if a hop rate that exceeds the information-symbol rate can be implemented. Slow frequency hopping is preferable because the transmitted waveform is much more spectrally compact (cf. Sect. 3.2) and the overhead cost of the switching time is reduced.

Let M denote the hopset size, B denote the bandwidth of frequency channels, and F_s denote the minimum separation between adjacent carriers in a hopset. For full protection against stationary narrowband interference and jamming, it is desirable that $F_s \geq B$ so that the frequency channels are nearly spectrally disjoint. A hop then enables the transmitted signal to escape the interference in a frequency channel. To obtain the full advantage of block or convolutional channel codes in a slow frequency-hopping system, the code symbols should be interleaved in such a way that the symbols of a block codeword or within a few free distances in a convolutional code fade independently. In frequency-hopping systems operating over a frequency-selective fading channel, the realization of this independence requires certain constraints among the system parameter values (Chap. 5).

Frequency-selective fading and Doppler shifts make it difficult to maintain phase coherence from hop to hop between frequency synthesizers in the transmitter and the receiver. Furthermore, the time-varying delay between the frequency changes of the received signal and those of the synthesizer output in the receiver causes the phase shift in the dehopped signal to differ for each hop interval. Thus, practical frequency-hopping systems use noncoherent or differentially coherent demodulators unless a pilot signal is available, the hop duration is very long, or elaborate iterative phase estimation (perhaps as part of turbo decoding) is used.

In military applications, the ability of frequency-hopping systems to avoid interference is potentially neutralized by a *repeater jammer* (also known as a *follower jammer*), which is a device that intercepts a signal, processes it, and then transmits jamming at the same center frequency. To be effective against a frequency-hopping system, the jamming energy must reach the victim receiver before it hops to a new set of frequency channels. Thus, the hop rate is the critical factor in protecting a system against a repeater jammer. Required hop rates and the limitations of repeater jamming are analyzed in Ref. [1].

3.2 Frequency Hopping with Orthogonal FSK

In a frequency-hopping system with FSK as its data modulation (FH/FSK system), one of a set S_q of q FSK frequencies is selected to offset the carrier frequency for each transmitted symbol within each hop dwell interval. The general transmitter of Fig. 3.2a can be simplified for an FH/FSK system, as illustrated in Fig. 3.5a, where the code-generator output bits, which define a frequency in S_q, and the digital control symbols, which define a carrier frequency, are combined to determine the

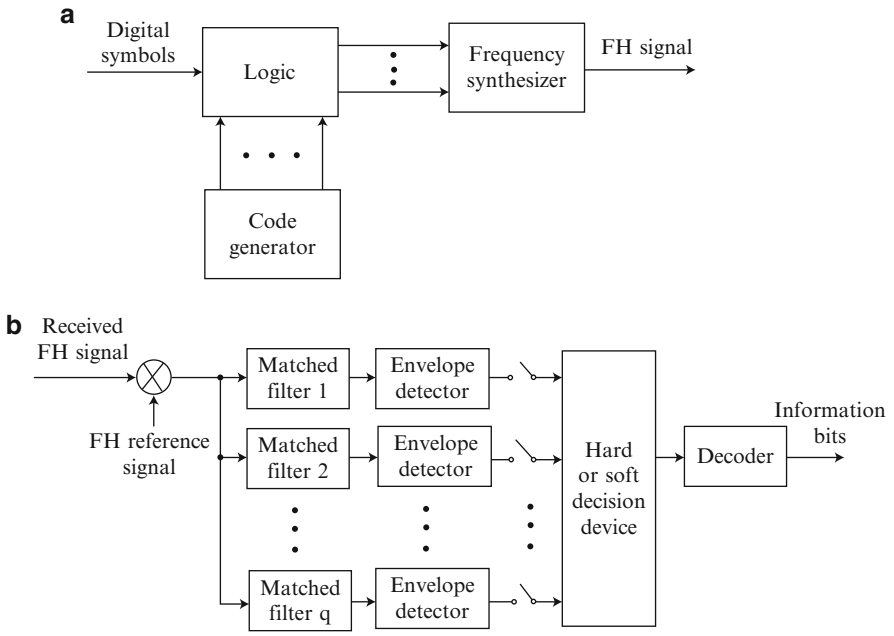

Fig. 3.5 FH/FSK (**a**) transmitter and (**b**) receiver

frequency generated by the synthesizer during a symbol interval. The implementation of phase continuity from symbol to symbol is highly desirable to prevent excessive spectral splatter outside a frequency channel (Sect. 3.3).

In an FH/FSK system, the carrier frequency plus each of the q frequencies or tones in S_q can be considered as the center frequency of an FSK subchannel. Therefore, the *effective number of frequency channels* is

$$M_e = qM \tag{3.2}$$

where M is the hopset size. In the standard implementation, the q subchannels of S_q are contiguous, and each set constitutes a frequency channel within the hopping band. For noncoherent orthogonal signals, the FSK tones must be separated enough that a received signal produces negligible responses in the incorrect subchannels. As shown subsequently, the frequency separation must be $f_d = k/T_s$, where k is a nonzero integer, and T_s denotes the symbol duration. To maximize the hopset size when the FSK subchannels are contiguous, $k = 1$ is selected. Consequently, the bandwidth of a frequency channel for slow frequency hopping with many symbols per dwell interval is

$$B \approx \frac{q}{T_s} = \frac{q}{T_b \log_2 q} \tag{3.3}$$

where T_b is the duration of a bit, and the factor $\log_2 q$ accounts for the increase in symbol duration when a nonbinary modulation is used. If the hopping band has bandwidth W and contiguous frequency channels are assigned, the hopset size is

$$M = \left\lfloor \frac{W}{B} \right\rfloor \tag{3.4}$$

where $\lfloor x \rfloor$ denotes the largest integer in x. Figure 3.5b depicts the main elements of a noncoherent FH/FSK receiver. Each matched filter corresponds to an FSK subchannel.

3.2.1 Soft-Decision Decoding

To illustrate some basic issues of frequency-hopping communications and the effectiveness of soft-decision decoding, we consider an FH/FSK system that uses a repetition code and the receiver of Fig. 3.5b. Each information symbol is transmitted as a codeword of n code symbols. The interference is modeled as wideband Gaussian noise uniformly distributed over part of the hopping band. Along with perfect dehopping, either slow frequency hopping with ideal interleaving or fast frequency hopping is assumed. Both ensure the independence of code-symbol errors. The optimal metric for the Rayleigh-fading channel (Chap. 5) and a good metric for the AWGN channel without fading is the Rayleigh metric defined by (1.80). For each of q possible information symbols, this metric is

$$U(l) = \sum_{i=1}^{n} R_{li}^2, \quad l = 1, 2, \ldots, q \tag{3.5}$$

where R_{li} is the sample value of the envelope-detector output that is associated with code symbol i of candidate information-symbol l. The diversity combining required by the Rayleigh metric is often called *linear square-law combining*. This metric has the advantage that no *side information*, which is specific information about the reliability of symbols, is required for its implementation. A performance analysis of a frequency-hopping system with BFSK and soft-decision decoding with the Rayleigh metric indicates that the system performs poorly against worst-case partial-band jamming [2] primarily because a single jammed frequency can corrupt the metrics. Furthermore, the repetition code is counterproductive because the *noncoherent combining loss* resulting from the fragmentation of the symbol energy is greater than any coding gain.

The difficulty of implementing the maximum-likelihood metric (1.75) leads to consideration of the approximation (1.79), which requires *nonlinear square-law combining:*

$$U(l) = \sum_{i=1}^{n} \frac{R_{li}^2}{N_{0i}^2}, \quad l = 1, 2, \ldots, q \tag{3.6}$$

where $N_{0i}/2$ is the two-sided power spectral density of the interference and noise over all the FSK subchannels during code symbol i. A plausible simplification [4], which is obtained by making the approximation that $N_{0i}^2 \approx N_{0i} N_0$ and then omitting the factor common to q symbol candidates, is the *variable-gain metric*:

$$U(l) = \sum_{i=1}^{n} \frac{R_{li}^2}{N_{0i}}, \quad l = 1, 2, \ldots, q \tag{3.7}$$

which is much easier to analyze. The advantage of both metrics is that they incorporate *side information* contained in the $\{N_{0i}\}$, which must be known. The subsequent analysis is for the variable-gain metric.

The union bound (1.56) implies that the information-symbol error probability satisfies

$$P_{is} \leq (q-1) P_2 \tag{3.8}$$

where P_2 is the probability of an error in comparing the metric associated with the transmitted information symbol with the metric associated with an alternative one. It is assumed that there are enough frequency channels that n distinct carrier frequencies are used for the n code symbols. Since the FSK tones are orthogonal, the symbol metrics $\{R_{li}^2/N_{0i}\}$ are independent and identically distributed for all values of l and i (Chap. 1). Therefore, the Chernoff bound given by (1.139) and (1.138) with $\alpha = 1/2$ yields

$$P_2 \leq \frac{1}{2} Z^n \tag{3.9}$$

$$Z = \min_{0<s<s_1} E\left[\exp\left\{\frac{s}{N_1}\left(R_2^2 - R_1^2\right)\right\}\right] \tag{3.10}$$

where R_1 is the sampled output of an envelope detector when the desired signal is present at the input of the associated matched filter, R_2 is the output when the desired signal is absent, and $N_1/2$ is the two-sided power-spectral density of the interference and noise over all the FSK subchannels during a code symbol. Since the FSK tones are orthogonal, and hence q-ary symmetric, (1.32), (3.8), and (3.9) give an upper bound on the information-bit error probability:

$$P_b \leq \frac{q}{4} Z^n. \tag{3.11}$$

For a Gaussian random variable X with mean m and variance σ^2, a direct calculation yields

$$E[\exp(aX^2)] = \frac{1}{\sqrt{1-2a\sigma^2}} \exp\left(\frac{am^2}{1-2a\sigma^2}\right), \quad a < \frac{1}{2\sigma^2}. \tag{3.12}$$

From the analysis of Chap. 1 leading to (1.91), it follows that

$$R_l^2 = x_l^2 + y_l^2, \quad l = 1, 2 \tag{3.13}$$

where x_l and y_l are the real and imaginary parts of R_l, respectively, and are independent Gaussian random variables with the moments

$$E[x_1] = \sqrt{\mathcal{E}_s T_s/2}\cos\theta, \quad E[y_1] = \sqrt{\mathcal{E}_s T_s/2}\sin\theta \tag{3.14}$$

$$E[x_2] = E[y_2] = 0 \tag{3.15}$$

$$\text{var}[x_l] = \text{var}[y_l] = N_1 T_s/4, \quad l = 1, 2 \tag{3.16}$$

where $\mathcal{E}_s$ is the energy per symbol. By conditioning on N_1, the expectation in (3.10) can be partially evaluated. Equations (3.12) to (3.16) and the substitution of $\lambda = s/2$ give

$$Z = \min_{0<\lambda<1} E\left[\frac{1}{1-\lambda^2}\exp\left(-\frac{\lambda\mathcal{E}_s/N_1}{1+\lambda}\right)\right] \tag{3.17}$$

where the remaining expectation is over the statistics of N_1.

To simplify the analysis, it is assumed that the thermal noise is negligible. When a repetition symbol encounters no interference, $N_1 = 0$; when it does, $N_1 = I_{t0}/\mu$, where μ is the fraction of the hopping band with interference, and I_{t0} is the spectral density that would exist if the interference power were uniformly spread over the entire hopping band. Since μ is the probability that interference is encountered, (3.17) becomes

$$Z = \min_{0<\lambda<1}\left[\frac{\mu}{1-\lambda^2}\exp\left(-\frac{\lambda\mu\gamma}{1+\lambda}\right)\right] \tag{3.18}$$

where

$$\gamma = \frac{\mathcal{E}_s}{I_{t0}} = \left(\frac{\log_2 q}{n}\right)\frac{\mathcal{E}_b}{I_{t0}} \tag{3.19}$$

$\log_2 q$ is the number of bits per information symbol, and $\mathcal{E}_b$ is the energy per information bit. Using calculus, we find that

$$Z = \frac{\mu}{1-\lambda_0^2}\exp\left(-\frac{\lambda_0\mu\gamma}{1+\lambda_0}\right) \tag{3.20}$$

where

$$\lambda_0 = -\left(\frac{1}{2}+\frac{\mu\gamma}{4}\right) + \left[\left(\frac{1}{2}+\frac{\mu\gamma}{4}\right)^2 + \frac{\mu\gamma}{2}\right]^{1/2}. \tag{3.21}$$

Substituting (3.20) and (3.19) into (3.11), we obtain

$$P_b \le \frac{q}{4}\left(\frac{\mu}{1-\lambda_0^2}\right)^n \exp\left[-\left(\frac{\lambda_0\mu\log_2 q}{1+\lambda_0}\right)\frac{\mathcal{E}_b}{I_{t0}}\right]. \tag{3.22}$$

Suppose that the interference is worst-case partial-band jamming. An upper bound on P_b is obtained by maximizing the right-hand side of (3.22) with respect to μ, where $0 \le \mu \le 1$. Calculus yields the maximizing value of μ:

$$\mu_0 = \min\left[\frac{3n}{\log_2 q}\left(\frac{\mathcal{E}_b}{I_{t0}}\right)^{-1},\ 1\right]. \tag{3.23}$$

Substituting (3.19), (3.21), and (3.23) into (3.22), we obtain an upper bound on P_b for worst-case partial-band jamming:

$$P_b \le \begin{cases} \dfrac{q}{4}\left[\dfrac{4n}{e\log_2 q}\left(\dfrac{\mathcal{E}_b}{I_{t0}}\right)^{-1}\right]^n, & n \le \dfrac{(\log_2 q)\mathcal{E}_b}{3I_{t0}} \\ \dfrac{q}{4}(1-\lambda_0^2)^{-n}\exp\left[-\left(\dfrac{\lambda_0 \log_2 q}{1+\lambda_0}\right)\dfrac{\mathcal{E}_b}{I_{t0}}\right], & n > \dfrac{(\log_2 q)\mathcal{E}_b}{3I_{t0}}. \end{cases} \tag{3.24}$$

Since μ_0 is obtained by maximizing a bound rather than an equality, it is not necessarily equal to the actual worst-case μ, which would provide a tighter bound than the one in (3.24).

If $\mathcal{E}_b/I_{t0}$ is known, then the number of repetitions can be chosen to minimize the upper bound on P_b for worst-case partial-band jamming. We treat n as a continuous variable such that $n \ge 1$ and let n_0 denote the minimizing value of n. A calculation indicates that the derivative with respect to n of the second line on the right-hand side of (3.24) is positive. Therefore, if $\mathcal{E}_b/I_{t0} < 3/\log_2 q$ so that the second line is applicable for $n \ge 1$, then $n_0 = 1$. If $\mathcal{E}_b/I_{t0} \ge 3/\log_2 q$, the continuity of (3.24) as a function of n implies that n_0 is determined by the first line in (3.24). Further calculation yields

$$n_0 = \max\left(\frac{(\log_2 q)\mathcal{E}_b}{4I_{t0}},\ 1\right). \tag{3.25}$$

Since n must be an integer, the optimal number of repetitions against worst-case partial-band jamming is approximately $\lfloor n_0 \rfloor$. If $\mathcal{E}_b/I_{t0} \ge 4/\log_2 q$, then (3.25) indicates that the optimal number of repetitions increases with both $\mathcal{E}_b/I_{t0}$ and q, the number of frequencies in the FSK set.

The upper bound on P_b for worst-case partial-band jamming when $n = n_0$ is given by

$$P_b \le \begin{cases} \dfrac{1}{4}\exp\left[-\log_2 q\left(\dfrac{\mathcal{E}_b}{4I_{t0}} - \ln 2\right)\right], & \dfrac{\mathcal{E}_b}{I_{t0}} \ge \dfrac{4}{\log_2 q} \\ \dfrac{q}{e\log_2 q}\left(\dfrac{\mathcal{E}_b}{I_{t0}}\right)^{-1}, & \dfrac{3}{\log_2 q} \le \dfrac{\mathcal{E}_b}{I_{t0}} < \dfrac{4}{\log_2 q} \\ \dfrac{q}{4}(1-\lambda_0^2)^{-1}\exp\left[-\left(\dfrac{\lambda_0 \log_2 q}{1+\lambda_0}\right)\dfrac{\mathcal{E}_b}{I_{t0}}\right], & \dfrac{\mathcal{E}_b}{I_{t0}} < \dfrac{3}{\log_2 q}. \end{cases} \tag{3.26}$$

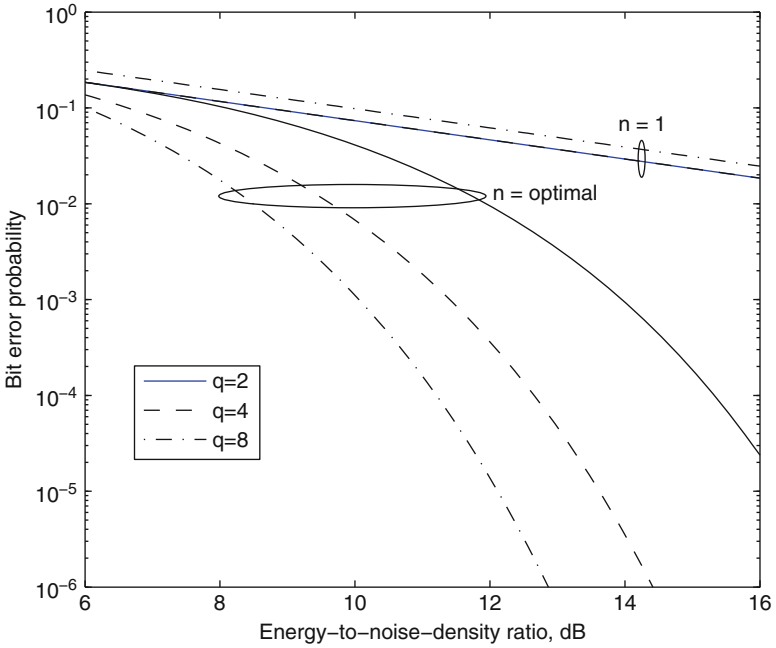

Fig. 3.6 Upper bound on bit error probability in the presence of worst-case partial-band jamming for $q = 2$, 4, and 8 and both the optimal number of repetitions and $n = 1$

This upper bound indicates that P_b decreases exponentially as either $\mathcal{E}_b/I_{t0}$ or q increases if the optimal number of repetitions is chosen and $\mathcal{E}_b/I_{t0} \geq 4\max(\ln 2, 1/\log_2 q)$. Figure 3.6 illustrates the upper bound on P_b for $q = 2$, 4, and 8 and both the optimal number of repetitions and $n = 1$. The figure indicates that the variable-gain metric and optimal repetitions sharply limit the performance degradation caused by worst-case partial-band jamming relative to full-band jamming. For example, setting $N_0 \to I_{t0}$ in (1.100) and $q = 2$ in (3.26) and then comparing the equations, we find that this degradation is approximately 3 dB for BFSK.

Substituting (3.25) into (3.23), we obtain

$$\mu_0 = \begin{cases} \dfrac{3}{4}, & \dfrac{\mathcal{E}_b}{I_{t0}} \geq \dfrac{4}{\log_2 q} \\ \dfrac{3}{\log_2 q}\left(\dfrac{\mathcal{E}_b}{I_{t0}}\right)^{-1}, & \dfrac{3}{\log_2 q} < \dfrac{\mathcal{E}_b}{I_{t0}} < \dfrac{4}{\log_2 q} \\ 1, & \dfrac{\mathcal{E}_b}{I_{t0}} \leq \dfrac{3}{\log_2 q}. \end{cases} \tag{3.27}$$

This result shows that if it is assumed that the optimal number of repetitions is used, then the worst-case jamming must cover three-fourths or more of the hopping band, a task that may not be a practical possibility for a jammer.

For frequency hopping with BFSK and the variable-gain metric, a more precise derivation [3] that does not use the Chernoff bound and allows $N_0 > 0$ confirms that (3.26) provides an approximate upper bound on the information-bit error rate caused by worst-case partial-band jamming when N_0 is small, although the optimal number of repetitions is much smaller than is indicated by (3.25). Thus, the appropriate weighting of terms in nonlinear square-law combining prevents the domination by a single corrupted term and limits the inherent noncoherent combining loss.

The implementation of the variable-gain metric requires the measurement of the interference power. One might attempt to measure this power in frequency channels immediately before the hopping of the signal into those channels, but this method will not be reliable if the interference is frequency-hopping or nonstationary. Another approach is to clip (soft-limit) each envelope-detector output R_{li} to prevent a single erroneous sample from undermining the metric. This method is potentially effective, but its implementation requires an accurate measurement of the signal power for properly setting the clipping level. A sufficiently accurate measurement is often impractical without iterative decoding (Chap. 8) because of fading or power variations across the hopping band. A metric that requires no side information is the *self-normalization metric* defined for BFSK as [4]

$$U(l) = \sum_{i=1}^{n} \frac{R_{li}^2}{R_{1i}^2 + R_{2i}^2}, \quad l = 1, 2. \tag{3.28}$$

Although it does not provide as good a performance against partial-band jamming as the variable-gain metric, the self-normalization metric is far more practical and is generally superior to hard-decision decoding.

The assumption was made that either all or none of the subchannels in an FSK set are jammed. However, this assumption ignores the threat of narrowband jamming signals that are randomly distributed over the frequency channels. Although (3.26) indicates that it is advantageous to use nonbinary signaling when $\mathcal{E}_b/I_{t0} \geq 4/\ln 2$, this advantage is completely undermined when distributed narrowband jamming signals are a threat. A fundamental problem, which also limits the applicability of FH/FSK in networks, is the reduced hopset size for nonbinary FSK indicated by (3.4) and (3.3).

3.2.2 Multitone Jamming

When the FSK subchannels are contiguous, it is not advantageous to a jammer to transmit the jamming in all the subchannels of an FSK set because only a single subchannel needs to be jammed to cause a symbol error. A sophisticated jammer with knowledge of the spectral locations of the FSK sets can cause increased system degradation by placing one jamming tone or narrowband jamming signal in every FSK set.

To assess the impact of this sophisticated *multitone jamming* on hard-decision decoding in the receiver of Fig. 3.5b, it is assumed that thermal noise is absent and that each jamming tone coincides with one FSK tone in a frequency channel encompassing q FSK tones. Whether a jamming tone coincides with the transmitted FSK tone or an incorrect one, there will be no symbol error if the desired-signal power S exceeds the jamming power. Thus, if I_t is the total available jamming power, then the jammer can maximize symbol errors by placing tones with power levels slightly above S whenever possible in approximately J frequency channels such that

$$J = \begin{cases} 1, & I_t < S \\ \left\lfloor \dfrac{I_t}{S} \right\rfloor, & S \le I_t \\ M, & MS < I_t. \end{cases} \tag{3.29}$$

If a transmitted tone enters a jammed frequency channel and $I_t \ge S$, then with probability $(q-1)/q$ the jamming tone will not coincide with the transmitted tone and will cause a symbol error after hard-decision decoding. If the jamming tone does coincide with the correct tone, it may cause a symbol error in the absence of thermal noise only if its power level is exactly S and it has exactly a 180° phase shift relative to the desired signal, an event with zero probability. Since J/M is the probability that a frequency channel is jammed, and no error occurs if $I_t < S$, the symbol error probability is

$$P_s = \begin{cases} 0, & I_t < S \\ \dfrac{J}{M}\left(\dfrac{q-1}{q}\right), & I_t \ge S. \end{cases} \tag{3.30}$$

Substitution of (3.3), (3.4), and (3.29) into (3.30) and the approximation $\lfloor x \rfloor \approx x$ yields

$$P_s = \begin{cases} \dfrac{q-1}{q}, & \dfrac{\mathcal{E}_b}{I_{t0}} < \dfrac{q}{\log_2 q} \\ \left(\dfrac{q-1}{\log_2 q}\right)\left(\dfrac{\mathcal{E}_b}{I_{t0}}\right)^{-1}, & \dfrac{q}{\log_2 q} \le \dfrac{\mathcal{E}_b}{I_{t0}} \le WT_b \\ 0, & \dfrac{\mathcal{E}_b}{I_{t0}} > WT_b \end{cases} \tag{3.31}$$

where $\mathcal{E}_b = ST_b$ denotes the energy per bit and $I_{t0} = I_t/W$ denotes the spectral density of the interference power that would exist if it were uniformly spread over the hopping band. This equation exhibits an inverse linear dependence of P_s on $\mathcal{E}_b/I_{t0}$, which indicates that the jamming has an impact qualitatively similar to that of Rayleigh fading and to what is observed in Fig. 3.6 for worst-case partial-band jamming and $n = 1$. The symbol error probability increases with q, which is the opposite of what is observed for worst-case partial-band jamming when n is optimized. The reason for this increase in P_s is the increase in the

bandwidth of each frequency channel as q increases, which provides a larger target for multitone jamming. Thus, BFSK is advantageous against this sophisticated multitone jamming.

To preclude this jamming, each FSK tone in an FSK set may be independently hopped. However, this approach demands a large increase in the amount of hardware, and uniformly distributed, narrowband jamming signals are almost as damaging as the worst-case multitone jamming. Thus, contiguous FSK subchannels are usually preferable, and the FH/FSK receiver has the form of Fig. 3.5b. An analysis of FH/FSK systems with hard-decision decoding in the presence of uniformly distributed, narrowband jamming signals confirms the superior robustness of BFSK relative to nonbinary FSK whether the FSK tones hop independently or not [5].

3.3 Frequency Hopping with CPM and DPSK

In a network of frequency-hopping systems, it is highly desirable to choose a spectrally compact modulation so that the number of frequency channels is large and, hence, the number of collisions between frequency-hopping signals is kept small. Binary orthogonal FSK allows more frequency channels than nonbinary orthogonal FSK and, hence, is advantageous against narrowband interference distributed throughout the hopping band. A spectrally compact modulation helps ensure that B is less than the coherence bandwidth (Chap. 5) so that equalization in the receiver is not necessary. This section considers spectrally compact alternatives to orthogonal FSK.

The demodulator transfer function following the dehopping in Fig. 3.2 is assumed to have a bandwidth approximately equal to B, the bandwidth of a frequency channel. The bandwidth is determined primarily by the percentage of the signal power that must be processed by the demodulator if the demodulated signal distortion and the intersymbol interference are to be negligible. In practice, this percentage must be at least 90% and is often more than 95%. The relation between B and the symbol duration may be expressed as

$$B = \frac{\zeta}{T_s} \tag{3.32}$$

where ζ is a constant determined by the signal modulation. For example, if minimum-shift keying is used, the transfer function is rectangular, and many symbols are transmitted during a dwell interval, then $\zeta = 0.8$ if 90% of the signal power is included in a frequency channel, and $\zeta = 1.2$ if 99% is included.

Spectral splatter is the interference produced in frequency channels other than the one being used by a frequency-hopping pulse. It is caused by the time-limited nature of transmitted pulses. The degree to which spectral splatter may cause errors depends primarily on the separation F_s (see Sect. 3.1) and the percentage of the signal power included in a frequency channel. Usually, only pulses in adjacent channels produce a significant amount of spectral splatter in a frequency channel.

The *adjacent splatter ratio* K_s is the ratio of the power due to spectral splatter from an adjacent channel to the corresponding power that arrives at the receiver in that channel. For example, if B is the bandwidth of a frequency channel that includes 97% of the signal power and $F_s \geq B$, then no more than 1.5% of the power from a transmitted pulse can enter an adjacent channel on one side of the frequency channel used by the pulse; therefore, $K_s \leq 0.015/0.97 = 0.155$. A given maximum value of K_s can be reduced by an increase in F_s, but eventually the value of M must be reduced if W is fixed. As a result, the rate at which users hop into the same channel increases. This increase may cancel any improvement due to the reduction of the spectral splatter. The opposite procedure (reducing F_s and B so that more frequency channels become available) increases not only the spectral splatter but also signal distortion and intersymbol interference, so the amount of useful reduction is limited.

To avoid spectral spreading due to amplifier nonlinearity, it is desirable for the signal modulation to have a constant envelope, as it is often impossible to implement a filter with the appropriate bandwidth and center frequency for spectral shaping of a signal after it emerges from the final power amplifier. Noncoherent demodulation is nearly always a practical necessity in frequency- hopping systems unless the dwell interval is large. Accordingly, good modulation candidates are DPSK and MSK or some other form of spectrally compact continuous-phase modulation (CPM).

The general form of a CPM signal is

$$s(t) = A\cos[2\pi f_c t + \phi(t, \boldsymbol{\alpha})] \tag{3.33}$$

where A is the amplitude, f_c is the carrier frequency, and $\phi(t, \boldsymbol{\alpha})$ is the *phase function* that carries the message. The phase function has the form

$$\phi(t, \boldsymbol{\alpha}) = 2\pi h \sum_{i=-\infty}^{n} \alpha_i \phi(t - iT_s), \quad nT_s \leq t \leq (n+1)\,T_s \tag{3.34}$$

where h is a constant called the *deviation ratio* or *modulation index*, T_s is the symbol duration, and the vector $\boldsymbol{\alpha}$ is a sequence of q-ary channel symbols. Each symbol α_i takes one of q values; if q is even, the values are $\pm 1, \pm 3, \ldots, \pm(q-1)$. The *phase response* is

$$\phi\,(t) = \int_0^t g(x)dx \tag{3.35}$$

where $g(t)$ is a *frequency pulse* such that $g(t) = 0$, $t < 0$. The phase function is continuous and (3.34) indicates that the phase in any specified symbol interval depends on the previous symbols.

It is assumed that the integrand in (3.34) is piecewise continuous so that $\phi(t, \boldsymbol{\alpha})$ is differentiable. The frequency function of the CPM signal, which is proportional to the derivative of $\phi(t, \boldsymbol{\alpha})$, is

$$\frac{1}{2\pi}\phi'(t, \boldsymbol{\alpha}) = h \sum_{i=-\infty}^{n} \alpha_i g(t - iT_s), \quad nT_s \leq t \leq (n+1)\,T_s. \tag{3.36}$$

The frequency pulse $g(t)$ is assumed to vanish outside an interval; that is,

$$g(t) = 0, \quad t < 0, \quad t > LT_s \tag{3.37}$$

where L is a positive integer and may be infinite. The presence of h as a multiplicative factor in the pulse function makes it convenient to normalize $g(t)$ by assuming that

$$\int_0^{LT_s} g(x)dx = \frac{1}{2}. \tag{3.38}$$

Thus, $\phi(t) = 1/2$ if $t \geq LT_s$. If $L = 1$, the CPM is called a *full-response modulation*; if $L > 1$, it is called a *partial-response modulation*, and each frequency pulse extends over two or more symbol intervals. The normalization condition for a full-response modulation implies that the phase change over a symbol interval is equal to $h\pi\alpha_i$.

Continuous-phase frequency-shift keying (CPFSK) is a subclass of CPM for which the instantaneous frequency is constant over each symbol interval. Because of the normalization, a CPFSK frequency pulse is given by

$$g(t) = \begin{cases} \dfrac{1}{2T_s}, & 0 \leq t \leq T_s \\ 0, & \text{otherwise.} \end{cases} \tag{3.39}$$

A binary CPFSK signal shifts between two frequencies separated by $f_d = h/T_s$ and has

$$\phi(t, \boldsymbol{\alpha}) = \pi h \sum_{i=-\infty}^{n-1} \alpha_i + \frac{\pi h}{T_s}\alpha_n(t - nT_s), \quad nT_s \leq t \leq (n+1)T_s. \tag{3.40}$$

The main difference between CPFSK and FSK is that h can have any positive value for CPFSK but is relegated to integer values for FSK so that the tones are orthogonal to each other. Both modulations may be detected with matched filters and envelope detectors, but CPFSK with $h < 1$ is often detected with a frequency discriminator. Although CPFSK explicitly requires phase continuity and FSK does not, FSK is usually implemented with phase continuity to avoid the generation of spectral splatter. Thus, FSK is usually implemented as CPFSK with $h = 1$. *Minimum-shift keying (MSK)* is defined as binary CPFSK with $h = 1/2$ and, hence, the two frequencies are separated by $f_d = 1/2T_s$.

Many communication signals are modeled as bandpass signals having the form

$$s(t) = A\text{Re}\left[s_l(t)\exp(j2\pi f_c t + \theta)\right] \tag{3.41}$$

where A is the amplitude and θ is an independent random variable that is uniformly distributed over $0 \leq \theta < 2\pi$. The complex envelope (Appendix A) of $s(t)$ is $As_l(t)\exp(j\theta)$. If

$$s_l(t) = Ad_1(t) + jAd_2(t) \tag{3.42}$$

then $s(t)$ may be expressed as

$$s(t) = Ad_1(t)\cos(2\pi f_c t + \theta) + Ad_2(t)\sin(2\pi f_c t + \theta). \tag{3.43}$$

We consider modulations with the form

$$d_i(t) = \sum_{k=-\infty}^{\infty} a_{ik}\psi(t - kT - T_0 - t_i), \quad i = 1, 2 \tag{3.44}$$

where $\{a_{ik}\}$ is a sequence of independent, identically distributed random variables, $a_{ik} = +1$ with probability 1/2 and $a_{ik} = -1$ with probability 1/2, $\psi(t)$ is a pulse waveform, T is the pulse duration, t_i is the relative pulse offset, and T_0 is an independent random variable that is uniformly distributed over the interval $(0, T)$ and reflects the arbitrariness of the origin of the coordinate system. Since a_{ik} is independent of a_{in} when $n \neq k$, it follows that $E[a_{ik}a_{in}] = 0, n \neq k$. Therefore, the autocorrelation of $d_i(t)$ is

$$\begin{aligned} R_{di}(\tau) &= E[d_i(t)d_i(t+\tau)] \\ &= \sum_{k=-\infty}^{\infty} E[\psi(t - kT - T_0 - t_i)\psi(t - kT - T_0 - t_i + \tau)]. \end{aligned} \tag{3.45}$$

Expressing the expected value as an integral over the range of T_0 and changing variables, we obtain

$$\begin{aligned} R_{di}(\tau) &= \sum_{k=-\infty}^{\infty} \frac{1}{T} \int_{t-kT-T-t_i}^{t-kT-t_i} \psi(x)\psi(x+\tau)dx \\ &= \frac{1}{T}\int_{-\infty}^{\infty} \psi(x)\psi(x+\tau)dx, \quad i = 1, 2. \end{aligned} \tag{3.46}$$

This equation indicates that $d_1(t)$ and $d_2(t)$ are wide-sense stationary processes with the same autocorrelation. The independence of $d_1(t)$ and $d_2(t)$ imply that the autocorrelation of $s_l(t)$ is

$$R_l(\tau) = \frac{A^2}{2}R_{d1}(\tau) + \frac{A^2}{2}R_{d2}(\tau). \tag{3.47}$$

The two-sided power spectral density $S_l(f)$ of the complex envelope $s_l(t)$, which is often called the *equivalent lowpass waveform,* is the Fourier transform of $R_l(\tau)$. From (3.47), (3.46), and the convolution theorem, we obtain the power spectral density

$$S_l(f) = A^2\frac{|G(f)|^2}{T} \tag{3.48}$$

where $G(f)$ is the Fourier transform of $\psi(t)$.

In a QPSK signal, $d_1(t)$ and $d_2(t)$ are usually modeled as independent random binary sequences with $t_1 = t_2 = 0$ and pulse duration $T = 2T_b$, where T_b is a bit duration. The component amplitude is $A = \sqrt{\mathcal{E}_b/T_b}$, where $\mathcal{E}_b$ is the energy per bit. If $\psi(t)$ is rectangular with unit amplitude over $[0, 2T_b]$, then (3.47), (3.46), and the convolution theorem yield the *power spectral density for QPSK:*

$$S_l(f) = 2\mathcal{E}_b \, sinc^2 2T_b f \tag{3.49}$$

which is the same as the density for BPSK.

A binary MSK signal with the same component amplitude can be represented by (3.43) and (3.44) with $t_1 = 0$, $t_2 = -\pi/2$, and

$$\psi(t) = \sqrt{2} \sin\left(\frac{\pi t}{2T_b}\right), \quad 0 \le t < 2T_b. \tag{3.50}$$

Therefore, the power spectral density for MSK is

$$S_l(f) = \frac{16\mathcal{E}_b}{\pi^2}\left[\frac{\cos(2\pi T_b f)}{16T_b^2 f^2 - 1}\right]^2. \tag{3.51}$$

A measure of the spectral compactness of signals is provided by the FOBP defined as

$$P_{ob}(f) = 1 - \frac{\int_{-f}^{f} S_l(f')df'}{\int_{-\infty}^{\infty} S_l(f')df'}, \quad f \ge 0. \tag{3.52}$$

The closed-form expressions for the power spectral densities of QPSK and binary MSK are used to generate Fig. 3.7. The graphs depict $P_{ob}(f)$ in decibels as a function of f in units of $1/T_b$, where $T_b = T_s/\log_2 q$ for a q-ary modulation. The *fractional power* within a transmission channel of bandwidth B is given by

$$K_0 = 1 - P_{ob}(B/2). \tag{3.53}$$

Usually, the fractional power K_0 must exceed at least 0.9 to prevent significant performance degradation in communications over a bandlimited channel. The transmission bandwidth for which $K_0 = 0.99$ is approximately $1.2/T_b$ for binary MSK, but approximately $8/T_b$ for PSK or QPSK. The adjacent splatter ratio, which is due to out-of-band power on one side of the center frequency, has the upper bound given by

$$K_s < \frac{1}{2} P_{ob}(B/2). \tag{3.54}$$

An even more compact spectrum than MSK is obtained by passing the MSK frequency pulses through a Gaussian filter with transfer function

$$H(f) = \exp\left[-\frac{(\ln 2)}{B^2} f^2\right] \tag{3.55}$$

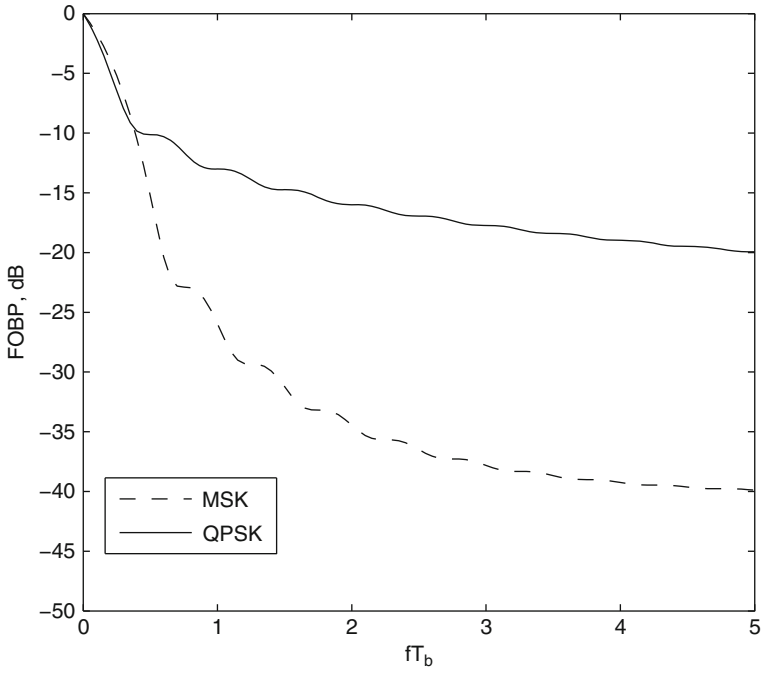

Fig. 3.7 Fractional out-of-band power (FOBP) for equivalent lowpass waveforms of QPSK and MSK

where B is the 3 dB bandwidth, which is the positive frequency such that $H(f) \geq H(0)/2, |f| \leq B$. The filter response to an MSK frequency pulse is the *Gaussian MSK (GMSK)* pulse:

$$g(t) = Q\left[\frac{2\pi B}{\sqrt{\ln 2}}\left(t - \frac{T_s}{2}\right)\right] - Q\left[\frac{2\pi B}{\sqrt{\ln 2}}\left(t + \frac{T_s}{2}\right)\right] \tag{3.56}$$

where $T_s = T_b$. As B decreases, the spectrum of a GMSK signal becomes more compact. However, each pulse has a longer duration and, hence, there is more intersymbol interference. If $BT_b = 0.3$, which is specified in the Global System for Mobile (GSM) cellular communication system, the bandwidth for which $K_0 = 0.99$ is approximately $0.92/T_b$. Each pulse may be truncated for $|\ t\ | > 1.5T_s$ with little loss. The performance loss relative to MSK is approximately 0.46 dB for coherent demodulation and presumably also for discriminator demodulation.

An FH/CPM signal has a continuous phase over each dwell interval with N symbols but has a phase discontinuity every $T_h = NT_s + T_{sw}$ seconds at the beginning of another dwell interval, where N is the number of symbols per dwell interval. The signal may be expressed as

$$s(t) = \sqrt{2S}\sum_{i=-\infty}^{\infty} w(t - iT_h, T_d)\cos\left[2\pi f_{ci}t + \phi(t, \boldsymbol{\alpha}) + \theta_i\right] \tag{3.57}$$

where $S = \mathcal{E}_s / T_s$ is the average signal power during a dwell interval, $w(t, T_d)$ as defined in (2.3) is a unit-amplitude rectangular pulse of duration $T_d = NT_s$, f_{ci} is the carrier frequency during hop-interval i, and θ_i is the phase at the beginning of dwell-interval i.

Consider multitone jamming of an FH/CPM or FH/CPFSK system in which the thermal noise is absent and each jamming tone is randomly placed within a single frequency channel. It is reasonable to assume that a symbol error occurs with probability $(q-1)/q$ when the frequency channel contains a jamming tone with power exceeding S. Thus, (3.24), (3.25), and (3.4) are applicable to FH/CPM or FH/CPFSK, but (3.3) is not. The substitution of (3.4), (3.24), $\mathcal{E}_b = ST_b$, and $I_{t0} = I_t / W$ into (3.25) yield

$$P_s = \begin{cases} \dfrac{q-1}{q}, & \dfrac{\mathcal{E}_b}{I_{t0}} < BT_b \\ \left(\dfrac{q-1}{q}\right) BT_b \left(\dfrac{\mathcal{E}_b}{I_{t0}}\right)^{-1}, & BT_b \le \dfrac{\mathcal{E}_b}{I_{t0}} \le WT_b \\ 0, & \dfrac{\mathcal{E}_b}{I_{t0}} > WT_b \end{cases} \tag{3.58}$$

for sophisticated multitone jamming. Since the orthogonality of the FSK tones is not a requirement for CPM or CPFSK, the bandwidth B for FH/CPM or FH/CPFSK may be much smaller than the bandwidth for FH/FSK given by (3.3). Thus, P_s may be much lower for FH/CPM, although still unfavorable. The symbol error probability increases with q because the enlarged frequency channels present better targets for the multitone jamming.

Consider multitone jamming of an FH/DPSK system with negligible thermal noise. Each tone is assumed to have a frequency identical to the center frequency of one of the frequency channels. A DPSK demodulator compares the phases of two successive received symbols. If the magnitude of the phase difference is less then $\pi/2$, then the demodulator decides that a 1 was transmitted; otherwise, it decides that a 0 was transmitted. The composite signal, consisting of the transmitted signal plus the jamming tone, has a constant phase over two successive received symbols in the same dwell interval, if a 1 was transmitted and the thermal noise is absent; thus, the demodulator will correctly detect the 1.

Suppose that a 0 was transmitted. Then the desired signal is $\sqrt{2S}\cos 2\pi f_c t$ during the first symbol and $-\sqrt{2S}\cos 2\pi f_c t$ during the second symbol, respectively, where f_c is the carrier frequency of the frequency-hopping signal during the dwell interval. When a jamming tone is present, trigonometric identities indicate that the composite signal during the first symbol may be expressed as

$$\begin{aligned} &\sqrt{2S}\cos 2\pi f_c t + \sqrt{2I}\cos(2\pi f_c t + \theta) \\ &\quad = \sqrt{2S + 2I_t + 4\sqrt{SI}\cos\theta}\cos(2\pi f_c t + \phi_1) \end{aligned} \tag{3.59}$$

where I is the average power of the tone, θ is the phase of the tone relative to the phase of the transmitted signal, and ϕ_1 is the phase of the composite signal:

$$\phi_1 = \tan^{-1}\left(\frac{\sqrt{I}\sin\theta}{\sqrt{S}+\sqrt{I}\cos\theta}\right). \tag{3.60}$$

Since the desired signal during the second symbol is $-\sqrt{2S}\cos 2\pi f_c t$, the phase of the composite signal during the second symbol is

$$\phi_2 = \tan^{-1}\left(\frac{\sqrt{I}\sin\theta}{-\sqrt{S}+\sqrt{I}\cos\theta}\right). \tag{3.61}$$

Using trigonometry, it is found that

$$\cos(\phi_2-\phi_1) = \frac{I-S}{\sqrt{S^2+I^2+2SI(1-2\cos^2\theta)}}. \tag{3.62}$$

If $I > S$, $|\phi_2 - \phi_1| < \pi/2$ so the demodulator incorrectly decides that a 1 was transmitted. If $I < S$, no mistake is made. Thus, multitone jamming with total power I_t is most damaging when J frequency channels given by (3.29) are jammed and each tone has power $I = I_t/J$. If the information bits 0 and 1 are equally likely, then the symbol error probability given that a frequency channel is jammed with $I > S$ is $P_s = 1/2$, the probability that a 0 was transmitted. Therefore, $P_s = J/2M$ if $I_t \geq S$, and $P_s = 0$, otherwise. Using (3.4) and (3.29) with $S = \mathcal{E}_b/T_b$, $I_t = I_{t0}W$, and $\lfloor x \rfloor \approx x$, we obtain the symbol error probability for DPSK and multitone jamming:

$$P_s = \begin{cases} \dfrac{1}{2}, & \dfrac{\mathcal{E}_b}{I_{t0}} < BT_b \\ \frac{1}{2}BT_b\left(\dfrac{\mathcal{E}_b}{I_{t0}}\right)^{-1}, & BT_b \leq \dfrac{\mathcal{E}_b}{I_{t0}} \leq WT_b \\ 0, & \dfrac{\mathcal{E}_b}{I_{t0}} > WT_b\,. \end{cases} \tag{3.63}$$

The same result holds for binary CPFSK.

As implied by Fig. 3.7, the bandwidth requirement of DPSK with $K_0 > 0.9$, which is the same as that of PSK or QPSK and less than that of orthogonal FSK, exceeds that of MSK. Thus, if the hopping bandwidth W is fixed, the number of frequency channels available for FH/DPSK is smaller than it is for noncoherent FH/MSK. This increase in B and reduction in frequency channels offsets the intrinsic performance advantage of DPSK and implies that noncoherent FH/MSK will give a lower P_s than FH/DPSK in the presence of worst-case multitone jamming, as indicated in (3.63). Alternatively, if the bandwidth of a frequency channel is fixed, an FH/DPSK signal will experience more distortion and spectral

splatter than an FH/MSK signal. Any pulse shaping of the DPSK symbols will alter their constant envelope. An FH/DPSK system is more sensitive to Doppler shifts and frequency instabilities than an FH/MSK system. Another disadvantage of FH/DPSK is due to the usual lack of phase coherence from hop to hop, which necessitates an extra phase-reference symbol at the start of every dwell interval. This extra symbol reduces $\mathcal{E}_s$ by a factor $(N_h - 1)/N_h$, where N_h is the number of symbols per hop or dwell interval and $N_h \geq 2$. Thus, DPSK does not appear to be as suitable a means of modulation as noncoherent MSK for most applications of frequency-hopping communications, and the main competition for MSK comes from other forms of CPM.

The *cross-correlation parameter* for two signals $s_1(t)$ and $s_2(t)$, each with energy $\mathcal{E}_s$, is defined as

$$C = \frac{1}{\mathcal{E}_s} \int_0^{T_s} s_1(t) s_2(t) dt. \tag{3.64}$$

For CPFSK, two possible transmitted signals, each representing a different channel symbol, are

$$s_1(t) = \sqrt{2\mathcal{E}_s/T_s} \cos(2\pi f_1 t + \phi_1), \quad s_2(t) = \sqrt{2\mathcal{E}_s/T_s} \cos(2\pi f_2 t + \phi_2). \tag{3.65}$$

The substitution of these equations into (3.64), a trigonometric expansion and discarding of an integral that is negligible if $(f_1 + f_2)T_s \gg 1$, and the evaluation of the remaining integral give

$$C = \frac{1}{2\pi f_d T_s} [\sin(2\pi f_d T_s + \phi_d) - \sin \phi_d], \quad f_d \neq 0 \tag{3.66}$$

where $f_d = f_1 - f_2$ and $\phi_d = \phi_1 - \phi_2$. Because of the phase synchronization in a coherent demodulator, we may take $\phi_d = 0$. Therefore, the orthogonality condition $C = 0$ is satisfied if $h = f_d T_s = k/2$, where k is any nonzero integer. The smallest value of h for which $C = 0$ is $h = 1/2$, which corresponds to MSK.

In a noncoherent demodulator, ϕ_d is a random variable that is assumed to be uniformly distributed over $[0, 2\pi)$. Equation (3.66) indicates that $E[C] = 0$ for all values of h. The variance of C is

$$\begin{aligned} var(C) &= \left(\frac{1}{2\pi f_d T_s}\right)^2 E\left[\sin^2(2\pi f_d T_s + \phi_d)\right. \\ &\qquad \left. + \sin^2 \phi_d - 2 \sin \phi_d \sin(2\pi f_d T_s + \phi_d)\right] \\ &= \left(\frac{1}{2\pi f_d T_s}\right)^2 (1 - \cos 2\pi f_d T_s) \\ &= \frac{1}{2} \left(\frac{\sin \pi h}{\pi h}\right)^2. \end{aligned} \tag{3.67}$$

Since $\text{var}(C) \neq 0$ for $h = 1/2$, MSK does not provide orthogonal signals for noncoherent demodulation. If h is any nonzero integer, then both (3.67) and (3.66) indicate that the two CPFSK signals are orthogonal for any ϕ_d. This result justifies the previous assertion that FSK tones must be separated by $f_d = k/T_s$ to provide noncoherent orthogonal signals.

An FH/CPM signal can be represented by (3.57). The power spectral density of the complex envelope of this signal, which is the same as the dehopped power spectral density, depends on the number of symbols per dwell interval N because of the finite dwell time. To simplify the derivation of the power spectral density, we neglect the switching time and set $T_h = T_d = NT_s$. Let $w(t) = 1, 0 \leq t < NT_s$, and $w(t) = 0$, otherwise. The normalized complex envelope of the FH/CPM signal is

$$F(t, \boldsymbol{\alpha}) = \sum_{i=-\infty}^{\infty} w(t - iNT_s) \exp[j\phi(t, \boldsymbol{\alpha}) + j\theta_i] \tag{3.68}$$

where $j = \sqrt{-1}$ and the $\{\theta_i\}$ are assumed to be independent and uniformly distributed over $[0, 2\pi)$. Therefore, $E[\exp(j\theta_i - j\theta_k)] = 0, i \neq k$, and the autocorrelation of $F(t, \boldsymbol{\alpha})$ is

$$\begin{aligned} R_f(t, t+\tau) &= E\left[F^*(t, \boldsymbol{\alpha}) F(t+\tau, \boldsymbol{\alpha})\right] \\ &= \sum_{i=-\infty}^{\infty} w(t - iNT_s) w(t + \tau - iNT_s) R_c(t, t+\tau) \end{aligned} \tag{3.69}$$

where the asterisk denotes the complex conjugate and the autocorrelation of the complex envelope of the underlying CPM signal is

$$R_c(t, t+\tau) = E\{\exp[j\phi(t+\tau, \boldsymbol{\alpha}) - j\phi(t, \boldsymbol{\alpha})]\}. \tag{3.70}$$

Equations (3.35), (3.37), and (3.38) imply that $\phi(t) = 0$ for $t \leq 0$ and $\phi(t) = 1/2$ for $t \geq LT_s$. The assumption that the symbols of $\boldsymbol{\alpha}$ are statistically independent and the substitution of (3.34) into (3.70) yields an infinite product. Using the properties of $\phi(t)$, if $k \geq \lfloor \max(t, t+\tau)/T_s \rfloor + 1$ or $k \leq \lfloor \min(t, t+\tau)/T_s \rfloor - L$, then $\phi(t + \tau - kT_s) - \phi(t - kT_s) = 0$, and the corresponding factors in the infinite product are unity. Thus, we obtain

$$\begin{aligned} R_c(t, t+\tau) &= \prod_{k=\lfloor t_l/T_s \rfloor + 1 - L}^{\lfloor t_u/T_s \rfloor} E\{\exp\{j2\pi h\alpha_k [\phi(t + \tau - kT_s) - \phi(t - kT_s)]\}\}, \\ t_u &= \max(t, t+\tau), \quad t_l = \min(t, t+\tau). \end{aligned} \tag{3.71}$$

Assuming that the symbols are identically distributed, a straightforward evaluation indicates that $R_c(t, t+\tau)$ is periodic in t with period T_s. A straightforward calculation using this periodicity and (3.69) indicates that $R_f(t, t+\tau)$ is periodic in t with period NT_s. The average autocorrelation of $F(t, \boldsymbol{\alpha})$, found by applying the definition (2.47) to (3.69), is

$$\begin{aligned} R_f(\tau) &= \frac{1}{NT_s} \int_0^{NT_s} R_f(t, t+\tau)\, dt \\ &= \begin{cases} \frac{1}{NT_s} \int_0^{NT_s-\tau} R_c(t, t+\tau)\, dt, & \tau \geq 0 \\ \frac{1}{NT_s} \int_{|\tau|}^{NT_s} R_c(t, t+\tau)\, dt, & \tau < 0. \end{cases} \end{aligned} \tag{3.72}$$

Equation (3.70) indicates that $R_c(t, t-\tau) = R_c^*(t-\tau, t)$. This equation and (3.72) imply that

$$R_f(-\tau) = R_f^*(\tau). \tag{3.73}$$

Since $w(t - iNT_s)w(t + \tau - iNT_s) = 0$ if $\tau \geq NT_s$ in (3.69),

$$R_f(\tau) = 0, \quad \tau \geq NT_s. \tag{3.74}$$

Thus, only $R_f(\tau)$ for $0 \leq \tau < NT_s$ remains to be evaluated. Let $\tau = \nu T_s + \epsilon$, where ν is a nonnegative integer, $0 \leq \nu < N$, and $0 \leq \epsilon < T_s$. Since $R_c(t, t+\tau)$ is periodic in t with period T_s, the integration interval in (3.72) can be divided into smaller intervals with similar integrals. Thus, we obtain

$$\begin{aligned} R_f(\nu T_s + \epsilon) = {} & \frac{N-\nu-1}{NT_s} \int_0^{T_s} R_c(t, t+\nu T_s+\epsilon)\, dt \\ & + \frac{1}{NT_s} \int_0^{T_s-\epsilon} R_c(t, t+\nu T_s+\epsilon)\, dt. \end{aligned} \tag{3.75}$$

If each symbol is equally likely to have any of the q possible values, then (3.71) with $0 \leq t < T_s$, $\tau \geq 0$ implies that

$$R_c(t, t+\tau) = \prod_{k=1-L}^{\lfloor (t+\tau)/T_s \rfloor} \left\{ \frac{1}{q} \sum_{l=-(q-1),odd}^{q-1} \exp\left\{ j2\pi hl \begin{bmatrix} \phi(t+\tau-kT_s) \\ -\phi(t-kT_s) \end{bmatrix} \right\} \right\}. \tag{3.76}$$

Table 3.1 Bandwidth (99%) for FH/CPFSK

	Deviation ratio	
Symbols/dwell	$h = 0.5$	$h = 0.7$
1	18.844	18.688
2	9.9375	9.9688
4	5.1875	5.2656
16	1.8906	2.1250
64	1.2813	1.8750
256	1.2031	1.8125
1024	1.1875	1.7969
No hopping	1.1875	1.7813

Evaluating the sum, which is a geometric series, we obtain

$$R_c(t, t+\tau) = \prod_{k=1-L}^{\lfloor (t+\tau)/T_s \rfloor} \left\{ \frac{1}{q} \frac{\sin 2\pi hq \left[\phi(t+\tau-kT_s) - \phi(t-kT_s)\right]}{\sin 2\pi h \left[\phi(t+\tau-kT_s) - \phi(t-kT_s)\right]} \right\},$$
$$0 \le t < T_s, \quad \tau \ge 0. \tag{3.77}$$

This equation indicates that $R_c(t, t+\tau)$ is real-valued, and then (3.72) and (3.73) indicate that $R_f(\tau)$ is a real-valued, even function. Therefore, the power spectral density of the dehopped signal, which is the Fourier transform of $R_f(\tau)$, is

$$S_f(f) = 2\int_0^{NT_s} R_f(\tau) \cos(2\pi f\tau)\, d\tau. \tag{3.78}$$

The power spectral density can be calculated by using (3.75), (3.77), and (3.78) and numerical integration of the integrals, which extend over finite intervals.

Using the preceding equations and numerical integration, the power spectral density has been calculated [6] for FH/CPFSK with binary CPFSK, assuming that the information symbols are ± 1 with equal probability. The 99-percent bandwidths of FH/CPFSK with deviation ratios $h = 0.5$ and $h = 0.7$ are listed in Table 3.1 for different values of N. As N increases, the power spectral density becomes more compact and approaches that of coherent CPFSK without frequency hopping. For $N \ge 64$, the frequency hopping causes little spectral spreading. However, fast frequency hopping, which corresponds to $N = 1$, entails a very large 99-percent bandwidth. This fact is the main reason why slow frequency hopping is preferable to fast frequency hopping and is the predominant form of frequency hopping. Consequently, frequency hopping is always assumed to be slow frequency hopping subsequently unless it is explicitly stated otherwise.

With multisymbol noncoherent detection [7], CPFSK systems can provide a better symbol error probability than coherent BPSK systems without multisymbol detection. For r-symbol detection, the optimal receiver correlates the received

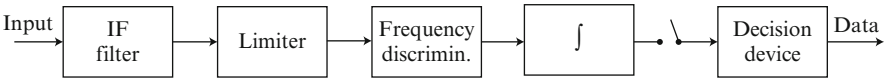

Fig. 3.8 Frequency discriminator for CPFSK

waveform over all possible r-symbol patterns before making a decision. The drawback is the considerable implementation complexity of multisymbol detection, even for three-symbol detection.

Symbol-by-symbol noncoherent detection after the dehopping of an FH/CPFSK signal can be inexpensively implemented by using a limiter and frequency discriminator, as illustrated in Fig. 3.8. Analysis of the *limiter-discriminator* or *frequency discriminator* [8] provides complicated expressions for the symbol error probability in the presence of white Gaussian noise. However, the theoretical P_s can be approximated to within a few tenths of a decibel by

$$P_s = \frac{1}{2} \exp\left(-\xi \frac{\mathcal{E}_s}{N_0}\right) \tag{3.79}$$

where the parameter ξ depends on h and the product BT_s, and $N_0/2$ is the two-sided power spectral density of the noise. If the frequency discriminator has a Gaussian IF filter, an integrate-and-dump postdetection filter, and $BT_s = 1$, then it is found that P_s is minimized when $h \approx 0.7$. For CPFSK with $h = 0.7$ and $BT_s = 1$, setting $\xi = 0.7$ in (3.79) provides an approximate least-squares fit to the theoretical curve for P_s over the range $10^{-6} \leq P_s \leq 10^{-2}$. If $BT_s = 1$, then $\xi = 0.5$ provides a close fit over the same range for orthogonal CPFSK with $h = 1$ and a fairly close fit for MSK($h = 0.5$). Thus, the discriminator demodulation of MSK or orthogonal CPFSK provides approximately the same performance as optimal noncoherent detection of orthogonal FSK. The favorable performance of the frequency discriminator is due to its ability to exploit the phase continuity from symbol to symbol of a CPFSK signal. In view of the known 0.46 dB loss of GMSK relative to MSK when coherent demodulation is used, it is expected that P_s for GMSK and discriminator demodulation is well approximated by (3.79) with $\xi = 0.45$.

The practical advantage of noncoherent MSK is that it requires roughly half the bandwidth of orthogonal FSK for specified levels of spectral splatter and intersymbol interference. The increased number of frequency channels due to the decreased value of B does not give FH/MSK an advantage over the AWGN channel. However, the increase is advantageous against a fixed number of interference tones, optimized jamming, and multiple-access interference in a network of frequency-hopping systems. A further increase in the number of frequency channels is possible with FH/GMSK.

Since $\xi = 0.7$ for an FH/CPFSK system with $h = 0.7$, this system has a potential 1.46 dB advantage in $\mathcal{E}_s$ relative to an FH/MSK system with $BT_s = 1$. However, since CPFSK with $h = 0.7$ does not have as compact a spectrum as MSK, the

FH/CPFSK system will have increased intersymbol interference due to bandlimiting and spectral splatter relative to the FH/MSK system. Only if these effects are negligible can the potential 1.46 dB advantage be realized. When $N_s \geq 64$, reducing the spectral splatter of the FH/CPFSK to the same level that it is for FH/MSK with $B = 1/T_s$ requires that $B = 1.4/T_s$. The increased bandwidth lowers ξ and decreases the number of frequency channels.

3.4 Hybrid Systems

Frequency-hopping systems reject interference by avoiding it, whereas direct-sequence systems reject interference by spreading it. Channel codes are more essential for frequency-hopping systems than for direct-sequence systems because partial-band interference is a more pervasive threat than high-power pulsed interference. When frequency-hopping and direct-sequence systems are constrained to use the same fixed bandwidth, then direct-sequence systems have an inherent advantage because they can use coherent PSK rather than a noncoherent modulation. Coherent PSK has an approximately 4 dB advantage relative to noncoherent MSK over the AWGN channel and an even larger advantage over fading channels. However, the potential performance advantage of direct-sequence systems is often illusory for practical reasons. A major advantage of frequency-hopping systems relative to direct-sequence systems is that it is possible to hop into noncontiguous frequency channels over a much wider band than can be occupied by a direct-sequence signal. This advantage more than compensates for the relatively inefficient noncoherent demodulation that is usually required for frequency-hopping systems. Other major advantages of frequency hopping are the possibility of excluding frequency channels with steady or frequent interference, the reduced susceptibility to the near-far problem (Chap. 6), and the relatively rapid acquisition of the frequency-hopping pattern (Chap. 4). A disadvantage of frequency hopping is that it is not amenable to transform-domain or nonlinear adaptive filtering (Sect. 2.7) to reject narrowband interference within a frequency channel. In practical systems, the dwell time is too short for adaptive filtering to have a significant effect.

A *hybrid frequency-hopping direct-sequence system* is a frequency-hopping system that uses direct-sequence spreading during each dwell interval or, equivalently, a direct-sequence system in which the carrier frequency changes periodically. In the transmitter of the hybrid system of Fig. 3.9, a single code generator controls both the spreading and the hopping pattern. The spreading sequence is added modulo-2 to the datasequence. Hops occur periodically after a fixed number of sequence chips. In the receiver, the frequency hopping and the spreading sequence are removed in succession to produce a carrier with the message modulation. Because of the phase changes due to the frequency hopping, noncoherent modulation, such as DPSK or noncoherent CPFSK, is usually required unless the hop rate is very low. Serial-search acquisition occurs in two stages. The first stage provides alignment of the hopping patterns, whereas the second stage over the unknown timing of the

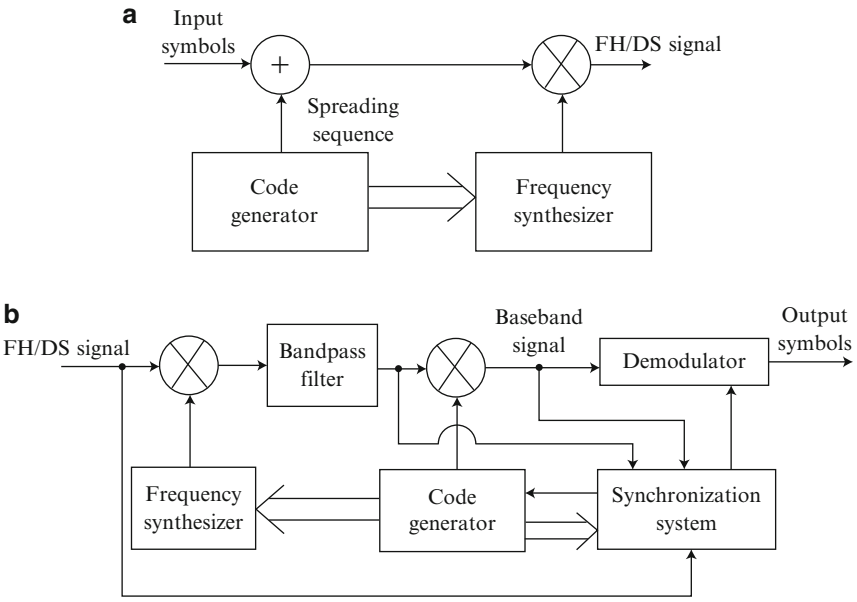

Fig. 3.9 Hybrid frequency-hopping direct-sequence system: (**a**) transmitter and (**b**) receiver

spreading sequence finishes acquisition rapidly because the timing uncertainty has been reduced by the first stage to a fraction of a hop duration.

A hybrid system curtails partial-band interference in two ways. The hopping allows the avoidance of the interference spectrum part of the time. When the system hops into the interference, the interference is spread and filtered as in a direct-sequence system. However, during a hop interval, interference that would be avoided by an ordinary frequency-hopping receiver is passed by the bandpass filter of a hybrid receiver because the bandwidth must be large enough to accommodate the direct-sequence signal that remains after the dehopping. This large bandwidth also limits the number of available frequency channels, which increases the susceptibility to narrowband interference and the near-far problem (Chap. 6). Thus, hybrid systems are seldom used except perhaps in specialized military applications because the additional direct-sequence spreading weakens the major strengths of frequency hopping.

3.5 Codes for Partial-Band Interference

When partial-band interference is present, let $I_{t0}/2$ denote the interference-power spectral density that would exist if the power were uniformly distributed over the hopping band. If a fixed amount of interference power is uniformly distributed over

J frequency channels out of M in the hopping band, then the fraction of the hopping band with interference is

$$\mu = \frac{J}{M} \tag{3.80}$$

and the interference-power spectral density in each of the interfered channels is $I_{t0}/2\mu$. When the frequency-hopping signal uses a carrier frequency that lies within the spectral region occupied by the partial-band interference, this interference is modeled as additional white Gaussian noise that increases the noise-power spectral density from N_0 to $N_0/2 + I_{t0}/2\mu$. Therefore, for hard-decision decoding, the symbol error probability is

$$P_s = \mu G\left(\frac{\mathcal{E}_s}{N_0 + I_{t0}/\mu}\right) + (1-\mu)G\left(\frac{\mathcal{E}_s}{N_0}\right) \tag{3.81}$$

where the conditional symbol error probability is a function $G(x)$ that depends on the modulation and fading. For noncoherent FH/FSK and the AWGN channel, (1.99) indicates that

$$G(x) = \sum_{i=1}^{q-1} \frac{(-1)^{i+1}}{i+1}\binom{q-1}{i} \exp\left[-\frac{ix}{(i+1)}\right] \tag{3.82}$$

where q is the alphabet size of the FSK symbols.

When frequency-nonselective or flat fading (Chap. 5) occurs, the symbol energy may be expressed as $\mathcal{E}_s\alpha^2$, where $\mathcal{E}_s$ represents the average energy and α is a random variable with $E[\alpha^2] = 1$. For Ricean fading, which is fully discussed in Sect. 5.2, the probability density function of α is

$$f_\alpha(r) = 2(\kappa+1)r \exp\{-\kappa - (\kappa+1)r^2\} I_0\left(\sqrt{\kappa(\kappa+1)}2r\right) u(r) \tag{3.83}$$

where κ is the Rice factor. Assuming ideal symbol interleaving and Ricean fading, P_s is given by (3.81) with $G(x)$ determined by averaging the symbol error probability in AWGN over the Ricean density. Replacing x by $x\alpha^2$ in (3.82), an integration over the density (3.83) and the use of (1.98) yield

$$G(x) = \sum_{i=1}^{q-1} (-1)^{i+1}\binom{q-1}{i} \frac{\kappa+1}{\kappa+1+(\kappa+1+x)i} \times \exp\left[-\frac{\kappa x i}{\kappa+1+(\kappa+1+x)i}\right]. \tag{3.84}$$

For the AWGN channel and binary CPFSK, P_s is given by (3.81), where (3.79) implies that

$$G(x) = \frac{1}{2}\exp(-\xi x). \tag{3.85}$$

For the AWGN channel, classical communication theory indicates that $G(x)$ for DPSK is given by (3.85) with $\xi = 1$. However, $\mathcal{E}_s$ in (3.81) must be reduced by the factor $N_h/(N_h + 1)$ because of the reference symbol that must be included in each dwell interval. For Ricean fading and binary CPFSK, (3.85) and (3.83) yield

$$G(x) = \frac{\kappa + 1}{2(\kappa + 1) + 2\xi x} \exp\left[-\frac{2\xi\kappa x}{2(\kappa + 1) + 2\xi x}\right]. \tag{3.86}$$

If μ is treated as a continuous variable over [0, 1] and $I_{t0} \gg N_0$, then the second term in (3.81) is negligible. Straightforward calculations using the first term of (3.81) and (3.85) indicate that the worst-case value of μ for the AWGN channel and binary CPFSK in the presence of strong interference is

$$\mu_0 = \min\left[\left(\frac{\xi\mathcal{E}_s}{I_{t0}}\right)^{-1}, \quad 1\right]. \tag{3.87}$$

The corresponding worst-case symbol error probability is

$$P_s = \begin{cases} \dfrac{1}{2e\xi}\left(\dfrac{\mathcal{E}_s}{I_{t0}}\right)^{-1}, & \dfrac{\mathcal{E}_s}{I_{t0}} \geq \dfrac{1}{\xi} \\ \dfrac{1}{2e}\exp\left(-\dfrac{\xi\mathcal{E}_s}{I_{t0}}\right), & \dfrac{\mathcal{E}_s}{I_{t0}} < \dfrac{1}{\xi} \end{cases} \tag{3.88}$$

which does not depend on M because of the assumption that μ is a continuous variable. This equation indicates that the symbol error probability in the presence of worst-case partial-band jamming exhibits an inverse linear dependence of P_s on $\mathcal{E}_b/I_{t0}$ that is qualitatively similar to the curves in Fig. 3.6 for $n = 1$. Thus, a channel code is needed.

For Rayleigh fading, similar calculations using (3.86) with $\kappa = 0$ indicate that the worst-case value of μ in the presence of strong interference is $\mu_0 = 1$. Thus, for frequency hopping with binary CPFSK in the presence of Rayleigh fading, strong interference spread uniformly over the entire hopping band hinders communications more than interference concentrated over part of the band.

Consider a frequency-hopping system with a fixed hop interval and negligible switching time. For FH/FSK with a channel code, the bandwidth of a frequency channel must be increased to $B = qB_u/2(\log_2 q)r$, where $r = k/n$ is the code rate and B_u is the bandwidth for BFSK in the absence of coding. If the bandwidth W of the hopping band is fixed, then the number of disjoint frequency channels available for hopping is reduced to

$$M = \left\lfloor \frac{2(\log_2 q)rW}{qB_u} \right\rfloor. \tag{3.89}$$

The energy per channel symbol is

$$\mathcal{E}_s = r(\log_2 q)\mathcal{E}_b. \tag{3.90}$$

When the interference is partial-band jamming, J and, hence, μ are parameters that may be varied by a jammer. It is assumed henceforth that M is large enough that μ in (3.81) may be treated as a continuous variable over [0, 1]. With this assumption, the error probabilities do not explicitly depend on M.

If a large amount of interference power is received over a small portion of the hopping band, then unless accurate channel state information is available, soft-decision decoding metrics for the AWGN channel may be ineffective because of the possible dominance of a path or code metric by a single symbol metric (cf. Sect. 2.5 on pulsed interference). This dominance is reduced by the use of a practical two- or three-bit quantization of symbol metrics instead of unquantized symbol metrics. For FH/FSK in the presence of partial-band interference, we consider codes that gives a strong performance when the decoder uses hard decisions (one-bit quantization) and/or erasures.

3.5.1 Reed–Solomon Codes

The use of a Reed–Solomon code with FSK is advantageous against partial-band interference for two principal reasons. First, a Reed–Solomon code is maximum-distance separable (Chap. 1) and, hence, accommodates many erasures. Second, the use of nonbinary FSK symbols to represent code symbols allows a relatively large symbol energy, as indicated by (3.90).

Consider an FH/FSK system that uses a Reed–Solomon code with no erasures in the presence of partial-band interference and Ricean fading. The demodulator comprises a parallel bank of noncoherent detectors and a device that makes hard decisions. In a slow frequency-hopping system, symbol interleaving among different dwell intervals and subsequent deinterleaving in the receiver may be needed to disperse errors due to the fading or interference and thereby facilitate their removal by the decoder. In a fast frequency-hopping system, symbol errors may be independent so that interleaving is unnecessary. The FSK modulation and hard decisions imply a q-ary symmetric channel. Therefore, for ideal symbol interleaving and hard-decision decoding of loosely packed codes, (1.30) and (1.32) indicate that

$$P_b \approx \frac{q}{2(q-1)} \sum_{i=t+1}^{n} \binom{n-1}{i-1} P_s^i (1-P_s)^{n-i}. \tag{3.91}$$

Figure 3.10 shows P_b for FH/FSK with $q = 32$ and an extended Reed–Solomon (32,12) code in the presence of Ricean fading. The bit SNR is $SNR = \mathcal{E}_b/N_0$, and the bit signal-to-interference ratio is $SIR = \mathcal{E}_b/I_{t0}$. The frequency channels are

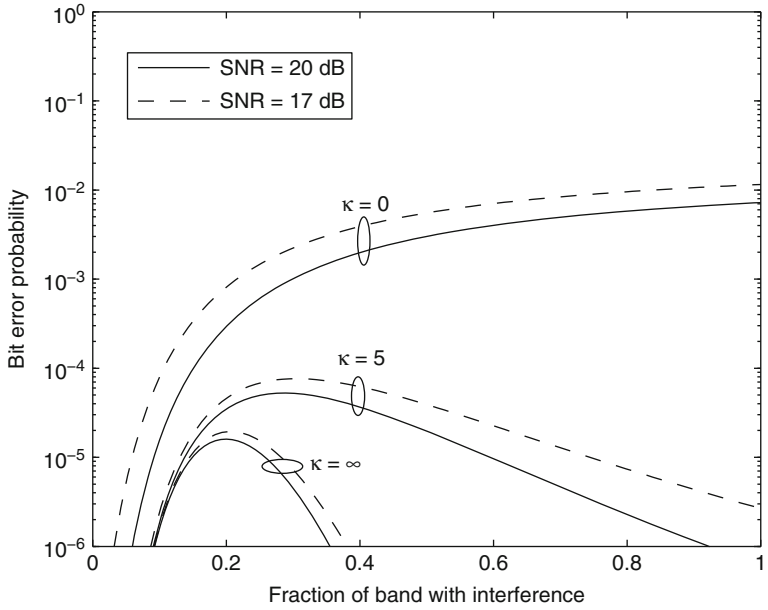

Fig. 3.10 Performance of FH/FSK with Reed–Solomon (32,12) code, $q = 32$, no erasures, $SIR = 10$ dB, and Ricean factor κ

assumed to be separated enough that fading events are independent. Thus, (3.81), (3.84), and (3.91) are applicable. For $\kappa > 0$, the graphs exhibit peaks as the fraction of the band with interference varies. These peaks indicate that for a sufficiently large value of $\mathcal{E}_b/I_{t0}$, the concentration of the interference power over part of the hopping band (perhaps intentionally by a jammer) is more damaging than uniformly distributed interference. The peaks become sharper and occur at smaller values of μ as $\mathcal{E}_b/I_{t0}$ increases. For Rayleigh fading, which corresponds to $\kappa = 0$, peaks are absent in the figure, and full-band interference is the most damaging. As κ increases, the peaks appear and become more pronounced.

Much better performance against partial-band interference can be obtained by inserting erasures (Chap. 1) among the demodulator output symbols before the symbol deinterleaving and hard-decision decoding. The decision to erase, which is made independently for each code symbol, is based on *side information*, which indicates which codeword symbols have a high probability of being incorrectly demodulated. The side information must be reliable so that only degraded symbols are erased, not correctly demodulated ones.

Side information about the channel state may be obtained from known *pilot symbols* that are transmitted along with the data symbols in each dwell interval of a slow frequency-hopping signal [9]. A dwell interval during which the signal is in partial-band interference is said to be *hit*. If one or more of the N_t pilot symbols are incorrectly demodulated, then the receiver decides that a hit has occurred, and

all codeword symbols in the same dwell interval are erased. Only one symbol of each codeword is erased if the interleaving ensures that only a single symbol of a codeword is in any particular dwell interval. Pilot symbols decrease the information rate, but this loss is negligible if $N_t \ll N_h$, which is assumed henceforth.

The probability of the erasure of a code symbol is

$$P_\epsilon = \mu P_{\epsilon 1} + (1-\mu) P_{\epsilon 0} \tag{3.92}$$

where $P_{\epsilon 1}$ is the erasure probability given that a hit occurred, and $P_{\epsilon 0}$ is the erasure probability given that no hit occurred. If δ or more errors among the N_t known pilot symbols causes an erasure, then

$$P_{\epsilon i} = \sum_{j=\delta}^{N_t} \binom{N_t}{j} P_{si}^j (1-P_{si})^{N_t - j}, \quad i = 0, 1 \tag{3.93}$$

where P_{s1} is the conditional channel-symbol error probability given that a hit occurred and P_{s0} is the conditional channel-symbol error probability given that no hit occurred.

A codeword symbol error can only occur if there is no erasure. Since pilot and codeword symbol errors are statistically independent when the partial-band interference is modeled as a white Gaussian process, the probability of a codeword symbol error is

$$P_s = \mu(1-P_{\epsilon 1}) P_{s1} + (1-\mu)(1-P_{\epsilon 0}) P_{s0} \tag{3.94}$$

and the conditional channel-symbol error probabilities are

$$P_{s1} = F\left(\frac{\mathcal{E}_s}{N_0 + I_{t0}/\mu}\right), \quad P_{s0} = F\left(\frac{\mathcal{E}_s}{N_0}\right) \tag{3.95}$$

where (3.84) is applicable for FSK symbols. To account for Ricean fading, one must integrate (3.94) and (3.92) over the Ricean density (3.83). In the remainder of this section, we assume the absence of fading.

The word error probability for errors-and-erasures decoding is upper-bounded in (1.38). Since most word errors result from decoding failures, it is reasonable to assume that $P_b \lesssim P_w/2$. Therefore, the information-bit error probability is given by

$$P_b \approx \frac{1}{2} \sum_{j=0}^{n} \sum_{i=i_0}^{n-j} \binom{n}{j} \binom{n-j}{i} P_s^i P_\epsilon^j (1-P_s-P_\epsilon)^{n-i-j} \tag{3.96}$$

where $i_0 = \max(0, \lceil (d_m - j)/2 \rceil)$ and $\lceil x \rceil$ denotes the smallest integer greater than or equal to x.

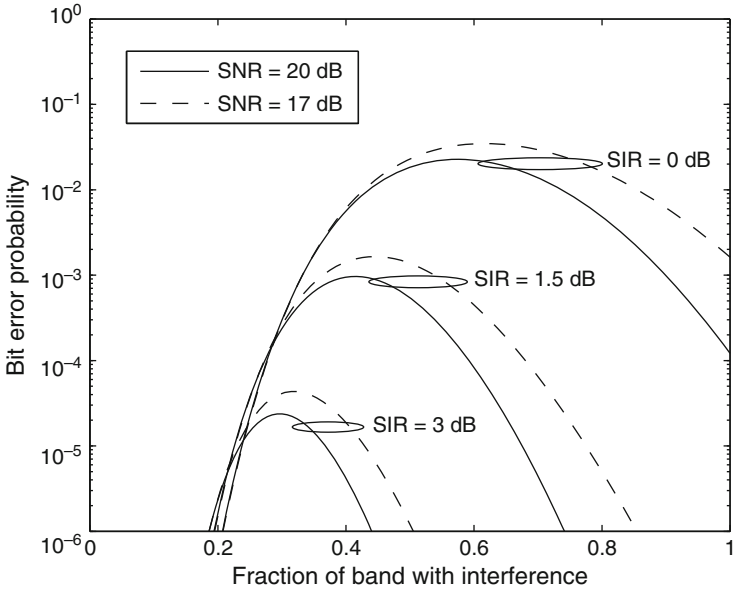

Fig. 3.11 Performance of FH/FSK with Reed–Solomon (32,12) code, $q = 32$, erasures, $N_t = 2$, and no fading

The P_b for FH/FSK with $q = 32$, an extended Reed–Solomon (32,12) code, and errors-and-erasures decoding with $N_t = 2$ and $\delta = 0$ is shown in Fig. 3.11. Fading is absent, and (3.92) to (3.96) are used. A comparison of this figure with the $\kappa = \infty$ graphs of Fig. 3.10 indicates that when $\mathcal{E}_b/N_0 = 20\,\text{dB}$, erasures provide nearly a 7 dB improvement in the required $\mathcal{E}_b/I_{t0}$ for $P_b = 10^{-5}$. The erasures also confer immunity to partial-band interference that is concentrated in a small fraction of the hopping band and decrease the sensitivity to $\mathcal{E}_b/N_0$.

There are other options for generating side information and, hence, erasure insertion in addition to demodulating pilot symbols. One might use a radiometer (Chap. 7) to measure the energy in the current frequency channel, a future channel, or an adjacent channel. Erasures are inserted if the energy is inordinately large. This method does not have the overhead cost in information rate that is associated with the use of pilot symbols. Other methods include attaching parity-check bits to each code symbol representing multiple bits to check whether the symbol was correctly received, using the soft information provided by the inner decoder of a concatenated code, or using the outputs of the parallel FSK envelope detectors.

The envelope-detector outputs provide several low-complexity schemes for erasure insertion [10]. Consider the decision variables applied to the FSK decision device of Fig. 3.5b. The *output threshold test* (OTT) compares the largest decision variable to a threshold to determine whether the corresponding demodulated symbol should be erased. The *ratio threshold test* (RTT) computes the ratio of the largest

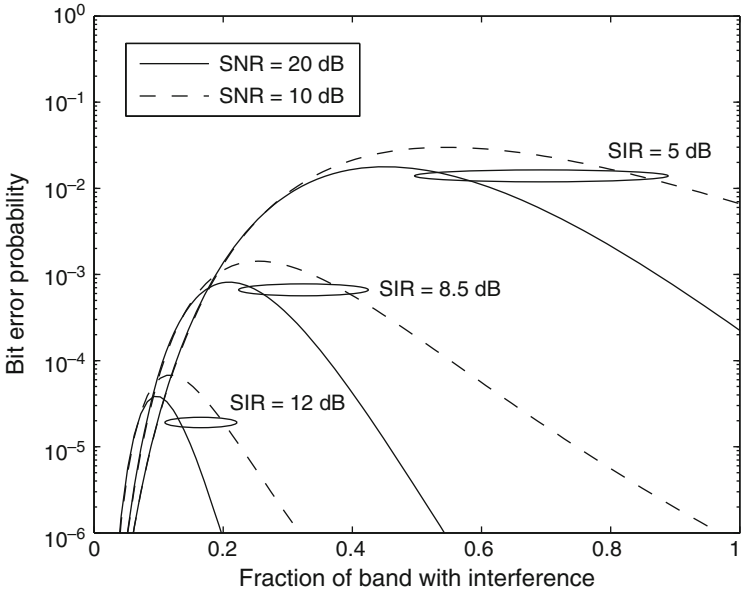

Fig. 3.12 Performance of FH/FSK with Reed–Solomon (8,3) code, $q = 8$, erasures, $N_t = 4$, and no fading

decision variable to the second largest one. This ratio is then compared to a threshold to determine an erasure. If the values of both $\mathcal{E}_b/N_0$ and $\mathcal{E}_b/I_{t0}$ are known, then optimum thresholds for the OTT, the RTT, or a hybrid method can be calculated. It is found that the OTT is resilient against fading and tends to outperform the RTT when $\mathcal{E}_b/I_{t0}$ is sufficiently low, but the opposite is true when $\mathcal{E}_b/I_{t0}$ is sufficiently high. The main disadvantage of the OTT and the RTT relative to the pilot-symbol method is the need to estimate $\mathcal{E}_b/N_0$ and either $\mathcal{E}_b/I_{t0}$ or $\mathcal{E}_b/(N_0 + I_{t0})$. Although the RTT suppresses partial-band interference, it is not as resilient against fading as OTT. The joint *maximum-output ratio threshold test* (MO-RTT) uses both the maximum and the second largest of the decision variables. It is robust against both fading and partial-band interference.

Proposed erasure methods are based on the use of FSK symbols, and their performances against partial-band interference improve as the alphabet size q increases. For a fixed hopping band, the number of frequency channels decreases as q increases, thereby making an FH/FSK system more vulnerable to narrowband jamming signals (Sect. 3.2) or multiple-access interference (Chap. 6).

Figure 3.12 depicts P_b for FH/FSK with $q = 8$, an extended Reed–Solomon (8,3) code, $N_t = 4$, and $\delta = 0$. A comparison of Figs. 3.12 and 3.11 indicates that reducing the alphabet size while preserving the code rate has increased the system sensitivity to $\mathcal{E}_b/N_0$, increased the susceptibility to interference concentrated in a small fraction of the hopping band, and raised the required $\mathcal{E}_b/I_{t0}$ for a specified P_b by 5 to 9 dB.

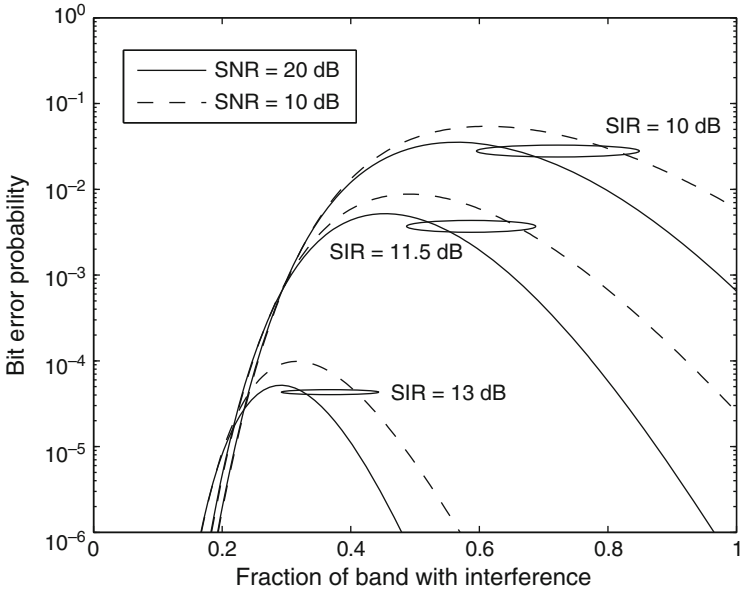

Fig. 3.13 Performance of FH/DPSK with Reed–Solomon (32,12) code, binary channel symbols, erasures, $N_t = 10$, and no fading

Another approach is to represent each nonbinary code symbol by a sequence of $\log_2 q$ consecutive binary channel symbols. Then an FH/MSK or FH/DPSK system can be implemented to provide a large number of frequency channels and, hence, better protection against multiple-access interference. Equations (3.92), (3.93), and (3.95) are still valid. However, since a code-symbol error occurs if any of its $\log_2 q$ component channel symbols is incorrect, (3.94) is replaced by

$$P_s = 1 - [1 - \mu(1 - P_{\epsilon 1})P_{s1} - (1 - \mu)(1 - P_{\epsilon 0})P_{s0}]^{\log_2 q} \tag{3.97}$$

and (3.82) is replaced by (3.85), where $\xi = 1/2$ for MSK and $\xi = 1$ for DPSK. The results for an FH/DPSK system with an extended Reed–Solomon (32,12) code, $N_t = 10$ binary pilot symbols, and $\delta = 0$ are shown in Fig. 3.13. It is assumed that $N_h \gg 1$ so that the loss due to the reference symbol in each dwell interval is negligible. The graphs in Fig. 3.13 are similar in form to those of Fig. 3.11, but the transmission of binary rather than nonbinary symbols has caused approximately a 10 dB increase in the required $\mathcal{E}_b/I_{t0}$ for a specified P_b. Figure 3.13 is applicable to orthogonal FSK and MSK if $\mathcal{E}_b/I_{t0}$ and $\mathcal{E}_b/N_0$ are both increased by 3 dB to compensate for the lower value of ξ.

An alternative to erasures that uses binary channel symbols is an FH/DPSK system with concatenated coding (Sect. 1.4). Although generally unnecessary in a fast frequency-hopping system, the channel interleaver and deinterleaver may be

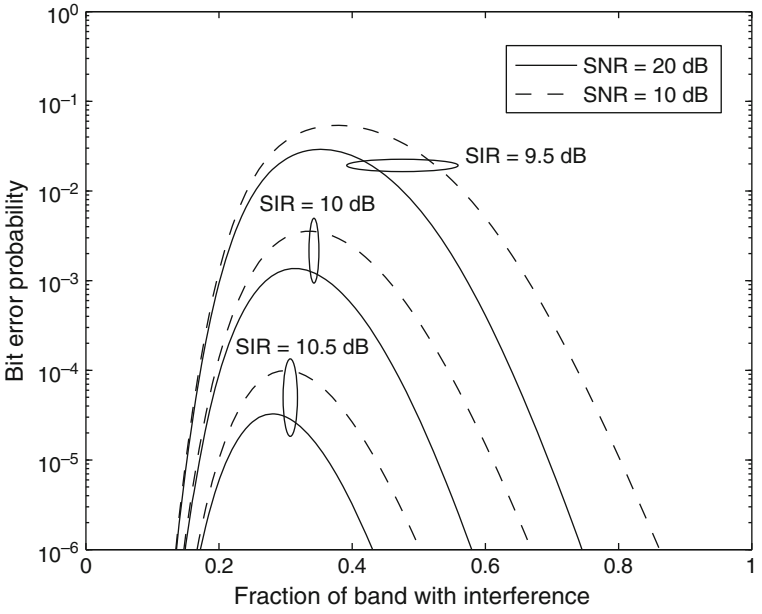

Fig. 3.14 Performance of FH/DPSK with concatenated code, binary channel symbols, hard decisions, and no fading. Inner code is convolutional (rate = 1/2, $K = 7$) code and outer code is Reed–Solomon (31,21) code

required in a slow frequency- hopping system to ensure independent symbol errors at the decoder input. Consider a concatenated code comprising a Reed–Solomon (n, k) outer code and a binary convolutional inner code. The inner Viterbi decoder performs hard- decision decoding to limit the impact of individual symbol metrics. Assuming that $N_h \gg 1$, the symbol error probability is given by (3.81) and (3.85) with $\xi = 1$. The probability of a Reed–Solomon symbol error, P_{s1}, at the output of the Viterbi decoder is upper-bounded by (1.142) and (1.112). Setting $P_s = P_{s1}$ in (3.91) then provides an upper bound on P_b. Figure 3.14 depicts this bound for an outer Reed–Solomon (31,21) code and an inner rate-1/2, $K = 7$ convolutional code. This concatenated code provides a better performance than the Reed–Solomon (32,12) code with binary channel symbols, but a much worse performance than the latter code with nonbinary channel symbols. Figures 3.11 through 3.14 indicate that a reduction in the alphabet size for channel symbols increases the system susceptibility to partial-band interference. The primary reason is the reduced energy per channel symbol.

3.5.2 Trellis-Coded Modulation

Trellis-coded modulation is a combined coding and modulation method that is usually applied to coherent digital communications over bandlimited channels

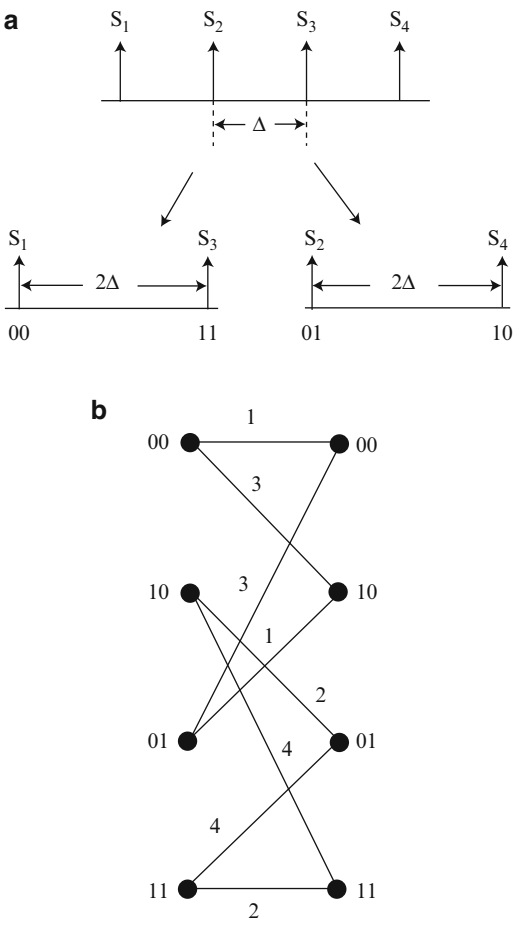

Fig. 3.15 Rate-1/2, four-state trellis-coded 4-ary FSK: (**a**) signal set partitioning and mapping of bits to signals, and (**b**) mapping of signals to state transitions

(Chap. 1). Multilevel and multiphase modulations are used to enlarge the signal constellation while not expanding the bandwidth beyond what is required for the uncoded signals. Since the signal constellation is more compact, there is some modulation loss that detracts from the coding gain, but the overall gain can be substantial. Since a noncoherent demodulator is usually required for frequency-hopping communications, the usual coherent trellis-coded modulations are not suitable. Instead, the trellis coding may be implemented by expanding the signal set for $q/2$-ary FSK to q-ary FSK. Although the frequency tones are uniformly spaced, they are allowed to be nonorthogonal to limit or avoid bandwidth expansion.

Trellis-coded 4-ary FSK is illustrated in Fig. 3.15 for a system that uses a 4-state, rate-1/2, convolutional code followed by a symbol mapper. The signal set partitioning, shown in Fig. 3.15a, partitions the set of four signals or tones into two subsets, each with two tones. The partitioning doubles the frequency separation between tones from Δ Hz to 2Δ Hz. The mapping of the code bits produced by the

convolutional encoder into signals is indicated. In Fig. 3.15b, the numerical labels denote the signal assignments associated with the state transitions in the trellis for a four-state encoder. The bandwidth of the frequency channel that accommodates the four tones is approximately $B = 4\Delta$.

There is a trade-off in the choice of Δ because a small Δ allows more frequency channels and thereby limits the effect of multiple-access interference or multitone jamming, whereas a large Δ tends to improve the system performance against partial-band interference. If a trellis code uses four orthogonal tones with spacing $\Delta = 1/T_b$, where T_b is the bit duration, then $B = 4/T_b$. The same bandwidth results when an FH/FSK system uses two orthogonal tones, a rate-1/2 code, and binary channel symbols since $B = 2/T_s = 4/T_b$. The same bandwidth also results when a rate-1/2 binary convolutional code is used and each pair of code symbols is mapped into a 4-ary channel symbol. The performance of the 4-state, trellis-coded, rate-1/2, 4-ary FSK frequency-hopping system [11] indicates that it is not as strong against worst-case partial-band interference as an FH/FSK system with a rate-1/2 convolutional code and 4-ary channel symbols or an FH/FSK system with a Reed–Solomon (32,16) code and errors-and-erasures decoding. Thus, trellis-coded modulation is relatively weak against partial-band interference. The advantage of trellis-coded modulation in a frequency-hopping system is its relatively low implementation complexity.

3.5.3 Turbo and LDPC Codes

Turbo and LDPC codes are potentially the most effective codes for suppressing partial-band interference if the system latency and computational complexity of these codes is acceptable. A turbo-coded frequency-hopping system that uses spectrally compact channel symbols will also resist multiple-access interference (Chap. 8). Accurate estimates of channel parameters such as the variance of the interference plus noise and the fading amplitude are needed in the iterative turbo decoding algorithms (Chap. 1). When the channel dynamics are slower than the hop rate, all the received symbols of a dwell interval may be used in estimating the channel parameters associated with that dwell interval.

The architecture of iterative turbo or LDPC decoding and channel estimation is illustrated in Fig. 3.16. For turbo decoding, the *log-likelihood ratio* (LLR) of a bit b_k conditioned on a received sequence $\mathbf{y}_i$ of demodulator outputs applied to decoder i is defined by (1.156) as

$$\Lambda_{ki} = \log\left[\frac{P(b_k = 1|\mathbf{y}_i)}{P(b_k = 0|\mathbf{y}_i)}\right], \quad i = 1, 2. \tag{3.98}$$

Successive estimates of the LLRs of the code bits are computed by each component decoder during the iterative decoding of the turbo code. The usual turbo decoding is extended to include the iterative updating of the LLRs of both

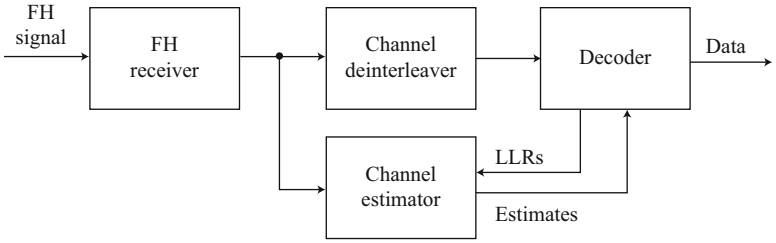

Fig. 3.16 Receiver and decoder architecture for frequency-hopping system with turbo or LDPC code

the information and parity bits. After each iteration by a component decoder, its LLRs are updated and the extrinsic information is transferred to the other component decoder. The fact that $P(b_k = 1|\mathbf{y}_i) = 1 - P(b_k = 0|\mathbf{y}_i)$ and (3.98) imply that the *a posteriori* probabilities are

$$p_{1ki} = P(b_k = 1|\mathbf{y}_i) = \frac{1}{1 + \exp(-\Lambda_{ki})} \tag{3.99}$$

$$p_{0ki} = P(b_k = 0|\mathbf{y}_i) = \frac{\exp(-\Lambda_{ki})}{1 + \exp(-\Lambda_{ki})}. \tag{3.100}$$

These equations indicate that the channel estimator can convert a LLR transferred after a component decoder iteration into the probabilities p_{1ki} and p_{0ki}. These probabilities can be used to improve the estimates of the fading attenuation and the noise variance for each dwell interval, which can be integrated into the iterative demodulation and decoding. The operation of a receiver with iterative LDPC decoding and channel estimation is similar.

Known symbols may be inserted into the transmitted code symbols to facilitate the estimation, but the energy per information bit is reduced. Increasing the number of symbols per hop N_h improves the estimates because they may be based on more observations and more known symbols can be accommodated. However, since the reduction in the number of independent hops per information block of fixed size decreases the diversity, and hence the independence of errors, there is a limit on N_h beyond which a performance degradation occurs. A full analysis of a robust frequency-hopping system that suppresses both partial-band and multiple-access interference and multitone jamming is presented in Chap. 8.

A turbo code can still provide a fairly good performance against partial-band interference even if only the presence or absence of strong interference is detected. For this purpose, turbo product codes (Chap. 1) are an attractive option because of their reduced complexity compared with other turbo codes. The outer encoder fills the block interleaver row-by-row with the outer codewords. Since the interleaver columns are read by the inner encoder to provide the channel symbols, there is interleaving of the outer-code symbols but no interleaving of the inner-code

symbols. In the absence of interleaving, severely corrupted inner codewords cannot provide significant information for decoding of the outer codewords during the iterative decoding of the turbo product code. Thus, the channel interleaver of Fig. 1.14 is an essential part of the transmitter of a turbo product code. The channel interleaver precludes the possibility that sufficiently corrupted inner codewords due to dwell intervals hit by interference can undermine the iterative process in the turbo decoder, which is illustrated in Fig. 1.20. Side information about whether or not a hit has occurred is obtained by hard-decision decoding of the inner codewords. The metric for determining a hit occurrence is the Hamming distance between the binary sequence resulting from the hard decisions and the codewords obtained by bounded-distance decoding. When full interleaving and side information are used, the turbo product code performs well except for a slight inferiority against partial-band interference occupying a small fraction of the hopping band [12].

3.6 Frequency Synthesizers

A *frequency synthesizer* [13–16] converts a standard reference frequency into a different desired frequency. In a frequency-hopping system, the frequencies of the hopset must be synthesized. In practical applications, the frequencies of the hopset have the form

$$f_{hi} = af_1 + b_i f_r, \quad i = 1, 2, ..., M \tag{3.101}$$

where a and the $\{b_i\}$ are rational numbers, f_r is the reference frequency, and f_1 is a frequency in the spectral band of the hopset. The *reference signal*, which is a tone at the reference frequency, is usually generated by dividing or multiplying by a positive integer the frequency of the tone produced by a stable source, such as an atomic or crystal oscillator. The use of a single reference signal, which even generates f_1, ensures that any output frequency of the synthesizer has the same stability and accuracy as the reference. The three fundamental types of frequency synthesizers are the direct, digital, and indirect synthesizers. Most practical synthesizers are hybrids of these fundamental types.

3.6.1 Direct Frequency Synthesizer

A *direct frequency synthesizer* uses frequency multipliers and dividers, mixers, bandpass filters, and electronic switches to produce signals with the desired frequencies. Direct frequency synthesizers provide both very fine resolution and high frequencies, but often require a very large amount of hardware and do not provide a phase-continuous output after frequency changes. Although a direct synthesizer can be realized with programmable dividers and multipliers, the standard approach is to use the *double-mix-divide* (DMD) system illustrated in Fig. 3.17. The reference

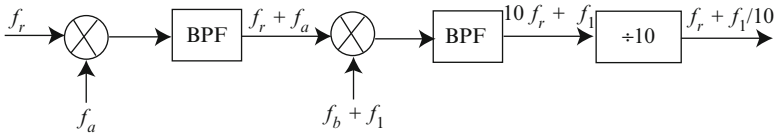

Fig. 3.17 Double-mix-divide module, where BPF = bandpass filter

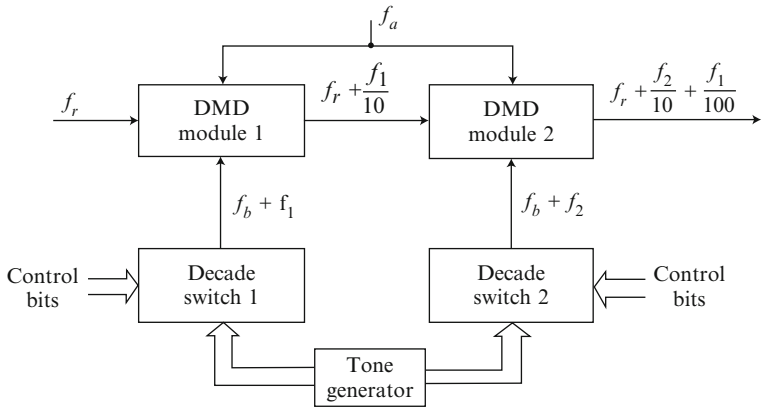

Fig. 3.18 Direct frequency synthesizer with two-digit resolution

signal at frequency f_r is mixed with a tone at the fixed frequency f_a. The bandpass filter selects the sum frequency $f_r + f_a$ produced by the mixer. Another mixing and filtering operation with a tone at $f_b + f_1$ produces the frequency $f_r + f_a + f_b + f_1$. If the fixed frequencies f_a and f_b are chosen so that

$$f_a + f_b = 9f_r \tag{3.102}$$

then the divider, which reduces the frequency of its input by a factor of 10, produces the output frequency $f_r + f_1/10$. In principle, a single mixer and bandpass filter could produce this output frequency, but two mixers and bandpass filters simplify the filters. Each bandpass filter must select the sum frequency while suppressing the difference frequency and the mixer input frequencies, which may enter the filter because of mixer leakage. If the sum frequency is too close to one of these other frequencies, the bandpass filter becomes prohibitively complex and expensive.

The DMD system of Fig. 3.17 can be used as a module in a direct frequency synthesizer that can achieve arbitrary frequency resolution by cascading enough DMD modules. A synthesizer that provides two-digit resolution is shown in Fig. 3.18. When the synthesizer is used in a frequency-hopping system, the control bits are produced by the code generator. Each set of control bits determines a single tone that the decade switch passes to a DMD module. The ten tones that are available to the decade switches may be produced by applying the reference

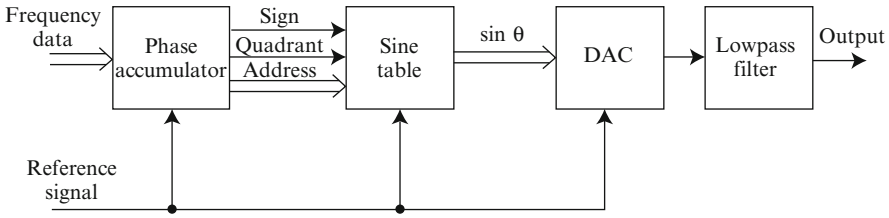

Fig. 3.19 Digital frequency synthesizer

frequency to appropriate frequency multipliers and dividers in the tone generator. Equation (3.102) ensures that the output frequency of the second bandpass filter in DMD module 2 is $10f_r + f_2 + f_1/10$. Thus, the final synthesizer output frequency is $f_r + f_2/10 + f_1/100$.

Example 3.1. It is desired to produce a 1.79 MHz tone. Let $f_r = 1$ MHz and $f_b = 5$ MHz. The ten tones provided to the decade switches are 5, 6, 7, ..., 14 MHz so that f_1 and f_2 can range from 0 to 9 MHz. Equation (3.102) yields $f_a = 4$ MHz. If $f_1 = 7$ MHz and $f_2 = 9$ MHz, then the output frequency is 1.79 MHz. The frequencies f_a and f_b are such that the designs of the bandpass filters inside the modules are reasonably simple. □

3.6.2 Direct Digital Synthesizer

A *direct digital synthesizer,* which is a discrete-time version of a voltage controlled oscillator, converts the stored sample values of a sine wave into an analog sine wave with a specified frequency. The periodic and symmetric character of a sine wave implies that only values for the first quadrant need to be stored. The basic elements of a digital frequency synthesizer are shown in Fig. 3.19. The *reference signal* is a sinusoidal signal with *reference frequency* f_r. A set of bits, which are produced by the code generator in a frequency-hopping system, determine the synthesized frequency by specifying a phase increment δ. The *phase accumulator,* which is a discrete-time integrator, converts the phase increment into successive samples of the phase by adding the increment to the content of an internal register at the rate f_r after every cycle of the reference signal. A phase sample θ, which is an integer multiple of δ, defines an address in the sine table or memory in which the values of $\sin\theta$ are stored. Each value is applied to a digital-to-analog converter (DAC), which performs a sample-and-hold operation at a sampling rate equal to the reference frequency f_r. The DAC output is applied to an anti-aliasing lowpass filter, the output of which is the desired analog signal.

Let ν denote the number of bits used to represent the $N \leq 2^\nu$ possible values of the phase accumulator contents. Since the contents are updated at the rate f_r, the longest period of distinct phase samples before repetition is N/f_r. Therefore,

since the sample values of sin θ are applied to the DAC at the rate f_r, the smallest frequency that can be generated by the direct digital synthesizer is the inverse of this period:

$$f_{\min} = \frac{f_r}{N}. \tag{3.103}$$

The output frequency f_{0k} is produced when every kth stored sample value of the phase θ is applied to the DAC at the rate f_r. Thus, if the phase sample is $\theta = k\delta = k2\pi/N$ after every cycle of the reference signal, then

$$f_{0k} = kf_{\min} \tag{3.104}$$

which implies that $f_{\min}$ is the frequency resolution.

The maximum frequency $f_{\max}$ that can be generated is produced by using only a few samples of sin θ per period. From the Nyquist sampling theorem, it is known that $f_{\max} < f_r/2$ is required to avoid aliasing. Practical DAC and lowpass filter requirements further limit $f_{\max}$ to approximately 0.4 f_r or less. Thus, $q \geq 2.5$ samples of sin θ per period are used in synthesizing $f_{\max}$, and

$$f_{\max} = \frac{f_r}{q}. \tag{3.105}$$

The lowpass filter may be implemented with a linear phase across a flat passband extending slightly above $f_{\max}$. The frequencies f_r and $f_{\max}$ are limited by the speed of the DAC.

Suppose that $f_{\min}$ and $f_{\max}$ are specified minimum and maximum frequencies that must be produced by a synthesizer. Equations (3.103) and (3.105) imply that $qf_{\max}/f_{\min} = N \leq 2^{\nu}$, and the required number of accumulator bits is

$$\nu = \lfloor \log_2(qf_{\max}/f_{\min}) \rfloor + 1 \tag{3.106}$$

where $\lfloor x \rfloor$ denotes the largest integer in x.

The sine table stores 2^n words, each comprising m bits, and hence has a memory requirement of $2^n m$ bits. The memory requirements of a sine table can be reduced by using trigonometric identities and hardware multipliers. Each stored word represents one possible value of sin θ in the first quadrant or, equivalently, one possible magnitude of sin θ. The input to the sine table comprises $n + 2$ parallel bits. The two most significant bits are the *sign bit* and the *quadrant bit*. The sign bit specifies the polarity of sin θ. The quadrant bit specifies whether sin θ is in the first or second quadrants or in the third or fourth quadrants. The n least significant bits of the input determine the address in which the magnitude of sin θ is stored. The address specified by the n least significant bits is appropriately modified by the quadrant bit when θ is in the second or fourth quadrants. The sign bit along with the m output bits of the sine table are applied to the DAC. The maximum number of table addresses that the phase accumulator can specify is 2^{ν}, but if ν input lines were applied to the

sine table, the memory requirement generally would be impractically large. Since $n+2$ bits are needed to address the sine table, the $\nu - n - 2$ least significant bits in the accumulator contents are not used to address the table.

If n is decreased, the memory requirement of the sine table is reduced, but the truncation of the potential accumulator output from ν to $n+2$ bits causes the table output to remain constant for $\nu - n - 2$ samples of $\sin\theta$ per period. Since the true phase $\theta(n)$ is only approximated by $\widehat{\theta}(n)$, the input to the sine table, there are spurious spectral lines in the spectrum of the table output. The phase error, $\delta(n) = \theta(n) - \widehat{\theta}(n)$, is a periodic ramp with a discrete spectrum. For $\delta(n) \ll 1$, a trigonometric expansion indicates that

$$\sin(\theta(n)) \approx \sin\left(\widehat{\theta}(n)\right) + \delta(n)\cos\left(\widehat{\theta}(n)\right). \tag{3.107}$$

The amplitudes of the spurious spectral lines are determined by the coefficients of the Fourier series of $\delta(n)$, and the largest amplitude is $2^{-(n+2)}$. The power in the largest of the spectral lines, which is often the limiting factor in applications, is

$$E_s = (2^{-(n+2)})^2 = (-6n - 12)\,dB. \tag{3.108}$$

There are several methods, each entailing an additional implementation cost, that can reduce the peak amplitudes of the spurious spectral lines. The *error feedforward method* computes the right-hand side of (3.107), which then provides a more accurate estimate of the desired $\sin(\theta(n))$. The computational requirements are a multiplication and an addition with m bits of precision at the sample rate. Other methods of reducing the peak amplitudes are based on dithering and error feedback.

Since m ROM output bits specify the magnitude of $\sin\theta$, the quantization error produces the worst-case *amplitude-quantization noise power*

$$E_q = (2^{-m})^2 \cong -6m\,dB \tag{3.109}$$

relative to the signal in the ROM output. Quantization noise increases the amplitudes of spurious spectral lines in the table output.

Example 3.2. A direct digital synthesizer is to be designed to cover 1 kHz to 1 MHz with $E_q \le -45$ dB and $E_s \le -60$ dB. According to (3.109), the use of 8-bit words in the sine table is adequate for the required quantization noise level. With $m = 8$, the table contains $2^8 = 256$ distinct words. According to (3.108), $n = 8$ is satisfactory, and hence the table has $n + 2 = 10$ input bits. If $2.5 \le q \le 4$, then since $f_{\max}/f_{\min} = 10^3$, (3.106) yields $\nu = 12$. Thus, a 12-bit phase accumulator is needed. Since $2^{12} = 4096$, we may choose $N = 4{,}000$. If the frequency resolution and smallest frequency is to be $f_{\min} = 1$ kHz, then (3.103) indicates that $f_r = 4$ MHz is required. When the frequency $f_{\min}$ is desired, the phase increments are so small that $2^{\nu-n-2} = 4$ increments occur before a new address is specified and a new value of $\sin\theta$ is produced. Thus, the four least-significant bits in the accumulator are not used in the addressing of the sine table. □

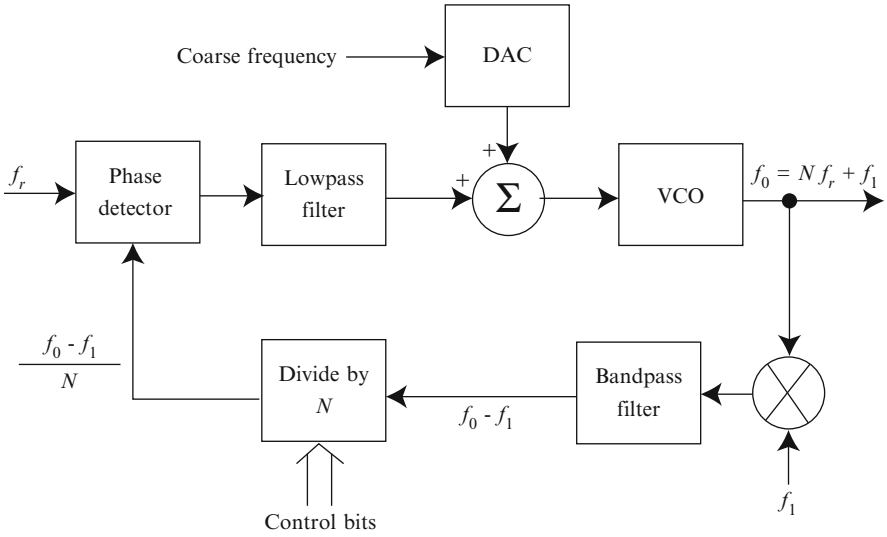

Fig. 3.20 Indirect frequency synthesizer with single loop

The direct digital synthesizer can be easily modified to produce a modulated output when high-speed digital data is available. For amplitude modulation, the table output is applied to a multiplier. Phase modulation may be implemented by adding the appropriate bits to the phase accumulator output. Frequency modulation entails a modification of the accumulator input bits. For a quaternary modulation, the quadrature signals may be generated by separate sine and cosine tables.

A direct digital synthesizer can produce nearly instantaneous, phase-continuous frequency changes and a very fine frequency resolution despite its relatively small size, weight, and power requirements. A disadvantage is the limited maximum frequency, which restricts the bandwidth of the covered frequencies following a frequency translation of the synthesizer output. For this reason, direct digital synthesizers are sometimes used as components in hybrid synthesizers. Another disadvantage is the stringent requirement for the lowpass filter to suppress frequency spurs generated during changes in the synthesized frequency.

3.6.3 Indirect Frequency Synthesizers

An *indirect frequency synthesizer* uses voltage-controlled oscillators and feedback loops. Indirect synthesizers usually require less hardware than comparable direct ones, but require more time to switch from one frequency to another. Like digital synthesizers, indirect synthesizers inherently produce phase-continuous outputs after frequency changes. The principal components of a single-loop indirect synthesizer, which is similar in operation to a phase-locked loop, are depicted in Fig. 3.20.

The control bits, which determine the value of the modulus or divisor N, are supplied by a code generator. The input signal at frequency f_1 may be provided by another synthesizer. Since the feedback loop forces the frequency of the divider output, $(f_0 - f_1)/N$, to closely approximate the reference frequency f_r, the output of the voltage-controlled oscillator (VCO) is a sine wave with frequency

$$f_0 = Nf_r + f_1 \tag{3.110}$$

where N is a positive integer. *Phase detectors* in frequency-hopping synthesizers are usually digital devices that measure zero-crossing times rather than the phase differences measured when mixers are used. Digital phase detectors have an extended linear range, are less sensitive to input-level variations, and simplify the interface with a digital divider.

Since the output frequencies change in increments of f_r, the frequency resolution of the single-loop synthesizer is f_r. For stable operation and the suppression of sidebands that are offset from f_0 by f_r, it is desirable that the loop bandwidth be on the order of 0.1 f_r. The *switching time* t_s for changing frequencies, which is inversely proportional to the loop bandwidth, is roughly approximated by

$$t_s = \frac{25}{f_r}. \tag{3.111}$$

This equation indicates that a low resolution and a low switching time may not be achievable by a single loop. The switching time t_s is less than or equal to T_{sw} defined previously for frequency-hopping pulses, which may have additional guard time inserted. To decrease the switching time while maintaining the frequency resolution of a single loop, a coarse steering signal can be stored in a ROM, converted into analog form by a DAC, and applied to the VCO (as shown in Fig. 3.20) immediately after a frequency change. The steering signal reduces the frequency step that must be acquired by the loop when a hop occurs. An alternative approach is to place a fixed divider with modulus M after the loop so that the output frequency is $f_0 = Nf_r/M + f_1/M$. By this means, f_r can be increased without sacrificing resolution provided that the VCO output frequency, which equals Mf_0, is not too large for the divider in the feedback loop. To limit the transmission of spurious frequencies, it may be desirable to inhibit the transmitter output during frequency transitions.

The switching time can be dramatically reduced by using two synthesizers that alternately produce the output frequency. One synthesizer produces the output frequency while the second one is being tuned to the next frequency following a command from the code generator. If the hop duration exceeds the switching time of each synthesizer, then the second synthesizer begins producing the next frequency before a control switch routes its output to a modulator or a dehopping mixer.

A *divider* is a binary counter that produces a square-wave output. The divider counts down by one unit every time its input crosses zero. If the modulus or divisor is the positive integer N, then after N zero crossings, the divider output crosses zero and changes state. The divider then resumes counting down from N.

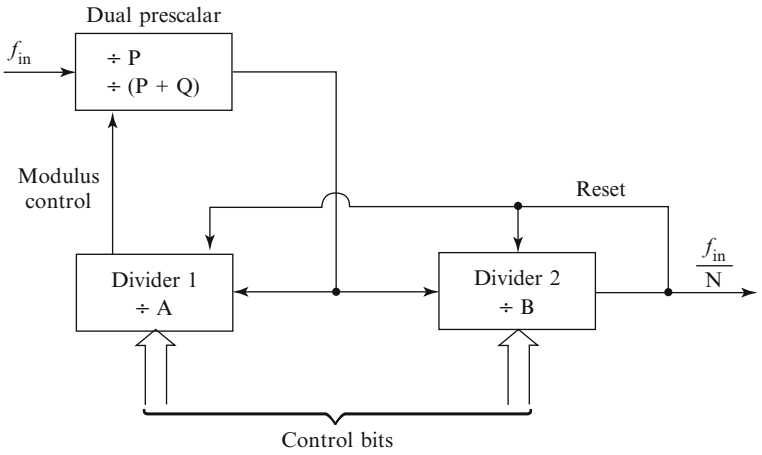

Fig. 3.21 Dual-modulus divider

Programmable dividers have limited operating speeds that impair their ability to accommodate a high-frequency VCO output. A problem is avoided by the down-conversion of the VCO output by the mixer shown in Fig. 3.20, but spurious components are introduced. Since fixed dividers can operate at much higher speeds than programmable dividers, one might consider placing a fixed divider before the programmable divider in the feedback loop. However, if the fixed divider has a modulus N_1, then the loop resolution becomes $N_1 f_r$ so this solution is usually unsatisfactory.

A *dual-modulus divider*, which is depicted in Fig. 3.21, allows synthesizer operation at high frequencies while maintaining the frequency resolution equal to f_r. The *dual prescalar* consists of two fixed dividers with divisors equal to the positive integers P and $P + Q$. The two programmable dividers count down from the integers A and B, where $B > A$ and A is nonnegative. These programmable dividers are only required to accommodate a frequency f_{in}/P. The dual prescalar initially divides by the modulus $P + Q$. This modulus changes whenever a programmable divider reaches zero. After $(P + Q)A$ input transitions, divider 1 reaches zero, and the modulus control causes the dual prescalar to divide by P. Divider 2 has counted down to $B-A$. After $P(B-A)$ more input transitions, divider 2 reaches zero and causes an output transition. The two programmable dividers are then reset, and the dual prescalar reverts to division by $P + Q$. Thus, each output transition corresponds to $A(P + Q) + P(B - A) = AQ + PB$ input transitions, which implies that the dual-modulus divider has a modulus

$$N = AQ + PB, \quad B > A \tag{3.112}$$

and produces the output frequency f_{in}/N.

If $Q = 1$ and $P = 10$, then the dual-modulus divider is called a *10/11 divider*, and

$$N = 10B + A, \quad B > A \tag{3.113}$$

which can be increased in unit steps by changing A in unit steps. Since $B > A$ is required, a suitable range for A and minimum value of B are

$$0 \leq A \leq 9, \qquad B_{\min} = 10. \tag{3.114}$$

The relations (3.110), (3.113), and (3.114) indicate that the range of a synthesized hopset is from $f_1 + 100f_r$ to $f_1 + (10B_{\max} + 9)f_r$. Therefore, a spectral band between f_{min} and f_{max} is covered by the hopset if

$$f_1 + 100f_r \leq f_{min} \tag{3.115}$$

and

$$f_1 + (10B_{\max} + 9)f_r \geq f_{max}. \tag{3.116}$$

Example 3.3. The *Bluetooth* communication system is used to establish wireless communications among portable electronic devices. The system has a hopset of 79 carrier frequencies, its hop rate is 1,600 hops per second, its hop band is between 2,400 and 2,483.5 MHz, and the bandwidth of each frequency channel is 1 MHz. Consider a system in which the 79 carrier frequencies are spaced 1 MHz apart from 2,402 MHz to 2,480 MHz. A 10/11 divider with $f_r = 1$ MHz provides the desired increment, which is equal to the frequency resolution. Equation (3.111) indicates that $t_s = 25\,\mu s$, which indicates that 25 potential data symbols will have to be omitted during each hop interval. Inequality (3.115) indicates that $f_1 = 2{,}300$ MHz is a suitable choice. Then (3.116) is satisfied by $B_{max} = 18$. Therefore, dividers A and B require 4 and 5 control bits, respectively, to specify their potential values. If the control bits are stored in a ROM, then each ROM location contains nine bits. The number of ROM addresses is at least 79, the number of frequencies in the hopset. Thus, a ROM input address requires seven bits. □

3.6.3.1 Multiple Loops

A *multiple-loop frequency synthesizer* uses two or more single-loop synthesizers to obtain both fine frequency resolution and fast switching. A three-loop frequency synthesizer is shown in Fig. 3.22. Loops A and B have the form of Fig. 3.20, but loop A does not have a mixer and filter in its feedback. Loop C has the mixer and filter, but lacks the divider. The reference frequency f_r is chosen to ensure that the desired switching time is realized. If $A > M$, then loop C does not appreciably degrade the switching time. The divisor M is chosen so that f_r/M is equal to the desired resolution. Loop A and the divider generate increments of f_r/M while loop

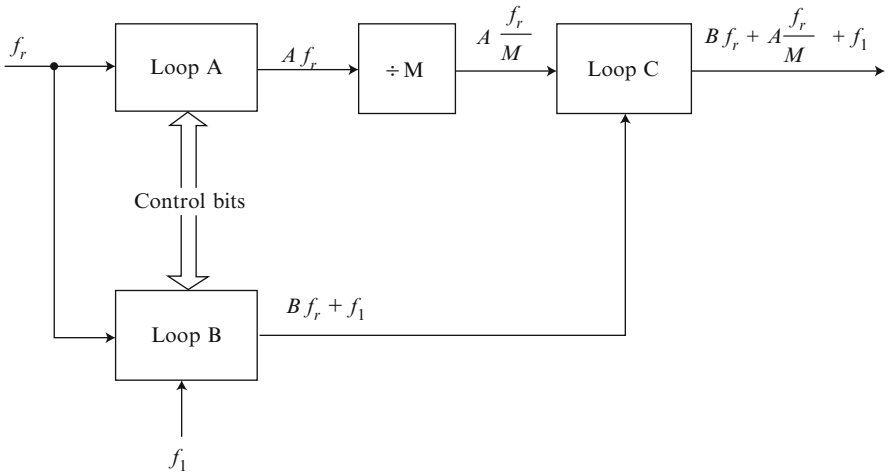

Fig. 3.22 Indirect frequency synthesizer with three loops

B generates increments of f_r. Loop C combines the outputs of loops A and B to produce the output frequency

$$f_0 = Bf_r + A\frac{f_r}{M} + f_1 \tag{3.117}$$

where B, A, and M are positive integers because they are produced by dividers. Loop C is preferable to a mixer and bandpass filter because the filter would have to suppress a closely spaced, unwanted component when Af_r/M and Bf_r were far apart. To ensure that each output frequency is produced by unique values of A and B, it is required that $A_{max} = A_{min} + M - 1$. To prevent degradation in the switching time, it is required that $A_{\min} > M$. Both requirements are met by choosing

$$A_{min} = M + 1, \qquad A_{max} = 2M. \tag{3.118}$$

According to (3.117), a range of frequencies from f_{min} to f_{max} is covered if

$$B_{min} f_r + A_{min}\frac{f_r}{M} + f_1 \leq f_{min} \tag{3.119}$$

and

$$B_{max} f_r + A_{max}\frac{f_r}{M} + f_1 \geq f_{max}. \tag{3.120}$$

Example 3.4. Consider the Bluetooth system of Example 3.3 but with the more stringent requirement that $t_s = 2.5\mu$s, which only sacrifices three potential data symbols per hop interval. The single-loop synthesizer of Example 3.3 cannot provide this short switching time. The required switching time is provided by a

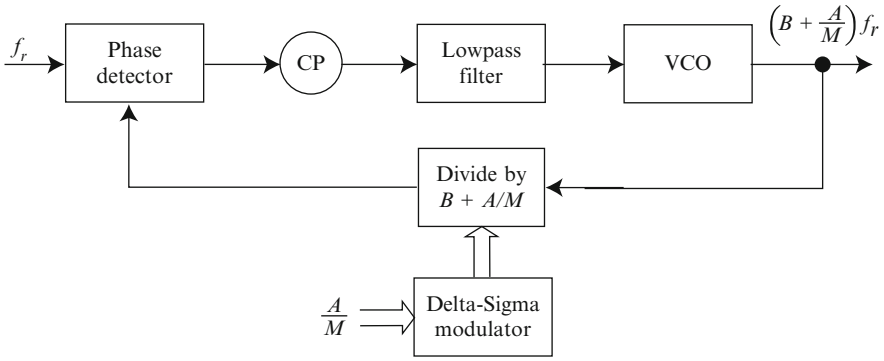

Fig. 3.23 Fractional-N frequency synthesizer

three-loop synthesizer with $f_r = 10\,\text{MHz}$. The resolution of 1 MHz is achieved by taking $M = 10$. Equations (3.118) indicate that $A_{min} = 11$ and $A_{max} = 20$. Inequalities (3.119) and (3.120) are satisfied if $f_1 = 2,300\,\text{MHz}$, $B_{min} = 9$, and $B_{max} = 16$. The maximum frequencies that must be accommodated by the dividers in loops A and B are $A_{max} f_r = 200\,\text{MHz}$ and $B_{max} f_r = 160\,\text{MHz}$, respectively. Dividers A and B require 5 and 4 control bits, respectively. □

3.6.3.2 Fractional-N Synthesizer

A *fractional-N synthesizer* uses a single loop and auxiliary hardware to produce an output frequency given by (3.117) with $0 \leq A \leq M - 1$. Although the switching time is inversely proportional to f_r, the resolution is f_r/M, which can be made arbitrarily small in principle. The synthesis method alters the loop feedback by changing the frequency division modulus every reference period according to a sequence of small integers $y[n]$ such that the effective divisor is $N = B + A/M$. The main disadvantage of the fractional-N synthesizer is its production of relatively high-level spurious signals and phase noise that frequency-modulate its output signal.

As shown in Fig. 3.23, the phase detector compares the arrival times of the rising edges of the frequency-divider output with those of the reference signal. A charge pump (CP) draws proportionate charge into the lowpass filter, the output of which is the control signal of the VCO. The output frequency of the VCO is $Nf_r = (B + A/M) f_r$. However, the reference signal and the divider output have an instantaneous frequency error equal to $(y[n] - A/M) f_r$ that causes spurious signals in the power spectral density of the VCO output. These spurious signals and the phase noise are partially suppressed by the lowpass loop filter. The delta-sigma modulator generates the sequence $y[n]$, which is a quantization of A/M. The loop bandwidth, which is usually less than $0.1 f_r$ to ensure stability, can be set to a high

value because the resolution is no longer limited to the reference frequency. As a result, there is better VCO phase-noise suppression at the cost of increased phase noise due to the quantization noise.

Example 3.5. Consider a fractional-N synthesizer for the Bluetooth system of Example 3.4 in which $t_s = 2.5\mu s$. If the output of the fractional-N synthesizer is frequency-translated by 2,300 MHz, then the synthesizer itself needs to cover 102 MHz to 180 MHz. The switching time is achieved by taking $f_r = 10$ MHz. The resolution is achieved by taking $M = 10$. Equation (3.117) indicates that the required frequencies are covered by varying B from 10 to 18 and A from 0 to 9. The integers B and A require 5 and 4 control bits, respectively. □

Problems

3.1. An n-stage feedback shift register is used as the code generator in the FH/FSK transmitter shown in Fig. 3.5a. What is the maximum number of effective frequency channels in the hopset? What is required for message privacy?

3.2. Consider FH/FSK with soft-decision decoding of repetition codes and $\mathcal{E}_b/I_{t0} \geq 3/(\log_2 q)$. Show that n_0 is given by (3.25).

3.3. Consider FH/FSK with soft-decision decoding of repetition codes and large values of $\mathcal{E}_b/I_{t0}$. Suppose that the number of repetitions is not chosen to minimize the potential impact of partial-band jamming. Show that a nonbinary modulation with $m = \log_2 q$ bits per symbol gives a better performance than binary modulation in the presence of worst-case partial-band jamming if $n > (m-1)\ln(2)/\ln(m)$.

3.4. Draw the block diagram of a receiver for an FH/FSK system with an independently hopped FSK set. This system precludes sophisticated multitone jamming.

3.5. How many symbols per hop are required for the loss due to a phase-reference symbol to be less than 0.1 dB in an FH/DPSK system?

3.6. For FH/CPM, use the procedures described in the text to verify (3.72), (3.75), and (3.77).

3.7. This problem illustrates the importance of a channel code to a frequency-hopping system in the presence of worst-case partial-band interference. Consider an FH/MSK system with limiter-discriminator demodulation. (a) Use (3.88) to calculate the required $\mathcal{E}_b/I_{t0}$ to obtain a bit error rate $P_b = 10^{-5}$ when no channel code is used. (b) Calculate the required $\mathcal{E}_b/I_{t0}$ for $P_b = 10^{-5}$ when a (23,12) Golay code is used. As a first step, use the first term in (1.29) to estimate the required symbol error probability. What is the coding gain?

3.8. Verify (3.87) for frequency hopping with binary CPFSK over the AWGN channel. Show that in the presence of Rayleigh fading, strong interference spread

uniformly over the entire hopping band hinders communications more than interference concentrated over part of the band.

3.9. It is desired to cover 198–200 MHz in 10 Hz increments using double-mix-divide modules. (a) What is the minimum number of modules required? (b) What is the range of acceptable reference frequencies? (c) Choose a reference frequency. What are the frequencies of the required tones? (d) If an upconversion by 180 MHz follows the DMD modules, what is the range of acceptable reference frequencies? Is this system more practical?

3.10. It is desired to cover 100–100.99 MHz in 10 kHz increments with an indirect frequency synthesizer containing a single loop and a dual-modulus divider. Let $f_1 = 0$ in Fig. 3.20 and $Q = 1$ in Fig. 3.21. (a) What is a suitable range of values of A? (b) What are a suitable value of P and a suitable range of values of B if it is required to minimize the highest frequency applied to the programmable dividers?

3.11. It is desired to cover 198–200 MHz in 10 Hz increments with a switching time equal to 2.5 ms. An indirect frequency synthesizer with three loops in the form of Fig. 3.22 is used. It is desired that $B_{\max} \leq 10^4$. (a) What are suitable values of the parameters f_r, M, $A_{\min}$, $A_{\max}$, $B_{\min}$, $B_{\max}$, and f_1? (b) If the desired switching time is reduced to 250 μs and f_1 is minimized, what are the values of these parameters?

3.12. Specify the design parameters of a fractional-N synthesizer that covers 198–200 MHz in 10 Hz increments with a switching time equal to 250 μs.

References

1. D. J. Torrieri "Fundamental Limitations on Repeater Jamming of Frequency-Hopping Communications," *IEEE J. Select. Areas Commun.*, vol. 7, pp. 569–578, May 1989.
2. J. S. Lee, R. H. French, and L. E. Miller, "Probability of Error Analyses of a BFSK Frequency-Hopping System with Diversity under Partial-Band Jamming Interference—Part I: Performance of Square-Law Linear Combining Soft Decision Receiver," *IEEE Trans. Commun.*, vol. 32, pp. 645–653, June 1984.
3. J. S. Lee, L. E. Miller, and Y. K. Kim, "Probability of Error Analyses of a BFSK Frequency-Hopping System with Diversity under Partial-Band Jamming Interference—Part II: Performance of Square-Law Nonlinear Combining Soft Decision Receivers," *IEEE Trans. Commun.*, vol. 32, pp. 1243–1250, Dec. 1984.
4. L. E. Miller, J. S. Lee, and A. P. Kadrichu, "Probability of Error Analyses of a BFSK Frequency-Hopping System with Diversity under Partial-Band Jamming Interference—Part III: Performance of Square-Law Self-Normalizing Soft Decision Receiver," *IEEE Trans. Commun.*, vol. 34, pp. 669–675, July 1986.
5. D. J. Torrieri, "Frequency Hopping with Multiple Frequency-Shift Keying and Hard Decisions," *IEEE Trans. Commun.*, vol. 32, pp. 574–583, May 1984.
6. Y. M. Lam and P. H. Wittke, "Frequency-Hopped Spread-Spectrum Transmission with Band-Efficient Modulations and Simplified Noncoherent Sequence Estimation," *IEEE Trans. Commun.*, vol. 38, pp. 2184–2196, Dec. 1990.
7. M. C. Valenti, S. Cheng, and D. Torrieri, "Iterative Multisymbol Noncoherent Reception of Coded CPFSK," *IEEE Trans. Commun.*, vol. 58, pp. 2046-2054, July 2010.

8. R. F. Pawula, "Refinements to the Theory of Error Rates for Narrow-Band Digital FM," *IEEE Trans. Commun.*, vol. 36, pp. 509-513, April 1988.
9. M. B. Pursley, "The Derivation and Use of Side Information in Frequency-Hop Spread Spectrum Communications," *IEICE Trans. Commun.*, vol. E76-B, pp. 814–824, August 1993.
10. S. Ahmed, L.-L. Yang, and L. Hanzo, "Erasure Insertion in RS-Coded SFH FSK Subjected to Tone Jamming and Rayleigh Fading," *IEEE Trans. Commun.*, vol. 56, pp. 3563-3571, Nov. 2007.
11. P. H. Wittke, Y. M. Lam, and M. J. Schefter, "The Performance of Trellis-Coded Nonorthogonal Noncoherent FSK in Noise and Jamming," *IEEE Trans. Commun.*, vol. 43, pp. 635–645, Feb./March/April 1995.
12. Q. Zhang and T. LeNgoc, "Turbo Product Codes for FH-SS with Partial-Band Interference," *IEEE Trans. Wireless Commun.*, vol. 1, pp. 513-520, July 2002.
13. J. R. Smith, *Modern Communication Circuits, 2nd ed*. Boston: McGraw-Hill, 1998.
14. U. L. Rohde, *Microwave and Wireless Synthesizers, Theory and Design*. New York: Wiley, 1997.
15. M. Rice, *Digital Communications: A Discrete-Time Approach*. Upper Saddle River, NJ: Pearson Prentice Hall, 2009.
16. P.-E. Su and S. Pamarti, "Fractional-N Phase-Locked Loop-Based Frequency Synthesis: A Tutorial," *IEEE Trans. Circuits Syst. II: Express Briefs,* vol. 56, pp.881-885, Dec. 2009.
17. D. Torrieri, *Principles of Secure Communication Systems*, 2nd ed. Boston: Artech House, 1992.

Chapter 4
Code Synchronization

A spread-spectrum receiver must generate a spreading sequence or frequency-hopping pattern that is synchronized with the received sequence or pattern; that is, the corresponding chips or dwell intervals must precisely or nearly coincide. Any misalignment causes the signal amplitude at the demodulator output to fall in accordance with the autocorrelation or partial autocorrelation function. Although the use of precision clocks in both the transmitter and the receiver limit the timing uncertainty in the receiver, clock drifts, range uncertainty, and the Doppler shift may cause synchronization problems. *Code synchronization*, which is either sequence or pattern synchronization, might be obtained from separately transmitted pilot or timing signals. It may be aided or enabled by feedback signals from the receiver to the transmitter. However, to reduce the cost in power and overhead, most spread-spectrum receivers achieve code synchronization by processing the received signal.

Both acquisition, which provides coarse synchronization, and tracking, which provides fine synchronization, are described in this chapter. The emphasis is on the acquisition system because this system is almost always the dominant design issue and most expensive component of a complete spread-spectrum system. By comparison, the implementation of a tracking system is generally considered straightforward.

4.1 Acquisition of Spreading Sequences

In the first part of this chapter, we consider direct-sequence systems. To derive the maximum-likelihood estimate of the *code phase* or timing offset of the spreading sequence, several assumptions are made. Since the presence of the data modulation impedes code synchronization, the transmitter is assumed to facilitate the synchronization by transmitting the spreading sequence without any data modulation. In nearly all applications, *noncoherent code synchronization* must precede carrier synchronization because the signal energy is spread over a wide spectral band. Prior

D. Torrieri, *Principles of Spread-Spectrum Communication Systems*,
DOI 10.1007/978-1-4419-9595-7_4, © Springer Science+Business Media, LLC 2011

to despreading, which requires code synchronization, the SNR is unlikely to be sufficiently high for successful carrier tracking by a phase-locked loop.

The received signal is

$$r(t) = s(t) + n(t), \quad 0 \le t \le T \tag{4.1}$$

where $s(t)$ is the desired signal, $n(t)$ is the additive white Gaussian noise, and T is the duration of the observation interval. For a direct-sequence system with PSK modulation, the desired signal is

$$s(t) = \sqrt{2S}\, p(t - \tau') \cos\left(2\pi f_c t + 2\pi f_d' t + \theta\right), \quad 0 \le t \le T \tag{4.2}$$

where S is the average power, $p(t)$ is the spreading waveform, f_c is the carrier frequency, θ is the random carrier phase, τ' is the received code phase or timing offset, and f_d' is the frequency offset. The frequency offset may be due to a Doppler shift or to a drift or instability in the transmitter oscillator. The values of τ' and f_d' must be estimated.

Consider the vector space of continuous-time, finite-energy signals defined over the observation interval [1]. A complete set of basis functions $\{\phi_i(t)\}, i = 1, 2, \ldots,$ that are orthonormal over the observation interval satisfy

$$\int_0^T \phi_i(t)\phi_k(t)dt = \delta_{ik}, \quad i \ne k. \tag{4.3}$$

The coefficients of the observed waveform in terms of N orthonormal basis functions of the signal space constitute the vector $\mathbf{r} = [r_1\ r_2 \ldots r_N]$. The *average likelihood function* for the unknown τ and f_d is the limit of the expectation with respect to θ of the conditional density function of $\mathbf{r}$ given that the timing and frequency offsets are τ and f_d:

$$\Lambda[r(t)] = \lim_{N\to\infty} E_\theta\left[f\left(\mathbf{r}|\tau, f_d, \theta\right)\right] \tag{4.4}$$

where $f(\mathbf{r}|\tau, f_d, \theta)$ is the conditional density function of $\mathbf{r}$ given the values of τ, f_d, and θ, and E_θ is the expectation with respect to θ. The maximum-likelihood estimates are those values of τ and f_d that maximize $\Lambda[r(t)]$. The waveforms $r(t)$, $s(t)$, and $n(t)$ have the expansions

$$r(t) = \lim_{N\to\infty} \sum_{i=1}^{N} r_i\phi_i(t), \quad s(t) = \lim_{N\to\infty} \sum_{i=1}^{N} s_i\phi_i(t), \quad n(t) = \lim_{N\to\infty} \sum_{i=1}^{N} n_i\phi_i(t). \tag{4.5}$$

Application of (4.3) and (4.5) yields the expansion coefficients:

$$r_i = \int_0^T r(t)\phi_i(t)dt, \quad s_i = \int_0^T s(t)\phi_i(t)dt, \quad n_i = \int_0^T n(t)\phi_i(t)dt,$$
$$i = 0, 1, \ldots, N. \tag{4.6}$$

The expansion coefficients are related by $r_i = s_i + n_i$.

Since the noise is zero-mean, the expected values of r_i is

$$E\left[r_i\right] = s_i\,. \tag{4.7}$$

The white Gaussian process $n(t)$ has autocorrelation (Appendix A)

$$R_n\left(\tau\right) = \frac{N_0}{2}\delta\left(\tau\right). \tag{4.8}$$

Using this equation, (4.3), and (4.6), we find that the Gaussian variables n_i and n_k, $i \neq k$, are uncorrelated, and hence statistically independent. The variance of r_i is

$$var\left[r_i\right] = E\left[n_i^2\right] = \frac{N_0}{2}. \tag{4.9}$$

The coefficients in the expansion of $r(t)$ in terms of the orthonormal basis functions are Gaussian, statistically independent, and have variance $N_0/2$. Therefore,

$$f\left(\mathbf{r}|\tau, f_d, \theta\right) = \lim_{N\to\infty}\prod_{i=1}^{N}\frac{1}{\sqrt{\pi N_0}}\exp\left[-\frac{\left(r_i - s_i\right)^2}{N_0}\right] \tag{4.10}$$

where the $\{s_i\}$ are the coefficients of the signal $s(t)$ when τ, f_d, and θ are given. Substituting this equation into (4.4), eliminating factors irrelevant to the maximum-likelihood estimation, and using the continuity of the exponential function, we obtain

$$\Lambda[r(t)] = E_\theta\left\{\exp\left[\frac{2}{N_0}\lim_{N\to\infty}\sum_{i=1}^{N} r_i s_i - \frac{1}{N_0}\lim_{N\to\infty}\sum_{i=1}^{N} s_i^2\right]\right\}. \tag{4.11}$$

By substituting the orthonormal expansions given by 4.5 into the integral, interchanging the limits and integrations, and then using (4.3), we obtain

$$\int_0^T r(t)s(t)dt = \lim_{N\to\infty}\sum_{i=1}^{N} r_i s_i\,, \quad \int_0^T s^2(t)dt = \lim_{N\to\infty}\sum_{i=1}^{N} s_i^2. \tag{4.12}$$

Therefore, the average likelihood function may be expressed in terms of the signal waveforms as

$$\Lambda[r(t)] = E_\theta\left\{\exp\left[\frac{2}{N_0}\int_0^T r(t)s(t)dt - \frac{\mathcal{E}}{N_0}\right]\right\} \tag{4.13}$$

where $\mathcal{E}$ is the energy in the signal waveform over the observation interval of duration T. Assuming that $\mathcal{E}$ does not vary significantly over the ranges of τ and

f_d considered, the factor involving $\mathcal{E}$ may be dropped from further consideration. The substitution of $s(t)$ in (4.2) with $\tau' = \tau$ and $f_d' = f_d$ into (4.13) then yields

$$\Lambda[r(t)] = E_\theta \left\{ \exp \left[\frac{2\sqrt{2S}}{N_0} \int_0^T r(t)\, p(t-\tau) \cos\left(2\pi f_c t + 2\pi f_d t + \theta\right) dt \right] \right\} . \tag{4.14}$$

For noncoherent estimation, the received carrier phase θ is assumed to be uniformly distributed over $[0, 2\pi)$. A trigonometric expansion and an integration of (4.14) over θ give

$$\Lambda[r(t)] = I_0 \left(\frac{2\sqrt{2SR\left(\tau, f_d\right)}}{N_0} \right) \tag{4.15}$$

where $I_0(\,)$ is the modified Bessel function of the first kind and order zero defined by (1.73), and

$$\begin{aligned} R\left(\tau, f_d\right) = & \left[\int_0^T r(t)\, p(t-\tau) \cos\left(2\pi f_c t + 2\pi f_d t\right) dt \right]^2 \\ & + \left[\int_0^T r(t)\, p(t-\tau) \sin\left(2\pi f_c t + 2\pi f_d t\right) dt \right]^2 . \end{aligned} \tag{4.16}$$

Since $I_0(x)$ is a monotonically increasing function of x, (4.15) implies that $R(\tau, f_d)$ is a sufficient statistic for maximum-likelihood estimation. Ideally, the estimates $\widehat{\tau}$ and $\widehat{f_d}$ are determined by considering all possible values of τ and f_d, and then choosing those values that maximize (4.16):

$$\left(\widehat{\tau}, \widehat{f_d}\right) = \arg \max_{(\tau, f_d)} R\left(\tau, f_d\right) . \tag{4.17}$$

A practical implementation of maximum-likelihood estimation or other type of estimation is greatly facilitated by dividing synchronization into the two operations of acquisition and tracking. *Acquisition* provides coarse synchronization by limiting the choices of the estimated values to a finite number of quantized candidates. Following the acquisition, *tracking* provides and maintains fine synchronization.

One method of acquisition is to use a *parallel array* of processors, each matched to candidate quantized values of the timing and frequency offsets. The largest processor output then indicates which candidates are selected as the estimates. An alternative method of acquisition, which is much less complex, but significantly increases the time needed to make a decision, is to serially search over the candidate offsets. Since the frequency offset is usually negligible, is easily tracked by a phase-locked loop, or requires only a few candidate values of a parallel array, the remainder of this chapter analyzes code synchronization in which only the timing

offset τ is estimated. Assuming that the instantaneous carrier frequency is known, the sufficient statistic for the received code phase or timing offset is

$$R_o(\tau) = \left[\int_0^T r(t)\,p(t-\tau)\cos(2\pi f_c t)\,dt\right]^2 + \left[\int_0^T r(t)\,p(t-\tau)\sin(2\pi f_c t)\,dt\right]^2 \tag{4.18}$$

and the estimate $\widehat{\tau}$ is the value of τ that maximizes (4.18). Search methods rather than parallel processing are examined. A device that generates (4.18) or (4.16) for various offsets is called a *noncoherent correlator*.

Code acquisition is the operation by which the phase of the receiver-generated sequence is brought to within a fraction of a chip of the phase of the received sequence. After this condition is detected and verified, the tracking system is activated. *Code tracking* is the operation by which synchronization errors are further reduced or at least maintained within certain bounds. Both the acquisition and tracking devices regulate the clock rate. Changes in the clock rate adjust the phase or timing offset of the *local sequence* generated by the receiver relative to the phase or timing offset of the received sequence.

In a benign environment, *sequential estimation* methods provide rapid acquisition [2]. Successive received chips are demodulated and then loaded into the receiver's code generator to establish its initial state. The tracking system then ensures that the code generator maintains synchronization. However, because chip demodulation is required, the usual despreading mechanism cannot be used to suppress interference during acquisition. Since an acquisition failure completely disables a communication system, an acquisition system must be capable of rejecting the anticipated level of interference. To meet this requirement, *matched-filter acquisition* and *serial-search acquisition* are the most effective techniques in general.

4.1.1 Matched-Filter Acquisition

Matched-filter acquisition provides potentially rapid acquisition when short programmable sequences give adequate security. The matched filter in an acquisition system is matched to one period of the spreading waveform, which is usually transmitted without modulation during the time interval allocated to acquisition. The sequence length or integration time of the matched filter is limited by frequency offsets and chip-rate errors. The output envelope, which ideally comprises triangular autocorrelation spikes, is compared with one or more thresholds, one of which is close to the peak value of the spikes. If the data-symbol boundaries coincide with the beginning and end of a spreading sequence, the occurrence of a threshold crossing provides timing information used for both symbol synchronization and acquisition. A major application of matched-filter acquisition is for *burst communications*, which are short and infrequent communications that do not require a long spreading sequence.

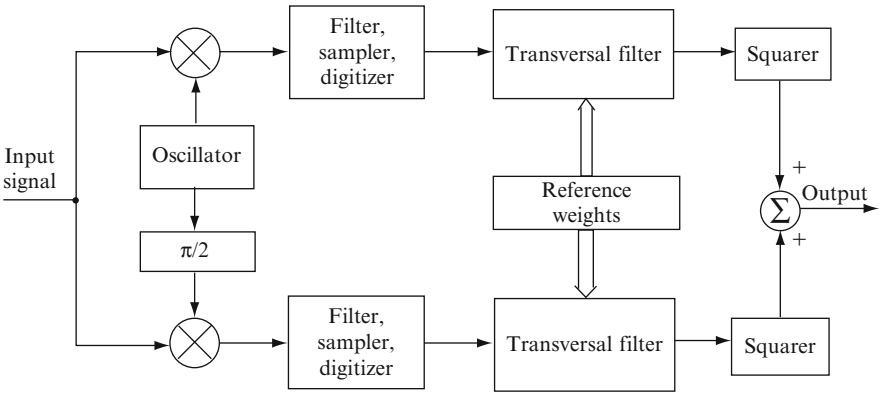

Fig. 4.1 Digital matched filter

A *digital matched filter* that generates $R_o(\tau)$ for noncoherent acquisition of a binary spreading waveform is illustrated in Fig. 4.1. The digital matched filter offers great flexibility, but is limited in the bandwidth it can accommodate. The received spreading waveform is decomposed into in-phase and quadrature baseband components, each of which is applied to a separate branch. The outputs of each digitizer are applied to a transversal filter. Tapped outputs of each transversal filter are multiplied by stored weights and summed. The two sums are squared and added together to produce the final matched-filter output. A *one-bit digitizer* makes hard decisions on the received chips by observing the polarities of the sample values. Each transversal filter is a shift register, and the reference weights are sequence chips stored in shift-register stages. The transversal filter contains G successive received spreading-sequence chips and a correlator that computes the number of received and stored chips that match. The correlator outputs are applied to the squarers.

Matched-filter acquisition for continuous communications is useful when serial-search acquisition with a long sequence fails or takes too long. A short sequence for acquisition is embedded within the long sequence. The short sequence may be a subsequence of the long sequence that is presumed to be ahead of the received sequence and is stored in the programmable matched filter. Figure 4.2 depicts the configuration of a matched filter for short-sequence acquisition and a serial-search system for long-sequence acquisition. The control signal provides the short sequence that is stored or recirculated in the matched filter. The control signal activates the matched filter when it is needed and deactivates it otherwise. The short sequence is detected when the envelope of the matched-filter output crosses a threshold. The threshold-detector output starts a long-sequence generator in the serial-search system at a predetermined initial state. The long sequence is used for verifying the acquisition and for despreading the received direct-sequence signal. Several matched filters in parallel may be used to expedite the process.

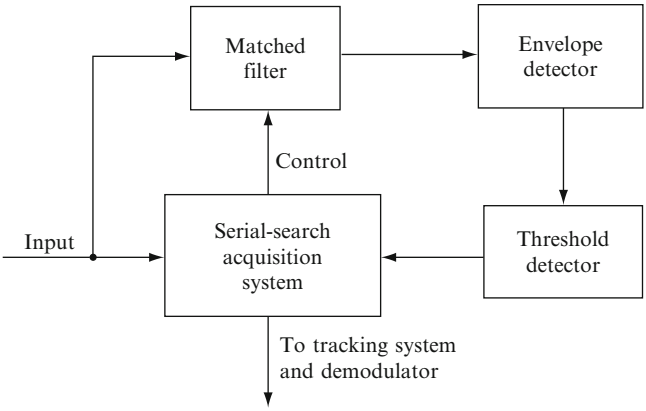

Fig. 4.2 Configuration of a serial-search acquisition system enabled by a matched filter

4.2 Serial-Search Acquisition

Serial-search acquisition consists of a search, usually in discrete steps, among candidate code phases of a local sequence until it is determined that the local sequence is nearly synchronized with the received spreading sequence. Conceptually, the timing uncertainty covers a region that is quantized into a finite number of *cells*, which are search positions of relative code phases or timing alignments. The cells are serially tested until it is determined that a particular cell corresponds to the alignment of the two sequences to within a fraction of a chip.

Figure 4.3 depicts the principal components of a serial-search acquisition system. The received direct-sequence signal and a local spreading sequence are applied to a noncoherent correlator that produces the statistic (4.18) associated with each cell. If the received and local spreading sequences are not aligned, the sampled correlator output is low. Therefore, the threshold is not exceeded, the cell under test is rejected, and the phase of the local sequence is retarded or advanced, possibly by generating an extra clock pulse or by blocking one. A new cell is then tested. If the sequences are nearly aligned, the sampled correlator output is high, the threshold is exceeded, the search is stopped, and the two sequences run in parallel at some fixed phase offset. Subsequent tests verify that the correct cell has been identified. If a cell fails the verification tests, the search is resumed. If a cell passes, the two sequences are assumed to be coarsely synchronized, demodulation begins, and the tracking system is activated. The threshold-detector output continues to be monitored so that any subsequent loss of synchronization activates the serial search.

There may be several cells that potentially provide a valid acquisition. However, if none of these cells corresponds to perfect synchronization, the detected energy is reduced below its potential peak value. The *step size* is the separation between cells. If the step size is one-half of a chip, then one of the cells corresponds to an alignment within one-fourth of a chip. On the average, the misalignment of this cell

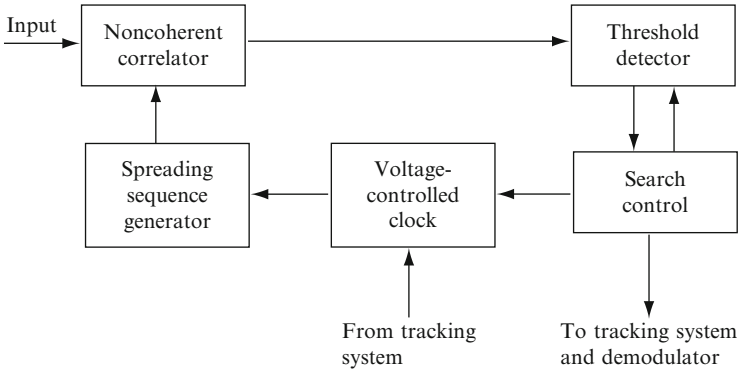

Fig. 4.3 Serial-search acquisition system

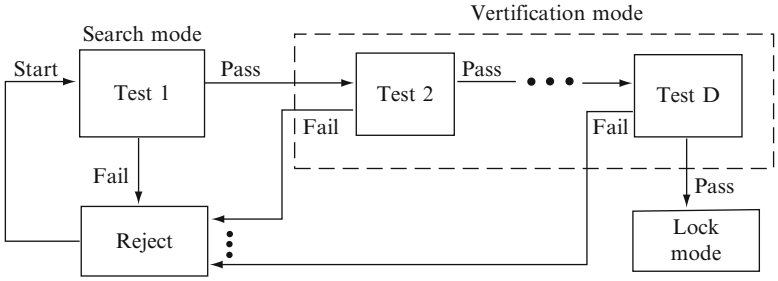

Fig. 4.4 Flow graph of multiple-dwell system with consecutive-count strategy

is one-eighth of a chip, which may cause a negligible degradation. As the step size decreases, both the average detected energy during acquisition and the number of cells to be searched increase.

The *dwell time* is the amount of time required for testing a cell and is approximately equal to the length of the integration interval in the noncoherent correlator (Sect. 4.3). An acquisition system is called a *single-dwell system* if a single test determines whether a cell is accepted as the correct one. If verification testing occurs before acceptance, the system is called a *multiple-dwell system*. The dwell times either are fixed or are variable but bounded by some maximum value. The dwell time for the initial test of a cell is usually designed to be much shorter than the dwell times for verification tests. This approach expedites the acquisition by quickly eliminating the bulk of the incorrect cells. In any serial-search system, the dwell time allotted to a test is limited by the Doppler shift, which causes the received and local chip rates to differ. As a result, an initial close alignment of the two sequences may disappear by the end of the test.

A multiple-dwell system may use a *consecutive-count strategy*, in which a failed test causes a cell to be immediately rejected, or an *up-down strategy*, in which a failed test causes a repetition of a previous test. Figures 4.4 and 4.5 depict the flow

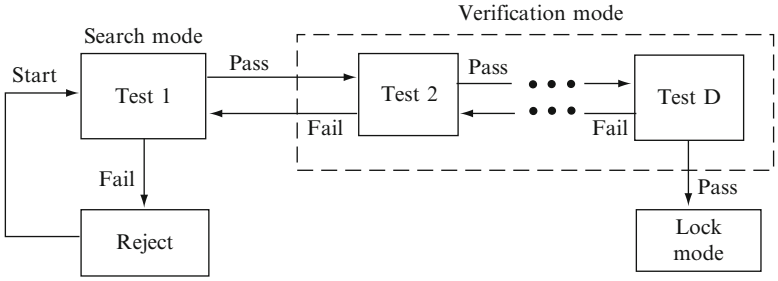

Fig. 4.5 Flow graph of multiple-dwell system with up-down strategy

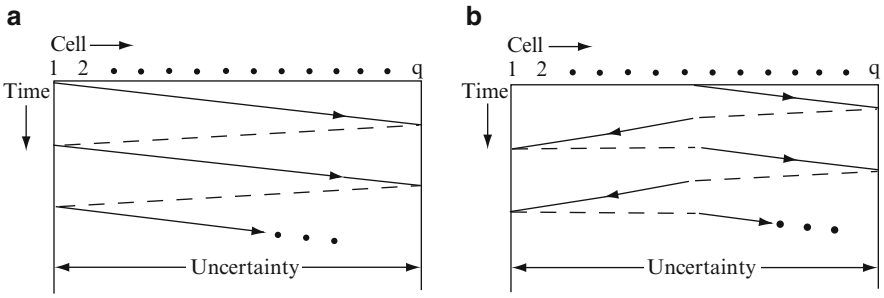

Fig. 4.6 Trajectories of search positions: (**a**) uniform search and (**b**) broken-center Z search

graphs of the consecutive-count and up-down strategies, respectively, that require D tests to be passed before acquisition is declared. If the threshold is not exceeded during test 1, the cell fails the test, and the next cell is tested. If it is exceeded, the cell passes the test, the search is stopped, and the system enters the *verification mode*. The same cell is tested again, but the dwell time and the threshold may be changed. Once all the verification tests have been passed, the code tracking is activated, and the system enters the *lock mode*. In the lock mode, the lock detector continually verifies that code synchronization is maintained. If the lock detector decides that synchronization has been lost, *reacquisition* begins in the search mode.

The order in which the cells are tested is determined by the general search strategy. Figure 4.6a depicts a *uniform search* over the q cells of the *timing uncertainty*. The broken lines represent the discontinuous transitions of the search from the one part of the timing uncertainty to another. The *broken-center Z search*, illustrated in Fig. 4.6b, is appropriate when *a priori* information makes part of the timing uncertainty more likely to contain the correct cell than the rest of the region. *A priori* information may be derived from the detection of a short preamble. If the sequences are synchronized with the time of day, then the receiver's estimate of the transmitter range combined with the time of day provide the *a priori* information.

The *acquisition time* is the amount of time required for an acquisition system to locate the correct cell and initiate the code tracking system. To derive the statistics

of the acquisition time [3], one of the q possible cells is considered the correct cell, and the other $(q-1)$ cells are incorrect. The difference in timing offsets among cells is ΔT_c, where the *step size* Δ is usually either 1 or 1/2. However, it is convenient to allow the correct cell to include two or more timing offsets or code phases. Let L denote the number of times the correct cell is tested before it is accepted and acquisition terminates. Let C denote the number of the correct cell and π_j denote the probability that $C = j$. Let $\nu(L, C)$ denote the number of incorrect cells tested during the acquisition process. The functional dependence is determined by the search strategy. Let $T_r(L, C)$ denote the total *rewinding time,* which is the time required for the search to move discontinuously to a different cell within the timing uncertainty. Since an incorrect cell is always ultimately rejected, there are only three types of events that occur during a serial search. Either the nth incorrect cell is dismissed after $T_{11}(n)$ seconds, a correct cell is falsely dismissed for the mth time after $T_{12}(m)$ seconds, or a correct cell is accepted after T_{22} seconds, where the first subscript is 1 if dismissal occurs, and 2 otherwise; the second subscript is 1 if the cell is incorrect, and 2 otherwise. Each of these decision times is a random variable. If an incorrect cell is accepted, the receiver eventually recognizes the mistake and reinitiates the search at the next cell. The wasted time expended in code tracking is a random variable called the *penalty time*. These definitions imply that the acquisition time is the random variable given by

$$T_a = \sum_{n=1}^{\nu(L,C)} T_{11}(n) + \sum_{m=1}^{L-1} T_{12}(m) + T_{22} + T_r(L, C). \tag{4.19}$$

The most important performance measures of the serial search are the mean and variance of T_a. Given $L = i$ and $C = j$, the conditional expected value of T_a is

$$E\left[T_a | i, j\right] = \nu(i, j)\bar{T}_{11} + (i-1)\bar{T}_{12} + \bar{T}_{22} + T_r(i, j) \tag{4.20}$$

where $\bar{T}_{11}, \bar{T}_{12}$, and $\bar{T}_{22}$ are the expected values of each $T_{11}(n), T_{12}(m)$, and T_{22}, respectively. Therefore, the mean acquisition time is

$$\bar{T}_a = \bar{T}_{22} + \sum_{i=1}^{\infty} P_L(i) \sum_{j=1}^{q} \pi_j \left[\nu(i, j)\bar{T}_{11} + (i-1)\bar{T}_{12} + T_r(i, j)\right] \tag{4.21}$$

where $P_L(i)$ is the probability that $L = i$. We assume that the test statistics are independent and identically distributed. Therefore,

$$P_L(i) = P_D\left(1 - P_D\right)^{i-1} \tag{4.22}$$

where P_D is the probability that the correct cell is detected when it is tested during a scan of the uncertainty region. After calculating the conditional expected value of T_a^2 given that $L = i$ and $C = j$, and using the identity $\overline{x^2} = var(x) + \bar{x}^2$, we obtain

$$\overline{T_a^2} = \sum_{i=1}^{\infty} P_L(i) \sum_{j=1}^{q} \pi_j \{[\nu(i,j)\bar{T}_{11} + (i-1)\bar{T}_{12} + \bar{T}_{22} + T_r(i,j)]^2 + \nu(i,j)var(T_{11}) + (i-1)var(T_{12}) + var(T_{22})\}. \tag{4.23}$$

The variance of T_a is

$$\sigma_a^2 = \overline{T_a^2} - \bar{T}_a^2. \tag{4.24}$$

4.2.0.1 Application of Chebyshev's Inequality

To derive Chebyshev's inequality, consider a random variable X with distribution $F(x)$. Let $E[X] = m$ denote the expected value of X and $P[A]$ denote the probability of event A. From elementary probability it follows that

$$E[|X-m|^k] = \int_{-\infty}^{\infty} |x-m|^k dF(x) \geq \int_{|x-m|\geq\alpha}^{\infty} |x-m|^k dF(x) \geq \alpha^k \int_{|x-m|\geq\alpha}^{\infty} dF(x) = \alpha^k P[|X-m| \geq \alpha]. \tag{4.25}$$

Therefore,

$$P[|X-m| \geq \alpha] \leq \frac{1}{\alpha^k} E[|X-m|^k]. \tag{4.26}$$

Let $\sigma^2 = E[(X-m)^2]$ denote the variance of X. If $k = 2$, then (4.26) becomes *Chebyshev's inequality*:

$$P[|X-m| \geq \alpha] \leq \frac{\sigma^2}{\alpha^2}. \tag{4.27}$$

In some applications, the serial-search acquisition must be completed within a specified period of duration T_{max}. If it is not, the serial search is terminated, and special measures such as the matched-filter acquisition of a short sequence are undertaken. The probability that $T_a \leq T_{max}$ can be bounded by using Chebyshev's inequality:

$$P[T_a \leq T_{\max}] \geq P[|T_a - \bar{T}_a| \leq T_{\max} - \bar{T}_a] \geq 1 - \frac{\sigma_a^2}{(T_{\max} - \bar{T}_a)^2} \tag{4.28}$$

where $P[A]$ denotes the probability of the event A.

4.2.1 Uniform Search with Uniform Distribution

As an important application, we consider the uniform search of Fig. 4.6a and a uniform *a priori* distribution for the location of the correct cell given by

$$\pi_j = \frac{1}{q}, \quad 1 \le j \le q. \tag{4.29}$$

If the cells in the figure are labeled consecutively from left to right, then

$$v(i, j) = (i - 1)(q - 1) + j - 1. \tag{4.30}$$

The rewinding time is

$$T_r(i, j) = T_r(i) = (i - 1)T_r \tag{4.31}$$

where T_r is the rewinding time associated with each broken line in the figure. If the timing uncertainty covers an entire sequence period, then the cells at the two edges are actually adjacent and $T_r = 0$.

To evaluate $\bar{T}_a$ and $\overline{T_a^2}$, we substitute (4.22), (4.29), (4.30), and (4.31) into (4.21) and (4.23) and use the following identities:

$$\begin{aligned} &\sum_{i=0}^{\infty} r^i = \frac{1}{1-r}, \quad \sum_{i=1}^{\infty} i r^i = \frac{r}{(1-r)^2}, \quad \sum_{i=1}^{\infty} i^2 r^i = \frac{r(1+r)}{(1-r)^3} \\ &\sum_{i=1}^{n} i = \frac{n(n+1)}{2}, \quad \sum_{i=1}^{n} i^2 = \frac{n(n+1)(2n+1)}{6} \end{aligned} \tag{4.32}$$

where $0 \le |r| < 1$. Defining

$$\alpha = (q - 1)\bar{T}_{11} + \bar{T}_{12} + T_r \tag{4.33}$$

we obtain

$$\bar{T}_a = (q - 1)\left(\frac{2 - P_D}{2P_D}\right)\bar{T}_{11} + \left(\frac{1 - P_D}{P_D}\right)\left(\bar{T}_{12} + T_r\right) + \bar{T}_{22} \tag{4.34}$$

and

$$\begin{aligned} \overline{T_a^2} = {} & (q - 1)\left(\frac{2 - P_D}{2P_D}\right) var\left(T_{11}\right) + \left(\frac{1 - P_D}{P_D}\right) var\left(T_{12}\right) + var\left(T_{22}\right) \\ & + \frac{(2q + 1)(q + 1)}{6}\bar{T}_{11}^2 + \frac{\alpha^2 (1 - P_D)(2 - P_D)}{P_D^2} + (q + 1)\alpha\left(\frac{1 - P_D}{P_D}\right) \\ & + (q + 1)\bar{T}_{11}\left(\bar{T}_{22} - \bar{T}_{11}\right) + 2\alpha\left(\frac{1 - P_D}{P_D}\right)\left(\bar{T}_{22} - \bar{T}_{11}\right) + \left(\bar{T}_{22} - \bar{T}_{11}\right)^2. \end{aligned} \tag{4.35}$$

In most applications, the number of cells to be searched is large, and simpler *asymptotic forms* for the mean and variance of the acquisition time are applicable. As $q \to \infty$, (4.34) gives

$$\bar{T}_a \to q\left(\frac{2-P_D}{2P_D}\right)\bar{T}_{11}, \quad q \to \infty. \tag{4.36}$$

Similarly, (4.35) and (4.24) yield

$$\sigma_a^2 \to q^2\left(\frac{1}{P_D^2}-\frac{1}{P_D}+\frac{1}{12}\right)\bar{T}_{11}^2, \quad q \to \infty. \tag{4.37}$$

These equations must be modified in the presence of a large uncorrected Doppler shift. The fractional change in the received chip rate of the spreading sequence is equal to the fractional change in the carrier frequency due to the Doppler shift. If the chip rate changes from $1/T_c$ to $1/T_c + \delta$, then the average change in the code or sequence phase during the test of an incorrect cell is $\delta\bar{T}_{11}$. The change relative to the step size is $\delta\bar{T}_{11}/\Delta$. The number of cells that are actually tested in a sweep of the timing uncertainty becomes $q(1+\delta\bar{T}_{11}/\Delta)^{-1}$. Since incorrect cells predominate, the substitution of the latter quantity in place of q in (4.36) and (4.37) gives approximate asymptotic expressions for $\bar{T}_a$ and σ_a^2 when the Doppler shift is significant.

4.2.2 Consecutive-Count Double-Dwell System

For further specialization, consider the consecutive-count double-dwell system described by Fig. 4.4 with $D = 2$. Assume that the *correct cell* actually subsumes two consecutive cells in the sense that the timing offsets of both cells are sufficiently low that either one of these cells could be considered a correct cell. The detection probabilities of the two consecutive cells are P_a and P_b, respectively. If the test results are assumed to be statistically independent, then

$$P_D = P_a + (1 - P_a)P_b. \tag{4.38}$$

Let τ_1, P_{F1}, P_{a1}, and P_{b1} denote the search-mode dwell time, false-alarm probability, and successive detection probabilities, respectively. Let τ_2, P_{F2}, P_{a2}, and P_{b2} denote the verification-mode dwell time, false-alarm probability, and successive detection probabilities, respectively. Let $\bar{T}_p$ denote the mean penalty time, which is incurred by the incorrect activation of the tracking mode. The flow graph indicates that since each cell must pass two tests,

$$P_a = P_{a1}P_{a2}, \quad P_b = P_{b1}P_{b2} \tag{4.39}$$

and

$$\bar{T}_{11} = \tau_1 + P_{F1}\left(\tau_2 + P_{F2}\bar{T}_p\right). \tag{4.40}$$

Equations (4.38) to (4.40) are sufficient for the evaluation of the asymptotic values of the mean and variance given by (4.36) and (4.37).

For a more accurate evaluation of the mean acquisition time, expressions for the conditional means $\bar{T}_{22}$ and $\bar{T}_{12}$ are needed. Expressing $\bar{T}_{22}$ as the conditional expectation of the correct-cell test duration given cell detection, and enumerating the three possible durations and their conditional probabilities, we obtain

$$\begin{aligned}\bar{T}_{22} &= \frac{1}{P_D}\sum_{i=1}^{3} t_i\, P\left(T_{22} = t_i \cap \text{detection}\right)\\ &= \frac{1}{P_D}\left[(\tau_1+\tau_2)\,P_a + (2\tau_1+\tau_2)\,(1-P_{a1})\,P_b + (2\tau_1+2\tau_2)\,P_{a1}\,(1-P_{a2})\,P_b\right]\end{aligned} \tag{4.41}$$

which simplifies to

$$\bar{T}_{22} = \tau_1 + \tau_2 + \tau_1\frac{(1-P_a)\,P_b}{P_D} + \tau_2\frac{P_{a1}\,(1-P_{a2})\,P_b}{P_D}. \tag{4.42}$$

Similarly,

$$\bar{T}_{12} = 2\tau_1 + \tau_2\left[\frac{P_{a1}\,(1-P_{a2})\,(1-P_b) + (1-P_a)\,P_{b1}\,(1-P_{b2})}{1-P_D}\right]. \tag{4.43}$$

4.2.3 Single-Dwell and Matched-Filter Systems

Results for a single-dwell system are obtained by setting $P_{a2} = P_{b2} = P_{F2} = 1$, $\tau_2 = 0$, $P_a = P_{a1}$, $P_b = P_{b1}$, $P_{F1} = P_F$, and $\tau_1 = \tau_d$ in (4.40) to (4.43). We obtain

$$\bar{T}_{11} = \tau_d + P_F\bar{T}_p,\quad \bar{T}_{22} = \tau_d\left[1 + \frac{(1-P_a)\,P_b}{P_D}\right],\quad \bar{T}_{12} = 2\tau_d. \tag{4.44}$$

Thus, (4.34) yields

$$\bar{T}_a = \frac{(q-1)\,(2-P_D)\left(\tau_d + P_F\bar{T}_p\right) + 2\tau_d\,(2-P_a) + 2\,(1-P_D)\,T_r}{2P_D}. \tag{4.45}$$

Since the single-dwell system may be regarded as a special case of the double-dwell system, the latter can provide a better performance by the appropriate setting of its additional parameters.

The approximate mean acquisition time for a matched filter can be derived in a similar manner. Suppose that many periods of a short spreading sequence with N chips per period are received, and the matched-filter output is sampled m times per chip. Then the number of cells that are tested is $q = mN$ and $T_r = 0$. Each sampled output is compared to a threshold so $\tau_d = T_c/m$ is the time duration associated with a test. For $m = 1$ or 2, it is reasonable to regard two of the cells as the correct ones. These cells are effectively tested when a signal period fills or nearly fills the matched filter. Thus, (4.38) is applicable with $P_a \approx P_b$, and (4.34) yields

$$\bar{T}_a \approx NT_c \left(\frac{2 - P_D}{2P_D} \right) (1 + mKP_F), \qquad q \gg 1 \tag{4.46}$$

where $K = \bar{T}_p / T_c$. Ideally, the threshold is exceeded once per period, and each threshold crossing provides a timing marker.

4.2.4 Up-Down Double-Dwell System

For the up-down double-dwell system with two correct cells, the flow graph of Fig. 4.5 with $D = 2$ indicates that

$$P_a = P_{a1} P_{a2} \sum_{i=0}^{\infty} [P_{a1} (1 - P_{a2})]^i = \frac{P_{a1} P_{a2}}{1 - P_{a1} (1 - P_{a2})}. \tag{4.47}$$

Similarly,

$$P_b = \frac{P_{b1} P_{b2}}{1 - P_{b1} (1 - P_{b2})} \tag{4.48}$$

and P_D is given by (4.38). If an incorrect cell passes the initial test but fails the verification test, then the cell begins the testing sequence again without any memory of the previous testing. Therefore, for an up-down double-dwell system, a recursive evaluation gives

$$\bar{T}_{11} = (1 - P_{F1}) \tau_1 + P_{F1} P_{F2} \left(\tau_1 + \tau_2 + \bar{T}_p \right) + P_{F1} (1 - P_{F2}) \left(\tau_1 + \tau_2 + \bar{T}_{11} \right). \tag{4.49}$$

Solving this equation yields

$$\bar{T}_{11} = \frac{\tau_1 + P_{F1} \left(\tau_2 + P_{F2} \bar{T}_p \right)}{1 - P_{F1} (1 - P_{F2})}. \tag{4.50}$$

Substitution of (4.47) to (4.50) into (4.36) to (4.38) gives the asymptotic values of the mean and variance of the acquisition time.

From the possible durations and their conditional probabilities, we obtain

$$\bar{T}_{22} = \tau_1 + \tau_2 + P_{a1}\,(1 - P_{a2})\,\bar{T}_{22} + \frac{(1 - P_{a1})\,P_{b1}\,P_{b2}}{P_D}\tau_1 + \frac{(1 - P_{a1})\,P_{b1}\,(1 - P_{b2})\,P_b}{P_D}\left(\tau_1 + \bar{T}'_{22}\right) \tag{4.51}$$

where $\bar{T}'_{22}$ is the expected delay for the detection of the correct cell given that the testing begins at the second correct cell. A recursive evaluation gives

$$\begin{aligned}\bar{T}'_{22} &= \tau_1 + \tau_2 + P_{b1}\,(1 - P_{b2})\,\bar{T}'_{22} \\ &= \frac{\tau_1 + \tau_2}{1 - P_{b1}\,(1 - P_{b2})}.\end{aligned} \tag{4.52}$$

Substituting this equation into (4.52) and solving for $\bar{T}_{22}$ yields

$$\begin{aligned}\bar{T}_{22} = [1 - P_{a1}\,(1 - P_{a2})]^{-1} \Bigg\{ &\tau_1 \left[1 + \frac{(1 - P_{a1})\,P_{b1}\,P_{b2}}{P_D} + \frac{(1 - P_{a1})\,P_{b1}\,(1 - P_{b2})\,P_b}{P_D}\left(1 + \frac{1}{1 - P_{b1}\,(1 - P_{b2})}\right)\right] \\ &+ \tau_2 \left[1 + \frac{(1 - P_{a1})\,P_{b1}\,(1 - P_{b2})\,P_b}{P_D\,[1 - P_{b1}\,(1 - P_{b2})]}\right]\Bigg\}.\end{aligned} \tag{4.53}$$

Similarly, $\bar{T}_{12}$ is determined by the recursive equation

$$\bar{T}_{12} = \tau_1 + \frac{(1 - P_{a1})\,(1 - P_{a2})}{1 - P_D}\tau_1 + P_{a1}\,(1 - P_{a2})\left(\tau_2 + \bar{T}_{12}\right) + \frac{(1 - P_{a1})\,P_{b1}\,(1 - P_{b2})\,(1 - P_b)}{1 - P_D}\left(\tau_1 + \tau_2 + \bar{T}'_{12}\right) \tag{4.54}$$

with

$$\bar{T}'_{12} = \frac{\tau_1 + P_{b1}\,(1 - P_{b2})\,\tau_2}{1 - P_{b1}\,(1 - P_{b2})}. \tag{4.55}$$

Substituting this equation into (4.54) and solving for $\bar{T}_{12}$ yields

$$\begin{aligned}\bar{T}_{12} = [1 - P_{a1}\,(1 - P_{a2})]^{-1} \Bigg\{ &\tau_1 \left[1 + \frac{(1 - P_{a1})\,(1 - P_{a2})}{1 - P_D} + \frac{(1 - P_{a1})\,P_{b1}\,(1 - P_{b2})\,(1 - P_b)}{1 - P_D}\left(1 + \frac{1}{1 - P_{b1}\,(1 - P_{b2})}\right)\right]\end{aligned}$$

$$+\tau_2\left[P_{a1}\left(1-P_{a2}\right)+\frac{\left(1-P_{a1}\right)P_{b1}\left(1-P_{b2}\right)\left(1-P_b\right)}{1-P_D}\right.$$
$$\left.+\frac{P_{b1}\left(1-P_{b2}\right)}{1-P_{b1}\left(1-P_{b2}\right)}\right]\Bigg\}. \tag{4.56}$$

4.2.5 Penalty Time

The *lock detector* that monitors the code synchronization in the lock mode performs tests to verify the lock condition. The time that elapses before the system incorrectly leaves the lock mode is called the *holding time*. It is desirable to have a large mean holding time and a small mean penalty time, but the realization of one of these goals tends to impede the realization of the other. As a simple example, suppose that each test has a fixed duration τ and that code synchronization is actually maintained. A single missed detection, which occurs with probability $1 - P_{DL}$, causes the lock detector to assume a loss of lock and to initiate a search. Assuming the statistical independence of the lock-mode tests, the *mean holding time* is

$$\begin{aligned}\bar{T}_h &= \sum_{i=1}^{\infty} i\tau\left(1-P_{DL}\right)P_{DL}^{i-1}\\ &= \frac{\tau}{1-P_{DL}}.\end{aligned} \tag{4.57}$$

This result may also be derived by recognizing that $\bar{T}_h = \tau + P_{DL}\bar{T}_h$ because once the lock mode is verified, the testing of the same cell is renewed without any memory of the previous testing. If the locally generated code phase is incorrect, the penalty time expires unless false alarms, each of which occurs with probability P_{FL}, continue to occur every τ seconds. Therefore, $\bar{T}_p = \tau + P_{FL}\bar{T}_p$, which yields the *mean penalty time* for a single-dwell lock detector:

$$\bar{T}_p = \frac{\tau}{1-P_{FL}}. \tag{4.58}$$

A trade-off between a high $\bar{T}_h$ and a low $\bar{T}_p$ exists because increasing P_{DL} tends to increase P_{FL}.

When a single test verifies the lock condition, the synchronization system is vulnerable to deep fades and pulsed interference. A preferable strategy is for the lock mode to be maintained until a number of consecutive or cumulative misses occur during a series of tests. The performance analysis is analogous to that of serial-search acquisition.

4.2.6 Other Search Strategies

In a *Z search*, no cell is tested more than once until all cells in the timing uncertainty have been tested. Both strategies of Fig. 4.6 are Z searches. A characteristic of the Z search is that

$$\nu(i, j) = (i - 1)(q - 1) + \nu(1, j) \tag{4.59}$$

where $\nu(1, j)$ is the number of incorrect cells tested when $P_D = 1$ and, hence, $L = 1$. For simplicity, we assume that q is even. For the broken-center Z search, the search begins with cell $q/2 + 1$, and

$$\nu(1, j) = \begin{cases} j - \frac{q}{2} - 1, & j \geq \frac{q}{2} + 1 \\ q - j, & j \leq \frac{q}{2} \end{cases} \tag{4.60}$$

whereas $\nu(1, j) = j - 1$ for the uniform search. If the rewinding time is negligible, then (4.21), (4.22), and (4.59) yield

$$\bar{T}_a = \frac{1 - P_D}{P_D} \left[(q - 1)\bar{T}_{11} + \bar{T}_{12} \right] + \bar{T}_{22} + \bar{T}_{11}\nu(1) \tag{4.61}$$

where

$$\nu(1) = \sum_{j=1}^{q} \nu(1, j)\pi_j \tag{4.62}$$

is the average number of incorrect cells tested when $P_D = 1$.

If C has a uniform distribution, then $\nu(1)$ and, hence, $\bar{T}_a$ are the same for both the uniform and broken-center-Z search strategies. If the distribution of C is symmetrical about a pronounced central peak and $P_D \approx 1$, then a uniform search gives $\nu(1) \approx q/2$. Since a broken-center Z search usually ends almost immediately or after slightly more than $q/2$ tests,

$$\nu(1) \approx 0 \left(\frac{1}{2} \right) + \frac{q}{2} \left(\frac{1}{2} \right) = \frac{q}{4} \tag{4.63}$$

which indicates that for large values of q and P_D close to unity, the broken-center Z search reduces $\bar{T}_a$ approximately by a factor of 2 relative to its value for the uniform search.

An *expanding-window search* attempts to exploit the information in the distribution of C by continually retesting cells with high *a priori* probabilities of being the correct cell. Tests are performed on all cells within a radius R_1 from the center. If the correct cell is not found, then tests are performed on all cells within an increased radius R_2. The radius is increased successively until the boundaries of the timing uncertainty are reached. The expanding-window search then becomes a Z search. If the rewinding time is negligible and C is centrally peaked, then the broken-center search of Fig. 4.7a is preferable to the continuous-center search of

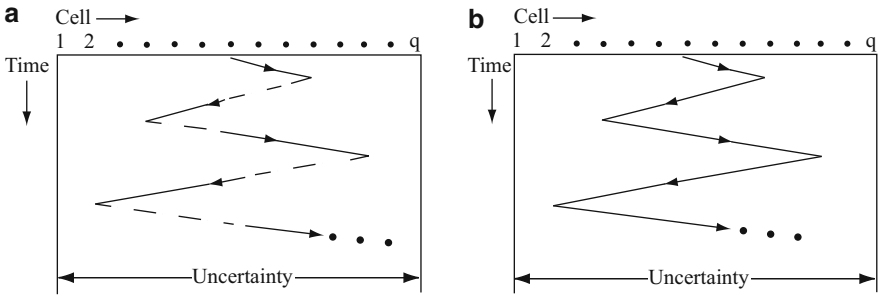

Fig. 4.7 Trajectories of expanding-window search positions: (**a**) broken-center and (**b**) continuous-center search

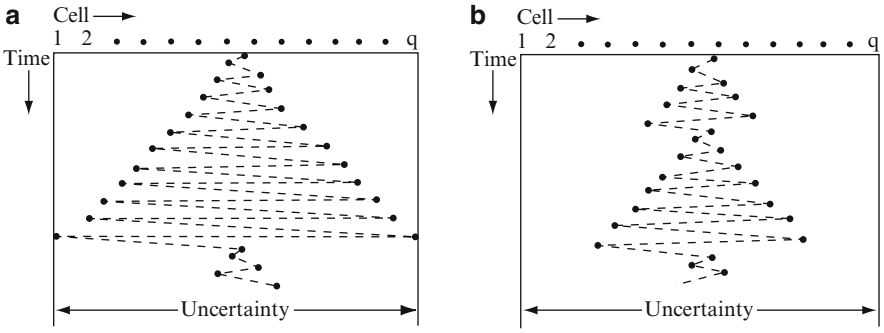

Fig. 4.8 Trajectories of alternating search positions: (**a**) uniform search and (**b**) nonuniform search

Fig. 4.7b because the latter retests cells before testing all the cells near the center of the timing uncertainty. In an *equiexpanding search*, the radii have the form

$$R_n = \frac{nq}{2N}, \quad n = 1, 2, \ldots, N \tag{4.64}$$

where N is the number of sweeps before the search becomes a Z search. If the rewinding time is negligible, then it can be shown [4] that the broken-center equiexpanding-window search is optimized for $P_D \leq 0.8$ by choosing $N = 2$. For this optimized search, $\bar{T}_a$ is moderately reduced relative to its value for the broken-center Z search.

When $T_r(i, j) = 0$ and $P_D = 1$, the optimal search, which is called a *uniform alternating search*, tests the cells in order of decreasing *a priori* probability. For a symmetric, unimodal, centrally peaked distribution of C, this optimal search has the trajectory depicted in Fig. 4.8a. Once all the cells in the timing uncertainty have been tested, the search repeats the same pattern. Equations (4.59) and (4.61) are applicable. If $P_D \approx 1$ and the distribution of C has a pronounced central peak, then $\nu(1)$ is small, and a comparison with (4.63) indicates that the uniform alternating

search has an advantage over the broken-center expanding-window search when $q \gg 4$ and the rewinding time for any discontinuous transition is much smaller than $\bar{T}_{11}$. However, computations show that this advantage dissipates as P_D decreases [3], which occurs because all cells are tested with the same frequency without accounting for the distribution of C.

In the *nonuniform alternating search*, illustrated in Fig. 4.8b, a uniform search is performed until a radius R_1 is reached. Then a second uniform search is performed within a larger radius R_2. This process continues until the boundaries of the timing uncertainty are reached and the search becomes a uniform alternating search. Computations show that for a centrally peaked distribution of C, the nonuniform alternating search can give a significant improvement over the uniform alternating search if $P_D < 0.8$, and the radii $R_n, n = 1, 2, \ldots$, are optimized [4]. However, if the radii are optimized for $P_D < 1$, then as $P_D \to 1$ the nonuniform search becomes inferior to the uniform search.

4.2.7 Density Function of the Acquisition Time

The density function of T_a, which is needed to accurately calculate $P[T_a \leq T_{max}]$ and other probabilities, may be decomposed as

$$f_a(t) = P_D \sum_{i=1}^{\infty} (1 - P_D)^{i-1} \sum_{j=1}^{q} \pi_j f_a(t|i, j) \tag{4.65}$$

where $f_a(t|i, j)$ is the conditional density of T_a given that $L = i$ and $C = j$. Let $*$ denote the convolution operation, $[f(t)]^{*n}$ denote the n-fold convolution of the density $f(t)$ with itself, $[f(t)]^{*0} = 1$, and $[f(t)]^{*1} = f(t)$. Using this notation, we obtain

$$f_a(t|i, j) = [f_{11}(t)]^{*\nu(i,j)} * [f_{12}(t)]^{*(i-1)} * [f_{22}(t)] \tag{4.66}$$

where $f_{11}(f)$, $f_{12}(t)$, and $f_{22}(t)$ are the densities associated with T_{11}, T_{12}, and T_{22}, respectively. If one of the decision times is a constant, then the associated density is a delta function.

The exact evaluation of $f_a(t)$ is difficult [5], but an approximation usually suffices. Since the acquisition time conditioned on $L = i$ and $C = j$ is the sum of independent random variables, it is reasonable to approximate $f_a(t|i, j)$ by a truncated Gaussian density with mean

$$\mu_{ij} = \nu(i, j)\bar{T}_{11} + (i - 1)\bar{T}_{12} + \bar{T}_{22} + T_r(i) \tag{4.67}$$

and variance

$$\sigma_{ij}^2 = \nu(i, j)var(T_{11}) + (i - 1)var(T_{12}) + var(T_{22}). \tag{4.68}$$

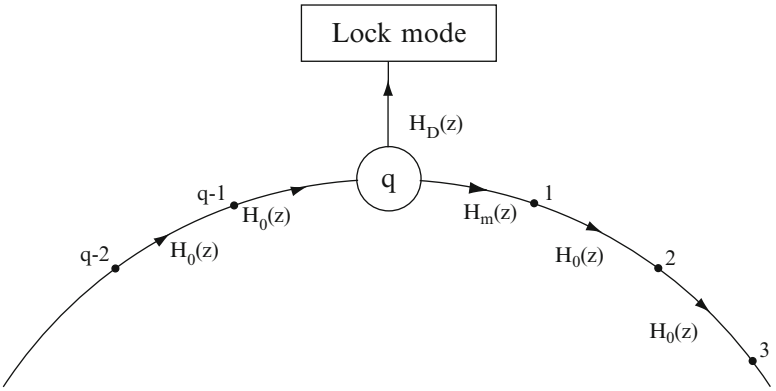

Fig. 4.9 Circular state diagram for serial-search acquisition

The truncation is such that $f_a(t|i,j) \neq 0$ only if $0 \leq t \leq T_{\max}$ or $0 \leq t \leq \mu_{ij} + 3\sigma_{ij}$. When P_D is large, the infinite series in (4.65) converges rapidly enough that the $f_a(t)$ can be accurately approximated by its first few terms.

4.2.8 *Alternative Analysis*

An alternative method of analyzing acquisition relies on transfer functions [6]. Each phase offset of the local code defines a *state* of the system. Of the total number of q states, $q-1$ are states that correspond to offsets (cells) that equal or exceed a chip duration. One state is a *collective state* that corresponds to all phase offsets that are less than a chip duration and, hence, cause acquisition to be terminated and code tracking to begin. The serial-search acquisition process is represented by its *circular state diagram*, a segment of which is illustrated in Fig. 4.9. The *a priori* probability distribution $\pi_j, j = 1, 2, \ldots, q$, gives the probability that the search begins in state j. The rewinding time is assumed to be negligible.

The branch labels between two states are transfer functions that contain information about the delays that may occur during the transition between the two states. Let z denote the unit-delay variable and let the power of z denote the time delay. A single-dwell system with dwell τ, false-alarm probability P_F, and constant penalty time T_p has transfer function $H_0(z) = (1-P_F)z^{\tau} + P_F z^{\tau+T_p}$ for all branches that do not originate in collective state q because the transition delay is τ with probability $1-P_F$ and $\tau + T_p$ with probability P_F. For a multiple-dwell system, $H_0(z)$ is determined by first drawing a subsidiary state diagram representing intermediate states and transitions that may occur as the system progresses from one state to the next one in the original circular state diagram. For example, Fig. 4.10 illustrates the subsidiary state diagram for a consecutive-count double-dwell system with false alarms P_{F1} and P_{F2} and delays τ_1 and τ_2 for the initial test and the

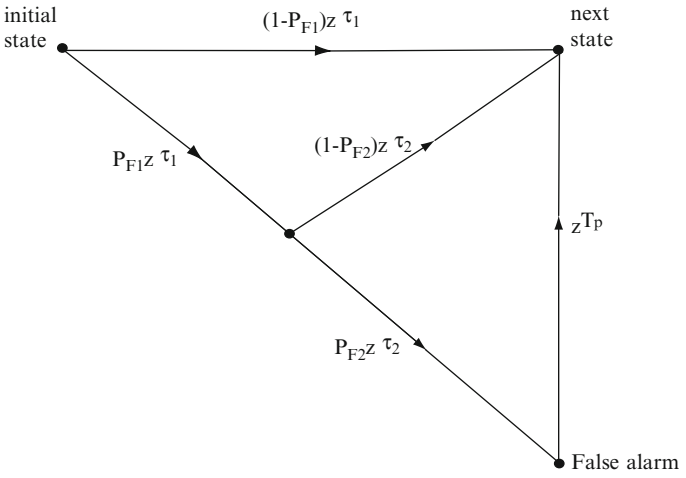

Fig. 4.10 Subsidiary state diagram for determination of $H_0(z)$ for consecutive-count double-dwell system

verification test, respectively. Examination of all possible paths between the initial state and the next state indicates that

$$\begin{aligned} H_0(z) &= (1 - P_{F1})\, z^{\tau_1} + P_{F1} z^{\tau_1} \left[(1 - P_{F2})\, z^{\tau_2} + P_{F2} z^{\tau_2 + T_P} \right] \\ &= (1 - P_{F1})\, z^{\tau_1} + P_{F1}\, (1 - P_{F2})\, z^{\tau_1 + \tau_2} + P_{F1} P_{F2} z^{\tau_1 + \tau_2 + T_p}. \end{aligned} \tag{4.69}$$

Let $H_D(z)$ denote the transfer function between the collective state q and the lock mode. Let $H_M(z)$ denote the transfer function between state q and state 1, which represents the failure to recognize code-phase offsets that are less than a chip duration. These transfer functions may be derived in the same manner as $H_0(z)$. For example, consider a consecutive-count, double-dwell system with a collective state that comprises two states. Figure 4.11 depicts the subsidiary state diagram representing intermediate states and transitions that may occur as the system progresses from state q (with subsidiary states a and b) to either the lock mode or state 1. Examination of all possible paths yields

$$\begin{aligned} H_D(z) = {} & P_{a1} P_{a2} z^{\tau_1 + \tau_2} + P_{a1}\, (1 - P_{a2})\, P_{b1} P_{b2} z^{2\tau_1 + 2\tau_2} \\ & + (1 - P_{a1})\, P_{b1} P_{b2} z^{2\tau_1 + \tau_2} \end{aligned} \tag{4.70}$$

$$\begin{aligned} H_M(z) = {} & (1 - P_{a1})\, (1 - P_{b1})\, z^{2\tau_1} + (1 - P_{a1})\, P_{b1}\, (1 - P_{b2})\, z^{2\tau_1 + \tau_2} \\ & + P_{a1}\, (1 - P_{a2})\, (1 - P_{b1})\, z^{2\tau_1 + \tau_2} \\ & + P_{a1}\, (1 - P_{a2})\, P_{b1}\, (1 - P_{b2})\, z^{2\tau_1 + 2\tau_2}. \end{aligned} \tag{4.71}$$

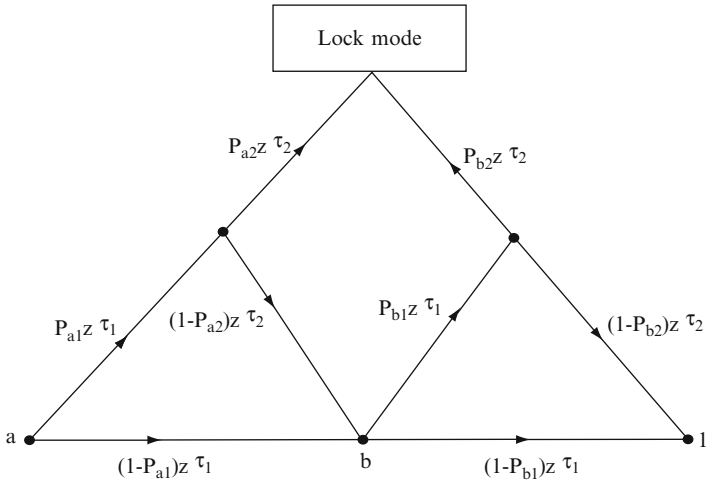

Fig. 4.11 Subsidiary state diagram for calculation of $H_D(z)$ and $H_M(z)$ for consecutive-count double-dwell system with two-state collective state

For a single-dwell system with a collective state that comprises N states,

$$H_D(z) = P_1 z^{\tau} + \sum_{j=2}^{N} P_j \left[\prod_{i=1}^{j-1} \left(1 - P_j\right) \right] z^{j\tau} \tag{4.72}$$

$$H_M(z) = \left[\prod_{j=1}^{N} \left(1 - P_j\right) \right] z^{N\tau} \tag{4.73}$$

$$H_0(z) = (1 - P_F)\, z^{\tau} + P_F z^{\tau + T_p} \tag{4.74}$$

where τ is the dwell time, P_F is the false-alarm probability, and P_j is the detection probability of state j within the collective state.

To calculate the statistics of the acquisition time, we seek the *generating function of the acquisition time* defined as the series

$$H(z) = \sum_{i=0}^{\infty} p_i\,(\tau_i)\, z^{\tau_i} \tag{4.75}$$

where $p_i(\tau_i)$ is the probability that the acquisition process will terminate in the lock mode after τ_i seconds. Since the probability that the lock mode is reached is equal

to or less than unity, $H(0) \leq 1$, and $H(z)$ converges at least for $|z| \leq 1$. If $H(z)$ is known, then a direct differentiation of (4.75) indicates that

$$\frac{dH(z)}{dz} = \sum_{i=0}^{\infty} \tau_i \, p_i(\tau_i) z^{\tau_i - 1}. \tag{4.76}$$

Therefore, the mean acquisition time is

$$\bar{T}_a = \sum_{i=0}^{\infty} \tau_i \, p_i(\tau_i) = \left. \frac{dH(z)}{dz} \right|_{z=1}. \tag{4.77}$$

Similarly, the second derivative of $H(z)$ gives

$$\left. \frac{d^2 H(z)}{dz^2} \right|_{z=1} = \sum_{i=0}^{\infty} \tau_i \, (\tau_i - 1) \, p_i \, (\tau_i) = \overline{T_a^2} - \bar{T}_a. \tag{4.78}$$

Therefore, the variance of the acquisition time is

$$\sigma_a^2 = \left\{ \frac{d^2 H(z)}{dz^2} + \frac{dH(z)}{dz} - \left[\frac{dH(z)}{dz} \right]^2 \right\} \Bigg|_{z=1}. \tag{4.79}$$

To derive $H(z)$, we observe that it may be expressed as

$$H(z) = \sum_{j=1}^{q} \pi_j \, H_j(z) \tag{4.80}$$

where $H_j(z)$ is the transfer function from an initial state j to the lock mode. Since the circular state diagram of Fig. 4.9 may be traversed an indefinite number of times during the acquisition process,

$$H_j(z) = H_0^{q-j}(z) H_D(z) \sum_{i=0}^{\infty} \left[H_M(z) H_0^{q-1}(z) \right]^i$$

$$= \frac{H_0^{q-j}(z) H_D(z)}{1 - H_M(z) H_0^{q-1}(z)}. \tag{4.81}$$

Substitution of this equation into (4.80) yields

$$H(z) = \frac{H_D(z)}{1 - H_M(z) H_0^{q-1}(z)} \sum_{j=1}^{q} \pi_j \, H_0^{q-j}(z). \tag{4.82}$$

For the uniform *a priori* distribution given by (4.29),

$$H(z) = \frac{H_D(z)\left[1 - H_0^q(z)\right]}{q\left[1 - H_M(z)H_0^{q-1}(z)\right][1 - H_0(z)]}. \tag{4.83}$$

Since the progression from one state to another is inevitable until the lock mode is reached, $H_0(1) = 1$. Since $H_D(1) + H_M(1) = 1$, (4.82) and (4.77) yield

$$\bar{T}_a = \frac{1}{H_D(1)}\left\{H_D'(1) + H_M'(1) + (q-1)H_0'(1)\left[1 - \frac{H_D(1)}{2}\right]\right\} \tag{4.84}$$

where the prime indicates differentiation with respect to z. As an example, consider a single-dwell system with a two-state collective state. The evaluation of (4.84) using (4.72) to (4.74) with $N = 2$ yields (4.45) with $T_r = 0$ if we set $P_1 = P_a$, $P_2 = P_b$, $T_p = \bar{T}_p$, $\tau = \tau_d$, and define P_D by (4.38).

4.2.9 Nonconsecutive and Sequential Searches

In the presence of frequency-selective fading with multiple resolvable multipath signals, the NMAT of serial-search acquisition is usually increased because the increased self-interference is more significant than the multiple correct or in-phase cells. The presence of the multipath signals may be exploited by using a *nonconsecutive serial search*, which can be shown to provide a lower NMAT than the conventional serial search in which cells are tested serially [7, 8]. The cost is increased computational complexity.

An alternative to acquisition tests of fixed dwell time or number of detector samples is *sequential detection*, which uses only the number necessary for a reliable decision. Thus, some sample sequences may allow a quick decision, while others may warrant using a large number of samples in the evaluation of a single phase of the spreading waveform. The *sequential probability ratio test* [2] entails the recalculation of the likelihood ratio after each new detector sample is produced. This ratio is compared with both upper and lower thresholds to determine if the test is terminated and no more samples need to be extracted. If the upper threshold is exceeded, the receiver declares acquisition and the lock mode is entered. If the likelihood ratio drops below the lower threshold, the test fails, and another code phase is tested. As long as the likelihood ratio lies between the two thresholds, a decision is postponed and the ratio continues to be updated. Although the sequential detector is capable of significantly reducing the mean acquisition time relative to detectors that use a fixed number of samples, it has a number of practical limitations. Chief among them is the computational complexity of calculating the likelihood ratio or log-likelihood ratio.

4.3 Acquisition Correlator

The noncoherent correlator of Fig. 4.3 provides the approximate generation of $R_o(\tau)$ given by (4.18). It is assumed that chip synchronization is established by one of the standard methods of symbol synchronization. Consequently, the test interval can be defined with boundaries that coincide with chip boundaries, and the receiver tests possible code phases of a locally generated spreading sequence to find the code phase of the received spreading sequence. Let MT_c denote the duration of the test interval, where M is a positive integer and T_c is the chip duration. The received spreading waveform has the form

$$p(t) = \sum_{i=-\infty}^{\infty} p_i \psi(t - iT_c) \tag{4.85}$$

where p_i is equal to +1 or −1 and represents one chip of a spreading sequence $\{p_i\}$. The chip waveform is normalized so that

$$\frac{1}{T_c} \int_0^{T_c} \psi^2(t)dt = 1. \tag{4.86}$$

The acquisition correlator has the form depicted in Fig. 4.12. The sequences $\{x_k\}$ and $\{y_k\}$ are obtained by in-phase and quadrature downconversions followed by chip-matched filters sampled at times $t = kT_c$. The decision variable is applied to a threshold detector to determine whether or not a test of a particular code phase is passed. If the locally generated spreading sequence is delayed by ν chips relative to an arbitrary time origin, where ν is an integer, then the test interval begins with chip -ν of the local spreading sequence. As indicated by (4.85) and shown in Fig. 4.12, the decision variable for one test of a specific code phase is

$$V = V_c^2 + V_s^2 \tag{4.87}$$

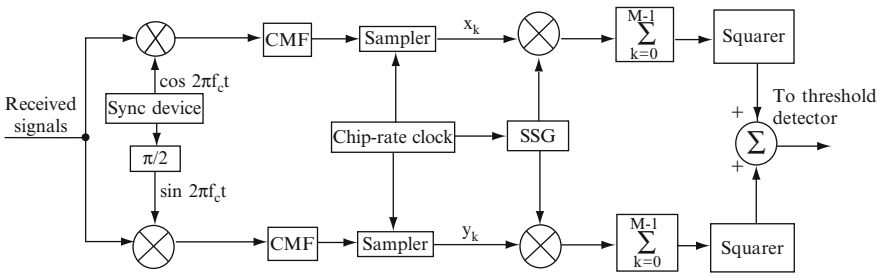

Fig. 4.12 Noncoherent correlator for acquisition system. *CMF* chip matched filter; *SSG* spreading sequence generator

where

$$V_c = \sum_{k=0}^{M-1} p_{k-\nu} x_k, \qquad V_s = \sum_{k=0}^{M-1} p_{k-\nu} y_k \tag{4.88}$$

$$x_k = \sqrt{2} \int_{kT_c}^{(k+1)T_c} r(t)\psi\,(t - kT_c) \cos 2\pi f_c t\, dt \tag{4.89}$$

$$y_k = \sqrt{2} \int_{kT_c}^{(k+1)T_c} r(t)\psi\,(t - kT_c) \sin 2\pi f_c t\, dt. \tag{4.90}$$

Sequences $\{x_k\}$ and $\{y_k\}$ associated with different values of ν can be applied to multiple parallel computations of $V(\nu)$ simultaneously. This procedure allows a parallel search of various code phases with a moderate amount of additional hardware or software. Since $p_k = \pm 1$, each of the inner products $V_c(\nu)$ and $V_s(\nu)$ may be computed by either adding or subtracting each component of $\{x_k\}$ or $\{y_k\}$.

To analyze the performance of the acquisition correlator for both the AWGN and the fading channels, we assume that the received signal is

$$r(t) = \sqrt{2\frac{\mathcal{E}_c}{T_c}} \alpha p(t - \tau) \cos(2\pi f_c t + \theta) + n(t) \tag{4.91}$$

where α is the attenuation due to fading with $E[\alpha^2] = 1$ so that $\mathcal{E}_c$ is the average energy per chip, f_c is the carrier frequency, θ is the random carrier phase, τ is the delay due to the unknown code phase, and $n(t)$ is the interference plus noise modeled as additive white Gaussian noise. The data modulation $d(t)$ is omitted because either it is not transmitted during acquisition or the test duration MT_c is much smaller than a symbol duration $T_s = GT_c$. In the latter case, the probability that a symbol transition occurs during a test is small, and the squaring operations eliminate the symbol value from V. The delay τ may be expressed in the form $\tau = \nu T_c - NT_c - \epsilon T_c$, where N is an integer and $0 \le \epsilon < 1$. For a rectangular chip waveform, (4.86), (4.88)–(4.91), $f_c T_c \gg 1$, and the definition of chip ν yield

$$V_c = \sqrt{\mathcal{E}_c T_c}\alpha \cos\theta \sum_{k=0}^{M-1} p_{k-\nu} \left[(1-\epsilon)\, p_{k-\nu+N} + \epsilon p_{k-\nu+N+1}\right] + N_{gc} \tag{4.92}$$

where

$$N_{gc} = \sum_{k=0}^{M-1} p_{k-\nu} n_{ck}, \quad n_{ck} = \sqrt{2} \int_{kT_c}^{(k+1)T_c} n(t)\psi\,(t - kT_c) \cos 2\pi f_c t\, dt \tag{4.93}$$

and

$$V_s = -\sqrt{\mathcal{E}_c T_c}\alpha \sin\theta \sum_{k=0}^{M-1} p_{k-\nu} \left[(1-\epsilon)\, p_{k-\nu+N} + \epsilon p_{k-\nu+N+1}\right] + N_{gs} \tag{4.94}$$

where

$$N_{gs} = \sum_{k=0}^{M-1} p_{k-\nu} n_{sk}, \; n_{sk} = \sqrt{2} \int_{kT_c}^{(k+1)T_c} n(t)\psi\left(t - kT_c\right) \sin 2\pi f_c t \; dt. \quad (4.95)$$

The alignment of the received and local spreading sequences is often close enough for acquisition if $N = -1$ or $N = 0$. If $N \neq -1, 0$, then the cell may be considered incorrect.

In the performance analysis, the spreading sequence $\{p_k\}$ is modeled as a zero-mean random binary sequence, ϵ is modeled as a random variable uniformly distributed over $[0, 1]$, and θ is modeled as a random variable uniformly distributed over $[0, 2\pi]$. Since $n(t)$ is zero-mean, white Gaussian noise, n_{ck} and n_{sk} are zero-mean Gaussian random variables. Therefore, the model implies that $E[V_c] = E[V_s] = 0$.

Since $p_{k-\nu} = \pm 1$ and is independent of n_{ck} and n_{sk}, the products $p_{k-\nu} n_{ck}$ and $p_{k-\nu} n_{sk}$ are zero-mean and Gaussian. The independence of the terms in the sum then indicates that N_{gc} and N_{gs} are zero-mean Gaussian random variables. Straightforward calculations using $f_c T_c \gg 1$ indicate that N_{gc} and N_{gs} are statistically independent with the same variance:

$$var\left(N_{gc}\right) = var\left(N_{gs}\right) = \frac{N_0 M T_c}{2}. \quad (4.96)$$

Straightforward calculations indicate that if the cell is incorrect and $N \neq -1, 0$, then $var\left(V_c\right) = var\left(V_s\right) = \sigma_0^2$, where

$$\sigma_0^2 = \frac{N_0 M T_c}{2}\left[1 + \left(\frac{2}{3}\right)\frac{\mathcal{E}_c}{N_0}\alpha^2\right], \; N \neq -1, 0. \quad (4.97)$$

The factor $(1 + 2\mathcal{E}_c/3N_0)$ indicates the presence of *self-interference,* which is due to the processing of the desired signal even when the cell is incorrect. The self-interference increases the probability of a false acquisition even if the noise term is negligible. The self-interference is negligible if $\mathcal{E}_c/N_0 \ll 1$, which may be true in practical systems, especially if N_0 incorporates the power spectral densities due to multiple-access interference and multipath signals. Straightforward calculations indicate that if $N = -1$ or 0, then $var\left(V_c\right) = var\left(V_s\right) = \sigma_1^2$, where

$$\sigma_1^2 = \frac{N_0 M T_c}{2}\left[1 + \left(\frac{M+1}{3}\right)\frac{\mathcal{E}_c}{N_0}\alpha^2\right], \; N = -1 \text{ or } 0. \quad (4.98)$$

Let V_1 denote the decision variable $V = V_c^2 + V_s^2$ when a correct cell is tested, and let V_0 denote V when an incorrect cell is tested. We assume that V_c and V_s have approximately Gaussian density functions. This assumption is most plausible when $M\mathcal{E}_c/N_0 < 1$ because then the terms N_{gc} and N_{gc} tend to dominate in (4.92) and

(4.94). It is also plausible when M is large because then we may invoke the central limit theorem, which indicates that the sums in (4.92) and (4.94) have approximately Gaussian densities, albeit these densities are distorted by the densities of the factors $\cos(\theta)$ and $\sin(\theta)$ in (4.92) and (4.94). Straightforward calculations indicate that V_c and V_s are uncorrelated, and hence independent Gaussian random variables. The decision variable is the sum of the squares of two independent, zero-mean Gaussian random variables. The results of Appendix B then indicate that V_i, $i = 0, 1$, has a central chi-square distribution with two degrees of freedom and probability density function

$$f_i(x) = \frac{1}{2\sigma_i^2} \exp\left(-\frac{x}{2\sigma_i^2}\right) u(x), \quad i = 0, 1 \tag{4.99}$$

where $u(x) = 1$, $x \geq 0$, and $u(x) = 0$, $x < 0$.

The false-alarm probability P_f for a test of an incorrect cell is the probability that $V_0 > V_t$, where V_t is the threshold. The detection probability P_d for a test of a correct cell is the probability that $V_1 > V_t$. The integration of (4.99) gives

$$P_f = \exp\left(-\frac{V_t}{2\sigma_0^2}\right) \tag{4.100}$$

$$P_d = \exp\left(-\frac{V_t}{2\sigma_1^2}\right). \tag{4.101}$$

Equation (4.100) indicates that the threshold needed to realize a specified P_f is

$$V_t = -2\sigma_0^2 \ln P_f \tag{4.102}$$

which requires an accurate estimate of N_0. If P_f is specified, then (4.100) and (4.101) yield

$$P_d = P_f^{\xi}, \quad \xi = \frac{1 + \left(\frac{2}{3}\right)\frac{\mathcal{E}_c}{N_0}\alpha^2}{1 + \left(\frac{M+1}{3}\right)\frac{\mathcal{E}_c}{N_0}\alpha^2}. \tag{4.103}$$

In the presence of Rayleigh fading, α has the Rayleigh probability density (Appendix B.4):

$$f_\alpha(x) = 2x \exp(-x^2) u(x) \tag{4.104}$$

and $E[\alpha^2] = 1$. For fast Rayleigh fading, it is assumed that α is approximately constant during a test, but independent between one test and another. Since (4.103) is implicitly conditioned on α, the detection probability in the presence of fast fading is determined by integrating the latter equation over the Rayleigh density. For slow Rayleigh fading with a coherence time much larger than the acquisition time, it is appropriate to use (4.103) in calculating the conditional mean acquisition time and then integrate the latter time over the Rayleigh density to obtain the mean acquisition time.

The step size Δ of the serial search is the separation in chips between cells. When $\Delta = 1/2$, the two consecutive cells that correspond to $N = -1$ and $N = 0$

are considered the two correct cells out of the q in the timing uncertainty region. When $\Delta = 1$, it is plausible to assume that there is only one correct cell, which corresponds to either $N = -1$ or $N = 0$. Let C_u denote the number of chip durations in the timing uncertainty. The *normalized mean acquisition time* (NMAT) is defined as $\bar{T}_a/C_uT_c$. The *normalized standard deviation* (NSD) is defined as σ_a/C_uT_c. For step size $\Delta = 1$, $q/C_u = 1$; for $\Delta = 1/2$, $q/C_u = 2$.

Example 4.1. As an example of the application of the preceding results, consider a single-dwell system with a uniform search and a uniform *a priori* correct-cell location distribution. Let $\tau_d = MT_c$, where M is the number of chips per test, and $\bar{T}_p = KT_c$, where K is the number of chip durations in the mean penalty time. For $\Delta = 1/2$, it is assumed that there are two independent correct cells with the common detection probability $P_d = P_a = P_b$. If $q \gg 1$, (4.45) and (4.38) yield the NMAT:

$$NMAT = \left(\frac{2 - P_D}{2P_D}\right)\frac{q}{C_u}(M + KP_F) \tag{4.105}$$

where

$$P_D = 2P_d - P_d^2, \ \Delta = 1/2. \tag{4.106}$$

For $\Delta = 1$, it is assumed that there one correct cell so that

$$P_D = P_d, \ \Delta = 1. \tag{4.107}$$

In a single-dwell system, $P_F = P_f$. In the absence of fading, (4.103) relates P_d and P_f.

Figure 4.13 shows the NMAT as a function of $\mathcal{E}_c/N_0$ in the absence of fading. At each value of $\mathcal{E}_c/N_0$, the values of P_f and M are selected to minimize the NMAT. The figure indicates the slight advantage of $\Delta = 1$ in a single-dwell system. From (4.37), it is found that each plot of the NSD has a shape similar to that of the corresponding NMAT plot. □

Example 4.2. Consider double-dwell systems with a uniform search, a uniform *a priori* correct-cell location distribution, $\Delta = 1/2$, and two independent correct cells with $P_d = P_a = P_b$, $P_{a1} = P_{b1}$, and $P_{a2} = P_{b2}$. The test durations are $\tau_1 = M_1T_c$ and $\tau_2 = M_2T_c$. If $q \gg 1$, the NMAT is obtained from (4.36) and (4.106), where $\bar{T}_{11}$ is given by (4.40) for a consecutive-count system and (4.50) for an up-down system. Since $q/C_u = 2$, a consecutive-count system has

$$NMAT = \left(\frac{2-2P_d + P_d^2}{2P_d - P_d^2}\right)[M_1 + P_{F1}(M_2 + P_{F2}K)] \tag{4.108}$$

and an up-down system has

$$NMAT = \left(\frac{2-2P_d + P_d^2}{2P_d - P_d^2}\right)\left[\frac{M_1 + P_{F1}(M_2 + P_{F2}K)}{1 - P_{F1}(1 - P_{F2})}\right]. \tag{4.109}$$

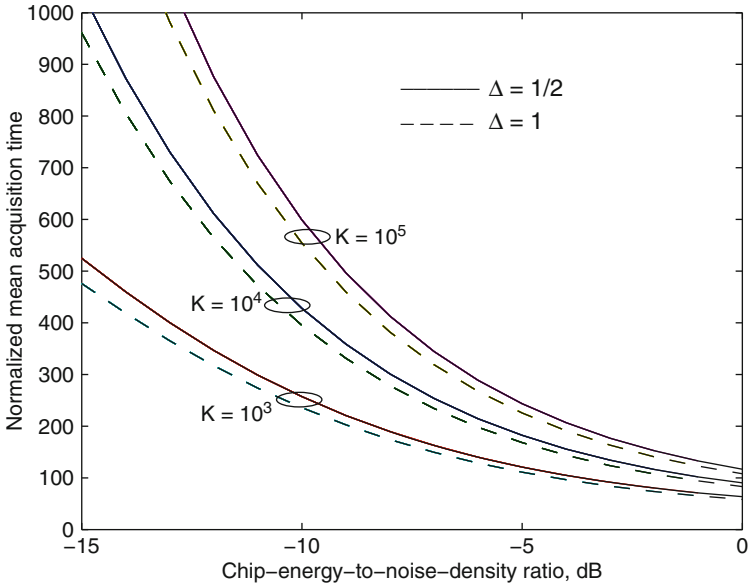

Fig. 4.13 NMAT versus $\mathcal{E}_c/N_0$ for single-dwell system in absence of fading. Values of P_f and M are optimized

By replacing P_d with P_{ai} and P_f with P_{Fi}, the probabilities P_{ai} and P_{Fi}, $i = 1$ or 2, are related through (4.103) in the absence of fading. Therefore, (4.39) implies that a consecutive-count system has

$$P_d = P_{F1}^{\xi_1} P_{F2}^{\xi_2} \text{ (consecutive-count)} \tag{4.110}$$

where

$$\xi_i = \frac{1 + \left(\frac{2}{3}\right)\frac{\mathcal{E}_c}{N_0}}{1 + \left(\frac{M_i+1}{3}\right)\frac{\mathcal{E}_c}{N_0}}, \quad i = 1, 2. \tag{4.111}$$

Equations (4.47) and (4.48) imply that an up-down system has

$$P_d = \frac{P_{F1}^{\xi_1} P_{F2}^{\xi_2}}{1 - P_{F1}^{\xi_1}(1 - P_{F2}^{\xi_2})} \text{ (up-down)}. \tag{4.112}$$

Figure 4.14 shows the NMAT as a function of $\mathcal{E}_c/N_0$ for double-dwell systems in the absence of fading. The step size is $\Delta = 1/2$, which is found to be slightly advantageous in typical double-dwell systems. At each value of $\mathcal{E}_c/N_0$, the values of P_{F1}, P_{F2}, M_1, and M_2 are selected to minimize the NMAT. The figure illustrates the advantage of the up-down system in most practical applications. From (4.37), it is found that each plot of the NSD has a shape similar to that of the corresponding NMAT plot. A comparison of Fig. 4.14 with Fig. 4.13 indicates that double-dwell

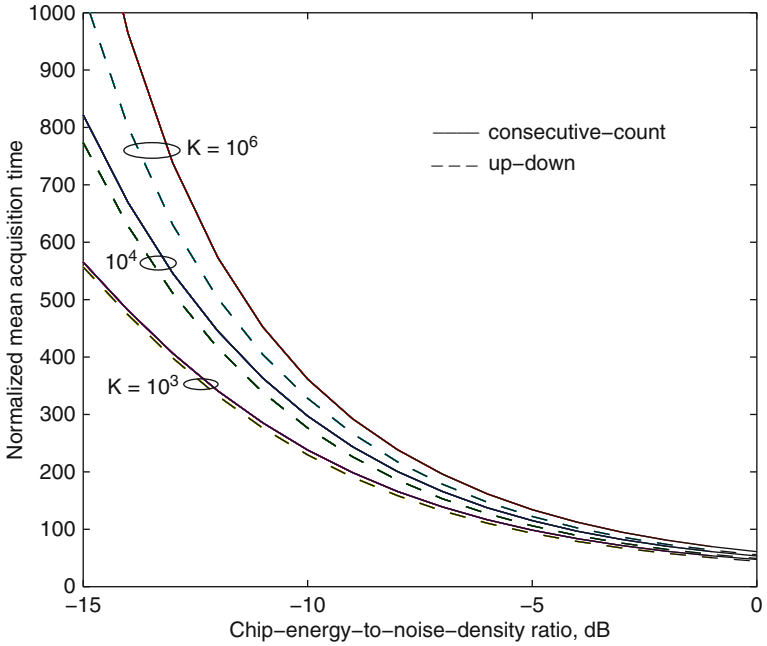

Fig. 4.14 NMAT versus $\mathcal{E}_c/N_0$ for double-dwell systems in absence of fading. Step size is $\Delta = 1/2$. Values of P_{F1}, P_{F2}, M_1, and M_2 are optimized

systems are capable of significantly lowering the NMAT relative to a single-dwell system if the penalty time is sufficiently large. □

The detection threshold of (4.102) depends on an estimate of N_0, the equivalent noise-power spectral density. An accurate estimate usually requires a long observation interval. When the instantaneous interference power may be rapidly varying, an adaptive threshold may be set by estimating the instantaneous received power [9]. As a result, the mean acquisition time is lowered relative to its value for nonadaptive schemes when Rayleigh fading or pulsed Gaussian noise jamming is present.

4.4 Code Tracking

Coherent code-tracking loops operate at baseband following the coherent removal of the carrier of the received signal. An impediment to their use is that the input SNR is usually too low for carrier synchronization prior to code synchronization and the subsequent despreading of the received signal. Furthermore, coherent loops cannot easily accommodate the effects of data modulation. Noncoherent loops, which predominate in spread-spectrum systems, operate directly on the received signals and are unaffected by the data modulation.

To motivate the design of the noncoherent loop, one may adapt the statistic $R_o(\tau)$ given by (4.18). If the maximum-likelihood estimate $\hat{\tau}$ is assumed to be within the interior of its timing uncertainty region and $R_o(\tau)$ is a differentiable function of τ, then the estimate $\hat{\tau}$ that maximizes $R_o(\tau)$ may be found by setting

$$\left.\frac{\partial R_o(\tau)}{\partial \tau}\right|_{\tau=\hat{\tau}} = 0. \tag{4.113}$$

Although $R_o(\tau)$ is not differentiable if the chip waveform is rectangular, this problem is circumvented by using a difference equation as an approximation of the derivative. Thus, for a positive δT_c, we set

$$\frac{\partial R_o(\tau)}{\partial \tau} \approx \frac{R_o(\tau + \delta T_c) - R_o(\tau - \delta T_c)}{2\delta T_c}. \tag{4.114}$$

This equation implies that the solution of (4.113) may be approximately obtained by a device that finds the $\hat{\tau}$ such that

$$R_o(\hat{\tau} + \delta T_c) - R_o(\hat{\tau} - \delta T_c) = 0. \tag{4.115}$$

To determine an implementation of this equation, we assume that no noise is present, and that

$$s(t) = Ap(t)\cos(2\pi f_c t + \theta) \tag{4.116}$$

where the correct timing offset of the received signal is $\tau = 0$. Substituting $r(t) = s(t)$ into (4.18) and using trigonometry, we obtain

$$R_o(\hat{\tau}) = \frac{A^2}{4}\left[\int_0^T p(t)p(t-\hat{\tau})dt\right]^2. \tag{4.117}$$

If $p(t)$ is modeled as the spreading waveform for a random binary sequence and the interval $[0, T]$ includes many chips, then the integral is reasonably approximated by its expected value, which is proportional to the autocorrelation $R_p(\hat{\tau})$. Substituting this result into (4.115), we find that the maximum-likelihood estimate is approximately obtained by a device that finds the $\hat{\tau}$ such that

$$R_p^2(\hat{\tau} + \delta T_c) - R_p^2(\hat{\tau} - \delta T_c) = 0. \tag{4.118}$$

The noncoherent *delay-locked loop* [10], which is diagrammed in Fig. 4.15, implements an approximate computation of the difference on the left-hand side of (4.118) and then continually adjusts $\hat{\tau}$ so that this difference remains near zero. The estimate is used to produce the synchronized local spreading sequence that is used for despreading the received direct-sequence signal. The code generator produces three sequences, one of which is the reference sequence used for acquisition and demodulation. The other two sequences are advanced and delayed, respectively,

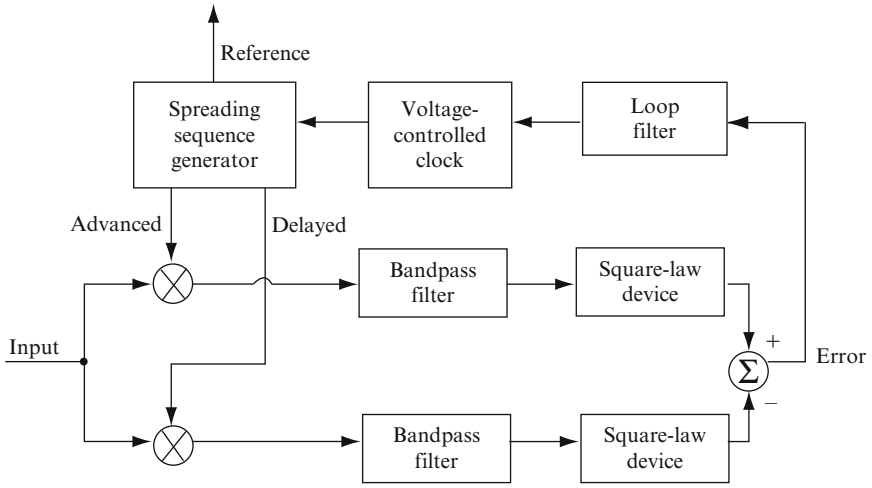

Fig. 4.15 Delay-locked loop

by δT_c relative to the reference sequence. The product δT_c is usually equal to the acquisition step size, and thus usually $\delta = 1/2$, but other values are plausible. The advanced and delayed sequences are multiplied by the received direct-sequence signal in separate branches.

For the received direct-sequence signal (4.116), the signal portion of the upper-branch mixer output is

$$s_{u1}(t) = Ad(t)p(t)p\left(t + \delta T_c - \epsilon T_c\right)\cos\left(2\pi f_c t + \theta\right) \tag{4.119}$$

where ϵT_c is the delay of the reference sequence relative to the received sequence. Although ϵ is a function of time because of the loop dynamics, the time dependence is suppressed for notational convenience. Since each bandpass filter has a bandwidth on the order of $1/T_s$, where T_s is the duration of each symbol, $d(t)$ is not significantly distorted by the filtering. Nearly all spectral components except the slowly varying expected value of $p(t)p(t + \delta T_c - \epsilon T_c)$ are blocked by the upper-branch bandpass filter. Since this expected value is the autocorrelation of the spreading sequence, the filter output is

$$s_{u2}(t) \approx Ad(t)R_p\left(\delta T_c - \epsilon T_c\right)\cos\left(2\pi f_c t + \theta\right). \tag{4.120}$$

Any double-frequency component produced by the square-law device is ultimately suppressed by the loop filter and thus is ignored. Since $d^2(t) = 1$, the data modulation is removed, and the upper-branch output is

$$s_{u3}(t) \approx \frac{A^2}{2}R_p^2\left(\delta T_c - \epsilon T_c\right). \tag{4.121}$$

Similarly, the output of the lower branch is

$$s_{l3}(t) \approx \frac{A^2}{2} R_p^2 \left(-\delta T_c - \epsilon T_c\right). \tag{4.122}$$

The difference between the outputs of the two branches is the *error signal*:

$$s_e(t) \approx \frac{A^2}{2} \left[R_p^2 \left(\delta T_c - \epsilon T_c\right) - R_p^2 \left(-\delta T_c - \epsilon T_c\right)\right]. \tag{4.123}$$

Since $R_p(\tau)$ is an even function, the error signal is proportional to the left-hand side of (4.118) with $\hat{\tau} = \epsilon T_c$.

If $p(t)$ is modeled as the spreading waveform for a random binary sequence, then (Sect. 2.2)

$$R_p(\tau) = \Lambda\left(\frac{\tau}{T_c}\right) = \begin{cases} 1 - |\frac{\tau}{T_c}|, & |\tau| \le T_c \\ 0, & |\tau| > T_c. \end{cases} \tag{4.124}$$

The substitution of this equation into (4.123) yields

$$s_e(t) \approx \frac{A^2}{2} S(\epsilon, \delta) \tag{4.125}$$

where $S(\epsilon, \delta)$ is the *discriminator characteristic* or *S-curve* of the tracking loop. For $0 \le \delta \le 1/2$,

$$S(\epsilon, \delta) = \begin{cases} 4\epsilon(1-\delta), & 0 \le \epsilon \le \delta \\ 4\delta(1-\epsilon), & \delta \le \epsilon \le 1-\delta \\ 1 + (\epsilon - \delta)(\epsilon - \delta - 2), & 1-\delta \le \epsilon \le 1+\delta \\ 0, & 1+\delta \le \epsilon. \end{cases} \tag{4.126}$$

For $1/2 \le \delta \le 1$,

$$S(\epsilon, \delta) = \begin{cases} 4\epsilon(1-\delta), & 0 \le \epsilon \le 1-\delta \\ 1 + (\epsilon - \delta)(\epsilon - \delta + 2), & 1-\delta \le \epsilon \le \delta \\ 1 + (\epsilon - \delta)(\epsilon - \delta - 2), & \delta \le \epsilon \le 1+\delta \\ 0, & 1+\delta \le \epsilon. \end{cases} \tag{4.127}$$

In both cases,

$$S(-\epsilon, \delta) = -S(\epsilon, \delta). \tag{4.128}$$

Figure 4.16 illustrates the discriminator characteristic for $\delta = 1/2$. The filtered error signal is applied to the voltage-controlled clock. Changes in the clock frequency cause the reference sequence to converge toward alignment with the received spreading sequence. When $0 < \epsilon(t) < 1 + \delta$, the reference sequence is delayed relative to the received sequence. As shown in Fig. 4.16, $S(\epsilon, \delta)$ is positive, so the clock rate is increased, and $\epsilon(t)$ decreases. The figure indicates that $s_e(t) \to 0$

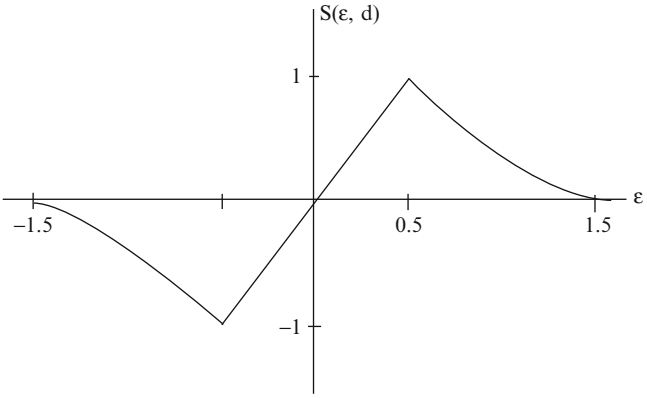

Fig. 4.16 Discriminator characteristic of delay-locked loop for $\delta = 1/2$

as $\epsilon(t) \to 0$. Similarly, when $\epsilon(t) < 0$, we find that $s_e(t) \to 0$ as $\epsilon(t) \to 0$. Thus, the delay-locked loop tracks the received code timing once the acquisition system has finished the coarse alignment.

The discriminator characteristic of code-tracking loops differs from that of phase-locked loops in that it is nonzero only within a finite range of ϵ. Outside that range, code tracking cannot be sustained, the synchronization system loses lock, and a reacquisition search is initiated by the lock detector. Tracking resumes once the acquisition system reduces ϵ to within the range for which the discriminator characteristic is nonzero.

When short spreading sequences are used in a synchronous direct-sequence network, the reduced randomness in the multiple-access interference (Chap. 6) may cause increased tracking jitter or even an offset in the discriminator characteristic [11]. For orthogonal sequences, the interference is zero when synchronization exists, but may become large when there is a code-phase error in the local spreading sequence. In the presence of a tracking error, the delay-locked-loop arm with the larger offset relative to the correct code phase receives relatively more noise power than the other arm. This disparity reduces the slope of the discriminator characteristic and, hence, degrades the tracking performance. Moreover, because of the nonsymmetric character of the cross-correlations among the spreading sequences, the discriminator characteristic may be biased in one direction, which will cause a tracking offset.

The noncoherent *tau-dither loop,* which is depicted in Fig. 4.17, is a lower-complexity alternative to the noncoherent delay-locked loop. The dither generator produces the *dither signal* $D(t)$, a square wave that alternates between $+1$ and -1. This signal controls a switch that alternately passes an advanced or delayed version of the spreading sequence. In the absence of noise, the output of the switch can be represented by

$$s_1(t) = \left[\frac{1 + D(t)}{2}\right] p\left(t + \delta T_c - \epsilon T_c\right) + \left[\frac{1 - D(t)}{2}\right] p\left(t - \delta T_c - \epsilon T_c\right) \quad (4.129)$$

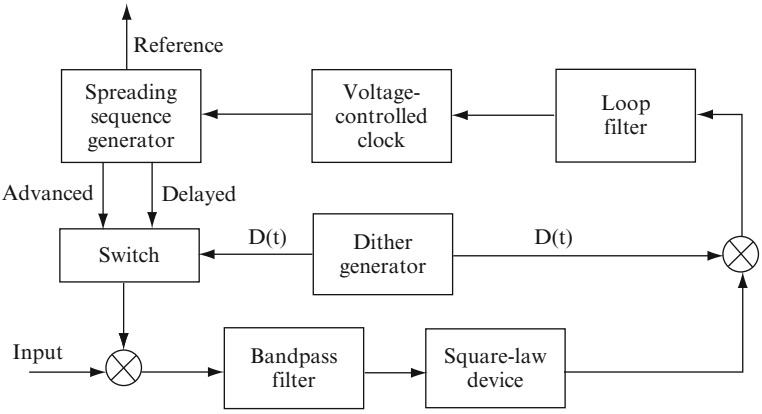

Fig. 4.17 Tau-dither loop

where the two factors within brackets are orthogonal functions of time and alternate between +1 and 0. Only one of the factors is nonzero at any instant. The received direct-sequence signal is multiplied by $s_1(t)$, filtered, and then applied to a square-law device. If the bandpass filter has a sufficiently narrow bandwidth, then a derivation similar to that of (4.121) indicates that the device output is

$$s_2(t) \approx \frac{A^2}{2}\left[\frac{1+D(t)}{2}\right] R_p^2\left(\delta T_c - \epsilon T_c\right) + \frac{A^2}{2}\left[\frac{1-D(t)}{2}\right] R_p^2\left(-\delta T_c - \epsilon T_c\right). \tag{4.130}$$

Since $D(t)[1+D(t)] = 1 + D(t)$ and $D(t)[1-D(t)] = -[1-D(t)]$, the input to the loop filter is

$$s_3(t) \approx \frac{A^2}{2}\left[\frac{1+D(t)}{2}\right] R_p^2\left(\delta T_c - \epsilon T_c\right) - \frac{A^2}{2}\left[\frac{1-D(t)}{2}\right] R_p^2\left(-\delta T_c - \epsilon T_c\right) \tag{4.131}$$

which is a rectangular wave if the time variation of ϵ is ignored. Since the loop filter has a narrow bandwidth relative to that of $D(t)$, its output is approximately the direct-current component of $s_3(t)$, which is the average value of $s_3(t)$. Averaging the two terms of (4.131), we obtain the clock input:

$$s_4(t) \approx \frac{A^2}{4}\left[R_p^2\left(\delta T_c - \epsilon T_c\right) - R_p^2\left(\delta T_c - \epsilon T_c\right)\right]. \tag{4.132}$$

The substitution of (4.124) yields the:

$$s_4(t) = \frac{A^2}{4} S(\epsilon, \delta) \tag{4.133}$$

where the discriminator characteristic is given by (4.126) to (4.128). Thus, the tau-dither loop can track the code timing in a manner similar to that of the delay-locked loop. A detailed analysis including the effects of noise indicates that the tau-dither loop provides less accurate code tracking [2]. However, the tau-dither loop requires less hardware than the delay-locked loop and avoids the need to balance the gains and delays in the two branches of the delay-locked loop.

In the presence of frequency-selective fading, the discriminator characteristics of tracking loops are severely distorted. Much better performance is potentially available from a noncoherent tracking loop with diversity and multipath-interference cancellation [12], but a large increase in implementation complexity is required.

4.5 Frequency-Hopping Patterns

The synchronization of the reference frequency-hopping pattern produced by the receiver synthesizer with the received pattern may be facilitated by precision clocks in both the transmitter and the receiver, feedback signals from the receiver to the transmitter, or transmitted pilot signals. However, in most applications, it is necessary or desirable for the receiver to be capable of obtaining synchronization by processing the received signal. During *acquisition*, the reference pattern is synchronized with the received pattern to within a fraction of a hop duration. The *tracking* system further reduces the synchronization error, or at least maintains it within certain bounds. For communication systems that require a strong capability to reject interference, *matched-filter acquisition* and *serial-search acquisition* are the most effective techniques. The matched filter provides rapid acquisition of short frequency-hopping patterns, but requires the simultaneous synthesis of multiple frequencies. The matched filter may also be used in the configuration of Fig. 4.2 to detect short patterns embedded in much longer frequency-hopping patterns. Such a detection can be used to initialize or supplement serial-search acquisition, which is more reliable and accommodates long patterns.

4.5.1 Matched-Filter Acquisition

Figure 4.18 shows a programmable *matched-filter acquisition system* that provides substantial protection against interference [13]. It is assumed that a single frequency channel is used during each hop interval that occurs during acquisition. One or more programmable frequency synthesizers produce tones at frequencies $f_1, f_2, \ldots, f_N$, which are offset by a constant frequency from the consecutive frequencies of the hopping pattern for code acquisition. Each tone multiplies the received frequency-hopping signal and the result is filtered so that most of the received energy is blocked, except the energy in a frequency-hopping pulse at a specific frequency.

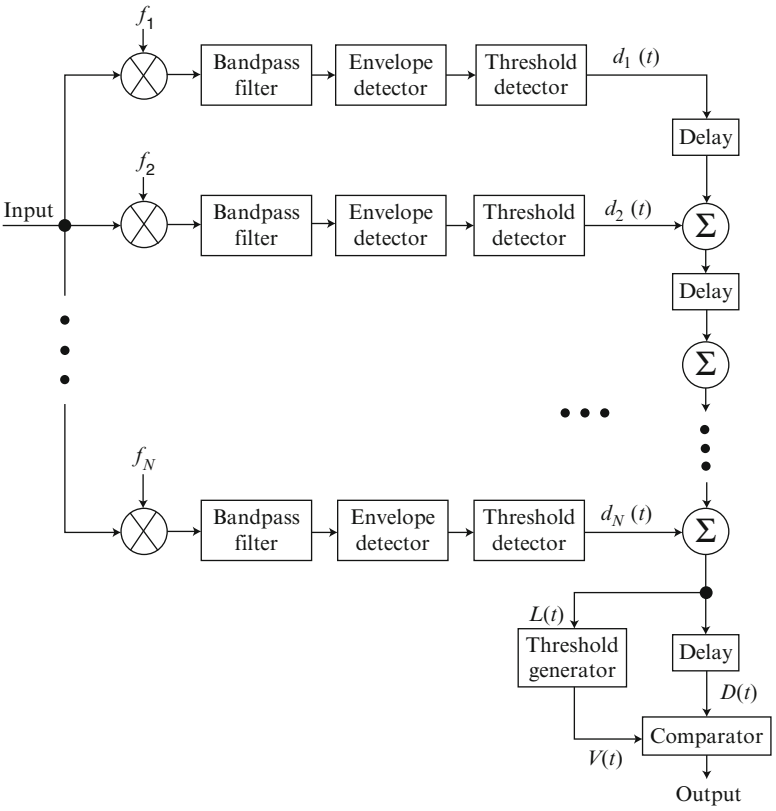

Fig. 4.18 Matched-filter acquisition system with protection against interference

The threshold detector of branch k produces $d_k(t) = 1$ if its threshold is exceeded, which ideally occurs only if the received signal hops to a specific frequency. Otherwise, the threshold detector produces $d_k(t) = 0$. The use of binary detector outputs prevents the system from being overwhelmed by a few strong interference signals. Input $D(t)$ of the comparator is the number of frequencies in the hopping pattern that were received in succession. This discrete-valued, continuous-time function is

$$D(t) = \sum_{k=1}^{N} d_k[t - (N - k + 1)T_h] \tag{4.134}$$

where T_h is the hop duration. These waveforms are illustrated in Fig. 4.19a for $N = 8$. The input to the threshold generator is

$$L(t) = D(t + T_h). \tag{4.135}$$

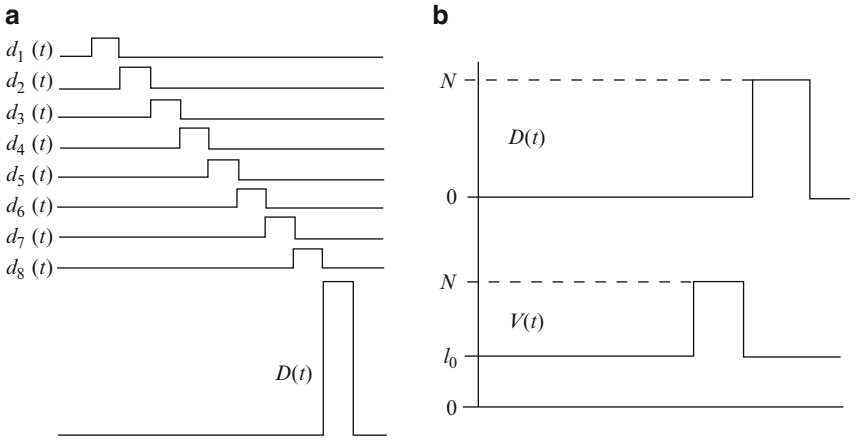

Fig. 4.19 Ideal acquisition system waveforms: (**a**) formation of $D(t)$ when $N = 8$, and (**b**) comparison of $D(t)$ and $V(t)$

Acquisition is declared when $D(t) \geq V(t)$, where $V(t)$ is an adaptive threshold that is a function of $L(t)$. An effective choice is

$$V(t) = \min[L(t) + l_0, N] \tag{4.136}$$

where l_0 is a positive integer.

In the absence of noise and interference, $L(t) = 0$ and $V(t) = l_0$ during the hop interval in which $D(t) = N$, as illustrated in Fig. 4.19b. If j of the N frequency channels monitored by the matched filter receive strong, continuous interference and $j \leq N - l_0$, then $L(t) = j$ and $V(t) = j + l_0$ during this hop, and $D(t) \geq V(t)$. During other intervals, $j + l_0 \leq V(t) \leq N$, but $D(t) = j$. Therefore, $V(t) > D(t)$, and the matched filter does not declare acquisition. False alarms are prevented because $L(t)$ provides an estimate of the number of frequency channels with continuous interference.

When acquisition tone k is received, the signal in branch k of the matched filter is

$$r_k(t) = \sqrt{2S}\cos 2\pi f_0 t + \sqrt{2I}\cos(2\pi f_0 t + \phi) + n(t) \tag{4.137}$$

where f_0 is the IF, the first term is the desired signal with average power S, the second term represents tone interference with average power I, $n(t)$ is zero-mean, stationary Gaussian noise and interference, and ϕ is the phase shift of the tone interference relative to the desired signal. The power in $n(t)$ is

$$N_1 = N_t + N_i \tag{4.138}$$

where N_t is power of the thermal noise and N_i is the power of the statistically independent noise interference.

Bandpass filters are used instead of filters matched to the acquisition tones because the appropriate sampling times are unknown. The passbands of the bandpass filters in the branches are assumed to be spectrally disjoint so that tone interference entering one branch has negligible effect on the other branches, and the filter outputs are statistically independent of each other. To prove the statistical independence of the noise, let $R_n(\tau)$ and $S_n(f)$ denote the autocorrelation and power spectral density, respectively, of the stationary Gaussian noise $n(t)$ in the input of the acquisition system. Let $h_1(t)$ and $h_2(t)$ denote the impulse responses and $H_1(f)$ and $H_2(f)$ the transfer functions of two bandpass filters. Since the same Gaussian noise process enters both filters, their outputs are jointly Gaussian. The cross-covariance of the jointly Gaussian, zero-mean filter outputs is

$$\begin{aligned} C &= E\left[\int_{-\infty}^{\infty} h_1(\tau_1)n(t-\tau_1)d\tau_1 \int_{-\infty}^{\infty} h_2(\tau_2)n(t-\tau_2)d\tau_2\right] \\ &= \int_{-\infty}^{\infty}\int_{-\infty}^{\infty} h_1(\tau_1)h_2(\tau_2)R_n(\tau_2-\tau_1)d\tau_1\, d\tau_2 \\ &= \int_{-\infty}^{\infty}\int_{-\infty}^{\infty}\int_{-\infty}^{\infty} h_1(\tau_1)h_2(\tau_2)S(f)\exp[j2\pi f(\tau_2-\tau_1)]df\, d\tau_1\, d\tau_2 \\ &= \int_{-\infty}^{\infty} S(f)H_1(f)H_2^*(f)df \end{aligned} \tag{4.139}$$

which is equal to zero if $H_1(f)$ and $H_2(f)$ are spectrally disjoint. If the noise is white and, hence, $S(f)$ is a constant, then $C = 0$ if $H_1(f)$ and $H_2(f)$ are orthogonal. When $C = 0$ for all pairs of bandpass filters, the threshold-detector outputs in the N branches are statistically independent.

Suppose that noise interference is present in a branch, but that tone interference is absent so that $I = 0$. The stationary Gaussian noise has the representation (Appendix A.2)

$$n(t) = n_c(t)\cos 2\pi f_0 t - n_s(t)\sin 2\pi f_0 t \tag{4.140}$$

where $n_c(t)$ and $n_s(t)$ are zero-mean Gaussian processes with noise powers equal to N_1. In practice, the matched filter of Fig. 4.18 would operate in continuous time so that acquisition might be declared at any moment. However, for analytical simplicity, the detection and false-alarm probabilities are calculated under the assumption that there is one sample taken per hop dwell time. From (4.137) with $I = 0$ and (4.140), it follows that

$$r_k(t) = \sqrt{Z_1^2(t) + Z_2^2(t)}\cos[2\pi f_0 t + \psi(t)] \tag{4.141}$$

where

$$Z_1(t) = \sqrt{2S} + n_c(t), \quad Z_2(t) = n_s(t), \quad \psi(t) = \tan^{-1}\left[\frac{n_s(t)}{n_c(t)}\right]. \tag{4.142}$$

Since $n_c(t)$ and $n_s(t)$ are statistically independent (Appendix A.2), the joint probability density function of Z_1 and Z_2 at any specific time is

$$g_1(z_1, z_2) = \frac{1}{2\pi N_1} \exp\left[- \frac{(z_1 - \sqrt{2S})^2 + z_2^2}{2N_1} \right]. \tag{4.143}$$

Let R and Θ be implicitly defined by $Z_1 = R\cos\Theta$ and $Z_2 = R\sin\Theta$. The joint density of R and Θ is

$$g_2(r, \theta) = \frac{r}{2\pi N_1} \exp\left(- \frac{r^2 - 2r\sqrt{2S}\cos\theta + 2S}{2N_1} \right), \; r \geq 0, \; |\theta| \leq \pi. \tag{4.144}$$

The probability density function of the envelope $R = \sqrt{Z_1^2(t) + Z_2^2(t)}$ is obtained by integration over θ. The application of (1.73) gives

$$f_1(r) = \frac{r}{N_1} \exp\left(- \frac{r^2 - 2S}{2N_1} \right) I_0\left(r\frac{\sqrt{2S}}{N_1} \right) u(r) \tag{4.145}$$

where $I_0(\;)$ is the modified Bessel function of the first kind and order zero, and $u(r) = 1$ if $r \geq 0$ and $u(r) = 0$ if $r < 0$.

The detection probability for the threshold detector in the branch is the probability that the envelope-detector output R exceeds the threshold η:

$$P_{11} = \int_{\eta}^{\infty} f_1(r) dr. \tag{4.146}$$

The *Marcum Q-function* is defined as

$$Q(\alpha, \beta) = \int_{\beta}^{\infty} x \exp\left(- \frac{x^2 + \alpha^2}{2} \right) I_0(\alpha x) dx. \tag{4.147}$$

Applying this definition,

$$P_{11} = Q\left(\sqrt{\frac{2S}{N_1}}, \frac{\eta}{\sqrt{N_1}} \right). \tag{4.148}$$

In the absence of noise interference, the detection probability is

$$P_{10} = Q\left(\sqrt{\frac{2S}{N_t}}, \frac{\eta}{\sqrt{N_t}} \right). \tag{4.149}$$

If the acquisition tone is absent so that $S = 0$, but the noise interference is present, the false-alarm probability is

$$P_{01} = \exp\left(-\frac{\eta^2}{2N_1}\right). \tag{4.150}$$

In the absence of both the acquisition tone and the noise interference, the false-alarm probability is

$$P_{00} = \exp\left(-\frac{\eta^2}{2N_t}\right). \tag{4.151}$$

In (4.148) to (4.151), the first subscript is 1 when the acquisition tone is present and 0 otherwise, whereas the second subscript is 1 when interference is present and 0 otherwise.

Suppose that tone interference is present in a branch. We make the pessimistic assumption that this tone has a frequency exactly equal to that of the acquisition tone, as indicted in (4.137). A trigonometric expansion of the interference term and a derivation similar to that of (4.148) indicates that given the value of ϕ, the conditional detection probability is

$$P_{11}(\phi) = Q\left(\sqrt{\frac{2(S + I + \sqrt{SI}\cos\phi)}{N_1}},\ \frac{\eta}{\sqrt{N_1}}\right). \tag{4.152}$$

If ϕ is modeled as a random variable uniformly distributed over $[0, 2\pi)$, then the detection probability is

$$P_{11} = \frac{1}{\pi}\int_0^{\pi} P_{11}(\phi)d\phi \tag{4.153}$$

where the fact that $\cos\phi$ takes all its possible values over $[0, \pi]$ has been used to shorten the integration interval. If the acquisition tone is absent, but the tone interference is present, the false-alarm probability is

$$P_{01} = Q\left(\sqrt{\frac{2I}{N_1}},\ \frac{\eta}{\sqrt{N_1}}\right). \tag{4.154}$$

It is convenient to define the function

$$\beta(i, N, m, P_a, P_b) = \sum_{n=0}^{i}\binom{m}{n}\binom{N-m}{i-n}P_a^n(1-P_a)^{m-n}P_b^{i-n}(1-P_b)^{N-m-i+n} \tag{4.155}$$

where $\binom{b}{a} = 0$ if $a > b$. Given that m of the N matched-filter branches receive interference of equal power, let the index n represent the number of interfered channels with detector outputs above η. If $0 \le n \le i$, there are $\binom{m}{n}$ ways to choose

n channels out of m and $\binom{N-m}{i-n}$ ways to choose $i-n$ channels with detector outputs above η from among the $N-m$ channels that are not interfered. Therefore, the conditional probability that $D(t)=i$ given that m channels receive interference is

$$P(D=i|m)=\beta(i,N,m,P_{h1},P_{h0}),\quad h=0,1 \tag{4.156}$$

where $h=1$ if the acquisition tones are present and $h=0$ if they are not. Similarly, given that m of N acquisition channels receive interference, the conditional probability that $L(t)=l$ is

$$P(L=l|m)=\beta(l,N,m,P_{h1},P_{h0}),\quad h=0,1. \tag{4.157}$$

If there are J interference signals randomly distributed among a hopset of M frequency channels, then the probability that m out of N matched-filter branches have interference is

$$P_m=\frac{\binom{N}{m}\binom{M-N}{J-m}}{\binom{M}{J}}. \tag{4.158}$$

The probability that acquisition is declared at a particular sampling time is

$$P_A=\sum_{m=0}^{\min(N,J)}P_m\sum_{l=0}^{N}P(L=l|m)\sum_{k=V(l)}^{N}P(D=k|m). \tag{4.159}$$

When the acquisition tones are received in succession, the probability of detection is determined from (4.156) to (4.159). The result is

$$P_D=\sum_{m=0}^{\min(N,J)}\frac{\binom{N}{m}\binom{M-N}{J-m}}{\binom{M}{J}}\sum_{l=0}^{N}\beta(l,N,m,P_{01},P_{00})\sum_{k=V(l)}^{N}\beta(k,N,m,P_{11},P_{10}). \tag{4.160}$$

For simplicity in evaluating the probability of a false alarm, we ignore the sampling time preceding the peak value of $D(t)$ in Fig. 4.19 because this probability is negligible at that time. Since the acquisition tones are absent, the probability of a false alarm is

$$P_F=\sum_{m=0}^{\min(N,J)}\frac{\binom{N}{m}\binom{M-N}{J-m}}{\binom{M}{J}}\sum_{l=0}^{N}\beta(l,N,m,P_{01},P_{00})\sum_{k=V(l)}^{N}\beta(k,N,m,P_{01},P_{00}). \tag{4.161}$$

If there is no interference so that $J=0$, then (4.160) and (4.161) reduce to

$$P_D=\sum_{l=0}^{N}\binom{N}{l}P_{00}^{l}(1-P_{00})^{N-l}\sum_{k=V(l)}^{N}\binom{N}{k}P_{10}^{k}(1-P_{10})^{N-k} \tag{4.162}$$

$$P_F = \sum_{l=0}^{N} \binom{N}{l} P_{00}^{l}(1-P_{00})^{N-1} \sum_{k=V(l)}^{N} \binom{N}{k} P_{00}^{k}(1-P_{00})^{N-k}. \tag{4.163}$$

The normalized channel threshold $\eta/\sqrt{N_t}$ is selected to maintain a required P_F when there is no interference and the value of l_0 is specified. The value of l_0 is then selected to maximize P_D given the value of S/N_t. The best choice is generally $l_0 = \lfloor N/2 \rfloor$. For example, suppose that $N = 8$, $P_F = 10^{-7}$, and the SNR is $S/N_t = 10\,\text{dB}$ when an acquisition tone is received. A numerical evaluation of (4.163) then yields $\eta/\sqrt{N_t} = 3.1856$ and $l_0 = 4$ as the parameter values that maintain $P_F = 10^{-7}$ while maximizing P_D in the absence of interference. The nearly identical threshold pair $\eta/\sqrt{N_t} = 3.1896$, $l_0 = 4$ is the choice when a fixed comparator threshold $V(t) = l_0$ is used instead of the adaptive threshold of (4.136). If $D(t)$ and $L(t)$ are sampled once every hop dwell interval, then the false-alarm rate is P_F/T_h.

As an example, suppose that noise jamming with total power N_{it} is uniformly distributed over J of the N matched-filter frequency channels so that

$$N_i = \frac{N_{it}}{J} \tag{4.164}$$

is the power in each of these channels. Interference tones are absent and $N = 8$, $M = 128$, and $S/N_t = 10\,\text{dB}$. To ensure that $P_F = 10^{-7}$ in the absence of jamming, we set $l_0 = 4$ and $\eta/\sqrt{N_t} = 3.1856$ when an adaptive comparator threshold is used, and set $l_0 = 4$ and $\eta/\sqrt{N_t} = 3.1896$ when a fixed comparator threshold is used. Since P_D is relatively insensitive to J, its effect is assessed by examining P_F. Figure 4.20 depicts P_F as a function of N_{it}/S, the jamming-to-signal ratio. The figure indicates that an adaptive threshold is much more resistant to partial-band jamming than a fixed threshold when N_{it}/S is large. When $N_{it}/S < 10\,\text{dB}$, the worst-case partial-band jamming causes a considerably higher P_F than full-band jamming. It is found that multitone jamming tends to produce fewer false alarms than noise jamming. Various other performance and design issues and the impact of frequency-hopping interference are addressed in [12].

4.5.2 *Serial-Search Acquisition*

As illustrated by Fig. 4.21, a *serial-search acquisition system* for frequency-hopping signals determines acquisition by downconverting the received frequency-hopping pattern to a fixed IF, and then comparing the output of an energy detector (Chap. 7) to a threshold. The energy detector comprises a bandpass filter, a squarer, and an integrator and sampler, where the latter may be implemented by an adder of sample values. A trial alignment of the frequency-hopping pattern synthesized by the receiver with the received pattern is called a *cell*. If a cell passes certain tests,

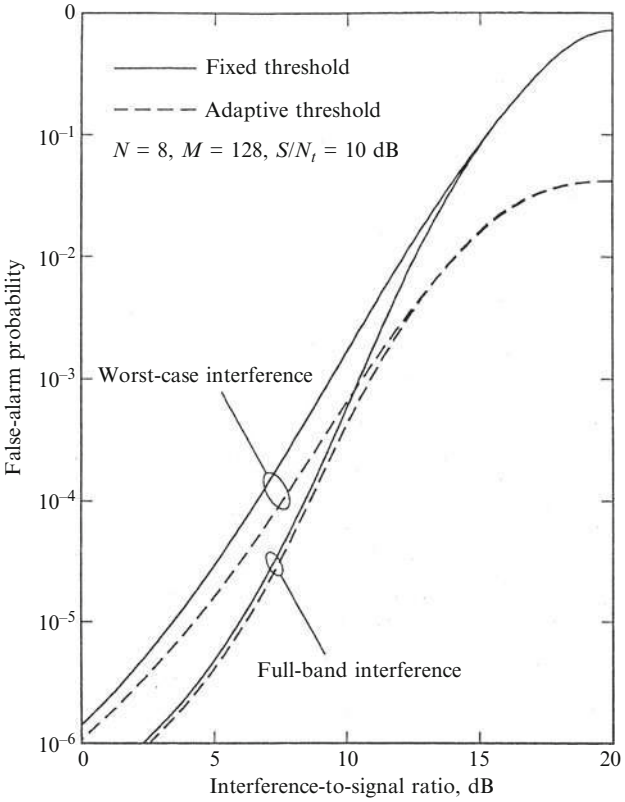

Fig. 4.20 False-alarm probability for matched-filter acquisition system

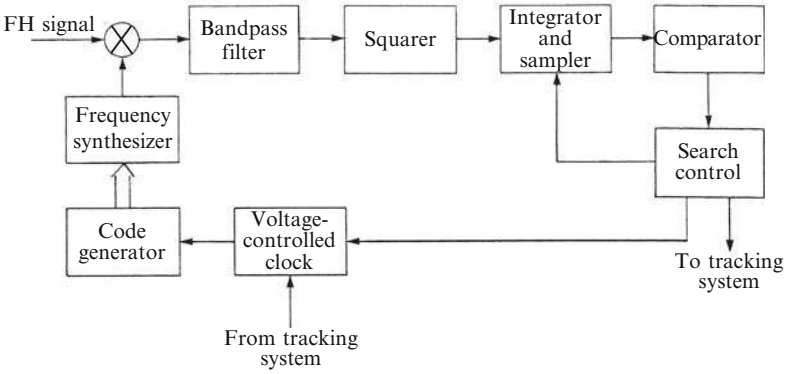

Fig. 4.21 Serial-search acquisition system

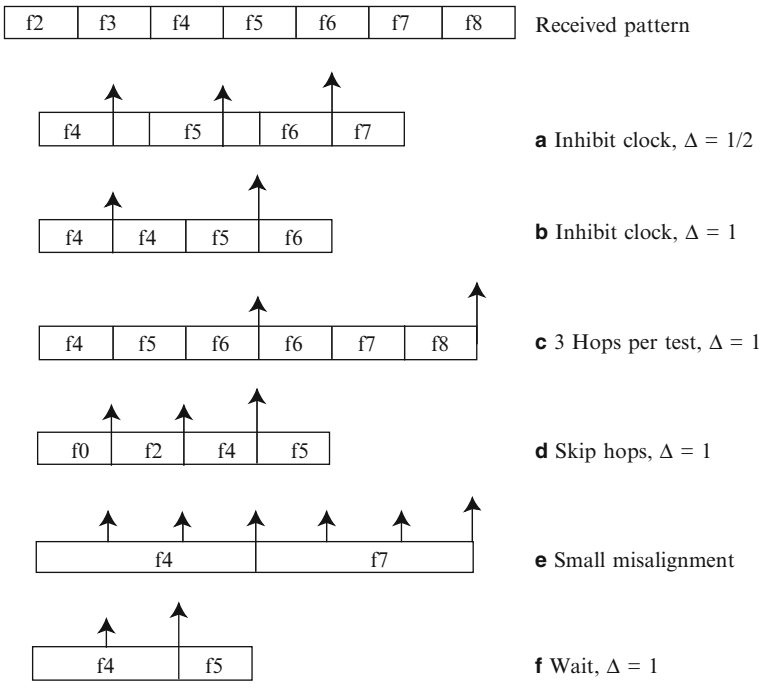

Fig. 4.22 Search techniques for acquisition

acquisition is declared and the tracking system is activated. If not, the cell is rejected. A new candidate cell is produced when the reference pattern synthesized by the receiver is either advanced or delayed relative to the received pattern.

A number of search techniques are illustrated in Fig. 4.22, which depicts successive frequencies in the received pattern and six possible receiver-generated patterns. Each search technique is implemented as part of a uniform or Z-search of the timing uncertainty. The small arrows indicate test times at which cells are usually rejected, and the large arrows indicate typical times at which acquisition is declared or subsequent verification testing begins. The step size, which is the separation in hop durations between cells, is denoted by Δ. Techniques (a) and (b) entail inhibiting the code-generator clock after each unsuccessful test. Technique (c) is the same as technique (b) but extends the test duration to three hops. Technique (d) advances the reference pattern by skipping frequencies in the pattern after each unsuccessful test. The inhibiting or advancing of techniques (a) to (d) or an alternation of them continues until acquisition is declared. The *small misalignment technique* (e) is effective when there is a high probability that the reference and received patterns are within r hops of each other, which usually is true immediately after the tracking system loses lock. The code generator temporarily forces the reference signal to remain at a frequency for $2r + 1$ hop intervals extending both before and after the interval in which the frequency would ordinarily be synthesized.

If the misalignment is less than r hops, then acquisition occurs within $2r + 1$ hop durations. In the figure, $r = 1$, the initial misalignment is one-half hop duration, and it is assumed that the first time the reference and received frequencies coincide, detection fails, but the second time results in acquisition. Technique (f) entails waiting at a fixed synchronization frequency until this frequency is received. The *wait technique* results in a rapid search if the reference frequency can be selected so that it is soon reached by the received pattern. The reference frequency is determined from an estimate of the timing uncertainty, the key bits, and the time-of-day (TOD) bits (Sect. 3.1), but must be periodically shifted by at least the coherence bandwidth so that neither fading nor interference in any particular frequency channel prevents acquisition.

When the period of the frequency-hopping pattern is large, special measures may be required to reduce the timing uncertainty. A reduced hopset with a short pattern period may be used temporarily to reduce the timing uncertainty and, hence, the acquisition time. A feedback signal from the receiver may be used to adjust the timing of the transmitted pattern. In a network, a separate communication channel or cueing frequency may provide the TOD to subscribers. After reception of the TOD, a receiver might use the small misalignment technique for acquisition.

Several frequencies might be dedicated synchronization frequencies. Prior to acquisition, the receiver waits at one of the synchronization frequencies and changes which one periodically. When a synchronization frequency is detected by the receiver, the data bits indicate the TOD of the network or transmitter and other information that facilitates acquisition of the timing or the maintenance of it. Once the appropriate TOD is known, the small misalignment technique completes the acquisition.

The *search control system* determines the integration intervals, the thresholds, and the logic of the tests to be conducted before acquisition is declared and the tracking system is activated. The details of the search control strategy determine the statistics of the acquisition time. The control system is usually a *multiple-dwell system* that uses an initial test to quickly eliminate improbable cells. Subsequent tests are used for verification testing of cells that pass the initial test. The multiple-dwell strategy may be a *consecutive-count strategy*, in which a failed test causes a cell to be immediately rejected, or an *up-down strategy*, in which a failed test causes a repetition of a previous test. The up-down strategy is preferable when the interference or noise level is high [14].

Since acquisition for frequency-hopping signals is analogous to acquisition for direct-sequence signals, the statistical description of acquisition given in Sect. 4.2 is applicable if the chips are interpreted as hops. Only the specific equations of the detection and false-alarm probabilities are sometimes different. For example, consider a single-dwell system with a uniform search, a uniform *a priori* correct-cell location distribution, two independent correct cells with the common detection probability P_d, and $q \gg 1$. By analogy with (4.105), the NMAT is

$$NMAT = \frac{\bar{T}_a}{C_h T_h} = \left(\frac{2 - P_D}{2P_D} \right) \frac{q_h}{C_h} \left(M_h + K_h P_F \right) \tag{4.165}$$

where M_h is the number of hops per test, K_h is the number of hop durations in the mean penalty time, C_h is the number of hop durations in the timing uncertainty, q_h is the number of cells, and

$$P_D = 2P_d - P_d^2. \tag{4.166}$$

For step size $\Delta = 1$, $q_h/C_h = 1$; for $\Delta = 1/2$, $q_h/C_h = 2$.

If the detector integration is over several hop intervals, strong interference or deep fading over a single hop interval can cause a false alarm with high probability. This problem is mitigated by making a hard decision after integrating over each hop interval. After N decisions, a test for acquisition is passed or failed if the comparator threshold has been exceeded l_0 or more times out of N. Let P_{dp} and P_{da} denote the probabilities that the comparator threshold is exceeded at the end of a hop interval when the correct cell is tested and interference is present and absent, respectively. Let P_d denote the probability that an acquisition test is passed when the correct cell is tested. If there are two independent correct cells, then P_D is given by (4.166); if there is a single correct cell, then $P_D = P_d$. If the N acquisition tones in a test are distinct, then a derivation similar to the one for matched filters yields

$$P_d = \sum_{m=0}^{\min(N,J)} \frac{\binom{N}{m}\binom{M-N}{J-m}}{\binom{M}{J}} \sum_{l=l_0}^{N} \beta(l, N, m, P_{dp}, P_{da}) \tag{4.167}$$

where $l_0 \geq 0$. Similarly, the probability that an acquisition test is passed when an incorrect cell is tested and no acquisition tones are present is

$$P_F = \sum_{m=0}^{\min(N,J)} \frac{\binom{N}{m}\binom{M-N}{J-m}}{\binom{M}{J}} \sum_{l=l_0}^{N} \beta(l, N, m, P_{fp}, P_{fa}) \tag{4.168}$$

where P_{fp} and P_{fa} are the probabilities that the threshold is exceeded when an incorrect cell is tested and interference is present and absent, respectively. A suitable choice for l_0 is $\lfloor N/2 \rfloor$. Since the serial-search system of Fig. 4.21 has an embedded radiometer, the performance analysis of the radiometer given in Chap. 7 can be used to obtain expressions for P_{dp}, P_{da}, P_{fp}, and P_{fa}.

Although a large step size limits the number of incorrect cells that must be tested before the correct cell is tested, it causes a loss in the average signal energy in the integrator output of Fig. 4.21 when a correct cell is tested. This issue and the role of the hop dwell time are illustrated by Fig. 4.23, which depicts the idealized output for a single pulse of the received and reference signals in the absence of noise. Let τ_e denote the delay of the reference pattern relative to the received pattern. Suppose that one tested cell has $\tau_e = -x$, where $0 \leq x \leq \Delta T_h$, and the next tested cell has $\tau_e = \Delta T_h - x$ following a cell rejection. The largest amplitude of the integrator output occurs when $|\tau_e| = y$, where

$$y = \min(x, \Delta T_h - x), \quad 0 \leq x < \Delta T_h. \tag{4.169}$$

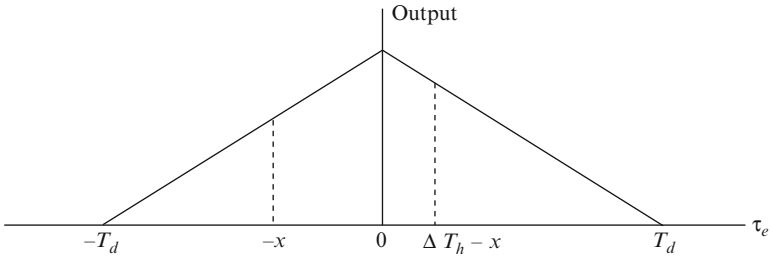

Fig. 4.23 Amplitude of integrator output as function of relative pattern delay

Assuming that x is uniformly distributed over $(0, \Delta T_h)$, y is uniformly distributed over $(0, \Delta T_h/2)$. Therefore,

$$E[y] = \frac{\Delta T_h}{4} \tag{4.170}$$

$$E[y^2] = \frac{\Delta^2 T_h^2}{12}. \tag{4.171}$$

The *correct cell* is considered to be the one for which $|\tau_e| = y$. If the output function approximates the triangular shape depicted in the figure, its amplitude when $|\tau_e| = y$ is

$$A = A_{\max}\left(1 - \frac{y}{T_d}\right). \tag{4.172}$$

Therefore, the average signal energy in the integrator output is attenuated by the factor

$$E\left[\left(1 - \frac{y}{T_d}\right)^2\right] = 1 - \frac{\Delta T_h}{2T_d} + \frac{\Delta^2 T_h^2}{12T_d^2} \tag{4.173}$$

which indicates the loss due to the misalignment of patterns when the correct cell is tested. For example, if $T_d = 0.9T_h$, then (4.173) indicates that the average loss is 1.26 dB when $\Delta = 1/2$; if $\Delta = 1$, then the loss is 2.62 dB. These losses should be taken into account when calculating P_{dp} and P_{da}.

The serial-search acquisition of frequency-hopping signals is faster than the acquisition of direct-sequence signals because the hop duration is much greater than a spreading-sequence chip duration for practical systems. Given the same timing uncertainty, fewer cells have to be searched to acquire frequency-hopping signals because each step covers a larger portion of the region.

4.5.3 Tracking System

The acquisition system ensures that the receiver-synthesized frequency-hopping pattern is aligned in time with the received pattern to within a fraction of a hop

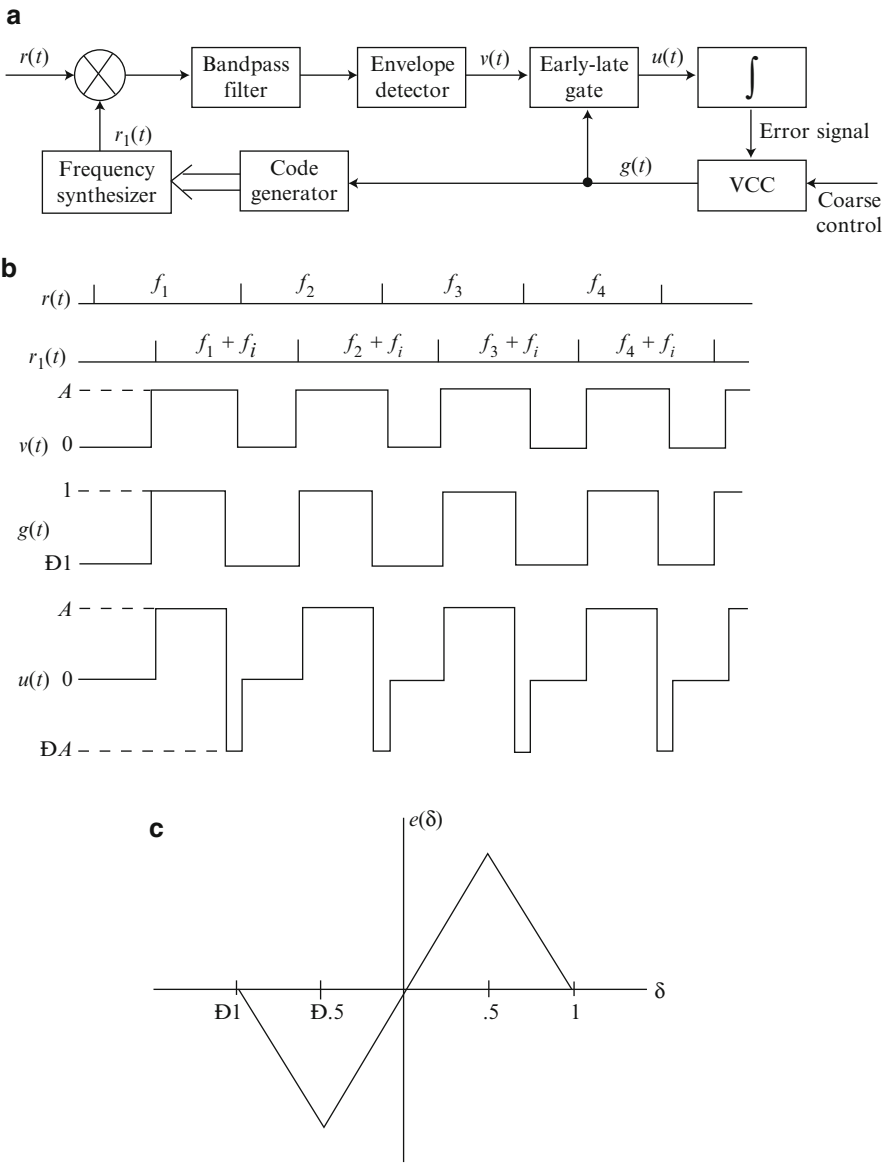

Fig. 4.24 Early-late gate: (**a**) loop, (**b**) signals, and (**c**) discriminator characteristic

duration. The tracking system must provide a fine synchronization by reducing the residual misalignment after acquisition. Although the delay-locked and tau-dither loops used for the tracking of direct-sequence signals can be adapted to frequency-hopping signals, the predominant form of tracking in frequency-hopping systems is provided by the *early-late gate* [15]. This loop is shown in Fig. 4.24 along with

the ideal associated waveforms for a typical example in which there is a single carrier frequency during a hop dwell interval. If the data modulation is FSK, then the outputs of parallel branches, each with a bandpass filter and envelope detector can be combined and applied to the early-late gate. In the absence of noise, the envelope detector produces a positive output only when the received frequency-hopping signal $r(t)$, and the receiver-generated frequency-hopping replica $r_1(t)$ are offset by the IF f_i. The *gating signal* $g(t)$ is a square-wave clock signal with transitions from -1 to $+1$ that control the frequency transitions of $r_1(t)$. The early-late gate functions as a signal multiplier. Its output $u(t)$ is the product of the gating signal and the envelope-detector output $v(t)$. The error signal is the time integral of $u(t)$ and is a function of τ_e, the delay of $r_1(t)$ relative to $r(t)$. The error signal can be expressed as the discriminator characteristic $e(\delta)$, which is a function of $\delta = \tau_e / T_h$, the normalized delay error. For the typical waveforms shown, δ is positive, and hence so is $e(\delta)$. Therefore, the voltage-controlled clock (VCC) will increase the transition rate of the gating signal, which will bring $r_1(t)$ into better time-alignment with $r(t)$. If the tracking system loses lock and the small-misalignment test fails, then the wait technique of Fig. 4.22 can be used to expedite the reacquisition.

After dehopping the received signal to baseband, demodulating, and producing oversampled information bits, the receiver establishes bit synchronization by searching for a special sequence of marker bits that match a stored reference sequence, as is often done for frame synchronization [16]. After this matching occurs, information is extracted from subsequent bits. The information could specify the time of occurrence and the spectral location of the next synchronization frequency at which the receiver waits.

Problems

4.1. Prove that for a random variable Y and a random variable X with density $f(x)$, the relation $\int var(Y/x) f(x) dx = var(Y)$ is not true in general. If it were, then σ_a^2 given by (4.23) and (4.24) could be simplified. Give a sufficient condition under which this relation is valid.

4.2. Consider a uniform search with a uniform a priori distribution for the location of the correct cell. (a) What is the average number of sweeps through the timing uncertainty during acquisition? (b) For a large number of cells, calculate an upper bound on $P(T_a > c\overline{T_a})$ as a function of P_D for $c > 1$. (c) For a large number of cells to be searched, show that the standard deviation of the acquisition time satisfies $\frac{\overline{T_a}}{\sqrt{3}} \leq \sigma_a \leq \overline{T_a}$.

4.3. (a) Derive (4.43) by first expressing $\overline{T}_{12}$ as a conditional expectation and then enumerating the possible values of $\overline{T}_{12}$ and their conditional probabilities. (b) Use a similar procedure to derive (4.51) to (4.55).

4.4. Derive P_D in (4.46) assuming the presence of zero-mean, white Gaussian noise with two-sided power spectral density N_0. Use (4.38) and assume that $P_a = P_b$. To determine P_a, begin by writing an expression for the matched-filter output when a target signal with energy $\mathcal{E}$ completely fills the filter.

4.5. Consider a lock detector that uses a double-dwell consecutive-count system with equal test durations. (a) Use a recursive relation to show that $\overline{T_h} = \tau[(1 - P_D)^{-1} + (1 - P_D)^{-2}]$. (b) Use a recursive relation to show that $\overline{T_p} = \tau[(1 - P_F)^{-1} + (1 - P_F)^{-2}]$.

4.6. Prove that if C has a uniform distribution and the rewinding time is negligible, then $\bar{T}_a$ is the same for both the uniform search and the broken-center Z search.

4.7. Starting with (4.92), derive σ_0^2 and σ_1^2 for the acquisition correlator.

4.8. Consider Example 2 of Sect. 4.3 leading to Fig. 4.14. Assume fast fading and that $\Delta = 1/2$, $E_c/N_0 = -10\,\text{dB}$, $K = 10{,}000$, $P_{F1} = 0.03$, $P_{F2} = 0.001$, and $M_2 = 10M_1$. Plot the NMAT versus M_1 for the consecutive-count and up-down systems to determine graphically what values of M_1 minimize the NMAT.

4.9. Derive (4.126) and (4.127).

4.10. Compare the NMAT for a frequency-hopping system given by (4.165) with the NMAT for a direct-sequence system given by (4.105) when the penalty times and test durations for both systems are equal. Under the latter condition, it is reasonable to assume that P_D and P_F are roughly equal for both systems. With these assumptions, what is the ratio of the direct-sequence NMAT to the frequency-hopping NMAT?

4.11. Reduce (4.167) to a single summation and simplify for the following cases. a) $l_0 = N$, and b) $J = 0, l_0 \geq 0$.

4.12. Derive P_D and P_F for serial-search acquisition of frequency-hopping signals when a single acquisition tone is used.

References

1. J. G. Proakis and M. Salehi, *Digital Communications, 5th ed.* New York: McGraw-Hill, 2008.
2. R. L. Peterson, R. E. Ziemer, and D. E. Borth, *Introduction to Spread Spectrum Communications*. Upper Saddle River, NJ: Prentice Hall, 1995.
3. H. Meyr and G. Polzer, "Performance Analysis for General PN Spread-spectrum Acquisition Techniques," *IEEE Trans. Commun.*, vol. 31, pp. 1317–1319, Dec. 1983.
4. V. M. Jovanovic, "Analysis of Strategies for Serial-Search Spread-Spectrum Code Acquisition—Direct Approach," *IEEE Trans. Commun.*, vol. 36, pp. 1208–1220, Nov. 1988.
5. S.-M. Pan, D. E. Dodds, and S. Kumar, "Acquisition Time Distribution for Spread-Spectrum Receivers, *IEEE J. Select. Areas Commun.*, vol. 8, pp. 800-808, June 1990.
6. A. Polydoros and C. L. Weber, "A Unified Approach to Serial-Search Spread Spectrum Code Acquisition," *IEEE Trans. Commun.*, vol. 32, pp. 542–560, May 1984.

7. W. Suwansantisuk and M. Z. Win, "Multipath Aided Rapid Acquisition: Optimal Search Strategies," I*EEE Trans. Inform. Theory*, vol. 53, pp. 174-193, Jan. 2007.
8. S. Gezici, "Mean Acquisition Time Analysis of Fixed-Step Serial Search Algorithms," *IEEE Trans. Commun.*, vol. 8, pp. 1096–1101, March 2009.
9. K. Choi, K. Cheun, and T. Jung, "Adaptive PN Code Acquisition Using Instantaneous Power-Scaled Detection Threshold under Rayleigh Fading and Pulsed Gaussian Noise Jamming," *IEEE Trans. Commun.*, pp. 1232–1235, Aug. 2001.
10. A. Polydoros and C. L. Weber, "Analysis and Optimization of Correlative Code-Tracking Loops in Spread-Spectrum Systems," *IEEE Trans. Commun.*, vol. 33, pp. 30–43, Jan. 1985.
11. W. R. Braun, "PN Acquisition and Tracking Performance in DS/CDMA Systems with Symbol-Length Spreading Sequence," *IEEE Trans. Commun.*, vol. 45, pp. 1595–1601, Dec. 1997.
12. J.-C. Lin, "A Modified PN Code Tracking Loop for Direct-Sequence Spread-Spectrum Communication Over Arbitrarily Correlated Multipath Fading Channels," *IEEE Trans. Selected Areas Commun.*, vol. 19, pp. 2381–2395, Dec. 2001.
13. L. E. Miller, J. S. Lee, R. H. French, and D. J. Torrieri, "Analysis of an Anti-jam FH Acquisition Scheme," *IEEE Trans. Commun.*, vol. 40, pp. 160-170, Jan. 1992.
14. C. A. Putman, S. S. Rappaport, and D. L. Schilling, "Comparison of Strategies for Serial Acquisition of Frequency-Hopped Spread-Spectrum Signals," *IEE Proc.*, vol. 133, pt. F, pp. 129–137, April 1986.
15. C. A. Putman, S. S. Rappaport, and D. L. Schilling, "Tracking of Frequency-Hopped Spread-Spectrum Signals in Adverse Environments," *IEEE Trans. Commun.*, vol. 31, pp. 955–963, Aug. 1983.
16. D. Torrieri, *Principles of Secure Communication Systems*, 2nd ed. Boston: Artech House, 1992.

Chapter 5
Fading and Diversity

Fading is the variation in received signal strength due to a time-varying communications channel. It is primarily caused by the interaction of multipath components of the transmitted signal that are generated and altered by changing physical characteristics of the propagation medium. The principal means of counteracting fading are *diversity methods*, which are based on the exploitation of the latent redundancy in two or more independently fading copies of the same signal. This chapter provides a general description of the most important aspects of fading and diversity methods. The rake demodulator, which is of central importance in most direct-sequence systems, is shown to be capable of exploiting undesired multipath signals rather than simply attempting to reject them. The multicarrier direct-sequence system, which is described in the final section, is an alternative method of exploiting multipath signals that has practical advantages.

5.1 Path Loss, Shadowing, and Fading

Free-space propagation losses of electromagnetic waves vary inversely with the square of the distance between a transmitter and a receiver. Analysis indicates that if a signal traverses a direct path and combines in the receiver with a multipath component that is perfectly reflected from a plane, then the composite received signal has a power loss proportional to the inverse of the fourth power of the distance. Thus, it is natural to seek a power-law variation for the average received power in a specified geographic area as a function of distance. For terrestrial wireless communications, measurements averaged over many different positions of a transmitter and a receiver in a specified geographic area confirm that the average received power, measured in decibels and called the *area-mean power*, does tend to vary linearly with the logarithm of the transmitter-receiver distance r. If the receiver lies in the far field of the transmitted signal, then it is found that the area-mean power, when expressed in decimal units, is approximately given by

D. Torrieri, *Principles of Spread-Spectrum Communication Systems*,
DOI 10.1007/978-1-4419-9595-7_5,

$$p_a = p_0 \left(\frac{r}{\delta}\right)^{-\beta}, \quad r \geq \delta \tag{5.1}$$

where p_0 is the average received power when the distance is $r = \delta$, β is the *attenuation power law*, and δ is a reference distance that exceeds the minimum distance at which the receiver lies in the far field. The parameters p_0 and β are functions of the carrier frequency, antenna heights, terrain characteristics, vegetation, and various characteristics of the propagation medium. Typically, the parameters vary with distance, but are constant within a range of distances. The attenuation power law increases with the carrier frequency. Typical values of the attenuation power law for urban areas and microwave frequencies are in the range $3 \leq \beta \leq 4$.

For a specific propagation path, the received *local-mean power* departs from the area-mean power due to *shadowing*, which is the effect of diffractions and propagation conditions that are path-dependent. Each diffraction due to obstructing terrain and each reflection from an obstacle causes the signal power to be multiplied by an attenuation factor. Thus, the received signal power is often the product of many factors, and hence the logarithm of the signal power is the sum of many factors. If each factor is modeled as a uniformly bounded, independent random variable that varies from path to path, then the central-limit theorem implies that the logarithm of the received signal power has an approximately normal distribution if the number of attenuation factors is large enough. Extensive empirical data confirms that the received local-mean power after transmission over a randomly selected propagation path with a fixed distance is approximately lognormally distributed. Thus, the shadowing model specifies that the local-mean power has the form

$$p_l = p_0 \left(\frac{r}{\delta}\right)^{-\beta} 10^{\xi/10}, \quad r \geq \delta \tag{5.2}$$

where the *shadowing factor* ξ is a zero-mean random variable with a normal distribution, and p_0 is the average received power when $\xi = 0$ and $r = \delta$. The shadowing factor is expressed in decibels and has a standard deviation denoted by σ_s. From (5.1) and (5.2), it follows that the probability distribution function of the normalized local-mean power, p_l/p_0, is

$$F(x) = 1 - Q\left\{\frac{10 \log_{10} e}{\sigma_s} \ln\left[x \left(\frac{r}{\delta}\right)^{\beta}\right]\right\} \tag{5.3}$$

where ln[ ] denotes the natural logarithm. The standard deviation σ_s increases with carrier frequency and terrain irregularity and sometimes exceeds 10 dB for terrestrial communications. The value of the shadowing factor for a propagation path is usually strongly correlated with its value for a nearby propagation path. For mobile communications, the typical time interval during which the shadowing factor is nearly constant corresponds to a movement of five to ten meters.

Fading, which is endemic in mobile, long-distance, high-frequency, and other communication channels, causes power fluctuations about the local-mean power.

Fading occurs at much faster rate than shadowing. During an observation interval in which the shadowing factor is nearly constant, the received signal power may be expressed as the product

$$p_r = p_0 \left(\frac{r}{\delta}\right)^{-\beta} 10^{\xi/10}\alpha^2(t), \quad r \geq \delta \tag{5.4}$$

where the factor $\alpha^2(t)$ is due to the fading and is normalized so that $E[\alpha^2(t)] = 1$. Since ξ is fixed, the local-mean power is

$$p_l = E[p_r] = p_0 \left(\frac{r}{\delta}\right)^{-\beta} 10^{\xi/10}, \quad r \geq \delta. \tag{5.5}$$

A signal experiences *fading* when the interaction of multipath components and time- or frequency-varying channel conditions cause significant fluctuations in its amplitude at a receiver. *Multipath components* of a signal are generated by inhomogeneities in the propagation medium or reflections from obstacles. These components travel along different paths before being recombined at the receiver. Because of the different time-varying delays and attenuations encountered by the multipath components, the recombined signal is a distorted version of the original transmitted signal. Fading may be classified as time-selective, frequency-selective, or both. *Time-selective fading* is fading caused by the movement of the transmitter or receiver or by changes in the propagation medium. *Frequency-selective fading* is fading caused by the different delays of the multipath components, which may affect certain frequencies more than others. The following concise development of fading theory [1–3] emphasizes basic physical mechanisms.

A bandpass transmitted signal can be expressed as

$$s_t(t) = \text{Re}[s(t)\exp(j2\pi f_c t)] \tag{5.6}$$

where $s(t)$ denotes its complex envelope, f_c denotes its carrier frequency, and Re[ ] denotes the real part. Transmission over a time-varying multipath channel of $N(t)$ paths produces a received bandpass signal that consists of the sum of $N(t)$ waveforms. The ith waveform is the transmitted signal delayed by time $\tau_i(t)$, attenuated by a factor $a_i(t)$ that depends on the path loss and shadowing, and shifted in frequency by the amount $f_{di}(t)$ due to the Doppler effect. Assuming that $f_{di}(t)$ is constant during the path delay $t - \tau_i(t)$, the received signal may be expressed as

$$s_r(t) = \text{Re}[s_1(t)\exp(j2\pi f_c t)] \tag{5.7}$$

where the received complex envelope is

$$s_1(t) = \sum_{i=1}^{N(t)} a_i(t)\exp[j\phi_i(t)]s[t - \tau_i(t)] \tag{5.8}$$

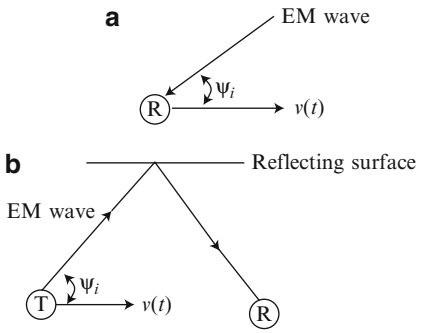

Fig. 5.1 Examples of the Doppler effect: (**a**) receiver motion and (**b**) transmitter motion and reflecting surface

and its phase is

$$\phi_i(t) = -2\pi f_c \tau_i(t) + 2\pi f_{di}(t)\left[t - \tau_i(t)\right]. \tag{5.9}$$

The Doppler shift arises because of the relative motion between the transmitter and the receiver. In Fig. 5.1a, the receiver is moving at speed $v(t)$ and the angle between the velocity vector and the propagation direction of an electromagnetic wave is $\psi_i(t)$. For this geometry, the received frequency is increased by the Doppler shift

$$f_{di}(t) = f_c \frac{v(t)}{c} \cos\psi_i(t) \tag{5.10}$$

where c is the speed of an electromagnetic wave. In Fig. 5.1b, the transmitter is moving at speed $v(t)$ and there is a reflecting surface that changes the arrival angle of the electromagnetic wave at the receiver. If $\psi_i(t)$ represents the angle between the velocity vector and the initial direction of the electromagnetic wave, then (5.10) again gives the Doppler shift.

5.2 Time-Selective Fading

To analyze time-selective fading, it is assumed that $N(t) = N$ for the time interval of interest and that the differences in the time delays along the various paths are small compared with the inverse of the signal bandwidth. Therefore, the received multipath components overlap in time and are called *unresolvable multipath components*. If the time origin is chosen to coincide with the average arrival time of the multipath components at a receiver, then the received complex envelope of (5.8) may be expressed as

$$s_1(t) \approx s(t) r(t) \tag{5.11}$$

where the *equivalent lowpass* or *equivalent baseband channel response* is

$$r(t) = \sum_{i=1}^{N} a_i(t) \exp[j\phi_i(t)] \tag{5.12}$$

The fluctuations in this factor cause signal fading at the receiver and increase the bandwidth of the received signal. If the transmitted signal is an unmodulated tone, then $s(t) = 1$ and (5.12) represents the complex envelope of the received signal.

The channel response can be decomposed as

$$r(t) = r_c(t) + jr_s(t) \tag{5.13}$$

where $j = \sqrt{-1}$ and

$$r_c(t) = \sum_{i=1}^{N} a_i(t) \cos[\phi_i(t)], \qquad r_s(t) = \sum_{i=1}^{N} a_i(t) \sin[\phi_i(t)]. \tag{5.14}$$

If the range of the delay values exceeds $1/f_c$, then the sensitivity of $\phi_i(t)$ to small variations in the delay $\tau_i(t)$ makes it plausible to model the phases $\phi_i(t), i = 1, 2, \ldots, N$, as random variables that are independent of each other and the amplitudes $\{a_i(t)\}$ and are uniformly distributed over $[0, 2\pi)$ at a specific time t. Therefore,

$$E[r_c(t)] = E[r_s(t)] = 0. \tag{5.15}$$

If the amplitude factors $a_i(t), i = 1, 2, \ldots, N$, are either identically distributed or uniformly bounded independent random variables at time t, then according to the central-limit theorem, the probability distributions of both $r_c(t)$ and $r_s(t)$ approach Gaussian distributions as N increases. Thus, if N is sufficiently large, then $r(t)$ at a specific time is well modeled as a *complex Gaussian random variable*. Since the phases are independent and uniformly distributed, it follows that

$$E[r_c(t)r_s(t)] = 0 \tag{5.16}$$

$$E[r_c^2(t)] = E[r_s^2(t)] = \sigma_r^2(t) \tag{5.17}$$

where we define

$$\sigma_r^2(t) = \frac{1}{2} \sum_{i=1}^{N} E[a_i^2(t)]. \tag{5.18}$$

This equation indicates that $\sigma_r^2(t)$ is equal to the sum of the local-mean powers of the multipath components. Equations (5.15) to (5.17) imply that $r_c(t)$ and $r_s(t)$ are independent, identically distributed, zero-mean Gaussian random variables.

Let $\alpha(t) = |r(t)|$ denote the envelope, and $\theta(t) = \tan^{-1}[r_s(t)/r_c(t)]$ the phase of $r(t)$ at a specific time t. Then

$$r(t) = \alpha(t)e^{j\theta(t)}. \tag{5.19}$$

From (5.13), (5.17), and (5.18), it follows that the average envelope power is

$$\Omega(t) = E[\alpha^2(t)] = 2\sigma_r^2(t) = \sum_{i=1}^{N} E[a_i^2(t)]. \tag{5.20}$$

As shown in Appendix B.4, since $r_c(t)$ and $r_s(t)$ are Gaussian and $\alpha^2(t) = r_c^2(t) + r_s^2(t)$, $\theta(t)$ has a uniform distribution over $[0, 2\pi)$, and $\alpha(t)$ has the *Rayleigh* probability density function:

$$f_\alpha(r) = \frac{2r}{\Omega} \exp\left(-\frac{r^2}{\Omega}\right) u(r) \tag{5.21}$$

where the time-dependence has been suppressed for convenience, and $u(r) = 1$, $r \geq 0$, and $u(r) = 0$, $r < 0$. The substitution of (5.19) and (5.11) into (5.7) gives

$$\begin{aligned} s_r(t) &= \mathrm{Re}[\alpha(t)s(t)\exp(j2\pi f_c t + j\theta(t))] \\ &= \alpha(t)\,A(t)\cos[2\pi f_c t + \phi(t) + \theta(t)] \end{aligned} \tag{5.22}$$

where $A(t)$ is the amplitude and $\phi(t)$ the phase of $s(t)$, and $s_r(t)$ experiences *Rayleigh fading*. Equations (5.20) and (5.22) indicate that the instantaneous local-mean power is $p_l = E[s_r^2(t)] = \Omega(t)\,A^2(t)/2$.

When a line-of-sight exists between a transmitter and a receiver, one of the received multipath components may be much stronger than the others. This strong component is called the *specular component* and the other unresolvable components are called *diffuse* or *scattered components*. As a result, the multiplicative channel response of (5.12) becomes

$$r(t) = a_0(t)\exp[j\phi_0(t)] + \sum_{i=1}^{N} a_i(t)\exp[j\phi_i(t)] \tag{5.23}$$

where the summation term is due to the diffuse components, and the first term is due to the specular component. If N is sufficiently large, then at time t the summation term is well-approximated by a zero-mean, complex Gaussian random variable. Thus, $r(t)$ at a specific time is a complex Gaussian random variable with a nonzero mean equal to the deterministic first term, and (5.13) implies that

$$E[r_c(t)] = a_0(t)\cos[\phi_0(t)], \qquad E[r_s(t)] = a_0(t)\sin[\phi_0(t)]. \tag{5.24}$$

From (5.18) and (5.23), it follows that the envelope $\alpha(t) = |r(t)|$ has the average power given by

$$\Omega(t) = E[\alpha^2(t)] = a_0^2(t) + 2\sigma_r^2(t). \tag{5.25}$$

As shown in Appendix B.3, since $r_c(t)$ and $r_s(t)$ are Gaussian and $\alpha^2(t) = r_c^2(t) + r_s^2(t)$, the envelope has the *Rice* probability density function:

$$f_\alpha(r) = \frac{r}{\sigma_r^2} \exp\left\{-\frac{r^2 + a_0^2}{2\sigma_r^2}\right\} I_0\left(\frac{a_0 r}{\sigma_r^2}\right) u(r) \tag{5.26}$$

where $I_0(\,)$ is the modified Bessel function of the first kind and order zero, and the time-dependence is suppressed for convenience. The type of fading modeled by (5.23) and (5.26) is called *Ricean fading*. At a specific time, the *Rice factor* is defined as

$$\kappa = \frac{a_0^2}{2\sigma_r^2}. \tag{5.27}$$

which is the ratio of the specular power to the diffuse power. In terms of κ and $\Omega = 2\sigma_r^2(\kappa + 1)$, the Rice density is

$$f_\alpha(r) = \frac{2(\kappa+1)}{\Omega} r \exp\left\{-\kappa - \frac{(\kappa+1)r^2}{\Omega}\right\} I_0\left(\sqrt{\frac{\kappa(\kappa+1)}{\Omega}}\,2r\right) u(r). \tag{5.28}$$

When $\kappa = 0$, Ricean fading is the same as Rayleigh fading. When $\kappa = \infty$, there is no fading.

A more flexible fading model, called *Nakagami fading*, is created by introducing a new parameter m; the *Nakagami-m* probability density function for the envelope $\alpha(t)$ is

$$f_\alpha(r) = \frac{2}{\Gamma(m)}\left(\frac{m}{\Omega}\right)^m r^{2m-1} \exp\left(-\frac{m}{\Omega} r^2\right) u(r), \quad m \geq \frac{1}{2} \tag{5.29}$$

where the gamma function $\Gamma(\,)$ is defined by (B.12) in Appendix B. When $m = 1$, the Nakagami density becomes the Rayleigh density, and when $m \to \infty$, there is no fading. When $m = 1/2$, the Nakagami density becomes the one-sided Gaussian density, which models fading that is more severe than Rayleigh fading. Integrating over (5.29), changing the integration variable, and using (B.12), we obtain

$$E[\alpha^n] = \frac{\Gamma(m + \frac{n}{2})}{\Gamma(m)}\left(\frac{\Omega}{m}\right)^{n/2}. \tag{5.30}$$

A measure of the severity of the fading is $\text{var}(\alpha^2)/(E[\alpha^2])^2 = 1/m$. Equating this ratio for the Rice and Nakagami densities, it is found that the Nakagami density approximates a Rice density with Rice factor κ if

$$m = \frac{(\kappa+1)^2}{2\kappa+1}, \quad \kappa \geq 0. \tag{5.31}$$

Since the Nakagami-m model essentially incorporates the Rayleigh and Rice models as special cases and provides for many other possibilities, it is not surprising that this model often fits well with empirical data.

Consider a time interval small enough that $N(t) = N$, $f_{di}(t) = f_{di}$, $\psi_i(t) = \psi_i$, $a_i(t) = a_i$, and $\tau_i(t) = \tau_i$ are approximately constants. Then (5.9) and (5.10) imply that

$$\phi_i(t + \tau) - \phi_i(t) = 2\pi f_d \tau \cos \psi_i \tag{5.32}$$

where $f_d = f_0 v/c$ is the maximum Doppler shift and τ is a time delay. The *autocorrelation of a wide-sense-stationary complex process* $r(t)$ is defined as

$$A_r(\tau) = E[r^*(t)r(t + \tau)] \tag{5.33}$$

where the asterisk denotes the complex conjugate. The variation of the autocorrelation of the equivalent baseband channel response defined by (5.12) provides a measure of the changing channel characteristics. To interpret the meaning of (5.33), we substitute (5.13) and decompose the autocorrelation as

$$\text{Re}\{A_r(\tau)\} = E[r_c(t)r_c(t + \tau)] + E[r_s(t)r_s(t + \tau)] \tag{5.34}$$

$$\text{Im}\{A_r(\tau)\} = E[r_c(t)r_s(t + \tau)] - E[r_s(t)r_c(t + \tau)]. \tag{5.35}$$

Thus, the real part of this autocorrelation is the sum of the autocorrelations of the real and imaginary parts of $r(t)$; the imaginary part is the difference between two cross-correlations of the real and imaginary parts of $r(t)$. Substituting (5.12) into (5.33), using the independence and uniform distribution of each ϕ_i and the independence of $a_i(t) = a_i$ and ϕ_i, and then substituting (5.32), we obtain

$$A_r(\tau) = \sum_{i=1}^{N} E[a_i^2] \exp(j 2\pi f_d \tau \cos \psi_i). \tag{5.36}$$

If all the received multipath components have approximately the same power and the receive antenna is omnidirectional, then (5.20) implies that $E[a_i^2] \approx \Omega/N$, $i = 1, 2, \ldots, N$, and (5.36) becomes

$$A_r(\tau) = \frac{\Omega}{N} \sum_{i=1}^{N} \exp(j 2\pi f_d \tau \cos \psi_i). \tag{5.37}$$

A communication system such as a mobile system that receives a signal from an elevated base station may be surrounded by many scattering objects. An *isotropic scattering* model assumes that multipath components of comparable power are reflected from many different scattering objects and hence arrive from many different directions. For two-dimensional isotropic scattering, N is large, and

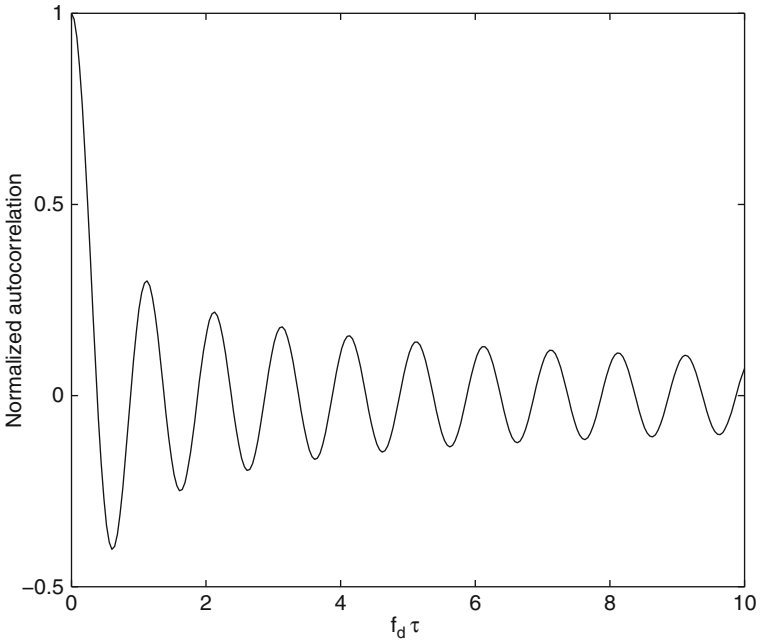

Fig. 5.2 Autocorrelation of r(t) for isotropic scattering

the $\{\psi_i\}$ lie in a plane and have values that are uniformly distributed over $[0, 2\pi)$. Therefore, the summation in (5.37) can be approximated by an integral; that is,

$$A_r(\tau) \approx \frac{\Omega}{2\pi} \int_0^{2\pi} \exp(j\,2\pi f_d\,\tau \cos\psi) d\psi. \tag{5.38}$$

This integral has the same form as the integral representation of $J_0(\ )$, the Bessel function of the first kind and order zero. Thus, the *autocorrelation of the channel response for two-dimensional isotropic scattering* is

$$A_r(\tau) = \Omega J_0(2\pi f_d\,\tau). \tag{5.39}$$

The normalized autocorrelation $A_r(\tau)/A_r(0)$, which is a real-valued function of $f_d\,\tau$, is plotted in Fig. 5.2. It is observed that its magnitude is less than 0.3 when $f_d\,\tau > 1$. This observation leads to the definition of the *coherence time* or *correlation time* of the channel as

$$T_{coh} = \frac{1}{f_d} \tag{5.40}$$

where f_d is the maximum Doppler shift or *Doppler spread*. The coherence time is a measure of the time separation between signal samples sufficient for the samples to be largely decorrelated. If the coherence time is much longer than the duration of

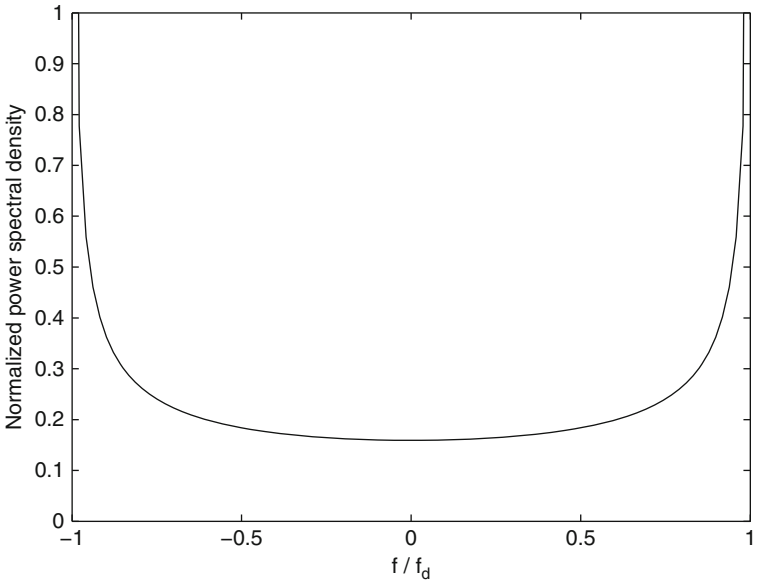

Fig. 5.3 Doppler spectrum for isotropic scattering

a channel symbol, then the fading is relatively constant over a symbol and is called *slow fading*. Conversely, if the coherence time is on the order of the duration of a channel symbol or less, then the fading is called *fast fading*.

The power spectral density of a complex process is defined as the Fourier transform of its autocorrelation. From (5.39) and tabulated Fourier transforms, we obtain the *Doppler power spectrum for two-dimensional isotropic scattering*:

$$S_r(f) = \begin{cases} \frac{\Omega}{\pi\sqrt{f_d^2 - f^2}}, & |f| < f_d \\ 0, & \textit{otherwise}. \end{cases} \tag{5.41}$$

The normalized Doppler spectrum $S_r(f)/S_r(0)$, which is plotted in Fig. 5.3 versus f/f_d, is bandlimited by the Doppler spread f_d and tends to infinity as f approaches $\pm f_d$. The Doppler spectrum is the superposition of contributions from multipath components, each of which experiences a different Doppler shift upper bounded by f_d.

The received signal power spectrum may be calculated from (5.7), (5.11), and (5.41). For an unmodulated carrier, $s(t) = 1$ and the received signal power spectrum is

$$S_{\text{rec}}(f) = \frac{1}{2}S_r(f - f_c) + \frac{1}{2}S_r(f + f_c). \tag{5.42}$$

In general, when the scattering is not isotropic, the imaginary part of the autocorrelation $A_r(\tau)$ is nonzero, and the amplitude of the real part decreases much more

slowly and less smoothly with increasing τ than (5.39). Both the real and imaginary parts often exhibit minor peaks for time shifts exceeding $1/f_d$. Thus, the coherence time provides only a rough characterization of the channel behavior.

5.2.1 Fading Rate and Fade Duration

The *fading rate* is the rate at which the envelope of a received fading signal crosses below a specified level. Consider a time interval over which the fading parameters are constant. For a level $r \geq 0$, isotropic scattering, and Ricean fading with density given by (5.28), it can be shown that the fading rate is [3]

$$f_r = \sqrt{2\pi(\kappa+1)}\, f_d \rho \exp[-\kappa-(\kappa+1)\rho^2] I_0\left(2\rho\sqrt{\kappa(\kappa+1)}\right) \tag{5.43}$$

where κ is the Rice factor,

$$\rho = \frac{r}{\sqrt{\Omega}} \tag{5.44}$$

and Ω is the average envelope power. For Rayleigh fading, $\kappa = 0$ and (5.43) becomes

$$f_r = \frac{\sqrt{2\pi} f_d r}{\sqrt{\Omega}} \exp(-r^2/\Omega). \tag{5.45}$$

Equations (5.43) and (5.45) indicate that the fading rate is proportional to the Doppler spread f_d. Thus, slow fading occurs when the Doppler spread is small, whereas fast fading occurs when the Doppler spread is large.

Let T_f denote the average envelope *fade duration*, which is the amount of time the envelope remains below the specified level $r \geq 0$. The product $f_r T_f$ is the fraction of the time between fades during which a fade occurs. If the time-varying envelope is assumed to be a stationary ergodic process, then this fraction is equal to $F_\alpha(r)$, the probability that the envelope is below or equal to the level r. Thus,

$$T_f = \frac{F_\alpha(r)}{f_r}. \tag{5.46}$$

If the envelope has a Ricean distribution, then integrating (5.28) and using (5.43) and (5.46), we obtain

$$T_f = \frac{1 - Q_1\left(\sqrt{2\kappa}, \sqrt{2(\kappa+1)}\rho\right)}{\sqrt{2\pi(\kappa+1)} f_d\, \rho \exp[-\kappa-(\kappa+1)\rho^2] I_0(2\rho\sqrt{\kappa(\kappa+1)})} \tag{5.47}$$

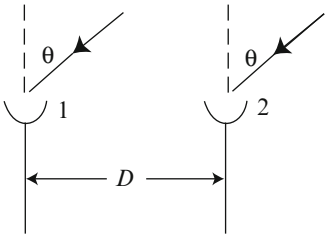

Fig. 5.4 Two antennas receiving plane wave that results in a signal copy at each antenna

where $Q_1(\ )$ is defined by (B.15). For Rayleigh fading, $\kappa = 0$ and (5.47) becomes

$$T_f = \frac{\exp(r^2/\Omega) - 1}{\sqrt{2\pi} f_d \, r/\sqrt{\Omega}}. \tag{5.48}$$

For both Ricean and Rayleigh fading, the fade duration is inversely proportional to f_d.

5.2.2 *Spatial Diversity and Fading*

To obtain spatial diversity in a fading environment, the antennas in an array at the receiver must be separated enough that there is little correlation between signal replicas or copies at the antennas. To determine what separation is needed, consider the reception of a signal at two antennas separated by a distance D, as illustrated in Fig. 5.4. If the signal arrives as an electromagnetic plane wave, then the signal copy at antenna 1 relative to antenna 2 is delayed by $D \sin\theta/c$, where θ is the arrival angle of the plane wave relative to a line perpendicular to the line joining the two antennas. Let $\phi_{ki}(t)$ denote the phase of the complex envelope of multipath component i at antenna k. Consider a time interval small enough that $N(t) = N$, the fading amplitudes are constants at the two antennas, and each multipath component arrives from a fixed angle. Thus, if multipath component i of a narrowband signal arrives as a plane wave at angle ψ_i, then the phase $\phi_{2i}(t)$ of the complex envelope of the component copy at antenna 2 is related to the phase $\phi_{1i}(t)$ at antenna 1 by

$$\phi_{2i}(t) = \phi_{1i}(t) + 2\pi \frac{D}{\lambda} \sin\psi_i \tag{5.49}$$

where $\lambda = c/f_c$ is the wavelength of the signal. If the multipath component propagates over a distance much larger than the separation between the two antennas, then it is reasonable to assume that the attenuation a_i is identical at the two antennas. If the range of the delay values exceeds $1/f_c$, then the sensitivity of the phases to small delay variations makes it plausible that the phases $\phi_{ki}(t)$, $i = 1, 2, \ldots, N$, $k = 1, 2$ are well modeled as independent random variables that are

uniformly distributed over $[0, 2\pi)$. From (5.12), the complex envelope r_k of the signal copy at antenna k when the signal is a tone is

$$r_k(t) = \sum_{i=1}^{N} a_i \exp[j\phi_{ki}(t)], \quad k = 1, 2. \tag{5.50}$$

The cross-correlation between $r_1(t)$ and $r_2(t)$ is defined as

$$C_{12}(D) = E[r_1^*(t)\, r_2(t)]. \tag{5.51}$$

Substituting (5.50) into (5.51), using the independence of each a_i and $\phi_{ki}(t)$, the independence of $\phi_{1i}(t)$ and $\phi_{2l}(t)$, $i \neq l$, and the uniform distribution of each $\phi_{ki}(t)$, and then substituting (5.49), we obtain

$$C_{12}(D) = \sum_{i=1}^{N} E[a_i^2] \exp(j 2\pi D \sin\psi_i/\lambda). \tag{5.52}$$

This equation for the cross-correlation as a function of spatial separation clearly resembles (5.36) for the autocorrelation as a function of time delay. If all the multipath components have approximately the same power so that $E[a_i^2] \approx \Omega/N$, $i = 1, 2, \ldots, N$, then

$$C_{12}(D) = \frac{\Omega}{N} \sum_{i=1}^{N} \exp(j 2\pi D \sin\psi_i/\lambda). \tag{5.53}$$

Applying the two-dimensional isotropic scattering model, (5.53) is approximated by an integral. As in the derivation of (5.39), the evaluation of the integral gives the real-valued cross-correlation

$$C_{12}(D) = \Omega J_0(2\pi D/\lambda). \tag{5.54}$$

This model indicates that an antenna separation of $D \geq \lambda/2$ ensures that the normalized cross-correlation $C_{12}(D)/C_{12}(0)$ is less than 0.3. A plot of the normalized cross-correlation is obtained from Fig. 5.2 if the abscissa is interpreted as D/λ. When the scattering is not isotropic or the number of scattering objects producing multipath components is small, then the real and imaginary parts of the cross-correlation decrease much more slowly with D/λ. For example, Fig. 5.5 shows the real and imaginary parts of the normalized cross-correlation when the $\{\psi_i\}$ are a nearly continuous band of angles between $7\pi/32$ and $9\pi/32$ radians so that (5.53) can be approximated by an integral. Figure 5.6 depicts the real and imaginary parts of the normalized cross-correlation when $N = 9$ and the $\{\psi_i\}$ are uniformly spaced throughout the first two quadrants: $\psi_i = (i-1)\pi/8$, $i = 1, 2, \ldots, 9$. In the example of Fig. 5.5, an antenna separation of at least 5λ is necessary

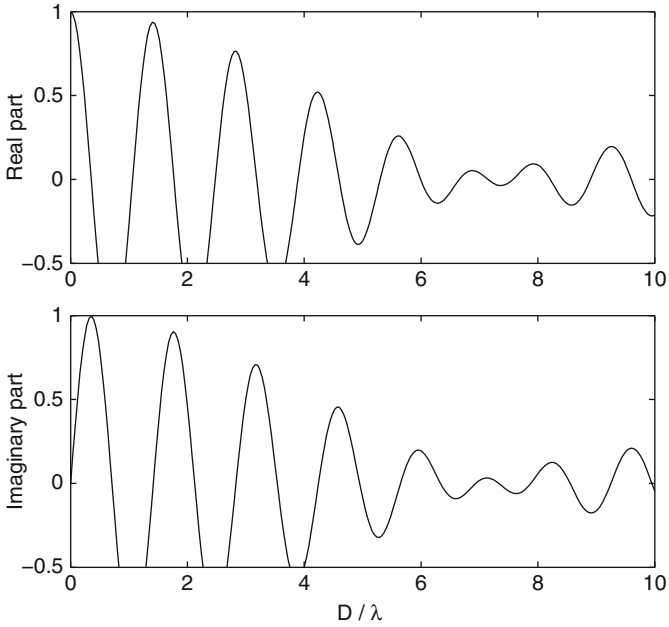

Fig. 5.5 Normalized cross-correlation for multipath components arriving between $7\pi/32$ and $9\pi/32$ radians: real and imaginary parts

to ensure approximate decorrelation of the signal copies and obtain spatial diversity. In the example of Fig. 5.6, not even a separation of 10λ is adequate to ensure approximate decorrelation.

5.3 Frequency-Selective Fading

Frequency-selective fading occurs because multipath components combine destructively at some frequencies, but constructively at others. The different path delays cause *dispersion* of a received pulse in time and cause intersymbol interference between successive symbols. When a multipath channel introduces neither time variations nor Doppler shifts, (5.8) and (5.9) indicate that the received complex envelope is

$$s_1(t) = \sum_{i=1}^{L_s} a_i \exp(-j2\pi f_c \tau_i) s(t - \tau_i). \tag{5.55}$$

The number of multipath components L_s includes only those components with power that is a significant fraction, perhaps 0.05 or more, of the power of the dominant component. The multipath *delay spread* T_d is defined as the maximum

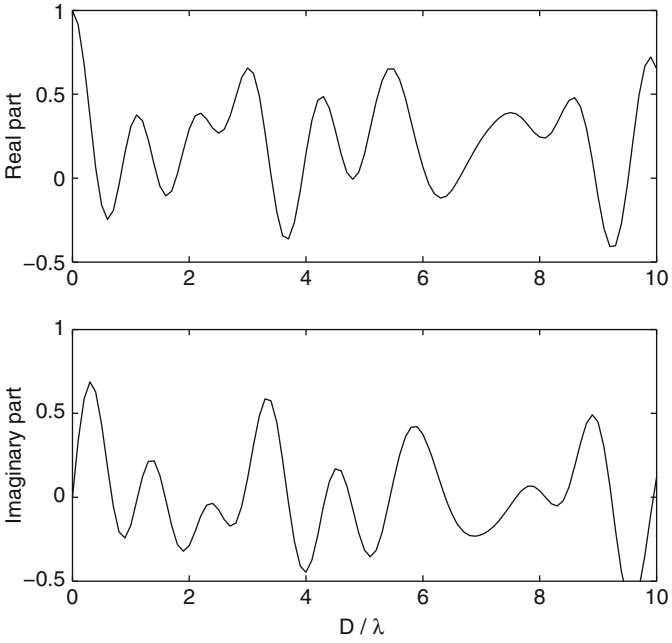

Fig. 5.6 Normalized cross-correlation for N = 9 multipath components arriving from uniformly spaced angles in the first two quadrants: real and imaginary parts

delay of a significant multipath component relative to the minimum delay of a component; that is,

$$T_d = \max_i \tau_i - \min_i \tau_i, \quad i = 1, 2, \ldots, L_s. \tag{5.56}$$

Suppose that $BT_d \ll 1$, where B is the bandwidth of the complex envelope $s(t)$. Since $B \approx 1/T_s$, where T_s is the symbol duration, $T_s \gg T_d$. Therefore, the multipath components are unresolvable, $s(t - \tau_i) \approx s(t - \tau_1)$, $i = 1, 2, \ldots, L_s$, and hence $s_1(t)$ is proportional to $s(t - \tau_1)$. Since all frequency components of the received signal fade nearly simultaneously, this type of fading is called *frequency-nonselective* or *flat fading* and occurs if $B \ll B_{coh}$, where the *coherence bandwidth* is defined as

$$B_{coh} = \frac{1}{T_d}. \tag{5.57}$$

In contrast, a signal is said to experience *frequency-selective fading* if $B > B_{coh}$, and hence $T_s < T_d$, because then the time variation or fading of the spectral components of $s(t)$ may be different. The large delay spread may cause intersymbol interference, which is accommodated by equalization in the receiver. However, if the time delays are sufficiently different among the multipath components that they are *resolvable* at

the demodulator or matched-filter output, then the independently fading components provide diversity that can be exploited by a rake demodulator (Sect. 5.5).

To illustrate frequency-selective fading, consider the reception of two multipath components. Calculating the Fourier transform $S_1(f)$ of $s_1(t)$ using (5.55) with $L_s = 2$, we obtain

$$|S_1(f)| = \left|a_1^2 + a_2^2 + 2a_1a_2\cos 2\pi\,(f + f_c)\,T_d\right|^{1/2} |S(f)| \tag{5.58}$$

where $T_d = \tau_1 - \tau_2$ and $S(f)$ is the Fourier transform of $s(t)$. This equation indicates that $|S_1(f)| / |S(f)|$ fluctuates over the range of f. If the range of f equals of exceeds $B_{coh} = 1/T_d$, then $|S_1(f)| / |S_1(f)|$ varies from $|a_1 - a_2|$ to $|a_1 + a_2|$, which is very large when $a_1 \approx a_2$.

5.3.1 Channel Impulse Response

A generalized impulse response may be used to characterize the impact of the transmission channel on the signal. The *equivalent complex-valued baseband impulse response* of the channel $h(t, \tau)$ is the response at time t due to an impulse applied τ seconds earlier. The complex envelope $s_1(t)$ of the received signal is the result of the convolution of the complex envelope $s(t)$ of the transmitted signal with the baseband impulse response:

$$s_1(t) = \int_{-\infty}^{\infty} h(t, \tau)s(t - \tau)d\tau. \tag{5.59}$$

In accordance with (5.8), the impulse response is usually modeled as a complex-valued stochastic process:

$$h(t, \tau) = \sum_{i=1}^{N(t)} h_i(t)\delta[\tau - \tau_i(t)]. \tag{5.60}$$

For most practical applications, the *wide-sense stationary, uncorrelated scattering* model is reasonably accurate. The impulse response is *wide-sense stationary* if the correlation between its value at t_1 and its value at t_2 depends only on $t_1 - t_2$. Thus, the autocorrelation of the impulse response is

$$R_h(t_1, t_2, \tau_1, \tau_2) = E[h^*(t_1, \tau_1)h(t_2, \tau_2)] = R_h(t_1 - t_2, \tau_1, \tau_2). \tag{5.61}$$

Uncorrelated scattering implies that the gains and phase shifts associated with two different delays are uncorrelated so that multipath components fade independently. Extending this notion, the wide-sense stationary, uncorrelated scattering model assumes that the autocorrelation has the form

$$R_h(t_1 - t_2, \tau_1, \tau_2) = R_h(t_1 - t_2, \tau_1)\delta(\tau_1 - \tau_2) \tag{5.62}$$

where $\delta(\ )$ is the Dirac delta function. The result of integrating this autocorrelation over τ_2 is the autocorrelation $R(t_1 - t_2, \tau_1)$.

The *multipath intensity profile* or *power delay spectrum*

$$S_h(\tau) = R_h(0, \tau) \tag{5.63}$$

can be interpreted as the channel output power due to an impulse applied τ seconds earlier. The range of the delay τ over which the multipath intensity profile has a significant magnitude is a measure of the multipath delay spread. The multipath intensity profile has *diffuse* components if it is a piecewise continuous function and has *specular* components if it includes delta functions at specific values of the delay. If the channel impulse response is modeled by (5.60) and it is time-invariant so that $h(t, \tau) = h(0, \tau) = h(\tau)$, then the multipath intensity profile has only specular components and

$$S_h(\tau) = \sum_{i=1}^{N} |h_i|^2 \delta(\tau - \tau_i). \tag{5.64}$$

A received signal from one source can often be decomposed into the sum of signals reflected from several clusters of scatterers. Each cluster is the sum of a number of multipath components with nearly the same delay. In this model, the impulse response can be expressed as (5.60) with $N(t) = L_c(t)$, where $L_c(t)$ is the number of clusters and $\tau_i(t)$ is the distinct delay associated with the ith cluster. Each complex process $h_i(t)$ has a magnitude with a Rayleigh, Rice, or Nakagami probability density function.

The Fourier transform of the impulse response gives the *time-varying channel frequency response*:

$$H(t, f) = \int_{-\infty}^{\infty} h(t, \tau) \exp(-j2\pi f \tau) d\tau. \tag{5.65}$$

Equation (5.61) implies that the autocorrelation of the frequency response for a wide-sense stationary channel is

$$R_H(t_1, t_2, f_1, f_2) = E[H^*(t_1, f_1) H(t_2, f_2)] = R_H(t_1 - t_2, f_1, f_2) \tag{5.66}$$

which depends only on $t_1 - t_2$. For the *wide-sense stationary, uncorrelated scattering* model, the substitution of (5.65), (5.61), and (5.62) into (5.66) yields

$$\begin{aligned} R_H(t_1, t_2, f_1, f_2) &= \int_{-\infty}^{\infty} R_h(t_1 - t_2, \tau) \exp[-j2\pi(f_1 - f_2)\tau] d\tau \\ &= R_H(t_1 - t_2, f_1 - f_2) \end{aligned} \tag{5.67}$$

which is a function only of the differences $t_1 - t_2$ and $f_1 - f_2$. If $t_1 = t_2$, then the autocorrelation of the frequency response is

$$R_H(0, f_1 - f_2) = \int_{-\infty}^{\infty} S_h(\tau) \exp[-j2\pi(f_1 - f_2)\tau] d\tau \tag{5.68}$$

which is the Fourier transform of the delay power spectrum. From a fundamental characteristic of the Fourier transform, it follows that the coherence bandwidth B_{coh} of the channel, which is a measure of the range of $f_1 - f_2$ for which $R_H(0, f_1 - f_2)$ has a significant value, is given by the reciprocal of the range of $S_h(\tau)$. Since this range is on the order of the multipath delay spread, (5.57) is confirmed as a suitable definition of B_{coh} for this channel model.

The Doppler shift is the main limitation on the channel coherence time or range of values of the difference $T_d = t_1 - t_2$ for which $R_h(T_d, 0)$ is significant. Thus, the *Doppler power spectral density* is defined as

$$S_D(f) = \int_{-\infty}^{\infty} R_h(t_d, 0) \exp(-j2\pi f t_d) dt_d. \tag{5.69}$$

The inverse Fourier transform of $S_D(f)$ gives the autocorrelation $R_h(t_d, 0)$. The coherence time T_{coh} of the channel, which is a measure of the range of t_d for which $R_h(t_d, 0)$ has a significant value, is given by the reciprocal of the spectral range of $S_D(f)$. Since this spectral range is on the order of the maximum Doppler shift, (5.40) is confirmed as a suitable definition of T_{coh} for this channel model.

5.4 Diversity for Fading Channels

Diversity combiners for fading channels are designed to combine independently fading copies of the same signal in different branches. The combining is done in such a way that the combiner output has a power level that varies much more slowly than that of a single copy. Although useless in improving communications over the AWGN channel, diversity improves communications over fading channels because the diversity gain is large enough to overcome any noncoherent combining loss. Diversity may be provided by signal redundancy that arises in a number of different ways. *Time diversity* is provided by channel coding or by signal copies that differ in time delay. *Frequency diversity* may be available when signal copies using different carrier frequencies experience independent or weakly correlated fading. If each signal copy is extracted from the output of a separate antenna in an antenna array, then the diversity is called *spatial diversity*. Although spatial diversity may be obtained by using multiple antennas in the transmitter, the receiver, or both, the use of the more efficient receive antennas is tacitly assumed in the subsequent development. *Polarization diversity* may be obtained by using two cross-polarized antennas at the same site. Although this configuration provides compactness, it

is not as potentially effective as spatial diversity because the received horizontal component of an electric field is usually much weaker than the vertical component.

The three most common types of diversity combining are selective, maximal-ratio, and equal-gain combining. The last two methods use linear combining with variable weights for each signal copy. Since they usually must eventually adjust their weights, maximal-ratio and equal-gain combiners can be viewed as types of adaptive arrays. They differ from other adaptive antenna arrays in that they are not designed to cancel interference signals.

5.4.1 Optimal Array

Consider a receiver array of L diversity branches, each of which processes a different signal copy. Each branch input is translated to baseband, and then either the baseband signal is applied to a matched filter and sampled or the sampled complex envelope is extracted (Appendix A.3). Alternatively, each branch input is translated to an IF, and the sampled analytic signal is extracted. The subsequent analysis is valid for any of these types of branch processing. It is simplest to assume that the branch outputs are sampled complex envelopes. The branch outputs provide the inputs to a linear combiner. Let $\mathbf{x}(l)$ denote the discrete-time vector of the L complex-valued combiner inputs, where the index denotes the sample number. This vector can be decomposed as

$$\mathbf{x}(l) = \mathbf{s}(l) + \mathbf{n}(l) \tag{5.70}$$

where $\mathbf{s}(l)$ and $\mathbf{n}(l)$ are the discrete-time vectors of the desired signal and the interference plus thermal noise, respectively. Let $\mathbf{W}$ denote the $L \times 1$ weight vector of a linear combiner applied to the input vector. The combiner output is

$$y(l) = \mathbf{W}^H \mathbf{x}(l) = y_s + y_n \tag{5.71}$$

where the superscript H denotes the conjugate transpose,

$$y_s(l) = \mathbf{W}^H \mathbf{s}(l) \tag{5.72}$$

is the output component due to the desired signal, and

$$y_n(l) = \mathbf{W}^H \mathbf{n}(l) \tag{5.73}$$

is the output component due to the interference plus noise. The components of both $\mathbf{s}(l)$ and $\mathbf{n}(l)$ are modeled as discrete-time jointly wide-sense-stationary processes.

The correlation matrix of the desired signal is defined as the $L \times L$ matrix

$$\mathbf{R}_{ss} = E\left[\mathbf{s}(l)\mathbf{s}^H(l)\right] \tag{5.74}$$

and the correlation matrix of the interference plus noise is defined as the $L \times L$ matrix

$$\mathbf{R}_{nn} = E\left[\mathbf{n}(l)\mathbf{n}^H(l)\right]. \tag{5.75}$$

The desired-signal power at the output is

$$p_{so} = E\left[|y_s(l)|^2\right] = \mathbf{W}^H \mathbf{R}_{ss} \mathbf{W}. \tag{5.76}$$

The interference plus noise power at the output is

$$p_n = E\left[|y_n(l)|^2\right] = \mathbf{W}^H \mathbf{R}_{nn} \mathbf{W}. \tag{5.77}$$

The SINR at the combiner output is

$$\rho_0 = \frac{p_{so}}{p_n} = \frac{\mathbf{W}^H \mathbf{R}_{ss} \mathbf{W}}{\mathbf{W}^H \mathbf{R}_{nn} \mathbf{W}}. \tag{5.78}$$

The definitions of $\mathbf{R}_{ss}$ and $\mathbf{R}_{nn}$ ensure that these matrices are Hermitian and nonnegative definite. Consequently, these matrices have complete sets of orthonormal eigenvectors, and their eigenvalues are real-valued and nonnegative. The noise power is assumed to be positive. Therefore, $\mathbf{R}_{nn}$ is positive definite and has positive eigenvalues. Since $\mathbf{R}_{nn}$ can be diagonalized, it can be expressed as [4].

$$\mathbf{R}_{nn} = \sum_{i=1}^{L} \lambda_i \mathbf{e}_i \mathbf{e}_i^H \tag{5.79}$$

where λ_i is an eigenvalue and $\mathbf{e}_i$ is the associated eigenvector.

To derive the weight vector that maximizes the SINR with no restriction on $\mathbf{R}_{ss}$, we define the Hermitian matrix

$$\mathbf{A} = \sum_{i=1}^{L} \sqrt{\lambda_i} \mathbf{e}_i \mathbf{e}_i^H \tag{5.80}$$

where the positive square root is used. Direct calculations verify that

$$\mathbf{R}_{nn} = \mathbf{A}^2 \tag{5.81}$$

and the inverse of $\mathbf{A}$ is

$$\mathbf{A}^{-1} = \sum_{i=1}^{L} \frac{1}{\sqrt{\lambda_i}} \mathbf{e}_i \mathbf{e}_i^H. \tag{5.82}$$

The matrix $\mathbf{A}$ specifies an invertible transformation of $\mathbf{W}$ into the vector

$$\mathbf{V} = \mathbf{A}\mathbf{W}. \tag{5.83}$$

We define the Hermitian matrix

$$\mathbf{C} = \mathbf{A}^{-1}\mathbf{R}_{ss}\mathbf{A}^{-1}. \tag{5.84}$$

Then (5.78), (5.81), (5.83), and (5.84) indicate that the SINR can be expressed as the *Rayleigh quotient*

$$\rho_0 = \frac{\mathbf{V}^H\mathbf{C}\mathbf{V}}{\|\mathbf{V}\|^2}. \tag{5.85}$$

where $\| \ \|$ denotes the *Euclidean norm* of a vector and $\|\mathbf{V}\|^2 = \mathbf{V}^H\mathbf{V}$.

Let $\mathbf{u}_1 \ldots \mathbf{u}_L$ denote the orthonormal eigenvectors of $\mathbf{C}$, and $\mu_1 \ldots \mu_L$ the corresponding eigenvalues. *The vector* $\mathbf{V}$ may be expressed $\mathbf{V} = V_1\mathbf{u}_1 + \ldots + V_L\mathbf{u}_L$. Then $\mathbf{V}^H\mathbf{C}\mathbf{V} = \mu_1 |V_1|^2 + \ldots + \mu_L |V_L|^2 \leq \mu_{\max}\left(|V_1|^2 + \ldots + |V_L|^2\right) = \mu_{\max}\|\mathbf{V}\|^2$, where $\mu_{\max}$ is the largest eigenvalue. Similarly, $\mathbf{V}^H\mathbf{C}\mathbf{V} \geq \mu_{\min}\|\mathbf{V}\|^2$, where $\mu_{\min}$ is the smallest eigenvalue. Thus, the Rayleigh quotient satisfies

$$\mu_{\min} \leq \frac{\mathbf{V}^H\mathbf{C}\mathbf{V}}{\|\mathbf{V}\|^2} \leq \mu_{\max}. \tag{5.86}$$

Since $\rho_0 \leq \mu_{\max}$, ρ_0 is maximized by $\mathbf{V} = \eta\mathbf{u}$, where $\mathbf{u}$ is the eigenvector of $\mathbf{C}$ associated with its largest eigenvalue $\mu_{\max}$, and η is an arbitrary constant. Thus, the maximum value of ρ_0 is

$$\rho_{\max} = \mu_{\max}. \tag{5.87}$$

From (5.83) with $\mathbf{V} = \eta\mathbf{u}$, it follows that the *optimal weight vector that maximizes the SINR* is

$$\mathbf{W}_0 = \eta\mathbf{A}^{-1}\mathbf{u}. \tag{5.88}$$

The purpose of an adaptive-array algorithm is to adjust the weight vector to converge to the optimal value, which is given by (5.88) when the maximization of the SINR is the performance criterion.

When the discrete-time dependence of $\mathbf{s}(l)$ is the same for all its components, (5.88) can be made more explicit. Let $s(l)$ denote the discrete-time sampled complex envelope of the desired signal in a fixed reference branch. It is assumed henceforth that the desired signal is sufficiently narrowband that the desired-signal copies in all the branches are nearly aligned in time, and the desired-signal input vector may be represented as

$$\mathbf{s}(l) = s(l)\mathbf{S}_0 \tag{5.89}$$

where the *steering vector* is

$$\mathbf{S}_0 = [\alpha_1 \exp(j\,\theta_1) \ \ \alpha_2 \exp(j\,\theta_2) \ \ \ldots \ \alpha_L \exp(j\,\theta_L)]^T. \tag{5.90}$$

For independent Rayleigh fading in each branch, each phase θ_i is modeled as a random variable with a uniform distribution over $[0, 2\pi)$, and each attenuation α_i has a Rayleigh distribution function, as explained in Sect. 1.3.

Example 5.1. Equation (5.90) can serve as a model for a narrowband desired signal that arrives at an antenna array as a plane wave and does not experience fading. Let $T_i, i = 1, 2, \ldots, L$, denote the arrival-time delay of the desired signal at the output of antenna i relative to a fixed reference point in space. Equations (5.89) and (5.90) are valid with $\theta_i = -2\pi f_c T_i, i = 1, 2, \ldots, L$, where f_c is the carrier frequency of the desired signal. The $\alpha_i, i = 1, 2, \ldots, L$, depend on the relative antenna patterns and propagation losses. If they are all equal, then the common value can be subsumed into $s(l)$. It is convenient to define the origin of a Cartesian coordinate system to coincide with the fixed reference point. Let (x_i, y_i) denote the coordinates of antenna i. If a single plane wave arrives from direction ψ relative to the normal to the array, then

$$\theta_i = \frac{2\pi}{c} f_c (x_i \sin\psi + y_i \cos\psi), \quad i = 1, 2, \ldots, L \tag{5.91}$$

where c is the speed of an electromagnetic wave. □

The substitution of (5.89) into (5.74) yields

$$\mathbf{R}_{ss} = p_s \mathbf{S}_0 \mathbf{S}_0^H \tag{5.92}$$

where

$$p_s = E[|s(l)|^2]. \tag{5.93}$$

After substituting (5.92) into (5.84), it is observed that $\mathbf{C}$ may be factored:

$$\mathbf{C} = p_s \mathbf{A}^{-1} \mathbf{S}_0 \mathbf{S}_0^H \mathbf{A}^{-1} = \mathbf{F}\mathbf{F}^H \tag{5.94}$$

where

$$\mathbf{F} = \sqrt{p_s}\mathbf{A}^{-1}\mathbf{S}_0. \tag{5.95}$$

This factorization explicitly shows that $\mathbf{C}$ is a rank-one matrix. Therefore, an eigenvector of $\mathbf{C}$ associated with the only nonzero eigenvalue is

$$\mathbf{u} = \mathbf{F} = \sqrt{p_s}\mathbf{A}^{-1}\mathbf{S}_0 \tag{5.96}$$

and the nonzero eigenvalue is

$$l_{\max} = \|\mathbf{F}\|^2. \tag{5.97}$$

Substituting (5.96) into (5.88), using (5.81), and then merging $\sqrt{p_s}$ into the arbitrary constant, we obtain the *Wiener–Hopf equation* (Sect. 2.7) for the optimal weight vector:

$$\mathbf{W}_0 = \eta \mathbf{R}_{nn}^{-1} \mathbf{S}_0 \tag{5.98}$$

where η is an arbitrary constant. The maximum value of the SINR, obtained from (5.87), (5.97), (5.95), and (5.81), is

$$\rho_{\max} = p_s \mathbf{S}_0^H \mathbf{R}_{nn}^{-1} \mathbf{S}_0. \tag{5.99}$$

5.4.2 Maximal-Ratio Combining

Suppose that the interference plus noise in a branch is zero-mean and uncorrelated with the interference plus noise in any of the other branches in the array. Then the correlation matrix $\mathbf{R}_{nn}$ is diagonal. The ith diagonal element has the value

$$\sigma_i^2 = E[|n_i|^2]. \tag{5.100}$$

Since $\mathbf{R}_{nn}^{-1}$ is diagonal with diagonal elements $1/2\sigma_i^2$, the Wiener–Hopf equation implies that the optimal weight vector that maximizes the SINR is

$$\mathbf{W}_m = \eta \left[\frac{S_{01}}{\sigma_1^2} \ \frac{S_{02}}{\sigma_2^2} \ \cdots \ \frac{S_{0L}}{\sigma_L^2} \right]^T. \tag{5.101}$$

Equations (5.72), (5.101), (5.89), and (5.90) yield the desired part of the combiner output:

$$y_s(l) = \mathbf{W}_m^H \mathbf{s}(l) = \eta s(l) \sum_{i=1}^{L} \frac{|S_{0i}|^2}{\sigma_i^2} \alpha_i^2 \tag{5.102}$$

and (5.99) and (5.90) yield

$$\rho_{\max} = \sum_{i=1}^{L} \frac{p_s}{\sigma_i^2} \alpha_i^2 \tag{5.103}$$

where each term is the SINR at a branch output. Linear combining that uses $\mathbf{W}_m$ is called *maximal-ratio combining* (MRC). It is the optimal linear combining only if the interference-plus-noise signals in all the diversity branches are uncorrelated. Since $y_s(l)$ is proportional to $s(l)$, MRC equalizes the phases of the signal copies in the array branches, a process called *cophasing*. As discussed subsequently, MRC can also be derived as the maximum-likelihood estimator associated with a multivariate Gaussian density function. The critical assumption in the derivation is that the noise process in each array branch is both Gaussian and independent of the noise processes in the other branches.

In most applications, the interference-plus-noise power in each array branch is approximately equal, and it is assumed that $\sigma_i^2 = \sigma^2$, $i = 1, 2, \ldots, L$. If this common value is merged with the constant in (5.98) or (5.101), then the MRC weight vector is

$$\mathbf{W}_m = \eta \mathbf{S}_0 \tag{5.104}$$

the desired part of the combiner output is

$$y_s(l) = \mathbf{W}_m^H \mathbf{s}(l) = \eta s(l) \sum_{i=1}^{L} \alpha_i^2 \tag{5.105}$$

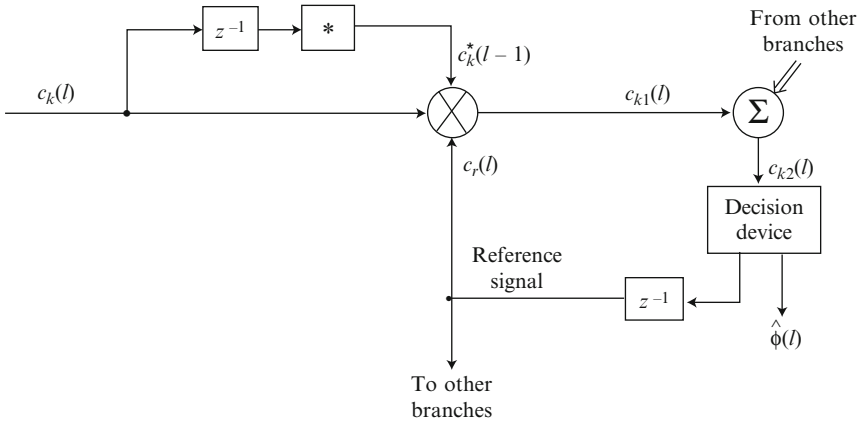

Fig. 5.7 Branch k of MRC with a phase stripper

and the corresponding maximum SINR is

$$\rho_{\max} = \frac{p_s}{\sigma^2} \sum_{i=1}^{L} \alpha_i^2. \tag{5.106}$$

Since the weight vector is not a function of the interference parameters, the combiner attempts no interference cancellation. The interference signals are ignored while the combiner does coherent combining of the desired signal. If each α_i, $i = 1, 2, \ldots, L$, is modeled as a random variable with an identical probability distribution function, then (5.106) implies that

$$E[\rho_{\max}] = L \frac{p_s}{\sigma^2} E[\alpha_1^2] \tag{5.107}$$

which indicates a gain in the mean SINR that is proportional to L.

There are several ways to implement cophasing [5]. Unlike most other cophasing systems, the *phase stripper* does not require a pilot signal. Figure 5.7 depicts branch k of a digital version of MRC with a phase stripper. It is assumed that the interference-plus-noise power in each branch is equal so that only cophasing and amplitude multiplication are required for the MRC. In the absence of noise, the angle-modulated input signal is assumed to have the form

$$c_k(l) = \alpha_k s(l) \exp[j\theta_k] = \alpha_k \exp[j\phi(l) + j\theta_k]. \tag{5.108}$$

where α_k is the amplitude, $\phi(l)$ is the angle modulation carried by all the signal copies in the diversity branches, and θ_k is the undesired phase shift in branch k, which is assumed to be constant for at least two consecutive samples. The signal $c_k^*(l-1)$ is produced by a delay and complex conjugation. During steady-state

operation following an initialization process, the reference signal is assumed to have the form

$$c_r(l) = \exp[j\phi(l-1) + j\psi] \tag{5.109}$$

where ψ is a phase angle. The three signals $c_r(l)$, $c_k(l)$, and $c_k^*(l-1)$ are multiplied together to produce

$$c_{k1}(l) = \alpha_k^2 \exp[j\phi(l) + j\psi] \tag{5.110}$$

which as been stripped of the undesired phase shift θ_k. This signal is combined with similar signals from the other diversity branches that use the same reference signal. The input to the decision device is

$$c_{k2}(l) = \sum_{k=1}^{L} \alpha_k^2 \exp[j\phi(l) + j\psi] = e^{j\psi} s(l) \sum_{k=1}^{L} \alpha_k^2 \tag{5.111}$$

which indicates that MRC has been obtained by phase equalization, as in (5.105). The normalization of $c_{k2}(l)$ and its delay produces $c_r(l)$,the reference signal. After extracting the phase $\phi(l) + \psi$ from the normalized $c_{k2}(l)$, the decision device produces the demodulated sequence $\hat{\phi}(l)$, which is an estimate of $\phi(l)$, by some type of phase-recovery loop [6].

5.4.3 Coherent Binary Modulations and Metrics

Suppose that the desired-signal modulation is BPSK and consider the reception of a single binary symbol or bit. Each bit is equally likely to be a 0 or a 1 and is represented by $+\psi(t)$ or $-\psi(t)$, respectively, where $\psi(t)$ is a unit-energy symbol waveform. Each received signal copy in a diversity branch experiences independent Rayleigh fading that is constant during the signal interval. The received signal in branch i is

$$r_i(t) = \text{Re}\left[\sqrt{2\mathcal{E}_b}\alpha_i e^{j\theta_i} x\psi(t) e^{j2\pi f_c t}\right] + n_i(t), \quad 0 \le t \le T_b, \quad i = 1, 2, \ldots, L \tag{5.112}$$

where $x = +1$ or -1 depending on the transmitted bit, each α_i is an amplitude, each θ_i is a phase shift, f_c is the carrier frequency, T_b is the bit duration, $\mathcal{E}_b$ is the desired-signal energy per bit in the absence of fading and diversity combining, and $n_i(t)$ is the noise. It is assumed that either the interference is absent or, more generally, that the received interference plus noise in each diversity branch can be modeled as independent, zero-mean, white Gaussian noise with the same two-sided power spectral density $N_0/2$.

Although MRC maximizes the SINR after linear combining, the theory of maximum-likelihood detection is needed to determine an optimal decision variable that can be compared to a threshold. The initial branch processing before sampling could entail passband matched-filtering followed by a downconversion to baseband,

or, equivalently, a downconversion followed by baseband matched-filtering [6], which is assumed in this analysis.

A derivation similar to that following (1.40) in Sect. 1.1 indicates that the matched filter in diversity branch i produces the sample

$$y_i = \sqrt{\mathcal{E}_b}\alpha_i e^{j\theta_i} x + N_i, \quad i = 1, 2, \ldots, L \tag{5.113}$$

where $\mathcal{E}_b$ is the desired-signal energy per bit in the absence of fading and diversity combining, and N_i is independent, zero-mean, complex Gaussian noise. These samples provide sufficient statistics that contain all the relevant information in the received signal copies in the L diversity branches.

If the two-sided noise-power spectral density in each branch is equal to $N_0/2$, then $E[|\ N_i\ |^2] = N_0$. Because of its circular symmetry, N_i has independent real and imaginary components with variance $N_0/2$. Given x, α_i, and θ_i, the branch likelihood function or conditional probability density function of y_i is

$$f(y_i|x, \alpha_i, \theta_i) = \frac{1}{\pi N_0} \exp\left[- \frac{|\ y_i - \sqrt{\mathcal{E}_b}\alpha_i e^{j\theta_i} x\ |^2}{N_0} \right], \quad i = 1, 2, \ldots, L. \tag{5.114}$$

Since the branch samples are statistically independent, the log-likelihood function for the vector $\mathbf{y} = (y_1\ y_2\ \ldots\ y_L)^T$ given $\alpha = (\alpha_1\ \alpha_2\ \ldots\ \alpha_L)^T$ and $\boldsymbol{\theta} = (\theta_1\ \theta_2\ \ldots\ \theta_L)^T$ is

$$\ln[f(\mathbf{y}|x, \boldsymbol{\alpha}, \boldsymbol{\theta})] = \sum_{i=1}^{L} \ln[f(y_i|x, \alpha_i, \theta_i)]. \tag{5.115}$$

The receiver decides in favor of a 0 or a 1 depending on whether $x = +1$ or $x = -1$ gives the larger value of the log-likelihood function. Substituting (5.114) into (5.115) and eliminating irrelevant terms and factors that do not depend on the value of x, we find that the *maximum-likelihood metric for BPSK is*

$$U = \sum_{i=1}^{L} \mathrm{Re}(\alpha_i e^{-j\theta_i} y_i) \tag{5.116}$$

which is compared with a threshold equal to zero to determine the bit state. Equations (5.104) and (5.90) indicate that the decision variable may be expressed as $U = Re[\mathbf{W}_m^H \mathbf{y}]$, where $\mathbf{y} = [y_1\ y_2\ \ldots\ y_L]^T$. Since the noise power is assumed to be identical in each diversity branch and taking the real part of $\mathbf{W}_m^H \mathbf{y}$ serves only to eliminate orthogonal noise, the decision variable U is equal to an MRC output. This decision variable or metric has the disadvantage that it requires phase synchronization in each branch and estimates of the $\{\alpha_i\}$.

Since (5.116) is computed in either case, the implementation of the maximum-likelihood detector may use either maximal-ratio *predetection combining* before the demodulation, as illustrated in Fig. 5.8a, or *postdetection combining* following

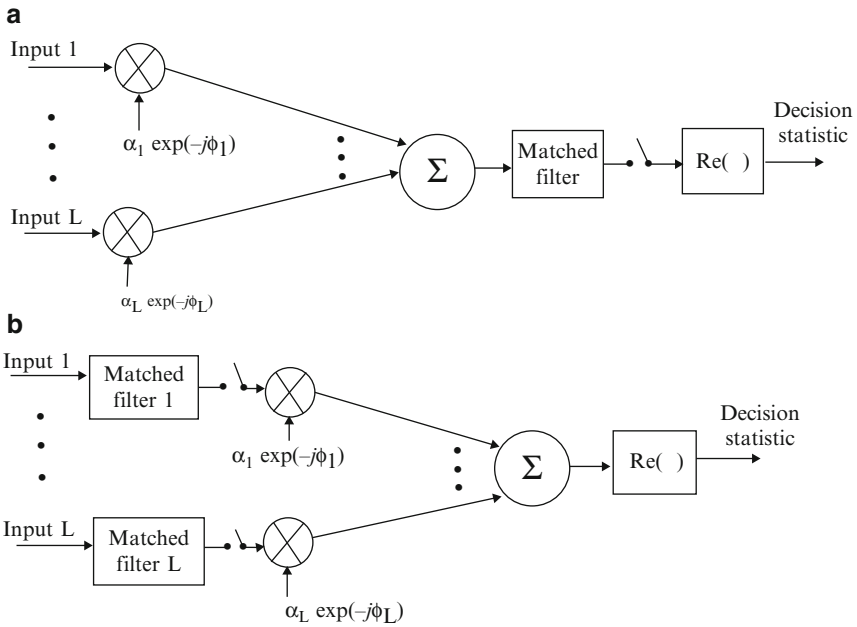

Fig. 5.8 Maximal-ratio combiner for PSK with (**a**) predetection combining and (**b**) postdetection combining. Coherent equal-gain combiner for PSK omits the factors $\{\alpha_i\}$

the demodulation, as illustrated in Fig. 5.8b. Since the optimal coherent matched-filter or correlation demodulator performs a linear operation on the $\{y_i\}$, both predetection and postdetection combining provide the same decision variable, and hence the same performance.

If the transmitted bit is represented by x, then the substitution of (5.113) into (5.116) yields

$$U = \sqrt{\mathcal{E}_b} \sum_{i=1}^{L} \alpha_i^2 + \sum_{i=1}^{L} \alpha_i N_{1i} \tag{5.117}$$

where N_{1i} is the zero-mean Gaussian random variable

$$N_{1i} = \text{Re}\left(e^{-j\theta_i} N_i\right). \tag{5.118}$$

If the $\{\alpha_i\}$ are given and the $\{\theta_i\}$ are uniformly distributed over $[0, 2\pi)$, then the decision variable has a Gaussian distribution with mean

$$E(U) = \sqrt{\mathcal{E}_b} \sum_{i=1}^{L} \alpha_i^2. \tag{5.119}$$

The $\{n_i(t)\}$ and, hence, the $\{N_{1i}\}$ are independent. The variance of N_{1i} is equal to $E[|\ N_i\ |^2]/2 = N_0/2$. Therefore, the variance of U is

$$\sigma_u^2 = \frac{N_0}{2}\sum_{i=1}^{L}\alpha_i^2. \tag{5.120}$$

Because of the symmetry, the bit error probability is equal to the conditional bit error probability given that $x = +1$, corresponding to a transmitted 0. A decision error is made if $U < 0$. Since the decision variable has a Gaussian conditional distribution, a standard evaluation indicates that the conditional bit error probability given the $\{\alpha_i\}$ is

$$P_{b|\boldsymbol{\alpha}}(\gamma_b) = Q(\sqrt{2\gamma_b}) \tag{5.121}$$

where $Q(x)$ is defined by (1.35) and the SNR for the bit is

$$\gamma_b = \sum_{i=1}^{L}\gamma_i, \quad \gamma_i = \frac{\mathcal{E}_b}{N_0}\alpha_i^2. \tag{5.122}$$

The bit error probability is determined by averaging $P_{b|\boldsymbol{\alpha}}(\gamma_b)$ over the distribution of γ_b, which depends on the $\{\alpha_i\}$ and embodies the statistics of the fading channel.

Suppose that independent Rayleigh fading occurs so that each of the $\{\alpha_i\}$ is independent with the identical Rayleigh distribution and $E[\alpha_i^2] = E[\alpha_1^2]$. As shown in Appendix B.4, α_i^2 is exponentially distributed. Therefore, γ_b is the sum of L independent, identically and exponentially distributed random variables. From (B.49), it follows that the probability density function of γ_b is

$$f_\gamma(x) = \frac{1}{(L-1)!\bar{\gamma}^L}x^{L-1}\exp\left(-\frac{x}{\bar{\gamma}}\right)u(x) \tag{5.123}$$

where the average SNR per branch is

$$\bar{\gamma} = \frac{\mathcal{E}_b}{N_0}E[\alpha_1^2]. \tag{5.124}$$

The bit error probability is determined by averaging (5.121) over the density given by (5.123). Thus,

$$P_b(L) = \int_0^\infty Q(\sqrt{2x})\frac{1}{(L-1)!\bar{\gamma}^L}x^{L-1}\exp\left(-\frac{x}{\bar{\gamma}}\right)dx. \tag{5.125}$$

Direct calculations verify that since L is a positive integer,

$$\frac{d}{dx}Q\left(\sqrt{2x}\right) = -\frac{1}{2\sqrt{\pi}}\frac{\exp(-x)}{\sqrt{x}} \tag{5.126}$$

$$\frac{d}{dx}\left[e^{-x/\bar{\gamma}}\sum_{i=0}^{L-1}\frac{(x/\bar{\gamma})^i}{i!}\right] = -\frac{1}{(L-1)!\bar{\gamma}^L}x^{L-1}\exp\left(-\frac{x}{\bar{\gamma}}\right). \tag{5.127}$$

Applying integration by parts to (5.125), using (5.126), (5.127), and $Q(0) = 1/2$, we obtain

$$P_b(L) = \frac{1}{2} - \sum_{i=0}^{L-1} \frac{1}{i!\bar{\gamma}^i 2\sqrt{\pi}} \int_0^\infty \exp\left[-x\left(1+\bar{\gamma}^{-1}\right)\right] x^{i-1/2}\, dx. \tag{5.128}$$

This integral can be evaluated in terms of the gamma function, which is defined in (B.12) of Appendix B. A change of variable in (5.128) yields

$$P_b(L) = \frac{1}{2} - \frac{1}{2}\sqrt{\frac{\bar{\gamma}}{1+\bar{\gamma}}} \sum_{i=0}^{L-1} \frac{\Gamma(i+1/2)}{\sqrt{\pi} i!(1+\bar{\gamma})^i}. \tag{5.129}$$

Since $\Gamma(1/2) = \sqrt{\pi}$, the bit error probability for no diversity or a single branch is

$$p = P_b(1) = \frac{1}{2}\left(1 - \sqrt{\frac{\bar{\gamma}}{1+\bar{\gamma}}}\right) \qquad \text{(BPSK, QPSK)}. \tag{5.130}$$

Since $\Gamma(x) = (x-1)\Gamma(x-1)$, it follows that

$$\Gamma(k+1/2) = \frac{\sqrt{\pi}\,\Gamma(2k)}{2^{2k-1}\Gamma(k)} = \frac{\sqrt{\pi}k!}{2^{2k-1}}\binom{2k-1}{k}, \quad k \geq 1. \tag{5.131}$$

Solving (5.130) to determine $\bar{\gamma}$ as a function of p and then using this result and (5.131) in (5.129) gives

$$P_b(L) = p - (1-2p)\sum_{i=1}^{L-1}\binom{2i-1}{i}[p(1-p)]^i. \tag{5.132}$$

This expression explicitly shows the change in the bit error probability as the number of diversity branches increases. Equations (5.130) and (5.132) are valid for QPSK because the latter can be transmitted as two independent BPSK waveforms in phase quadrature.

An alternative expression for $P_b(L)$, which may be obtained by a far more complicated calculation entailing the use of the properties of the Gauss hypergeometric function, is [2]

$$P_b(L) = p^L \sum_{i=0}^{L-1}\binom{L+i-1}{i}(1-p)^i. \tag{5.133}$$

By using mathematical induction, this equation can be derived from (5.132) without invoking the hypergeometric function.

To derive an upper bound on $P_b(L)$ that facilitates analysis of its asymptotic behavior, we use an identity for the sum of binomial coefficients:

$$\sum_{i=0}^{L-1} \binom{L+i-1}{i} = \binom{2L-1}{L}. \tag{5.134}$$

To prove (5.134), observe that $\binom{2L-1}{L} = \binom{2L-1}{L-1}$ is the number of ways of choosing $L-1$ distinct objects out of $2L-1$. For $0 \le k \le L$, a choice could also be made by selecting the first k objects, not selecting the next object, and then selecting $L-k-1$ distinct objects from the remaining $2L-1-(k+1) = 2L-k-2$ objects. Thus,

$$\binom{2L-1}{L} = \sum_{k=0}^{L-1} \binom{2L-k-2}{L-k-1} = \sum_{i=0}^{L-1} \binom{L+i-1}{i} \tag{5.135}$$

which proves the identity. Since $1-p \le 1$, (5.133) and (5.134) imply that

$$P_b(L) \le \binom{2L-1}{L} p^L. \tag{5.136}$$

This upper bound becomes tighter as $p \to 0$.

If $\bar{\gamma} > 1$, a Taylor series expansion of (5.130) implies that $p \le 1/4\bar{\gamma}$, which becomes tighter as $\bar{\gamma}$ increases, and (5.136) indicates that

$$P_b(L) \le \binom{2L-1}{L} \left(\frac{1}{4^L}\right) \bar{\gamma}^{-L}, \quad \bar{\gamma} > 1. \tag{5.137}$$

When the upper bound is tight, then

$$P_b(L+1) \approx P_b(L) \left(\frac{2L+1}{2L+2}\right) \bar{\gamma}^{-1}, \quad \bar{\gamma} > 1 \tag{5.138}$$

which demonstrates the potential performance improvement provided by diversity when $\bar{\gamma} > 1$.

Inequality (5.137) motivates the following general measure of diversity. The *diversity order* is defined as

$$D_o = -\lim_{\bar{\gamma} \to \infty} \frac{\partial \log P_b(L)}{\partial \bar{\gamma}}. \tag{5.139}$$

When the upper bound in (5.137) is tight, then $D_o = L$.

The advantage of MRC is critically dependent on the assumption of uncorrelated fading in each diversity branch. If there is complete correlation so that the $\{\alpha_i\}$ are

all equal and the fading occurs simultaneously in all the diversity branches, then $\gamma_b = L\mathcal{E}\alpha_1^2/N_0$. Therefore, γ_b has an exponential probability density function:

$$f_\gamma^c(x) = \frac{1}{L\bar{\gamma}} \exp\left(-\frac{x}{L\bar{\gamma}}\right) u(x) \tag{5.140}$$

where $\bar{\gamma}$ is defined by (5.124) and the superscript c denotes correlated fading. A derivation similar to that of (5.129) yields

$$P_b^c(L) = \frac{1}{2}\left(1 - \sqrt{\frac{L\bar{\gamma}}{1 + L\bar{\gamma}}}\right) \quad \text{(BPSK, QPSK)}. \tag{5.141}$$

When $L\bar{\gamma} \gg 1$,

$$P_b^c(L) \approx \frac{1}{4L\bar{\gamma}} \approx \frac{p}{L}, \quad p \ll 1 \quad \text{(BPSK, QPSK)} \tag{5.142}$$

where p is given by (5.130). A comparison of (5.142) with (5.136) indicates that

$$P_b(L) \lessapprox P_b^c(L) L \binom{2L-1}{L} \left(\frac{1}{4^{L-1}}\right) \bar{\gamma}^{-L+1}, \quad \bar{\gamma} > 1 \tag{5.143}$$

which shows the large disparity in performance between a system with completely correlated fading and one with uncorrelated fading when $\bar{\gamma}$ is sufficiently large.

This result has an important application to receive antennas, which can be used for different purposes. Receive antennas can provide MRC diversity, but instead they can be used for beamforming. If the receive antennas are used for beamforming, then their phase-shifted outputs are completely correlated. Consequently, when $\bar{\gamma}$ is sufficiently large in an environment of fading and noise, beamforming entails a performance loss relative to the potential performance with diversity combining. The main advantage of beamforming is its suppression of interference entering the sidelobes of the receive antenna pattern.

Graphs of the bit error probability for a single branch with no fading, L branches with independent fading and MRC, and L branches with completely correlated fading and MRC are shown in Fig. 5.9. Equations (5.121), (5.130), (5.132), and (5.141) are used in generating the graphs. The independent variable is the average SNR per branch for a bit, which is equal to $\bar{\gamma}$ for MRC and is equal to $\gamma_b = \mathcal{E}/N_0$ for the single branch with no fading. The average SNR per bit for MRC is $L\bar{\gamma}$. The figure demonstrates the advantage of diversity combining and independent fading.

For FSK, one of q equal-energy orthogonal signals $s_1(t), s_2(t), \ldots, s_q(t)$, each representing $\log_2 q$ bits, is transmitted. The maximum-likelihood detector generates q decision variables corresponding to the q possible nonbinary symbols. The decoder decides in favor of the symbol associated with the largest of the decision

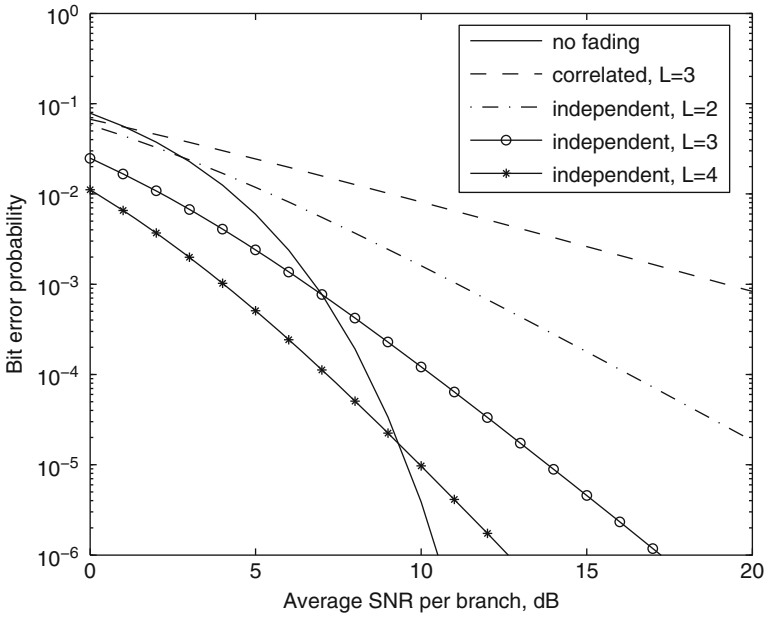

Fig. 5.9 Bit error probability of PSK for no fading, completely correlated fading, and independent fading

variables. Matched filters for the q orthogonal signals are needed in every diversity branch. Because of the orthogonality, each filter matched to $s_k(t)$ has a zero response to $s_l(t)$, $l \neq k$, at the sampling time. A derivation similar to that following (1.60) in Sect. 1.1 indicates that when symbol l represented by $s_l(t)$ is received in the presence of white Gaussian noise, matched-filter k of branch i produces the sample

$$y_{ki} = \sqrt{\mathcal{E}_s}\alpha_i e^{j\theta_i}\delta_{kl} + N_{ki}, \quad k = 1, 2, \ldots, q, \quad i = 1, 2, \ldots, L \tag{5.144}$$

where $\mathcal{E}_s$ is the desired-signal energy per symbol in the absence of fading and diversity combining, and each N_{ki} is an independent, zero-mean, complex-valued Gaussian noise variable. These samples provide sufficient statistics that contain all the relevant information in the received signal copies in the L diversity branches.

Assuming that the two-sided noise-power spectral density in each branch is equal to $N_0/2$, then $E[\mid N_{ki} \mid^2] = N_0$. Because of its circular symmetry, N_{ki} has independent real and imaginary components with variance $N_0/2$. The conditional probability density function of y_{ki} given the values of l, α_i, and θ_i is

$$f(y_{ki}|l, \alpha_i, \theta_i) = \frac{1}{\pi N_0} \exp\left[-\frac{|y_{ki} - \sqrt{\mathcal{E}_s}\alpha_i e^{j\theta_i}\delta_{kl}|^2}{N_0}\right]. \tag{5.145}$$

For coherent FSK, the $\{\alpha_i\}$ and the $\{\theta_i\}$ are assumed to be known. Since the noise in each branch is assumed to be independent, the likelihood function is the product of qL densities given by (5.145) for $k = 1, 2, \ldots, q$ and $i = 1, 2, \ldots, L$. Forming the log-likelihood function, observing that $\sum_k \delta_{kl}^2 = 1$, and eliminating irrelevant terms and factors that are independent of l, we find that the maximization of the log-likelihood function is equivalent to selecting the largest of q metrics, one for each of $s_1(t), s_2(t), \ldots, s_q(t)$. The *maximum-likelihood metric for coherent FSK is*

$$U_l = \sum_{i=1}^{L} \mathrm{Re}\left(\alpha_i e^{-j\theta_i} y_{li}\right) , \quad l = 1, 2, \ldots, q. \tag{5.146}$$

These metrics have the disadvantage that they require phase synchronization in each branch and estimates of the $\{\alpha_i\}$.

Consider coherent binary frequency-shift keying (BFSK). Because of the symmetry of the model, $P_b(L)$ can be calculated by assuming that $s_1(t)$ was transmitted. With this assumption, the two decision variables become

$$U_1 = \sqrt{\mathcal{E}_b} \sum_{i=1}^{L} \alpha_i^2 + \sum_{i=1}^{L} \alpha_i N_{1i}^d \tag{5.147}$$

$$U_2 = \sum_{i=1}^{L} \alpha_i N_{2i}^d \tag{5.148}$$

where N_{1i}^d and N_{2i}^d are independent, real-valued, Gaussian noise variables given by

$$N_{ki}^d = \mathrm{Re}\left[e^{-j\theta_i} N_{ki}\right] , \quad k = 1, 2. \tag{5.149}$$

Because of the symmetry, the bit error probability is equal to the conditional bit error probability given that $x = +1$, corresponding to a transmitted 0. A decision error is made if $U_1 - U_2 < 0$. Since the decision variable $U_1 - U_2$ has a Gaussian conditional distribution, a standard evaluation indicates that the conditional bit error probability given the $\{\alpha_i\}$ is

$$P_{b|\boldsymbol{\alpha}}(\gamma_b) = Q(\sqrt{\gamma_b}) \tag{5.150}$$

where the SNR for the bit is given by (5.122). The bit error probability is determined by averaging $P_{b|\boldsymbol{\alpha}}(\gamma_b)$ over the distribution of γ_b, which depends on the $\{\alpha_i\}$ and embodies the statistics of the fading channel. Suppose that independent Rayleigh fading occurs so that each of the $\{\alpha_i\}$ is independent with the identical Rayleigh distribution and $E[\alpha_i^2] = E[\alpha_1^2]$. A derivation similar to the one for coherent BPSK indicates that (5.132) and (5.133) are again valid for coherent BFSK provided that

$$p = \frac{1}{2}\left(1 - \sqrt{\frac{\bar{\gamma}}{2 + \bar{\gamma}}}\right) \qquad \text{(coherent BFSK)} \tag{5.151}$$

where the average SNR per branch is defined by (5.124). Equation (5.151) can also be obtained by observing the presence of two independent noise variables and, hence, substituting $\bar{\gamma}/2$ in place of $\bar{\gamma}$ in (5.130). Thus, in a fading environment, BPSK retains its usual 3 dB advantage over coherent BFSK, although (5.139) indicates that both provide the same diversity order $D_o = L$ when $\bar{\gamma} \gg 1$.

The preceding analysis for independent, identical Rayleigh fading can be extended to independent Nakagami fading if the parameter m is a positive integer. From (5.29) and elementary probability, it follows that the probability density function of each random variable $\gamma_i = \mathcal{E}_b \alpha_i^2 / N_0$ is

$$f_{\gamma i}(x) = \frac{m^m}{(m-1)!\,\bar{\gamma}^m} x^{m-1} \exp\left(-\frac{mx}{\bar{\gamma}}\right) u(x), \quad m = 1, 2, \ldots \tag{5.152}$$

where $\bar{\gamma}$ is defined by (5.124). As indicated in Appendix B.2, the characteristic function of γ_i is

$$C_{\gamma i}(j\,\nu) = \frac{1}{(1 - j\frac{\bar{\gamma}}{m}\,\nu)^m}. \tag{5.153}$$

If γ_b in (5.122) is the sum of L independent, identically-distributed random variables, then it has the characteristic function

$$C_{\gamma}(j\,\nu) = \frac{1}{(1 - j\frac{\bar{\gamma}}{m}\,\nu)^{mL}}. \tag{5.154}$$

The inverse Fourier transform of this function yields the probability density function

$$f_{\gamma}(x) = \frac{1}{(mL-1)!\,(\bar{\gamma}/m)^{mL}} x^{mL-1} \exp\left(-\frac{m\,x}{\bar{\gamma}}\right) u(x), \; m = 1, 2, \ldots \tag{5.155}$$

The form of this expression is the same as that in (5.123) except that L and $\bar{\gamma}$ are replaced by mL and $\bar{\gamma}/m$, respectively. Consequently, the derivation following (5.123) is valid once the replacements are made, and

$$P_b(L) = p - (1-2p) \sum_{i=1}^{mL-1} \binom{2i-1}{i} [p(1-p)]^i \tag{5.156}$$

where

$$p = \frac{1}{2}\left(1 - \sqrt{\frac{\bar{\gamma}}{m + \bar{\gamma}}}\right) \quad \text{(BPSK, QPSK)} \tag{5.157}$$

$$p = \frac{1}{2}\left(1 - \sqrt{\frac{\bar{\gamma}}{2m + \bar{\gamma}}}\right) \quad \text{(coherent BFSK)}. \tag{5.158}$$

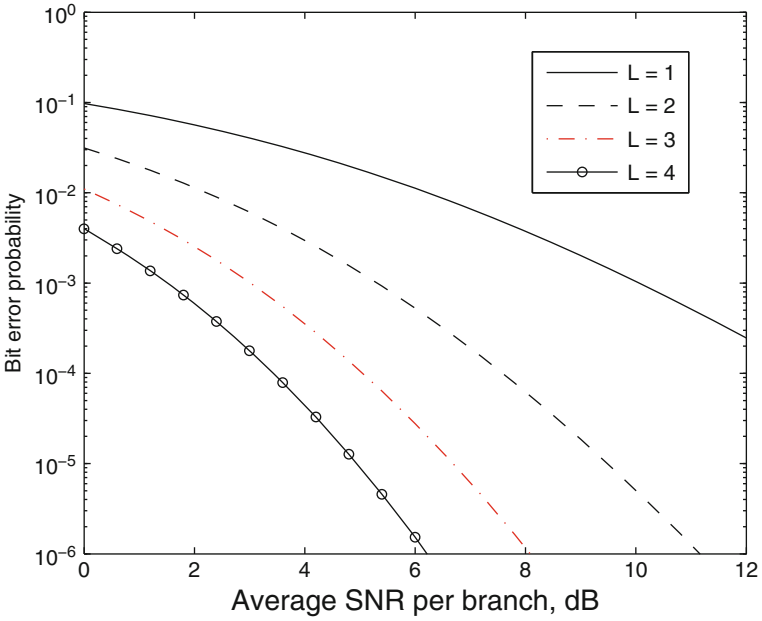

Fig. 5.10 Bit error probability of PSK for Nakagami fading with $m = 4$

The diversity order is $D_o = mL$ when $\bar{\gamma} \gg 1$. These results can be approximately related to Ricean fading by using (5.31). Figure 5.10 displays the bit error probability for Nakagami fading with $m = 4$, PSK, and $L = 1, 2, 3$, and 4 diversity branches.

5.4.4 *Equal-Gain Combining*

Let $\mathbf{x}$ and $\mathbf{y}$ denote $N \times 1$ vectors. Then $||\mathbf{x}-\alpha\mathbf{y}||^2 \geq 0$ for any complex scalar α. Expanding the squared norm and substituting $\alpha = \mathbf{x}^H\mathbf{y}/\,||\mathbf{x}||^2\,||\mathbf{y}||^2$, where $\mathbf{y} \neq \mathbf{0}$, we obtain the *Cauchy–Schwarz inequality for vectors*:

$$\left|\mathbf{x}^H\mathbf{y}\right| \leq ||\mathbf{x}|| \cdot ||\mathbf{y}|| \tag{5.159}$$

which is valid when $\mathbf{y} = \mathbf{0}$. Equality is achieved if and only if $\mathbf{x} = k\mathbf{y}$ for some complex scalar k. Let x_i and y_i denote the ith components of $\mathbf{x}$ and $\mathbf{y}$, respectively. Then substitution into (5.159) give the *Cauchy–Schwarz inequality for complex numbers or discrete-time sequences:*

$$\left|\sum_{i=1}^{N} x_i^* y_i\right| \leq \left(\sum_{i=1}^{N} |x_i|^2\right)^{1/2} \left(\sum_{i=1}^{N} |y_i|^2\right)^{1/2} \tag{5.160}$$

where equality is achieved if and only if $x_i = k y_i$, $i = 1, 2, \ldots, N$, for some complex scalar k.

Coherent equal-gain combining (EGC) performs cophasing, but does not compensate for unequal values of the SNR in each branch. Thus, when a narrowband desired signal experiences fading, instead of (5.101) and (5.90), the EGC weight vector is

$$\mathbf{W}_e = \eta[\exp(j\theta_1) \quad \exp(j\theta_2) \quad \ldots \quad \exp(j\theta_L)]^T \tag{5.161}$$

where θ_i is the phase shift of the desired signal in branch i. When MRC is optimal and the values of the $\{\alpha_i/\sigma_i^2\}$ are unequal, EGC is suboptimal, but requires much less information about the channel. If the interference plus noise in each array branch is zero-mean and uncorrelated with the other branches and $E[|n_i|^2] = \sigma^2, i = 1, 2, \ldots, L$, then $\mathbf{R}_{nn}$ is diagonal, and (5.78), (5.90), and (5.92) with $\mathbf{W} = \mathbf{W}_e$ give the output SINR

$$\rho_0 = \frac{p_s}{L\sigma^2}\left(\sum_{i=1}^{L}\alpha_i\right)^2. \tag{5.162}$$

It can be verified by applying the Cauchy–Schwarz inequality (5.160) that this SINR is less than or equal to $\rho_{\max}$ given by (5.106). Figure 5.8 displays EGC with predetection and postdetection combining if the factors $\{\alpha_i\}$ are omitted.

In a Rayleigh-fading environment, each α_i, $i = 1, 2, \ldots, L$, has a Rayleigh probability distribution function. If the desired signal in each array branch is uncorrelated with the other branches and has identical average power, then using (B.36), we obtain

$$E[\alpha_i^2] = E[\alpha_1^2], \quad E[\alpha_i] = \left\{\frac{\pi}{4}E[\alpha_1^2]\right\}^{1/2}, \; i = 1, 2, \ldots, L \tag{5.163}$$

$$E[\alpha_i\alpha_k] = E[\alpha_i]\,E[\alpha_k] = \frac{\pi}{4}E[\alpha_1^2], \; i \neq k. \tag{5.164}$$

These equations and (5.162) give

$$E[\rho_0] = \left[1 + (L-1)\frac{\pi}{4}\right]\frac{p_s}{\sigma^2}\,E[\alpha_1^2] \tag{5.165}$$

which exceeds $\pi/4$ times $E[\rho_{\max}]$ given by (5.107) for MRC. Thus, the loss associated with using EGC instead of MRC is on the order of 1 dB.

Example 5.2. In some environments, MRC is identical to EGC but distinctly suboptimal because of interference correlations among the branches. Consider narrowband desired and interference signals that do not experience fading and arrive as plane waves. The array antennas are sufficiently close that the steering vector $\mathbf{S}_0$ of the desired signal and the steering vector $\mathbf{J}_0$ of the interference signal can be represented by

$$\mathbf{S}_0 = \left[e^{-j2\pi f_0 \tau_1} \quad e^{-j2\pi f_0 \tau_2} \quad \ldots \quad e^{-j2\pi f_0 \tau_L}\right]^T \tag{5.166}$$

$$\mathbf{J}_0 = \left[e^{-j2\pi f_0 \delta_1} \quad e^{-j2\pi f_0 \delta_2} \quad \ldots \quad e^{-j2\pi f_0 \delta_L}\right]^T. \tag{5.167}$$

The correlation matrix for the interference plus noise is

$$\mathbf{R}_{nn} = \sigma^2 \, \mathbf{I} + p_i \, \mathbf{J}_0 \, \mathbf{J}_0^H \tag{5.168}$$

where σ^2 and p_i are the noise and interference powers, respectively, in each array branch. This equation shows explicitly that the interference in one branch is correlated with the interference in the other branches. A direct matrix multiplication using $\|\mathbf{J}_0\|^2 = L$ verifies that

$$\mathbf{R}_{nn}^{-1} = \frac{1}{\sigma^2}\left(\mathbf{I} - \frac{g \, \mathbf{J}_0 \mathbf{J}_0^H}{Lg + 1}\right) \tag{5.169}$$

where $g = p_i/\sigma^2$ is the interference-to-noise ratio in each array branch. After merging $1/\sigma^2$ with the constant in (5.98), it is found that the optimal weight vector is

$$\mathbf{W}_0 = \eta\left(\mathbf{S}_0 - \frac{\xi L g}{Lg + 1}\mathbf{J}_0\right) \tag{5.170}$$

where ξ is the normalized inner product

$$\xi = \frac{1}{L}\mathbf{J}_0^H \mathbf{S}_0. \tag{5.171}$$

The corresponding maximum SINR, which is calculated by substituting (5.166), (5.169), and (5.171) into (5.99), is

$$\rho_{\max} = L\,\gamma\left(1 - \frac{|\xi|^2 L g}{Lg + 1}\right) \tag{5.172}$$

where $\gamma = p_s/\sigma^2$ is the SNR in each branch. Equations (5.166), (5.167), and (5.171) indicate that $0 \le |\xi| \le 1$ and $|\xi| = 1$ if $L = 1$. Equation (5.172) indicates that $\rho_{\max}$ decreases as $|\xi|$ increases if $L \ge 2$ and is nearly directly proportional to L if $g \gg 1$.

Since the values of the SNRs in the branches are all equal, both MRC and EGC use the weight vector of (5.161) with $\theta_i = -2\pi f_c \tau_i, i = 1, 2, \ldots, L$, which gives $\mathbf{W} = \eta \mathbf{S}_0$. Substituting (5.92), (5.166)–(5.168), and (5.171) into (5.78) gives the SINR for MRC and EGC:

$$\rho_0 = \frac{L\,\gamma}{1 + |\xi|^2 L g}. \tag{5.173}$$

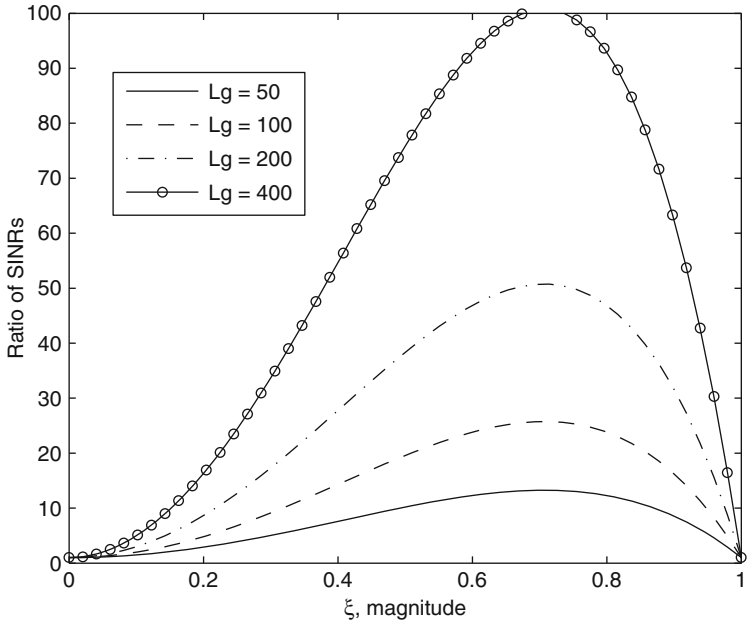

Fig. 5.11 Ratio of the maximum SINR to the maximal-ratio-combiner SINR

Both $\rho_{\max}$ and ρ_0 equal $L\gamma$, the peak value, when $\xi = 0$. They both equal $L\gamma/(1+Lg)$ when $|\xi| = 1$, which occurs when both the desired and interference signals arrive from the same direction or $L = 1$. Using calculus, it is determined that the maximum value of $\rho_{\max}/\rho_0$, which occurs when $|\xi| = 1/\sqrt{2}$, is

$$\left(\frac{\rho_{\max}}{\rho_0}\right)_{\max} = \frac{(Lg/2+1)^2}{Lg+1}, \quad L \geq 2. \tag{5.174}$$

This ratio approaches $Lg/4$ for large values of Lg. Thus, an adaptive array based on the maximization of the SINR has the potential to significantly outperform MRC or EGC if $Lg \gg 1$ under the conditions of the nonfading environment assumed. Figure 5.11 displays $\rho_{\max}/\rho_0$ as a function of $|\xi|$ for various values of Lg. □

When accurate phase estimation is unavailable so that neither cophasing nor coherent demodulation is possible, then postdetection combining following noncoherent demodulation can provide a significant performance improvement over a system with no diversity. For BFSK or MSK, postdetection combining with a frequency discriminator is illustrated in Fig. 5.12. Each IF signal is sampled, converted to a discrete-time complex baseband signal, and then demodulated by a digital frequency discriminator [7]. The square of the magnitude or possibly the magnitude of the discrete-time complex baseband signal is used to weight the output of each branch. If the noise power in each branch is approximately the same

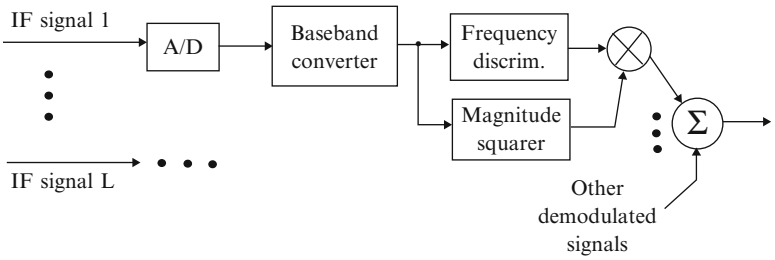

Fig. 5.12 Postdetection combining with frequency discriminator

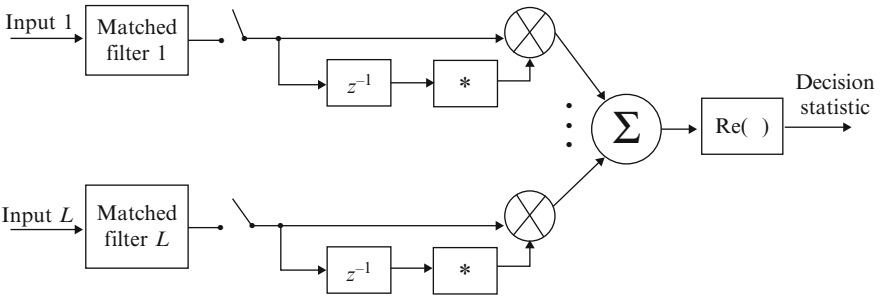

Fig. 5.13 Equal-gain combiner for DPSK with postdetection combining

and much smaller then the desired-signal power, then this weighting is a good approximation of the weighting used in MRC, but it is suboptimal since cophasing is absent.

An alternative is postdetection EGC. However, when the desired-signal power is very low in a branch, then that branch contributes only noise to the EGC output. This problem is eliminated if each branch has a threshold device that blocks the output of that branch if the desired-signal power falls below the threshold.

A block diagram of a DPSK receiver with postdetection EGC is depicted in Fig. 5.13. For equally likely binary symbols, the error probability is the same regardless of whether two consecutive symbols are the same or different. Assuming that they are the same and that the fading is constant over two symbols, the EGC decision variable is

$$U = \text{Re}\left[\sum_{i=1}^{L} y_{1i} y_{2i}^*\right] \tag{5.175}$$

where y_{1i} and y_{2i} are received symbols in branch i arising from two consecutive symbol intervals. This decision variable or metric has the advantage that it requires neither phase synchronization nor channel-state estimation. A derivation [2] indicates that if the $\{\alpha_i\}$ are independent but have identical Rayleigh distributions, then

$P_b(L)$ is given by (5.132), (5.133), and (5.136) with the single-branch bit error probability

$$p = \frac{1}{2(1+\bar{\gamma})} \quad (DPSK) \tag{5.176}$$

where $\bar{\gamma}$ is given by (5.124). Equation (5.176) can be directly derived by observing that the conditional bit error probability for DPSK with no diversity is $\frac{1}{2}\exp(-\gamma_b)$ and then integrating the equation over the density (5.123) with $L = 1$. DPSK provides the diversity order $D_o = L$ when $\bar{\gamma} \gg 1$. A comparison of (5.176) with (5.151) indicates that DPSK with EGC and coherent BFSK with MRC give nearly the same performance in a Rayleigh-fading environment if $\bar{\gamma} \gg 1$.

To derive a noncoherent FSK receiver from the maximum-likelihood criterion, we assume that the $\{\alpha_i\}$ and the $\{\theta_i\}$ in (5.144) are random variables. We expand the argument of the exponential function in (5.145), assume that θ_i is uniformly distributed over $[0, 2\pi)$, and integrate over the density of θ_i. The integral may be evaluated by expressing y_{ki} in polar form, using (B.30), and observing that the integral is over one period of a periodic integrand. Thus, we obtain the conditional density function

$$f(y_{ki}|l, \alpha_i) = \frac{1}{\pi N_0} \exp\left[-\frac{|y_{ki}|^2 + \mathcal{E}_s\alpha_i^2\delta_{kl}}{N_0}\right] I_0\left(\frac{2\sqrt{\mathcal{E}_s}\alpha_i|y_{ki}|\delta_{kl}}{N_0}\right). \tag{5.177}$$

Assuming that α_i has the Rayleigh probability density function given by (5.21) with $2\sigma_r^2 = E[\alpha_i^2]$, the density $f(y_{ki}|l)$ may be evaluated by using the identity (B.33). The likelihood function is the product of qL densities for $k = 1, 2, \ldots, q$, and $i = 1, 2, \ldots, L$. Forming the log-likelihood function and eliminating irrelevant terms and factors that are independent of l, we find that the maximization of the log-likelihood function is equivalent to selecting the largest of q branch metrics. The maximum-likelihood branch metric is

$$U_l = \sum_{i=1}^{L} |y_{li}|^2 \left(\frac{\bar{\gamma}_i}{1+\bar{\gamma}_i}\right), \quad l = 1, 2, \ldots, q \tag{5.178}$$

where

$$\bar{\gamma}_i = \frac{\mathcal{E}_s}{N_0} E[\alpha_i^2], \quad i = 1, 2, \ldots, L. \tag{5.179}$$

Thus, maximum-likelihood detection requires the estimation of $\bar{\gamma}_i$ for each branch. If it is assumed that all the $\{\bar{\gamma}_i\}$ are equal, then we obtain the *Rayleigh metric*:

$$U_l = \sum_{i=1}^{L} |y_{li}|^2, \quad l = 1, 2, \ldots, q. \tag{5.180}$$

This metric implies a noncoherent FSK receiver with postdetection square-law EGC, which is illustrated in Fig. 5.14. Each branch contains filters matched to the equal-energy orthogonal signals $s_1(t), s_2(t), \ldots, s_q(t)$.

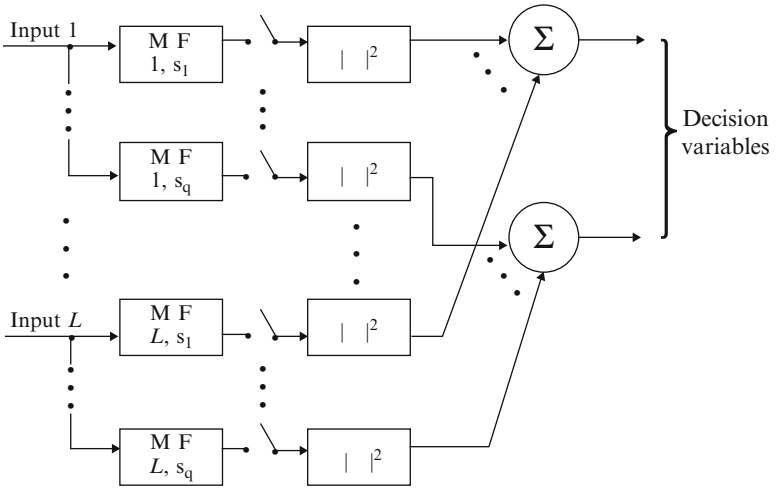

Fig. 5.14 Equal-gain combiner for noncoherent FSK with postdetection combining

A major advantage of the Rayleigh metric is that it does not require knowledge of $\bar{\gamma}_i$ or any channel state information. If the $\{\bar{\gamma}_i\}$ are unequal, then the Rayleigh metric is inferior to the maximum-likelihood metric of (5.178). However, when $\bar{\gamma}_i$ is large, the corresponding terms in the two metrics are nearly equal; when $\bar{\gamma}_i$ is small, the corresponding terms in the two metrics both tend to be insignificant. Thus, there is little penalty in using the Rayleigh metric, as is confirmed by numerical evaluations [1].

Consider noncoherent BFSK. Because of the symmetry of the signals, $P_b(L)$ can be calculated by assuming that $s_1(t)$ was transmitted. Given that $s_1(t)$ was transmitted, the two decision variables at the combiner output are

$$\begin{aligned} U_1 &= \sum_{i=1}^{L} |\sqrt{\mathcal{E}_b}\alpha_i e^{j\theta_i} + N_{1i}|^2 \\ &= \sum_{i=1}^{L} \left(\sqrt{\mathcal{E}_b}\alpha_i \cos\theta_i + N_{1i}^R\right)^2 + \sum_{i=1}^{L} \left(\sqrt{\mathcal{E}_b}\alpha_i \sin\theta_i + N_{1i}^I\right)^2 \end{aligned} \tag{5.181}$$

$$U_2 = \sum_{i=1}^{L} |N_{2i}|^2 = \sum_{i=1}^{L} \left(N_{2i}^R\right)^2 + \sum_{i=1}^{L} \left(N_{2i}^I\right)^2 \tag{5.182}$$

where N_{1i} and N_{2i} are the independent, complex-valued, zero-mean, Gaussian noise variables and N_{ki}^R and N_{ki}^I are the real and imaginary parts of N_{ki}, respectively. Assuming that the noise-power spectral density in each branch is equal to N_0, then

$E[|\ N_{ki}\ |^2] = N_0$. Because of its circular symmetry, N_{ki} has independent real and imaginary components, and

$$E[(N_{ki}^R)^2] = E[(N_{ki}^I)^2] = N_0/2, \quad k = 1, 2, \quad i = 1, 2, \ldots, L. \tag{5.183}$$

When independent, identically distributed, Rayleigh fading occurs in each branch, $\alpha_i \cos\theta_i$ and $\alpha_i \sin\theta_i$ are zero-mean, independent, Gaussian random variables with the same variance equal to $E[\alpha_i^2]/2 = E[\alpha_1^2]/2$, $i = 1, 2, \ldots, L$, as shown in Sect. B.4. Therefore, both U_1 and U_2 have central chi-square distributions with $2L$ degrees of freedom. From (B.18), the density function of U_k is

$$f_k(x) = \frac{1}{(2\sigma_k^2)^L (L-1)!} x^{L-1} \exp\left(-\frac{x}{2\sigma_k^2}\right) u(x), \quad k = 1, 2 \tag{5.184}$$

where (5.183) and (5.124) give

$$\sigma_2^2 = E[(N_{2i}^R)^2] = N_0/2 \tag{5.185}$$

$$\sigma_1^2 = E[(\sqrt{\mathcal{E}_b}\alpha_1 \cos\theta_i + N_{Ii}^R)^2] = N_0(1 + \bar{\gamma})/2. \tag{5.186}$$

Since an erroneous decision is made if $U_2 > U_1$,

$$P_b(L) = \int_0^\infty \frac{x^{L-1} \exp\left(-\frac{x}{2\sigma_1^2}\right)}{(2\sigma_1^2)^L (L-1)!} \left[\int_x^\infty \frac{y^{L-1} \exp\left(-\frac{y}{2\sigma_2^2}\right)}{(2\sigma_2^2)^L (L-1)!}\, dy \right] dx. \tag{5.187}$$

Using (5.127) inside the brackets and integrating, we obtain

$$P_b(L) = \int_0^\infty \exp\left(-\frac{x}{2\sigma_1^2}\right) \sum_{i=0}^{L-1} \frac{(x/2\sigma_2^2)^i}{i!} \frac{x^{L-1} \exp\left(-\frac{x}{2\sigma_2^2}\right)}{(2\sigma_1^2)^L (L-1)!}\, dx. \tag{5.188}$$

Changing variables, applying (B.12) of Appendix B, and simplifying gives (5.133), where the bit error probability for $L = 1$ is

$$p = \frac{1}{2 + \bar{\gamma}} \qquad \text{(noncoherent BFSK)} \tag{5.189}$$

and $\bar{\gamma}$ is given by (5.124). Thus, $P_b(L)$ is once again given by (5.132), and the diversity order is $D_o = L$ when $\bar{\gamma} \gg 1$. Equations (5.189) and (5.176) indicate that 3 dB more power is needed for noncoherent BFSK to provide the same performance as DPSK. As discussed subsequently in Chap. 6, the performance of DPSK is approximately equaled by using MSK and the configuration shown in Fig. 5.12.

Equation (5.132) is valid for MRC and BPSK or coherent BFSK and also for EGC and DPSK or noncoherent BFSK. Once the bit error probability in the absence of diversity combining, p, is determined, the bit error probability for

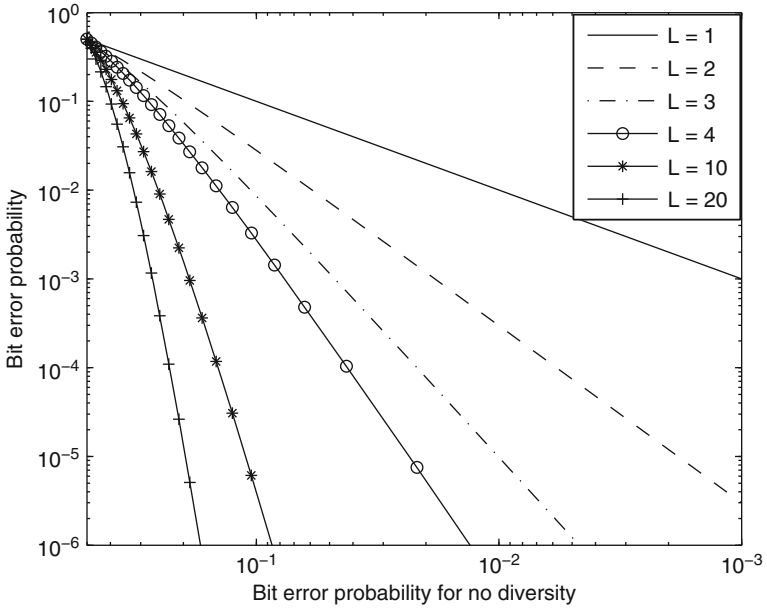

Fig. 5.15 Bit error probability for MRC with PSK and coherent FSK and for EGC with DPSK and noncoherent FSK

diversity combining in the presence of independent Rayleigh fading, $P_b(L)$, can be calculated from (5.132). A plot of $P_b(L)$ versus p for different values of L is displayed in Fig. 5.15. This figure illustrates the diminishing returns obtained as L increases. A plot of $P_b(L)$ versus $\bar{\gamma}$, the SNR per branch for one bit, is displayed in Fig. 5.16 for MRC with BPSK and EGC with DPSK and noncoherent BFSK. The plot for MRC with coherent BFSK is nearly the same as that for EGC with DPSK. Since (5.136) is valid for all these modulations, we find that $P_b(L)$ is asymptotically proportional to $\bar{\gamma}^{-L}$ with only the proportionality constant differing among the modulation types.

For noncoherent q-ary orthogonal signals such as FSK with $L \geq 2$, it can be shown that the symbol error probability $P_s(L)$ decreases slightly as q increases [2]. The price for this modest improvement is an increase is transmission bandwidth.

5.4.5 Selection Diversity

A *selection-diversity system* or *predetection selection-combining system* selects the diversity branch that has the largest SNR and forwards the signal in this branch for further processing. In a fading environment, selection diversity is sensible only if the selection rate is much faster than the fading rate. If the noise and interference levels in all the branches are nearly the same, then the total signal-plus-noise power in each branch rather than the SNR can be measured to enable the selection process,

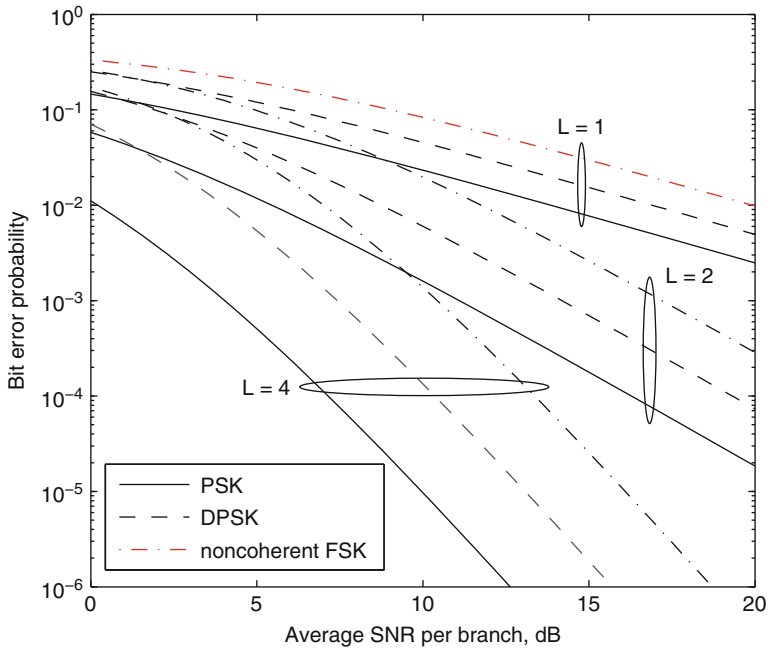

Fig. 5.16 Bit error probability for MRC with PSK and for EGC with DPSK and noncoherent FSK

thereby allowing a major simplification. Selection diversity does not provide a performance as good as MRC or EGC when the interference plus noise in each branch is uncorrelated with that in the other branches. However, selection diversity requires only a single demodulator, and when noises or interference signals are correlated, then selection diversity may become more competitive.

The average power of the desired-signal component of the complex envelope in each diversity branch is $p_s = E[|s(l)|^2]$. If the noise in each diversity branch is zero-mean and $E[|n_i|^2] = \sigma_i^2$, then the SNR in branch i is $\rho_i = \mathcal{E}_s\alpha_i^2/\sigma_i^2$. If each of the $\{\alpha_i\}$ has a Rayleigh distribution and $\sigma_i^2 = \sigma^2$, $i = 1, 2, \ldots, L$, then the SNR in each branch has the same expected value

$$\bar{\rho} = \frac{p_s}{\sigma^2} E[\alpha_1^2]. \tag{5.190}$$

The results of Appendix B.4 for the square of a Rayleigh-distributed random variable indicate that each SNR has the exponential probability density function

$$f_\rho(x) = \frac{1}{\bar{\rho}} \exp\left(-\frac{x}{\bar{\rho}}\right) u(x). \tag{5.191}$$

The corresponding probability distribution function is

$$F_\rho(x) = \left[1 - \exp\left(-\frac{x}{\bar{\rho}}\right)\right] u(x). \tag{5.192}$$

The branch with the largest SNR is selected. Let ρ_0 denote the SNR of the selected branch:

$$\rho_0 = \frac{p_s}{N_0} \max_i \left(\alpha_i^2\right). \tag{5.193}$$

The probability that ρ_0 is less than or equal to x is equal to the probability that all the branch SNRs are simultaneously less than or equal to x. If the interference plus noise in each branch is independent, the probability distribution function of ρ_0 is

$$F_{\rho 0}(x) = \left[1 - \exp\left(-\frac{x}{\bar{\rho}}\right)\right]^L u(x). \tag{5.194}$$

The corresponding probability density function is

$$f_{\rho 0}(x) = \frac{L}{\bar{\rho}} \exp\left(-\frac{x}{\bar{\rho}}\right)\left[1 - \exp\left(-\frac{x}{\bar{\rho}}\right)\right]^{L-1} u(x). \tag{5.195}$$

The average SNR obtained by selection diversity is calculated by integrating the SNR over the density given by (5.195). The result is

$$\begin{aligned} E[\rho_0] &= \int_0^\infty \frac{L}{\bar{\rho}} x \exp\left(-\frac{x}{\bar{\rho}}\right)\left[1 - \exp\left(-\frac{x}{\bar{\rho}}\right)\right]^{L-1} dx \\ &= \bar{\rho} L \int_0^\infty x e^{-x} \left(\sum_{i=0}^{L-1} \binom{L-1}{i} (-1)^i e^{-xi}\right) dx \\ &= \bar{\rho} \sum_{i=1}^{L} \binom{L}{i} \frac{(-1)^{i+1}}{i}. \end{aligned} \tag{5.196}$$

The second equality results from a change of variable and the substitution of the binomial expansion. The third equality results from a term-by-term integration using (B.12) and an algebraic simplification. Substituting (5.190) and applying the method of mathematical induction to prove a series identity, we obtain

$$E[\rho_0] = \frac{p_s}{\sigma^2} E[\alpha_1^2] \sum_{i=1}^{L} \frac{1}{i}. \tag{5.197}$$

Thus, the average SNR for selection diversity with $L \geq 2$ is less than that for MRC and EGC, as indicated by (5.107) and (5.165), respectively. Approximating the summation in (5.197) by an integral, it is observed that the ratio of the average SNR for MRC to that for selection diversity is approximately $L/\ln L$ for $L \geq 2$.

Suppose that the modulation is BPSK and optimal coherent demodulation follows the selection process. Then the conditional bit error probability given the value of ρ_0 is

$$P_{b|\boldsymbol{\rho}}(\rho_0) = Q(\sqrt{2\rho_0}) \tag{5.198}$$

and $p_s = \mathcal{E}_b$. Therefore, using the binomial expansion, the bit error probability is

$$P_b(L) = \int_0^\infty Q(\sqrt{2x}) \frac{L}{\bar{\gamma}} \exp\left(-\frac{x}{\bar{\gamma}}\right) \left[1 - \exp\left(-\frac{x}{\bar{\gamma}}\right)\right]^{L-1} dx$$
$$= \sum_{i=0}^{L-1} \binom{L-1}{i} (-1)^i \frac{L}{\bar{\gamma}} \int_0^\infty Q(\sqrt{2x}) \exp\left[-x\left(\frac{1+i}{\bar{\gamma}}\right)\right] dx \quad (5.199)$$

where

$$\bar{\gamma} = \frac{\mathcal{E}_b}{N_0} E[\alpha_1^2]. \quad (5.200)$$

The last integral in (5.199) can be evaluated in the same manner as the one in (5.125). After regrouping factors and using the fact that $\sum_{i=0}^{n} \binom{n}{i} (-1)^i = (1-1)^i = 0$, the result is

$$P_b(L) = \frac{1}{2} \sum_{i=1}^{L} \binom{L}{i} (-1)^i \sqrt{\frac{\bar{\gamma}}{i+\bar{\gamma}}} \qquad \text{(BPSK, QPSK)}. \quad (5.201)$$

This equation is valid for QPSK since it can be implemented as two parallel BPSK waveforms.

To obtain the diversity order, we use the upper bound $[1 - \exp(-x)]^{L-1} \leq x^{L-1}$, $x \geq 0$, which is proved by using a Taylor-series expansion with a remainder. Substitution of this bound into the integral in (5.199) indicates that $P_b(L)$ is upper bounded by $L!$ times the right-hand side of (5.125). Therefore, a derivation similar to the one leading to (5.137) yields

$$P_b(L) \leq L! \binom{2L-1}{L} \left(\frac{1}{4^L}\right) \bar{\gamma}^{-L}, \quad \bar{\gamma} > 1 \quad (5.202)$$

which indicates that the diversity order is $D_o = L$ when $\bar{\gamma} > 1$. Thus, selection combining provides the same diversity order as MRC, but a bit error probability that is roughly $L!$ larger when $\bar{\gamma} \gg 1$.

For coherent BFSK, the conditional bit error probability is $P_{b|\boldsymbol{\rho}}(\rho_0) = Q(\sqrt{\rho_0})$. Therefore, it is found that

$$P_b(L) = \frac{1}{2} \sum_{i=1}^{L} \binom{L}{i} (-1)^i \sqrt{\frac{\bar{\gamma}}{2i+\bar{\gamma}}} \qquad \text{(coherent BFSK)}. \quad (5.203)$$

Again, 3 dB more power is needed to provide to the same performance as BPSK, and the diversity order is $D_o = L$ when $\bar{\gamma} > 1$.

When DPSK is the data modulation, the conditional bit error probability is $\exp(-\gamma_b)/2$. Thus, selection diversity provides the bit error probability

$$P_b(L) = \int_0^\infty \frac{L}{2\bar{\gamma}} \exp\left[\left(-x\frac{1+\bar{\gamma}}{\bar{\gamma}}\right)\right]\left[1-\exp\left(-\frac{x}{\bar{\gamma}}\right)\right]^{L-1} dx. \tag{5.204}$$

The *beta function* is defined as

$$B(x,y) = \int_0^1 t^{x-1}(1-t)^{y-1}\, dt\,, \quad x>0, \quad y>0. \tag{5.205}$$

If y is a positive integer n, then the substitution of the binomial expansion of $(1-t)^{n-1}$ and the evaluation of the resulting integral yields

$$B(x,n) = \sum_{i=0}^{n-1} \binom{n-1}{i} \frac{(-1)^i}{i+x}, \quad n \geq 1, \quad x>0. \tag{5.206}$$

Using $t = \exp(-x/\bar{\gamma})$ to change the integration variable in (5.204) and then using (5.205) gives

$$P_b(L) = \frac{L}{2} B(\bar{\gamma}+1, L) \qquad \text{(DPSK)}. \tag{5.207}$$

For noncoherent FSK, the conditional symbol error probability given the value of ρ_0 is obtained from (1.99):

$$P_{s|\boldsymbol{\rho}}(\rho_0) = \sum_{i=1}^{q-1} \frac{(-1)^{i+1}}{i+1} \binom{q-1}{i} \exp\left(-\frac{i\rho_0}{i+1}\right). \tag{5.208}$$

Therefore, a derivation similar to that of (5.207) yields the symbol error probability

$$P_s(L) = L\sum_{i=1}^{q-1} \frac{(-1)^{i+1}}{i+1} \binom{q-1}{i} B\left(1+\frac{i\bar{\gamma}}{i+1}, L\right) \qquad \text{(noncoherent FSK)}. \tag{5.209}$$

For BFSK, the bit error probability is

$$P_b(L) = \frac{L}{2} B\left(\frac{\bar{\gamma}}{2}+1, L\right) \qquad \text{(noncoherent BFSK)} \tag{5.210}$$

which exhibits the usual 3 dB disadvantage compared with DPSK.

Asymptotic forms of (5.207) and (5.210) may be obtained by substituting

$$B(a,b) = \frac{\Gamma(a)\Gamma(b)}{\Gamma(a+b)}. \tag{5.211}$$

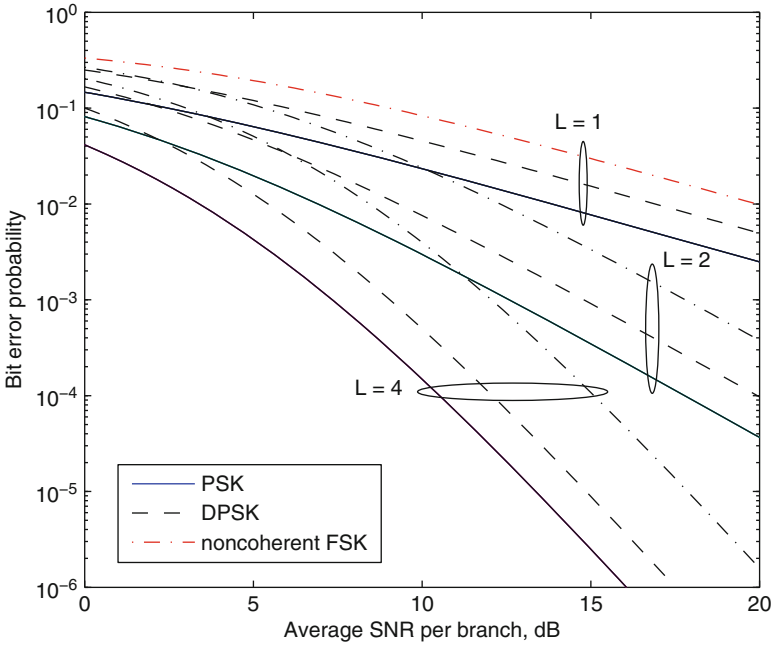

Fig. 5.17 Bit error probability for selection diversity with PSK, DPSK, and noncoherent FSK

To prove this identity, let $y = z^2$ in the integrand of the gamma function defined in (B.12) of Appendix B. Express the product $\Gamma(a)\Gamma(b)$ as a double integral, change to polar coordinates, integrate over the radius to obtain a result proportional to $\Gamma(a + b)$, and then change the variable in the remaining integral to obtain $B(a, b)\Gamma(a+b)$.

For DPSK, the substitution of (5.211) and (5.176) into (5.207) and the use of $\Gamma(\bar{\gamma} + L + 1) = (\bar{\gamma} + L)(\bar{\gamma} + L - 1) \ldots (\bar{\gamma} + 1)\Gamma(\bar{\gamma} + 1) \geq (\bar{\gamma} + 1)^L \Gamma(\bar{\gamma} + 1)$ give

$$P_b(L) \leq 2^{L-1} L \,!\, p^L. \tag{5.212}$$

For noncoherent BFSK, a similar derivation using (5.189) and (5.210) yields the same upper bound, which is tight when $\bar{\gamma} \gg L$. The upper bound on $P_b(L)$ for DPSK and noncoherent BFSK with EGC is given by (5.136). Comparing the latter with (5.212) indicates the disadvantage of selection diversity relative to EGC when $\bar{\gamma} \gg L$ and $L \geq 2$.

Figure 5.17 shows $P_b(L)$ as a function of the average SNR per branch, assuming selection diversity with BPSK, DPSK, and noncoherent BFSK. A comparison of Figs. 5.17 and 5.16 indicates the reduced gain provided by selection diversity relative to MRC and EGC.

A fundamental limitation of selection diversity is made evident by the plane-wave example in which the signal and interference steering vectors are given by (5.166) and (5.167). In this example, the SNRs are equal in all the diversity branches.

Consequently, selection diversity can give no better performance than no diversity combining or the use of a single branch. In contrast, (5.173) indicates that EGC can improve the SINR significantly.

Other types of selection diversity besides predetection selection combining are sometimes of interest. *Postdetection selection combining* entails the selection of the diversity branch with the largest signal plus noise power after detection. It outperforms predetection selection combining in general but requires as many matched filters as diversity branches. Thus, its complexity is not much less than that required for EGC. *Switch-and-stay combining (SSC)* or *switched combining* entails processing the output of a particular diversity branch as long as its quality measure remains above a fixed threshold. When it does not, the receiver selects another branch output and continues processing this output until the quality measure drops below the threshold. In *predetection SSC*, the quality measure is the instantaneous SNR of the connected branch. Since only one SNR is measured, predetection SSC is less complex than selection combining but suffers a performance loss. In *postdetection SSC*, the quality measure is the same output quantity used for data detection. The optimal threshold depends on the average SNR per branch. Postdetection SSC provides a lower bit error rate than predetection SSC, and the improvement increases with both the average SNR and less severe fading [1].

5.4.6 Transmit Diversity

Spatial diversity may be implemented as either *transmit diversity*, which uses an antenna array at the transmitter, *receive diversity*, which uses an array at the receiver, or both. Receive diversity is more effective than transmit diversity because the latter requires a power division among the transmit antennas prior to transmission. However, economics and practical issues may motivate the use of transmit diversity. For example, since multiple antennas are much more feasible at a base station than at a mobile, transmit diversity is usually the only type of spatial diversity in the downlink from a base station to a mobile (Chap. 8).

Delay diversity, frequency-offset diversity, and transmit beamforming are elementary forms of transmit diversity [6] that have significant practical limitations. *Delay diversity* entails the transmission of the same symbol successively from multiple antennas after appropriate delays. The received signal is equivalent to a set of artificial multipath signals that are generated at considerable cost in power and cause multiple-access interference in other systems. *Frequency-offset diversity* transforms the spatial diversity into time diversity by requiring each transmit antenna to use a different carrier frequency. The main practical issue is the bandwidth expansion. *Transmit beamforming* entails the use of weights by the transmit antennas to steer a beam in the direction of the receiver. However, feedback from the receiver is required to appropriately choose the weights.

Orthogonal transmit diversity, which is included in the CDMA2000 standard, transmits alternating even and odd symbols on two antennas. The diversity gain

from this method stems from the increased diversity embedded in the codewords or trellis paths by the deinterleaved bits generated by the different antennas. The gain relative to no diversity is substantial provided that the fading is slow and the channel code is strong [8].

Space-time codes transmitted by multiple antennas improve the performance of a communication system in a fading environment without the need for multiple receive antennas or channel-state information at the transmitter [2, 6, 9]. Space-time codes include *space-time block codes* and *space-time trellis codes*. The Alamouti code is by far the most widely used space-time code and is included in the CDMA2000 standard. The *Alamouti code* is the an orthogonal space-time block code (STBC) that uses two transmit antennas and provides full diversity at full transmission rate and maximum-likelihood decoding that entails only linear processing. However, rate-1 orthogonal STBCs for complex constellations exist only for two transmit antennas. Orthogonal STBCs for more than two transmit antennas require a code rate that is less than unity, which implies a reduced spectral efficiency.

The Alamouti STBC uses two antennas and two signaling intervals to transmit two complex symbols from a PSK or QAM constellation. The transmitted space-time codeword of length two has a code rate equal to one, the number of information symbols conveyed per signaling interval. A direct-sequence system multiplies each symbol by a spreading sequence prior to the modulation and transmission. Let $p_1(t)$ and $p_2(t)$ denote the spreading sequences used during successive signaling intervals. The 2×2 *generator matrix* representing a transmitted codeword for information symbols d_1 and d_2 is

$$\mathbf{G} = \begin{bmatrix} d_1 p_1(t) & d_2 p_1(t) \\ -d_2^* p_2(t) & d_1^* p_2(t) \end{bmatrix} \tag{5.213}$$

where each row identifies the symbols transmitted during a signaling interval, and each column identifies the successive symbols transmitted by one of the antennas.

Assuming a single receive antenna, the demodulated signal during the first observation interval is $r_1(t) = h_1 d_1 p_1(t) + h_2 d_2 p_1(t) + n_1(t)$, where h_i, $i = 1, 2$, is the complex channel response from transmit antenna i to the receive antenna, and $n_1(t)$ is a complex, zero-mean, white Gaussian noise process. After despreading, sampling, and an amplitude normalization, the observation at the end of the first signaling interval is $r_1 = h_1 d_1 + h_2 d_2 + n_1$, where n_1 is complex zero-mean Gaussian noise. Similarly, assuming that the channel does not change during two signaling intervals, the observation at the end of the second signaling interval is $r_2 = -h_1 d_2^* + h_2 d_1^* + n_2$, where n_2 is complex zero-mean Gaussian noise that is independent of n_1. These two observations are combined in the vector $\mathbf{y}_r = \left[r_1 \; r_2^*\right]^T$. Then

$$\mathbf{y}_r = \mathbf{H}\mathbf{d} + \mathbf{n} \tag{5.214}$$

where

$$\mathbf{H} = \begin{bmatrix} h_1 & h_2 \\ -h_2^* & -h_1^* \end{bmatrix} \tag{5.215}$$

and $\mathbf{n} = \begin{bmatrix} n_1 & n_2^* \end{bmatrix}^T$. Let $\mathcal{E}_s$ denote the average energy per symbol transmitted by both transmit antennas. Then $E\left[|d_k|^2\right] = \mathcal{E}_s/2, k = 1, 2$. In the presence of additive white Gaussian noise with spectral-density $N_0/2$, $\mathbf{n}$ is the zero-mean noise vector with covariance matrix $E\left[\mathbf{n}\mathbf{n}^H\right] = N_0\mathbf{I}$.

The matrix $\mathbf{H}$ satisfies the *orthogonality condition*:

$$\mathbf{H}^H\mathbf{H} = ||\mathbf{h}||^2\mathbf{I} \tag{5.216}$$

where $||\mathbf{h}||$ denotes the Euclidean norm of $\mathbf{h}$ and $\mathbf{I}$ is the 2×2 identity matrix. The receiver computes the 2×1 vector

$$\mathbf{y} = \mathbf{H}^H\mathbf{y}_r = \mathbf{d}||\mathbf{h}||^2 + \mathbf{n}_1 \tag{5.217}$$

where $E\left[\mathbf{n}_1\mathbf{n}_1^H\right] = N_0||\mathbf{h}||^2\mathbf{I}$. Because the orthogonality condition is satisfied, (5.217) indicates that the maximum-likelihood decision for d_k is separately obtained by finding the value of d_k that minimizes $\left|y_k - d_k||\mathbf{h}||^2\right|, k = 1, 2$. Since each noise component is independent, each symbol decision is decoupled from the other one, and there is no intersymbol interference. Let $\alpha_i = |h_i|$. Then

$$y_k = d_k \sum_{i=1}^{2} \alpha_i^2 + n_{1k}, \quad k = 1, 2 \tag{5.218}$$

which has the same form as MRC and indicates order-2 diversity. Thus, the bit error probabilities for BPSK, DPSK, and QPSK in the preceding section are valid with one important change. Since $E\left[|d_k|^2\right] = \mathcal{E}_s/2$, $\bar{\gamma}$ must be replaced by $\bar{\gamma}/2$ in the equations applicable to fading. The ultimate source of the change is the power splitting between the two transmit antennas.

The Alamouti STBC with generator matrix given by (5.213) provides order-$2L$ diversity when there are L receive antennas. Let $\mathbf{h}_i, i = 1, 2$, denote an $L \times 1$ vector, each component of which is the complex channel response from transmit antenna i to a receive antenna. The observation at the end of the first signaling interval is the $L \times 1$ vector $\mathbf{r}_1 = \mathbf{h}_1 d_1 + \mathbf{h}_2 d_2 + \mathbf{n}_{a1}$, where each component of $\mathbf{n}_{a1}$ is complex zero-mean Gaussian noise. Similarly, assuming that the channel does not change during two signaling intervals, the observation at the end of the second signaling interval is $\mathbf{r}_2 = -\mathbf{h}_1 d_2^* + \mathbf{h}_2 d_1^* + \mathbf{n}_{a2}$, where each component of $\mathbf{n}_{a2}$ is complex zero-mean Gaussian noise, and all components of $\mathbf{n}_{a1}$ and $\mathbf{n}_{a2}$ are independent of each other. These two observations are combined in the vector $\mathbf{y}_r = \begin{bmatrix} \mathbf{r}_1 & \mathbf{r}_2^* \end{bmatrix}^T$. Then (5.214) is applicable with the $2L \times 1$ noise vector $\mathbf{n} = \begin{bmatrix} \mathbf{n}_{a1} & \mathbf{n}_{a2}^* \end{bmatrix}^T$ and the $2L \times 2$ matrix

$$\mathbf{H} = \begin{bmatrix} \mathbf{h}_1 & \mathbf{h}_2 \\ -\mathbf{h}_2^* & -\mathbf{h}_1^* \end{bmatrix}. \tag{5.219}$$

The noise vector $\mathbf{n}$ is zero-mean with the $2L \times 2L$ covariance matrix $E\left[\mathbf{n}\mathbf{n}^H\right] = N_0\mathbf{I}$, where is $\mathbf{I}$ the $2L \times 2L$ identity matrix. The orthogonality condition (5.216) is satisfied if $||\mathbf{h}||$ denotes the norm of the $2L \times 1$ channel vector $\mathbf{h} = \left[\mathbf{h}_1^T \ \mathbf{h}_2^T\right]^T$ for which $||\mathbf{h}||^2 = ||\mathbf{h}_1||^2 + ||\mathbf{h}_2||^2$. The receiver computes the 2×1 vector given by (5.217), and the maximum-likelihood decision for d_k is separately obtained by finding the value of d_k that minimizes $\left|y_k - d_k||\mathbf{h}||^2\right|, k = 1, 2$. Let $\alpha_i = |h_i|$. Then

$$y_k = d_k \sum_{i=1}^{2L} \alpha_i^2 + n_{1k}, \quad k = 1, 2 \tag{5.220}$$

which has the same form as MRC and indicates order-$2L$ diversity and no intersymbol interference. Again the bit error probabilities for BPSK, DPSK, and QPSK in the preceding section are valid if $\bar{\gamma}$ is replaced by $\bar{\gamma}/2$ in the equations applicable to fading.

STBCs exist that can provide full diversity at full rate but require more complex decoding than the decoupled decoding of each real-valued symbol that is possible with orthogonal STBCs [9]. Nearly orthogonal, full rate STBCs exist that use the decoupled decoding at the cost of a performance loss only at high SNRs [10]. When the spectral efficiency is specified, an efficient outer code is used, and the fading is severe, these codes provide better performance than orthogonal STBCs.

5.5 Channel Codes

If the channel symbols are interleaved to a depth beyond the coherence time of the channel, then the symbols fade independently. As a result, a channel code provides a form of time diversity for direct-sequence systems. Interleaving over many hop intervals enables a channel code to provide a form of frequency diversity for frequency-hopping systems with frequency channels separated by more than the coherence bandwidth of the channel.

The subsequent analysis for BPSK is applicable to direct-sequence signals if it is assumed that the despread interference and noise are well approximated by white Gaussian noise. With this assumption, the analysis may be applied by substituting N_{0e}, the equivalent noise-power spectral density, in place of N_0 in the subsequent results.

Consider an (n, k) linear block code with soft-decision decoding, where n is the number of code symbols and k is the number of information symbols. For BPSK over a fading channel in which the fading is constant over a symbol interval, the received signal representing symbol i of codeword l is

$$r_i(t) = \mathrm{Re}\left[\sqrt{\mathcal{E}_s}\alpha_i e^{j\theta_i} x_{li}\psi(t)e^{j2\pi f_c t}\right] + n_i(t), \quad i = 1, 2, \ldots, n, \quad l = 1, 2, \ldots, 2^k \tag{5.221}$$

where α_i is a random variable that includes the effects of the fading, $x_{li} = +1$ when binary symbol i is a 1 and $x_{li} = -1$ when binary symbol i is a 0, $\mathcal{E}_s$ is the desired-signal energy per symbol in the absence of fading and diversity combining, and $\psi(t)$ is the unit-energy symbol waveform. When codeword l is received in the presence of white Gaussian noise, it is downconverted, and then the matched-filter or correlator, which is matched to $\psi(t)$, produces symbol-rate samples. A derivation similar to that following (1.40) in Sect. 1.1 indicates that the matched filter for symbol i produces the sample

$$y_i = \sqrt{\mathcal{E}_s}\alpha_i e^{j\theta_i} x_{li} + N_i, \quad i = 1, 2, \ldots, n \tag{5.222}$$

where N_i is an independent, zero-mean, complex Gaussian random variable. Since $\psi(t)$ is the sole basis function for the signal space, these samples provide sufficient statistics; that is, they contain all the relevant information in the received signal [6].

If the noise-power spectral density during each symbol interval is equal to $N_0/2$, then $E[|\ N_i\ |^2] = N_0$. Because of its circular symmetry, N_i has independent real and imaginary components with variance $N_0/2$. Therefore, the conditional probability density function of y_i given the values of x_{li}, α_i, and θ_i is,

$$f(y_i|x_{li}, \alpha_i, \theta_i) = \frac{1}{\pi N_0} \exp\left[- \frac{|y_i - \sqrt{\mathcal{E}_s}\alpha_i e^{j\theta_i} x_{li}|^2}{N_0} \right], \quad i = 1, 2, \ldots, n,$$
$$l = 1, 2, \ldots, 2^k. \tag{5.223}$$

In the subsequent analysis, it is always assumed that perfect symbol interleaving or sufficiently fast fading ensures the statistical independence of the demodulator outputs so that the log-likelihood function for the vector $\mathbf{y} = (y_1\ y_2\ \ldots\ y_L)^T$ given $\boldsymbol{\alpha} = (\alpha_1\ \alpha_2\ \ldots\ \alpha_L)^T$ and $\boldsymbol{\theta} = (\theta_1\ \theta_2\ \ldots\ \theta_L)^T$ is

$$\ln[f(\mathbf{y}|x, \boldsymbol{\alpha}, \boldsymbol{\theta})] = \sum_{i=1}^{L} \ln[f(y_i|x, \alpha_i, \theta_i)]. \tag{5.224}$$

Substituting (5.223) into this equation and then eliminating irrelevant terms and factors that do not depend on the codeword l, we obtain the *maximum-likelihood metric for BPSK*:

$$U(l) = \sum_{i=1}^{n} \mathrm{Re}\left[y_i \alpha_i e^{-j\theta_i} x_{li} \right], \quad l = 1, 2, \ldots, 2^k. \tag{5.225}$$

The 2^k metrics serve as the decision variables and require knowledge of the $\{x_{li}\}$, $\{\alpha_i\}$, and $\{\theta_i\}$.

For a linear block code, the error probabilities may be calculated by assuming that the all-zero codeword denoted by $l = 1$ was transmitted. The comparison of

the metrics $U(1)$ and $U(l)$, $l \neq 1$, depends only on the d terms that differ, where d is the weight of codeword l. The two-codeword error probability is equal to the probability that $U(1) < U(l)$. If each of the $\{\alpha_i\}$ is independent with the identical Rayleigh distribution and $E[\alpha_i^2] = E[\alpha_1^2]$, $i = 1, 2, \ldots, n$, the average SNR per binary code symbol is

$$\bar{\gamma}_s = \frac{\mathcal{E}_s}{N_0} E[\alpha_1^2] = \frac{r\mathcal{E}_b}{N_0} E[\alpha_1^2] = r\bar{\gamma}_b \quad \text{(binary symbols)} \tag{5.226}$$

where $\mathcal{E}_b$ is the information-bit energy, r is the code rate, and $\bar{\gamma}_b$ is the average SNR per bit. A derivation similar to the one leading to (5.132) indicates that the two-codeword error probability is

$$P_2(d) = P_s - (1 - 2P_s) \sum_{i=1}^{d-1} \binom{2i-1}{i} [P_s(1 - P_s)]^i \tag{5.227}$$

where the symbol error probability is

$$P_s = \frac{1}{2}\left(1 - \sqrt{\frac{\bar{\gamma}_s}{1 + \bar{\gamma}_s}}\right) \quad \text{(BPSK, QPSK)}. \tag{5.228}$$

The same equations are valid for both PSK and QPSK because the latter can be transmitted as two independent BPSK waveforms in phase quadrature. A derivation analogous to that of (5.136) indicates that

$$P_2(d) \leq \binom{2d-1}{d} P_s^d. \tag{5.229}$$

As indicated in (1.56), an upper bound on the information-symbol error probability for soft-decision decoding is given by

$$P_{is} \leq \sum_{d=d_m}^{n} \frac{d}{n} A_d P_2(d) \tag{5.230}$$

and the information-bit error probability P_b is given by (1.32). A comparison of (5.132) with (5.227) and the first term on the right-hand side of (5.230) indicates that a binary block code with maximum-likelihood decoding provides the diversity order $D_o = d_m$ when $P_b = P_{is}$ is low enough that the first term in (5.230) dominates.

For q-ary orthogonal symbol waveforms $s_1(t), s_2(t), \ldots, s_q(t)$, q matched filters are needed. The observation vector is $\mathbf{y} = [\mathbf{y}_1 \ \mathbf{y}_2 \ldots \mathbf{y}_q]$, where each $\mathbf{y}_k$ is an n-dimensional row vector of output samples y_{ki}, $i = 1, 2, \ldots, n$, from matched-filter k, which is matched to $s_k(t)$. Suppose that symbol i of codeword l uses $s_v(t)$. A derivation similar to that following (1.57) in Sect. 1.1 indicates that when

codeword l is received in the presence of white Gaussian noise, matched-filter k produces the samples

$$y_{ki} = \sqrt{\mathcal{E}_s}\alpha_i e^{j\theta_i}\delta_{kv_{li}} + N_{ki}, \quad i = 1, 2, \ldots, n, \quad k = 1, 2, \ldots, q \tag{5.231}$$

where $\delta_{kv_{li}} = 1$ if $k = v_{li}$ and $\delta_{kv_{li}} = 0$ otherwise, $\mathcal{E}_s$ is the desired-signal energy per symbol in the absence of fading and diversity combining, and each N_{ki} is an independent, zero-mean, complex-valued Gaussian noise variable. These samples provide sufficient statistics that contain all the relevant information in the received symbols. Since each symbol waveform represents $\log_2 q$ code bits, the average SNR per code symbol is

$$\bar{\gamma}_s = (\log_2 q) r \bar{\gamma}_b \tag{5.232}$$

which reduces to (5.226) when $q = 2$.

Assuming that the two-sided noise-power spectral density in each branch is equal to $N_0/2$, then $E[|\ N_{ki}\ |^2] = N_0$. Because of its circular symmetry, N_{ki} has independent real and imaginary components with variance $N_0/2$. Therefore, the conditional probability density function of y_{ki} given the values of l, α_i, and θ_i is

$$f(y_{ki}|l, \alpha_i, \theta_i) = \frac{1}{\pi N_0} \exp\left[- \frac{|y_{ki} - \sqrt{\mathcal{E}_s}\alpha_i e^{j\theta_i}\delta_{kv_{li}}|^2}{N_0} \right]. \tag{5.233}$$

The orthogonality of the $\{s_k(t)\}$ and the independence of the white noise from symbol to symbol imply the conditional independence of the $\{y_{ki}\}$.

For coherent FSK, the $\{\alpha_i\}$ and the $\{\theta_i\}$ are assumed to be known, and the likelihood function is the product of qn densities given by (5.233) for $k = 1, 2, \ldots, q$ and $i = 1, 2, \ldots, n$. Forming the log-likelihood function and eliminating irrelevant terms that are independent of l, we obtain the *maximum-likelihood metric for coherent FSK*:

$$U(l) = \sum_{i=1}^{n} \mathrm{Re}\left[\alpha_i e^{-j\theta_i} V_{li} \right], \quad l = 1, 2, \ldots, q^k \tag{5.234}$$

where $V_{li} = y_{v_{li}}$ is the sampled output of the filter matched to $s_{v_{li}}(t)$, the signal representing symbol i of codeword l. A disadvantage of the maximum-likelihood metric is that it requires channel state information.

For independent, identically distributed Rayleigh fading of each codeword symbol, a derivation similar to the one for BPSK indicates that the two-codeword error probability $P_2(d)$ is again given by (5.227) provided that

$$P_s = \frac{1}{2}\left(1 - \sqrt{\frac{\bar{\gamma}_s}{2 + \bar{\gamma}_s}} \right) \quad \text{(coherent BFSK)} \tag{5.235}$$

where $\bar{\gamma}_s$ is given by (5.232), and P_{is} is given by (5.230). The diversity order is $D_o = d_m$ when $\bar{\gamma}_s \gg 1$. A comparison of (5.228) and (5.235) indicates that for large values of $\bar{\gamma}_s$ and the same block code, BPSK and QPSK have the usual 3 dB advantage over coherent BFSK in a fading environment. However, BPSK and 4-FSK provide the same performance, and FSK provides superior performance if $q \geq 8$.

The preceding analysis can be extended to Nakagami fading if the fading parameter m is a positive integer. An analysis similar to that following (5.153) indicates that $P_2(d)$ is given by (5.227) with d replaced by md,

$$P_s = \frac{1}{2}\left(1 - \sqrt{\frac{r\bar{\gamma}_b}{m + r\bar{\gamma}_b}}\right) \quad \text{(BPSK, QPSK)} \tag{5.236}$$

$$P_s = \frac{1}{2}\left(1 - \sqrt{\frac{r\bar{\gamma}_b}{2m + r\bar{\gamma}_b}}\right) \quad \text{(coherent BFSK)} \tag{5.237}$$

and P_{is} is given by (5.230).

When fast fading makes it impossible to obtain accurate estimates of the $\{\alpha_i\}$ and $\{\theta_i\}$, noncoherent FSK is a suitable modulation. Expanding the argument of the exponential function in (5.233), assuming that θ_i is uniformly distributed over $[0, 2\pi)$, expressing y_{ki} in polar form, observing that the integral over θ_i is over one period of the integrand, and using the identity (B.30), we obtain the conditional probability density function of y_{ki} given l and α_i:

$$f(y_{ki}|l, \alpha_i) = \frac{1}{\pi N_0} \exp\left[-\frac{|y_{ki}|^2 + \mathcal{E}_s\alpha_i^2\delta_{kv_{li}}}{N_0}\right] I_0\left(\frac{2\sqrt{\mathcal{E}_s}\alpha_i|y_{ki}|\delta_{kv_{li}}}{N_0}\right). \tag{5.238}$$

Assuming that each α_i is statistically independent and has the same Rayleigh probability density function given by (5.21), $f(y_{ki}|l)$ can be evaluated by using the identity (B.33). Calculating the log-likelihood function and eliminating irrelevant terms and factors, we obtain the *Rayleigh metric* for noncoherent FSK:

$$U(l) = \sum_{i=1}^{n} R_{li}^2, \quad l = 1, 2, \ldots, q^k \tag{5.239}$$

where $R_{li} = |y_{v_{li}}|$ denotes the envelope produced by the filter matched to the transmitted signal for symbol i of codeword l. A major advantage of the Rayleigh metric is that it does not require any channel state information.

Assuming that the all-zero codeword was transmitted, a derivation similar to the one preceding (5.189) again verifies (5.227) with

$$P_s = \frac{1}{2 + \bar{\gamma}_s} \quad \text{(noncoherent FSK)} \tag{5.240}$$

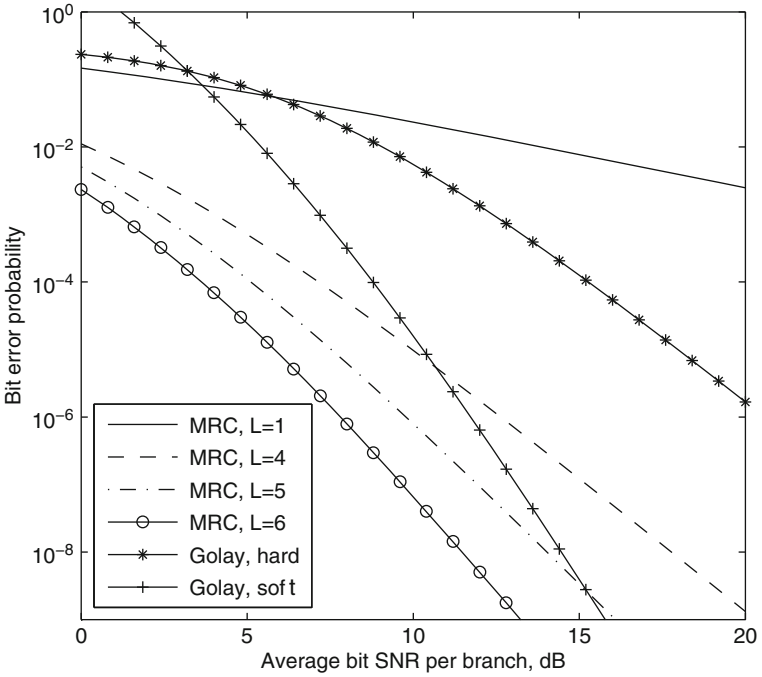

Fig. 5.18 Information-bit error probability for extended Golay (24,12) code with soft and hard decisions, coherent PSK modulation, and Rayleigh fading, and for MRC with $L = 1, 4, 5$, and 6

where $\bar{\gamma}_s$ is given by (5.232), and P_{is} is given by (5.230). The diversity order is $D_o = d_m$ when $\bar{\gamma}_s \gg 1$. A comparison of (5.228) and (5.240) indicates that for large values of $\bar{\gamma}_b$ and the same block code, BPSK and QPSK have an approximate 6 dB advantage over noncoherent BFSK in a fading environment. Thus, the fading accentuates the advantage that exists for the AWGN channel. However, BPSK and noncoherent 16-FSK provide approximately the same performance, and noncoherent FSK provides superior performance if $q \geq 32$ at the cost of bandwidth.

For hard-decision decoding, the symbol error probability P_s is given by (5.228) for coherent PSK, (5.235) for coherent FSK, (5.240) for noncoherent FSK, or (5.176) for DPSK. For loosely packed codes, P_{is} is approximated by (1.30) whereas it is approximated by (1.29) for tightly packed codes.

Figure 5.18 illustrates $P_b = P_{is}$ for an extended Golay (24,12) code with $L = 1$ and P_b for MRC with $L = 1, 4, 5$, and 6 diversity branches. A Rayleigh fading channel and BPSK are assumed. The extended Golay (24,12) code is tightly packed with 12 information bits, $r = 1/2$, $d_m = 8$, and $t = 3$. The values of A_d in (5.230) are listed in Table 1.3. The MRC graphs assume that a single bit is transmitted. The SNR per code symbol $\bar{\gamma}_s = \bar{\gamma}/2$, where $\bar{\gamma}$ is the average SNR per bit and branch. The figure indicates the benefits of coding particularly when the

desired P_b is low. At $P_b = 10^{-3}$, the (24,12) code with hard decisions provides on 11 dB advantage over uncoded BPSK; with soft decisions, the advantage becomes 16 dB. The advantage of soft-decision decoding relative to hard-decision decoding increases to more than 10 dB at $P_b = 10^{-7}$, a vast gain over the approximately 2 dB advantage of soft-decision decoding for the AWGN channel. At $P_b = 10^{-9}$, the Golay (24,12) code with soft decisions outperforms MRC with $L = 5$ and is nearing the performance of MRC with $L = 6$. However, since $A_{d_m} = A_8 = 759$, the diversity order will not reach the theoretical limit $D_o = d_m = 8$ even for very low P_b. For noncoherent BFSK, all the graphs in the figure are shifted approximately 6 dB to the right when $P_b \leq 10^{-3}$.

Since the soft-decision decoding of long block codes is usually impractical, convolutional codes are more likely to give a good performance over a fading channel. The metrics are basically the same as they are for block codes with the same modulation, but they are evaluated over path segments that diverge from the correct path through the trellis and then merge with it subsequently. The linearity of binary convolutional codes ensures that all-zero path can be assumed to be the correct one when calculating the decoding error probability. Let d denote the Hamming distance of an incorrect path from the correct all-zero path. If perfect symbol interleaving is used, then the probability of error in the pairwise comparison of two paths with an unmerged segment is $P_2(d)$, which is given by (5.227). As shown in Sect. 1.2, the probability of an information-bit error in soft-decision decoding is upper bounded by

$$P_b \leq \frac{1}{k} \sum_{d=d_f}^{\infty} B(d) P_2(d) \tag{5.241}$$

where $B(d)$ is the number of information-bit errors over all paths with unmerged segments at Hamming distance d, k is the number of information bits per trellis branch, and d_f is the minimum free distance, which is the minimum Hamming distance between any two convolutional codewords. This upper bound approaches $B_{d_f} P_2(d_f)/k$ as $P_b \to 0$ so the diversity order is $D_o = d_f$ if P_b and $B(d_f)/k$ are small.

In general, d_f increases with the constraint length of the convolutional code. However, if each encoder output bit is repeated n_r times, then the minimum distance of the convolutional code increases to $n_r d_f$ without a change in the constraint length, but at the cost of a bandwidth expansion by the factor n_r. From (5.241), we infer that for the code with repeated bits,

$$P_b \leq \frac{1}{k} \sum_{d=d_f}^{\infty} B(d) P_2(n_r d) \tag{5.242}$$

where $B(d)$ refers to the original code. The diversity order is $D_o = n_r d_f$ if P_b and $B(d_f)/k$ are small.

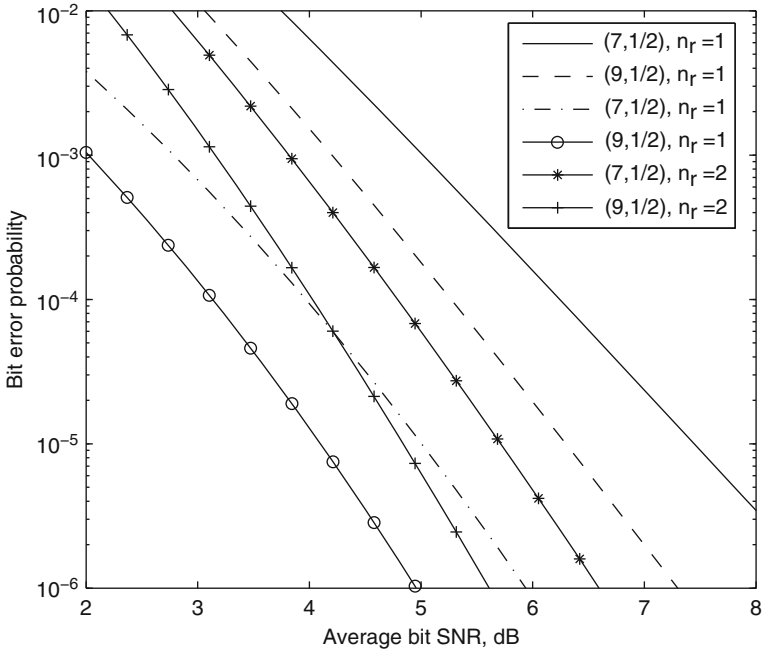

Fig. 5.19 Information-bit error probability for Rayleigh fading, coherent PSK, and binary convolutional codes with various values of (K, r) and n_r

Figure 5.19 illustrates P_b as a function of $\bar{\gamma}_b$ for the Rayleigh-fading channel and binary convolutional codes with different values of the constraint length K, the code rate r, and the number of repetitions n_r. Relations (5.242) and (5.227) with $k = 1$ are used, and the $\{B(d)\}$ are taken from the listings for seven terms in Tables 1.4 and 1.5. The figure indicates that an increase in the constraint length provides a much greater performance improvement for the Rayleigh-fading channel than the increase does for the AWGN channel [19]. For a fixed constraint length, the rate-1/4 codes give a better performance than the rate-1/2 codes with $n_r = 2$, which require the same bandwidth but are less complex to implement. The latter two codes require twice the bandwidth of the rate-1/2 code with no repetitions.

The issues are similar for trellis-coded modulation (Chap. 1), which provides a coding gain without a bandwidth expansion. However, if parallel state transitions occur in the trellis, then $d_f = 1$, which implies that the code provides no diversity protection against fading. Thus, for fading communications, a conventional trellis code with distinct transitions from each state to all other states must be selected. Since Rayleigh fading causes large amplitude variations, multiphase PSK is usually a better choice than multilevel QAM for the symbol modulation. However, the optimum trellis decoder uses coherent detection and requires an estimate of the channel attenuation.

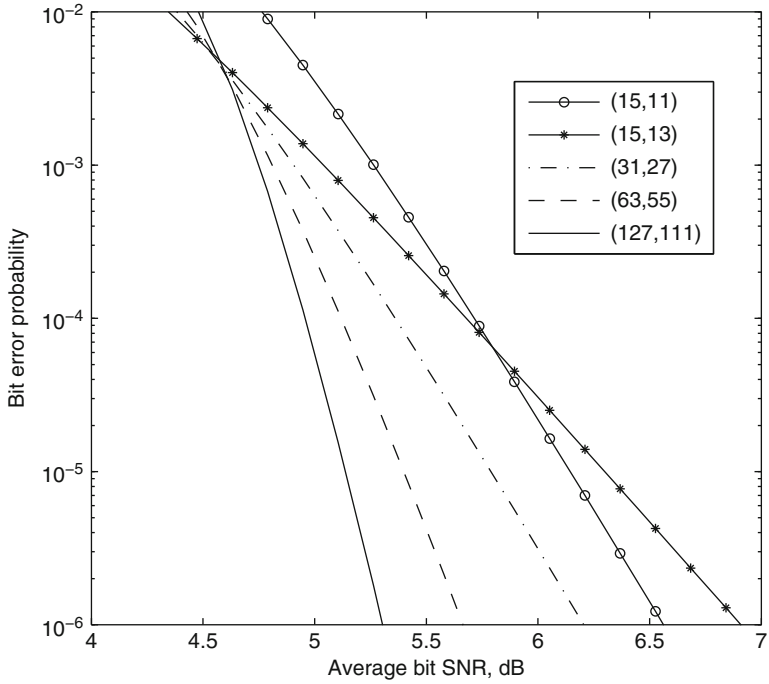

Fig. 5.20 Information-bit error probability for Rayleigh fading, coherent PSK, soft decisions, and concatenated codes comprising an inner binary convolutional code with K = 7 and $r_1 = 1/2$, and various Reed–Solomon (n, k) outer codes

Whether a block, convolutional, or trellis code is used, the results of this section indicate that the minimum Hamming distance rather than the minimum Euclidean distance is the critical parameter in designing an effective code for the Rayleigh fading channel.

Turbo codes or serially concatenated codes with iterative decoding based on the *maximum a posteriori* (MAP) criterion can provide excellent performance. However, the system must be able to accommodate considerable decoding delay and computational complexity. Even without iterative decoding, a serially concatenated code with an outer Reed–Solomon code and an inner binary convolutional code (Sect. 1.4) can be effective against Rayleigh fading. In the worst case, each output bit error of the inner decoder causes a separate symbol error at the input to the Reed–Solomon decoder. Therefore, an upper bound on P_b is given by (1.143) and (1.142). For coherent BPSK modulation with soft-decision decoding, $P_2(d)$ is given by (5.227) and (5.228), and $\bar{\gamma}_s$ is given by (5.226). The concatenated code has a code rate $r = r_1 r_0$, where r_1 is the inner-code rate and r_0 is the outer-code rate.

Figure 5.20 depicts examples of the upper bound on P_b as a function $\bar{\gamma}_b$ for Rayleigh fading, coherent BPSK, soft decisions, an inner binary convolutional code with $K = 7$, $r_1 = 1/2$, and $k = 1$, and various Reed–Solomon (n, k) outer codes.

The required bandwidth is B_u/r, where B_u is the uncoded BPSK bandwidth. Thus, the codes of the figure require a bandwidth less than $3B_u$.

5.5.1 Bit-Interleaved Coded Modulation

The performance of a channel code over a fading channel depends on the minimum Hamming distance, whereas the performance over the AWGN channel depends on the Euclidean distance. For binary modulations, such as BPSK and BFSK, the two distances are proportional to each other. For nonbinary modulations, the increase in one of these distances often decreases the other one. Bit-interleaved coded modulation (BICM), which is described in Sect. 1.7, increases the minimum Hamming distance, and hence the diversity order, of a code because two trellis paths or codewords tend to have more distinct bits than distinct nonbinary symbols. To compensate for the increase in the minimum Euclidean distance, BICM with iterative decoding and demodulation (BICM-ID) may be used, as explained in Sect. 1.7. BICM-ID introduces flexibility into communication systems using nonbinary alphabets over an AWGN channel with a variable level of fading. Since small alphabets are used in BPSK and QPSK modulations, BICM and BICM-ID are inherent or add little to direct-sequence systems. In contrast, frequency-hopping systems can exploit large alphabets and noncoherent CPFSK modulation, and hence BICM and BICM-ID are often effective (Chap. 8).

5.6 Rake Demodulator

In a fading environment, the principal means for a direct-sequence system to obtain the benefits of diversity combining is by using a rake demodulator. A *rake demodulator* provides *path diversity* by coherently combining resolvable multipath components that are often present during frequency-selective fading. This receiver is the standard type for direct-sequence systems used in mobile communication networks.

Consider a multipath channel with frequency-selective fading slow enough that its time variations are negligible over a signaling interval. To harness the energy in all the multipath components, a receiver should decide which signal was transmitted among M candidates, $s_1(t), s_2(t), \ldots, s_M(t)$, only after processing all the received multipath components of the signal. If the channel impulse response of (5.60) is time-invariant over the time interval of interest, the receiver selects among the M baseband signals or complex envelopes:

$$v_k(t) = \sum_{i=1}^{L} C_i s_k(t - \tau_i), \quad k = 1, 2, \ldots, M, \quad 0 \le t \le T + T_d \tag{5.243}$$

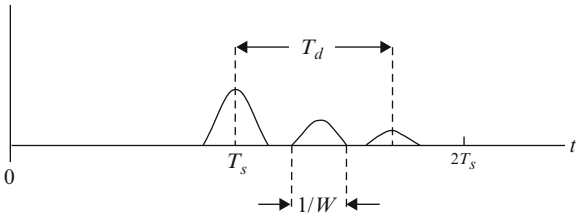

Fig. 5.21 Response of matched filter to input with three resolvable multipath components

where T is the duration of the transmitted signal, T_d is the multipath delay spread, L is the number of multipath components, τ_i is the delay of component i, and the channel parameter C_i is the *complex fading amplitude* or *fading coefficient* that represents the attenuation and phase shift of component i. An idealized sketch of the output of a baseband matched filter that receives three multipath components of the signal to which it is matched is shown in Fig. 5.21. If a signal has bandwidth W, then the duration of the matched-filter response to this signal is on the order of $1/W$. Multipath components that produce distinguishable matched-filter output pulses are said to be *resolvable*. Thus, three multipath components are resolvable if their relative delays are greater than $1/W$, as depicted in the figure. A necessary condition for at least two resolvable multipath components is that duration $1/W$ is less than the delay spread T_d. From (5.57) it follows that $W > B_{coh}$ is required, which implies that both frequency-selective fading and resolvable multipath components are associated with wideband signals. There are at most $\lfloor T_d W \rfloor + 1$ resolvable components, where $\lfloor x \rfloor$ denotes the largest integer in x. As observed in the figure, intersymbol interference at the sampling times is not significant if $T_d + 1/W$ is less than the symbol duration T_s.

For the following analysis, it is assumed that the M possible signals are orthogonal to each other. The receiver uses a separate baseband matched filter or correlator for each possible desired signal including its multipath components. Thus, if $s_k(t)$ is the kth symbol waveform, $k = 1, 2, \ldots, M$, then the kth matched filter is matched to the signal $v_k(t)$ in (5.243) with $T = T_s$, the symbol duration. Each matched-filter output sampled at $t = T_s + T_d$ provides a decision variable. A derivation similar to that of (5.146) indicates that the kth decision variable is

$$U_k = \text{Re}\left[\sum_{i=1}^{L} C_i^* \int_0^{T_s+T_d} r(t) s_k^*(t-\tau_i)\,dt\right] \tag{5.244}$$

where $r(t)$ is the received signal, including the noise, after downconversion to baseband. A receiver implementation based on this equation would require a separate transversal filter or delay line and a matched filter for each possible waveform $s_k(t)$. An alternative form that requires only a single transversal filter

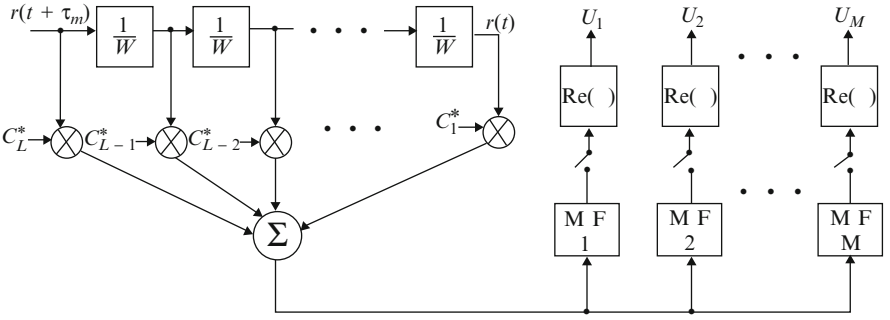

Fig. 5.22 Rake demodulator for M orthogonal pulses. MF denotes a matched filter

and M matched filters is derived by changing variables in (5.244) and using the fact that $s_k(t)$ is zero outside the interval $[0, T_s)$. The result is

$$U_k = \text{Re}\left[\sum_{i=1}^{L} C_i^* \int_0^{T_s} r(t+\tau_i) s_k^*(t) dt\right]. \tag{5.245}$$

For frequency-selective fading and resolvable multipath components, a simplifying assumption is that each delay is an integer multiple of $1/W$. Accordingly, L is increased to equal the maximum number of resolvable components, and we set $\tau_i = (i-1)/W$, $i = 1, 2, \ldots, L$, and $(L-1)/W \approx \tau_m$, where τ_m is the maximum delay. As a result, some of the $\{C_i\}$ may be equal to zero. The decision variables become

$$U_k = \text{Re}\left[\sum_{i=1}^{L} C_i^* \int_0^{T_s} r(t+(i-1)/W) s_k^*(\tau) dt\right], \quad k = 1, 2, \ldots, M. \tag{5.246}$$

A receiver based on these decision variables, which is called a *rake demodulator*, is diagrammed in Fig. 5.22. Since $r(t)$ is designated as the output of the final tap, the sampling occurs at $t = T_s$. Each tap output contains at most one multipath component of $r(t)$.

An alternative configuration to that of Fig. 5.22 uses a separate transversal filter for each of the M decision variable and has the corresponding matched filter in the front, as shown in Fig. 5.23a. Each matched-filter or correlator output is applied to L_s parallel *fingers*, the outputs of which are recombined and sampled to produce one of the decision variables. The number of fingers L_s, where $L_s \leq L$, is equal to the number the resolvable components that have significant power. The matched filter produces a number of output pulses in response to the multipath components, as illustrated in Fig. 5.21. Each finger delays and weights one of these pulses by the appropriate amount so that all the finger output pulses are aligned in time and can

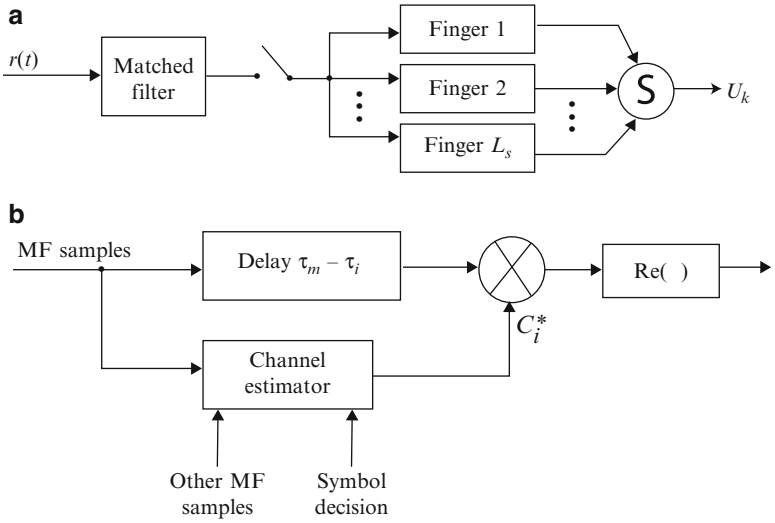

Fig. 5.23 Rake demodulator: (**a**) basic configuration for generating each of the M decision variables and (**b**) a single finger

be constructively combined after weighting, as shown in Fig. 5.23b. Digital devices can be used because the sampling immediately follows the matched filtering.

When a direct-sequence signal is transmitted, the delay of each significant multipath component may be estimated and tracked by using devices similar to the acquisition and tracking systems of Chap. 4. Let t_e denote the time required to estimate the relative delay of a multipath component, and let v denote the relative radial velocity of a receiver relative to a transmitter. Then vt_e/c is the change in delay that occurs during the estimation procedure, where c is the speed of an electromagnetic wave. This change must be much less than the duration of a multipath output pulse shown in Fig. 5.21 if the delay estimate is to be useful. Thus, with v interpreted as the maximum speed of a mobile in a mobile communications network,

$$t_e \ll \frac{c}{vW} \tag{5.247}$$

is required of the multipath-delay estimation.

The channel estimator in Fig. 5.23b delays its inputs by one or more symbols, depending on the duration of a constant complex fading amplitude. A previous symbol decision by the rake demodulator is sent to the channel estimator to enable it to select the delayed sampled matched-filter output corresponding to that symbol. The selected sample is applied to a lowpass filter that provides the estimate $\widehat{C}_i^*$ of the complex conjugate of the complex fading amplitude. The estimates produced by the channel estimator must be updated at a rate exceeding the fade rate of (5.43) or (5.45).

An unmodulated direct-sequence pilot signal with a distinct spreading sequence may be transmitted to facilitate the channel estimation. Since transmitted energy must be diverted from the modulated direct-sequence signals, a pilot signal is a useful option primarily when it is shared by many users so that the energy allocation to the pilot signal is a minor loss. The downlink from a base station to the users of a cellular network (Chap. 6) is an example of an application that warrants the use of a pilot signal for channel estimation.

Path crosstalk is interference in a rake finger associated with one multipath component due to a multipath component that is associated with another rake finger. Suppose that $s_k(t)$ is a direct-sequence signal with chip duration $T_c = 1/W$. If the spreading sequence has a small autocorrelation when the relative delay is T_c or more, then

$$\int_0^{T_s} s_k(t + (i-1)/W)s_k(t)dt \ll \int_0^{T_s} |s_k(t)|^2 dt \ , \quad i \geq 2. \tag{5.248}$$

When this condition is satisfied, the path crosstalk tends to be negligible.

When the data modulation is binary antipodal or PSK, only a single symbol waveform $s_1(t)$ and its associated decision variable U_1, which is defined by (5.246), are needed. After downconversion to baseband, the received signal is

$$r(t) = \left\{ \mathrm{Re}\left[v_1(t)e^{j2\pi f_c t} \right] + n(t) \right\} 2e^{-j2\pi f_c t} \tag{5.249}$$

where $v_1(t)$ is given by (5.243) and $n(t)$ is zero-mean white Gaussian noise. Let $\alpha_i = |h_i|$ and set $k = 1$ and $\tau_i = (i-1)/W, i = 1, 2, \ldots, L$ in (5.243). Substituting (5.249) and (5.243) into (5.246) with $k = 1$ and then using (5.248) and a derivation similar to that of (5.117), we obtain

$$U_1 = 2\mathcal{E}_s \sum_{i=1}^{L} \alpha_i^2 + \sum_{i=1}^{L} \alpha_i N_i \tag{5.250}$$

where $\mathcal{E}_s$ is the average energy per symbol and N_i is a zero-mean Gaussian random variable. Thus, the ideal rake demodulator with no path crosstalk produces MRC. In many practical applications, there is a significant loss due to the path crosstalk.

If hard decisions are made on the received symbols, then a derivation similar to that of (5.121) yields the conditional symbol error probability given the $\{\alpha_i\}$:

$$P_{s|\boldsymbol{\alpha}}(\gamma_b) = Q\left(\sqrt{2\gamma_s}\right) \tag{5.251}$$

$$\gamma_s = \sum_{i=1}^{L} \gamma_i, \quad \gamma_i = \frac{\mathcal{E}_s}{N_0}\alpha_i^2. \tag{5.252}$$

For a rake demodulator, each of the $\{\alpha_i\}$ is associated with a different multipath component that fades independently. If each α_i has a Rayleigh distribution, then each γ_i has the exponential probability density function (Appendix B.4)

$$f_{\gamma_i}(x) = \frac{1}{\bar{\gamma}_i} \exp\left(-\frac{x}{\bar{\gamma}_i}\right) u(x), \quad i = 1, 2, \ldots, L \tag{5.253}$$

where the average SNR for a symbol in branch i is

$$\bar{\gamma}_i = \frac{\mathcal{E}_s}{N_0} E[\alpha_i^2], \; i = 1, 2, \ldots, L. \tag{5.254}$$

If each multipath component fades independently so that each of the $\{\gamma_i\}$ is statistically independent, then γ_s is the sum of independent, exponentially distributed random variables. The results of Appendix B.5 indicate that the probability density function of γ_s is

$$f_{\gamma_s}(x) = \sum_{i=1}^{L} \frac{A_i}{\bar{\gamma}_i} \exp\left(-\frac{x}{\bar{\gamma}_i}\right) u(x) \tag{5.255}$$

where

$$A_i = \begin{cases} \displaystyle\prod_{\substack{k=1 \\ k \neq i}}^{L} \frac{\bar{\gamma}_i}{\bar{\gamma}_i - \bar{\gamma}_k}, & L \geq 2 \\ 1, & L = 1. \end{cases} \tag{5.256}$$

The symbol error probability is determined by averaging the conditional bit error probability $P_{s|\boldsymbol{\alpha}}(\gamma_b)$ over the density given by (5.255). A derivation similar to that leading to (5.129) yields

$$P_s(L) = \frac{1}{2} \sum_{i=1}^{L} A_i \left(1 - \sqrt{\frac{\bar{\gamma}_i}{1 + \bar{\gamma}_i}}\right) \qquad \text{(BPSK, QPSK)}. \tag{5.257}$$

When a rake demodulator is used, each finger of the receiver must acquire the timing of a separate multipath signal. Whether matched filtering or a serial search is used, some mechanism is needed to ensure that each finger acquires a distinct multipath signal [11].

The number of fingers in an ideal rake demodulator equals the number of significant resolvable multipath components, which is constantly changing in a mobile communications receiver. Rather than attempting to implement all the required fingers that may sometimes be required, a more practical alternative is to implement a fixed number of fingers independent of the number of multipath components. *Generalized selection diversity* entails selecting the L_c strongest resolvable components among the L available ones and then applying MRC or EGC of these L_c components, thereby discarding the $L - L_c$ components with the lowest SNRs. Analysis [1] indicates that diminishing returns are obtained as L_c increases, but for a fixed value of L_c, the performance improves as L increases.

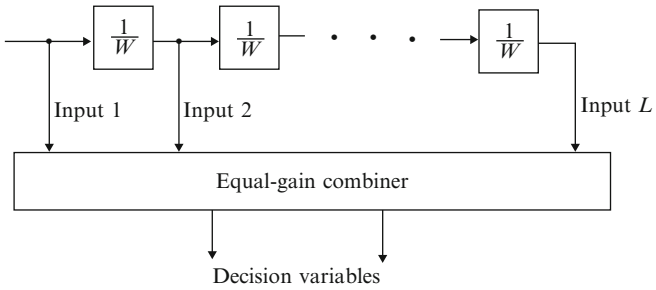

Fig. 5.24 Rake demodulator that uses equal-gain combiner to avoid channel-parameter estimation

An increase in the number of resolved components L is potentially beneficial if it is caused by natural changes in the physical environment that generate additional multipath components. However, an increase in L due to an increase in the bandwidth W is not always beneficial [12]. Although new components provide additional diversity and may exhibit the more favorable Ricean fading rather than Rayleigh fading, the average power per multipath component decreases because some composite components fragment into more numerous but weaker components. Hence, the estimation of the channel parameters becomes more difficult, and the fading of some multipath components may be highly correlated rather than independent.

The estimation of the channel parameters needed in a rake demodulator becomes more difficult as the fading rate increases. When the estimation errors are large, it may be preferable to use a rake demodulator that avoids channel-parameter estimation by abandoning MRC and using noncoherent postdetection EGC. The form of this rake demodulator for binary signals is depicted in Fig. 5.24. Each tap output of the transversal filter provides an input to the equal-gain combiner, which may have the form of Fig. 5.13 or Fig. 5.14.

Consider the rake demodulator of Figs. 5.24 and 5.14 and two symbols represented by orthogonal signals that satisfy (5.248). The two decision variables are defined by (5.246). A derivation similar to that of (5.181)–(5.183) proves that the decision variables may be expressed as

$$U_1 = \sum_{i=1}^{L} \left[\left(\sqrt{\mathcal{E}_s}\alpha_i \cos\theta_i + N_{1i}^R \right)^2 + \left(\sqrt{\mathcal{E}_s}\alpha_i \sin\theta_i + N_{1i}^I \right)^2 \right] \tag{5.258}$$

$$U_2 = \sum_{i=1}^{L} \left[\left(N_{2i}^R \right)^2 + \left(N_{2i}^I \right)^2 \right] \tag{5.259}$$

where N_{1i}^R, N_{1i}^I, N_{2i}^R, and N_{2i}^I are independent, zero-mean, Gaussian random variables with a common variance equal to $N_0/2$. Each phase θ_i is assumed to be statistically independent and uniformly distributed over $[0, 2\pi)$. Since each α_i has a Rayleigh distribution, $\alpha_i \cos\theta_i$ and $\alpha_i \sin\theta_i$ have zero-mean, independent,

Gaussian distributions. Therefore, as indicated in Appendix B.4, each term of U_1 has an exponential distribution with mean

$$m_i = N_0(1 + \bar{\gamma}_i) \tag{5.260}$$

where $\bar{\gamma}_i$ is defined by (5.254). Each term of U_2 has an exponential distribution with mean N_0. Since the terms of U_2 are statistically independent and the statistical independence of the $\{\alpha_i\}$ and $\{\theta_i\}$ implies the statistical independence of the terms of U_1, the probability density functions of U_1 and U_2 for distinct values of the $\{\bar{\gamma}_i\}$ are given by (B.45), (B.46), and (B.49) with $N = L$. If hard decisions are made on the received symbols, an erroneous decision is made if $U_2 > U_1$, and hence the symbol error probability is

$$P_s(L) = \sum_{i=1}^{L} \frac{B_i}{m_i} \int_0^\infty \exp\left(-\frac{x}{m_i}\right) \int_x^\infty \frac{y^{L-1} \exp\left(-\frac{y}{N_0}\right)}{(N_0)^L (L-1)!} dy\, dx. \tag{5.261}$$

Integrating by parts to eliminate the inner integral, changing the remaining integration variable, applying (B.12), and simplifying yields the symbol error probability for orthogonal signals and a rake demodulator with noncoherent postdetection EGC:

$$P_s(L) = \sum_{i=1}^{L} B_i \left[1 - \left(\frac{1 + \bar{\gamma}_i}{2 + \bar{\gamma}_i}\right)^L\right] \quad \text{(orthogonal signals)} \tag{5.262}$$

where

$$B_i = \begin{cases} \prod\limits_{\substack{k=1 \\ k \neq i}}^{L} \dfrac{1 + \bar{\gamma}_i}{\bar{\gamma}_i - \bar{\gamma}_k}, & L \geq 2 \\ 1, & L = 1. \end{cases} \tag{5.263}$$

An alternative derivation of (5.262) using the direct-conversion receiver modeled in Appendix A.3 is given in [13]. Equation (5.262) is more compact and considerably easier to evaluate than the classical formula [2], which is derived in a different way.

For dual rake combining with orthogonal signals, (5.262) reduces to

$$P_s(2) = \frac{8 + 5\bar{\gamma}_1 + 5\bar{\gamma}_2 + 3\bar{\gamma}_1\bar{\gamma}_2}{(2 + \bar{\gamma}_1)^2(2 + \bar{\gamma}_2)^2}. \tag{5.264}$$

If $\bar{\gamma}_2 = 0$, then

$$P_s(2) = \frac{2 + \frac{5}{4}\bar{\gamma}_1}{(2 + \bar{\gamma}_1)^2} \geq \frac{1}{2 + \bar{\gamma}_1} = P_s(1). \tag{5.265}$$

This result illustrates the performance degradation that results when a rake combiner uses an input that provides no desired-signal component, which may occur when EGC is used rather than MRC. In the absence of a desired-signal component, this

input contributes only noise to the combiner. For large values of $\bar{\gamma}_1$, the extraneous noise causes a loss of almost 1 dB.

A way to avoid the necessity of estimation of the $\{c_i\}$ is to use DPSK and the diversity receiver of Fig. 5.13 in Fig. 5.24. The classical analysis [2] verifies that $P_s(L)$ is given by (5.262) and (5.263) with $\bar{\gamma}_i$ replaced by $2\bar{\gamma}_i$.

If an adaptive array produces a directional beam to reject interference or enhance the desired signal, it also reduces the delay spread of the significant multipath components of the desired signal because components arriving from angles outside the beam are greatly attenuated. As a result, the potential benefit of a rake demodulator diminishes. Another procedure is to assign a separate set of adaptive weights to each significant multipath component. Consequently, the adaptive array can form separate array patterns, each of which enhances a particular multipath component while nulling other components. The set of enhanced components are then applied to the rake demodulator [14].

5.7 Diversity and Spread Spectrum

Some form of diversity is crucial in compensating for the effects of fading. Spread-spectrum systems exploit the different types of diversity that are available. Consider a direct-sequence signal that is accompanied by multipath components in addition to the direct-path signal. If the multipath components are delayed by more than one chip, then the independence of the chips ensures that the multipath interference is suppressed by at least the processing gain. However, since multipath signals carry information, they are a potential resource to be exploited rather than merely rejected. A *rake demodulator* provides *path diversity* by coherently combining the resolvable multipath components present during frequency-selective fading, which occurs when the chip rate of the spreading sequence exceeds the coherence bandwidth.

A direct-sequence system exploits time diversity through the branches or demodulators in its rake demodulator, which is inserted prior to the despreading in the receiver as depicted in Fig. 5.25. These demodulators must be synchronized to the path delays of the multipath components. The effectiveness of the rake demodulator depends on the concentration of strong diffuse and specular components in the vicinity of resolvable path delays, which becomes more likely as the chip rate increases. A large Doppler spread is beneficial to a direct-sequence system because it decreases the channel coherence time. If the coherence time is less than the

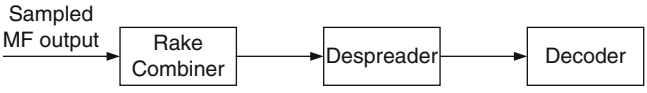

Fig. 5.25 Rake demodulator for direct-sequence system

interleaving depth, the performance of the channel decoder is enhanced. Equation (5.10) indicates that the Doppler spread increases with the carrier frequency and the speed of the receiver relative to the transmitter.

Consider a multipath channel with frequency-selective fading slow enough that its time variations are negligible over a signaling interval. When the data modulation is BPSK, only a single symbol waveform and its associated decision variable are needed. Assume the presence of zero-mean, white Gaussian noise with two-sided power spectral density $N_{0e}/2$. As indicated in Sect. 5.5, if $\alpha_i = |h_i|$, then for an ideal rake demodulator with no path crosstalk and perfect tap weights, the conditional bit or symbol error probability given the $\{\alpha_i\}$ is

$$P_{s|\alpha}(\gamma_s) = Q\left(\sqrt{2\gamma_s}\right). \tag{5.266}$$

For a rake demodulator, each of the $\{\alpha_i\}$ is associated with a different multipath component, and hence each $E[\alpha_i^2]$ has a different value in general. Therefore,

$$\gamma_s = \sum_{i=1}^{L} \gamma_i, \quad \gamma_i = \frac{\mathcal{E}_s}{N_{0e}} \alpha_i^2. \tag{5.267}$$

The average SNR for a symbol in branch i is

$$\bar{\gamma}_i = \frac{\mathcal{E}_s}{N_{0e}} E\left[\alpha_i^2\right], \quad i = 1, 2, \ldots, L. \tag{5.268}$$

If each multipath component experiences independent Rayleigh fading so that each of the $\{\gamma_i\}$ is statistically independent, then the analysis of Sect. 5.5 gives the symbol error probability:

$$P_s(L) = \frac{1}{2} \sum_{i=1}^{L} A_i \left(1 - \sqrt{\frac{\bar{\gamma}_i}{1 + \bar{\gamma}_i}}\right) \tag{5.269}$$

where

$$A_i = \begin{cases} \prod_{\substack{k=1 \\ k \neq i}}^{L} \frac{\bar{\gamma}_i}{\bar{\gamma}_i - \bar{\gamma}_k}, & L \geq 2 \\ 1, & L = 1. \end{cases} \tag{5.270}$$

Since only white Gaussian noise is present, the processing gain of the system is irrelevant under this model.

The processing of a multipath component requires channel estimation. When a practical channel estimator is used, measurements indicate that only four or fewer components are likely to have a sufficient signal-to-interference ratio to be useful in the rake combining [12]. To assess the potential performance of the rake demodulator, it is assumed that the largest multipath component has $\bar{\gamma}_1 = \bar{\gamma}$ and that $L \leq 4$ components are received and processed. The other three or fewer

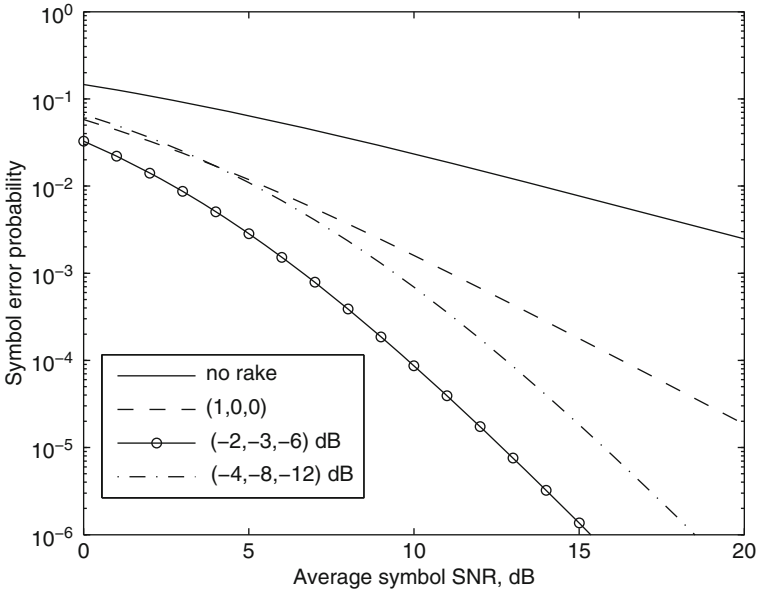

Fig. 5.26 Symbol error probability for single-carrier systems and $L \leq 4$ multipath components with different multipath intensity vectors

minor multipath components have relative average symbol SNRs specified by the *multipath intensity vector*

$$\Gamma = \left(\frac{\bar{\gamma}_2}{\bar{\gamma}_1}, \frac{\bar{\gamma}_3}{\bar{\gamma}_1}, \frac{\bar{\gamma}_4}{\bar{\gamma}_1}\right) = \left(\frac{\overline{\alpha_2^2}}{\overline{\alpha_1^2}}, \frac{\overline{\alpha_3^2}}{\overline{\alpha_1^2}}, \frac{\overline{\alpha_4^2}}{\overline{\alpha_1^2}}\right) \tag{5.271}$$

where $\overline{\alpha_i^2} = E\left[\alpha_i^2\right]$.

Figure 5.26 plots the symbol error probability of the ideal rake demodulator as a function of $\bar{\gamma}_1 = \mathcal{E}_s \overline{\alpha_1^2} / N_{0e}$, the average symbol SNR of the main component, for multipath intensity vectors occurring in mobile networks. Typically, three significant multipath components are available. The multipath intensity vector $(1, 0, 0)$ represents the hypothetical environment in which a single additional multipath component has the same power as the main component. Expressing the components in decibels, the multipath intensity vector $(-4, -8, -12)$ dB represents the minor multipath intensities typical of a rural environment. The vector $(-2, -3, -6)$ dB represents a typical urban environment. The figure indicates that despite 2.1 dB less power in the minor components, the rural environment generally provides a lower symbol error probability than the hypothetical one. The superior performance in the urban environment relative to the rural environment is primarily due to its 3.5 dB additional power in the minor multipath components.

This figure and other numerical data establish two basic features of single-carrier direct-sequence systems with ideal rake demodulators that experience negligible path crosstalk.

1. System performance improves as the total energy in the minor multipath components increases. The underlying reason is that the rake demodulator of the single-carrier system harnesses energy that would otherwise be unavailable.
2. When the total energy in the minor multipath components is fixed, the system performance improves as the number of resolved multipath components L increases and as the energy becomes uniformly distributed among these components.

Rake demodulators are not useful in frequency-hopping systems because of the relatively narrow bandwidth of the frequency channels. Frequency-hopping systems rely on the inherent frequency diversity provided by the frequency changes. Interleaving of the code symbols over many dwell intervals provides a large level of diversity to slow frequency-hopping systems operating over a frequency-selective fading channel. Codeword symbol errors are independent if the fading is independent in each frequency channel and each symbol is transmitted in a different frequency channel. Let F_s denote the minimum separation between adjacent carrier frequencies in a hopset. A necessary condition for nearly independent symbol errors is

$$F_s \geq B_{coh} \tag{5.272}$$

where B_{coh} is the coherence bandwidth of the fading channel. For a hopping band with bandwidth W, a frequency channel with bandwidth B, a hopset with M carrier frequencies, and a uniform carrier separation, $F_s = W/M \geq B$. Thus, (5.272) implies that the number of frequency channels is constrained by

$$M \leq \frac{W}{\max(B, B_{coh})} \tag{5.273}$$

if nearly independent symbol errors are to be ensured. If (5.273) is not satisfied, there will be a performance loss due to the correlated symbol errors. Frequency-hopping systems are usually insensitive to variations in the Doppler spread of the channel because any additional diversity due to improved time-selective fading is insignificant.

If $B < B_{coh}$, equalization will not be necessary because the channel transfer function is nearly flat over each frequency channel. If $B \geq B_{coh}$, either equalization may be used to prevent intersymbol interference or a multicarrier modulation may be combined with the frequency hopping.

Let n denote the number of code symbols in a block codeword or the constraint length of a convolutional code. For each of these symbols to fade independently with a high probability, $n \leq M$ is necessary. Let T_{del} denote the maximum tolerable

processing delay. Since the delay caused by coding and ideal interleaving over n hops is $(n-1)T_h + T_s$, and n distinct frequencies are desired,

$$n \leq \min\left(M, 1 + \frac{T_{\text{del}} - T_s}{T_h}\right) \tag{5.274}$$

is required. If this inequality is not satisfied, then the interleaving is not ideal, and some performance degradation results.

Instead of providing diversity, an antenna array may be used to adaptively suppress interference. The *maximin algorithm* is an adaptive-array algorithm that exploits the characteristics of spread-spectrum signals to provide a much larger degree of protection against strong interference than could be provided by spread spectrum alone [15, 16].

5.8 Multicarrier Direct-Sequence Systems

A direct-sequence system is called *wideband* or *broadband* if it uses a spectral band with a bandwidth that exceeds the coherence bandwidth of a frequency-selective fading channel. The two most commonly proposed types of wideband direct-sequence systems are single-carrier and multicarrier systems. A *single-carrier system* uses a single carrier frequency to transmit signals. A *multicarrier system* partitions the available spectral band among multiple direct-sequence signals, each of which has a distinct subcarrier frequency. Whereas a single-carrier system provides diversity by using a rake demodulator that combines several multipath signals, a multicarrier system provides diversity by the combining of parallel correlator outputs, each of which is associated with a different subcarrier. Two of the main attractions of the multicarrier system are its potential ability to operate over disjoint, noncontiguous spectral regions and its ability to avoid transmissions in spectral regions with strong interference or where the multicarrier signal might interfere with other signals. These features have counterparts in frequency-hopping systems.

A typical multicarrier system divides a spectral band of bandwidth W into L frequency channels or *subchannels*, each of bandwidth W/L. The carrier associated with a subchannel is called a *subcarrier*. In one type of system, which is diagrammed in Fig. 5.27, this bandwidth is approximately equal to the coherence bandwidth because a larger one would allow frequency-selective fading in each subchannel, while a smaller one would allow correlated fading among the subcarriers [17]. It is assumed that the spacing between adjacent subcarriers is β/T_c, where $\beta \geq 1$. The coherence bandwidth (Sect. 5.3) is approximately $1/T_d$, where T_d is the delay spread. Thus, $T_c \leq \beta T_d$ is required to ensure that each subcarrier signal is subject to independent fading. If the bandwidth of a subcarrier signal is on the order of $1/T_c$, then $T_c \geq T_d$ is required for the subcarrier signals to experience no significant frequency-selective fading. The two preceding inequalities

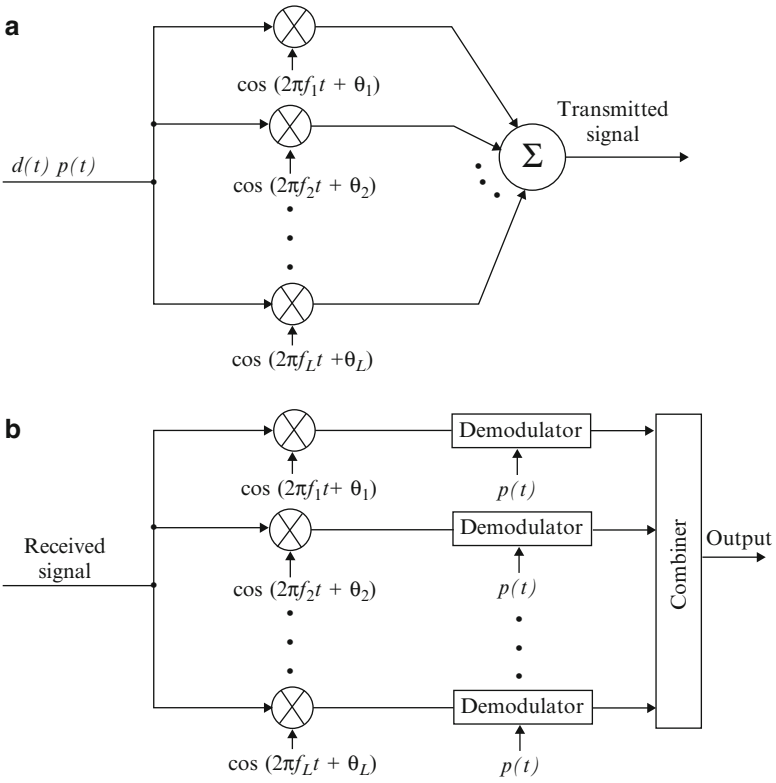

Fig. 5.27 Multicarrier direct-sequence system: (**a**) transmitter and (**b**) receiver

imply that $1 \leq \beta \leq 2$ is required. If the chip waveforms are rectangular and $\beta = 1$ or $\beta = 2$, then the subcarrier frequencies are orthogonal, which can be verified by a calculation similar to that leading to (3.66). Although the orthogonality prevents *self-interference* among the subcarrier signals, its effectiveness is reduced by multipath components and Doppler shifts. One may use bandlimited subcarrier signals to minimize the self-interference without requiring orthogonality. If $\beta = 2$ and the chip waveforms are rectangular, then the spectral mainlobes of the subcarrier signals have no overlap. Furthermore, a spacing of $2/T_c$ limits the significant multiple-access interference in a subchannel to subcarrier signals from other users that have the same subcarrier frequency.

In the transmitter, the product $d(t)p(t)$ of the data modulation $d(t)$ and the spreading waveform $p(t)$ simultaneously modulates L subcarriers, each of which has its frequency in the center of one of the L spectral regions, as illustrated in Fig. 5.27a. The receiver has L parallel demodulators, one for each subcarrier, the outputs of which are suitably combined, as indicated in Fig. 5.27b. The total signal power is divided equally among the L subcarriers. The chip rate and, hence, the processing gain for each subcarrier of a multicarrier direct-sequence system is

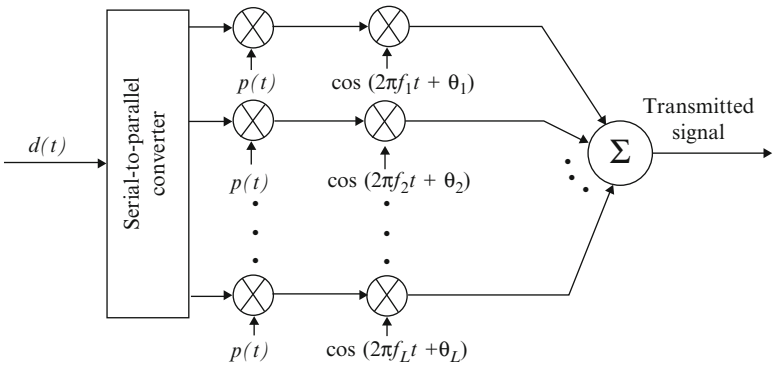

Fig. 5.28 Multicarrier DS/CDMA transmitter

reduced by the factor L. However, if strong interference exists in a subchannel, the gain used in MRC is small. Alternatively, the associated subcarrier can be omitted and the saved power redistributed among the remaining subcarriers. Channel codes and interleaving can be used to provide both time diversity and coding gain. Since the spectral regions are defined so that the fading in each of them is independent and frequency nonselective, the frequency diversity provided by the spectral regions can be exploited in a diversity combiner.

Another version of the transmitter of a *multicarrier direct-sequence system* is shown in Fig. 5.28. This system uses a serial-to-parallel converter to convert a stream of data symbols into multiple parallel substreams of different data symbols. The multicarrier modulation reduces the data-symbol rate and, hence, the intersymbol interference of the direct-sequence signal in each subchannel. The receiver is similar in form to that of Fig. 5.27b except that the combiner is replaced by a parallel-to-serial converter. If the subcarriers are separated by $2/T_c$, then the interchannel interference and multiple-access interference from subcarrier signals are minimized. The cost of this efficiency is a high peak-to-average power ratio (PAPR) for the transmitted signal. In contrast to the system of Fig. 5.27, the multicarrier system of Fig. 5.28 cannot exploit frequency diversity because each subcarrier is modulated by a different data symbol. However, the processing gain of each subchannel signal is increased by the factor L, which can be exploited in the suppression of multiple-access interference.

5.8.1 MC-CDMA System

A *code-division multiple-access* (CDMA) system (Chap. 6) is one that uses a spreading sequence or frequency-hopping pattern to accommodate multiple users. The multicarrier systems of Figs. 5.27 and 5.28 are very expensive and impractical because of their hardware requirements. A much more practical multicarrier system

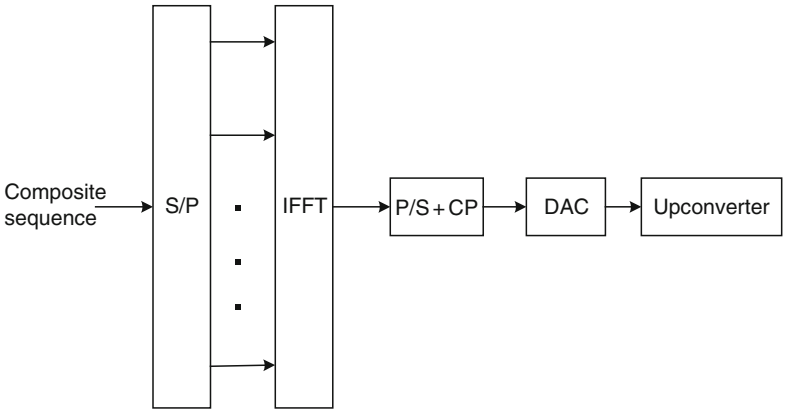

Fig. 5.29 Principal components of the transmitter of an MC-CDMA system

that can be used as a CDMA system is called the *multicarrier CDMA* (MC-CDMA) system. This system adapts the efficient processing of orthogonal frequency-division multiplexing [6], but differs from OFDM in that substantial diversity gain is provided. In an MC-CDMA system [18, 19], the sampled direct-sequence signal is converted into G parallel data-modulated chip samples, where G is the number of chips per data symbol. Each of these G samples modulates a different sampled subcarrier so that the spreading occurs in the frequency domain.

The principal components of the transmitter of an MC-CDMA system are depicted in Fig. 5.29. The data symbols of each of the N users are spread by a separate orthogonal spreading sequence with spreading factor G. Users that require higher data rates may use more than one spreading sequence, thereby becoming equivalent to more than one user. We consider a synchronous MC-CDMA system for downlink communications in which the data symbols and the spreading-sequence chips are all aligned in time. The sampling rate is $1/T_c$, where T_c is the chip duration. Consider a *block* of G samples and one data-symbol per user. The input samples applied to the serial-to-parallel converter (S/P) constitute the composite sequence

$$s(i) = \sum_{n=0}^{N-1} d_n p_n(i), \quad i = 0, 1, ..., G-1 \tag{5.275}$$

where d_n is the data symbol of user n during the block, and $p_n(i)$ is sample i of the G samples of the spreading-sequence of user n. The G parallel converter outputs may be represented by the vector

$$\mathbf{b} = \mathbf{Pd} = \sum_{n=0}^{N-1} \mathbf{p}_n d_n \tag{5.276}$$

where column n of the $G \times G$ matrix $\mathbf{P}$ is the vector $\mathbf{p}_n$ that represents the spreading sequence of user n, and $\mathbf{d}$ is the N-dimensional vector representing the data symbols:

$$\mathbf{p}_n = [p_n(G-1)\ p_n(G-2)\ \ldots\ p_n(0)]^T, \quad \mathbf{d} = [d_0\ d_1\ \ldots\ d_{N-1}]^T. \tag{5.277}$$

Orthogonality of the spreading sequences implies that

$$\mathbf{p}_i^H \mathbf{p}_k = \mathbf{0},\ k \neq i \quad \text{(orthogonal sequences)}. \tag{5.278}$$

The G serial-to-parallel converter outputs are applied to an *inverse fast Fourier transformer* (IFFT), which implements an *inverse discrete Fourier transform*. A G-point *discrete Fourier transform* may be represented by the $G \times G$ matrix

$$\mathbf{F} = \frac{1}{\sqrt{G}} \begin{bmatrix} 1 & 1 & 1 & \cdots & 1 \\ 1 & W & W^2 & \cdots & W^{G-1} \\ \vdots & \vdots & \vdots & \vdots & \vdots \\ 1 & W^{G-1} & W^{2(G-1)} & \cdots & W^{(G-1)^2} \end{bmatrix} \tag{5.279}$$

where $W = \exp(-j2\pi/G)$ and $j = \sqrt{-1}$. Thus, $\mathbf{F}^H$ represents the G-point inverse discrete Fourier transform. The G parallel outputs of the IFFT are represented as components of the vector $\mathbf{x} = [x_{G-1}, x_{G-2}, \ldots, x_0]^T$, which transforms $\mathbf{b}$ according to

$$\mathbf{x} = \mathbf{F}^H \mathbf{b}. \tag{5.280}$$

Because of the IFFT transformation, each component of $\mathbf{b}$ is transmitted through a distinct sampled subcarrier and experiences flat fading. A straightforward evaluation verifies that

$$\mathbf{F}^H \mathbf{F} = \mathbf{F}\mathbf{F}^H = \mathbf{I} \tag{5.281}$$

which indicates that $\mathbf{F}$ is a unitary matrix, and hence $\mathbf{F}^{-1} = \mathbf{F}^H$. The parallel-to-serial converter (P/S) converts the components of $\mathbf{x}$ into a serial stream.

The channel impulse response is assumed to have the form

$$h(\tau) = \sum_{i=0}^{m} h_i \delta(\tau - iT_c) \tag{5.282}$$

where some of the coefficients $\{h_i\}$ may be zero, depending on how many significant multipath components exist, and mT_c is the *multipath delay spread* or duration of the impulse response. A *guard interval* of duration mT_c or larger must be inserted between blocks to prevent *interblock interference* due to the multipath delay spread. The guard interval is implemented by appending an m-sample *cyclic prefix* (CP) prior to the samples of the data stream. It is assumed that G is chosen so that

$$G \geq m + 1. \tag{5.283}$$

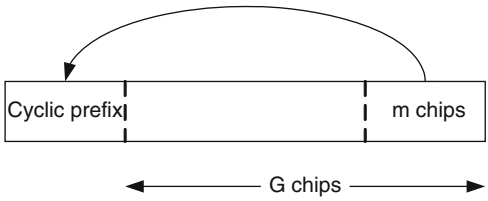

Fig. 5.30 Appending the cyclic prefix prior to the data stream

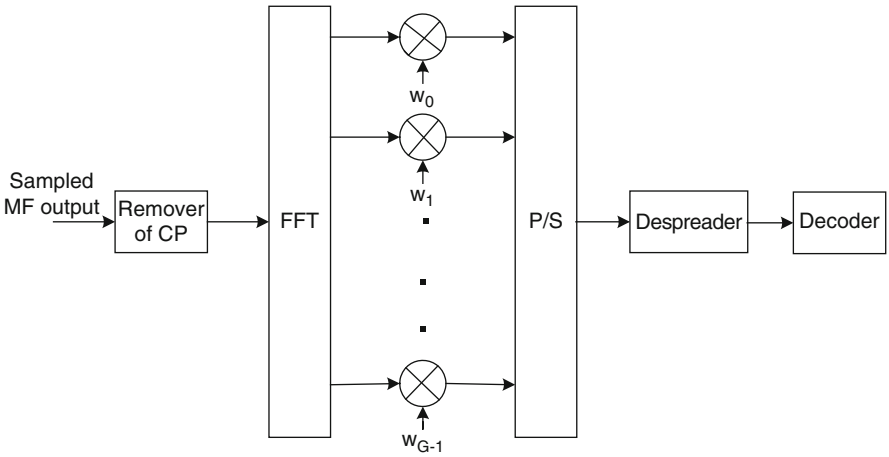

Fig. 5.31 Principal components of the MC-CDMA receiver

After the insertion of the cyclic prefix, the resultant sequence is represented by the vector $\overline{\mathbf{x}}$ with $G + m$ components defined by

$$\overline{x}_i = x_k, \quad k = i \text{ modulo-}G, \quad -m \leq i \leq G - 1 \tag{5.284}$$

which is illustrated in Fig. 5.30, this sequence is applied to a DAC and then a modulator for transmission, as shown in Fig. 5.29.

The duration of the time interval during which the data block is transmitted is $T = T_c(m + G) = T_s(1 + m/G)$, where $T_s = GT_c$ is the data-symbol duration. If the data rate is fixed, then the extended sequence causes a reduction in the energy per data symbol that is processed by the receiver, as explained subsequently. The reduction is by the *prefix factor*

$$c = \frac{G}{m + G}. \tag{5.285}$$

Since m is determined by the multipath delay spread and cannot be reduced without introducing interblock interference, c is increased by increasing G.

The principal components of the MC-CDMA receiver are diagrammed in Fig. 5.31. Assuming nearly ideal chip waveforms, chip-matched filters, and sampling timing, there is negligible intersymbol interference. The m-sample cyclic prefix (CP) of the matched-filter output samples is discarded because these samples

are corrupted by the prior data block. The remaining G-dimensional received vector is

$$\overline{\mathbf{y}} = \overline{\mathbf{H}}_1 \overline{\mathbf{x}} + \overline{\mathbf{n}} \tag{5.286}$$

where $\overline{\mathbf{y}} = [y_{G-1}\ y_{G-2}\ \ldots\ y_0]^T$, $\overline{\mathbf{x}} = [\overline{x}_{G-1}\ \overline{x}_{G-2}\ \ldots\ \overline{x}_{-m}]^T$, $\overline{\mathbf{n}}$ is the G-dimensional vector of Gaussian noise samples, $\overline{\mathbf{H}}_1$ is the $G \times (G+m)$ matrix

$$\mathbf{H}_1 = \begin{bmatrix} h_0 & h_1 & \cdots & h_m & 0 & \cdots & 0 \\ 0 & h_0 & \cdots & h_{m-1} & h_m & \cdots & 0 \\ \vdots & \vdots & \vdots & \vdots & \vdots & \vdots & \vdots \\ 0 & \cdots & 0 & h_0 & \cdots & h_{m-1} & h_m \end{bmatrix} \tag{5.287}$$

and the $\{h_i\}$ represent the coefficients of the channel impulse response. Since the final m components of $\overline{\mathbf{x}}$ constitute the cyclic prefix, which is derived from $\mathbf{x}$, we find that the received vector may be represented by

$$\overline{\mathbf{y}} = \mathbf{H}\mathbf{x} + \overline{\mathbf{n}} \tag{5.288}$$

where $\mathbf{H}$ is the $G \times G$ matrix

$$\mathbf{H} = \begin{bmatrix} h_0 & h_1 & \cdots & h_m & 0 & \cdots & 0 \\ 0 & h_0 & \cdots & h_{m-1} & h_m & \cdots & 0 \\ \vdots & \vdots & \vdots & \vdots & \vdots & \vdots & \vdots \\ 0 & \cdots & 0 & h_0 & \cdots & h_{m-1} & h_m \\ \vdots & \vdots & \vdots & \vdots & \vdots & \vdots & \vdots \\ h_2 & h_3 & \cdots & h_{m-2} & \cdots & h_0 & h_1 \\ h_1 & h_2 & \cdots & h_{m-1} & \cdots & 0 & h_0 \end{bmatrix}. \tag{5.289}$$

This matrix has the form of a *circulant* matrix, which is a matrix in which each row is obtained from the previous one by circularly shifting the latter to the right by one element. The form of $\mathbf{H}$ indicates that although the cyclic prefix has been removed, it affects $\mathbf{H}$, and hence influences the received vector $\mathbf{y}$. As shown in Sect. 1.1 for pulse-amplitude and orthogonal modulations, $\overline{\mathbf{n}}$ has zero-mean, circularly symmetric components. Therefore, $\overline{\mathbf{n}}$ is a zero-mean, circularly symmetric, complex-valued, Gaussian noise vector with $E\left[\overline{\mathbf{n}}\overline{\mathbf{n}}^T\right] = 0$. The covariance of $\overline{\mathbf{n}}$ is

$$E\left[\overline{\mathbf{n}}\overline{\mathbf{n}}^H\right] = N_0\mathbf{I} \tag{5.290}$$

where $N_0/2$ is the two-sided noise-power spectral density, and $\mathbf{I}$ is the $G \times G$ identity matrix.

Each column of $\mathbf{F}^H$ has the form

$$\mathbf{f}_i = \frac{1}{\sqrt{G}}[1\ \ W^{-i}\ \ W^{-2i}\ \ \cdots\ \ W^{-(G-1)i}]^T,\ \ i = 0, 1, \cdots, G-1. \tag{5.291}$$

A substitution of (5.289) and (5.291) into the eigenvector equation

$$\mathbf{H}\mathbf{f}_i = \lambda_i \mathbf{f}_i, \quad i = 0, 1, \cdots, G-1 \tag{5.292}$$

and the use of the fact that $W^G = 1$ prove that $\mathbf{f}_i$ is an eigenvector of $\mathbf{H}$ with the associated eigenvalue

$$\lambda_i = \sum_{k=0}^{m} h_k W^{-ki}, \quad i = 0, 1, \cdots, G-1. \tag{5.293}$$

Let

$$\mathbf{h} = [h_0 \ \ldots \ h_m \ \ldots \ 0]^T \tag{5.294}$$

denote the $G \times 1$ vector of impulse-response coefficients, at least $G-m-1$ of which are zero. Let $\boldsymbol{\lambda}$ denote the $G \times 1$ vector of eigenvalues:

$$\boldsymbol{\lambda} = [\lambda_0 \ \lambda_1 \ \ldots \ \lambda_{G-1}]^T. \tag{5.295}$$

Then (5.293) implies that

$$\boldsymbol{\lambda} = \sqrt{G}\mathbf{F}^H\mathbf{h}, \quad \mathbf{h} = \frac{1}{\sqrt{G}}\mathbf{F}\boldsymbol{\lambda} \tag{5.296}$$

and λ_i is component i of the discrete Fourier transform of the channel impulse response.

Since $\mathbf{F}$ is nonsingular, the $\{\mathbf{f}_i\}$ are linearly independent. Therefore, $\mathbf{H}$ is diagonalizable, and (5.292) implies that

$$\mathbf{H} = \mathbf{F}^H \boldsymbol{\Lambda} \mathbf{F} \tag{5.297}$$

where

$$\boldsymbol{\Lambda} = diag(\boldsymbol{\lambda}) \tag{5.298}$$

is the diagonal matrix with λ_i as its ith diagonal element, $i = 0, 1, \cdots, G-1$. This diagonalization is possible because of the way the cyclic prefix is defined, and hence provides the motivation for the definition of the cyclic prefix.

As indicated in Fig. 5.31, after a serial-to-parallel conversion, the received vector is applied to a *fast Fourier transformer* (FFT), which implements the *discrete Fourier transform*. The G parallel FFT outputs constitute the vector

$$\mathbf{y} = \mathbf{F}\bar{\mathbf{y}}. \tag{5.299}$$

The substitution of (5.288), (5.297), (5.280), and (5.281) into (5.299) yields

$$\mathbf{y} = \boldsymbol{\Lambda}\mathbf{b} + \mathbf{n} \tag{5.300}$$

where $\mathbf{n} = \mathbf{F}\overline{\mathbf{n}}$ is zero-mean, independent of $\mathbf{b}$, and has covariance

$$E\left[\mathbf{n}\mathbf{n}^H\right] = N_0\mathbf{I}. \tag{5.301}$$

Let $\mathcal{E}_{sn}$ denote the transmitted energy in the data symbol of user n when there is no cyclic prefix. Then

$$\| d_n\mathbf{p}_n \|^2 = c\mathcal{E}_{sn} \tag{5.302}$$

where the *prefix factor* c takes into account the energy loss due to the cyclic prefix. Normalizing the chip magnitudes so that

$$|p_n(i)| = \frac{1}{\sqrt{G}}, \quad 0 \le n \le N-1, \quad 0 \le i \le G-1 \tag{5.303}$$

we obtain

$$|d_n|^2 = c\mathcal{E}_{sn}. \tag{5.304}$$

5.8.1.1 Equalization

Equalization is the process by which the effect of the channel on $\mathbf{b}$ and $\mathbf{d}$ is compensated. The *linear equalizer* computes the estimator

$$\widehat{\mathbf{b}} = \mathbf{W}\mathbf{y} \tag{5.305}$$

where $\mathbf{W}$ is a $G \times G$ diagonal matrix with diagonal elements $w_i = W_{ii}$, $i = 0, 1, \cdots, G-1$, and $\widehat{\mathbf{b}} = [\widehat{b}_0 \;\; \widehat{b}_1 \; \ldots \; \widehat{b}_{N-1}]^T$. The diagonal elements are called the *weights* of the equalizer. As shown in Fig. 5.31, the equalized FFT outputs $\{\hat{b}_i\}$ are applied to a parallel-to-serial converter (P/S) that feeds its output to the despreader. The despreader computes the estimator of the data symbols $\mathbf{d} = [d_0 \;\; d_1 \; \ldots \; d_{N-1}]^T$ according to

$$\widehat{\mathbf{d}} = \mathbf{P}^H\widehat{\mathbf{b}}. \tag{5.306}$$

The substitution of (5.305), (5.300), and (5.276) into (5.306) indicates that

$$\widehat{\mathbf{d}} = \mathbf{P}^H\mathbf{W}\mathbf{\Lambda}\mathbf{P}\mathbf{d} + \mathbf{P}^H\mathbf{W}\mathbf{n} \tag{5.307}$$

which shows the relation between $\widehat{\mathbf{d}}$ and $\mathbf{d}$ after linear equalization and despreading. Using this equation, the fact that $\mathbf{W}\mathbf{\Lambda}$ is a diagonal matrix, (5.303), and (5.276), we find that the estimator of a symbol of an arbitrary user k is

$$\widehat{d_k} = d_k G^{-1} tr\,(\mathbf{W}\mathbf{\Lambda}) + \sum_{n=0, n\neq k}^{N-1} d_n\mathbf{p}_k^H\mathbf{W}\mathbf{\Lambda}\mathbf{p}_n + \mathbf{p}_k^H\mathbf{W}\mathbf{n}. \tag{5.308}$$

The first term is the desired part of the estimator while the remaining terms constitute noise and multiple-access interference.

A *zero-forcing* (ZF) equalizer estimates $\mathbf{d}$ by using

$$\mathbf{W} = \mathbf{\Lambda}^{-1} \quad \text{(ZF)}. \tag{5.309}$$

This equation, (5.307), and the orthogonality specified by (5.278) imply that the zero-forcing equalizer and despreading provide $\widehat{\mathbf{d}} = \mathbf{d} + \mathbf{P}^H \mathbf{\Lambda}^{-1} \mathbf{n}$. Thus, the zero-forcing equalizer allows the recovery of the data symbols of all users without interference among their symbols. For an arbitrary user k, we have the unbiased estimator

$$\widehat{d_k} = d_k + \mathbf{p}_k^H \mathbf{\Lambda}^{-1} \mathbf{n}. \tag{5.310}$$

The problem with the zero-forcing equalizer is that if $|\lambda_i|$ is low for some value of i, then the noise term in (5.310) is greatly amplified and degrades the estimator $\widehat{d_k}$. The *SNR for the data symbol of user k provided by the zero-forcing equalizer* is proportional to the ratio of the squared magnitude of the first term in (5.310) to the variance of the second term:

$$\gamma_{sk} = \frac{|d_k|^2}{var\left(\widehat{d_k}\right)} \tag{5.311}$$

where $var\left(\widehat{d_k}\right) = E\left[\left|\mathbf{p}_k^H \mathbf{\Lambda}^{-1} \mathbf{n}\right|\right]^2$. From this equation, (5.301), and (5.303), we obtain

$$var\left(\widehat{d_k}\right) = N_0 G^{-1} tr\left(\mathbf{\Lambda}^{-1} \mathbf{\Lambda}^{-*}\right) \quad \text{(ZF)} \tag{5.312}$$

where $\mathbf{\Lambda}^{-*}$ denotes the complex conjugate of $\mathbf{\Lambda}^{-1}$ and tr($\mathbf{A}$) denotes the trace of matrix $\mathbf{A}$, which is the sum of its diagonal elements. Substituting (5.304) and (5.312) into (5.311), we find that

$$\gamma_{sk} = \frac{c\mathcal{E}_{sk}}{N_0} \frac{G}{tr\left(\mathbf{\Lambda}^{-1} \mathbf{\Lambda}^{-*}\right)}, \quad \text{(ZF)}. \tag{5.313}$$

The noise amplification of the zero-forcing equalizer is avoided by using MRC equalization. An *MRC equalizer* maximizes the SNR of the data symbol of a single user. To assess the SNR when an arbitrary user k is the sole user, we discard the middle term of (5.308) and substitute the diagonal elements of $\mathbf{W}$ and $\mathbf{\Lambda}$. We obtain

$$\widehat{d_k} = d_k G^{-1} \sum_{i=0}^{G-1} w_i \lambda_i + \sum_{i=0}^{G-1} w_i p_{ki} n_i \tag{5.314}$$

where p_{ki} denotes component i of $\mathbf{p}_k$. The noise samples of $\mathbf{n}$ are independent, identically distributed, zero-mean Gaussian random variables with covariance given

by (5.301). Therefore, after applying (5.301), (5.303), and (5.304), we find that the SNR is proportional to

$$\gamma_{sk} = \frac{c\mathcal{E}_{sk}}{N_0 G} \frac{\left|\sum_{i=0}^{G-1} w_i \lambda_i\right|^2}{\sum_{i=0}^{G-1} |w_i|^2} \tag{5.315}$$

where $\mathcal{E}_{sk}$ is the energy of user k. Application of the Cauchy–Schwarz inequality for complex numbers given by (5.160) indicates that γ_{sk} is maximized if

$$w_i = \eta \lambda_i^* \quad \text{(MRC)} \tag{5.316}$$

where η is an arbitrary constant. Equivalently, $\mathbf{W}$ is a diagonal matrix with diagonal elements

$$\mathbf{W} = \eta \mathbf{\Lambda}^* \quad \text{(MRC)} \tag{5.317}$$

which is independent of the particular user. Therefore, the *SNR for the data symbol of user k provided by the MRC equalizer* is

$$\gamma_{sk} = \frac{c\mathcal{E}_{sk} \|\boldsymbol{\lambda}\|^2}{N_0 G} \quad \text{(sole user, MRC)}. \tag{5.318}$$

The *minimum mean-square error (MMSE) equalizer or linear detector* equalizes with a diagonal matrix $\mathbf{W}$ such that the mean squared error $\text{MSE} = E[\| \mathbf{Wy} - \mathbf{b} \|^2]$ is minimized. The MSE can be expressed as $\text{MSE} = tr(\mathbf{R})$, which is the trace of matrix

$$\mathbf{R} = E[(\mathbf{Wy} - \mathbf{b})(\mathbf{Wy} - \mathbf{b})^H]. \tag{5.319}$$

Let $\mathbf{R}_b = E[\mathbf{bb^H}]$ and $\mathbf{R}_y = E[\mathbf{yy}^H]$. It is assumed that the nonnegative-definite correlation matrix $\mathbf{R}_y$ is positive definite, and hence invertible. An expansion of (5.319) and the substitution of (5.300) yields

$$\begin{aligned} \mathbf{R} &= \mathbf{W}\,\mathbf{R}_y\,\mathbf{W}^H - \mathbf{W}\,\mathbf{\Lambda}\,\mathbf{R}_b - \mathbf{R}_b\,\mathbf{\Lambda}^*\,\mathbf{W}^* + \mathbf{R}_b \\ &= (\mathbf{W} - \mathbf{R}_b\,\mathbf{\Lambda}^*\,\mathbf{R}_y^{-1})\mathbf{R}_y\,(\mathbf{W} - \mathbf{R}_b\,\mathbf{\Lambda}^*\,\mathbf{R}_y^{-1})^H + \mathbf{R}_b - \mathbf{R}_b\,\mathbf{\Lambda}^*\,\mathbf{R}_y^{-1}\mathbf{\Lambda}\,\mathbf{R}_b. \end{aligned} \tag{5.320}$$

Only the first term of the second equation depends on $\mathbf{W}$. The *trace identity* is $tr(\mathbf{AB}) = tr(\mathbf{BA})$ for compatible matrices $\mathbf{A}$ and $\mathbf{B}$, which is proved by direct substitution of the definitions of matrix multiplication and the trace of a matrix. Using $\mathbf{R}_y = E[\mathbf{yy}^H]$ and the trace identity, we find that the first term of the second equation is nonnegative. Therefore, the MMSE estimate is obtained by using the matrix $\mathbf{W} = \mathbf{R}_b\,\mathbf{\Lambda}^*\,\mathbf{R}_y^{-1}$. Using (5.300) to evaluate $\mathbf{R}_y$, we obtain

$$\mathbf{W} = \mathbf{R}_b\,\mathbf{\Lambda}^*\,[\mathbf{R}_n + \mathbf{\Lambda}\,\mathbf{R}_b\,\mathbf{\Lambda}^*]^{-1}. \tag{5.321}$$

To evaluate $\mathbf{R}_b$, each chip in a spreading sequence is modeled as an independent, zero-mean random variable. Then (5.276), (5.303), and (5.304) imply that $\mathbf{R}_b = \sigma_b^2 \mathbf{I}$, and

$$\sigma_b^2 = \sum_{n=0}^{N-1} \frac{c\mathcal{E}_{sn}}{G} = \frac{cN\overline{\mathcal{E}}_s}{G}, \quad \overline{\mathcal{E}}_s = \frac{1}{N} \sum_{n=0}^{N-1} \mathcal{E}_{sn} \tag{5.322}$$

where $\overline{\mathcal{E}}_s$ is the average value of $\mathcal{E}_{sn}$ over all N users. Substituting these results and $\mathbf{R}_n = \sigma_n^2 \mathbf{I}$ into (5.321), we obtain

$$\mathbf{W} = \mathbf{\Lambda}^* \left[\frac{\sigma_n^2}{\sigma_b^2} \mathbf{I} + \mathbf{\Lambda}\mathbf{\Lambda}^* \right]^{-1} \quad \text{(MMSE)} \tag{5.323}$$

which is a diagonal matrix with diagonal elements $w_i = W_{ii}$, $i = 0, 1, \cdots, G-1$, given by

$$w_i = \frac{\lambda_i^*}{|\lambda_i|^2 + \left(\frac{cN\overline{\mathcal{E}}_s}{GN_0} \right)^{-1}} \quad \text{(MMSE)}. \tag{5.324}$$

Since $\mathbf{W}\mathbf{\Lambda} \neq \mathbf{I}$ when MRC and MMSE equalizers are used, these equalizers at least partially forego the advantage of spreading-sequence orthogonality and produce an estimator $\widehat{\mathbf{d}}$ that is not proportional to $\mathbf{d}$ in the absence of noise. However, the noise is usually not amplified by the processing, and hence these equalizers are usually preferred over the zero-forcing equalizer. If the number of users is sufficiently large that

$$\frac{cN\overline{\mathcal{E}}_s}{N_0} \gg \frac{G}{\min\limits_i |\lambda_i|^2} \tag{5.325}$$

then (5.324) and (5.309) indicate that the MMSE equalizer approximates the zero-forcing equalizer.

If it is assumed that

$$\frac{c\mathcal{E}_{sk}}{N_0} \ll \frac{G}{\max\limits_i |\lambda_i|^2} \tag{5.326}$$

where $\mathcal{E}_{sk}$ is the energy of the single user k, then (5.324) with $N = 1$ indicates that the MMSE equalizer has $w_i \approx c\mathcal{E}_{sk}\lambda_i^*/N_0 G$, which is proportional to the MRC equalizer weight, as indicated by (5.316). Therefore, when the assumption is valid and there is only one user, γ_{sk} is given by (5.318) for both the MRC and MMSE equalizers.

5.8.1.2 Performance Analysis

The approximate symbol error rate for a user with MRC or MMSE equalization in the presence of multiple-access interference can be obtained by assuming that

the chips of each spreading sequence are independent, zero-mean random variables. Therefore, (5.303) indicates that

$$E\left[p_n^*(i)\,p_m(k)\right] = \begin{cases} G^{-1}, & n = m,\ \ i = k \\ 0, & \text{otherwise} \end{cases} \tag{5.327}$$

where $0 \le n, m \le N-1$, $0 \le i, k \le G-1$, and $p_n(i)$ is the ith component of spreading-sequence n. Since the noise is independent of the spreading sequences, (5.308) implies that

$$\begin{aligned} var\left(\widehat{d}_k\right) &= \sum_{n=0, n\neq k}^{N-1} c\mathcal{E}_{sn} E\left[\left|\mathbf{p}_k^H(\mathbf{W}\Lambda)\mathbf{p}_n\right|^2\right] + N_0 G^{-1} tr\left(\mathbf{W}\mathbf{W}^*\right) \\ &= c\mathcal{E}_t G^{-2} tr\left(\mathbf{W}\mathbf{\Lambda}\mathbf{\Lambda}^*\mathbf{W}^*\right) + N_0 G^{-1} tr\left(\mathbf{W}\mathbf{W}^*\right) \end{aligned} \tag{5.328}$$

where $\mathcal{E}_t$ is the *total energy of the multiple-access interference*:

$$\mathcal{E}_t = \sum_{n=0, n\neq k}^{N-1} \mathcal{E}_{sn}. \tag{5.329}$$

The *SNR for the data symbol of user k provided by the equalizer* is proportional to the ratio of the squared magnitude of the first term in (5.308) to $var\left(\widehat{d}_k\right)$. Therefore,

$$\gamma_{sk} = \frac{\frac{c\mathcal{E}_{sk}}{G}\left|tr\left(\mathbf{W}\mathbf{\Lambda}\right)\right|^2}{\frac{c\mathcal{E}_t}{G} tr\left(\mathbf{W}\mathbf{\Lambda}\mathbf{\Lambda}^*\mathbf{W}^*\right) + N_0 tr\left(\mathbf{W}\mathbf{W}^*\right)}, \quad \text{(MRC, MMSE)}. \tag{5.330}$$

A comparison of (5.330) and (5.313) indicates that although the MRC and MMSE equalizers tend to avoid the enhancement of noise, they allow multiple-access interference that increases with the number of users.

Matrix $\mathbf{W}\mathbf{\Lambda}$ has real-valued components for all the equalizers when $\eta = 1$ in (5.317). Therefore, if the data modulation is binary antipodal or BPSK, then $d_k = \pm 1$ and the sign of $Re\left(\widehat{d}_k\right)$ determines the symbol decision for user k. Since the noise is Gaussian, the symbol error probability is (Sect. 1.2)

$$P_s = Q(\sqrt{2\gamma_{sk}}) \tag{5.331}$$

where γ_{sk} is given by (5.330) for the MRC and MMSE equalizers and (5.313) for the zero-forcing equalizer. To assess the performance of the MC-CDMA system with the MRC and MMSE equalizers when user k is the sole user, we set $\mathcal{E}_t = 0$. Then (5.330) reduces to (5.318) for the MRC equalizer and the MMSE equalizer if (5.326) is satisfied.

Equation (5.296) indicates that the impulse-response vector $\mathbf{h}$ has the squared norm

$$\| \mathbf{h} \|^2 = \frac{\| \mathbf{\Lambda} \|^2}{G}. \tag{5.332}$$

This equation indicates that *the energy in the time-domain components of the impulse response has been distributed among the eigenvalues of the matrix* $\mathbf{H}$ *of* (5.289).

If there are at most $m + 1$ nonzero elements of $\mathbf{h}$ and $\alpha_i = |h_{i+1}|$ denotes each magnitude, then (5.318) and (5.332) imply that for a single user and an MRC or MMSE equalizer

$$\gamma_{sk} \approx \frac{c\mathcal{E}_{sk}}{N_0} \sum_{i=1}^{m+1} \alpha_i^2 \tag{5.333}$$

provided that (5.326) is satisfied. Equation (5.333) is the same as (5.267) derived for the single-carrier direct-sequence system with a rake demodulator that has $L = m + 1$, $N_{0e} = N_0$ and $\mathcal{E}_s = c\mathcal{E}_{sk}$. Therefore, if the $\{\alpha_i\}$ have Rayleigh distributions, then (5.269) and (5.270) are valid for the single-user MC-CDMA system with an MRC or MMSE equalizer provided that (5.326) and (5.283) are satisfied. As indicated by the equations, the single-carrier direct-sequence system with rake combining and the MC-CDMA system with an MRC or MMSE equalizer give approximately the same performance for a single user except for two principal factors. One is the MC-CDMA system loss due to the prefix factor $c \leq 1$, which accounts for the energy wasted in the cyclic prefix. The other, which is generally much more significant, is the loss in the single-carrier direct-sequence system due to path crosstalk, which has been neglected in the derivation of the performance of the rake demodulator.

As an example of the performance of a single-user MC-CDMA system with an MRC or MMSE equalizer, we assume that a (63, 36) BCH channel code with $n = 63$, $k = 36$, $t = 5$, and ideal channel-symbol interleaving is used. For this loosely packed, binary block code and hard-decision decoding with a bounded-distance decoder, the information-bit error probability P_b as a function of the symbol error probability P_s is approximated by (1.30). The signal energy per channel symbol is $\mathcal{E}_s = c\mathcal{E}_{sk} = cr\mathcal{E}_b$, where $r = k/n = 4/7$ is the code rate, and $\mathcal{E}_b$ is the energy per information bit. We evaluate P_s for the frequency-selective fading channel by using (5.269) and (5.270) with $L = m+1 = 4$, $\bar{\gamma}_1 = cr\bar{\gamma}_b$, where $\bar{\gamma}_b = \mathcal{E}_b\overline{\alpha_1^2}/N_0$ is the average bit SNR. Figure 5.32 plots P_b as a function of $\bar{\gamma}_b$ for a multicarrier system with $\Gamma_1 = (-4, -8, -12)$ dB, and $\Gamma_2 = (-2, -3, -6)$ dB, which are typical for rural and urban environments, respectively. It is assumed that $G \geq 4$ and that G is large enough that (5.326) is satisfied for $\bar{\gamma}_b \geq 0$ dB. If $P_b = 10^{-5}$ is required, then the multicarrier system in an urban environment characterized by Γ_2 has an approximate 2.5 dB advantage relative to a similar system in a rural environment characterized by Γ_1. The loss when $c = 0.75$, which is due to a cyclic prefix that is $1/4$ of the total symbol duration, is roughly 1 dB.

If the $\{\lambda_i\}$ are subject to fading that varies from symbol to symbol, then the symbol error probability can be calculated by integrating (5.331) over the

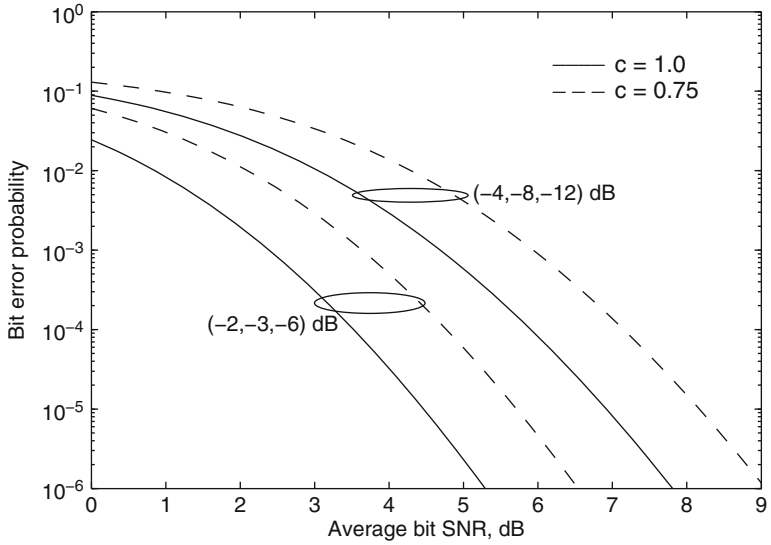

Fig. 5.32 Information-bit error probability for single-user MC-CDMA system with typical rural and urban multipath intensity vectors. Error-control code is BCH (63, 36)

distributions of the $\{\lambda_i\}$. Simulation and analytical results indicate that the MRC and MMSE equalizers provide nearly the same performance for a few users, but MMSE equalizers gain the advantage as the number of users increases [15, 16].

5.8.1.3 Channel Estimation

The implementation of equalization requires *channel estimates*, which comprise estimates of the components of $\boldsymbol{\lambda}$. The channel estimates may be obtained by transmitting known pilot symbols during some of the blocks. Accordingly, let $\mathbf{b}_a = [b_{a0}\ b_{a1} \ldots b_{a,G-1}]^T$ denote a known G-dimensional data vector of pilot symbols such that $|b_{ai}| = 1$, and let $\mathbf{B}$ denote a $G \times G$ diagonal matrix with diagonal elements

$$B_{ii} = b_{ai}^*, \quad i = 0, 1, \ldots, G-1. \tag{5.334}$$

When $\mathbf{b}_a$ is the received vector, the FFT output vector at the input to the equalizer is

$$\mathbf{y} = \boldsymbol{\Lambda}\mathbf{b}_a + \mathbf{n}. \tag{5.335}$$

A rough estimator of $\boldsymbol{\lambda}$ is

$$\widehat{\boldsymbol{\lambda}}_r = \mathbf{B}\mathbf{y} \tag{5.336}$$

since (5.335) and (5.336) indicate that $\widehat{\boldsymbol{\lambda}}_r = \boldsymbol{\lambda} + \mathbf{B}\mathbf{n}$.

This rough estimator may be refined by using the value of the delay spread mT_c, which is needed to determine the length of the cyclic prefix and is assumed to be known. The FFT is applied to $\widehat{\boldsymbol{\lambda}}_r$, which gives a rough estimator of $\mathbf{h}$:

$$\widehat{\mathbf{h}}_r = G^{-1/2}\mathbf{F}\widehat{\boldsymbol{\lambda}}_r. \tag{5.337}$$

Substituting (5.334)–(5.336) into (5.337) and using (5.296), we find that $\widehat{\mathbf{h}}_r = \mathbf{h} + G^{-1/2}\mathbf{FBn}$. The final $G-m-1$ components of $\widehat{\mathbf{h}}_r$ would be zero, like those of $\mathbf{h}$, in the absence of noise but are nonzero in the presence of noise. The final $G-m-1$ components are set to zero by the refined estimator

$$\widehat{\mathbf{h}} = \mathbf{I}_{m+1}\widehat{\mathbf{h}}_r \tag{5.338}$$

where $\mathbf{I}_{m+1}$ is the diagonal matrix with its first $m+1$ diagonal values equal to 1 and its remaining diagonal values set equal to 0. Since $\mathbf{I}_{m+1}$ has no effect on $\mathbf{h}$,

$$\widehat{\mathbf{h}} = \mathbf{h} + G^{-1/2}\mathbf{I_{m+1}FBn}. \tag{5.339}$$

The IFFT is applied to $\widehat{\mathbf{h}}$ to obtain the refined estimator of $\boldsymbol{\lambda}$, which is

$$\widehat{\boldsymbol{\lambda}} = G^{1/2}\mathbf{F}^H\widehat{\mathbf{h}}. \tag{5.340}$$

Substituting (5.336) -(5.338) into (5.340), we obtain the *channel estimator*:

$$\widehat{\boldsymbol{\lambda}} = \mathbf{F}^H\mathbf{I}_{m+1}\mathbf{FBy} \tag{5.341}$$

where the $G \times G$ product matrix $\mathbf{F}^H\mathbf{I}_{m+1}\mathbf{FB}$ can be stored in the receiver since the pilot symbols are known. When the pilot symbols are received, the product matrix is applied to the FFT output vector $\mathbf{y}$ to determine the channel estimator, which is used to calculate the weights in Fig. 5.31.

Substituting (5.339) and (5.296) into (5.340), we find that

$$\widehat{\boldsymbol{\lambda}} = \boldsymbol{\lambda} + \mathbf{n}_e \tag{5.342}$$

where $\mathbf{n}_e = \mathbf{F}^H\mathbf{I}_{m+1}\mathbf{FBn}$. Since $\mathbf{n}_e$ is zero-mean, $\widehat{\boldsymbol{\lambda}}$ is an unbiased estimator of $\boldsymbol{\lambda}$. The covariance matrix of $\mathbf{n}_e$ is $\mathbf{R}_{ne} = N_0\mathbf{F}^H\mathbf{I}_{m+1}\mathbf{F}$. Using (5.283), it is found that the noise power is

$$\begin{aligned} E\left[\| \mathbf{n}_e \|^2\right] &= tr\left[\mathbf{R}_{ne}\right] = (m+1)N_0 \\ &\le GN_0 = E\left[\| \mathbf{n} \|^2\right]. \end{aligned} \tag{5.343}$$

This inequality shows that the estimator (5.341) is corrupted by less total noise power than is present at the input to the equalizer.

5.8.1.4 PAPR

Since the IFFT outputs in the MC-CDMA transmitter have potentially large amplitude variations, the transmitter's power amplifier must either have its average output power reduced to maintain inefficient operation in its linear region with a high probability or operate in its nonlinear region. Although operation in the nonlinear region allows higher power levels, it causes signal distortion, excessive radiation into other spectral regions, and a performance loss due to intermodulation interference among the subcarriers. Another problem with the large amplitude variations in the IFFT outputs is the increase in the demands on the DAC, which increases its expense or introduces losses.

The PAPR of a transmitted signal over an interval is defined as the ratio of the maximum instantaneous power of a signal to its average value during the interval. If $x(t)$ represents the complex envelope of a signal and the interval $\mathcal{I}$ has duration T, then this ratio is

$$PAPR = \frac{\max\limits_{\mathcal{I}} |x(t)|^2}{\frac{1}{T}\int_{\mathcal{I}} |x(t)|^2\, dt}. \tag{5.344}$$

In an MC-CDMA system, the pulse shaping of each transmitted IFFT sample generates non-rectangular transmitted pulses or waveforms that increase the PAPR relative to its value without pulse shaping. If we ignore the effect of pulse shaping or assume that there is none, then the PAPR for a transmitted block of an MC-CDMA system is

$$PAPR \approx 2\frac{\max\limits_{-m\le i\le G-1} |\overline{x}_i|^2}{\frac{1}{G+m}\sum_{i=-m}^{G-1} |\overline{x}_i|^2} \tag{5.345}$$

where the $\{\overline{x}_i\}$ are defined in terms of $\mathbf{b}$ by (5.280) and (5.284), and the factor of "2" arises because the square of a sinusoidal waveform is averaged in the denominator of (5.344).

In the technical literature, the factor of "2" is often ignored. Thus, the subsequent analysis is in terms of the *discrete-time PAPR* defined as $\overline{PAPR} = PAPR/2$. To derive an approximate probability distribution function for $\overline{PAPR}$, we replace the denominator in (5.345) with $E\left[|\overline{x}_i|^2\right]$ and assume that each component of $\mathbf{b}$ is an independent, identically distributed, zero-mean random variable with variance equal to $E\left[|b|^2\right]$. Calculations using (5.280) and (5.284) yield $E\left[|\overline{x}_i|^2\right] = E\left[|x_i|^2\right] = E\left[|b|^2\right]$, and hence

$$\overline{PAPR} \approx \max_{-m\le i\le G-1}\left\{\frac{|\overline{x}_i|^2}{E\left[|b|^2\right]}\right\}. \tag{5.346}$$

If $G + m$ is large, the central-limit theorem indicates that the real and imaginary parts of $\overline{x}_i$ have distributions that are approximately Gaussian with variances equal to $E\left[|b|^2\right]/2$. As shown in Appendix B, $|\overline{x}_i|$ then has a Rayleigh distribution with a variance equal to $E\left[|b|^2\right]$, and $|\overline{x}_i|^2 / E\left[|b|^2\right]$ has an exponential distribution function $F(z) = 1 - \exp(-z)$ and a mean equal to 1. Equation (5.346) then implies that $\overline{PAPR}$ has a distribution function given by $[1 - \exp(-z)]^{G+m}$, and the probability that $\overline{PAPR}$ exceeds z is given by

$$P\left[\overline{PAPR} > z\right] \approx 1 - [1 - \exp(-z)]^{G+m}. \tag{5.347}$$

For large values of z,

$$P\left[\overline{PAPR} > z\right] \approx (G + m)\exp(-z) \tag{5.348}$$

which indicates that the probability that an excessively large value of $\overline{PAPR}$ occurs is proportional to the value of $G + m$. Thus, *the selection of the value of G is constrained by the level of the PAPR that can be tolerated.*

Numerous PAPR reduction techniques for OFDM systems have been proposed [20], and these techniques are generally applicable to MC-CDMA systems. The cost of PAPR reduction is an increase in the transmitted power, an increase in the bit error rate, an increase in the computational complexity, or a decrease in the throughput. The PAPR problem makes single-carrier direct-sequence code-division multiple-access (DS-CDMA) more suitable than MC-CDMA for uplink communications in a cellular network.

5.8.2 DS-CDMA System with Frequency-Domain Equalization

Instead of using rake combining to exploit frequency-selective fading, a single-carrier DS-CDMA system may use *frequency-domain equalization* (FDE) in the receiver [18, 19]. This type of equalization is applied to subcarrier components obtained from an FFT in the receiver. The DS-CDMA system with FDE preserves a favorable PAPR while eliminating the problem of interpath interference that exists in a rake demodulator. Although subsequently we set the spreading factor equal to the FFT window size, this equality is not required. By allowing the spreading factor to differ from the FFT window size, FDE can be applied to a multi-rate DS-CDMA system that uses OVSF sequences (Sect. 6.1).

The DS-CDMA system with FDE directly transmits the vector $\mathbf{b}$ defined by (5.276) without an application of an IFFT. The cyclic prefix is obtained from the composite chip sequence formed from the components of $\mathbf{b}$. The receiver is diagrammed in Fig. 5.33. Assuming nearly ideal chip waveforms, chip-matched filters, and sampling timing, there is negligible intersymbol interference in the

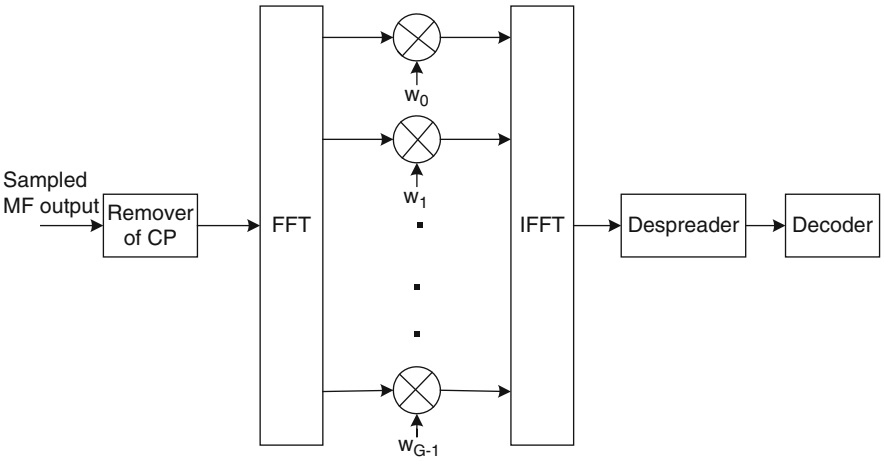

Fig. 5.33 Receiver of DS-CDMA system with FDE

sampled matched-filter output. The m-sample cyclic prefix (CP) of the matched-filter output samples is discarded because these samples are corrupted by the prior data block. The remaining samples constitute the components of the received vector

$$\bar{\mathbf{y}} = \mathbf{H}\mathbf{b} + \bar{\mathbf{n}}. \tag{5.349}$$

As indicated in the figure, after a serial-to-parallel conversion, the received vector is applied to an FFT. The G parallel FFT outputs constitute the vector $\mathbf{y} = \mathbf{F}\bar{\mathbf{y}}$. The substitution of (5.280) and (5.297) into this equation yields

$$\mathbf{y} = \mathbf{\Lambda}\mathbf{x} + \mathbf{n} \tag{5.350}$$

where $\mathbf{n} = \mathbf{F}\bar{\mathbf{n}}$, and $\mathbf{x} = \mathbf{F}\mathbf{b}$ is a discrete Fourier transform. Assuming that $E[\bar{\mathbf{n}}\bar{\mathbf{n}}^H] = N_0\mathbf{I}$, it follows that $E[\mathbf{n}\mathbf{n}^H] = N_0\mathbf{I}$.

The *equalizer* computes

$$\widehat{\mathbf{x}} = \mathbf{W}\mathbf{y} \tag{5.351}$$

where $\mathbf{W}$ is a diagonal matrix with diagonal elements $w_i = W_{ii}$. The substitution of (5.350) into (5.351) yields

$$\widehat{\mathbf{x}} = \mathbf{W}\mathbf{\Lambda}\mathbf{x} + \mathbf{W}\mathbf{n}. \tag{5.352}$$

As shown in Fig. 5.33, the equalized FFT outputs $\{\widehat{x}_i\}$ are applied to an IFFT that produces

$$\begin{aligned} \widehat{\mathbf{b}} &= \mathbf{F}^H \widehat{\mathbf{x}} \\ &= \mathbf{F}^H \mathbf{W}\mathbf{\Lambda}\mathbf{F}\mathbf{b} + \mathbf{F}^{\mathbf{H}}\mathbf{W}\mathbf{n}. \end{aligned} \tag{5.353}$$

The IFFT outputs are applied to a parallel-to-serial converter that feeds its output stream to the despreader. The despreader computes

$$\widehat{\mathbf{d}} = \mathbf{P}^H \widehat{\mathbf{b}}. \tag{5.354}$$

The substitution of (5.353) and (5.276) into this equation gives

$$\widehat{\mathbf{d}} = \mathbf{P}^H \mathbf{F}^H \mathbf{W} \mathbf{\Lambda} \mathbf{F} \mathbf{P} \mathbf{d} + \mathbf{P}^H \mathbf{F}^H \mathbf{W} \mathbf{n}. \tag{5.355}$$

The estimator of a symbol of an arbitrary user k is

$$\widehat{d_k} = d_k \mathbf{p}_k^H \mathbf{F}^H \mathbf{W} \mathbf{\Lambda} \mathbf{F} \mathbf{p}_k + \sum_{n=0, n \neq k}^{N-1} d_n \mathbf{p}_k^H \mathbf{F}^H \mathbf{W} \mathbf{\Lambda} \mathbf{F} \mathbf{p}_n + \mathbf{p}_k^H \mathbf{F}^H \mathbf{W} \mathbf{n}. \tag{5.356}$$

5.8.2.1 Equalization

A *zero-forcing* (ZF) equalizer uses weights determined by (5.309). The orthogonality of the N spreading sequences implies that symbol estimator for user k is

$$\widehat{d_k} = d_k + \mathbf{p}_k^H \mathbf{F}^H \mathbf{\Lambda}^{-1} \mathbf{n}. \tag{5.357}$$

Thus, the zero-forcing equalizer allows the recovery of the data symbols of all users without interference among these symbols at the cost of noise enhancement when one of the $\{\lambda_i\}$ is small.

An *MRC equalizer* maximizes the SNR of the data symbol of a single user. To assess the SNR when an arbitrary user k is the sole user, we discard the middle term of (5.356) and obtain

$$\widehat{d_k} = d_k \mathbf{u}^H \mathbf{m} + \mathbf{u}^H \mathbf{n} \tag{5.358}$$

where $\mathbf{u}$ and $\mathbf{m}$ are the $G \times 1$ vectors defined as

$$\mathbf{u} = \mathbf{W}^* \mathbf{F} \mathbf{p}_k, \quad \mathbf{m} = \mathbf{\Lambda} \mathbf{F} \mathbf{p}_k. \tag{5.359}$$

The noise samples of $\overline{\mathbf{n}}$, and hence $\mathbf{n}$, are independent, identically distributed, zero-mean Gaussian random variables with variance N_0. Using (5.304), we find that the SNR is proportional to

$$\gamma_{sk} = \frac{c\mathcal{E}_{sk}}{N_0} \frac{\left| \sum_{i=0}^{G-1} u_i^* m_i \right|^2}{\sum_{i=0}^{G-1} |u_i|^2} \tag{5.360}$$

where $\mathcal{E}_{sk}$ is the energy of user k. Application of the Cauchy–Schwarz inequality for complex numbers indicates that γ_{sk} is maximized if $u_i = \eta m_i$, where η is an arbitrary constant. Equations (5.359) indicate that the latter equality is satisfied if $\mathbf{W}$ is the diagonal matrix

$$\mathbf{W} = \eta \mathbf{\Lambda}^* \quad \text{(MRC)} \tag{5.361}$$

which is independent of the particular user. Therefore, the *SNR for the data symbol of user k provided by the MRC equalizer* is

$$\gamma_{sk} = \frac{c\mathcal{E}_{sk} \|\mathbf{m}\|^2}{N_0} \text{ (sole user, MRC).} \tag{5.362}$$

The *MMSE equalizer or linear detector* equalizes with a diagonal matrix $\mathbf{W}$ such that the mean squared error $\text{MSE} = E[\| \mathbf{Wy} - \mathbf{x} \|^2]$ is minimized. If each chip in a spreading sequence is modeled as an independent, zero-mean random variable, then (5.276), (5.303), and (5.304) imply that $\mathbf{R}_x = E\left[\mathbf{x}\mathbf{x}^H\right] = \mathbf{R}_b = \sigma_b^2\mathbf{I}$. Therefore, a derivation similar to the previous one for the MC-CDMA system indicates that the MMSE equalizer uses the matrix given by (5.323). Thus, the ZF, MRC, and MMSE equalizers are the same for the MC-CDMA system and the DS-CDMA system with FDE provided that both have the spreading factor equal to the FFT window size.

5.8.2.2 Performance Analysis

The approximate symbol error rate for a user with MRC or MMSE equalization in the presence of multiple-access interference can be obtained by assuming that the spreading sequences are statistically independent of each other and that the chips of each spreading sequence are independent, zero-mean random variables characterized by (5.327). Under this model, (5.356) and the identity $\mathbf{p}_k^H\mathbf{F}^H\mathbf{W}\mathbf{\Lambda}\mathbf{F}\mathbf{p}_k = tr\left(\mathbf{W}\mathbf{\Lambda}\mathbf{F}\mathbf{p}_k\mathbf{p}_k^H\mathbf{F}^H\right)$ imply that the estimator of a symbol of an arbitrary user k has

$$E\left[\widehat{d}_k\right] = d_k G^{-1} tr\left(\mathbf{W}\mathbf{\Lambda}\right) \tag{5.363}$$

and (5.356) may be expressed as

$$\begin{aligned}\widehat{d}_k &= d_k G^{-1} tr\left(\mathbf{W}\mathbf{\Lambda}\right) + d_k\left[\mathbf{p}_k^H\mathbf{D}\mathbf{p}_k - G^{-1} tr\left(\mathbf{W}\mathbf{\Lambda}\right)\right] \\ &\quad + \sum_{n=0, n\neq k}^{N-1} d_n \mathbf{p}_k^H\mathbf{D}\mathbf{p}_n + \mathbf{p}_k^H\mathbf{F}^H\mathbf{W}\mathbf{n}\end{aligned} \tag{5.364}$$

where

$$\mathbf{D} = \mathbf{F}^H\mathbf{W}\mathbf{\Lambda}\mathbf{F}. \tag{5.365}$$

The first term of (5.364) represents the desired part of the estimator, the second term represents the *self-interference*, the third term represents the multiple-access interference, and the final term represents the noise. The model implies that the

final three terms and all the terms within the sum are zero-mean and uncorrelated. Using (5.304), we obtain

$$var\left(\widehat{d_k}\right) = c\mathcal{E}_{sk} E\left[\left|\mathbf{p}_k^H \mathbf{D}\mathbf{p}_k - G^{-1} tr\left(\mathbf{W}\boldsymbol{\Lambda}\right)\right|^2\right] + \sum_{n=0, n\neq k}^{N-1} c\mathcal{E}_{sn} E\left[\left|\mathbf{p}_k^H \mathbf{D}\mathbf{p}_n\right|^2\right] + E\left[\left|\mathbf{p}_k^H \mathbf{F}^H \mathbf{W}\mathbf{n}\right|^2\right]. \tag{5.366}$$

Using (5.327) and (5.301), a straightforward evaluation yields

$$var\left(\widehat{d_k}\right) = c\mathcal{E}_{sk} G^{-2} D_s + c\mathcal{E}_t G^{-2} tr\left(\mathbf{W}\boldsymbol{\Lambda}\boldsymbol{\Lambda}^*\mathbf{W}^*\right) + N_0 G^{-1} tr\left(\mathbf{W}\mathbf{W}^*\right) \tag{5.367}$$

where

$$D_s = \sum_{i=0}^{G-1} \sum_{k=0, k\neq i}^{G-1} \left[|D_{ik}|^2 + D_{ik} D_{ki}^*\right] \tag{5.368}$$

and $\mathcal{E}_t$ is defined by (5.329).

Assuming that BPSK symbols are transmitted by all users and that $\widehat{d_k}$ has an approximately Gaussian distribution, the symbol error probability is given by (5.331) with

$$\gamma_{sk} = \frac{\frac{c\mathcal{E}_{sk}}{G} |tr\left(\mathbf{W}\boldsymbol{\Lambda}\right)|^2}{\frac{c\mathcal{E}_t}{G} tr\left(\mathbf{W}\boldsymbol{\Lambda}\Lambda^*\mathbf{W}^*\right) + N_0 tr\left(\mathbf{W}\mathbf{W}^*\right) + \frac{c\mathcal{E}_{sk}}{G} D_s} \quad \text{(MRC, MMSE)}. \tag{5.369}$$

If the $\{\lambda_i\}$, which constitute the nonzero elements of $\boldsymbol{\Lambda}$, are subject to fading that varies from symbol to symbol, then the symbol error probability can be calculated by integrating (5.331) over the distributions of the $\{\lambda_i\}$. Even if $\mathcal{E}_t = 0$, the denominator of (5.369) indicates that there is self-interference in addition to the noise. The self-interference exists in the DS-CDMA system with FDE but does not exist in the MC-CDMA system. However, numerical calculations indicate that when $\mathcal{E}_t > \mathcal{E}_{sk}$, the self-interference is typically negligible, and the symbol error probabilities for the two systems are nearly identical.

For the zero-forcing equalizer, (5.357) and the preceding assumptions indicate that P_s is given by (5.331) and (5.313).

5.8.2.3 Channel Estimation

The implementation of equalization requires channel estimation, which can be accomplished in the DS-CDMA system with FDE by a method similar to that

used in the MC-CDMA system. Let $\mathbf{b}_a = [b_{a0}\ b_{a1} \ldots b_{a,G-1}]^T$ denote a known G-dimensional vector of pilot symbols transmitted during some block, and let $\mathbf{x}_a = [x_{a0}\ x_{a1} \ldots x_{a,G-1}]^T$ denote the corresponding G-dimensional discrete Fourier transform vector. Let $\mathbf{X}$ denote a $G \times G$ diagonal matrix with diagonal elements

$$X_{ii} = x_{ai}^* / |x_{ai}|^2, \quad i = 0, 1, \ldots, G-1. \tag{5.370}$$

When $\mathbf{b}_a$ is the received vector, (5.350) indicates that the FFT output vector at the input of the equalizer is

$$\mathbf{y} = \mathbf{\Lambda}\mathbf{x}_a + \mathbf{n}. \tag{5.371}$$

A rough estimator of $\boldsymbol{\lambda}$ is

$$\widehat{\boldsymbol{\lambda}}_r = \mathbf{X}\mathbf{y} \tag{5.372}$$

since the last two equations indicate that $\widehat{\boldsymbol{\lambda}}_r = \boldsymbol{\lambda} + \mathbf{X}\mathbf{n}$. Using the same estimation method as used for the MC-CDMA system, the rough estimator leads to the more refined *channel estimator*:

$$\widehat{\boldsymbol{\lambda}} = \mathbf{F}^H \mathbf{I}_{m+1} \mathbf{F}\mathbf{X}\mathbf{y} \tag{5.373}$$

where the $G \times G$ product matrix $\mathbf{F}^H \mathbf{I}_{m+1} \mathbf{F}\mathbf{X}$ can be stored in the receiver. Straightforward calculations using (5.294) and (5.296) indicate that

$$\widehat{\boldsymbol{\lambda}} = \boldsymbol{\lambda} + \mathbf{n}_e \tag{5.374}$$

where $\mathbf{n}_e = \mathbf{F}^H \mathbf{I}_{m+1} \mathbf{F}\mathbf{X}\mathbf{n}$. Since $\mathbf{n}_e$ is zero-mean, $\widehat{\boldsymbol{\lambda}}$ is an unbiased estimator of $\boldsymbol{\lambda}$. The noise power is

$$E\left[\| \mathbf{n}_e \|^2\right] = tr\left[\mathbf{R}_{ne}\right] = N_0 tr\left[\mathbf{I}_{m+1} \mathbf{F}\mathbf{X}\mathbf{X}^* \mathbf{F}^H\right]. \tag{5.375}$$

5.8.2.4 Comparisons

Simulation and numerical results indicate that when the same equalizers are used, the DS-CDMA system with FDE and the MC-CDMA system provide nearly the same performance [18, 19]. Both systems benefit from the use of joint antenna diversity and equalization, but the performance improvement hinges on accurate calculations of the discrete Fourier transforms.

Although FDE using MRC is essentially rake combining in the spectral domain, there are practical differences. As the frequency selectivity increases, the number of paths with significant power increases, thereby increasing the required number of rake fingers. In contrast, the FDE implementation complexity is independent of the frequency selectivity. When (5.326) is not satisfied, simulation results indicate that FDE with MMSE usually provides much better performance than FDE with MRC.

Since each symbol is transmitted over a different subcarrier, OFDM does not provide the diversity gain of the DS-CDMA system with FDE and the MC-CDMA system. However, OFDM provides more coding gain.

Problems

5.1. Give an alternative derivation of (5.41). First, observe that the total received Doppler power $S_r(f) \mid df \mid$in the spectral band $[f, f + df]$ corresponds to arrival angles determined by $f_d \cos\theta = f$. Since $\cos\theta$ is an even function over angles $\mid \theta \mid \leq \pi$, $S_r(f) \mid df \mid = P(\theta) \mid d\theta \mid + P(-\theta) \mid d\theta \mid$, where $P(\theta)$ is the power density arriving from angle θ. Assume that the received power arrives uniformly spread over all angles $\mid \theta \mid \leq \pi$.

5.2. Following the guidance in the text, derive the maximum-likelihood decision variable (5.116) and its variance (5.120) for PSK over the Rayleigh fading channel.

5.3. Consider the maximum-likelihood detection of *coherent* FSK for the Rayleigh fading channel. The independent noise in each diversity branch has power spectral density N_{0i}, $i = 1, 2, \ldots, L$. Find the q decision variables and show that they are given by (5.146) when the $\{N_{0i}\}$ are all equal.

5.4. Consider the maximum-likelihood detection of *noncoherent* FSK for the Rayleigh fading channel. The independent noise in each diversity branch has power spectral density N_{0i}, $i = 1, 2, \ldots, L$. Find the q decision variables and show that they are given by (5.178) when the $\{N_{0i}\}$ are all equal.

5.5. Suppose that diversity L is achieved by first dividing the symbol energy into L equal parts so that the SNR per branch in (5.124) is reduced by the factor L. For the four modulations of Fig. 5.15 and $p \to 0$, by what factor does $\mathrm{P}_b(L)$ increase relative to its value when the energy is not divided?

5.6. For noncoherent q-ary orthogonal signals such as those with FSK, use the union bound to derive an upper bound on the symbol error probability as a function of q and the diversity L.

5.7. For dual rake combining, PSK, MRC, and Rayleigh fading, find $P_b(2)$ as both γ_1 and $\gamma_2 \to \infty$. Find $P_b(2)$ for dual rake combining, noncoherent orthogonal signals, EGC, and Rayleigh fading as both γ_1 and $\gamma_2 \to \infty$. What advantage does PSK have?

5.8. Three multipath components arrive at a direct-sequence receiver moving at $30\,\mathrm{m\,s^{-1}}$ relative to the transmitter. The second and third multipath components travel over paths 200 m and 250 m longer than the first component. If the chip rate is equal to the bandwidth of the received signal, what is the minimum chip rate required to resolve all components? How much time can the receiver allocate to the estimation of the component delays?

5.9. Consider a system that uses PSK or FSK, an (n, k) block code, and the maximum-likelihood metric in the presence of Rayleigh fading. Show by successive applications of various bounds that the word error probability for soft-decision decoding satisfies

$$P_w < q^k \binom{2d_m - 1}{d_m} P_s^{d_m}$$

where q is the alphabet size and d_m is the minimum distance between codewords.

5.10. Verify that (5.293) gives the eigenvalues of $\mathbf{H}$.

5.11. Use $\mathbf{R}_y = E[\mathbf{y}\mathbf{y}^H]$ and the trace identity to verify that the first term of (5.320) is nonnegative.

5.12. Verify (5.343).

5.13. Use (5.280), (5.284), and the model preceding (5.346) to prove that $E\left[|\overline{x}_i|^2\right] = E\left[|x_i|^2\right] = E\left[|b|^2\right]$.

5.14. Use the methods described in the text to verify (5.363) and (5.367).

References

1. M. K. Simon and M.-S. Alouini, *Digital Communication over Fading Channels, 2nd ed.* New York: Wiley, 2004.
2. J. G. Proakis and M. Salehi, *Digital Communications, 5th ed.* New York: McGraw-Hill, 2008.
3. G. Stuber, *Principles of Mobile Communication, 2nd ed.* Boston: Kluwer Academic, 2001.
4. S. J. Leon, *Linear Algebra with Applications, 8th ed.* Upper Saddle River, NJ: Pearson Prentice-Hall, 2009.
5. J. D. Parsons and J. G. Gardiner, *Mobile Communication Systems.* New York: Halsted Press, 1989.
6. D. R. Barry, E. A. Lee, and D. G. Messerschmitt, *Digital Communication, 3rd ed.* Boston: Kluwer Academic, 2004.
7. B. Porat, *A Course in Digital Signal Processing*. New York: Wiley, 1997.
8. R. A. Soni and R. M. Buehrer, "On the Performance of Open-Loop Transmit Diversity Techniques for IS-2000 Systems: A Comparative Study," *IEEE Trans. Wireless Commun.*, vol. 3, pp. 1602-1615, Sept. 2004.
9. E. G. Larsson and P. Stoica, *Space-Time Block Coding for Wireless Communications*. New York: Cambridge Univ. Press, 2003.
10. D. Torrieri and M.C. Valenti, "Efficiently Decoded Full-Rate Space-Time Block Codes," *IEEE Trans. Communications*, vol. 58, pp. 480-488, Feb. 2010.
11. S. Glisic and M. D. Katz, "Modeling of the Code Acquisition Process for Rake Receivers in CDMA Wireless Networks with Multipath and Transmitter Diversity," *IEEE J. Select. Areas Commun.*, vol. 19, pp. 21–32, Jan. 2001.
12. K. Higuchi et al., "Experimental Evaluation of Combined Effect of Coherent Rake Combining and SIR-Based Fast Transmit Power Control for Reverse Link of DS-CDMA Mobile Radio," *IEEE J. Select. Areas Commun.*, vol. 18, pp. 1526–1535, Aug. 2000.

13. D. Torrieri, "Simple Formula for Error Probability of Rake Demodulator for Noncoherent Binary Orthogonal Signals and Rayleigh Fading," *IEEE Trans. Commun.*, vol. 50, pp. 1734-1735, Nov. 2002.
14. S. Tanaka, A. Harada, and F. Adachi, "Experiments on Coherent Adaptive Antenna Array Diversity for Wideband DS-CDMA Mobile Radio," *IEEE J. Select. Areas Commun.*, vol. 18, pp. 1495–1504, Aug. 2000.
15. D. Torrieri and K. Bakhru, "The Maximin Adaptive-Array Algorithm for Direct-Sequence Systems," *IEEE Trans. Signal Processing*, vol. 55, pp.1853-1861, May 2007.
16. D. Torrieri and K. Bakhru, "Anticipative Maximin Adaptive-Array Algorithm for Frequency-Hopping Systems," *Proc. IEEE Military Commun. Conf.*, Nov. 2006.
17. L. B. Milstein, "Wideband Code Division Multiple Access," *IEEE J. Select. Areas Commun.*, vol. 48, pp. 1318–1327, Aug. 2000.
18. F. Adachi, D. Garg, S. Takaoka, and K. Takeda, "Broadband CDMA Techniques," *IEEE Wireless Commun.*, vol. 44, pp. 8-18, April 2005.
19. F. Adachi and K. Takeda, "Bit Error Rate Analysis of DS-CDMA with Joint Frequency-Domain Equalization and Antenna Diversity Combining," *IEICE Trans. Commun.*, vol. E87-B, pp. 2291-3001, Oct. 2004.
20. T. Jiang and Y. Wu, "An Overview: Peak-to-Average Power Ratio Reduction Techniques for OFDM Signals," *IEEE Trans. Broadcasting*, vol. 54, pp. 257-268, June 2008.

Chapter 6
Code-Division Multiple Access

Multiple access is the ability of many users to communicate with each other while sharing a common transmission medium. Wireless multiple-access communications are facilitated if the transmitted signals are orthogonal or separable in some sense. Signals may be separated in time (*time-division multiple access* or TDMA), frequency (*frequency-division multiple access* or FDMA), or code (*code-division multiple access* or CDMA). CDMA is realized by using spread-spectrum modulation while transmitting signals from multiple users in the same frequency band at the same time. All signals use the entire allocated spectrum, but the spreading sequences or frequency-hopping patterns differ. Information theory indicates that in an isolated cell, CDMA systems achieve the same spectral efficiency as TDMA or FDMA systems only if optimal multiuser detection is used. However, even with single-user detection, CDMA is advantageous for cellular networks because it eliminates the need for frequency and time-slot coordination among cells, allows carrier-frequency reuse in adjacent cells, and imposes no sharp upper bound on the number of users.

A major CDMA advantage exists in networks accommodating voice communications. A *voice-activity detector* activates the transmitter only when the user is talking. Since typically fewer than 40% of the users are talking at any given time, the number of telephone users can be increased while maintaining a specified average interference power. Another major CDMA advantage is the ease with which it can be combined with multibeamed antenna arrays that are either adaptive or have fixed patterns covering cell sectors. There is no practical means of reassigning time slots in TDMA systems or frequencies in FDMA systems to increase capacity by exploiting intermittent voice signals or multibeamed arrays, and reassignments to accommodate variable data rates are almost always impractical. Inactive systems in a network reduce the interference received by an active CDMA system, but provide little or no benefit to TDMA or FDMA systems. These general advantages and its resistance to interference, interception, and frequency-selective fading make spread-spectrum CDMA an attractive choice for many mobile communication networks. The two principal types of spread-spectrum CDMA are *direct-sequence* CDMA (DS/CDMA) and *frequency-hopping* CDMA (FH/CDMA). The multicarrier CDMA systems of Sect. 5.8 are examples of DS/CDMA systems.

D. Torrieri, *Principles of Spread-Spectrum Communication Systems*,
DOI 10.1007/978-1-4419-9595-7_6, © Springer Science+Business Media, LLC 2011

This chapter presents the general characteristics of spreading sequences and frequency-hopping patterns that are suitable for CDMA systems. The impact of multiple-access interference in DS/CDMA and FH/CDMA systems and networks is analyzed. The role of power control in DS/CDMA networks is examined. Multiuser detectors, which have great potential usefulness but are fraught with practical difficulties, are described in the final section.

6.1 Spreading Sequences for DS/CDMA

Consider a DS/CDMA network with K users in which BPSK is used and every receiver has the form of Fig. 2.14. The desired signal that arrives at a receiver is

$$s(t) = \sqrt{2\mathcal{E}_s}d(t)p_0(t)\cos 2\pi f_c t \tag{6.1}$$

where $\mathcal{E}_s$ is the energy per binary channel symbol. The multiple-access interference that enters a receiver synchronized to a desired signal is modeled as

$$i(t) = \sum_{i=1}^{K-1} \sqrt{2I_i T_s}d_i(t-\tau)q_i(t-\tau_i)\cos(2\pi f_c t + \phi_i) \tag{6.2}$$

where $K-1$ is the number of interfering direct-sequence signals, and I_i is the average power of interference signal i, $d_i(t)$ is the code-symbol modulation, $q_i(t)$ is the spreading waveform, τ_i is the relative delay, and ϕ_i is the phase shift of interference signal i including the effect of carrier time delay. The spreading waveform of the desired signal is

$$p_0(t) = \sum_{n=-\infty}^{\infty} p_{0n}\psi(t-nT_c) \tag{6.3}$$

where $p_{0n} \in \{-1, 1\}$, and $\psi(t)$ is the chip waveform. Each spreading waveform of an interference signal has the form

$$q_i(t) = \sum_{n=-\infty}^{\infty} q_n^{(i)}\psi(t-nT_c), \quad i = 1, 2, \ldots, K-1 \tag{6.4}$$

where $q_n^{(i)} \in \{-1, 1\}$. The chip waveforms are assumed to be identical throughout the network and normalized so that

$$\int_0^{T_c} \psi^2(t)dt = \frac{T_c}{T_s}. \tag{6.5}$$

In a DS/CDMA network, the spreading sequences are often called *signature sequences*.

As shown in Sect. 2.3, after ideal carrier removal and chip-matched filtering, the demodulated sequence associated with a received symbol is given by (2.76):

$$Z_v = d_0 p_{0v} \sqrt{\mathcal{E}_s} \frac{T_c}{T_s} + J_v + N_{sv}, \ v = 0, 1, \ldots, G-1 \tag{6.6}$$

where d_0 is the desired symbol,

$$J_v = \sqrt{2} \int_{vT_c}^{(v+1)/T_c} i(t) \psi(t - vT_c) \cos 2\pi f_c t \ dt \tag{6.7}$$

and the noise component of the sequence is

$$N_{sv} = \sqrt{2} \int_{vT_c}^{(v+1)/T_c} n(t) \psi(t - vT_c) \cos 2\pi f_c t \ dt \tag{6.8}$$

Assuming that $n(t)$ is zero-mean white Gaussian noise, (6.8) and (6.5) imply that $E\left[N_{sv}^2\right] = N_0/2G$.

The despread correlator output is applied to the decision device in Fig. 2.14. The interference component of the despread correlator output due to a received symbol is

$$V_1 = \sum_{v=0}^{G-1} p_{0v} J_v. \tag{6.9}$$

Substituting (6.2), (6.3), and (6.7), we obtain

$$V_1 = \sum_{i=1}^{K-1} \sqrt{I_i T_s} \cos \phi_i \int_0^{T_s} d_i (t - \tau_i) \, q_i (t - \tau_i) \, p_0 (t) \, dt \tag{6.10}$$

where a double-frequency term is neglected, assuming that $f_c T_c \gg 1$.

Let $\mathbf{a} = (\ldots, a_0, a_1, \ldots)$ and $\mathbf{b} = (\ldots, b_0, b_1, \ldots)$ denote binary sequences with components in $GF(2)$. The sequences $\mathbf{a}$ and $\mathbf{b}$ are mapped into antipodal sequences $\mathbf{p}$ and $\mathbf{q}$, respectively, with components in $\{-1, +1\}$ by means of the transformation

$$p_i = (-1)^{a_i + 1}, \ \ q_i = (-1)^{b_i + 1}. \tag{6.11}$$

The periodic autocorrelation of a periodic binary sequence with period N is defined by (2.34). The *periodic cross-correlation* of periodic binary sequences $\mathbf{a}$ and $\mathbf{b}$ with the same period N is defined as the periodic cross-correlation of the antipodal sequences $\mathbf{p}$ and $\mathbf{q}$, which is defined as

$$\theta_{pq}(l) = \frac{1}{N} \sum_{n=0}^{N-1} p_{n+l} q_n. \tag{6.12}$$

Sequences are *orthogonal* if $\theta_{pq}(0) = 0$. Substitution of (6.11) into (6.12) indicates that the periodic cross-correlation of **a** and **b** is given by

$$\theta_{pq}(l) = \frac{A_l - D_l}{N} \tag{6.13}$$

where A_l denotes the number of agreements in the corresponding components of **b** and the shifted sequence $\mathbf{a}(l)$, and D_l denotes the number of disagreements.

6.1.1 Synchronous Communications

Synchronous communication signals are generated typically when a single station transmits to mobiles, as in the downlinks of cellular networks (Sect. 6.4). We consider synchronous communication signals such that all data symbols have duration T_s, symbol and chip transitions are aligned at the receiver input, and short spreading sequences with period G extend over each data symbol. Then $\tau_i = 0$, $i = 1, 2, \ldots, K-1$, and $d_i(t) = d_i$ is constant over the integration interval $[0, T_s]$. Thus, for synchronous communications, the substitution of (6.3), (6.4), and (6.5) into (6.10) and the use of (6.12) with $N = G$ yields

$$V_1 = \frac{1}{G} \sum_{i=1}^{K-1} \lambda_i \sum_{n=0}^{G-1} p_{0n} q_n^{(i)} = \sum_{i=1}^{K-1} \lambda_i \theta_{0i}(0) \tag{6.14}$$

where

$$\lambda_i = \sqrt{I_i T_s} d_i \cos\phi_i \tag{6.15}$$

and $\theta_{0i}(l)$ is the periodic cross-correlation of the desired sequence and interfering sequence i. If the K spreading sequences are all orthogonal to each other, then $V_1 = 0$ and the multiple-access interference $i(t)$ is suppressed at the receiver. A large number of multiple-access interference signals can be suppressed in a network if each such signal has its chip transitions aligned and the spreading sequences are mutually orthogonal.

Two binary sequences, each of length two, are orthogonal if each sequence is described by one of the rows of the 2×2 matrix

$$\mathbf{H}_1 = \begin{bmatrix} 0 & 0 \\ 0 & 1 \end{bmatrix}. \tag{6.16}$$

A set of 2^n mutually orthogonal sequences, each of length 2^n, is obtained by using the rows of the matrix

$$\mathbf{H}_n = \begin{bmatrix} \mathbf{H}_{n-1} & \mathbf{H}_{n-1} \\ \mathbf{H}_{n-1} & \bar{\mathbf{H}}_{n-1} \end{bmatrix}, \quad n = 2, 3, \ldots \tag{6.17}$$

where $\bar{\mathbf{H}}_{n-1}$ is the *complement* of $\mathbf{H}_{n-1}$, obtained by replacing each 1 and 0 by 0 and 1, respectively, and $\mathbf{H}_1$ is defined by (6.16). Any pair of rows in $\mathbf{H}_n$ differ in exactly 2^{n-1} columns, thereby ensuring orthogonality of the corresponding sequences. The $2^n \times 2^n$ matrix $\mathbf{H}_n$, which is called a *Hadamard matrix*, can be used to generate 2^n orthogonal spreading sequences for synchronous direct-sequence communications. The orthogonal spreading sequences generated from a Hadamard matrix are called *Walsh sequences*.

In CDMA networks for multimedia applications, the data rates for various services and users often differ. One way to accommodate different data rates is to use spreading sequences that are orthogonal to each other despite differences in the processing gains, which are often called *spreading factors* in CDMA networks. The chip rates of all the spreading sequences are equal, but the different data rates cause the spreading factors to differ. A tree-structured set of orthogonal sequences called the *orthogonal variable-spreading-factor* $(OVSF)$ *codes* can be generated recursively and enable the receiver to completely avoid multiple-access interference [1].

Starting with $\mathbf{C}_1(1) = 1$, let $\mathbf{C}_N(n)$ denote the row vector representing the *nth* sequence with spreading factor N, where $n = 1, 2, \ldots, N$, and $N = 2^k$ for some nonnegative integer k. The set of N sequences with N chips is derived by concatenating sequences from the set of $N/2$ sequences with $N/2$ chips:

$$\begin{aligned}
\mathbf{C}_N(1) &= [\mathbf{C}_{N/2}(1)\ \mathbf{C}_{N/2}(1)] \\
\mathbf{C}_N(2) &= [\mathbf{C}_{N/2}(1)\ \overline{\mathbf{C}}_{N/2}(1)] \\
&\vdots \\
\mathbf{C}_N(N-1) &= [\mathbf{C}_{N/2}(N/2)\ \mathbf{C}_{N/2}(N/2)] \\
\mathbf{C}_N(N) &= [\mathbf{C}_{N/2}(N/2)\ \overline{\mathbf{C}}_{N/2}(N/2)].
\end{aligned} \tag{6.18}$$

For example, $\mathbf{C}_{16}(4)$ is produced by concatenating $\mathbf{C}_8(2)$ and $\overline{\mathbf{C}}_8(2)$, thereby doubling the number of chips per data symbol to 16. A sequence used in the recursive generation of a longer sequence is called a *mother code* of the longer sequence. Equation (6.18) indicates that all the sequences with N chips are orthogonal to each other, and these sequences constitute a set of orthogonal Walsh sequences. Let R denote the data rate supported by an OVSF sequence of length N. As the spreading factor decreases from N to 1, the corresponding data rate increases from R to NR. A tree diagram illustrating the hierarchy of sequences is shown in Fig. 6.1. Each $\mathbf{C}_N(n)$ is orthogonal to concatenations of all sequences $\mathbf{C}_{N/2}(n'), \mathbf{C}_{N/4}(n''), \ldots$ and their complements except for its mother codes. For example, $\mathbf{C}_{16}(3)$ is not orthogonal to its mother codes $\mathbf{C}_8(2)$, $\mathbf{C}_4(1)$, or $\mathbf{C}_2(1)$. If $\mathbf{C}_8(3)$ is assigned to a user requesting a data rate twice that of a user assigned a sequence of 16 chips, then the sequences $\mathbf{C}_{16}(5)$ and $\mathbf{C}_{16}(6)$ descended from $\mathbf{C}_8(3)$ can not be assigned to other users requesting lower data rates, and the mother codes of $\mathbf{C}_8(3)$ can not be assigned to other users requesting higher data rates.

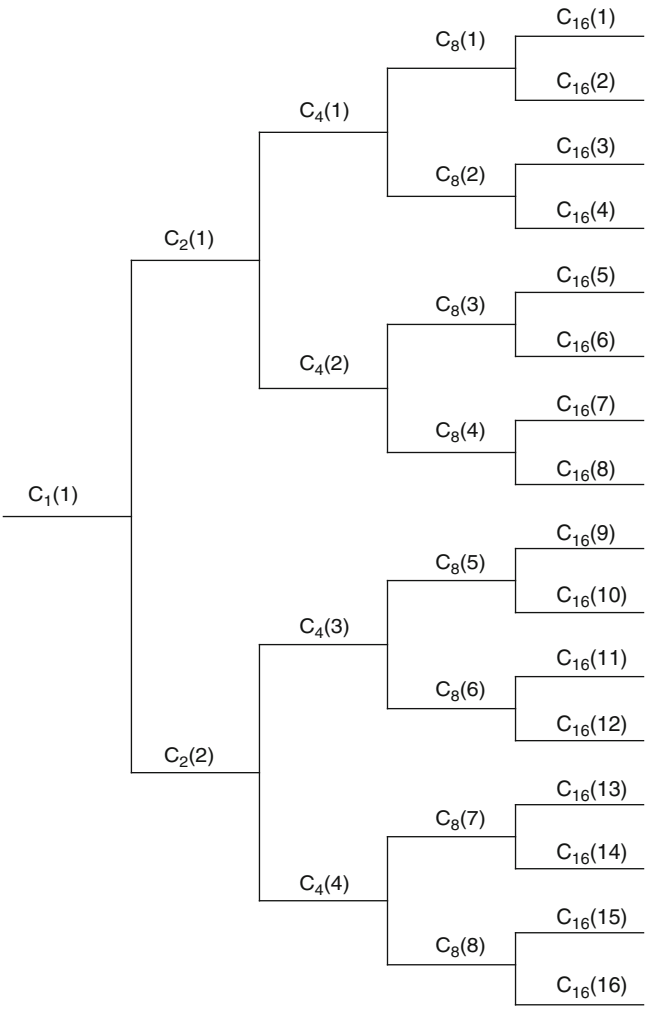

Fig. 6.1 Tree diagram of orthogonal variable-spreading-factor code

The capacity of a system using an OVSF code is the maximum data rate that the system can accommodate. The unavailability or *blocking* of ancestors and descendants causes new calls to be rejected even though the system has a sufficient capacity to accept them. Thus, potential capacity is wasted. Another source of wasted capacity is due to the quantization of data rates and spreading factors that must be powers of 2. A number of code assignment schemes have been proposed to reduce or even eliminate the wasted capacity. Flexible data services of different rates could be provided by an *orthogonal multicode assignment* of multiple orthogonal sequences to each user according to the data rate requested [2]. However,

a multicode assignment requires each user to have multiple rake demodulators, each of which responds to a different sequence. The resulting increase in the implementation complexity of each receiver is substantial.

6.1.2 Asynchronous Communications

Asynchronous communication signals are generated typically when mobiles independently transmit to a station, as in the uplinks of cellular networks (Sect. 6.3). The symbol transitions of *asynchronous* multiple-access signals at a receiver are not simultaneous, usually because of changing path-length differences among the various communication links. Since the spreading sequences are shifted relative to each other, sets of periodic sequences with small cross-correlations for any relative shifts are desirable to limit the effect of multiple-access interference. Walsh sequences, orthogonal variable-spreading-factor codes, and maximal sequences usually do not provide sufficiently small cross-correlations for practical applications.

In the presence of asynchronous multiple-access interference for which $\tau_i \neq 0$, the interference component of the despread correlator output is given by (6.10). We assume that either the data modulation of each interfering signal is absent or does not change during a symbol interval so that we may set $d_i(t) = d_i$ in this equation. Let $\tau_i = \nu_i T_c + \epsilon_i$, where ν_i is an integer and $0 \leq \epsilon_i < T_c$. Assuming rectangular chip waveforms, a derivation similar to the one leading to (2.42) gives

$$V_1 = \sum_{i=1}^{K-1} \lambda_i \left[\left(1 - \frac{\epsilon_i}{T_c} \right) \theta_{0i}(\nu_i) + \frac{\epsilon_i}{T_c} \theta_{0i}(\nu_i + 1) \right] \tag{6.19}$$

where $\theta_{0i}(\nu_i)$ is the periodic cross-correlation of the sequence $\mathbf{p}_0$ of desired-user 0 and the sequence $\mathbf{q}^{(i)}$ of interfering user i. As illustrated by this equation, ensuring that the cross-correlations are always small is a critical *necessary* condition for the success of asynchronous multiple-access communications. Since $d_i(t)$ may change polarity during an integration interval, the effect of asynchronous multiple-access interference will often vary from symbol to symbol.

For a set S of M periodic antipodal sequences of length N, let $\theta_{\max}$ denote the peak magnitude of the cross-correlations or autocorrelations:

$$\theta_{\max} = \max \left\{ \left| \theta_{pq}(k) \right| : \ 0 \leq k \leq N-1; \ \mathbf{p}, \mathbf{q} \in S; \ \mathbf{p} \neq \mathbf{q} \text{ or } k \neq 0 \right\}. \tag{6.20}$$

Theorem. *A set S of M periodic antipodal sequences of length N has*

$$\theta_{\max} \geq \sqrt{\frac{M-1}{MN-1}}. \tag{6.21}$$

Proof. Consider an extended set S_e of MN sequences $\mathbf{p}^{(i)}, i = 1, 2, \ldots, MN$, that comprises the N distinct shifted sequences derived from each of the sequences in S. The cross-correlation of sequences $\mathbf{p}^{(i)}$ and $\mathbf{p}^{(j)}$ in S_e is

$$\psi_{ij} = \frac{1}{N} \sum_{n=1}^{N} p_n^{(i)} p_n^{(j)} \tag{6.22}$$

and

$$\theta_{\max} = \max \left\{ \left| \psi_{ij} \right| : \mathbf{p}^{(i)} \epsilon\, S_e,\ \mathbf{p}^{(j)} \epsilon\, S_e, i \neq j \right\}.$$

Define the double summation

$$Z = \sum_{i=1}^{MN} \sum_{j=1}^{MN} \psi_{ij}^2. \tag{6.23}$$

Separating the MN terms for which $\psi_{ii} = 1$and then bounding the remaining $MN(MN-1)$ terms yields

$$Z \leq MN + MN(MN-1)\theta_{\max}^2. \tag{6.24}$$

Substituting (6.22) into (6.23), interchanging summations, and omitting the terms for which $m \neq n$, we obtain

$$Z = \frac{1}{N^2} \sum_{n=1}^{N} \sum_{m=1}^{N} \sum_{i=1}^{MN} p_n^{(i)} p_m^{(i)} \sum_{j=1}^{MN} p_n^{(j)} p_m^{(j)} = \frac{1}{N^2} \sum_{n=1}^{N} \sum_{m=1}^{N} \left(\sum_{i=1}^{MN} p_n^{(i)} p_m^{(i)} \right)^2$$

$$\geq \frac{1}{N^2} \sum_{n=1}^{N} \left[\sum_{n=1}^{MN} \left(p_n^{(i)} \right)^2 \right]^2 = M^2 N.$$

Combining this inequality with (6.24) gives (6.21). □

The lower bound in (6.21) is known as the *Welch bound*. It approaches $1/\sqrt{N}$ for large values of M and N. Only small subsets of maximal sequences or Gold sequences can be found with $\theta_{\max}$ close to this lower bound.

Large sets of sequences with $\theta_{\max}$ approaching the Welch bound can be obtained by combining maximal sequences with sampled versions of these sequences. If q is a positive integer, the new binary sequence $\mathbf{b}$ formed by taking every qth bit of binary sequence $\mathbf{a}$ is known as a *decimation* of $\mathbf{a}$ by q, and the components of the two sequences are related by $b_i = a_{qi}$. Let $gcd(x, y)$ denote the greatest common divisor of x and y. If the original sequence $\mathbf{a}$ has a period N and the new sequence $\mathbf{b}$ is not identically zero, then $\mathbf{b}$ has period $N/gcd(N, q)$. If $gcd(N, q) = 1$, then the decimation is called a *proper decimation*. Following a proper decimation, the bits of $\mathbf{b}$ do not repeat themselves until every bit of $\mathbf{a}$ has been sampled. Therefore,

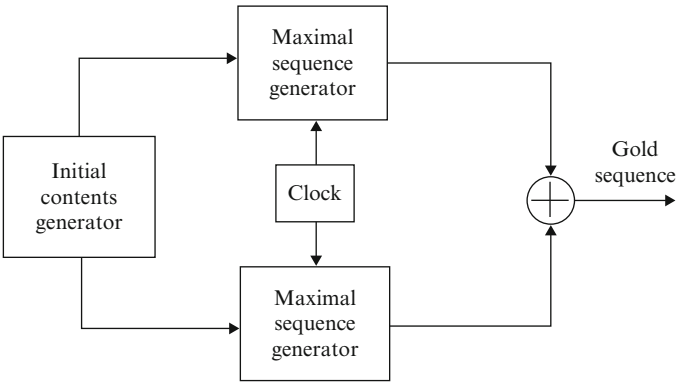

Fig. 6.2 Gold sequence generator

b and **a** have the same period N, and it can be shown that if **a** is maximal, then **b** is a maximal sequence [3]. A *preferred pair* of maximal sequences with period $2^m - 1$ are a pair with a periodic cross-correlation that takes only the three values $-t(m)/N, -1/N$, and $[t(m) - 2]/N$, where

$$t(m) = 2^{\lfloor (m+2)/2 \rfloor} + 1 \tag{6.25}$$

and $\lfloor x \rfloor$ denotes the integer part of the real number x.

The *Gold sequences* are a large set of sequences with period $N = 2^m - 1$ that may be generated by the modulo-2 addition of preferred pairs when m is odd or $m = 2$ modulo-4 [3]. One sequence of the preferred pair is a decimation by q of the other sequence. The positive integer q is either $q = 2^k + 1$ or $q = 2^{2k} - 2^k + 1$, where k is a positive integer such that $gcd(m, k) = 1$ when m is odd and $gcd(m, k) = 2$ when $m = 2$ modulo-4. Since the cross-correlation between any two Gold sequences in a set can take only three values, the peak magnitude of the periodic cross-correlation between any two Gold sequences of period $N = 2^m - 1$ is

$$\theta_{\max} = \frac{t(m)}{2^m - 1}. \tag{6.26}$$

For large values of m, $\theta_{\max}$ for Gold sequences exceeds the Welch bound by a factor of $\sqrt{2}$ for m odd and a factor of 2 for m even.

One form of a Gold sequence generator is shown in Fig. 6.2. If each maximal sequence generator has m stages, different Gold sequences in a set are generated by selecting the initial state of one maximal sequence generator and then shifting the initial state of the other generator. Since any shift from 0 to $2^m - 2$ results in a different Gold sequence, $2^m - 1$ different Gold sequences can be produced by the system of Fig. 6.2. Gold sequences identical to maximal sequences are produced by setting the state of one of the maximal sequence generators to zero. Altogether, there are $2^m + 1$ different Gold sequences, each with a period of $2^m - 1$, in the set.

An example of a set of Gold sequences is the set generated by the preferred pair specified by the primitive characteristic polynomials

$$f_1(x) = 1 + x^3 + x^7, \quad f_2(x) = 1 + x + x^2 + x^3 + x^7. \tag{6.27}$$

Since $m = 7$, there are 129 Gold sequences of period 127 in this set, and (6.26) gives $\theta_{\max} = 0.134$. Equation (2.62) indicates that there are only 18 maximal sequences with $m = 7$. For this set of 18 sequences, calculations [3] indicate that $\theta_{\max} = 0.323$. If $\theta_{\max} = 0.134$ is desired for a set of maximal sequences with $m = 7$, then one finds that the set has only 6 sequences. This result illustrates the much greater utility of Gold sequences in CDMA networks with many subscribers.

Consider a Gold sequence generated by using the characteristic functions $f_1(x)$ and $f_2(x)$ of degree m. The *generating function for the Gold sequence* is

$$\begin{aligned} G(x) &= \frac{\phi_1(x)}{f_1(x)} + \frac{\phi_2(x)}{f_2(x)} \\ &= \frac{\phi_1(x) f_2(x) + \phi_2(x) f_1(x)}{f_1(x) f_2(x)} \end{aligned} \tag{6.28}$$

where $\phi_1(x)$ and $\phi_2(x)$ have the form specified by the numerator of (2.56). Since the degrees of both $\phi_1(x)$ and $\phi_2(x)$ are less than m, the degree of the numerator of $G(x)$ must be less than $2m$. Since the product $f_1(x) f_2(x)$ has the form of a characteristic function of degree $2m$ given by (2.52), this product defines the feedback coefficients of a single linear feedback shift register with $2m$ stages that can generate the Gold sequences. The initial state of the register for any particular sequence can be determined by equating each coefficient in the numerator of (6.28) with the corresponding coefficient in (2.56) and then solving $2m$ linear equations.

A *small set of Kasami sequences* comprises $2^{m/2}$ sequences with period $2^m - 1$ if m is even [3]. To generate a set, a maximal sequence **a** with period $N = 2^m - 1$ is decimated by $q = 2^{m/2} + 1$ to form a binary sequence **b** with period $N/gcd(N, q) = 2^{m/2} - 1$. The modulo-2 addition of **a** and any cyclic shift of **b** from 0 to $2^{m/2} - 2$ provides a Kasami sequence. By including sequence **a**, we obtain a set of $2^{m/2}$ Kasami sequences with period $2^m - 1$. The periodic cross-correlation between any two Kasami sequences in a set can only take the values $-s(m)/N, -1/N$, or $[s(m) - 2]/N$, where

$$s(m) = 2^{m/2} + 1. \tag{6.29}$$

The peak magnitude of the periodic cross-correlation between any two Kasami sequences is

$$\theta_{\max} = \frac{s(m)}{N} = \frac{1}{2^{m/2} - 1}. \tag{6.30}$$

For $m \geq 2$ and $M = 2^{m/2}$, the use of $NM - 1 > NM - N$ in the Welch bound gives $\theta_{\max} > 1/\sqrt{N}$. Since $N = 2^m - 1$,

$$N\theta_{\max} > \sqrt{2^m - 1} > 2^{m/2} - 1. \tag{6.31}$$

Since N is an odd integer, $A_l - D_l$ in (6.13) must be an odd integer. Therefore, the definition of $\theta_{\max}$ and (6.13) indicate that $N\theta_{\max}$ must be an odd integer. Inequality (6.31) then implies that for $M = 2^{m/2}$, $N = 2^m - 1$, and even values of m, *a set of* M periodic antipodal sequences of length N *has*

$$N\theta_{\max} \geq 2^{m/2} + 1. \tag{6.32}$$

A comparison of this result with (6.30) indicates that the Kasami sequences are optimal in the sense that $\theta_{\max}$ has the minimum value for any set of sequences of the same size and period.

As an example, let $m = 10$. There are 60 maximal sequences, 1025 Gold sequences, and 32 Kasami sequences with period 1023. The peak cross-correlations are 0.37, 0.06, and 0.03, respectively.

A *large set of Kasami sequences* comprises $2^{m/2}(2^m + 1)$ sequences if $m = 2$ modulo-4 and $2^{m/2}(2^m + 1) - 1$ sequences if $m = 0$ modulo-4 [3]. The sequences have period $2^m - 1$. To generate a set, a maximal sequence $\mathbf{a}$ with period $N = 2^m - 1$ is decimated by $q = 2^{m/2} + 1$ to form a binary sequence $\mathbf{b}$ with period $N/gcd(N, q) = 2^{m/2} - 1$ and then decimated by $q_1 = 2^{(m+2)/2} + 1$ to form another binary sequence $\mathbf{c}$ with period $N/gcd(N, q_1)$. The modulo-2 addition of $\mathbf{a}$, a cyclic shift of $\mathbf{b}$, and a cyclic shift of $\mathbf{c}$ provides a Kasami sequence with period N. The periodic cross-correlations between any two Kasami sequences in a set can only take the values $-1/N, -t(m)/N, [t(m)-2]/N, -s(m)/N$, or $[s(m)-2]/N$. A large set of Kasami sequences includes both a small set of Kasami sequences and a set of Gold sequences as subsets. Since $t(m) \geq s(m)$, the value of $\theta_{\max}$ for a large set is the same as that for Gold sequences, and is given by (6.26). This value is suboptimal, but the large size of these sets makes them an attractive option for asynchronous CDMA networks.

A generator of a large set of 4111 Kasami sequences with $m = 8$ and period 255 is illustrated in Fig. 6.3. The two shift registers at the top of the figure by themselves generate a small set of 16 Kasami sequences with $m = 8$ and period 15. The top 8-stage shift register generates a maximal sequence with period 255, and the 4-stage shift register below it generates a maximal sequence with period 15. The bottom shift register generates a nonmaximal sequence with period 85.

In a network of similar systems, interfering sequences are substantially suppressed during acquisition if the cross-correlations among sequences are small, as they are if all the sequences are Gold or Kasami sequences.

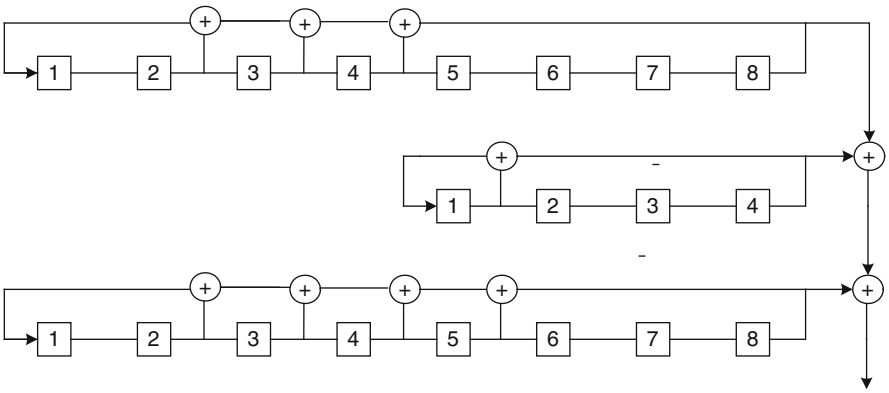

Fig. 6.3 Generator of Kasami sequences with period 255

6.1.3 Symbol Error Probability

Let $\mathbf{d}_i = (d_{-1}^{(i)}, d_0^{(i)})$ denote the vector of the two symbols of asynchronous multiple-access interference signal i that are received during the detection of a symbol of the desired signal. Equation (6.10) implies that

$$V_1 = \sum_{i=1}^{K-1} \sqrt{I_i T_s} \cos\phi_i \left[d_{-1}^{(i)} R_{0i}(\tau_i) + d_0^{(i)} \hat{R}_{0i}(\tau_i) \right], \ 0 \le \tau_i \le T_s \tag{6.33}$$

where the *continuous-time partial cross-correlation functions* are

$$R_{0i}(\tau) = \int_0^{\tau} p_0(t) q_i(t - \tau_i) dt \tag{6.34}$$

$$\hat{R}_{0i}(\tau) = \int_{\tau}^{T_s} p_0(t) q_i(t - \tau_i) dt. \tag{6.35}$$

Let $\tau_i = \nu_i T_c + \epsilon_i$, where ν_i is an integer such that $0 \le \nu_i \le G-1$, and $0 \le \epsilon_i < T_c$. For rectangular chip waveforms and spreading sequences of period G, a derivation using the periodicity of the spreading sequences and analogous to the one leading to (2.42) gives

$$R_{0i}(\tau_i) = A_{0i}(\nu_i - G) + [A_{0i}(\nu_i + 1 - G) - A_{0i}(\nu_i - G)] \frac{\epsilon_i}{T_c} \tag{6.36}$$

$$\hat{R}_{0i}(\tau_i) = A_{0i}(\nu_i) + [A_{0i}(\nu_i + 1) - A_{0i}(\nu_i)] \frac{\epsilon_i}{T_c} \tag{6.37}$$

where the *aperiodic cross-correlation function* is defined by

$$A_{0i}(\nu) = \begin{cases} \dfrac{1}{G} \displaystyle\sum_{n=0}^{G-1-\nu} p_{0,n+\nu} q_n^{(i)}, & 0 \le \nu \le G \\ \dfrac{1}{G} \displaystyle\sum_{n=0}^{G-1+\nu} p_{0n} q_{n-\nu}^{(i)}, & G \le \nu < 0 \end{cases} \tag{6.38}$$

and $A_{0i}(\nu) = 0$ for $|\nu| \ge G$. These equations indicate that the aperiodic cross-correlations are more important than the related periodic cross-correlations defined by (6.12) in determining the interference level and, hence, the symbol error probability. For most sets of sequences, the aperiodic cross-correlations are larger than the periodic cross-correlations. By the proper selection of the sequences and their relative phases, one can obtain a system performance slightly better than that attainable with sequences with good periodic cross-correlations or random sequences. However, the number of suitable sequences is too small for most applications. If all the spreading sequences are short, and the power levels of all received signals are equal, then the symbol error probability can be approximated and bounded [4, 5], but the process is complicated. An alternative approach is to model the spreading sequences as random binary sequences, as is done for long sequences.

In a network with multiple-access interference, code acquisition depends on both the periodic and aperiodic cross-correlations. In the absence of data modulations, V_c in (4.92) and V_s in (4.94) have additional terms, each of which is proportional to the periodic cross-correlation between the desired signal and an interference signal. When data modulations are present, some or all of these terms entail aperiodic cross-correlations.

6.1.4 Complex-Valued Quaternary Sequences

Quaternary direct-sequence system may use pairs of short binary sequences, such as Gold or Kasami sequences, to exploit the favorable periodic autocorrelation and cross-correlation functions. However, Gold sequences do not attain the Welch bound, and Kasami sequences that do are limited in number. To support many users and to facilitate the unambiguous synchronization to particular signals in a CDMA network, one might consider complex-valued quaternary sequences that are not derived from pairs of standard binary sequences but have better periodic correlation functions.

For q-ary PSK modulation, sequence symbols are powers of the complex rth root of unity, which is

$$\Omega = \exp\left(j\frac{2\pi}{q}\right) \tag{6.39}$$

where $j = \sqrt{-1}$. The complex spreading or signature sequence $\mathbf{p}$ of period N has symbols given by

$$p_i = \Omega^{a_i} e^{j\phi}, \qquad a_i \in Z_q = \{0, 1, 2, \ldots, q-1\}, \qquad i = 1, 2, \ldots, N \tag{6.40}$$

where ϕ is an arbitrary phase chosen for convenience. If p_i is specified by the exponent a_i and q_i is specified by the exponent b_i, then the periodic cross-correlation between sequences $\mathbf{p}$ and $\mathbf{q}$ is defined as

$$\theta_{pq}(k) = \frac{1}{N} \sum_{i=0}^{N-1} p_{i+k} q_i^* = \frac{1}{N} \sum_{i=0}^{N-1} \Omega^{a_{i+k} - b_i}. \tag{6.41}$$

The maximum magnitude θ_{max} defined by (6.20) must satisfy the Welch bound of (6.21). For a positive integer m, a family $\mathcal{A}$ of $M = N + 2$ quaternary or Z_4 sequences, each of period $N = 2^m - 1$, with θ_{max} that asymptotically approaches the Welch bound has been identified [6]. In contrast, a small set of binary Kasami sequences has only $\sqrt{N+1}$ sequences.

The sequences in a family $\mathcal{A}$ are determined by the *characteristic polynomial*, which is defined as

$$f(x) = 1 + \sum_{i=0}^{m} c_i x^i \tag{6.42}$$

where each coefficient $c_i \in Z_4$ and $c_m = 1$. The output sequence satisfies the linear recurrence relation of (2.21). For example, the characteristic polynomial $f(x) = 1 + 2x + 3x^2 + x^3$ has $m = 3$ and generates a family with period $N = 7$. A feedback shift register that implements the sequence of the family is depicted in Fig. 6.4a, where all operations are modulo-4. The generation of a particular sequence is illustrated in Fig. 6.4b. Different sequences may be generated by loading the shift register with any nonzero initial contents and then cycling the shift register through its full period $N = 2^m - 1$. Since the shift register has $4^m - 1$ nonzero states, there are $M = (4^m - 1)/(2^m - 1) = 2^m + 1$ *cyclically distinct* members of the family. Each family member may be generated by loading the shift register with any nonzero triple that is not a state occurring during the generation of another family member.

By setting $\phi = \pi/4$ in (6.40), a complex-valued data symbol in the family $\mathcal{A}$ may be represented by $d = d_1 + jd_2$, where d_1 and d_2 are antipodal symbols with values $\pm 1/\sqrt{2}$. If a complex-valued chip of the spreading sequence is $p = p_1 + jp_2$, then the complex multiplication of the data and spreading sequences produces a complex-valued sequence with each chip of the form $y = y_1 + jy_2 = dp$. The implementation of this product is shown in Fig. 6.5, in which real-valued inputs d_1, d_2, p_1 and p_2 produce the two real-valued outputs y_1 and y_2. The equation $y = dp$ gives a compact complex-variable representation of the real-variable equations $y_1 = d_1 p_1 - d_2 p_2$ and $y_2 = d_2 p_1 + d_1 p_2$. Each chip y_1 modulates the in-phase

a

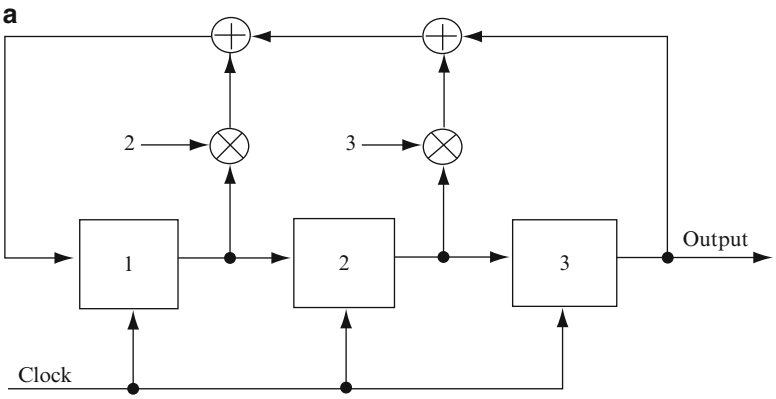

b

Shift	Contents		
	Stage 1	Stage 2	Stage 3
Initial	0	0	1
1	1	0	0
2	2	1	0
3	3	2	1
4	1	3	2
5	1	1	3
6	0	1	1
7	0	0	1

Fig. 6.4 (**a**) Feedback shift register for a quaternary sequence and (**b**) contents after successive shifts

carrier, and each chip y_2 modulates the quadrature carrier. The transmitted signal may be represented as

$$s(t) = \mathrm{Re}\left\{Ad(t)p(t)e^{j2\pi f_c t}\right\} \tag{6.43}$$

where $\mathrm{Re}\{x\}$ denotes the real part of x, A is the amplitude, and $d(t)$ and $p(t)$ are waveforms modulated by the data and spreading sequences.

A representation of the receiver in terms of complex variables is illustrated in Fig. 6.6. If $f_c T_c \gg 1$, two cross-correlation terms are negligible, and the actual implementation can be done by the architectures of Figs. 2.17 and 2.19 except that the

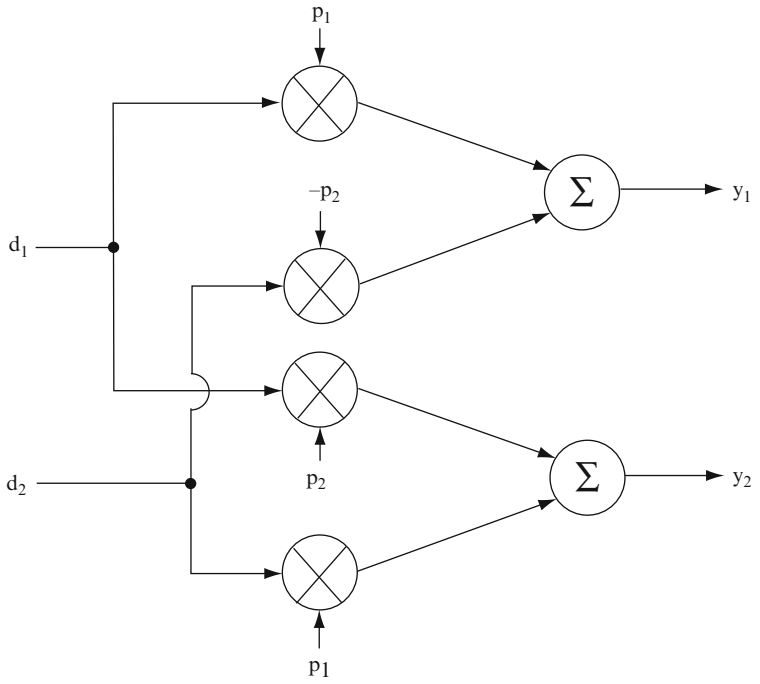

Fig. 6.5 Product of quaternary data and spreading sequences

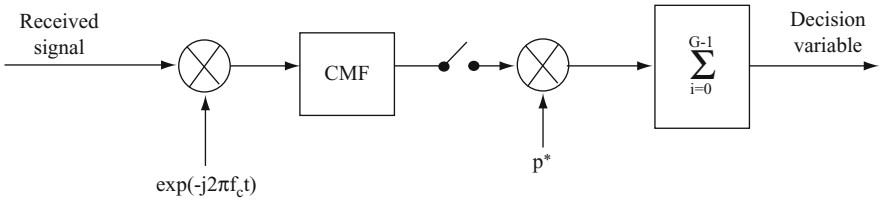

Fig. 6.6 Receiver for direct-sequence system with complex quaternary spreading sequences. CMF is chip-matched filter

final multiplications in the two branches are replaced by a complex multiplication. Thus, y is extracted by separate in-phase and quadrature demodulation. Since the complex quaternary symbols have unity magnitude, the despreading entails the complex multiplication of y by p^* to produce $d|p|^2 = d$ along with the residual interference and noise. As illustrated in Fig. 6.6, the summation of G multiplications produces the decision variable, where G is the number of chips per bit.

Although some complex-valued quaternary sequences have more favorable periodic autocorrelations and cross-correlations than pairs of standard binary sequences, they do not provide significantly smaller error probabilities in multiple-access systems [7,8]. The reason is that system performance is determined by the complex aperiodic functions. However, complex sequences have the potential to provide better acquisition performance than the Gold or Kasami sequences because of their superior periodic autocorrelations.

Complex-valued quaternary sequences ensure balanced power in the in-phase and quadrature branches of the transmitter, which limits the peak-to-average power fluctuations. Let $d(t) = d_1(t) + jd_2(t)$ represent a complex-valued data signal. Suppose that different bit rates or quality-of-service requirements make it desirable for $d_1(t)$ and $d_2(t)$ to have unequal amplitudes. Multiplication by a complex-valued spreading waveform $p(t) = p_1(t) + jp_2(t)$ produces $y(t) = y_1(t) + jy_2(t) = p(t)d(t)$. If the symbols of $d_1(t)$ and $d_2(t)$ are zero-mean, antipodal, and independent, and $p_1^2(t) = p_2^2(t) = p_1^2$, a constant, then $E[y_1^2(t)] = E[y_2^2(t)] = p_1^2(d_1^2 + d_2^2)$. This result indicates that the power in the in-phase and quadrature components after the spreading are equal despite any disparity between d_1^2 and d_2^2.

6.2 Systems with Random Spreading Sequences

If all the spreading sequences in a network of asynchronous CDMA systems have a common period equal to the data-symbol duration, then by the proper selection of the sequences and their relative phases, one can obtain a system performance better than that theoretically attainable with random sequences. However, the performance advantage is small, the number of suitable sequences is too small for many applications, and long sequences that extend over many data symbols provide more system security. Furthermore, long sequences ensure that successive data symbols are covered by different sequences, thereby limiting the time duration of an unfavorable cross-correlation due to multiple-access interference. Even if short sequences are used, the random-sequence model gives fairly accurate performance predictions.

The analysis and comparisons of CDMA systems are greatly facilitated by applying Jensen's inequality.

6.2.1 Jensen's Inequality

A function $g(x)$ defined on an open interval I is *convex* if

$$g(px + (1-p)y) \le pg(x) + (1-p)g(y) \tag{6.44}$$

for x, y in I and $0 \le p \le 1$. Suppose that $g(x)$ has a continuous, nondecreasing derivative $g'(x)$ on I. The inequality is valid if $p = 0$ or 1. If $x \ge y$ and $0 \le p < 1$,

$$\begin{aligned} g(px + (1-p)y) - g(y) &= \int_y^{px+(1-p)y} g'(z)dz \le p(x-y)g'(px+(1-p)y) \\ &\le \frac{p}{1-p}\int_{px+(1-p)y}^{x} g'(z)dz \\ &= \frac{p}{1-p}[g(x) - g(px+(1-p)y)]. \end{aligned} \tag{6.45}$$

Simplifying this result, we obtain (6.44). If $y \ge x$, a similar analysis again yields (6.44). Thus, *if $g(x)$ has a continuous, nondecreasing derivative on I, it is convex.*

Lemma. *If $g(x)$ is a convex function on the open interval I, then*

$$g(y) \ge g(x) + g^-(x)(y-x) \tag{6.46}$$

for all y, x in I, where $g^-(x)$ is the left derivative of $g(x)$.

Proof. If $y - x \ge z > 0$, then substituting $p = 1 - z/(y-x)$ into (6.44) gives

$$g(x+z) \le \left(1 - \frac{z}{y-x}\right) g(x) + \frac{z}{y-x} g(y)$$

which yields

$$\frac{g(x+z) - g(x)}{z} \le \frac{g(y) - g(x)}{y-x}, \quad y - x \ge z > 0. \tag{6.47}$$

If $v > 0$ and $z > 0$, then (6.44) implies that

$$g(x) \le \frac{z}{v+z} g(x-v) + \frac{v}{v+z} g(x+z)$$

which yields

$$\frac{g(x) - g(x-v)}{v} \le \frac{g(x+z) - g(x)}{z}, \quad v, z > 0. \tag{6.48}$$

Inequality (6.47) indicates that the ratio $[g(y) - g(x)]/(y-x)$ decreases monotonically as $y \to x$ from above and (6.48) implies that this ratio has a lower bound. Therefore, the right derivative $g^+(x)$ exists on I. If $x - y \ge v > 0$, then (6.44) with $p = 1 - v/(x-y)$ implies that

$$g(x-v) \le \left(1 - \frac{v}{x-y}\right) g(x) + \frac{v}{x-y} g(y)$$

which yields

$$\frac{g(x)-g(y)}{x-y} \le \frac{g(x)-g(x-v)}{v}, \quad x-y \ge v > 0. \tag{6.49}$$

This inequality indicates that the ratio $[g(x)-g(y)]/(x-y)$ increases monotonically as $y \to x$ from below and (6.48) implies that this ratio has an upper bound. Therefore, the left derivative $g^-(x)$ exists on I, and (6.48) yields

$$g^-(x) \le g^+(x) \tag{6.50}$$

Taking the limits as $z \to 0$ and $v \to 0$ in (6.47) and (6.49), respectively, and then using (6.50), we find that (6.46) is valid for all y, x in I. □

Jensen's inequality. If X is a random variable with a finite expected value $E[X]$, and $g(\ )$ is a convex function on an open interval containing the range of X, then

$$E[g(X)] \ge g(E[X]). \tag{6.51}$$

Proof. Set $y = X$ and $x = E[X]$ in (6.46), which gives $g(X) \ge g(E[X]) + g^-(E[X])(X - E[X])$. Taking the expected values of the random variables on both sides of this inequality gives Jensen's inequality. □

6.2.2 Direct-Sequence Systems with BPSK

Consider the direct-sequence receiver of Fig. 2.14 when the modulation is PSK and multiple-access interference is present. The spreading sequence of the desired signal is modeled as a random binary sequence and the chip waveform is confined to $[0, T_c)$. From (6.6), it follows that the despread correlator output V, which is the input to the decision device, is

$$V = \sum_{\nu=0}^{G-1} p_{0\nu} Z_\nu = d_0 \sqrt{\mathcal{E}_s} + V_1 + V_2 \tag{6.52}$$

where the multiple-access interference V_1 is given by (6.9), the noise is

$$V_2 = \sum_{\nu=0}^{G-1} p_{0\nu} N_{s\nu} \tag{6.53}$$

the mean value is

$$E[V] = d_0 \sqrt{\mathcal{E}_s} \tag{6.54}$$

and the noise variance is

$$var\,(V_2) = \frac{N_0}{2}. \tag{6.55}$$

Since the data modulation $d_i(t)$ in an interference signal is modeled as a random binary sequence, it can be subsumed into the spreading sequence with no loss of generality. Since $q_i(t)$ is determined by an independent, random spreading sequence, only time delays modulo-T_c are significant and, thus, we can assume that $0 \le \tau_i < T_c$ in (6.10) without loss of generality.

Since $\psi(t)$ is confined to $[0, T_c]$ and $f_c T_c \gg 1$, the substitution of (6.2) and (6.4) into (6.7) yields

$$J_\nu = \sum_{i=1}^{K-1} \sqrt{I_i T_s} \cos\phi_i \quad \left\{ q_{\nu-1}^{(i)} \int_{\nu T_c}^{\nu T_c + \tau_i} \psi(t - \nu T_c)\psi[t - (\nu-1)T_c - \tau_i]dt \right.$$
$$\left. + q_\nu^{(i)} \int_{\nu T_c + \tau_i}^{(\nu+1)T_c} \psi(t - \nu T_c)\psi(t - \nu T_c - \tau_i)dt \right\}. \tag{6.56}$$

The *partial autocorrelation* for the normalized chip waveform is defined as

$$R_\psi(s) = T_s \int_0^s \psi(t)\psi(t + T_c - s)dt, \quad 0 \le s < T_c. \tag{6.57}$$

Substitution into (6.56) and appropriate changes of variables in the integrals yield

$$J_\nu = \sum_{i=1}^{K-1} \sqrt{\frac{I_i}{T_s}} \cos\phi_i \left[q_{\nu-1}^{(i)} R_\psi(\tau_i) + q_\nu^{(i)} R_\psi(T_c - \tau_i) \right]. \tag{6.58}$$

For rectangular chips in the spreading waveform,

$$\psi(t) = \begin{cases} \dfrac{1}{\sqrt{T_s}}, & 0 \le t \le T_c \\ 0, & \text{otherwise.} \end{cases} \tag{6.59}$$

Consequently,

$$R_\psi(s) = s, \quad \textit{rectangular chip.} \tag{6.60}$$

For *sinusoidal chips* in the spreading waveform,

$$\psi(t) = \begin{cases} \sqrt{\dfrac{2}{T_s}} \sin\left(\dfrac{\pi}{T_c} t\right), & 0 \le t \le T_c \\ 0, & \text{otherwise.} \end{cases} \tag{6.61}$$

Substituting this equation into (6.57), using a trigonometric identity, and performing the integrations, we obtain

$$R_\psi(s) = \frac{T_c}{\pi} \sin\left(\frac{\pi}{T_c} s\right) - s\cos\left(\frac{\pi}{T_c} s\right), \quad \textit{sinusoidal chip.} \tag{6.62}$$

Since both J_v and J_{v+1} contain the same random variable $q_v^{(i)}$, it does not appear at first that the terms in (6.58) are statistically independent even when $\boldsymbol{\phi} = (\phi_1, \phi_2, \ldots, \phi_{K-1})$ and $\boldsymbol{\tau} = (\tau_1, \tau_2, \ldots, \tau_{K-1})$ are given. The following lemma [6] resolves this issue.

Lemma. *Suppose that $\{\alpha_i\}$ and $\{\beta_i\}$ are statistically independent, random binary sequences. Let x and y denote arbitrary constants. Then $\alpha_i\beta_j x$ and $\alpha_i\beta_k y$ are statistically independent random variables when $j \neq k$.*

Proof. Let $P(\alpha_i\beta_j x = a, \alpha_i\beta_k y = b)$ denote the joint probability that $\alpha_i\beta_j x = a$ and $\alpha_i\beta_k y = b$ where $|a| = |x|$ and $|b| = |y|$. From the theorem of total probability, it follows that

$$\begin{aligned} P(\alpha_i\beta_j x = a, \alpha_i\beta_k y = b) &= P(\alpha_i\beta_j x = a, \alpha_i\beta_k y = b, \alpha_i = 1) \\ &\quad + P(\alpha_i\beta_j x = a, \alpha_i\beta_k y = b, \alpha_i = -1) \\ &= P(\beta_j x = a, \beta_k y = b, \alpha_i = 1) \\ &\quad + P(\beta_j x = -a, \beta_k y = -b, \alpha_i = -1). \end{aligned}$$

From the independence of $\{\alpha_i\}$ and $\{\beta_j\}$ and the fact that they are random binary sequences, we obtain a simplification for $j \neq k$, $x \neq 0$, and $y \neq 0$:

$$\begin{aligned} P(\alpha_i\beta_j x = a, \alpha_i\beta_k y = b) &= P(\beta_j x = a)P(\beta_k y = b)P(\alpha_i = 1) \\ &\quad + P(\beta_j x = -a)P(\beta_k y = -b)P(\alpha_i = -1) \\ &= \frac{1}{2}P\left(\beta_j = \frac{a}{x}\right)P\left(\beta_k = \frac{b}{y}\right) + \frac{1}{2}P\left(\beta_j = -\frac{a}{x}\right)P\left(\beta_k = -\frac{b}{y}\right). \end{aligned}$$

Since β_j equals $+1$ or -1 with equal probability, $P(\beta_j = a/x) = P(\beta_j = -a/x)$ and thus

$$\begin{aligned} P(\alpha_i\beta_j x = a, \alpha_i\beta_k y = b) &= P\left(\beta_j = \frac{a}{x}\right)P\left(\beta_k = \frac{b}{y}\right) \\ &= P(\beta_j x = a)P(\beta_k y = b). \end{aligned}$$

A similar calculation gives

$$P(\alpha_i\beta_j x = a)P(\alpha_i\beta_k y = b) = P(\beta_j x = a)P(\beta_k y = b).$$

Therefore,

$$P(\alpha_i\beta_j x = a, \alpha_i\beta_k y = b) = P(\alpha_i\beta_j x = a)P(\alpha_i\beta_k y = b)$$

which satisfies the definition of statistical independence of $\alpha_i \beta_j x$ and $\alpha_i \beta_k y$. The same relation is trivial to establish for $x = 0$ or $y = 0$. □

The lemma indicates that when $\boldsymbol{\phi}$ and $\boldsymbol{\tau}$ are given, the terms in (6.9) are statistically independent. Since $p_{0\nu}^2 = 1$, the conditional variance is

$$\text{var}(V_1) = \sum_{\nu=0}^{G-1} \text{var}(J_\nu). \tag{6.63}$$

The independence of the K spreading sequences, the independence of successive terms in each random binary sequence, and (6.58) imply that the conditional variance of J_ν is independent of ν and, therefore,

$$\text{var}(V_1) = \sum_{i=1}^{K-1} \frac{I_i}{T_c} \cos^2 \phi_i [R_\psi^2(\tau_i) + R_\psi^2(T_c - \tau_i)]. \tag{6.64}$$

Since the terms of V_1 in (6.9) are independent, zero-mean random variables that are uniformly bounded and $\text{var}(V_1) \to \infty$ as $G \to \infty$, the central limit theorem implies that $V_1 / \sqrt{\text{var}(V_1)}$ converges in distribution to a Gaussian random variable with mean 0 and variance 1. Thus, when $\boldsymbol{\phi}$ and $\boldsymbol{\tau}$ are given, the conditional distribution of V_1 is approximately Gaussian when G is large. Since the noise component has a Gaussian distribution and is independent of V_1, V has an approximate Gaussian distribution with mean given by (6.54), $\text{var}(V_2)$ given by (6.55), and $\text{var}(V) = \text{var}(V_1) + \text{var}(V_2)$.

A straightforward derivation using the Gaussian distribution of the decision statistic V indicates that the conditional symbol error probability given $\boldsymbol{\phi}$ and $\boldsymbol{\tau}$ is

$$P_s(\phi, \tau) = Q\left(\sqrt{\frac{2\mathcal{E}_s}{N_{0e}(\boldsymbol{\phi}, \boldsymbol{\tau})}}\right) \tag{6.65}$$

where $Q(x)$ is defined by (1.35) and the *equivalent noise-power spectral density* is defined as

$$N_{0e}(\boldsymbol{\phi}, \boldsymbol{\tau}) = N_0 + \sum_{i=1}^{K-1} 2\frac{I_i}{T_c} \cos^2 \phi_i [R_\psi^2(\tau_i) + R_\psi^2(T_c - \tau_i)]. \tag{6.66}$$

For a rectangular chip waveform, this equation simplifies to

$$N_{0e}(\boldsymbol{\phi}, \boldsymbol{\tau}) = N_0 + \sum_{i=1}^{K-1} 2I_i T_c \cos^2 \phi_i \left(1 - 2\frac{\tau_i}{T_c} + 2\frac{\tau_i^2}{T_c^2}\right). \tag{6.67}$$

Numerical evaluations [9] give strong evidence that the error in (6.65) due to the Gaussian approximation is negligible if $G \geq 50$. For an asynchronous network, it is

assumed that the time delays are independent and uniformly distributed over $[0, T_c)$ and that the phase angles θ_i, $i = 1, 2, \ldots, K-1$, are uniformly distributed over $[0,2\pi)$. Therefore, the symbol error probability is

$$P_s = \left(\frac{2}{\pi T_c}\right)^{K-1} \int_0^{\pi/2} \cdots \int_0^{\pi/2} \int_0^{T_c} \cdots \int_0^{T_c} P_s(\boldsymbol{\phi}, \boldsymbol{\tau}) d\boldsymbol{\phi}\, d\boldsymbol{\tau} \tag{6.68}$$

where the fact that $\cos^2 \phi_i$ takes all its possible values over $[0, \pi/2)$ has been used to shorten the integration intervals. The absence of sequence parameters ensures that the amount of computation required for (6.68) is much less than the amount required to compute P_s for a short deterministic spreading sequence. Nevertheless, the computational requirements are large enough that it is highly desirable to find an accurate approximation that entails less computation. The conditional symbol error probability given $\boldsymbol{\phi}$ is defined as

$$P_s(\boldsymbol{\phi}) = \left(\frac{1}{T_c}\right)^{K-1} \int_0^{T_c} \cdots \int_0^{T_c} P_s(\boldsymbol{\phi}, \boldsymbol{\tau}) d\boldsymbol{\tau}. \tag{6.69}$$

A closed-form approximation to $P_s(\boldsymbol{\phi})$ greatly simplifies the computation of P_s, which reduces to

$$P_s = \left(\frac{2}{\pi}\right)^{K-1} \int_0^{\pi/2} \cdots \int_0^{\pi/2} P_s(\boldsymbol{\phi}) d\boldsymbol{\phi}. \tag{6.70}$$

To approximate $P_s(\boldsymbol{\phi})$, we first obtain upper and lower bounds on it.

For either rectangular or sinusoidal chip waveforms, elementary calculus establishes that

$$R_\psi^2(\tau_i) + R_\psi^2(T_c - \tau_i) \le T_c^2. \tag{6.71}$$

Using this upper bound successively in (6.66), (6.65), and (6.69), and performing the trivial integrations that result, we obtain

$$P_s(\boldsymbol{\phi}) \le Q\left(\sqrt{\frac{2\mathcal{E}_s}{N_{0u}(\boldsymbol{\phi})}}\right) \tag{6.72}$$

where

$$N_{0u}(\boldsymbol{\phi}) = N_0 + \sum_{i=1}^{K-1} 2I_i T_c \cos^2 \phi_i. \tag{6.73}$$

To apply Jensen's inequality, the successive integrals in (6.68) are interpreted as the evaluation of expected values. Consider the random variable

$$X = R_\psi^2(\tau_i) + R_\psi^2(T_c - \tau_i). \tag{6.74}$$

Since τ_i is uniformly distributed over $[0, T_c)$, straightforward calculations using (6.60) and (6.62) give

$$E[X] = \frac{1}{T_c}\int_0^{T_c} [R_\psi^2(\tau_i) + R_\psi^2(T_c - \tau_i)]d\tau_i = hT_c^2 \tag{6.75}$$

where the *chip factor* is

$$h = \begin{cases} \dfrac{2}{3}, & \textit{rectangular chip} \\ \dfrac{1}{3} + \dfrac{5}{2\pi^2}, & \textit{sinusoidal chip}. \end{cases} \tag{6.76}$$

The function (6.65) has the form

$$g(x) = Q\left(\sqrt{\frac{1}{a + bx}}\right). \tag{6.77}$$

Since the second derivative of $g(x)$ is nonnegative over the interval such that $0 < a + bx \leq 1/3$, $g(x)$ is a convex function over that interval, and Jensen's inequality is applicable. Relations (6.66), (6.71), and $\cos^2\phi_i \leq 1$ yield a sufficient condition for convexity:

$$\mathcal{E}_s \geq \frac{3}{2}\left[N_0 + \sum_{i=1}^{K-1} 2I_i T_c\right]. \tag{6.78}$$

Application of Jensen's inequality successively to each component of $\boldsymbol{\tau}$ in (6.69) yields

$$P_s(\boldsymbol{\phi}) \geq Q\left(\sqrt{\frac{2\mathcal{E}_s}{N_{0l}(\boldsymbol{\phi})}}\right) \tag{6.79}$$

where

$$N_{0l}(\boldsymbol{\phi}) = N_0 + \sum_{i=1}^{K-1} 2hI_i T_c \cos^2\phi_i. \tag{6.80}$$

If N_0 is negligible, then (6.80) and (6.73) give $N_{0l}/N_{0u} = h$. Thus, a good approximation is provided by

$$P_s(\boldsymbol{\phi}) \approx Q\left(\sqrt{\frac{2\mathcal{E}_s}{N_{0a}(\phi)}}\right) \tag{6.81}$$

where

$$N_{0a}(\boldsymbol{\phi}) = N_0 + \sum_{i=1}^{K-1} 2\sqrt{h}I_i T_c \cos^2\phi_i. \tag{6.82}$$

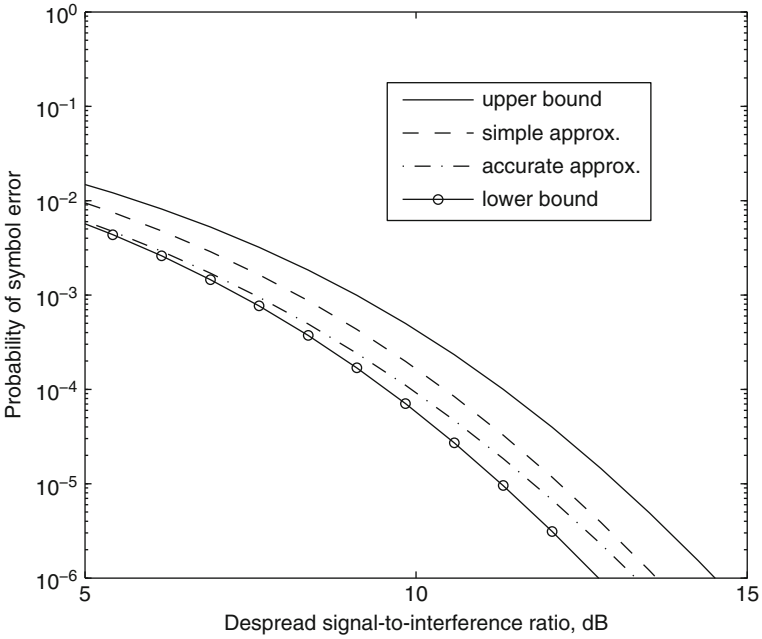

Fig. 6.7 Symbol error probability of direct-sequence system with PSK in presence of single multiple-access interference signal and $\mathcal{E}_s/N_0 = 15\,\text{dB}$

Since $I_i T_c = I_i T_s/G$, this equation explicitly indicates that the symbol energy of each multiple-access signal is suppressed by the factor G. If N_0 is negligible, then $N_{0u}/N_{0a} = N_{0a}/N_{0l} = 1/\sqrt{h}$. Therefore, in terms of the value of $\mathcal{E}_s$ needed to ensure a given $P_s(\phi)$, the error in using approximation (6.81) instead of (6.69) is bounded by $10\log_{10}(1/\sqrt{h})$ in decibels, which equals 0.88 dB for rectangular chip waveforms and 1.16 dB for sinusoidal chip waveforms. In practice, the error is expected to be only a few tenths of a decibel because $N_0 \neq 0$ and P_s coincides with neither the upper nor the lower bound.

As an example, suppose that rectangular chip waveforms are used, $\mathcal{E}_s/N_0 = 15\,\text{dB}$, and $K = 2$. Figure 6.7 illustrates four different evaluations of P_s as a function of $G\mathcal{E}_s/IT_s$, the *despread signal-to-interference ratio*, which is the signal-to-interference ratio after taking into account the beneficial results from the despreading in the receiver. The accurate approximation is computed from (6.65) and (6.68), the upper bound from (6.72) and (6.70), the lower bound from (6.79) and (6.70), the simple approximation from (6.81) and (6.70). The figure shows that the accurate approximation moves from the lower bound toward the simple approximation as the symbol error probability decreases. For $P_s = 10^{-5}$, the simple approximation is less than 0.3 dB in error relative to the accurate approximation.

Figure 6.8 compares the symbol error probabilities for $K = 2$ to $K = 4$, rectangular chip waveforms and $\mathcal{E}_s/N_0 = 15\,\text{dB}$. The simple approximation is used

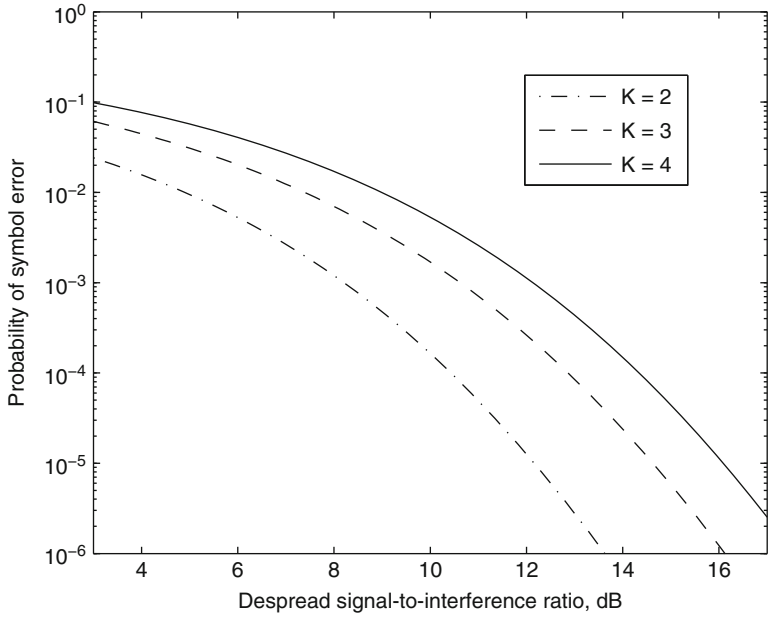

Fig. 6.8 Symbol error probability of direct-sequence system with PSK in presence of $K-1$ equal-power multiple-access interference signals and $\mathcal{E}_s/N_0 = 15$ dB

for P_s, and the abscissa shows $G\mathcal{E}_s/IT_s$, where I is the interference power of each equal-power interfering signal. The figure shows that P_s increases with K, but the shift in P_s is mitigated somewhat because the interference signals tend to partially cancel each other.

The preceding bounding methods can be extended to the bounds on $P_s(\boldsymbol{\phi})$ by observing that $\cos^2\phi_i \leq 1$ and setting $X = \cos^2\phi_i$ during the successive applications of Jensen's inequality, which is applicable if (6.78) is satisfied. After evaluating (6.73), we obtain

$$Q\left(\sqrt{\frac{2\mathcal{E}_s}{N_0 + hI_tT_c}}\right) \leq P_s \leq Q\left(\sqrt{\frac{2\mathcal{E}_s}{N_0 + 2I_tT_c}}\right) \tag{6.83}$$

where

$$I_t = \sum_{i=1}^{K-1} I_i. \tag{6.84}$$

A simple approximation is provided by

$$P_s \approx Q\left(\sqrt{\frac{2\mathcal{E}_s}{N_0 + \sqrt{2h}\, I_tT_c}}\right). \tag{6.85}$$

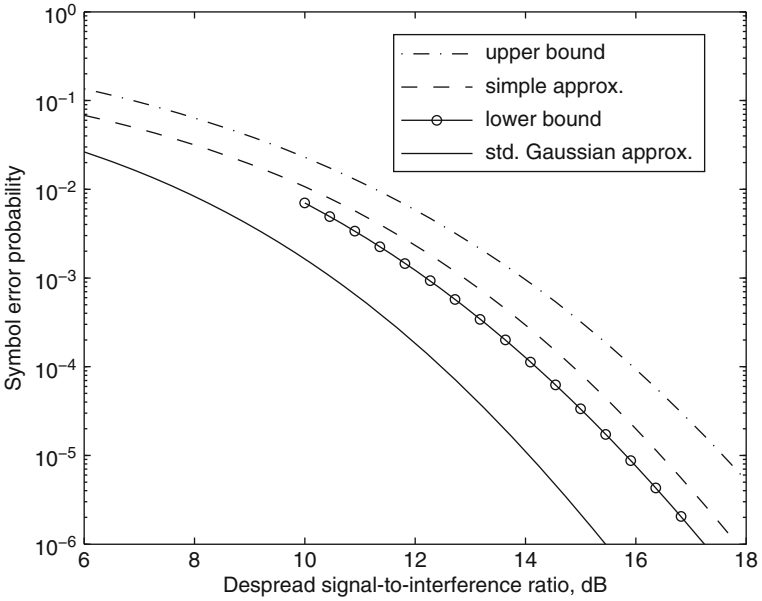

Fig. 6.9 Symbol error probability of direct-sequence system with PSK in presence of three equal-power multiple-access interference signals and $\mathcal{E}_s/N_0 = 15\,\text{dB}$

If P_s is specified, then the error in the required $\mathcal{E}_s/I_t$ caused by using (6.85) instead of (6.68) is bounded by $10\log_{10}\sqrt{2/h}$ in decibels. Thus, the error is bounded by 2.39 dB for rectangular chip waveforms and 2.66 dB for sinusoidal ones.

The lower bound in (6.83) gives the same result as that often called the *standard Gaussian approximation*, in which V_1 in (6.9) is assumed to be approximately Gaussian, each ϕ_i in (6.58) is assumed to be uniformly distributed over $[0, 2\pi)$, and each τ_i is assumed to be uniformly distributed over $[0, T_c)$. This approximation, gives an optimistic result for P_s that can be as much as 4.77 dB in error for rectangular chip waveforms according to (6.83). The substantial improvement in accuracy provided by (6.81) or (6.65) is due to the application of the Gaussian approximation only after conditioning V_1 on given values of $\boldsymbol{\phi}$ and $\boldsymbol{\tau}$. The accurate approximation given by (6.65) is a version of what is often called the *improved Gaussian approximation*.

Figure 6.9 illustrates the symbol error probability for 3 interferers, each with power I, rectangular chip waveforms, and $\mathcal{E}_s/N_0 = 15\,\text{dB}$ as a function of $G\mathcal{E}_s/IT_s$. The graphs show the standard Gaussian approximation of (6.83), the simple approximation of (6.85), and the upper and lower bounds given by (6.72), (6.79), and (6.70). The large error in the standard Gaussian approximation is evident. The simple approximation is reasonably accurate if $10^{-6} \le P_s \le 10^{-2}$.

For *synchronous* networks, (6.65) and (6.66) can be simplified because the $\{\tau_i\}$ are all zero. For either rectangular or sinusoidal chip waveforms, we obtain

$$P_s(\boldsymbol{\phi}) = Q\left(\sqrt{\frac{2\mathcal{E}_s}{N_{0e}(\boldsymbol{\phi})}}\right) \tag{6.86}$$

where

$$N_{0e}(\boldsymbol{\phi}) = N_0 + \sum_{i=1}^{K-1} 2I_i T_c \cos^2 \phi_i . \tag{6.87}$$

A comparison with (6.72) and (6.73) indicates that the *symbol error probability for a synchronous network equals or exceeds the symbol error probability for a similar asynchronous network when random spreading sequences are used.* This phenomenon is due to the increased bandwidth of a despread asynchronous interference signal, which allows increased filtering in the receiver.

The accurate approximation of (6.65) follows from the standard central limit theorem, which is justified by the lemma. This lemma depends on the restriction of the chip waveform to the interval $[0, T_c]$. If the chip waveform extends beyond this interval but is time-limited, as is necessary for implementation with digital hardware, then an extension of the central limit theorem for m-dependent sequences can be used to derive an improved Gaussian approximation [10]. Alternatives to the analysis in this section and the next one abound in the literature, but they are not as amenable to comparisons among systems.

6.2.3 Quadriphase Direct-Sequence Systems

Consider a network of quadriphase direct-sequence systems, each of which uses dual QPSK and random spreading sequences. As described in Sect. 2.4, each direct-sequence signal is given by

$$s(t) = \sqrt{\mathcal{E}_s} d_1(t) p_1(t) \cos 2\pi f_c t + \sqrt{\mathcal{E}_s} d_2(t) p_2(t) \sin 2\pi f_c t \tag{6.88}$$

where $\mathcal{E}_s$ is the energy per binary channel symbol. The multiple-access interference is

$$i(t) = \sum_{i=1}^{K-1} \Big[\sqrt{I_i T_s}\, q_{1i}(t - \tau_i) \cos(2\pi f_c t + \phi_i) + \sqrt{I_i T_s}\, q_{2i}(t - \tau_i) \sin(2\pi f_c t + \phi_i) \Big] \tag{6.89}$$

where $q_{1i}(t)$ and $q_{2i}(t)$ both have the form of (6.4) and incorporate the data modulation, and I_i is the average power of a binary channel symbol of interference signal i. The decision variables are given by

$$V = d_{10}\sqrt{2\mathcal{E}_s} + \sum_{\nu=0}^{2G-1} p_{1\nu} J_\nu + \sum_{\nu=0}^{2G-1} p_{1\nu} N_{s\nu} \tag{6.90}$$

$$U = d_{20}\sqrt{2\mathcal{E}_s} + \sum_{\nu=0}^{2G-1} p_{2\nu} J'_\nu + \sum_{\nu=0}^{2G-1} p_{2\nu} N'_\nu \tag{6.91}$$

where $G = T_s/T_c$. A straightforward calculation using (6.7) indicates that

$$J_\nu = \sum_{i=1}^{K-1} \sqrt{\frac{I_i}{2T_s}} \left\{ \cos\phi_i \left[q_{\nu-1}^{(1i)} R_\psi(\tau_i) + q_\nu^{(1i)} R_\psi(T_c - \tau_i) \right] \right.$$
$$\left. - \sin\phi_i \left[q_{\nu-1}^{(2i)} R_\psi(\tau_i) + q_\nu^{(2i)} R_\psi(T_c - \tau_i) \right] \right\}. \tag{6.92}$$

The statistical independence of the two sequences, the preceding lemma, and analogous results for J'_ν defined by (2.122) yield the variances of the interference terms of the decision variables:

$$\mathrm{var}(V_1) = \mathrm{var}(U_1) = \sum_{i=1}^{K-1} \frac{I_i}{T_c} \left[R_\psi^2(\tau_i) + R_\psi^2(T_c - \tau_i) \right]. \tag{6.93}$$

The noise variances and the means are given by (2.124) and (2.123). Since all variances and means are independent of $\boldsymbol{\phi}$, the Gaussian approximation yields a $P_s(\boldsymbol{\phi}, \boldsymbol{\tau})$ that is independent of $\boldsymbol{\phi}$:

$$P_s = \left(\frac{1}{T_c}\right)^{K-1} \int_0^{T_c} \cdots \int_0^{T_c} Q\left(\sqrt{\frac{2\mathcal{E}_s}{N_{0e}(\boldsymbol{\tau})}} \right) d\boldsymbol{\tau} \tag{6.94}$$

where

$$N_{0e}(\boldsymbol{\tau}) = N_0 + \sum_{i=1}^{K-1} \frac{I_i}{T_c} \left[R_\psi^2(\tau_i) + R_\psi^2(T_c - \tau_i) \right]. \tag{6.95}$$

Since a similar analysis for direct-sequence systems with balanced QPSK yields (6.95) again, *both quadriphase systems perform equally well against multiple-access interference*.

Application of the previous bounding and approximation methods to (6.94) yields

$$Q\left(\sqrt{\frac{2\mathcal{E}_s}{N_0 + hI_tT_c}} \right) \le P_s \le Q\left(\sqrt{\frac{2\mathcal{E}_s}{N_0 + I_tT_c}} \right) \tag{6.96}$$

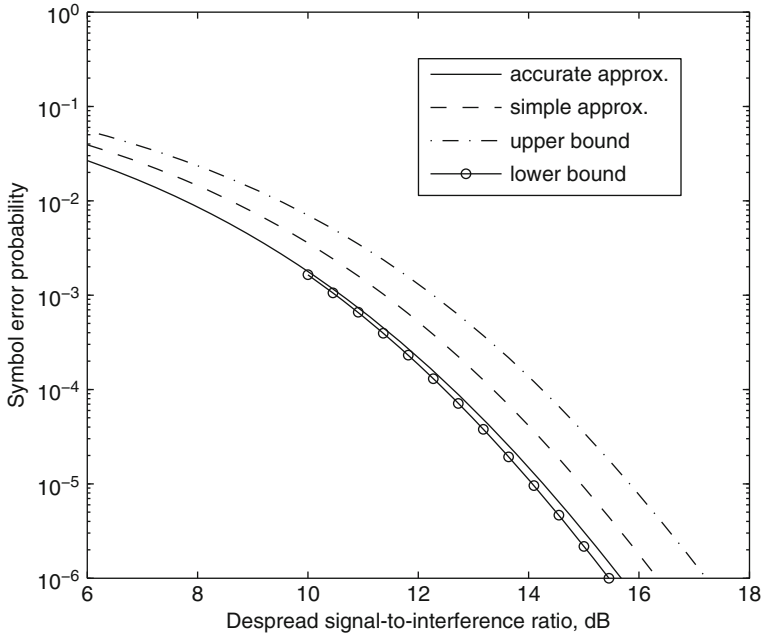

Fig. 6.10 Symbol error probability of quadriphase direct-sequence system in presence of three equal-power multiple-access interference signals and $\mathcal{E}_s/N_0 = 15\,\text{dB}$

where the total interference power I_t is defined by (6.84). A sufficient condition for the validity of the lower bound is

$$\mathcal{E}_s \geq \frac{3}{2}\left(N_0 + I_t T_c\right). \tag{6.97}$$

A simple approximation that limits the error in the required $\mathcal{E}_s/I_t$ for a specified P_s to $10\log_{10}(1/\sqrt{h})$ is

$$P_s \approx Q\left(\sqrt{\frac{2\mathcal{E}_s}{N_0 + \sqrt{h} I_t T_c}}\right). \tag{6.98}$$

This approximation introduces errors bounded by 0.88 dB and 1.16 dB for rectangular and sinusoidal chip waveforms, respectively. In (6.96) and (6.98), only the total interference power is relevant, not how it is distributed among the individual interference signals.

Figure 6.10 illustrates P_s for a quadriphase direct-sequence system in the presence of three interferers, each with power I, rectangular chip waveforms, and $\mathcal{E}_s/N_0 = 15\,\text{dB}$. The graphs represent the accurate approximation of (6.94), the simple approximation of (6.98), and the bounds of (6.96) as functions of $G\mathcal{E}_s/IT_s$. A comparison of Figs. 6.10 and 6.9 indicates the advantage of a quadriphase system.

For *synchronous networks* with either rectangular or sinusoidal chip waveforms, we set the $\{\tau_i\}$ equal to zero in (6.94) and obtain

$$P_s = Q\left(\sqrt{\frac{2\mathcal{E}_s}{N_0 + I_t T_c}}\right). \tag{6.99}$$

Since this equation coincides with the upper bound in (6.96), we conclude that *asynchronous networks accommodate more multiple-access interference than similar synchronous networks using quadriphase direct-sequence signals with random spreading sequences.*

To compare asynchronous quadriphase direct-sequence systems with asynchronous systems using BPSK, we find a lower bound on P_s for direct-sequence systems with PSK. Substituting (6.65) into (6.68) and applying Jensen's inequality successively to the integrations over ϕ_i, $i = 1, 2, \ldots, K-1$, we find that a lower bound on P_s is given by the right-hand side of (6.94) if (6.97) is satisfied. This result implies that *asynchronous quadriphase direct-sequence systems are more resistant to multiple-access interference than asynchronous direct-sequence systems with BPSK.*

The equations for P_s allow the evaluation of the information-bit error probability P_b for channel codes with hard-decision decoders. To facilitate the analysis of soft-decision decoding, two assumptions are necessary. Assume that K is large enough that the multiple-access interference after despreading is approximately Gaussian rather than conditionally Gaussian. Since the equivalent noise is a zero-mean process, the equivalent noise-power spectral density N_{0e} can be obtained by averaging $N_{0e}(\boldsymbol{\phi}, \boldsymbol{\tau})$ over the distributions of $\boldsymbol{\phi}$ and $\boldsymbol{\tau}$. For asynchronous communications, (6.95) and (6.75) yield

$$N_{0e} = N_0 + hI_t T_c \tag{6.100}$$

where h is given by (6.76). This equation is also valid for synchronous communications if we set $h = 1$. Thus, for a binary convolutional code with rate r, constraint length K, and minimum free distance d_f, P_b is upper-bounded by (1.110) with

$$P_2(l) = Q\left(\sqrt{\frac{2\mathcal{E}_s l}{N_{0e}}}\right) = Q\left(\sqrt{\frac{2r\mathcal{E}_b l}{N_0 + hI_t T_c}}\right). \tag{6.101}$$

The *network user capacity* is the number of equal-power users in a network of identical systems that can be accommodated while achieving a specified P_b. For equal-power users, $I_t = (K-1)\mathcal{E}_s/T_s$. Let γ_1 denote the value of $\mathcal{E}_s/N_{0e}$ necessary for a specific channel code to achieve the specified P_b. Equation (6.100) implies that the network user capacity is

$$K = \left\lfloor 1 + \frac{G}{h}\left(\frac{1}{\gamma_1} - \frac{1}{\gamma_0}\right)\right\rfloor, \quad \gamma_0 \geq \gamma_1 \tag{6.102}$$

where $\lfloor x \rfloor$ is the integer part of x, $\gamma_0 = \mathcal{E}_s/N_0$, $G = T_s/T_c$ is the processing gain, and the requirement $\gamma_0 \geq \gamma_1$ is necessary to ensure that the specified P_b can be achieved for some value of K. Since $h < 1$ in general, the factor G/h reflects the increased gain due to the random distributions of interference phases and delays. If they are not random but $\boldsymbol{\phi} = \boldsymbol{\tau} = \mathbf{0}$, then $h = 1$ and the number of users accommodated is reduced.

For equal-power users subject to the same fading statistics, $I_t = (K-1)\mathcal{E}_s\overline{\alpha^2}/T_s$ and the network user capacity is

$$K = \left\lfloor 1 + \frac{G_0}{h}\left(\frac{1}{\overline{\gamma}_1} - \frac{1}{\overline{\gamma}_0}\right)\right\rfloor, \quad \overline{\gamma}_0 \geq \overline{\gamma}_1 \tag{6.103}$$

where $\overline{\gamma}_0 = \mathcal{E}_s\overline{\alpha^2}/N_0$ and $\overline{\gamma}_1$ is the required $\mathcal{E}_s\overline{\alpha^2}/N_{0e}$ necessary for a specific channel code to achieve the specified P_b.

As an example, consider a network with systems that resemble those used for the synchronous downlinks of an IS-95 CDMA network. We assume the absence of fading and calculate the network user capacity for power-controlled users within a single cell. The data modulation is balanced QPSK. $G = 64$, and $h = 1$. The channel code is a rate-1/2 binary convolutional code with constraint length 9. If $P_b = 10^{-5}$ or better is desired, the performance curve of Fig. 1.9 for the convolutional code indicates that $\mathcal{E}_b/N_{0e} \approx 3.5\,\mathrm{dB}$ and thus $\gamma_1 \approx 0.5\,\mathrm{dB}$ is required. Equation (6.102) then indicates that the network user capacity is $K = 51$ if $\gamma_0 = 10\,\mathrm{dB}$ and $K = 57$ if $\gamma_0 = 20\,\mathrm{dB}$.

6.3 Cellular Networks and Power Control

In a *cellular network*, a geographic region is partitioned into cells, as illustrated in Fig. 6.11. A base station that includes a transmitter and receiver is located at the center of each cell. Ideally, the cells have equal hexagonal areas. Each *mobile*

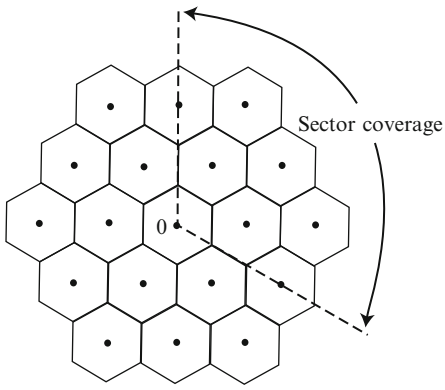

Fig. 6.11 Geometry of cellular network with base station at center of each hexagon. Two concentric tiers of cells surrounding a central cell are shown

(user or subscriber) in the network transmits omnidirectionally and is associated with a specific base station that handles the radio communications of the mobile. That base station is the one that receives the largest average power from the mobile. The base stations act as a switching center for the mobiles and communicate among themselves by wirelines in most applications. By comparing the received signals from a single mobile at several base stations, the switching center may decide which version of the mobile's signal is strongest at any instant in a process known as *soft handoff*. Typically, most of the mobiles in a cell are associated with the base station at the center of the cell. Cellular networks with DS/CDMA allow universal frequency reuse in that the same carrier frequency and spectral band is shared by all the cells. Distinctions among the direct-sequence signals are possible because each signal is assigned a unique spreading sequence.

Cells may be divided into *sectors* by using several directional sector antennas or arrays at the base stations. Only mobiles in the directions covered by a sector antenna can cause multiple-access interference on the *reverse link* or *uplink* from a mobile to its associated sector antenna. Only a sector antenna serving a cell sector oriented toward a mobile can cause multiple-access interference on the *forward link* or *downlink* from the mobile's associated sector antenna to the mobile. Thus, the numbers of interfering signals on both the uplink and the downlink are reduced approximately by a factor equal to the number of sectors.

To facilitate the identification of a base station controlling communications with a mobile, each spreading sequence for a downlink is formed as the product or concatenation of two sequences often called the scrambling and channelization codes. A *scrambling code* is a sequence that identifies a particular base station when the code is acquired by mobiles associated with the base station and its cell or sector. A long sequence is preferable to ensure small periodic cross-correlations among the scrambling codes. If the set of base stations use the Global Positioning System or some other common timing source, then each scrambling code may be a known phase shift of a common long pseudonoise sequence. If a common timing source is not used, then at the cost of increased acquisition time or complexity, the scrambling codes may comprise a set of long Gold sequences that approximate random binary sequences. A *channelization code* is designed to allow each mobile receiver to extract its messages while blocking messages intended for other mobiles within the same cell or sector. Walsh or other orthogonal sequences are suitable as channelization codes for synchronous downlinks. For the uplinks, channelization codes are not strictly necessary, and the scrambling codes that identify the mobiles may be drawn from a set of long Gold sequences.

The principal difficulty of DS/CDMA is called the *near-far problem*. If all mobiles transmit at the same power level, then the received power at a base station is higher for transmitters near the receiving antenna. There is a near-far problem because transmitters that are far from the receiving antenna may be at a substantial power disadvantage, and the spread-spectrum processing gain may not be enough to allow satisfactory reception of their signals. A similar problem may also result from large differences in received power levels due to differences in the shadowing experienced by signals traversing different paths or due to independent fading.

In cellular communication networks, the near-far problem is critical only on the uplink because on the downlink, the base station transmits orthogonal signals synchronously to each mobile associated with it. For cellular networks, the usual solution to the near-far problem of uplinks is *power control*, whereby all mobiles regulate their power levels. By this means, power control potentially ensures that the power arriving at a common receiving antenna is almost the same for all transmitters. Since solving the near-far problem is essential to the viability of a DS/CDMA network, the accuracy of the power control is a crucial issue.

An *open-loop method* of power control in a cellular network causes a mobile to adjust its transmitted power to be inversely proportional to the received power of a *pilot signal* transmitted by the base station. Open-loop power control is effective if the propagation losses on the uplinks and downlinks are nearly the same. Whether they are or not depends on the duplexing method used to allow transmissions on both links. *Frequency-division duplexing* assigns different frequencies to an uplink and its corresponding downlink. *Time-division duplexing* assigns closely spaced but distinct time slots to the two links. When frequency-division duplexing is used, as in the IS-95 and Global System for Mobile (GSM) standards, the frequency separation is generally wide enough that the channel transfer functions of the uplink and downlink are different. This lack of *link reciprocity* implies that power measurements over the downlink do not provide reliable information for subsequent uplink transmissions. When time-division duplexing is used, the received local-mean power levels for the uplink and the downlink will usually be nearly equal when the transmitted powers are the same, but the Rayleigh fading may subvert link reciprocity.

A *closed-loop* method of power control, which is more flexible than the open-loop method, requires the base station to transmit power-control information to each mobile based on the power level received from the mobile or the signal-to-interference ratio. Each base station attempts to either directly or indirectly track the received power of a desired signal from a mobile and dynamically transmit a power-control signal. The effect of increasing the carrier frequency or the mobile speeds is to increase the fading rate. As the fading rate increases, the tracking ability and, hence, the power-control accuracy decline. This problem might be discounted because the large fade durations during slow fading enable effective power control, whereas the imperfect power control in the presence of fast fading is compensated by the increased time diversity provided by the interleaving and channel coding. However, this argument ignores both the potential severity of the near-far problem and the limits of compensation as the fading rate increases. If the power control breaks down completely, then close interfering mobiles can cause frequent error bursts of duration long enough to overwhelm the ability of the deinterleaver to disperse the errors so that the decoder can eliminate them. Thus, some degree of power control must be maintained as the vehicle speeds or the carrier frequency increases. The degree required when the interleaving is perfect is quantified subsequently.

In *ad hoc networks* (Sect. 6.4), there is no cellular or hierarchical structure. Communications between two mobiles are either direct or are relayed by other

mobiles. Since there is no feasible method of power control to prevent the near-far problem, DS/CDMA systems are not as attractive an option as FH/CDMA systems in these networks.

6.3.1 Intercell Interference of Uplink

The following performance analysis of the uplink [11] begins with the derivation of the intercell interference factor, which is the ratio of the intercell interference power to the intracell interference power. The *intercell interference* arrives from mobiles associated with different base stations than the one receiving a desired signal. The *intracell interference* arrives from mobiles that are associated with the same base station receiving a desired signal. The performance is evaluated using two different criteria: the outage and the bit error rate. The outage criterion has the advantage that it simplifies the analysis and does not require specification of the data modulation or channel coding. The bit-error-rate criterion has the advantage that the impact of the channel coding can be calculated. For both criteria, the fading is flat and no explicit diversity or rake combining is assumed. Since the interference signals arrive asynchronously, they cannot be suppressed by using orthogonal spreading sequences.

To account for the fading and instantaneous power control in a mathematically tractable way, the product of the shadowing and fading factors in (5.4) is approximated [12] by a lognormal random variable. Thus, it is assumed that the *equivalent shadowing factor* η implicitly defined by

$$10^{\eta/10} = 10^{\xi/10}\alpha^2 \tag{6.104}$$

has a probability density function that is approximately Gaussian. This approximation is reasonable if the power variations due to the shadowing are more significant than those due to the fading and if the first two moments of both sides of (6.104) are equal. Since $\eta = \xi + 20\log_{10}\alpha$, the statistical independence of ξ and α and the shadowing assumption that $E[\xi] = 0$ imply that

$$E[\eta] = \frac{2}{b}E[ln\,\alpha] \tag{6.105}$$

$$E[\eta^2] = E[\xi^2] + \frac{4}{b^2}E[(ln\,\alpha)^2] \tag{6.106}$$

where $b = (ln\,10)/10$. To evaluate these equations when α has the Nakagami-m density function of (5.29) with $E[\alpha^2] = \Omega = 1$ and m equal to a positive integer, we express the expectations as integrals, change the integration variables, and apply the identities [13]

$$\int_0^\infty x^{\nu-1}e^{-\mu x}ln\,x\,dx = \frac{\Gamma(\nu)}{\mu^\nu}[\psi(\nu) - ln\,\mu] \tag{6.107}$$

$$\int_0^\infty x^{\nu-1} e^{-\mu x} (ln\, x)^2\, dx = \frac{\Gamma(\nu)}{\mu^\nu} \left\{ [\psi(\nu) - ln\, \mu]^2 + \zeta(2, \nu) \right\} \tag{6.108}$$

where $\mu > 0$, ν is a positive integer, $\zeta(2, \nu)$ is the Riemann zeta function given by

$$\zeta(2, \nu) = \sum_{i=0}^{\infty} \frac{1}{(\nu + i)^2}, \quad \nu \neq 0, -1, -2, \ldots \tag{6.109}$$

and $\psi(\nu)$ is the psi function given by

$$\psi(\nu) = \sum_{i=1}^{\nu-1} \frac{1}{i} - C, \quad \nu = 1, 2, \ldots, \quad C \cong 0.5772. \tag{6.110}$$

Let σ_η^2 denote the variance of η. Since $E[\xi^2] = \sigma_s^2$, the variance of ξ, we find that

$$E[\eta] = \frac{1}{b} [\psi(m) - ln(m] \tag{6.111}$$

$$\sigma_\eta^2 = \sigma_s^2 + \frac{\zeta(2, m)}{b^2}. \tag{6.112}$$

The impact of the fading declines with increasing values of the positive integer m, and hence the approximation that the equivalent shadowing factor η has a Gaussian density becomes more accurate. The approximation is close if $\sigma_s \geq 6$ dB, which are usually true in practical applications. For Rayleigh fading, $m = 1$ and $\zeta(2, 1) = 1.645$, so $E[\eta] = -2.5$ and $\sigma_\eta^2 = \sigma_s^2 + 31.0$. For $m = 5$, which approximates Ricean fading with Rice factor $\kappa = 8.47$, $E[\eta] = -0.45$ and $\sigma_\eta^2 = \sigma_s^2 + 4.2$.

Consider a cellular network in which each base station is located at the center of a hexagonal area, as illustrated in Fig. 6.11. To analyze uplink interference, it is assumed that the desired signal arrives at base station 0, while the other base stations are labeled 1, 2, ..., N_B. The directions covered by one of three sectors associated with base station 0 are indicated in the figure. Each mobile in the network transmits omnidirectionally and is associated with the base station from which it receives the largest average short-term or *instantaneous power*. This base station establishes the uplink power control of the mobile. If a mobile is associated with base station i, then (5.1), (5.4), and (6.104) indicate that the instantaneous power received by base station n is

$$D_{in} = p_{0i} \left(\frac{r_n}{\delta} \right)^{-\beta} 10^{\eta_n/10} = p_{0i} \left(\frac{r_n}{\delta} \right)^{-\beta} \exp(b\, \eta_n) \tag{6.113}$$

where r_n is the distance to base station n, η_n is the equivalent shadowing factor, p_{0i} is the area-mean power at $r_n = \delta$, and it is assumed that the attenuation power-law β is the same throughout the network and that the restriction $r_n \geq \delta$ can be omitted with negligible effect on the subsequent analysis. If the power control exerted by

base station i ensures that it receives unit instantaneous power from each mobile associated with it, then $D_{ii} = 1$. Consequently, $p_{0i} = (r_i/\delta)^{\beta} \exp(-b\,\eta_i)$, and

$$D_{in} = \left(\frac{r_i}{r_n}\right)^{\beta} \exp[b(\eta_n - \eta_i)]. \tag{6.114}$$

Assuming a common fading model for all of the $\{\eta_i\}$, (6.105) implies that they all have the same mean value. The form of (6.114) then indicates that this common mean value is irrelevant to the statistics of D_{in} and hence can be ignored without penalty in the subsequent statistical analysis of D_{in}.

The simplifying approximation is made that the base station with which a mobile is associated receives more instantaneous power from the mobile than any other base station. Since $D_{ii} = 1$, the approximation implies that $D_{in} \leq 1, 0 \leq n \leq N_B$, which is exact if the power control is perfect and the propagation losses over the uplink and downlink are identical. Given the approximation, the probability distribution function of the interference power D_{i0} at base station 0 is

$$F_i(x) = P[D_{i0} \leq x \mid D_{in} \leq 1, 0 \leq n \leq N_B] = \frac{\phi_i(x)}{\phi_i(1)} \tag{6.115}$$

where

$$\phi_i(x) = P[D_{i0} \leq x; D_{in} \leq 1, 0 \leq n \leq N_B]. \tag{6.116}$$

$P[A]$ denotes the probability of the event A, and $F_i(x) = 0$ if $x < 0$. Let

$$\phi_i(x \mid \eta_i, r_i, \theta_i) = P[D_{i0} \leq x; D_{in} \leq 1, 0 \leq n \leq N_B \mid \eta_i, r_i, \theta_i] \tag{6.117}$$

where this probability is conditioned on η_i, the equivalent shadowing factor for the controlling base station, and the polar coordinates r_i, θ_i of the mobile relative to base station i. It is assumed that each of the $\{\eta_n\}$ is statistically independent with the common variance σ_η^2. Therefore, given η_i, D_{in} and D_{ik}, $n \neq k$, are statistically independent. Let $Q_c(x) = 1 - Q(x)$, where $Q(x)$ is defined by (1.35). Since each of the $\{\eta_n\}$ has a Gaussian probability density function, (6.114) implies that for $0 \leq x \leq 1$,

$$\begin{aligned}\phi_i(x \mid \eta_i, r_i, \theta_i) = {} & Q_c\left(\frac{b\eta_i + \beta\, ln(r_0/r_i) + ln\, x}{b\sigma_\eta}\right) \\ & \times \prod_{n=1 n\neq i}^{N_B} Q_c\left(\frac{b\eta_i + \beta\, ln(r_n/r_i)}{b\sigma_\eta}\right)\end{aligned} \tag{6.118}$$

where $r_n, 0 \leq n \leq N_B$, is a function of r_i, θ_i, and the location of base station n.

The probability $\phi_i(x)$, and hence the distribution $F_i(x)$, can be determined by evaluating the expected value of (6.118) with respect to the random variables η_i, r_i,

and θ_i. If a mobile is associated with base station i, then its location is assumed to be uniformly distributed within a circle of radius R_b surrounding the base station. Therefore,

$$\phi_i(x) = \int_0^{2\pi} d\theta \int_0^{R_b} dr \int_{-\infty}^{\infty} d\eta \, \frac{r \exp\left(-\dfrac{\eta^2}{2\sigma_\eta^2}\right)}{\sqrt{2\pi}\,\sigma_\eta\,\pi R_b^2} \phi_i(x \mid \eta, r, \theta) \tag{6.119}$$

which determines the distribution function in (6.115).

Let I_{te} denote the total intercell interference relative to the unit desired-signal power that each base station maintains by power control of each mobile within its cell. Let K_i denote the number of active mobiles associated with a base station i or sector antenna i, which may be a random variable because of voice-activity detection or the movement of mobiles among the cells. Then

$$I_{te} = \sum_{i=1}^{N_B} \sum_{k=1}^{K_i} D_{i0k} \tag{6.120}$$

where D_{i0k} is the interference due to mobile k associated with base station i. It is assumed that the $\{D_{i0k}\}$ are statistically independent, that $E[K_i] = E[K]$ for all base stations, and that $E[D_{i0k}] = E[D_{i0}]$ and $var[D_{i0k}] = var[D_{i0}]$ are the same for all mobiles associated with base station i. Let $\mathbf{K}$ represent the set $\{K_i\}$, and let $E_{\mathbf{K}}\{\cdot\}$ denote the expectation with respect to $\mathbf{K}$. With the preceding assumptions and the expansion $var\,(I_{te}) = E_{\mathbf{K}}\{E[I_{te}^2 \,|\mathbf{K}\,\}-(E_{\mathbf{K}}\{E[I_{te}\,|\mathbf{K}\,\})^2$, straightforward calculations yield

$$E[I_{te}] = E[K] \sum_{i=1}^{N_B} E[D_{i0}] \tag{6.121}$$

$$\text{var}[I_{te}] = E[K] \sum_{i=1}^{N_B} \text{var}[D_{i0}] + \text{var}[K] \left(\sum_{i=1}^{N_B} E[D_{i0}] \right)^2 . \tag{6.122}$$

In general, $E[I_{te}]$ and $\text{var}[I_{te}]$ decrease as the attenuation power law β increases. The *intercell interference factor*, $g = E[I_{te}]/E[K]$, is the ratio of the average intercell interference power to the average intracell interference power. Table 6.1, calculated in [14], lists g versus σ_η when $N_B = 60$ cells in four concentric tiers surrounding a central cell, R_b is five times the distance from a base station to the corner of its surrounding hexagonal cell, and $\beta = 4$. The dependence of g on the specific fading model is exerted through (6.112), which relates σ_η to m and σ_s. Table 6.1 also lists the *variance factor* $g_1 = \text{var}[I_{te}]/E[K]$ assuming that $\text{var}[K] = 0$.

The results in Table 6.1 depend on the pessimistic assumption that the equivalent shadowing factors η_n and η_i from a mobile to two different base stations are independent random variables. Suppose, instead, that each factor is the sum of a

Table 6.1 Interference and variance factors when var[K] = 0

σ_η, dB	g	g_1
3	0.460	0.137
4	0.486	0.143
$6/\sqrt{2}$	0.493	0.145
5	0.519	0.153
$8/\sqrt{2}$	0.544	0.162
6	0.558	0.167
7	0.598	0.183
$10/\sqrt{2}$	0.601	0.184
8	0.634	0.189

common component and an equal-power independent component that depends on the receiving base station. Then (6.114) implies that the common component cancels. As a result, in determining g from Table 6.1, the effective value of σ_η is reduced by a factor of $\sqrt{2}$ relative to what it would be without the common component.

6.3.2 *Outage Analysis*

For a DS/CDMA system, it is assumed that the total power I_t of the multiple-access interference after the despreading is approximately uniformly distributed over its bandwidth, which is approximately equal to $1/T_c$. For instantaneous power control, the *instantaneous signal-to-interference-plus-noise ratio* (SINR) is defined to be $\mathcal{E}_s/(N_0+I_tT_c)$, the ratio of the energy per symbol $\mathcal{E}_s$ to the equivalent power spectral density of the interference plus noise. An *outage* is said to occur if the instantaneous SINR of a system is less than a specified threshold Z, which may be adjusted to account for any diversity, rake combining, or channel code. Initially, the interference is assumed to be *intracell interference* that arises from $K-1$ other active mobiles in the cell or sector occupied by a mobile of interest; subsequently, the intercell interference factor is used to account for the intercell interference. Let $\mathcal{E}_i = I_iT_s$, $i = 1, 2, \ldots, K-1$, denote the received energy in a symbol due to interference signal i with power I_i. These definitions imply that an outage occurs if

$$\mathcal{E}_s Z^{-1} < N_0 + \frac{1}{G}\sum_{i=1}^{K-1}\mathcal{E}_i \tag{6.123}$$

where $G = T_s/T_c$ is the processing gain. Let $\mathcal{E}_{s0}$ denote the common desired energy per symbol for all the signals associated with the base station of a single cell sector. When instantaneous power control is used, $\mathcal{E}_s = \mathcal{E}_{s0}\epsilon_0$ and $\mathcal{E}_i = \mathcal{E}_{s0}\epsilon_i$, $i = 1, 2, \ldots, K-1$, where ϵ_0 and ϵ_i are random variables that account for imperfections in the power control. Substitution into (6.123) yields the outage condition

$$G(Z^{-1}\epsilon_0 - \gamma_0^{-1}) < X \tag{6.124}$$

where $\gamma_0 = \mathcal{E}_{s0}/N_0$ is the energy-to-noise density ratio of the desired signal when the power control is perfect, and we define

$$X = \sum_{i=1}^{K-1} \epsilon_i . \tag{6.125}$$

By analogy with the lognormal spatial variation of the local-mean power, each of the $\{\epsilon_i\}$ is modeled as an independent lognormal random variable. Therefore,

$$\epsilon_i = 10^{\xi_i/10} = \exp(b\xi_i) , \quad i = 0, 1, 2, \ldots, K-1 \tag{6.126}$$

where each of the $\{\xi_i\}$ is a zero-mean Gaussian random variable with common variance σ_e^2. The moments of ϵ_i can be derived by direct integration or from the moment-generating function of ξ_i. We obtain

$$E[\epsilon_i] = \exp\left(\frac{b^2\sigma_e^2}{2}\right) , \quad E[\epsilon_i^2] = \exp(2b^2\sigma_e^2). \tag{6.127}$$

If K is a constant, then the mean $\bar{X}$ and the variance σ_x^2 of X in (6.125) are

$$\bar{X} = (K-1)\exp\left(\frac{b^2\sigma_e^2}{2}\right), \quad \sigma_x^2 = (K-1)\left[\exp(2b^2\sigma_e^2) - \exp(b^2\sigma_e^2)\right]. \tag{6.128}$$

The random variable X is the sum of $K-1$ lognormally distributed random variables. Since the distribution of X cannot be compactly expressed in closed form when $K > 3$, two approximate methods are adopted. The first method is based on the central limit theorem, and the second method is based on the assumption that σ_e is small. Since X is the sum of $K-1$ independent, identically distributed random variables, each with a finite mean and variance, the central limit theorem implies that the probability distribution function of X is approximately Gaussian when K is sufficiently large. Consequently, given the values of K and ϵ_0, the conditional probability of outage may be calculated from (6.124). Using (6.126) and integrating over the Gaussian density function of ξ_0, we then obtain the *conditional probability of outage* given the value of $K \gg 1$:

$$P_{\text{out}}(K) = \int_{-\infty}^{\infty} Q\left[\frac{G(Z^{-1}e^{b\xi} - \gamma_0^{-1}) - \bar{X}}{\sigma_x}\right] \frac{\exp(-\xi^2/2\sigma_e^2)}{\sqrt{2\pi}\sigma_e}\, d\xi. \tag{6.129}$$

As $\sigma_e \to 0$ and hence $\sigma_x \to 0$, $P_{\text{out}}(K)$ approaches a step function.

In the second approximate method, it is assumed that σ_e is sufficiently small and K is sufficiently large that $\sigma_x \ll \bar{X}$. From (6.128), it is observed that a sufficient condition for this assumption is that

$$\sqrt{K-1} \gg \exp\left(\frac{b^2\sigma_e^2}{2}\right). \tag{6.130}$$

The assumption implies that X is well approximated by the constant $\bar{X}$ given by (6.128). Since the only remaining random variable in (6.124) is $\epsilon_0 = \exp(b\xi_0)$, it follows that

$$P_{\text{out}}(K) = Q\left\{-\frac{ln[(K-1)G^{-1}Z\exp(b^2\sigma_e^2/2) + Z\gamma_0^{-1}]}{b\sigma_e}\right\}. \tag{6.131}$$

6.3.2.1 Variations in the Number of Active Mobiles

In the derivations of (6.129) and (6.131), the number of mobiles actively transmitting, K, is held constant. However, it is appropriate to model K as a random variable because of the movement of mobiles into and out of each sector and the changing of the cell or sector antenna with which a mobile communicates. Furthermore, a potentially active mobile may not be transmitting; for voice communications with voice-activity detection, energy transmission typically is necessary only roughly 40% of the time. As is shown below, a discrete random variable K with a Poisson distribution incorporates both of these effects.

To simplify the analysis, it is assumed that the average number of mobiles associated with each cell or sector antenna is the same and that the location of a mobile is uniformly distributed throughout a region comprising multiple cells. Let q denote the probability that a potentially transmitting mobile is actively transmitting, and let μ denote the average number of mobiles per sector. Thus, the average number of active mobiles in a sector is $E[K] = \mu q$. The probability that an active mobile is associated with a particular cell or sector antenna is $\mu q/N_r$, where N_r is the number of mobiles in the region. If the N_r mobiles are independently located in the region, then the probability of $K = k$ active mobiles being associated with a sector antenna is given by the binomial distribution

$$P(N_r, k) = \binom{N_r}{k}\left(\frac{\lambda}{N_r}\right)^k\left(1-\frac{\lambda}{N_r}\right)^{N_r-k} \tag{6.132}$$

where $\lambda = \mu q$ is assumed to be a constant. This equation can be expressed as

$$P(N_r, k) = \frac{(1-1/N_r)(1-2/N_r)\ldots(1-(k-1)/N_r)}{k!}\lambda^k\left(1-\frac{\lambda}{N_r}\right)^{-k}\left(1-\frac{\lambda}{N_r}\right)^{N_r}. \tag{6.133}$$

As $N_r \to \infty$, the initial fraction $\to 1/k!$, $(1-\lambda/N_r)^{-k} \to 1$, and $(1-\lambda/N_r)^{N_r} \to \exp(-\lambda)$. Therefore, $P(N_r, k)$ approaches

$$P_u(k) = \frac{\exp(-\lambda)\lambda^k}{k!}, \quad k = 0, 1, 2, \ldots \tag{6.134}$$

which is the *Poisson* distribution function.

Since the desired mobile is assumed to be present, it is necessary to calculate the conditional probability that $K = k$ given that $K \geq 1$. From the definition of a conditional probability and (6.134), it follows that this probability is

$$P_c(k) = \frac{\exp(-\lambda)\lambda^k}{[1 - \exp(-\lambda)]k!}, \; k = 1, 2, \ldots \tag{6.135}$$

and $P_c(0) = 0$. Using this equation, the probability of outage is

$$P_{\text{out}} = \sum_{k=1}^{\infty} \frac{\exp(-\lambda)\lambda^k}{[1 - \exp(-\lambda)]k!} P_{\text{out}}(k) \tag{6.136}$$

where $P_{\text{out}}(k)$ is given by (6.129) or (6.131).

The intercell interference from mobiles associated with other base stations introduces an additional average power equal to $g\mu q(\mathcal{E}_{s0}/T_s)$ into a given base station, where g is the intercell interference factor. Accordingly, the impact of the intercell interference is modeled as equivalent to an average of $g\mu$ additional mobiles in a sector [19]. When intercell interference is taken into account, the equations for a single cell or sector are modified. The parameter μ is replaced by $\mu(1 + g)$, and λ becomes the *equivalent number of mobiles defined as*

$$\lambda = \mu q(1 + g) = E[K](1 + g). \tag{6.137}$$

Figure 6.12 illustrates the probability of no outage, $1 - P_{\text{out}}$, as a function of λ for various values of σ_e. Both approximate models, which give (6.129) and (6.131), are used in (6.136) to calculate the graphs. Equations (6.129) and (6.131) indicate that the outage probability depends on the ratios G/Z and γ_0/G rather than on G, Z, and γ_0 separately. The parameter values for Fig. 6.15 are $G/Z = 40$ and $\gamma_0/G = 0.5$, which could correspond to $Z = 7$ dB, $G = 23$ dB, and $\gamma_0 = 20$ dB. The closeness of the results for the two models indicates that when $\sigma_e \leq 2$ dB both models give accurate outage probabilities. As an example of the application of the figure, suppose that the attenuation power law is $\beta = 4$, $\sigma_\eta = 8$ dB, $\sigma_e = 1.0$ dB, and $1 - P_{\text{out}} = 0.95$ is desired. Table 6.1 gives $g = 0.63$. The figure indicates that $\lambda = 23$ is needed. Thus, the average number of active mobiles per sector that can be accommodated is $E[K] = 14.1$. If $q = 0.4$ due to voice-activity detection, the average number of mobiles per sector that can be accommodated is $\mu = 35.3$.

6.3.3 Local-Mean Power Control

When the instantaneous signal power cannot be tracked because of the fast multipath fading, one might consider measuring the local-mean power, which is defined by (5.2) and is a long-term-average power obtained by averaging out the fading

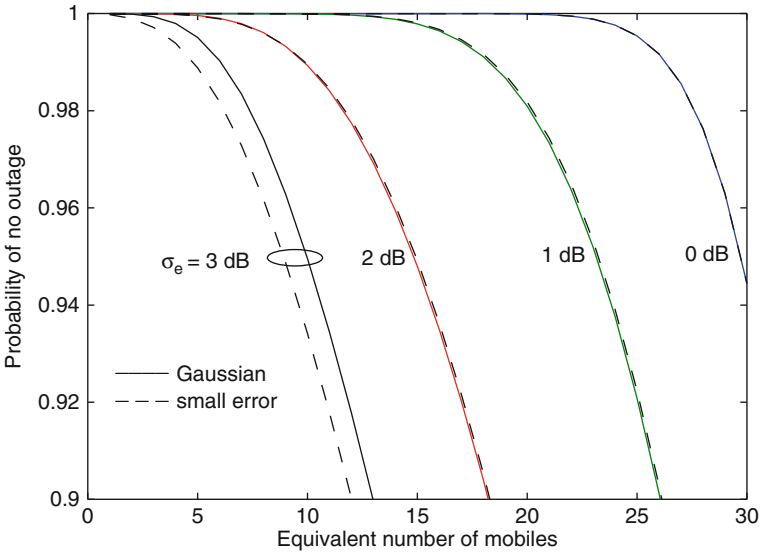

Fig. 6.12 Probability of no outage for instantaneous power control, $G/Z = 40$, $\gamma_0/G = 0.5$, and $\sigma_e = 0, 1, 2, 3$ dB

component. This measurement enables the system to implement *local-mean power control,* which ideally causes the received power to fluctuate only because of the fading. Two different analyses of the effects of local-mean power control are presented [11].

In the first analysis, which explores the potential effectiveness of local-mean power control, all received signals experience Rayleigh fading and the local-mean power control is perfect. Therefore, the received energy levels are proportional to the squares of Rayleigh-distributed random variables and, hence, are exponentially distributed, as shown in Appendix B.4. Thus, $\mathcal{E}_s = \mathcal{E}_{s0}\,\epsilon_0$ and $\mathcal{E}_i = \mathcal{E}_{s0}\,\epsilon_i$, where $\mathcal{E}_{s0}$ is the common local-mean energy per symbol and each ϵ_i, $i = 0, 1, 2, \ldots, K-1$, is an independent random variable with the exponential probability density function:

$$f_s(x) = \exp(-x)u(x) \tag{6.138}$$

and $\mathcal{E}_{s0}$ is the desired value of the average energy per symbol after averaging over the fading. The probability distribution function of the sum of $K-1$ independent random variables, each with the exponential density of (6.138), is given by (B.49) of Appendix B. Therefore, X in (6.125) has the distribution

$$F_X(x) = 1 - \exp(-x) \sum_{i=0}^{K-2} \frac{x^i}{i!}, \quad x \geq 0 \tag{6.139}$$

and

$$\bar{X} = (K-1), \quad \sigma_x^2 = (K-1). \tag{6.140}$$

Conditioning on the value of ϵ_0, using (6.139) to evaluate the probability of the outage condition (6.124), and then removing the conditioning by using (6.138) yields

$$P_{\text{out}}(K) = \int_0^\infty e^{-\xi} \exp[-c(\xi)] \sum_{i=0}^{K-2} \frac{[c(\xi)]^i}{i!}\, d\xi \tag{6.141}$$

where

$$c(\xi) = GZ^{-1}\xi - G\gamma_0^{-1}. \tag{6.142}$$

Replacing $[c(\xi)]^i$ by its binomial expansion, we obtain a double summation of integrals that can be evaluated using the gamma function defined by (B.12) of Appendix B. After simplification, we obtain

$$P_{\text{out}}(K) = \sum_{i=0}^{K-2} \sum_{l=0}^{i} \frac{\exp(G\gamma_0^{-1})(GZ^{-1})^l(-G\gamma_0^{-1})^{i-l}}{(i-l)!(1+GZ^{-1})^{l+1}}. \tag{6.143}$$

Interchanging the two sums and changing their limits accordingly, the inner sum is over a geometric series. Evaluating it, we obtain the final result:

$$P_{\text{out}}(K) = \exp(G\gamma_0^{-1}) \sum_{l=0}^{K-2} \frac{(-G\gamma_0^{-1})^l}{l!} \left[1 - \left(\frac{GZ^{-1}}{1+GZ^{-1}}\right)^{K-1-l}\right]. \tag{6.144}$$

The probability of outage is determined by substitution into (6.136). When $\gamma_0 = \infty$, only the $l = 0$ term in (6.144) is nonzero. Substitution into (6.136) and evaluation of the sum yields

$$P_{\text{out}} = 1 - \frac{\exp\left(\frac{\lambda}{1+G^{-1}Z}\right) - 1}{\exp(\lambda) - 1}(1 + G^{-1}Z), \quad \gamma_0 = \infty. \tag{6.145}$$

For perfect local-mean power control and Rayleigh fading, (6.140) indicates that a sufficient condition for $\sigma_x \ll \bar{X}$ is that $\sqrt{K-1} \gg 1$. If this condition is satisfied, then X is well approximated by $\bar{X} = K - 1$, which is equivalent to ignoring the fading of the multiple-access interference signals. With this approximation, the only remaining random variable in (6.124) is exponentially distributed, and hence the conditional probability of outage given K is

$$P_{\text{out}}(K) = 1 - \exp[-(K-1)G^{-1}Z - \gamma_0^{-1}Z]. \tag{6.146}$$

Substituting this equation into (6.136) and evaluating the sum, we obtain the approximation

$$P_{\text{out}} = 1 - \frac{\exp(-\gamma_0^{-1}Z + G^{-1}Z)[\exp(\lambda \exp(-G^{-1}Z)) - 1]}{\exp(\lambda) - 1}. \tag{6.147}$$

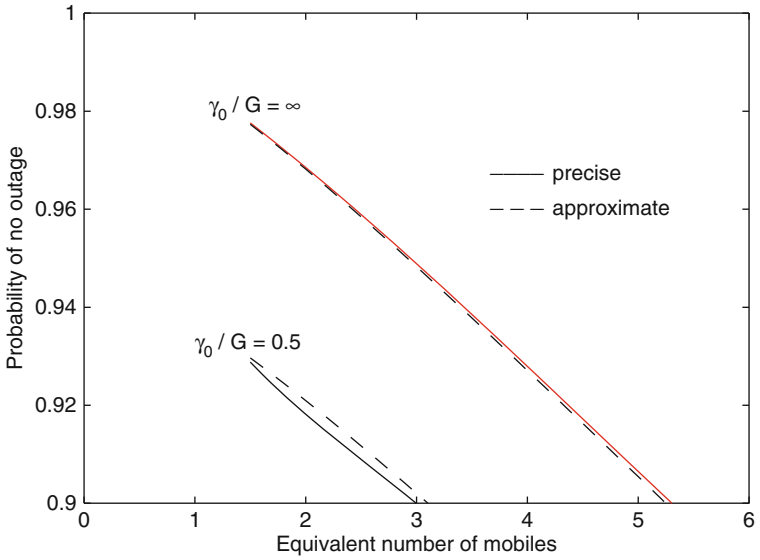

Fig. 6.13 Probability of no outage for perfect local-mean power control, $G/Z = 40$, and $\gamma_0/G = 0.5, \infty$

Figure 6.13 illustrates the probability of no outage as a function of the equivalent number of mobiles λ for $G/Z = 40$ and two values of γ_0/G using either the approximation (6.147) or the more precise (6.145), (6.144), and (6.136). It is observed that neglecting the fading of the interference signals and using the approximation makes little difference in the results. The effect of $\gamma_0 = \mathcal{E}_{s0}/N_0$ is considerable. A comparison of Figs. 6.13 and 6.12 indicates that when Rayleigh fading occurs, even perfect local-mean power control is not as useful as imperfect instantaneous power control unless σ_e is very large.

Since accurate power measurements require a certain amount of time, whether a power-control scheme is instantaneous, local mean, or something intermediate depends on the fading rate. To reduce the fading rate so that the power control is instantaneous and accurate, one might minimize the carrier frequency or limit the size of cells if these options are available.

The second analysis of the effects of local-mean power control uses the preceding results to develop a simple approximation to alternative performance calculations. This analysis has the advantages that the fading statistics do not have to be explicitly defined and the effect of imperfect local-mean power control is easily calculated. Let $\mathcal{E}_{sl}$ denote the local-mean energy per symbol, which is defined as the average energy per symbol after averaging over the fading. Similarly, let I_{tl} denote the total local-mean interference power in the receiver, and let $\mathcal{E}_{il}$ denote the local-mean energy per symbol due to interference signal i. The *local-mean SINR* is defined to be $\mathcal{E}_{sl}/(N_0 + I_{tl}T_c)$. For this analysis, a *local-mean outage* is said to occur if the local-mean SINR is less than a specified threshold Z_l, which may be adjusted to

account for the fading statistics and any diversity or rake combining. When the local-mean power control is imperfect, $\mathcal{E}_{sl} = \mathcal{E}_{s0}\epsilon_0$ and $\mathcal{E}_{il} = \mathcal{E}_{s0}\epsilon_i$, $i = 1, 2, \ldots, K-1$, where ϵ_0 and ϵ_i are lognormally distributed random variables with the common variance σ_{le}^2. A derivation similar to that leading to (6.131) indicates that if (6.130) is satisfied, then the *probability of a local-mean outage* is

$$P_{l\text{out}}(K) = Q\left\{-\frac{\ln[(K-1)G^{-1}Z_l \exp(b^2\sigma_{le}^2/2) + Z_l\gamma_0^{-1}]}{b\sigma_{le}}\right\} \tag{6.148}$$

and $P_{l\text{out}}$ is calculated by using (6.136) and (6.137). The intercell interference factor g can be determined by setting $\sigma_\eta = \sigma_s$ since the fading statistics do not affect the local-mean SINR. For adequate network performance in practical applications, $P_{l\text{out}}(K)$ must be much lower than $P_{\text{out}}(K)$ in (6.144) because the instantaneous SINR fluctuates rapidly relative to the local-mean SINR. Thus, the threshold Z_l must be set much higher than the threshold Z.

6.3.4 Bit-Error-Probability Analysis

Uplink capacity is the average number of mobiles per cell or sector that can be accommodated over the uplink at a specified information-bit error rate. Assuming a conventional correlation receiver and typical conditions for cellular communications, the subsequent results indicate that when imperfect power control causes the standard deviation of the received power from each mobile to increase beyond 2 dB, the uplink capacity rapidly collapses. When the instantaneous signal level cannot be tracked, one might consider measuring the local-mean power. Accurate local-mean power control eliminates the near-far problem and shadowing effects, but not the effects of the fading. In the subsequent analysis, it is confirmed that tracking the local-mean power is less useful than attempting to track the instantaneous signal level even if the latter results in large errors.

Consider a CDMA cell or sector with K active mobiles. The direct-sequence signals use QPSK modulation. Equation (6.98) indicates that the conditional symbol error probability given $\mathcal{E}_s$ and $\mathcal{E}_t = I_t T_s$ is approximately given by

$$P_s(\mathcal{E}_s, \mathcal{E}_t) = Q\left(\sqrt{\frac{2\mathcal{E}_s}{N_0 + \sqrt{h}G^{-1}\mathcal{E}_t}}\right). \tag{6.149}$$

It is assumed that the distribution of $\mathcal{E}_s$ and $\mathcal{E}_t$ and the values of $G = T_s/T_c$ and N_0 are such that (6.97), which is used in the derivation of (6.98), is satisfied with high probability in the subsequent analysis. We consider three models for power control: *perfect instantaneous power control (perfect ipc), imperfect instantaneous power control (imperfect ipc) with lognormally distributed errors, and perfect local-mean power control (perfect lmpc).*

If the power control is instantaneous and perfect, then $\mathcal{E}_i = \mathcal{E}_s = \mathcal{E}_{s0}$, $i = 1, 2, \ldots, K-1$, and $\mathcal{E}_t = (K-1)\mathcal{E}_{s0}$. Equation (6.149) implies that the conditional symbol error probability given K is

$$P_s(K) = Q\left(\sqrt{\frac{2}{\gamma_0^{-1} + \sqrt{h}G^{-1}(K-1)}}\right) \quad \text{(perfect ipc)} \tag{6.150}$$

where $\gamma_0 = \mathcal{E}_{s0}/N_0$ is the energy-to-noise-density ratio when the power control is perfect. If the power control is imperfect with lognormally distributed errors, then

$$\mathcal{E}_s = \mathcal{E}_{s0}\epsilon_0, \ \mathcal{E}_t = \mathcal{E}_{s0}X \tag{6.151}$$

and (6.125) to (6.128) are applicable. If (6.130) is satisfied, then $\bar{X} \gg \sigma_x$, and X is well-approximated by $\bar{X}$. Since $\epsilon_0 = \exp(b\xi_0)$ and ξ_0 has a Gaussian density, (6.149) and an integration over this density yield

$$P_s(K) = \int_{-\infty}^{\infty} \frac{\exp(-x^2/2\sigma_e^2)}{\sqrt{2\pi}\sigma_e} Q\left(\sqrt{\frac{2\exp(bx)}{\gamma_0^{-1} + \sqrt{h}G^{-1}(K-1)\exp(b^2\sigma_e^2/2)}}\right) dx$$

(imperfect ipc). (6.152)

Suppose that instead of the instantaneous signal power, the local-mean power averaged over the fast fading is tracked. If this tracking provides perfect power control of the local-mean power at a specific level, then a received signal still exhibits fast fading relative to this level. If the fast fading has a Rayleigh distribution but the fading level is constant over a symbol interval, then the energy per symbol is $\mathcal{E}_s = \mathcal{E}_{s0}\epsilon_0$, where ϵ_0 has the exponential probability density function given by (6.138). Therefore, (6.149) implies that the conditional symbol error probability given $\mathcal{E}_t$ is

$$\begin{aligned} P_s(\mathcal{E}_t) &= \int_0^{\infty} \exp(-x) Q\left(\sqrt{\frac{2x}{\gamma_0^{-1} + \sqrt{h}G^{-1}\mathcal{E}_t/\mathcal{E}_{s0}}}\right) dx \\ &= \frac{1}{2} - \frac{1}{2}\left(1 + \gamma_0^{-1} + \sqrt{h}G^{-1}\mathcal{E}_t/\mathcal{E}_{s0}\right)^{-1/2} \end{aligned} \tag{6.153}$$

where the integral is evaluated in the same way as (5.125). The total interference energy $\mathcal{E}_t$ is given by (6.151) and (6.125), where each ϵ_i is an independent, exponentially distributed random variable with mean equal to unity. Therefore, $\mathcal{E}_t/\mathcal{E}_{s0}$ has a gamma probability density function given by (B.49) of Appendix B with $N = K-1$, and for $K \geq 2$ the conditional symbol error probability given K is

$$P_s(K) = \frac{1}{2} - \frac{1}{2}\int_0^{\infty} \frac{x^{K-2}\exp(-x)}{(K-2)!\left(1 + \gamma_0^{-1} + \sqrt{h}G^{-1}x\right)^{1/2}} dx \quad \text{(perfect lmpc).} \tag{6.154}$$

Perfect symbol interleaving is defined as interleaving that causes independent symbol errors in a codeword. When the fading rate is sufficiently high, the error in the instantaneous power control approximates an independent random variable for each symbol of a codeword, and the symbol interleaving becomes nearly perfect. Assuming that fast fading enables perfect symbol interleaving, the information-bit error probability $P_b(K)$ can be calculated by substituting (6.150), (6.152), or (6.154) into the equations of Sect. 1.1. If r is the code rate of a binary code and E_b is the energy per bit that is available when the channel symbols are uncoded, then $\gamma_0 = rE_b/N_0$.

The impact of the intercell interference is modeled by assuming that K is constant during a codeword and using the equivalent number of mobiles λ given by (6.137), where g is obtained from Table 6.1. Averaging over K by using (6.135) to account for the change in $P_b(K)$ from one codeword to the next one, we obtain the information-bit error probability

$$P_b = \sum_{k=1}^{\infty} \frac{\exp(-\lambda)\lambda^k}{[1-\exp(-\lambda)]k!} P_b(k). \tag{6.155}$$

As an example of $P_b(k)$, assume a loosely packed, binary block code and hard-decision decoding with a bounded-distance decoder. Then $P_b(k)$ is approximated by (1.30), and the information-bit error probability is

$$P_b \approx \sum_{k=1}^{\infty} \frac{\exp(-\lambda)\lambda^k}{[1-\exp(-\lambda)]k!} \sum_{i=t+1}^{n} \binom{n-1}{i-1} P_s^i(k)(1-P_s(k))^{n-i} \tag{6.156}$$

where n is the code length, and t is the number of symbol errors that the decoder can correct.

Suppose that the fading is slow enough that the interleaving is ineffective and, hence, the error in the instantaneous power control is fixed over a codeword duration. Since K is constant during a codeword but varies from one codeword to the next one, the information-bit error probability is

$$P_b = \sum_{k=1}^{\infty} \frac{\exp(-\lambda)\lambda^k}{[1-\exp(-\lambda)]k!} \int_{-\infty}^{\infty} \frac{\exp(-x^2/2\sigma_e^2)}{\sqrt{2\pi}\sigma_e} P_b(P_s(k,x))\, dx \tag{6.157}$$

where $P_b(P_s(K,x))$ is the probability of a bit error given $P_s(K,x)$, which is the channel-symbol error probability given K and that $X = x$: An approximation similar to that preceding (6.152) implies that

$$P_s(K,x) = Q\left(\sqrt{\frac{2\exp(bx)}{\gamma_0^{-1} + \sqrt{h}G^{-1}(K-1)\exp(b^2\sigma_e^2/2)}}\right). \tag{6.158}$$

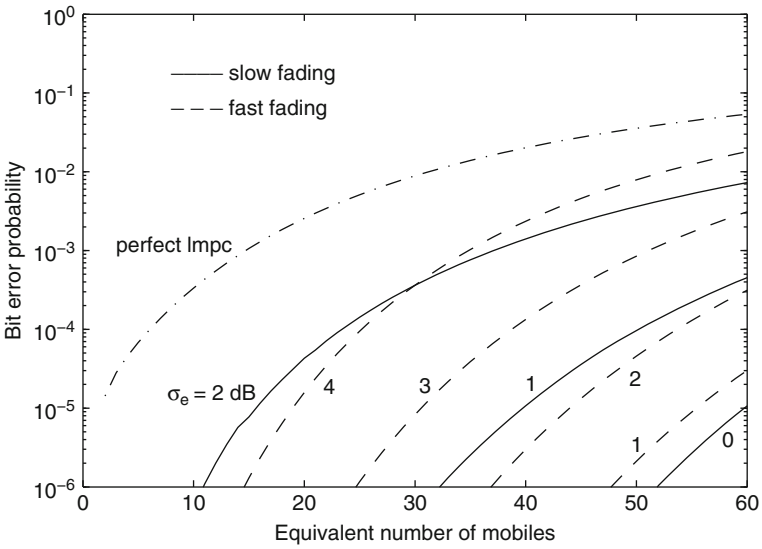

Fig. 6.14 Information-bit error probability for instantaneous power control and perfect local-mean power control, $\gamma_0 = 13\,\text{dB}$, G = 128, and the BCH (63,30) code with various values of σ_e in decibels

As an example of $P_b(P_s(K,x))$, assume a loosely packed, binary block code and hard-decision decoding with a bounded-distance decoder. Then (1.30) implies that the information-bit error probability is

$$P_b(P_s(K,x)) \approx \sum_{i=t+1}^{n} \binom{n-1}{i-1} P_s^i(K,x)(1-P_s(K,x))^{n-i} \tag{6.159}$$

where n is the code length, and t is the number of symbol errors that the decoder can correct.

Graphs of the information-bit error probability versus λ for instantaneous power control, $\gamma_0 = 13\,\text{dB}$, $G = 128$, a rectangular chip waveform with $h = 2/3$, and various values of σ_e, which is a measure of power-control accuracy, are illustrated in Fig. 6.14. The block code is the binary (63,30) BCH code, for which $d_m = 21$ and $t = 10$. Equations (6.157), (6.158), and (6.159) are used for slow fading, for which the power control is likely to be accurate. Equations (6.150), (6.152), and (6.156) are used for fast fading, for which the power control is likely to be inaccurate. When the fading is slow and the interleaving is ineffective, the coding is, as expected, less effective than when the fading is fast and the interleaving is perfect, provided that σ_e remains the same. However, σ_e increases with the fading rate, as shown subsequently. The figure indicates that as σ_e increases, there is a rapid uplink capacity loss for slow fading and a slower one for fast fading. The results for other block codes are qualitatively similar.

The use of spatial diversity or, in the presence of frequency-selective fading, a rake demodulator will improve the performance of a DS/CDMA system during both slow and fast fading, but the improvement is much greater when the fading is slow. As the fading rate increases, the accuracy of the estimation of the channel parameters used in the rake or diversity combiner becomes more difficult. When the channel-parameter estimation errors are too large to be accommodated, coherent MRC must be replaced by suboptimal noncoherent EGC, which does not require the estimation of channel parameters.

In Fig. 6.14, the information-bit error probability is depicted for perfect local-mean power control with the same parameter values and coding as for instantaneous power control. It is assumed that fast fading permits perfect interleaving so that (6.154) and (6.156) are applicable. The figure confirms that tracking of the local-mean power level is an inferior strategy for obtaining a large capacity compared with tracking of the instantaneous power level unless the inaccuracy of the latter is substantial. Another problem with local-mean power control is that it requires time that may be unavailable for sporadic data.

Suppose that the required information-bit error probability is 10^{-5}. There is instantaneous power control with fast fading and $\sigma_e = 2\,\text{dB}$. The figure indicates that $\lambda = 39$ is needed. If $\sigma_\eta = 8\,\text{dB}$, Table 6.1 gives $g = 0.63$, and the uplink capacity is $E[K] = 23.9$. If $q = 0.4$ due to voice-activity detection, the average number of mobiles per sector that can be accommodated is $\mu = 59.8$.

Apart from power control, instantaneous power measurements can be used to facilitate adaptive coding or adaptive transmit diversity. Both of these techniques require timely information about the impact of the fading, and this information is inherent in the instantaneous power measurements.

6.3.5 *Impact of Doppler Spread on Power-Control Accuracy*

When the received instantaneous power of the desired signal from a mobile is tracked, there are four principal error components. They are the quantization error due to the stepping of the transmitted power level, the error introduced in the decoding of the power-control information at the mobile, the error in the power measurement at the base station, and the error caused by the processing and propagation delay. Let $\sigma_q, \sigma_d, \sigma_m$, and σ_p denote the standard deviations of these errors, respectively, expressed in decibels relative to the received power measured in decibels. Usually, σ_m and σ_p are much larger than σ_q and σ_d, and $\sigma_m > 1.5\,\text{dB}$ [15]. The processing and propagation delay is a source of error because the multipath propagation conditions change during the execution of the closed-loop power-control algorithm.

Assuming that the error sources are independent, the variance of the power-control error can be decomposed as

$$\sigma_e^2 = \sigma_m^2 + \sigma_p^2 + \sigma_q^2 + \sigma_d^2. \tag{6.160}$$

If σ_e is to be less than 2 dB and $\sigma_m > 1.5$ dB, then even if σ_q and σ_d are small, $\sigma_p < 1.3$ dB is required. Let v denote the maximum speed of a mobile in the network, f_c the carrier frequency of its direct-sequence transmitted signal, and c the speed of an electromagnetic wave. It is assumed that this signal has a bandwidth that is only a few percent of f_c so that the effect of the bandwidth is negligible. The maximum Doppler shift or Doppler spread is

$$f_d = f_c v/c \tag{6.161}$$

which is proportional to the fading rate. To obtain $\sigma_p < 1.3$ dB requires nearly constant values of the channel attenuation during the processing and propagation delay. Thus, this delay must be much less than the coherence time, which is approximately equal to $1/f_d$ (Sect. 5.2). Examination of attenuation graphs for representative multipath scenarios indicates that this delay must be less than α/f_d, where $\alpha \approx 0.1$ or less if $\sigma_p < 1.3$ dB is to be attained. The propagation delay for closed-loop power control is $2d/c$, where d is the distance between the mobile and the base station. Therefore, the processing delay T_p must satisfy

$$T_p < \frac{\alpha}{f_d} - \frac{2d}{c}. \tag{6.162}$$

Since T_p must be positive, this inequality and (6.161) imply that $\sigma_p < 1.3$ dB is only possible if $f_c < \alpha c^2/2dv$. Thus, if the carrier frequency or maximum vehicle speed is too high, then the propagation delay alone makes it impossible for the system to attain the required σ_p throughout the network. If $v = 25\,\mathrm{m\,s^{-1}}$, $d = 10$ km, $\alpha = 0.1$, and $f_c = 850$ MHz, then (6.162) and (6.161) give $T_p < 1.34$ ms. The IS-95 system, which must accommodate similar parameter values, uses $T_p = 1.25$ ms.

Let p_m denote the measured power level of a received signal in decibels; thus, p_m is an estimate of $10 \log_{10} p_0$, where p_0 is the average received signal power from a mobile. Let σ_{m1}^2 denote the variance of an estimate of $\ln p_0$, the natural logarithm of p_0. It follows that the variance of p_m is

$$\sigma_m^2 = (10 \log_{10} e)^2 \sigma_{m1}^2. \tag{6.163}$$

It is assumed that power variations in a received signal at the base station are negligible during the measurement interval T_m, which is a large component of the processing delay T_p. Errors in the power measurement occur because of the presence of multiple-access interference and white Gaussian noise. A lower bound on σ_{m1}^2 can be determined by assuming that the power control is effective enough that the received powers from the mobiles in the cell or sector are approximately equal. The multiple-access interference is modeled as a Gaussian process that increases the noise-power spectral density from $N_0/2$ to $N_t/2$ with

$$N_t = N_0 + \frac{p_0}{B}(K-1)(1+g) \tag{6.164}$$

where p_0 is the common signal power of each mobile at the base station, K is the fixed number of active users in the cell or sector, and B is the bandwidth of the receiver.

The received signal from a mobile that is to be power-controlled has the form $\sqrt{p_0}s(t)$, where $s(t)$ has unity power. Thus,

$$\int_0^{T_m} s^2(t)dt = T_m. \tag{6.165}$$

The received signal can be expressed as

$$\sqrt{p_0}s(t) = \exp\left(\frac{y}{2}\right)s(t) \tag{6.166}$$

where $y = \ln p_0$. The Cramer-Rao bound [16] provides a lower bound on the variance of any unbiased estimate or measurement of $\ln p_0$. This bound and (6.166) give

$$\sigma_{m1}^2 \geq \left\{\frac{2}{N_t}\int_0^{T_m}\left[\frac{\partial}{\partial y}e^{y/2}s(t)\right]^2 dt\right\}^{-1}. \tag{6.167}$$

Evaluating (6.167) and using (6.165) and (6.166), we obtain

$$\sigma_m^2 \geq \frac{200(\log_{10} e)^2}{T_m}\left[\frac{N_0}{p_0} + \frac{(K-1)(1+g)}{B}\right]. \tag{6.168}$$

Let $T_1 = T_p - T_m$ denote the part of the processing delay in excess of the measurement interval. Substituting (6.160) and (6.162) into (6.168), we obtain

$$\sigma_e^2 > 200(\log_{10} e)^2\left(\frac{\alpha}{f_d} - \frac{2d}{c} - T_1\right)^{-1}\left[\frac{N_0}{p_0} + \frac{(K-1)(1+g)}{B}\right] + \sigma_p^2 + \sigma_q^2 + \sigma_d^2. \tag{6.169}$$

This lower bound indicates that σ_e^2 increases with f_d and, hence, the fading rate when the power estimation is ideal.

Inequality (6.169) indicates that an increase in the Doppler spread f_d, which could result from an increase in the carrier frequency, can be offset by an increase in the bandwidth B. The physical reason is that an expansion of the bandwidth of the direct-sequence signals allows enough interference suppression to more than compensate for the increased Doppler spread.

Consider a network of CDMA systems that do not expand the bandwidth when the Doppler spread changes, but adjust T_p so that (6.162) provides a tight bound. Ideal power estimation is assumed so that the lower bound in (6.169) approximates σ_e^2. If the other parameters are unchanged as the Doppler spread changes from f_{d1} to f_{d2}, then σ_e^2 is only affected by the *Doppler factor* defined as

$$D = \frac{f_{d2}}{f_{d1}}. \tag{6.170}$$

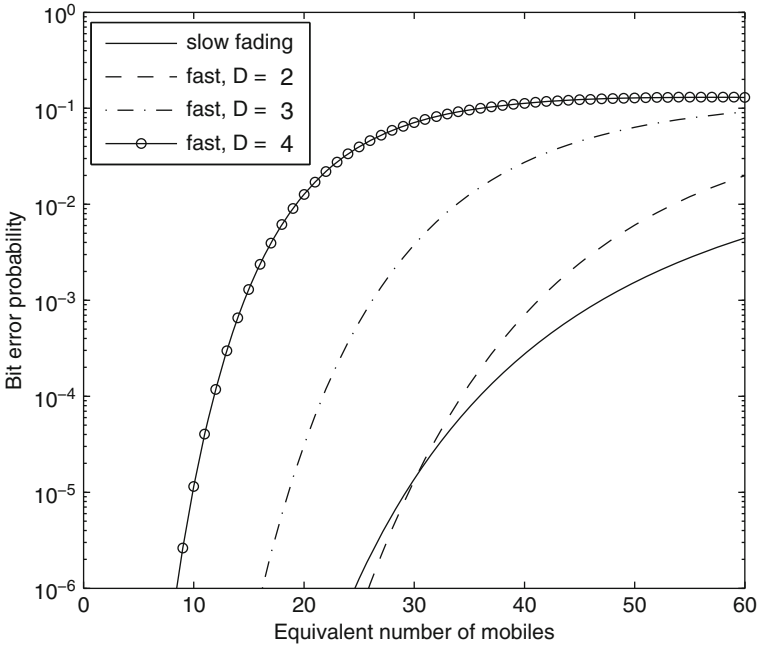

Fig. 6.15 Information-bit error probability for slow fading and fast fading with different Doppler factors D. Instantaneous power control and the BCH (63,30) code are used

An example of the impact of the Doppler factor is illustrated in Fig. 6.15, which shows the upper bounds on the bit error probability for instantaneous power control and the (63,30) BCH code. The network experiences slow fading and a Doppler spread $f_{d1} = 100\,\text{Hz}$ when the Doppler factor is $D = 1$. When the Doppler factor is $D = 2$, 3, or 4, perhaps because of increased vehicular speeds, the network is assumed to experience fast fading. The parameter values are $\alpha = 0.1$, $d = 10\,\text{km}$, $T_1 = 100\ \mu\text{s}$, $B = 1/T_c = 1.25\,\text{MHz}$, $N_0/p_0 = 5\,\mu\text{s}$, $\sigma_p^2 + \sigma_q^2 + \sigma_d^2 = 0.5\ (\text{dB})^2$, $h = 2/3$, $G = 128$, and $\gamma_0 = p_0 T_s/N_0 = (p_0/N_0)(G/B) = 20 = 13\,\text{dB}$. The calculations use (6.157), (6.158), and (6.159) for slow fading, and (6.150), (6.152), and (6.156) for fast fading. In this example, $D \geq 2.5$ causes a significant performance degradation despite the improved time diversity during the fast fading.

When fast fading causes large power-control errors, a DS/CDMA network exhibits a significant performance degradation, notwithstanding the exploitation of time diversity by interleaving and channel coding. Adopting long-term-average instead of instantaneous power control will not cure the problem. A better approach is to increase the bandwidth of the direct-sequence signals. If the bandwidth cannot be increased enough, then the Doppler spread might be reduced by minimizing the carrier frequency of the direct-sequence signals. Another strategy is to limit the size of cells so that the network must cope with the more benign Ricean fading rather than Rayleigh fading, which is more likely to cause large power-control errors.

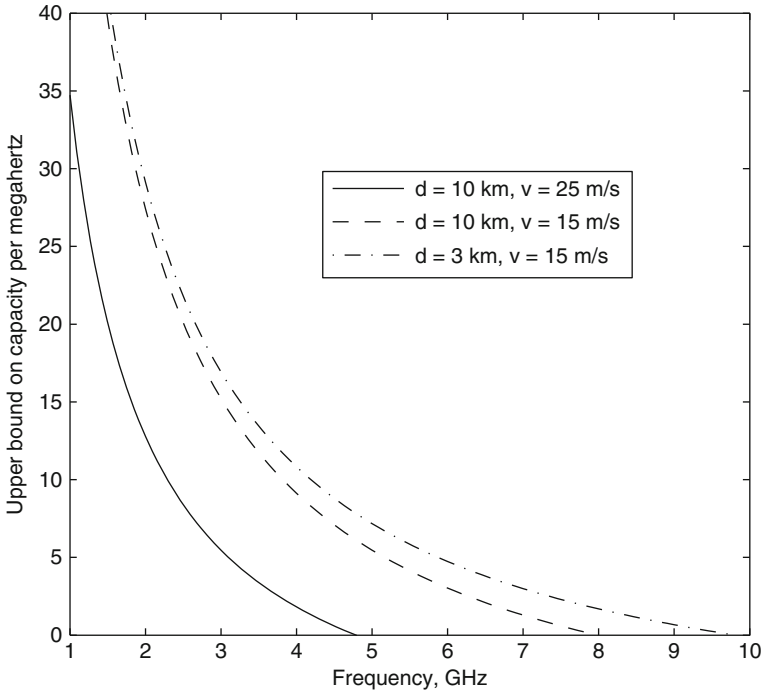

Fig. 6.16 Upper bound on number of active users per megahertz for $\sigma_e < 2\,\text{dB}$, $\alpha = 0.1$, $\sigma_m = 1.5\,\text{dB}$, g = 0.634, $\text{N}_0/p_0 = 5\,\mu\text{s}$, and $\text{T}_1 = 100\,\mu\text{s}$

It follows from (6.168) and $T_p = T_m + T_1$ that a specified σ_m can be attained if

$$T_p \geq \frac{200(\log_{10} e)^2}{\sigma_m^2}\left[\left(\frac{N_0}{p_0}\right) + K_1(1+g)\right] + T_1 \tag{6.171}$$

where $K_1 = (K-1)/B$ is the number of interfering active mobiles per unit bandwidth in the cell or sector. Inequalities (6.171) and (6.162) restrict the range of feasible values for T_p. Combining (6.161), (6.162), and (6.171) and assuming that K is large enough that $K_1 \approx K/B$, we conclude that to attain $\sigma_e < 2\,\text{dB}$ for vehicles at speed v or less, an approximate upper bound on the uplink capacity per unit bandwidth in a cell or sector is given by

$$K_1 < (1+g)^{-1}\left[\frac{\sigma_m^2}{200(\log_{10} e)^2}\left(\frac{\alpha c}{v f_c} - \frac{2d}{c} - T_1\right) - \left(\frac{N_0}{p_0}\right)\right]. \tag{6.172}$$

For typical parameter values, this upper bound is approximately inversely proportional to both the carrier frequency f_c and the maximum vehicle speed v.

Figure 6.16 illustrates the upper bound on the uplink capacity per megahertz as a function of frequency f_c for $\alpha = 0.1$, $\sigma_m = 1.5\,\text{dB}$, $\sigma_\eta = 8\,\text{dB}$, $N_0/p_0 = 5\,\mu\text{s}$,

$T_1 = 100\,\mu$s, and representative values of d and v. Table 6.1 gives $g = 0.634$. The figure indicates the limitations on K_1 due to power control as the carrier frequency increases if σ_m and the other parameters remain fixed. If K_1 exceeds the upper bound, then the network performance will be severely degraded. The uplink capacity $K_1 B$ can be maintained by expanding the bandwidth.

6.3.6 Downlink Power Control and Outage

Along with all the signals transmitted to mobiles associated with it, a base station transmits a pilot signal over the downlinks. A mobile, which is usually associated with the base station from which it receives the largest pilot signal, uses the pilot to identify a base station or sector, to initiate uplink power control, to estimate the attenuation, phase shift, and delay of each significant multipath component, and to assess the power-allocation requirement of the mobile.

A base station synchronously combines and transmits the pilot and all the signals destined for mobiles associated with it. Consequently, all the signals fade together, and the use of orthogonal spreading sequences will prevent intracell interference and, hence, a near-far problem on a downlink, although there will be interference caused by asynchronously arriving multipath components. The orthogonal sequences can be generated from the rows of a Hadamard matrix. The orthogonality, the energy-saving sharing of the same pilot at all covered mobiles, and the coherent demodulation of all transmitted signals are major advantages of the downlinks. However, interference signals from other base stations arrive at a mobile asynchronously and fade independently, thereby significantly degrading performance.

Although there is no near-far problem on the downlinks, power control is still desirable to enhance the received power during severe fading or when a mobile is near a cell edge. However, this power enhancement increases intercell interference. Downlink power control entails power allocation by the base station in a manner that meets the requirements of the individual mobiles associated with it. Let C_{in} denote the total power received by mobile i from base station n. If this mobile is associated with base station 0, then (6.100) indicates that the SINR at the mobile is

$$\text{SINR} = \frac{\Delta\,\phi_i\,C_{i0}\,T_s}{N_0 + h\sum_{n=1}^{N_B-1} C_{in}\,T_c} \tag{6.173}$$

where N_B is the total number of base stations that produce significant power at mobiles in a cell or sector, Δ is the fraction of the base-station power that is assigned to mobiles rather than to the pilot, and ϕ_i is the fraction of the total power for mobiles in a cell or sector that is allocated to mobile i. Typically, one might set $\Delta = 0.8$, which entails a 1 dB loss due to the pilot. Let R denote the SINR required

by network mobiles for acceptable performance. Inverting (6.173), it is found that R is achieved by all mobiles in a cell or sector if

$$\phi_i \geq \frac{R}{\Delta\, C_{i0}\, G}\left(\frac{N_0}{T_c} + h\sum_{n=1}^{N_B-1} C_{in}\right), \quad i = 1, 2, \ldots, K. \tag{6.174}$$

An outage occurs if the demands of all K mobiles in a cell or sector cannot be met simultaneously. Thus, no outage occurs if (6.174) is satisfied and

$$\sum_{i=1}^{K} \chi_i\, \phi_i \leq 1 \tag{6.175}$$

where χ_i is the voice-activity indicator such that $\chi_i = 1$ with probability q and $\chi_i = 0$ with probability $1-q$. If the left-hand side of (6.175) is strictly less than unity, then the transmitted power produced by base station 0 can be safely lowered to reduce the interference in other cells or sectors. Combining (6.174) and (6.175), a necessary condition for no outage is

$$\sum_{i=1}^{K} \frac{\chi_i}{C_{i0}}\left(\frac{N_0}{T_c} + h\sum_{n=1}^{N_B-1} C_{in}\right) \leq \frac{\Delta\, G}{R}. \tag{6.176}$$

The assignment of mobile i to base station 0 implies the constraint that $C_{in} \leq C_{i0}$, $n = 1, 2, \ldots, N_B - 1$. A complete performance analysis with this constraint is difficult. Simulation results [17] indicate that the downlink capacity potentially exceeds the uplink capacity if the orthogonal signaling is not undermined by excessive multipath.

6.4 Frequency-Hopping Multiple Access

Two major advantages of frequency hopping are that it can be implemented over a much larger frequency band than it is possible to implement direct-sequence spreading, and that the band can be divided into noncontiguous segments. Another major advantage is that frequency hopping provides resistance to multiple-access interference, while not requiring power control to prevent the near-far problem. Since direct-sequence systems cannot escape the near-far problem by hopping, accurate power control is crucial but becomes much less effective as the fading rate increases. These advantages of frequency hopping are decisive in many applications. For example, the Bluetooth system and combat net radios use frequency hopping to avoid the near-far problem. Frequency hopping may be added to almost any communication system to strengthen it against interference or fading. Thus, frequency hopping may be applied to the set of carriers used in a multicarrier DS/CDMA system or the subcarriers of an OFDM system.

Frequency-hopping systems are usually part of a *frequency-hopping code-division multiple-access* (FH/CDMA) network in which all systems share the same M frequency channels. In a *synchronous* FH/CDMA network, the systems coordinate their frequency transitions and hopping patterns. Consequently, by choosing frequency-hopping patterns that are circularly rotated versions of each other, as many as M frequency-hopping signals can be simultaneously accommodated by the network with insignificant multiple-access interference at any of the active receivers. Network coordination is much simpler to implement than for a DS/CDMA network because the timing alignments must be within a small fraction of a hop duration instead of a small fraction of a spreading-sequence chip. Multipath signals and errors in range estimates can be accommodated at some cost in the energy per information bit by increasing the switching time between frequency-hopping pulses. However, some type of centralized or cellular architecture is required, and such an architecture is often unavailable.

6.4.1 Asynchronous FH/CDMA Networks

An *asynchronous* FH/CDMA network has systems that transmit and receive frequency-hopping signals autonomously and asynchronously. When two or more frequency-hopping signals using the same frequency channel are received simultaneously, they are said to *collide*. To maximize the throughput of the asynchronous FH/CDMA network, we have to minimize the number of collisions. The primary method of minimization is to assume that all frequency transitions coincide and then optimize the choice of the set of frequency-hopping patterns or sequences that are used by the network systems. The main criterion is the minimization of cross-correlations among the patterns because this criterion is mathematically tractable. However, in actual network operation, it is the partial cross-correlations that have the most impact on throughput.

Consider the hopset of M frequencies: $F = \{f_1, f_2, \ldots, f_M\}$. Let P denote the set of all patterns of period or length n over F. For two periodic frequency-hopping patterns $X = \{x_i\}, Y = \{y_i\} \in P$, their *Hamming correlation* is defined as

$$H_{X,Y}(k) = \sum_{i=1}^{n-1} h[x_i y_{i+k}], \quad 0 \le k < n \tag{6.177}$$

where position indices are computed modulo-n and $h[x_i y_{i+k}] = 1$ if $x_i = y_{i+k}$, and 0 otherwise. The Hamming correlation of $X = \{x_i\}$ is $H_{X,X}(k)$. The Hamming correlation $H_{X,Y}(k)$ is a measure of the number of collisions between two patterns, and it is desirable to use a set of long frequency-hopping patterns with good Hamming correlations.

Let P_N denote a subset of P containing N patterns. The maximum nontrivial Hamming correlation of the sequence set is defined as

$$\mathcal{M}(P_N) = \max\left\{\max_{X\in P_N} H(X), \max_{X,Y\in P_N, X\neq Y} H(X,Y)\right\} \tag{6.178}$$

where

$$H(X) = \max_{0\le k<n} H_{X,X}(k) \tag{6.179}$$

$$H(X,Y) = \max_{0\le k<n} H_{X,Y}(k). \tag{6.180}$$

The minimization of $\mathcal{M}(P_N)$ tends to minimize both collisions among network signals and undesirable peaks in the autocorrelation of a pattern that might hinder frequency-hopping synchronization in a receiver. Lower bounds on $\mathcal{M}(P_N)$ have been derived [18, 19]:

$$\mathcal{M}(P_N) \ge \left\lceil \frac{(nN-M)n}{(nN-1)M} \right\rceil \tag{6.181}$$

$$\mathcal{M}(P_N) \ge \left\lceil \frac{2InN-(I+1)IM}{(nN-1)N} \right\rceil \tag{6.182}$$

where $I = \lfloor nN/M \rfloor$. A subset of patterns P_N is considered *optimal* if $\mathcal{M}(P_N)$ is equal to one of these two lower bounds, which are equal when nN/M is an integer. Only a few optimal sets of patterns are known. To ensure that all frequencies in the hopset are used, it is necessary that $n \ge M$.

As an example, consider the selection of frequency-hopping patterns when $N = M = 4$ and $n = 7$, which imply that $\mathcal{M}(P_4) \ge 2$. The hopset is $F = \{f_1, f_2, f_3, f_4\}$, and the set of patterns is $P_4 = \{X_1, X_2, X_3, X_4\}$. An optimal set of patterns for which $\mathcal{M}(P_4) = 2$ is

$$\begin{aligned} X_1 &= f_1, f_2, f_3, f_2, f_4, f_4, f_3 \quad & X_2 &= f_2, f_1, f_4, f_1, f_3, f_3, f_4 \\ X_3 &= f_3, f_4, f_1, f_4, f_2, f_2, f_1 \quad & X_4 &= f_4, f_3, f_2, f_3, f_1, f_1, f_2. \end{aligned} \tag{6.183}$$

Since $\mathcal{M}(P_N)$ is a measure of the maximum number of collisions between two patterns during n hops, the *maximum collision rate* for optimal patterns is $C(n,M) = \mathcal{M}(P_N)/n$. Equation (6.181) indicates that $C(n,M) < 1/M$ if $M > 1$. To protect against pattern reproduction by an opponent (Sect. 3.1), a large linear span (Sect. 3.1) of the sequence generating the pattern is required, which implies that $n \gg M$. Both lower bounds imply that $C(n,M) \cong 1/M$ if $n \gg M/N$. Thus, the maximum collision rate when optimal patterns are used is approximately equal to $1/M$ per hop, which equals the probability of a collision when random frequency-hopping patterns are used. A straightforward calculation of the variance of $H_{X,Y}(k)/n$ for independent, random frequency-hopping patterns proves that the standard deviation is $\sqrt{1/M}$. This result indicates that the collision

rate for n hops of random patterns seldom differs much from $1/M$, the probability of a collision between two patterns, if $M \gg 1$. Since the collision rate for random patterns is nearly the same as $C(n, M)$, the use of random frequency-hopping patterns in an asynchronous network is a viable option that is almost as effective as the use of optimal patterns. An advantage of random patterns is that planning and network coordination, which are necessary when optimal patterns are used, are not required. Even if optimal patterns are used, modeling the patterns as random is a good approximation, and this model is used in the subsequent analyses.

Since the probability of a collision in an asynchronous network can be decreased by increasing the number of frequency channels in the hopset, it is highly desirable to choose a data modulation that has a compact spectrum and produces little spectral splatter. Good candidates are FH/CPFSK systems. The CPFSK may be binary, such as MSK, or nonbinary with alphabet size $q = 4$ or $q = 8$. In Chap. 8, the nonbinary modulations are shown to be important parts of robust frequency-hopping systems.

Let d represent the *duty factor*, which is defined as the probability that an interferer using the same frequency channel will degrade the reception of a symbol. The duty factor is the product

$$d = q_1 q_2 \tag{6.184}$$

where q_1 is the probability that an interferer is transmitting, and q_2 is the probability that a significant portion of the interferer's transmitted waveform occurs during the symbol interval. The probability q_2 is upper bounded and well approximated by the probability that there is any overlap in time of the interference and the symbol interval. For synchronous frequency hopping, $q_2 = 1$. Since the switching time $T_{sw} > T_s$, it follows from elementary probability that for asynchronous frequency hopping, $q_2 \approx (T_d + T_s)/T_h$, where T_d is the dwell time, and T_h is the hop duration. For voice communications with voice-activity detection, $q_1 = 0.4$ is a typical value.

For asynchronous frequency hopping, the fact that $T_{sw} > T_s$ ensures that each potentially interfering frequency-hopping signal transmits power in at most one frequency channel during the reception of one symbol of a desired signal. Therefore, assuming that an interferer may transmit in any frequency channel with equal probability, the probability that a potentially interfering signal collides with the desired signal during a symbol interval is

$$P_t = \frac{d}{M}. \tag{6.185}$$

When a collision occurs, the symbol is said to be *hit* by the interfering signal.

6.4.2 Ad Hoc and Cellular Mobile Networks

FH/CDMA systems [20] are suitable for both ad hoc and cellular mobile communication networks. An *ad hoc network* or *peer-to-peer network* comprises autonomous systems that communicate without a centralized control or assistance. Ad hoc

networks include mobile communication networks that possess no supporting infrastructure, fixed or mobile; usually each user has identical signal processing capability. Ad hoc networks have both commercial applications and important military applications, the latter primarily because of their robustness in the presence of node losses. Power control and, hence, DS/CDMA are not viable for ad hoc networks because of the lack of a centralized architecture. Multiuser detection in DS/CDMA networks, such as interference cancellation (Sect. 6.5), reduces but does not eliminate the need for power control, which is usually essential for the synchronization. Even if an interference canceller can suppress a large amount of interference, the residual interference due to imperfect channel estimation may cause a severe performance degradation. Thus, DS/CDMA ad hoc networks can only compete with FH/CDMA ad hoc networks, which are largely immune to the near-far problem, if there is at least some degree of coordination among nearby nodes.

In contrast, DS/CDMA cellular networks are potentially preferable to FH/CDMA cellular networks because power control and coherent demodulation are available. However, the theoretical gap closes because of imperfect power control, and FH/CDMA cellular networks have the capability of exploiting larger, possibly disjoint, spectral bands.

A unified evaluation of the potential performance of both ad hoc and cellular FH/CDMA networks is presented by analysis and simulation in the remainder of this section. Multiple receive antennas that provide diversity combining (Chap. 5) are assumed to be available.

One method of combining antenna outputs is predetection combining, which requires the estimation of the signal and interference-plus-noise power levels at each antenna for MRC or selection diversity and requires the cophasing of the L antenna outputs for maximal-ratio or coherent equal-gain combining. Since the relative phases and power levels of the signals at the L antennas change after every hop, it is almost always impractical to implement predetection combining. As a much more practical alternative, a receiver can combine the demodulated outputs rather than the signals from the L antennas. This postdetection combining eliminates the cophasing and does not require the time alignment of L signals in practical applications because any misalignment is much smaller than a symbol duration. The estimation of power levels can be eliminated by the use of a fixed combining rule, such as equal-gain or square-law combining.

In the receiver of a frequency-hopping system, each antenna output is dehopped and filtered. The interference plus noise in each dehopped signal is approximated by independent bandlimited white Gaussian noise, with equivalent power given by

$$\sigma_1^2 = \sigma_n^2 + \sum_{i=1}^{K-1} p_{ui} \tag{6.186}$$

where σ_n^2 is the thermal noise power, $K - 1$ is the number of active frequency-hopping interference signals, and p_{ui} is the local-mean interference power received

from source i. The Gaussian model is reasonable for large numbers of interference signals that generally fade independently and experience different Doppler shifts. The total interference power is approximately uniform (white) over the receiver passband following dehopping if $BT_s \leq 1$. The L diversity antennas are assumed to be close enough to each other that the power-law losses and shadowing are nearly the same, and thus the local-mean power from a source is the same at each antenna. Each active interfering source may actually represent a cluster of mobiles. In this cluster, some discipline such as carrier-sense multiple access is used to ensure that there is at most one transmitted signal at any time.

The desired signal is assumed to experience flat Rayleigh fading. The Rayleigh fading model is appropriate under the pessimistic assumption that the propagation paths are often obstructed, and thus, the power of the direct line-of-sight signal is small compared with the reflected signal power. Flat fading occurs if $B < B_{\text{coh}}$, where B_{coh} is the coherence bandwidth. Rayleigh fading may be negligible if mobile speeds are very low, which would occur if each mobile consisted of a person walking. Shadowing would still occur but would be slowly varying over time.

We consider binary MSK with discriminator demodulation. For postdetection diversity, the outputs of L discriminators are weighted and combined. The weighting is by the square of the envelope at the input to each discriminator. When the desired signal undergoes independent Rayleigh fading at each antenna and the channel parameters remain constant for at least one symbol duration, a calculation using the results of [21] yields the symbol error probability:

$$P_s = \binom{2L-1}{L} \left(\frac{1}{4} + \frac{1}{3}\zeta^2\right)^L (\bar{\rho})^{-L} \tag{6.187}$$

where $\zeta = BT_s$, $\bar{\rho} = p_s/\sigma_1^2 \gg 1$, and p_s is the local-mean power of the desired signal. A comparison of this equation with (5.136) and (5.176) when $\zeta = 1$ so that $\bar{\rho} = \overline{\gamma}$ verifies that MSK with discriminator demodulation and square-law postdetection combining provides nearly the same P_s as ideal DPSK. The slowly varying shadowing in practical networks ensures that P_s is almost always nearly constant over an interleaved codeword or constraint length. The information-bit error rate following hard-decision decoding can be calculated from P_s with the equations of Chap. 1. The theoretical loss due to using postdetection rather than predetection combining is less than a decibel [21].

The propagation path losses are modeled as the result of power-law losses, shadowing, and fading. Equation (5.1) of Sect. 5.1 implies that the probability distribution function of the normalized local-mean power p_l/p_0 may be expressed as

$$F(x) = 1 - \mathrm{Q}\left\{\frac{10\log_{10} e}{\sigma_s} \ln\left[x\left(\frac{r}{R_0}\right)^{\beta}\right]\right\} \tag{6.188}$$

where p_0 is the average received power when the distance is $r = R_0$, β is the *attenuation power law,* and σ_s is the standard deviation in decibels. Although (6.188)

is only valid for $r \geq \delta$, where δ exceeds the minimum distance of the far field, the simplifying but pessimistic assumption is made that (6.188) is valid for all values of r. The fading causes a power fluctuation about the local-mean power.

6.4.3 Ad Hoc Networks

Consider an ad hoc network of independent, identical, frequency-hopping systems that have L omnidirectional antennas, generate the same output power, share the same carriers and frequency channels, and are nearly stationary in location over a single symbol duration. The antennas are separated from each other by several wavelengths, so that the fading of both the desired signal and the interfering signals at one antenna is independent of the fading at the other antennas. A few wavelengths are adequate because mobiles, in contrast to base stations, tend to receive superpositions of reflected waves arriving from many random angles. Because of practical physical constraints, spatial diversity will ordinarily be effective only if the carrier frequencies exceed roughly 1 GHz. Polarization diversity and other forms of adaptive array processing are alternatives.

Since in an ad hoc network it is assumed that an interfering mobile may transmit in any frequency channel with equal probability, the probability that power from an interferer enters the transmission channel of the desired signal is given by (6.185). It is assumed that M is sufficiently large that we may neglect the fact that a channel at one of the ends of the hopping band has only one adjacent channel instead of two. Consequently, the probability that the power from an interferer enters one of the two adjacent channels of the desired signal is

$$P_a = \frac{2d}{M}. \tag{6.189}$$

The probability that the power enters neither the transmission channel nor the adjacent channels is $(1 - 3d/M)$. These equations make it apparent that the performance of a frequency-hopping system depends primarily on the ratio $M_1 = M/d$. This ratio is called the *equivalent number of channels* because any decrease in the duty factor has the same impact as an increase in the number of frequency channels; what matters most for performance is this ratio.

In the simulation, the locations of the mobiles are assumed to be uniformly distributed in a circular region surrounding a specific mobile receiver, as illustrated in Fig. 6.17. Therefore, the radial distance of a mobile from the receiver has the probability distribution function

$$G(r) = \frac{r^2}{R^2}, \qquad 0 < r \leq R \tag{6.190}$$

where R is the radius of the circle. The distance of the desired mobile is randomly selected according to this distribution with $R = R_0$, where R_0 is the maximum

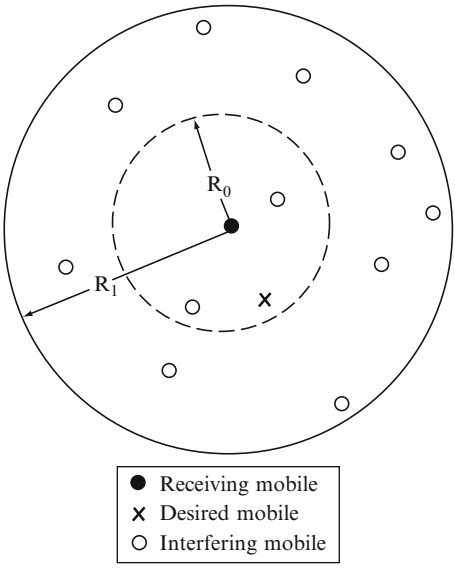

Fig. 6.17 Geometry of an ad hoc communication network

communication range and corresponds to a received area-mean signal power equal to p_0. The distance of each interfering mobile is randomly selected according to this distribution with $R = R_1$. The selected distance of the desired mobile is substituted into the distribution given by (6.188) as the value of r, and then this distribution is used to randomly select the local-mean power of the desired signal at the receiver. The probabilities given by (6.185) and (6.189) are used to determine if an interfering mobile produces power in the transmission channel or in one of the adjacent channels of the desired signal. The pessimistic assumption is made that any collision occurs over an entire symbol, not just part of it. If the power enters the transmission channel, then the power level is randomly selected according to (6.188) with the distance of the mobile substituted. If the power enters one of the adjacent channels, then the potential local-mean power level is first randomly selected via (6.188) and then multiplied by the adjacent-splatter ratio K_s (Sect. 3.2) to determine the net interference power p_{ui} that appears in (6.186). The effects of p_0 and σ_n^2 are determined solely by the *minimum area-mean SNR*, which occurs at the maximum range $r = R_0$ of the desired signal and is equal to p_0/σ_n^2.

Once the local-mean power levels and the noise power are calculated, the symbol error probability P_s is calculated with (6.186) and (6.187) subject to the constraint that $P_s \leq 1/2$. Each simulation experiment was repeated for 10,000 trials, with different randomly selected mobile locations in each trial. The performance measure is the *spatial reliability*, which is defined as the fraction of trials for which P_s is less than a specified performance threshold E. The appropriate value of the threshold depends on the desired information-bit error probability and the channel code. The spatial reliability is essentially the probability that an outage does not occur.

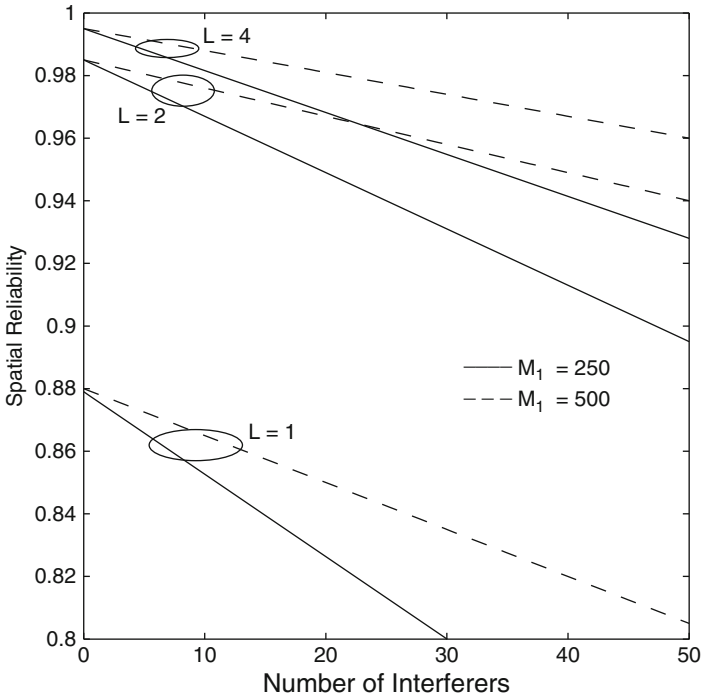

Fig. 6.18 Spatial reliability for $M_1 = 250$ and 500 and minimum area-mean SNR = 20 dB

Figures 6.18 and 6.19 depict the spatial reliability as a function of $K - 1$ for ad hoc networks. The figures, which are obtained by applying linear regression to the results of simulation experiments, plot the spatial reliability for various values of L, assuming Rayleigh fading and MSK. The parameter values are $\beta = 4$, $\sigma_s = 8$ dB, $E = 0.01$, $\zeta = 1$, $K_s = 0.015$, $R_0 = 1$, and $R_1 = 2$. The value of K_s results from assuming contiguous frequency channels with center frequencies separated by B, which is the frequency-channel bandwidth that captures 97% of the power of desired signal. The units of R_0 and R_1 are immaterial to the calculation of the spatial diversity.

In Fig. 6.18, the minimum area-mean SNR $= 20$ dB, and $M_1 = 250$ or 500. The number of equivalent frequency channels $M_1 = 250$ could model voice communications with $M = 90$ channels and $d = 0.36$; alternatively, it could model continuous data communications with $M = 225$ and $d = 0.9$. The figure illustrates the dramatic performance improvement provided by dual spatial diversity when Rayleigh fading occurs. Further increases in diversity yield diminishing returns. One can assess the impact of the spectral splatter in this example by setting $K_s = 0$ and observing the change in the spatial reliability. The change is small, and nearly imperceptible if $K < 25$. The figure illustrates the effect of increasing the number of equivalent channels from $M_1 = 250$ to $M_1 = 500$. Let the *capacity* of the network be defined as

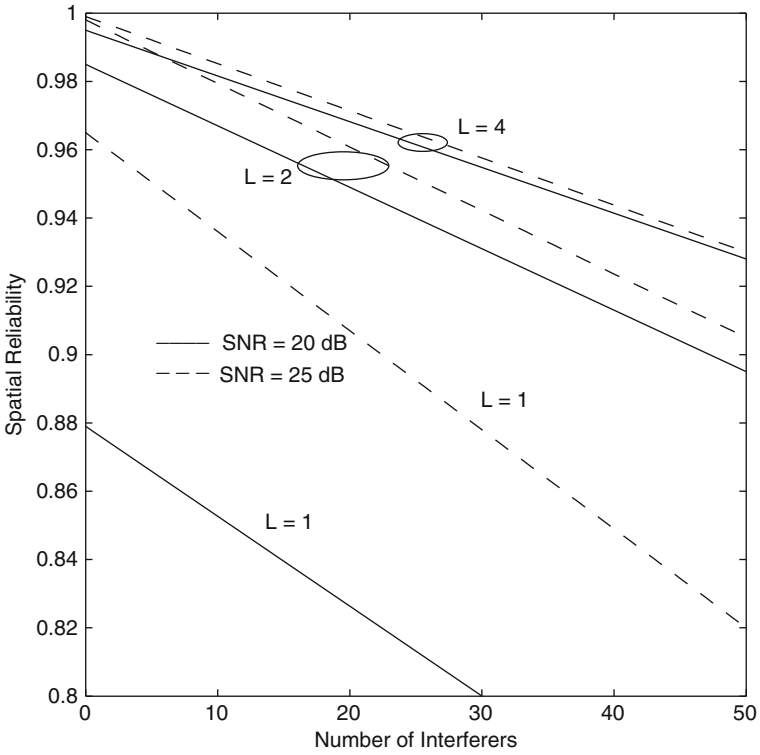

Fig. 6.19 Spatial reliability for $M_1 = 250$ and minimum area-mean SNR $= 20$ dB and 25 dB

the maximum number of interfering mobiles for which the spatial reliability exceeds 0.95. This figure and other simulation results indicate that for the parameter values selected, the capacity C for dual spatial diversity is approximately proportional to M_1; specifically, $C \approx 0.07\ M_1$ for $100 \leq M_1 \leq 1{,}000$. If E is increased to 0.02, the capacity for dual spatial diversity increases by approximately 20%

Figure 6.19 illustrates the sensitivity of the network to an increase in the minimum area-mean SNR, which may be due to a change in p_0 or σ_n^2. For no spatial diversity or dual diversity, a substantial performance improvement occurs when the minimum area-mean SNR $= 25$ dB. Other simulation results indicate that a decrease in the minimum area-mean SNR below 20 dB severely degrades performance. Since (6.187) relates P_s to $\bar{\rho}$, the local-mean SINR, the spatial reliability has an alternative and equivalent definition as the fraction of trials for which the SINR exceeds a specified threshold Z_l. Thus, the graphs labeled $L = 1$, 2, and 4 in Figs. 6.18, 6.19, and subsequent figures correspond to $Z_l = 17.7$ dB, 10.0 dB, and 6.5 dB, respectively. The desired value of Z_l is determined by the desired information-bit error probability, which depends on the channel code.

The performance of FH/CDMA communications in a mobile ad hoc network is greatly improved by the use of spatial diversity, which usually requires carrier frequencies in excess of 1 GHz. A crucial parameter is the number of equivalent frequency channels, which can be increased not only by an increase in the number of frequency channels, but also by a decrease in the duty factor of the network mobiles. The data modulation method that is most suitable appears to be some form of CPM or CPFSK. For these modulations, $BT_s \approx 1$, and the scenario modeled, the spectral splatter from adjacent channels, is not an important factor if the number of active interferers is much smaller than the number of equivalent channels.

6.4.4 Cellular Networks

In a cellular network, each base station assigns separate directional sector antennas or separate outputs of a phased array to cover disjoint angular sectors in both the transmitting and receiving modes. Typically, there are three sectors, and $2\pi/3$ radians are in each angular sector. The mobile antennas are assumed to be omnidirectional. An ideal sector antenna has a uniform gain over the covered sector and negligible sidelobes. With these antennas, only mobiles in the covered sector can cause multiple-access interference on an uplink from a mobile to a base station, and the number of interfering signals on the link is reduced by a factor s approximately equal to the number of sectors. Only the antenna serving a cell sector oriented toward a mobile can cause multiple-access interference on a downlink from the controlling base station to a mobile. Therefore, the number of interfering signals is reduced approximately by a factor s on both the uplinks and downlinks. Practical sector antennas have patterns with sidelobes that extend into adjacent sectors, but the performance degradation due to overlapping sectors is significant only for a small percentage of mobile locations. Ideal sector antennas are assumed in the subsequent simulation results.

Spatial diversity may be obtained through the deployment of L antennas in each mobile and L antenna elements for each sector antenna of each base station. The antennas are separated from each other enough that the fading of both the desired signal and the interfering signals at one antenna is independent of the fading at the other antennas. A few wavelengths are adequate for a mobile because it tends to receive superpositions of reflected waves arriving from many random angles. Many wavelengths separation may be necessary for a base station located at a high position, and polarization diversity may sometimes be a more practical means of obtaining diversity.

In a cellular network, synchronous frequency-hopping patterns can be chosen so that at any given instant in time, the frequencies of the mobiles within a cell sector are all different and, hence, the received signals are all orthogonal if the mobile transmissions are properly synchronized. Exact synchronization on a downlink is possible because a common timing is available. The advancing or retarding of the transmit times of the mobiles enables the arrival times at the

base station of the uplink signals to be synchronized. The uplink synchronization should be accurate enough that a small synchronization error can not subvert the orthogonality. The appropriate transmit times of a mobile can be determined from position information provided by the Global Positioning System and the known location of the base station. Alternatively, the transmit times can be determined from arrival-time measurements at the base station that are sent to the mobile. These measurements may be based on the adaptive thresholding [22] of the leading and/or trailing edges of a sequence of frequency-hopping pulses.

Let N_s denote the number of mobiles assigned to a cell sector. To ensure orthogonality of N_s received signals within a cell sector, a simple procedure is to generate a periodic frequency-hopping pattern that does not repeat until all the carrier frequencies in a hopset of size $M \geq N_s$ have been used. Mobile n is assigned this pattern with a delay of $n-1$ hop durations, where $n = 1, 2, \ldots, N_s$. The patterns associated with different sectors should be selected so that any two asynchronous signals from different cells or sectors will have few collisions during a period of the hopping patterns. However, this selection throughout a network requires frequency planning, which may be too costly in some applications.

It is possible to ensure not only the orthogonality of N_s signals in a sector but also that the received carrier frequencies in any two patterns are separated by at least νB, where ν is a positive integer, so that the spectral splatter is greatly reduced or negligible. Let $k = 0, 1, 2, \ldots, M - 1$ label the hopset frequencies in ascending order. Suppose that a frequency-hopping pattern is generated that does not repeat until all the carrier frequencies in a hopset of size $M \geq \nu N_s$ have been used. When mobile 1 hops to frequency k, mobile n hops to frequency $[k + \nu\ (n - 1)]$ modulo M. Frequency-hopping signals that use frequencies determined by this procedure are called *separated orthogonal signals*. Choosing $\nu = 2$ will generally be adequate because spectral splatter from channels that are not adjacent will be nearly always insignificant if a spectrally compact data modulation is used.

FH/CDMA networks largely avoid the near-far problem by continually changing the carrier frequencies so that frequency collisions become brief, unusual events. Thus, power control in a FH/CDMA network is unnecessary, and all mobiles may transmit at the same power level. When power control is used, it tends to benefit signals from mobiles far from an associated sector antenna, while degrading signals from mobiles close to it so that even perfect power control typically increases system capacity by only a small amount. There are good reasons to forego this slight potential advantage and not use power control. The required overhead may be excessive. If geolocation of mobiles is done by using measurements at two or more base stations, then the power control may result in significantly less signal power arriving at one or more base stations and the consequent loss of geolocation accuracy.

Consider communications between a base station and a mobile assigned to sector A of a particular cell, as illustrated in Fig. 6.20 for a hexagonal grid of cells. Because of orthogonality, no other signal in sector A will use the same carrier frequency at the same time and thereby cause interference in the transmission channel (current frequency channel) of either the uplink or downlink. Consider

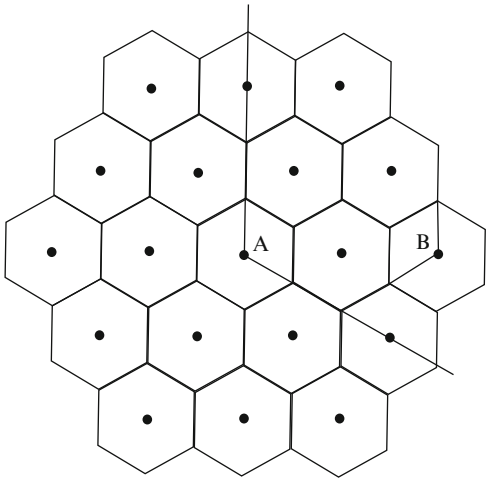

Fig. 6.20 Hexagonal grid of cells. Communicators are in sector A. Sector B is an interfering sector

another sector covered by the sector antenna of sector A; an example is sector B. Assuming that an interfering signal may independently and asynchronously use any frequency in the network hopset with equal probability, the probability that a mobile in the covered sector B produces interference in the transmission channel of the uplink and degrades a particular symbol is

$$P_m = \frac{dN_s}{M}. \tag{6.191}$$

This equation also gives the probability that a sector antenna serving another sector that is oriented toward the desired mobile degrades a symbol by producing interference in the transmission channel of the downlink. Because of orthogonality within each sector, no more than one signal from a sector will produce interference in the transmission channel of either link. A sector with mobiles that may interfere with communications over an uplink or a sector with an antenna that may produce interference over a downlink is called an *interfering sector*.

It is assumed that M is sufficiently large that we may neglect the fact that a channel at one of the ends of the hopping band has only one adjacent channel within the band instead of two. Let $N_1 = 1$ if a signal from an interfering sector uses the transmission channel of communicators in sector A; let $N_1 = 0$ if it does not. The probability distribution of N_1 is

$$P\,[N_1 = 1] = N_s/M, \quad P\,[N_1 = 0] = 1 - N_s/M. \tag{6.192}$$

The $N_s - N_1$ interference signals from a sector that do not enter the transmission channel are assumed to be randomly distributed among the $M - 1$ frequency channels excluding the transmission channel. There are $\binom{M-1}{N_s-N_1}$ ways to choose the channels with interference signals. There are $\binom{2}{1}$ ways to choose one of the

two adjacent channels to have an interference signal and $\binom{M-3}{N_s-N_1-1}$ ways to choose $N_s - N_1 - 1$ channels with interference signals out of the $M-3$ channels excluding both the transmission channel and the adjacent channels. The probability that an adjacent channel with an interference signal actually receives interference power is q_1. Similarly, there is one way to choose both adjacent channels with interference signals and $\binom{M-3}{N_s-N_1-2}$ ways to choose $N_s - N_1 - 2$ channels with interference signals out of $M-3$ channels. The probability that exactly one of the two adjacent channels with interference signals actually receives interference power is $2q_1(1-q_1)$. Because of the sector synchronization, either all of the signals from a sector overlap a desired symbol with probability q_2 or none of them do. Therefore, the probability that a symbol is degraded by interference in exactly one of the adjacent channels of the communicators is

$$\begin{aligned} P_{a1} &= \frac{\binom{2}{1}\binom{M-3}{N_s-N_1-1}}{\binom{M-1}{N_s-N_1}} q_1 q_2 + \frac{\binom{M-3}{N_s-N_1-2}}{\binom{M-1}{N_s-N_1}} 2\, q_1(1-q_1) q_2 \\ &= \frac{2d(N_s-N_1)}{(M-1)(M-2)}[M-2-q_1(N_s-N_1-1)], \quad M \geq N_s \geq 3. \end{aligned} \tag{6.193}$$

Similarly, the probability that a symbol is degraded by interference in both adjacent channels is

$$\begin{aligned} P_{a2} &= \frac{\binom{M-3}{N_s-N_1-2}}{\binom{M-1}{N_s-N_1}} q_1^2 q_2 \\ &= \frac{d q_1 (N_s-N_1)(N_s-N_1-1)}{(M-1)(M-2)}, \quad M \geq N_s \geq 3. \end{aligned} \tag{6.194}$$

For adjacent-channel interference from within sector A, P_{a1} and P_{a2} are given by the same equations with $N_1 = 1$ to reflect the fact that one of the mobiles is the communicating mobile.

Suppose that separated orthogonal frequency-hopping patterns with $\nu = 2$ are used. There is no adjacent-channel interference from sector A. If a signal from an interfering sector B uses the transmission channel so that $N_1 = 1$, an event with probability N_s/M, then the carrier separation of the signals generated in sector B ensures that there is no adjacent-channel interference from sector B, that is,

$$P_{a1} = P_{a2} = 0, \quad N_1 = 1. \tag{6.195}$$

Suppose that no signal from sector B uses the transmission channel so that $N_1 = 0$. Interference in exactly one adjacent channel results if the transmission channel of the desired signal in sector A, which may be any of $M - N_s$ channels, is located next to one of the two end channels of a set of $N_s \geq 1$ separated channels being used in sector B, neglecting hopset end effects. It also results if the transmission channel is located between two separated channels, of which only one is currently being used

in sector B, again neglecting hopset end effects. Therefore, the probability that a symbol is degraded by interference in exactly one of the adjacent channels of the communicators is

$$P_{a1} = \left[\frac{2q_1}{M - N_s} + \frac{N_s - 1}{M - N_s} 2q_1(1 - q_1)\right] q_2$$
$$= \frac{d}{M - N_s} \left[2\left(N_s - 1\right)\left(1 - q_1\right) + 2\right], \quad M \geq 2N_s\,,\ N_1 = 0,\ N_s \geq 1. \tag{6.196}$$

Interference in both adjacent channels results if the transmission channel is located between two separated channels of sector B and both are being used, neglecting hopset end effects. Therefore, the probability that a symbol is degraded by interference in both adjacent channels is

$$P_{a2} = \frac{dq_1\left(N_s - 1\right)}{M - N_s}, \quad M \geq 2N_s\,,\ N_1 = 0,\ N_s \geq 1. \tag{6.197}$$

If $N_s = 0$, then $P_{a1} = P_{a2} = 0$.

In the simulation, the spatial configuration consists of a hexagonal grid of cells with base stations at their centers. Each cell has a radius R_0 from its center to a corner. A central cell is surrounded by an inner concentric tier of 6 cells and an outer concentric tier of 12 cells, as depicted in Fig. 6.20. Other tiers are assumed to generate insignificant interference in the central cell. An equal number of mobiles, each transmitting at the same power level, is located in each sector and served by that sector's antenna. This assumption is pessimistic since slightly improved performance may be possible if a mobile is served by the sector antenna providing a signal with the least attenuation. Each signal transmitted by a sector antenna is allocated the same power. The set of frequency-hopping patterns used in each sector is assumed to be selected independently of the other sectors. Since the parameter R_0 in (6.188) is equal to the maximum communication range, p_0 is the minimum received area-mean power of a desired signal. The location of each mobile within a sector is assumed to be uniformly distributed.

In each simulation trial for communications in sector A of the central cell, the location of the desired mobile is randomly selected according to the uniform distribution. The selected distance of the desired mobile is substituted into (6.188) as the value of r, and then this equation is used to randomly select the local-mean power of the desired signal at the receiver. Each transmitting and receiving beam produced by a sector antenna is assumed to have a constant gain over its sector and zero gain elsewhere.

For an uplink of sector A, interference is assumed to arrive from mobiles within sector A, mobiles in the 6 sectors of the two cells in the inner tier that were covered by the beam of sector A, and mobiles in the 11 complete sectors and 2 half-sectors of the five cells in the outer tier completely or partially covered by the beam. The 2 half-sectors are approximated by an additional complete sector in the outer tier.

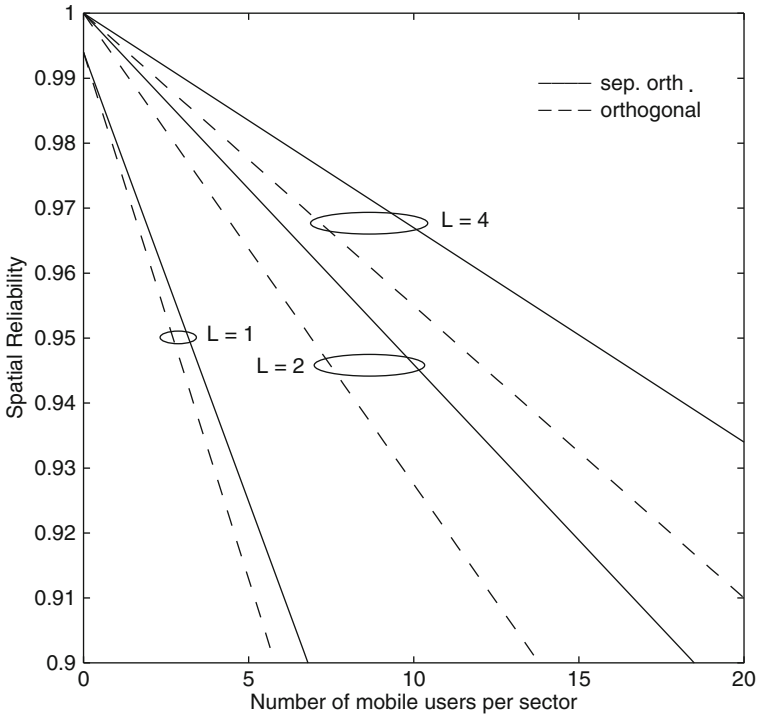

Fig. 6.21 Spatial reliability for uplinks, $M = 100$, minimum area-mean SNR $= 30$ dB, and orthogonal and separated orthogonal hopping

Equations (6.191) to (6.197) are used to determine if a sector contains mobiles that produce power in the transmission channel or in one or both of the adjacent channels. If the sector does, then the locations of the three or fewer interfering mobiles are randomly selected according to the uniform distribution, and their distances from the central cell's base station are computed.

For a downlink of sector A, interference is assumed to arrive from the two facing sector antennas of the inner tier and the five facing sector antennas of the outer tier. Equations (6.191) to (6.197) are used to determine if a signal generated by an interfering sector antenna produces power in the transmission channel or the adjacent channels of the desired signal. If so, then the distance between the sector antenna and the desired mobile is computed.

The pessimistic assumption is made that any collision occurs over an entire symbol, not just part of it. If the power from an interferer enters the transmission channel, then the power level is randomly selected according to (6.188), with the appropriate distance substituted. If the power enters an adjacent channel, then the potential local-mean power level is first randomly selected via (6.188) and then multiplied by K_s to determine the net interference power p_{ui} that appears in (6.186). The shadowing parameter σ_s is assumed to be the same for all signals originating

from all cells. The effects of p_0 and σ_n^2 are determined solely by p_0/σ_n^2, the minimum area-mean SNR. Since only ratios affect the performance, the numerical value of R_0 in the simulation is immaterial and is set equal to unity.

Once the local-mean power levels and the noise power are calculated, the symbol error probability is calculated with (6.186) and (6.187) subject to the constraint that $P_s \leq 1/2$. Each simulation experiment was repeated for 20,000 trials, with different randomly selected mobile locations in each trial. The performance measure is the spatial reliability, which is a function of $\bar{\rho}$, the SINR. The appropriate value of the threshold E depends on the desired information-bit error probability and the channel code.

Figures 6.21–6.24 depict the results of simulation experiments for the uplinks of a cellular network. The figures plot spatial reliability as a function of N_s for various values of L, assuming Rayleigh fading, MSK, three sectors, and that $\beta = 4$, $q_1 = 0.4$, $q_2 = 1.0$, $\sigma_s = 8$ dB, $E = 0.01$, $\zeta = 1$, and $K_s = 0.015$. The value of K_s results from assuming contiguous frequency channels with the center frequencies separated by the bandwidth of a frequency channel.

Figure 6.21 illustrates the spatial reliability for orthogonal and separated orthogonal frequency hopping with $\nu = 2$, $M = 100$ ($M_1 = 250$), and minimum area-mean SNR $= 30$ dB. The figure illustrates the dramatic performance improvement provided by dual spatial diversity when Rayleigh fading occurs. Further increases in diversity yield diminishing returns. The figure shows the effect of using orthogonal rather than separated orthogonal frequency hopping. The performance loss is significant in this example and becomes more pronounced as M decreases. One can assess the impact of the spectral splatter on the separated orthogonal frequency hopping by setting $K_s = 0$ and observing the change in spatial reliability. The change is insignificant because by far the most potentially damaging splatter arises from mobiles in the same sector as the desired mobile, and the separated orthogonality has eliminated it.

Figure 6.22 illustrates the effect of increasing M to 200, and hence increasing M_1 to 500, while the minimum area-mean SNR $= 30$ dB. The *uplink capacity* C_u of a cellular network is defined as the maximum number of interfering mobiles per cell for which the spatial reliability exceeds 0.95. This figure and other simulation results indicate that for three sectors per cell, dual diversity, and the other parameter values selected, the uplink capacity is $C_u \approx 0.108\, M_1$ for $50 \leq M_1 \leq 1{,}000$. This equation is sensitive to parameter variations. If the shadowing standard deviation σ_s is lowered to 6 dB, it is found that C_u increases by roughly 57%. Alternatively, if the threshold E is raised to 0.04, corresponding to SINR $= 7$ dB, it is found that C_u increases by roughly 59%.

Figure 6.23 illustrates the sensitivity of the network to a decrease in the minimum area-mean SNR, which may be due to a change in either p_0 or σ_n^2. A substantial performance loss occurs when the minimum area-mean SNR is reduced to 20 dB, particularly for no spatial diversity or dual diversity. Other simulation results indicate that an increase in the minimum area-mean SNR beyond 30 dB barely improves performance.

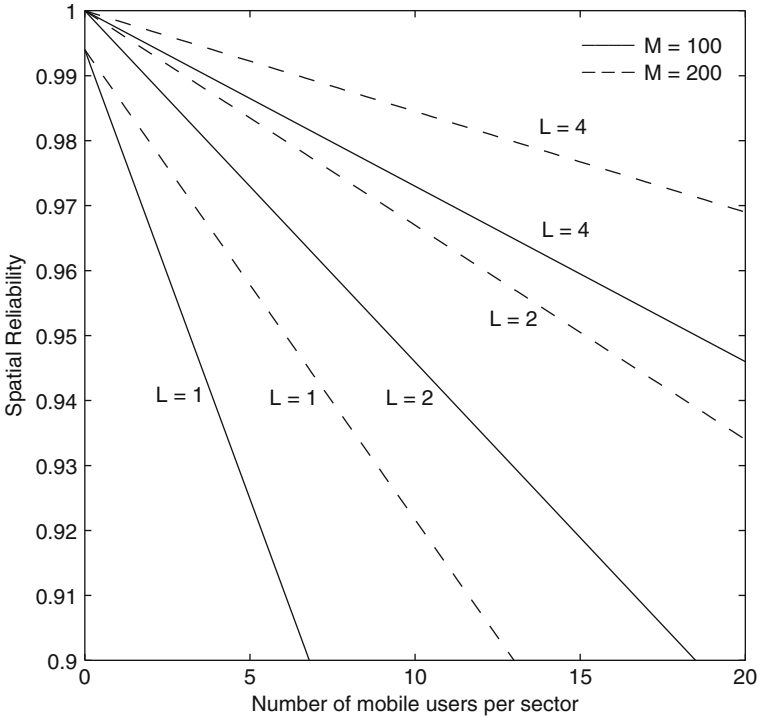

Fig. 6.22 Spatial reliability for uplinks, separated orthogonal hopping, $M = 100$ and 200, and minimum area-mean SNR = 30 dB

The performance is worse for the downlinks than for the uplinks because of the relative proximity of some of the interfering sector antennas to the desired mobile. The *downlink capacity* C_d, which is defined analogously to the uplink capacity, is $C_d \approx 0.072\ M_1$ for $50 \leq M_1 \leq 1{,}000$. A more realistic comparison of the downlinks and uplinks must take into account the differences between the high-power amplifiers and low-noise amplifiers in the base station and those in the mobiles. Assuming a net 10 dB advantage in the minimum area-mean SNR for the downlinks, Fig. 6.24 provides a performance comparison of the two links. The performance of the downlinks is slightly worse if $L \geq 2$ and $N_s \geq 5$. The difference in performance is increased if physical constraints in the mobiles limit the downlinks to $L = 1$ or 2 while $L = 4$ for the uplinks.

Compared with direct-sequence systems, frequency-hopping systems have a bandwidth advantage in that frequency hopping over a large, possibly noncontiguous, spectral band is as practical as direct-sequence spreading over a much smaller, necessarily contiguous, spectral band. Even deprived of its bandwidth advantage and power control, FH/CDMA can provide nearly the same multiple-access capacity over the uplinks as DS/CDMA subject to realistic power-control imperfections. For a numerical example, consider a cellular network with three

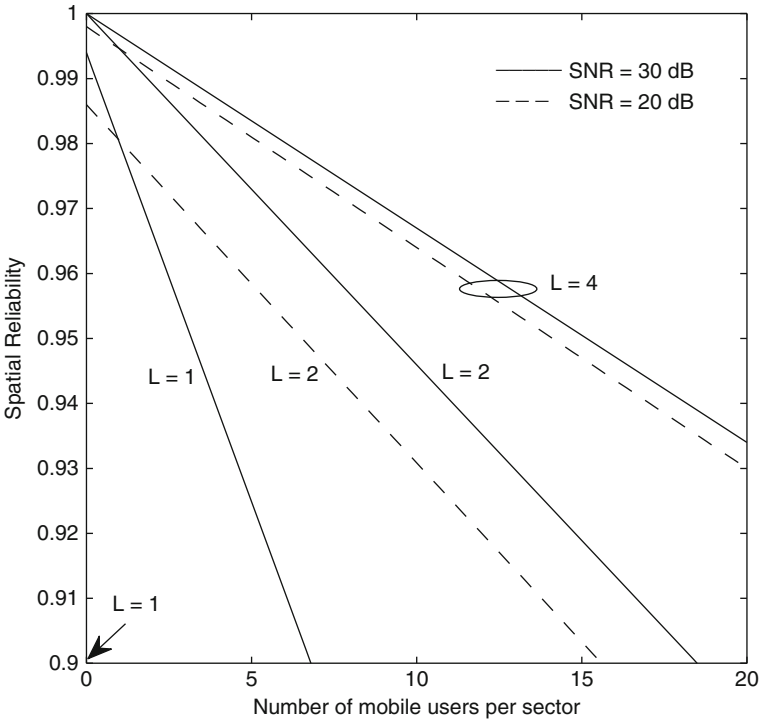

Fig. 6.23 Spatial reliability for uplinks, separated orthogonal hopping, $M = 100$, and minimum area-mean SNR $= 20$ dB and 30 dB

sectors, shadowing standard deviation $\sigma_s = 6$ dB, and $d = q_1 = 3/8$ due to the voice activity. A contiguous spectral band of bandwidth $W = 1.25$ MHz is occupied by the CDMA signals. The symbol rate is $1/T_s = 8$ kb/s so that the processing gain is 156.5 for DS/CDMA, and the number of frequency channels for FH/CDMA with $\zeta = BT_s = 1$ is $M = 156$. For DS/CDMA, it is assumed that p_0 is the received power at the base station from all associated mobiles when the power control is perfect and that the SNR before the despreading is -1 dB. Therefore, the SNR is 20.94 dB after the despreading. For FH/CDMA without power control, the minimum area-mean SNR is assumed to be 20.94 dB. The uplink capacity C_u is calculated as the number of mobiles per cell that can be accommodated while maintaining an SINR above a specified threshold Z with 95% probability. For FH/CDMA with dual diversity and $Z = 10$ dB, it is found that $C_u \approx 60$. For DS/CDMA with dual diversity and coherent phase-shift keying, a comparison of ((6.187) with (5.137) indicates that a comparable performance can be obtained when the SINR is roughly 3 dB less. Thus, the threshold for DS/CDMA is set at $Z = 7$ dB. Using (6.131) with $Z = 7$ dB, it is found that $C_u \approx 60$ when the power-control error has $\sigma_e = 2$ dB.

The performance of an FH/CDMA system is greatly enhanced if coherent demodulation is possible, which is highly unlikely in practical applications. For

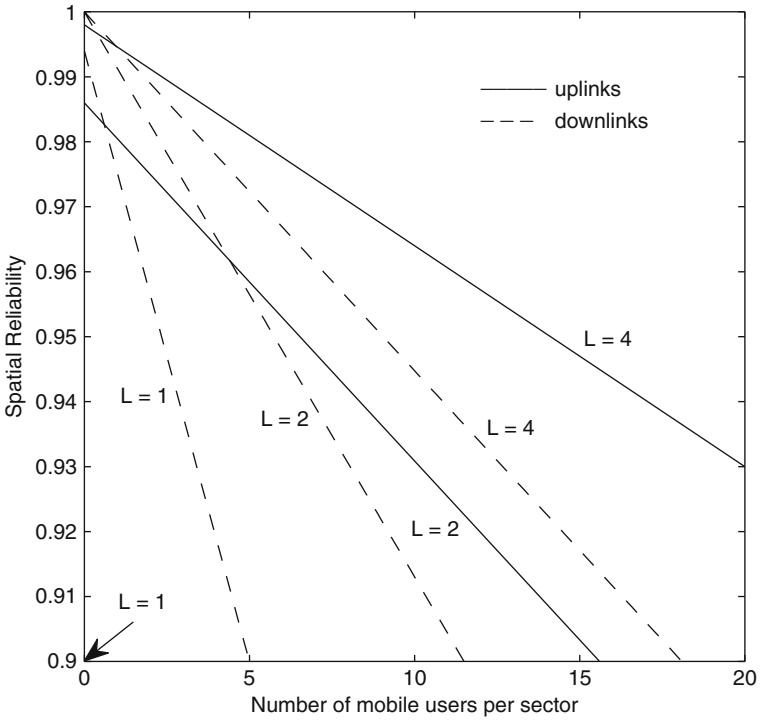

Fig. 6.24 Spatial reliability for uplinks and downlinks, separated orthogonal hopping, $M = 100$, and minimum area-mean SNR $= 30$ dB

coherent demodulation of a signal that hops over a wide band to be a practical possibility in a fading environment, either a pilot signal must be available, turbo or other iterative decoding with phase estimation must be feasible, or the dwell time must be large enough that a small portion of it can be dedicated to carrier synchronization. The implementation degradation due to the latter measures and the occasional failure to achieve carrier synchronization for a frequency-hopping pulse must be less than the potential gain due to the coherent demodulation. If ideal coherent demodulation is assumed in the preceding example so that $\mathrm{Z} = 7$ dB, and the implementation degradation is ignored, then it is found that $C_u \approx 108$, an increase of 80%. This uplink capacity is approximately obtained by DS/CDMA with $\mathrm{Z} = 7$ dB when $\sigma_e = 0.4$ dB, an impractically low value.

For a specified sectorization, diversity, and waveform, the capacity of a cellular FH/CDMA network is approximately proportional to the equivalent number of frequency channels. Thus, a desired capacity can be attained by choosing a sufficiently large number of frequency channels. A major advantage of frequency hopping is that these channels do not have to be spectrally contiguous but can be scattered throughout a large spectral band. Another advantage is that power control is not required. Its absence allows a substantial reduction of system complexity

and overhead cost and facilitates geolocation. Sectorization, orthogonality, and dual diversity are invaluable, but higher levels of diversity offer sharply decreasing gains. If spectral splatter is a problem, separated orthogonal signaling can be used to eliminate it. The overall limit on the capacity of a FH/CDMA network appears to be set more by the downlinks than the uplinks.

6.5 Multiuser Detectors

The conventional single-user direct-sequence receiver of Fig. 2.14 is optimal against multiple-access interference only if the spreading sequences of all the interfering signals and the desired signal are orthogonal. Orthogonality is possible in a synchronous communication network, but in an asynchronous network, it is not possible to find sequences that remain orthogonal for all relative delays. Thus, the conventional single-user receiver, which only requires knowledge of the spreading sequence of the desired signal, is suboptimal against asynchronous multiple-access interference. The price of the suboptimality might be minor if the spreading sequences are carefully chosen and the noise is relatively high, especially if a channel code and a sector antenna or adaptive array are used. If a potential near-far problem exists, power control may be used to limit its impact. However, power control is imperfect, entails a substantial overhead cost, and is not feasible for ad hoc communication networks. Even if the power control is perfect, the remaining interference causes a nonzero *error floor*, which is a minimum bit error probability that exists when the thermal noise is zero. Thus, an alternative to the conventional receiver is desirable.

A *multiuser detector* [23, 24] is a receiver that exploits the deterministic structure of multiple-access interference or uses joint processing of a set of multiple-access signals. An optimum multiuser detector almost completely eliminates the multiple-access interference and, hence, the near-far problem, thereby rendering power control unnecessary, but such a detector is prohibitively complex to implement, especially when long spreading sequences are used. A more practical multiuser detector alleviates but does not eliminate the power-control requirements of a cellular network on its uplinks. Even if a multiuser detector at a base station rejects *intracell interference* from mobiles within its cell, it generally cannot reject *intercell interference*, which arrives from mobiles associated with different base stations and located in different cells, and is typically more than one-third of the total interference on an uplink. Multipath components can be accommodated as separate interference signals or rake combining may precede the multiuser detection.

Though suboptimal compared with ideal multiuser detection, multiuser interference cancellers bear a much more moderate implementation burden and still provide considerable interference suppression. However, accurate power control is still needed at least for initial synchronization and to avoid overloading the front end of the receiver. Third-generation CDMA systems use adaptive interference cancellation but retain a closed-loop power-control subsystem.

6.5.1 Optimum Detectors

Consider a DS/CDMA network with K users, each of which uses BPSK to transmit a block of N binary symbols. A *jointly optimum* detector makes collective symbol decisions for K received signals based on the *maximum a posteriori* (MAP) criterion. The *individually optimum* detector selects the most probable set of symbols of a single desired signal based on the MAP criterion, thereby providing the minimum symbol error probability. In nearly all applications, jointly optimum decisions are preferable because of their lower complexity and because both types of decisions agree with very high probability unless the symbol error probability is very high. Assuming equally likely symbols are transmitted, the jointly optimum MAP detector is the same as the jointly optimum maximum-likelihood detector, which is henceforth referred to as the *optimum detector*.

For *synchronous communications* in the presence of white Gaussian noise, the symbols are aligned in time, and the detection of each symbol of the desired signal is independent of the other symbols. Thus, the optimum detector can be determined by considering a single symbol interval $0 \le t \le T_s$. Let d_k denote the symbol transmitted by user k. It is assumed that each of the K signals has a common carrier frequency but a distinct phase θ_k relative to the phase of the receiver-generated synchronization signal used to extract the complex envelope. The chip waveform is assumed to have unit energy in a symbol interval, as in (1.41), and cause negligible intersymbol interference. The complex envelope of the received signal is applied to a chip-matched filter, the output of which is sampled at the chip rate. A derivation similar to those in Sect. 1.1 indicates that the received discrete-time sequence associated with a received symbol is

$$y_\nu = \sum_{k=0}^{K-1} A_k d_k p_k(\nu) + n_{s\nu}, \quad \nu = 0, 1, \ldots, G-1 \tag{6.198}$$

where $A_k = \sqrt{\mathcal{E}_k/G}\exp(j\theta_k)$ is the complex symbol amplitude for user k, $\mathcal{E}_k$ is the energy in the data symbol for user k, G is the number of spreading-sequence chips per symbol, $p_k(\nu) = \pm 1$ is chip ν of the spreading sequence of user k, $d_k = \pm 1$, and

$$n_{s\nu} = \sqrt{2}\int_{\nu T_c}^{(\nu+1)/T_c} n(t)\psi(t - \nu T_c)\exp(-j2\pi f_c t)\, dt \tag{6.199}$$

is Gaussian noise.

Let $\mathbf{y} = [y_0 \;\; y_1 \ldots y_{G-1}]^T$, $\mathbf{p}_k = [p_k(0)\; p_k(1) \ldots p_k(G-1)]^T$, $\mathbf{d} = [d_0 \ldots d_{K-1}]^T$, and $\mathbf{n} = [n_{s0} \;\; n_{s1} \ldots n_{s,G-1}]^T$. Then the received vector is

$$\mathbf{y} = \mathbf{PAd} + \mathbf{n} \tag{6.200}$$

where column n of the $G \times K$ matrix $\mathbf{P}$ is the vector $\mathbf{p}_n$ that represents the spreading sequence of user n, and $\mathbf{A}$ is the diagonal matrix with A_i as its ith diagonal element.

Assuming that $n(t)$ is zero-mean white Gaussian noise, calculations similar to those in Sect. 1.1 indicate that $\mathbf{n}$ is a zero-mean, circularly symmetric, Gaussian noise vector with $E[\mathbf{n}\mathbf{n}^T] = 0$ and that

$$E\left[\mathbf{n}\mathbf{n}^H\right] = N_0\mathbf{I}. \tag{6.201}$$

Assuming that all possible values of the symbol vector $\mathbf{d}$ are equally likely, the optimum detector is the *maximum-likelihood detector*, which selects the value of $\mathbf{d}$ that minimizes the log-likelihood function

$$\Lambda(\mathbf{d}) = ||\mathbf{y} - \mathbf{PAd}||^2 \tag{6.202}$$

subject to the constraint that $\mathbf{d} \in \mathbf{D}$, where $\mathbf{D}$ is the set of vectors such that each $d_k = +1$ or -1. Thus, we may express the maximum-likelihood decision as

$$\widehat{\mathbf{d}} = \arg\min_{\mathbf{d}\in\mathbf{D}} ||\mathbf{y} - \mathbf{PAd}||^2 . \tag{6.203}$$

In contrast, a conventional single-user detector ignores the other users and uses a single correlator that is matched to the spreading sequence of the desired user. Thus, the *conventional matched-filter detector* for user k computes $r = \mathbf{p}_k^T\mathbf{y}$. The maximum-likelihood decision is

$$\widehat{d}_k = \arg\min_{\mathbf{d_k}\in(+\mathbf{1},-\mathbf{1})} |r - A_k d_k G|^2 . \tag{6.204}$$

The optimum detector of (6.203) uses G successive samples of the output of a chip-matched filter. Equation (6.203) indicates that the K spreading sequences must be known so that $\mathbf{P}$ can be calculated, and the K complex signal amplitudes must be estimated. Short spreading sequences are necessary or $\mathbf{P}$ must change with each symbol, which greatly increases the implementation complexity. The optimum detector is capable of making joint symbol decisions for all K signals or merely the symbol decisions for a single signal.

Equation (6.203) can be solved by an exhaustive search of all possible values of $\mathbf{d}$, but this search is only feasible or small values of K and G. However, if the spreading sequences are orthogonal, then this equation can be solved in closed form. Expanding this equation, using $\mathbf{p}_i^T\mathbf{p}_k = 0, i \neq k, i, k = 0, 1, \ldots, K-1$, dropping irrelevant terms, and recognizing that $\mathbf{d}$ and $\mathbf{P}$ are real-valued, we find that

$$\widehat{\mathbf{d}} = \arg\max_{\mathbf{d}\in\mathbf{D}} \left[\mathbf{d}^T\left(\mathrm{Re}(\mathbf{A}^*\mathbf{P}^\mathbf{T}\mathbf{y})\right]. \right. \tag{6.205}$$

The Cauchy–Schwarz inequality for vectors indicates that $\left|\mathbf{d}^T\mathbf{x}\right| \leq ||\mathbf{d}||\,||\mathbf{x}||$ with equality only if $\mathbf{d}$ is a constant times $\mathbf{x}$. Therefore, $\widehat{\mathbf{d}}$ must be a constant times $\mathrm{Re}(\mathbf{A}^*\mathbf{P}^\mathbf{T}\mathbf{y})$, and the constant must be such that $\mathbf{d} \in \mathbf{D}$. This requirement implies that

$$\widehat{\mathbf{d}} = \mathrm{sgn}[\mathrm{Re}(\mathbf{A}^*\mathbf{P}^\mathbf{T}\mathbf{y})] \tag{6.206}$$

where $sgn(\mathbf{x})$ is the vector of signum functions of the components of the vector $\mathbf{x}$. The *signum function* is defined as $sgn(x) = 1$, $x \geq 0$, and $sgn(x) = -1$, $x < 0$. For the symbol of user k,

$$\widehat{d}_k = \text{sgn}[\text{Re}(A_k^* \mathbf{p}_k^T \mathbf{y})]. \tag{6.207}$$

This detector requires knowledge of both the spreading sequence $\mathbf{p}_k$ and the amplitude A_k. However, if the receiver is phase-synchronized with the carrier of user k, then the phase of A_k is removed, and A_k may be assumed to be real-valued with zero phase. As a result, A_k does not affect the decision, and the detected symbol is

$$\widehat{d}_k = \text{sgn}[\mathbf{p}_k^T \mathbf{y}_r] \tag{6.208}$$

where $\mathbf{y}_r$ is the real part of $\mathbf{y}$.

For asynchronous communications, the design of the maximum-likelihood detector is complicated by the phase and timing offsets of each user's signal. Even if the dubious assumption is made that the relative phase offsets are negligible, the detector implementation remains formidable. A timing offset implies a desired symbol overlaps two consecutive symbols from each interference signal. Consequently, an entire message or codeword of N correlated data symbols from each of the K users must be processed, and decisions must be made about NK binary symbols. The vector $\mathbf{d}$ is $NK \times 1$ with the first N elements representing the symbols of signal 1, the second N elements representing the symbols of signal 2, and so forth. The detector must estimate the transmission delays of all K multiple-access signals and estimate the partial cross-correlations among the signals. The detector must select K symbol sequences, each of length N, corresponding to the maximum-likelihood criterion. The Viterbi algorithm simplifies computations by exploiting the fact that each received symbol overlaps at most $2(K-1)$ other symbols. Nevertheless, the computational complexity increases exponentially with K.

In view of both the computational requirements and the parameters that must be estimated, it is highly unlikely that the optimum multiuser detector will have practical applications. Subsequently, alternative suboptimal multiuser detectors with complexities that increase linearly with K are considered. All of them apply the chip-matched filter outputs to a filter bank of correlators.

6.5.2 Decorrelating Detector

Expanding (6.203), dropping the term $||\mathbf{y}||^2$ that is irrelevant to the selection of $\mathbf{d}$, and using the fact that $\mathbf{A^H} = \mathbf{A}^*$, we find that the maximum-likelihood detector for synchronous communications selects the value of $\mathbf{d}$ that minimizes the *correlation metric*

$$C = \mathbf{d}^H \mathbf{A}^* \mathbf{P^T} \mathbf{P} \mathbf{A} \boldsymbol{d} - \mathbf{y}^H \mathbf{P} \mathbf{A} \mathbf{d} - \mathbf{d}^H \mathbf{A}^* \mathbf{P^T} \mathbf{y} \tag{6.209}$$

subject to the constraint that $d_k = +1$ or $-1, k = 0, 1, \ldots, K-1$. The decorrelating detector may be derived by initially maximizing the correlation metric without any constraint on $\mathbf{d}$. For this purpose, the complex gradient of C with respect to the K-dimensional vector $\mathbf{d}$, which is denoted by $\nabla_{\mathbf{d}} C$, is defined as described in Sect. 2.7. Applying the necessary condition that $\nabla_{\mathbf{d}} C = \mathbf{0}$ implies that C has the stationary point $\mathbf{d} = \widehat{\mathbf{d}}_1$, where

$$\widehat{\mathbf{d}}_1 = \mathbf{A}^{-1} \left(\mathbf{P}^{\mathbf{T}} \mathbf{P}\right)^{-1} \mathbf{P}^{\mathbf{T}} \mathbf{y} \tag{6.210}$$

provided that all amplitudes have positive magnitudes and $\mathbf{P}^{\mathbf{T}}\mathbf{P}$ is invertible. If $G \geq K$, then the $G \times K$ matrix $\mathbf{P}$ is generally full rank, which implies that the $K \times K$ matrix $\mathbf{P}^{\mathbf{T}}\mathbf{P}$ is full rank and, hence, invertible and positive definite. The solution $\widehat{\mathbf{d}}_1$ corresponds to the minimum of C because its Hessian matrix is $\mathbf{A}^* \mathbf{P}^{\mathbf{T}} \mathbf{P} \mathbf{A} = \mathbf{A}^{\mathbf{H}} \mathbf{P}^{\mathbf{T}} \mathbf{P} \mathbf{A}$, which is a positive definite matrix because $\mathbf{P}^{\mathbf{T}}\mathbf{P}$ is. For an alternative proof, (6.209) may be expressed in terms of $\widehat{\mathbf{d}}_1$ as

$$C = \left(\mathbf{d} - \widehat{\mathbf{d}}_1\right)^H \mathbf{A}^* \left(\mathbf{P}^{\mathbf{T}} \mathbf{P}\right) \mathbf{A} \left(\mathbf{d} - \widehat{\mathbf{d}}_1\right) - \mathbf{y}^H \mathbf{P} \left(\mathbf{P}^{\mathbf{T}} \mathbf{P}\right)^{-1} \mathbf{P}^{\mathbf{T}} \mathbf{y}. \tag{6.211}$$

Since $\mathbf{A}^* \mathbf{P}^{\mathbf{T}} \mathbf{P} \mathbf{A}$ is a positive definite matrix, C has a unique minimum at $\mathbf{d} = \widehat{\mathbf{d}}_1$.

Substituting (6.200) into (6.210), we obtain

$$\widehat{\mathbf{d}}_1 = \mathbf{d} + \mathbf{A}^{-1} \left(\mathbf{P}^{\mathbf{T}} \mathbf{P}\right)^{-1} \mathbf{P}^{\mathbf{T}} \mathbf{n} \tag{6.212}$$

which shows that the data symbols have been decorrelated from each other in $\widehat{\mathbf{d}}_1$, and that $\widehat{\mathbf{d}}_1$ given by (6.210) is a type of zero-forcing estimator. Since $d_k = +1$ or -1, the imaginary part of $\widehat{\mathbf{d}}_1$ may be discarded in (6.210), and a suitable set of detected symbols based on hard decisions is

$$\widehat{\mathbf{d}} = \operatorname{sgn}[\operatorname{Re}(\mathbf{A}^{-1} \left(\mathbf{P}^{\mathbf{T}} \mathbf{P}\right)^{-1} \mathbf{P}^{\mathbf{T}} \mathbf{y})]. \tag{6.213}$$

Since the decorrelator completely removes the multiple-access interference, the near-far problem does not exist, and the *decorrelating detector*, which implements (6.213), is *near-far resistant*.

The decorrelating detector for user k is synchronized with this user's signal, and hence A_k is assumed to be real-valued with zero phase. Since the real-valued component A_k^{-1} of $\mathbf{A}^{-1}$ does not affect the decision, the decision for symbol k is

$$\widehat{d}_k = \operatorname{sgn}[(\left(\mathbf{P}^{\mathbf{T}} \mathbf{P}\right)^{-1} \mathbf{P}^{\mathbf{T}} \mathbf{y}_r)_k] \tag{6.214}$$

where $\mathbf{y}_r$ is the real part of $\mathbf{y}$, and the kth component of $\left(\mathbf{P}^{\mathbf{T}} \mathbf{P}\right)^{-1} \mathbf{P}^{\mathbf{T}} \mathbf{y}_r$ is computed. This equation indicates that the complex amplitudes do not need to be estimated. It reduces to (6.208) when the spreading sequences are mutually orthogonal.

The complete decorrelating detector that implements (6.213) has the form diagrammed in Fig. 6.25. The G sampled outputs of the chip-matched filter are applied

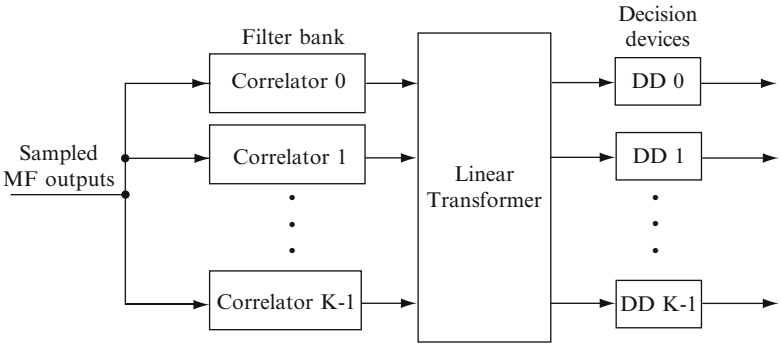

Fig. 6.25 Architecture of complete decorrelating or MMSE detector for synchronous communications. Filter bank comprises K parallel correlators

to a filter bank of K parallel correlators. Correlator n implements $r_n = \mathbf{p}_n^T \mathbf{y}$, and the filter-bank outputs constitute the vector $\mathbf{r} = \mathbf{P^T y}$. The linear transformer computes the vector $\mathrm{Re}(\mathbf{A}^{-1} \left(\mathbf{P}^T \mathbf{P}\right)^{-1} \mathbf{P}^T y)$. Each decision device applies the signum function to one component of this vector. For asynchronous communications, each of the K correlators in the filter bank must process N successive sets of G sampled outputs of the chip-matched filter, which is generally impractical.

Consider the detection of symbol d_k of user k. The receiver synchronizes with this user's signal, and hence A_k is assumed to be real-valued with zero phase. Using (6.200), (6.214) may be expressed as

$$\widehat{d}_k = \mathrm{sgn}\left[A_k d_k + \left(\left(\mathbf{P^T P}\right)^{-1} \mathbf{P^T n}_r\right)_k\right]. \tag{6.215}$$

The noise that affects $\widehat{d}_k$ is $\mathbf{n}_1 = \left(\mathbf{P^T P}\right)^{-1} \mathbf{P^T n}_r$, where $\mathbf{n}_r$ is the real part of $\mathbf{n}$. From (6.201) and the circular symmetry of $\mathbf{n}$, it follows that the covariance matrix of the noise vector $\mathbf{n}_r$ is

$$E\left[\mathbf{n}_r {\mathbf{n}_r}^T\right] = \frac{N_0}{2}\mathbf{I}. \tag{6.216}$$

Therefore, the covariance matrix of $\mathbf{n}_1$ is

$$E\left[\mathbf{n}_1 {\mathbf{n}_1}^T\right] = \frac{N_0}{2}\left(\mathbf{P^T P}\right)^{-1}. \tag{6.217}$$

The *correlation matrix* is defined as the real-valued matrix

$$\mathbf{R} = \frac{1}{G}\mathbf{P^T P}. \tag{6.218}$$

The variance of the kth component of $\mathbf{n}_{1r}$ is $(N_0/2G)R_{kk}^{-1}$, where R_{kk}^{-1} denotes element k, k of $\mathbf{R}^{-1}$. The noise causes an error if it causes the argument of the

signum function in (6.215) to have a different sign than d_k. Since this noise has a Gaussian density function, the symbol error probability at the output of decision-device k is

$$P_s(k) = Q\left(\sqrt{\frac{2\mathcal{E}_k}{N_0 R_{kk}^{-1}}}\right), \quad k = 0, 1, \ldots, K-1 \tag{6.219}$$

where $\mathcal{E}_k = A_k^2 G$ is the symbol energy. In the absence of multiple-access interference, $R_{kk}^{-1} = 1$. Thus, the presence of multiple-access interference requires an increase of energy by the factor R_{kk}^{-1} if a specified symbol error probability is to be maintained.

Element i, k of $\mathbf{R}$ is

$$R_{ik} = \frac{\mathbf{p}_i^T \mathbf{p}_k}{G} = \frac{\mathcal{A}_{ik} - \mathcal{D}_{ik}}{G} \tag{6.220}$$

where $\mathcal{A}_{ik}$ denotes the number of agreements in the corresponding bits of $\mathbf{p}_i$ and $\mathbf{p}_k$, and $\mathcal{D}_{ik}$ denotes the number of disagreements. As the spreading factor G increases, it becomes increasingly likely that R_{ik} is small, and hence $\mathbf{R}$ approximates a diagonal matrix, even if the spreading sequences are not selected to be orthogonal. If the spreading sequences are modeled as random binary sequences, then $E[R_{ik}] = 0$ and $var[R_{ik}] = G^{-1}, i \neq k$, which shows the advantage of a large spreading factor.

As an example, consider synchronous communications with $K = 2$ and $R_{01} = R_{10} = \rho$. The correlation matrix and its inverse are

$$\mathbf{R} = \begin{bmatrix} 1 & \rho \\ \rho & 1 \end{bmatrix}, \qquad \mathbf{R}^{-1} = \frac{1}{1-\rho^2}\begin{bmatrix} 1 & -\rho \\ -\rho & 1 \end{bmatrix}. \tag{6.221}$$

Equation (6.214) indicates that the symbol estimates are $\widehat{d}_0 = \text{sgn}(z_1 - \rho z_2)$ and $\widehat{d}_1 = \text{sgn}(z_2 - \rho z_1)$, where $z_i = \mathbf{p}_i^T \mathbf{y}$, $i = 1, 2$, are the correlator outputs. Since $R_{00}^{-1} = R_{11}^{-1} = (1-\rho^2)^{-1}$,

$$P_s(k) = Q\left(\sqrt{\frac{2\mathcal{E}_k\,(1-\rho^2)}{N_0}}\right), \qquad k = 0, 1. \tag{6.222}$$

If $\rho \leq 1/2$, the required energy increase or shift in each $P_s(k)$ curve to accommodate multiple-access interference is less than 1.25 dB.

To demonstrate analytically the advantage of the decorrelating detector, consider synchronous communications and a conventional receiver with a filter bank of K correlators. Each correlator is a matched filter for a single user. The receiver synchronizes with the signal of user k, and hence A_k is assumed to be real-valued with zero phase. Equation (6.200) implies that the output of correlator k is

$$r_k = \mathbf{p}_k^T \mathbf{y} = GA_k d_k + G \sum_{\substack{i=0 \\ i \neq k}}^{K-1} R_{ki} A_i d_i + \mathbf{p}_k^T \mathbf{n}. \tag{6.223}$$

The set of K symbols is determined by

$$\widehat{\mathbf{d}} = \text{sgn}[\text{Re}(\mathbf{P}^{\mathbf{T}}\mathbf{y})]. \tag{6.224}$$

By symmetry, we can assume that $d_k = 1$ in the evaluation of the symbol error probability. Let $\mathbf{D}_k$ denote the $(K-1)$-dimensional vector of all the d_i, $i \neq k$. Conditioning on $\mathbf{D}_k$, we find that a symbol error occurs if $Re(\mathbf{p}_k^T \mathbf{n})$ exceeds the real part of the first two terms in (6.223). Since $var[Re(\mathbf{p}_k^T \mathbf{n})] = GN_0/2$, the conditional symbol error probability for user k is

$$P_s\,(k|\mathbf{D}_k) = Q\left(\sqrt{\frac{2\mathcal{E}_k}{N_0}}(1 + B_k)\right) \tag{6.225}$$

where

$$B_k = \sum_{\substack{i=0 \\ i\neq k}}^{K-1} d_i\, R_{ki} \frac{\text{Re}(A_i)}{A_k}. \tag{6.226}$$

If all symbol sets are equally likely, then the symbol error probability for user k is

$$P_s(k) = 2^{-(K-1)} \sum_{n=1}^{2^{K-1}} P_s\,(k|\,\mathbf{D}_{kn}) \tag{6.227}$$

where $\mathbf{D}_{kn}$ is the nth choice of the vector $\mathbf{D}_k$, which can take 2^{K-1} values.

For $K = 2$ with $R_{01} = R_{10} = \rho$ and $C = \text{Re}(A_1)/A_0$, the preceding equations yield the symbol error probability for user 0 and the conventional detector:

$$\begin{aligned} P_s(0) &= \frac{1}{2}Q\left(\sqrt{\frac{2\mathcal{E}_1}{N_0}}\,(1-\rho C)\right) + \frac{1}{2}Q\left(\sqrt{\frac{2\mathcal{E}_1}{N_0}}\,(1+\rho C)\right) \\ &= \frac{1}{2}Q\left(\sqrt{\frac{2\mathcal{E}_1}{N_0}}\,(1-|\rho| C)\right) + \frac{1}{2}Q\left(\sqrt{\frac{2\mathcal{E}_1}{N_0}}\,(1+|\rho| C)\right). \end{aligned} \tag{6.228}$$

The symbol error probability for user 2 is given by a similar equation. Since the second term in (6.228) is less than or equal to the first term, $P_s(0)$ is upper bounded by twice the first term. Using this upper bound and comparing (6.228) with (6.222), we observe that if

$$C > \frac{1-\sqrt{1-\rho^2}}{|\rho|}, \quad \rho \neq 0 \tag{6.229}$$

then the decorrelating detector usually outperforms the conventional detector. Since $0 < \rho \leq 1$, the right-hand side of (6.229) is upper bounded by unity, and hence

$C > 1$ or $\mathrm{Re}(A_1) > A_0$ is usually sufficient for the decorrelating detector to be advantageous relative to the conventional detector.

If a direct-sequence system applies the output of a decorrelating detector to a channel decoder, then it is desirable for the detector to make soft rather than hard decisions. Soft estimated symbols can be produced by eliminating the signum function in (6.214) or replacing it with a different nonlinear function. To exploit the fact that $d_k = +1$ or -1, $k = 0, 1, \ldots, K-1$, a plausible choice for the nonlinear function is the *clipping function* defined as

$$cl(x) = \begin{cases} +1, & x \geq 1 \\ x, & -1 < x < 1 \\ -1, & x \leq -1. \end{cases} \tag{6.230}$$

The input to the decoder becomes

$$\widehat{d}_k = \mathrm{cl}\left[\left(\left(\mathbf{P}^{\mathbf{T}}\mathbf{P}\right)^{-1}\mathbf{P}^{\mathbf{T}}\mathbf{y}_r\right)_k\right] \tag{6.231}$$

and the final decision about a symbol value is made by applying the signum function to the corresponding decoder output.

For asynchronous communications, an entire message or codeword of N correlated data symbols from each of the K users must be processed because of the timing offsets. The data vector $\mathbf{d}$ and the correlation matrix $\mathbf{R}$ of the decorrelating detector are $NK \times 1$ and $NK \times NK$, respectively. Compared with the optimum detector, the decorrelating detector offers greatly reduced, but still formidable, computational requirements. There is no need to estimate the complex signal amplitudes, but the transmission delays of asynchronous signals must still be estimated, and the computational requirements increase rapidly as N and K increase.

6.5.3 Minimum-Mean-Square-Error Detector

The *minimum-mean-square-error* (MMSE) detector is the receiver that results from a linear transformation of $\boldsymbol{y}$ by the $K \times K$ matrix $\mathbf{L}_0$ such that the metric

$$M = E\left[\|\mathbf{d} - \mathbf{L}\boldsymbol{y}\|^2\right] \tag{6.232}$$

is minimized when $\mathbf{L} = \mathbf{L}_0$. Since $\mathbf{d}$ is a vector, rather than a scalar, the matrix $\mathbf{L}_0$ is not determined by the Wiener–Hopf equation. Let $\mathbf{L}_0$ denote the solution of the equation

$$E\left[\left(\mathbf{d} - \mathbf{L}_0\boldsymbol{y}\right)\boldsymbol{y}^H\right] = \mathbf{0}. \tag{6.233}$$

Let $tr(\mathbf{B})$ denote the trace of the matrix $\mathbf{B}$. Since $\|\mathbf{x}\|^2 = tr(\mathbf{x}\mathbf{x}^H)$ for a vector $\mathbf{x}$,

$$\begin{aligned}\|\mathbf{d}-\mathbf{L}\boldsymbol{y}\|^2 &= tr\left\{[\mathbf{d}-\mathbf{L}_0\boldsymbol{y}+(\mathbf{L}_0-\mathbf{L})\,\boldsymbol{y}]\,[\mathbf{d}-\mathbf{L}_0\boldsymbol{y}+(\mathbf{L}_0-\mathbf{L})\,\boldsymbol{y}]^H\right\}\\ &= \|\mathbf{d}-\mathbf{L}_0\boldsymbol{y}\|^2+\|(\mathbf{L}_0-\mathbf{L})\,\boldsymbol{y}\|^2\\ &\quad +2tr\left[\mathrm{Re}((\mathbf{d}-\mathbf{L}_0\boldsymbol{y})\,\boldsymbol{y}^H\,(\mathbf{L}_0-\mathbf{L})^H)\right].\end{aligned} \tag{6.234}$$

Substitution of this equation into (6.232) and the application of (6.233) yields

$$M = E\left[\|\mathbf{d}-\mathbf{L}_0\boldsymbol{y}\|^2\right]+E\left[\|(\mathbf{L}_0-\mathbf{L})\,\boldsymbol{y}\|^2\right]\geq E\left[\|\mathbf{d}-\mathbf{L}_0\boldsymbol{y}\|^2\right]. \tag{6.235}$$

If $\mathbf{L}=\mathbf{L}_0$, then M is equal to its lower bound. Thus, $\mathbf{L}_0$ minimizes the metric M.

Equation (6.233) has the solution

$$\mathbf{L}_0=\mathbf{R}_{\mathbf{dy}}\mathbf{R}_{\mathbf{y}}^{-1},\quad \mathbf{R}_{\mathbf{dy}}=E\left[\mathbf{d}\boldsymbol{y}^H\right],\quad \mathbf{R}_y=\left\{E\left[\boldsymbol{y}\boldsymbol{y}^H\right]\right\} \tag{6.236}$$

if $\mathbf{R}_{\mathbf{y}}^{-1}$ exists. If the data symbols are independent and equally likely to be $+1$ or -1, then $E[\mathbf{d}\mathbf{d}^{\mathbf{T}}]=\mathbf{I}$, where $\mathbf{I}$ is the identity matrix. Using this result, (6.200), (6.201), $E[\mathbf{n}]=\mathbf{0}$, and the independence of $\mathbf{d}$ and $\mathbf{n}$, we obtain

$$\mathbf{R}_{\mathbf{dy}}=\mathbf{A}^*\mathbf{P}^T,\quad \mathbf{R}_y=\mathbf{P}\,|\mathbf{A}|^2\,\mathbf{P}^T+\frac{N_0}{2}\mathbf{I} \tag{6.237}$$

where $|\mathbf{A}|^2$ is the diagonal matrix with $|A_k|^2$ as its kth component. Substitution of these equations into (6.236) yields

$$\mathbf{L}_0=\mathbf{A}^*\mathbf{P}^T\left(\mathbf{P}\,|\mathbf{A}|^{\mathbf{2}}\,\mathbf{P}^T+\frac{N_0}{2}\mathbf{I}\right)^{-1} \tag{6.238}$$

provided that the inverse exists. Direct matrix multiplication proves the identity

$$\left(\mathbf{P}^T\mathbf{P}+\frac{N_0}{2}|\mathbf{A}|^{-2}\right)|\mathbf{A}|^2\mathbf{P}^T=\mathbf{P}^T\left(\mathbf{P}\,|\mathbf{A}|^2\mathbf{P}^T+\frac{N_0}{2}\mathbf{I}\right). \tag{6.239}$$

Combining this identity with (6.238), we obtain

$$\mathbf{L}_0=\mathbf{A}^{-1}\left(\mathbf{P}^T\mathbf{P}+\frac{N_0}{2}|\mathbf{A}|^{-2}\right)^{-1}\mathbf{P}^T. \tag{6.240}$$

The MMSE decisions are

$$\widehat{\mathbf{d}} = \text{sgn}\left[\text{Re}\left(\mathbf{A}^{-1}\left(\mathbf{P}^T\mathbf{P}+\frac{N_0}{2}|\mathbf{A}|^{-2}\right)^{-1}\mathbf{P}^T\boldsymbol{y}\right)\right] \tag{6.241}$$

and the complete MMSE detector has the structure of Fig. 6.25.

The decorrelating detector for user k is synchronized with this user's signal, and hence A_k is assumed to be real-valued with zero phase. Since the real-valued component A_k^{-1} of $\mathbf{A}^{-1}$ does not affect the decision, the decision for symbol k is

$$\widehat{d}_k = \text{sgn}\left[\left(\left(\mathbf{P}^T\mathbf{P}+\frac{N_0}{2}|\mathbf{A}|^{-2}\right)^{-1}\mathbf{P}^{\mathbf{T}}\boldsymbol{y}_r\right)_k\right] \tag{6.242}$$

where the kth component of $\left(\mathbf{P}^T\mathbf{P}+\frac{N_0}{2}|\mathbf{A}|^{-2}\right)^{-1}\mathbf{P}^{\mathbf{T}}\mathbf{y}_r$ is computed. This equation indicates that the MMSE detector, in contrast to the decorrelating detector, requires estimates of the magnitudes of the signal amplitudes.

Since the received vector is $\mathbf{y} = \mathbf{PAd} + \mathbf{n}$, (6.242) may be expressed as $\widehat{d}_k = \text{sgn}[r_k]$, where

$$r_k = (\mathbf{QR})_{kk}A_k d_k + \sum_{\substack{i=0\\ i\neq k}}^{K-1}(\mathbf{QR})_{ki}\,\text{Re}(A_i)d_i + (\mathbf{n}_{1r})_k \tag{6.243}$$

$(\mathbf{n}_{1r})_k$ is the kth component of $\mathbf{n}_{1r}$, $\mathbf{R}$ is defined by (6.218), and

$$\mathbf{Q} = \left(\mathbf{R}+\frac{N_0}{2G}|\mathbf{A}|^{-2}\right)^{-1}, \quad \mathbf{n}_{1r} = \frac{\mathbf{QP^T}}{G}\mathbf{n}_r. \tag{6.244}$$

Using (6.216), we find that the variance of $(\mathbf{n}_{1r})_k$ is $(N_0/2G)(\mathbf{QRQ})_{kk}$. By symmetry, we can assume that $d_k = 1$ in the evaluation of the symbol error probability. Conditioning on $\mathbf{D}_k$, the $(K-1)$-dimensional vector of all the d_i, $i \neq k$, we find that a symbol error occurs if $(\mathbf{n}_{1r})_k$ causes r_k to have a different sign than d_k. Since the noise has a Gaussian density function, the conditional symbol error probability at the output of decision-device k is

$$P_s(k|\mathbf{D}_k) = Q\left(\sqrt{\frac{2\mathcal{E}_k}{N_0(\mathbf{QRQ})_{kk}}}((\mathbf{QR})_{kk} + B_k)\right), \quad k = 0, 1, \ldots, K-1 \tag{6.245}$$

where $\mathcal{E}_k = A_k^2\,G$ is the symbol energy and

$$B_k = \sum_{\substack{i=0\\ i\neq k}}^{K-1}(\mathbf{QR})_{ki}\frac{\text{Re}(A_i)}{A_k}d_i. \tag{6.246}$$

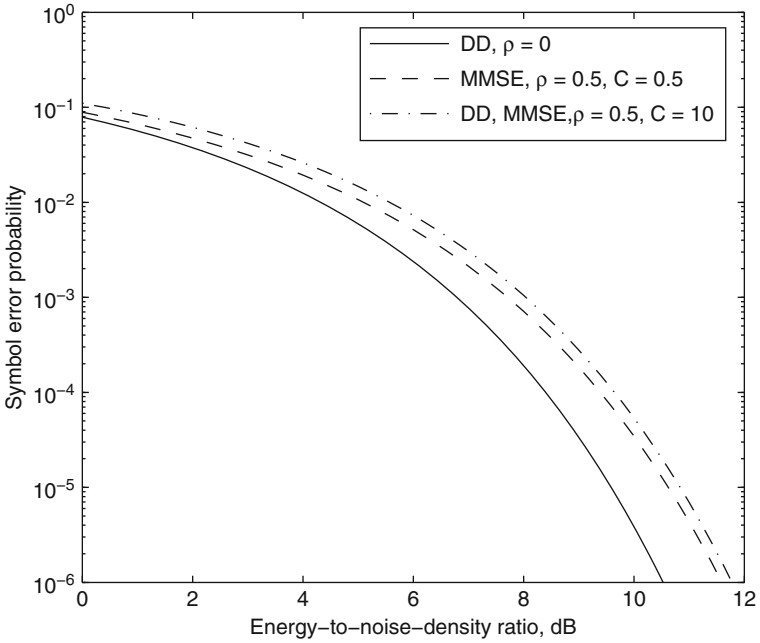

Fig. 6.26 Symbol error probability for decorrelating detector (DD) and MMSE detector when there is one multiple-access interference signal (K = 2)

If all symbol sets are equally likely, then the symbol error probability for user k is given by (6.227). In contrast to the decorrelating detector, the MMSE detector has a symbol error probability that depends on the amplitudes, the symbols, and the spreading sequences of the other users.

As an example, consider multiuser detection for $K = 2$ with $R_{01} = R_{10} = \rho$, $\mathrm{Re}(A_1) = A_1$, and $C = A_1/A_0$. Calculations of the symbol error probability using (6.228), (6.245), and (6.227) indicate that the performance of the MMSE detector degrades with increasing $|\rho|$ but is nearly identical to that of the decorrelating detector, which does not depend on C, when $C \geq 1$. In contrast, if the conventional detector is used, (6.228) indicates that the symbol error probability rapidly degrades as C increases and the signal-to-interference ratio decreases. Representative plots are illustrated in Fig. 6.26. The decorrelating detector (DD) with $\rho = 0$ has the same symbol error probability as a system with no multiuser detection and no multiple-access interference.

If a direct-sequence system applies the output of an MMSE detector to a channel decoder, then it is desirable for the detector to make soft rather than hard decisions. A logical choice for the soft estimated symbol that provides the decoder input is

$$\widehat{d}_k = \mathrm{cl}\left[\left(\left(\mathbf{P}^T\mathbf{P} + \frac{N_0}{2}|\mathbf{A}|^{-2}\right)^{-1}\mathbf{P}^{\mathbf{T}}\boldsymbol{y}_r\right)_k\right] \tag{6.247}$$

and the final decision about a symbol value is made by applying the signum function to the corresponding decoder output.

The MMSE and decorrelating detectors have almost the same computational requirements, and they both have equalizer counterparts, but they differ in several ways. The MMSE detector does not obliterate the multiple-access interference, and hence does not completely eliminate the near-far problem, but does not accentuate the noise to the degree that the decorrelating detector does. Although the MMSE detector tends to suppress strong interference signals, it also suppresses the desired signal to the degree that its spreading sequence is correlated with the spreading sequences of strong interference signals. For practical scenarios, the symbol error probability of the MMSE detector generally tends to be lower than that provided by the decorrelating detector. As $N_0 \to 0$, the MMSE estimate approaches the decorrelating detector estimate. Therefore, the MMSE detector is *asymptotically near-far resistant*. As N_0 increases, the MMSE estimate approaches that of the conventional detector given by (6.224), and hence provides diminished near-far resistance.

For either the MMSE or decorrelating linear detectors to be practical, it is desirable for the spreading sequences to be short. Short sequences ensure that the correlation matrix $\mathbf{R}$ is constant for multiple symbols. The price of short sequences is a security loss and the occasional but sometimes persistent performance loss due to a particular set of relative signal delays. Even with short spreading sequences, variations in $|\mathbf{A}|^2$ make the nonadaptive versions of the MMSE detector much less practical than the adaptive versions.

A major problem with the synchronous versions of the MMSE or decorrelating linear detectors is that they are seldom applicable to practical systems. The synchronous model certainly is applicable to a base station in a cellular network. In that case, however, the use of short orthogonal spreading sequences makes the use of a multiuser detector unnecessary, as a correlator in each receiver suffices to eliminate the multiple-access interference. When an asynchronous multiuser detector is necessary, the computational requirements increase rapidly as N and K increase. Even more significant is the requirement that the receiver must know the delays of the spreading sequences at the receiver input.

6.5.4 Adaptive Multiuser Detection

An *adaptive multiuser detector* [24] is an adaptive system that does not require explicit receiver knowledge of either the spreading sequences or the timing of the multiple-access interference signals. The receiver samples the output of a wideband filter at the chip rate. The use of short spreading sequences affords the opportunity for the adaptive filter to essentially learn the sequence cross-correlations and thereby to suppress the interference. The learning is accomplished by processing a known *training sequence* of L_t pilot symbols for the desired signal during a *training phase*. The LMS algorithm described in Sect. 2.7 may be used as the adaptive filter.

The nth symbol of the known training sequence for user k is denoted by $d_k(n)$, $n = 0, 1, \ldots, L_t - 1$. The nth output vector of the chip-matched filter, which is produced during the reception of symbol n, is denoted by $\mathbf{y}(n)$, $n = 0, 1, \ldots, L_t - 1$. Assuming that chip synchronization has been established with the desired signal, the LMS algorithm iteratively updates the G-dimensional weight vector $\mathbf{W}(n)$ according to the complex form of the LMS algorithm:

$$\mathbf{W}(n+1) = \mathbf{W}(n) + 2\mu\epsilon^*(n)\mathbf{y}(n), \quad n = 0, 1, \ldots, L_t - 1 \tag{6.248}$$

where μ is a constant that regulates the algorithm convergence rate, and

$$\epsilon(n) = d_k(n) - \mathbf{W}^H(n)\mathbf{y}(n). \tag{6.249}$$

This training phase is followed by a *decision-directed phase* that continues the adaptation by feeding back symbol decisions, which are computed as

$$\widehat{d}_k(n) = \text{sgn}[\text{Re}(\mathbf{W}^H(n)\mathbf{y}(n))]. \tag{6.250}$$

Adaptive detectors potentially can achieve much better performance than conventional ones at least if the transmission channel is time-invariant, but coping with fast fading and interference changes sometimes requires elaborate modifications. Appendix C derives the convergence characteristics of the LMS algorithm.

6.5.4.1 Adaptive Blind Multiuser Detector

A *blind multiuser detector* [25] is one that does not require pilot symbols or training sequences. Short spreading sequences are desirable, as long spreading sequences do not possess the cyclostationarity that makes possible many of the advanced signal processing techniques used for blind multiuser detection. *Adaptive blind multiuser detectors* are desirable for accommodating changing channel conditions and for applications such as system recovery, but entail some performance loss and complexity increase relative to adaptive detectors that are trained. Instead of training, adaptive blind multiuser detectors require explicit receiver knowledge of the spreading sequence of the desired signal. Several different adaptive filters [22, 26] can be used as adaptive blind multiuser detectors.

A performance criterion that inherently limits the inadvertent cancellation of the desired signal is the *constrained minimum-power criterion.* For multiuser detection, we assume the components of $\mathbf{y}$, which is a G-dimensional output vector of the chip-matched filter for one symbol, are derived from stationary stochastic processes. The output of a linear detector for user k is $\overline{d}_k = \mathbf{W}^H\mathbf{y}$. The criterion requires that the G-dimensional weight vector $\mathbf{W}$ minimizes the mean output power

$$E\left[\left|\overline{d}_k\right|^2\right] = \mathbf{W}^H\mathbf{R}_y\mathbf{W} \tag{6.251}$$

subject to the constraint

$$\mathbf{W}^H \mathbf{p}_k = 1 \tag{6.252}$$

where $\mathbf{p}_k$ is the vector of the spreading sequence of user k. The constraint prevents distortion of the desired signal.

Applying the method of Lagrange multipliers, we minimize the real scalar

$$H = \mathbf{W}^H \mathbf{R}_y \mathbf{W} + \gamma_1 \left[\text{Re}\left(\mathbf{W}^H \mathbf{p}_k\right)\right] + \gamma_2 \left[\text{Im}\left(\mathbf{W}^H \mathbf{p}_k\right)\right] \tag{6.253}$$

where γ_1 and γ_2 are real-valued Lagrange multipliers. Defining $\gamma = \gamma_1 - j\gamma_2$, we obtain

$$\begin{aligned} H &= \mathbf{W}^H \mathbf{R}_y \mathbf{W} + \text{Re}\left(\gamma \mathbf{W}^H \mathbf{p}_k\right) \\ &= \mathbf{W}^H \mathbf{R}_y \mathbf{W} + \frac{1}{2}\gamma \mathbf{W}^H \mathbf{p}_k + \frac{1}{2}\gamma^* \mathbf{W}^T \mathbf{p}_k. \end{aligned} \tag{6.254}$$

It is assumed that the Hermitian matrix $\mathbf{R}_y$ is positive definite, and hence its inverse exists. Let $\nabla_{\mathbf{w}}$ denote the complex gradient with respect to the weight vector (Sect. 2.7). Setting $\nabla_{\mathbf{w}} H = 0$ and applying the constraint to eliminate γ gives the optimal weight vector:

$$\mathbf{W}_0 = \frac{\mathbf{R}_y^{-1} \mathbf{p}_k}{\mathbf{p}_k^T \mathbf{R}_y^{-1} \mathbf{p}_k} \tag{6.255}$$

where the denominator is a scalar. Combining this equation with (6.251) and (6.252), we find that

$$E\left[\left|\overline{d}_k\right|^2\right] = (\mathbf{W} - \mathbf{W}_0)^H \mathbf{R}_y (\mathbf{W} - \mathbf{W}_0) + \left(\mathbf{p}_k^T \mathbf{R}_y^{-1} \mathbf{p}_k\right)^{-1}. \tag{6.256}$$

Since $\mathbf{R}_y$ is positive definite, this equation indicates that $\mathbf{W}_0$ is the unique weight vector that minimizes $E\left[\left|\overline{d}_k\right|^2\right]$.

The *Frost algorithm* or *linearly constrained minimum-variance algorithm* is an adaptive algorithm that approximates the constrained optimal weight. By the method of steepest descent (Sect. 2.7), the weight vector $\mathbf{W}(n)$ is updated according to

$$\begin{aligned} \mathbf{W}(n+1) &= \mathbf{W}(n) - \mu \nabla_{\mathbf{w}} H\,(n) \\ &= \mathbf{W}(n) - \mu \left[2\mathbf{R}_y \mathbf{W}(n) + \gamma\,(n)\,\mathbf{p}_k\right] \end{aligned} \tag{6.257}$$

where μ is a constant that regulates the algorithm convergence rate. The Lagrange multiplier is chosen so that

$$\mathbf{W}^H(n+1)\mathbf{p}_k = 1. \tag{6.258}$$

Combining this equation with (6.257) and using $\mathbf{p}_k^T \mathbf{p}_k = G$, we find that

$$\gamma(n) = \frac{1}{\mu G}\left[\mathbf{p}_k^T \mathbf{W}(n) - 2\mu \mathbf{p}_k^T \mathbf{R}_y \mathbf{W}(n) - 1\right]. \tag{6.259}$$

Substituting this equation into (6.257) and exploiting that $\mathbf{p}_k^T \mathbf{W}(n)$ and $\mathbf{p}_k^T \mathbf{R}_y \mathbf{W}(n)$ are scalars, we obtain

$$\mathbf{W}(n+1) = \left(\mathbf{I} - \frac{1}{G}\mathbf{p}_k \mathbf{p}_k^T\right)\left[\mathbf{W}(n) - 2\mu \mathbf{R}_y \mathbf{W}(n)\right] + \frac{1}{G}\mathbf{p}_k. \tag{6.260}$$

This equation provides a deterministic algorithm that would be used if $\mathbf{R}_y$ were known. Since it is not, the Frost algorithm approximates $\mathbf{R}_y$ by $\mathbf{y}(n)\mathbf{y}^H(n)$ and uses the linear detector output

$$\overline{d}_k(n) = \mathbf{W}^H(n)\mathbf{y}(n). \tag{6.261}$$

A suitable choice for the initial weight vector is $\mathbf{W}(0) = \mathbf{p}_k / G$ because this choice satisfies the constraint. Thus, the Frost algorithm is

$$\mathbf{W}(0) = \frac{1}{G}\mathbf{p}_k \tag{6.262}$$

$$\mathbf{W}(n+1) = \left(\mathbf{I} - \frac{1}{G}\mathbf{p}_k \mathbf{p}_k^T\right)\left[\mathbf{W}(n) - 2\mu \mathbf{y}(n)\overline{d}_k^*(n)\right] + \frac{1}{G}\mathbf{p}_k. \tag{6.263}$$

The symbol decisions are made according to

$$\widehat{d}_k(n) = \operatorname{sgn}\left\{\operatorname{Re}\left[\overline{d}_k(n)\right]\right\}. \tag{6.264}$$

An important feature of the algorithm is that each iteration automatically corrects for computational errors in the weight vector that prevented exact satisfaction of the constraint during the preceding iteration. These errors often occur during an iteration because of truncation, rounding, or quantization errors in the computer implementation of the algorithm. If the errors are not corrected, they may have a significant cumulative effect after a few iterations. The error-correcting capability of the algorithm is due to the fact that the factor $\mathbf{W}^H(n)\mathbf{p}_k$ was not set to unity in deriving (6.259). Thus, apart from other sources of error, $\mathbf{W}^H(n+1)\mathbf{p}_k = 1$ even if $\mathbf{W}^H(n)\mathbf{p}_k \neq 1$. The convergence characteristics of the Frost algorithm are derived in Appendix C.

6.5.5 *Interference Cancellers*

An *interference canceller* is a multiuser detector that explicitly estimates the interference signals and then subtracts them from the received signal to produce the desired signal. Interference cancellers may be classified as *successive interference*

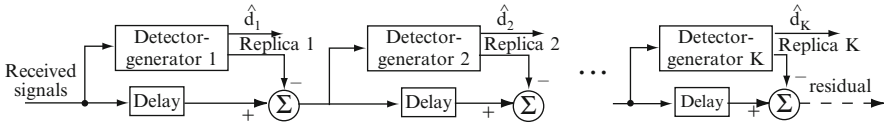

Fig. 6.27 Successive interference canceller with K detector-generators to produce signal estimates for subtraction

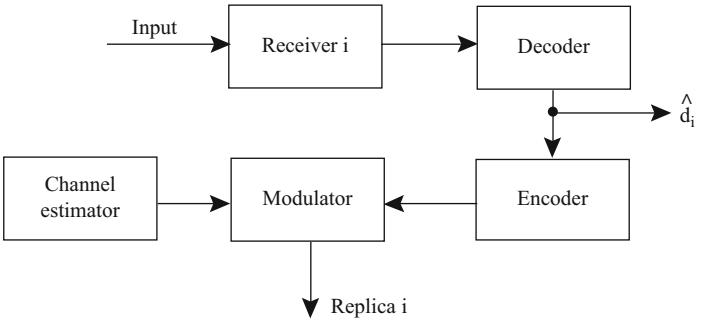

Fig. 6.28 Structure of detector-generator for signal i

cancellers in which the subtractions are done sequentially, *parallel interference cancellers* in which the subtractions are done simultaneously, or hybrids of these types. Only the basic structures and features of the successive and parallel cancellers are presented subsequently. A large number of alternative versions, some of them hybrids, adaptive, or blind, have been proposed [25]. Some type of interference canceller is by far the most practical multiuser detector for an asynchronous DS/CDMA network, especially if long spreading sequences are planned. The computational complexity of an interference canceller is proportional to spreading factor G, whereas the computational complexity of a decorrelating or MMSE detector is proportional to G^3.

6.5.5.1 Successive Interference Canceller

Figure 6.27 is a functional block diagram of a successive interference canceller, which uses nonlinear replica generations and subtractions to produce estimates of the symbol streams transmitted by the K users. The outputs of a set of K receivers with correlators are applied to level detectors that order the K received signals according to their estimated power levels. This ordering determines the placement of the detector-generators in Fig. 6.22, which are ordered according to descending power levels. Detector-generator i, $i = 1, 2, \ldots, K$, corresponds to the ith strongest signal.

Detector-generator i, which has structure depicted in Fig. 6.28, produces a replica of each received symbol of signal i. Receiver i has the form of Fig. 2.14 for

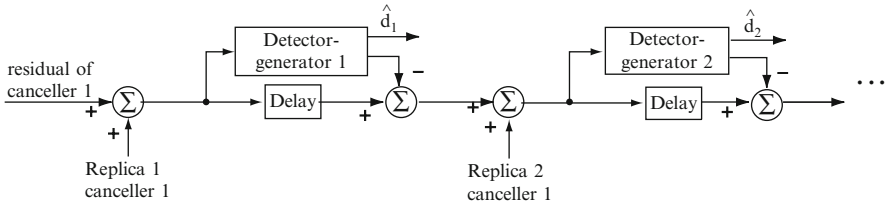

Fig. 6.29 Second canceller of multistage canceller using successive interference cancellers

BPSK modulation or the form of Fig. 2.17 for quaternary modulation. The decoder provides a hard estimate $\widehat{d}_i$ of each symbol. These symbols are encoded and applied to a modulator. The modulator generates a replica of signal i by adding the spreading sequence and modulating the chip waveforms. The channel estimator provides the channel amplitude and phase information that are applied to the modulator to compensate for the effects of the propagation channel. The channel estimator may use known pilot or training symbols to determine the channel response.

If the decoder makes a symbol error, then the amplitude of the interference that enters the next stage of the canceller of Fig. 6.27 is doubled. Any error in the replica generation adversely affects subsequent symbol estimates and replicas. The replica of signal i is generated and sent to the corresponding subtracter, which produces a difference signal with most of the interference due to signals i, $i-1,\ldots,1$ eliminated. Each difference signal is applied to the detector-generator for the next strongest received signal. Since each delay in Fig. 6.27 exceeds one symbol in duration, the overall processing delay of the successive interference canceller is one of its disadvantages.

The first canceller stage eliminates the strongest signal, thereby immediately alleviating the near-far problem for weaker signals while exploiting the superior detectability of the strongest signal. The amount of interference removal from a signal increases from the strongest received signal to the weakest one. Any imperfections in the interference cancellation rapidly reduce its value. In a DS/CDMA network, only a few interference signals need to be canceled to obtain the bulk of the available performance gain [27]. The delay introduced, the impact of cancellation errors, and the implementation complexity may limit the number of useful canceller stages to fewer than K, and a set of conventional detectors may be needed to estimate some of the symbol streams. At low SINRs, inaccurate cancellations may cause the canceller to lose its advantage over the conventional detector. The successive interference canceller requires known spreading sequences and timing of all signals. The computational complexity and the overall processing delay both increase linearly with the number of users.

A *multistage interference canceller* comprising more than one successive interference canceller potentially improves performance by repeated cancellations if the delay and complexity can be accommodated. The second canceller or stage of a multistage canceller is illustrated in Fig. 6.29. The input is the residual of canceller 1, which is shown in Fig. 6.27. As shown in Fig. 6.29, replica 1 of canceller 1 is added

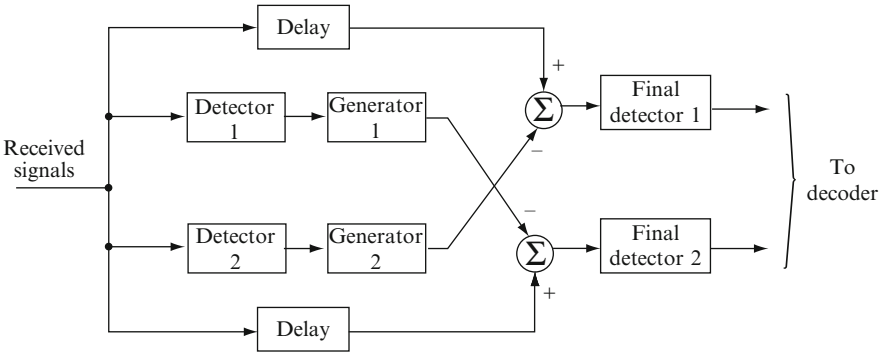

Fig. 6.30 Parallel interference canceller for two signals

to the residual to produce a sum signal that is applied to detector-generator 1. Since most of the interference has been removed from the residual, detector-generator 1 can produce an improved estimate $\widehat{d}_1$ and an improved replica of signal 1, which is then subtracted from the sum signal. The resulting difference signal contains less interference than the corresponding difference signal in Fig. 6.27. Subsequently, other replicas from canceller 1 are added and corresponding improved replicas are subtracted. The final estimated symbol streams are produced by the final canceller. Rake combining of multipath components may be incorporated into a multistage or single-stage interference canceller to improve performance in a fading environment [28].

6.5.5.2 Parallel Interference Canceller

A parallel interference canceller detects, generates, and then subtracts all multiple-access interference signals simultaneously, thereby avoiding the delay inherent in successive interference cancellers. A parallel interference canceller for two signals is diagrammed in Fig. 6.30. Each detector-generator pair may be implemented as shown in Fig. 6.28. Each of the final detectors includes a digital matched filter and a decision device that produce soft or hard decisions, which are applied to the decoder. Since each strong signal enters each detector-generator simultaneously and the initial detections influence the final ones, the parallel interference canceller is not as effective in suppressing the near-far problem as the successive interference canceller. However, if a CDMA network uses power control, the first several stages of a successive interference canceller may provide less accurate detected symbols than those provided by a one-stage parallel interference canceller. The primary reason is the presence of uncanceled multiple-access interference in each replica generated by a successive interference canceller. Power control also relieves the timing synchronization requirements in cancellers.

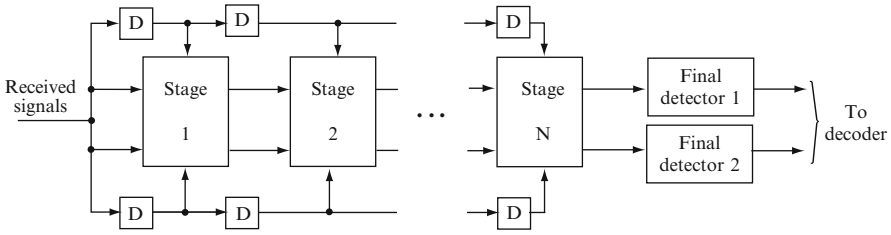

Fig. 6.31 Multistage parallel interference canceller for two signals. D = delay

A better suppression of the near-far problem is provided by the *multistage parallel interference canceller*, in which each stage is similar but has an improved input that results in an improved output. Figure 6.31 shows the multistage canceller for two signals. The initial stage may consist of a parallel interference canceller, successive interference canceller, decorrelating detector, or MMSE detector. Each subsequent stage has the form of Fig. 6.30.

6.5.6 Multiuser Detector for Frequency Hopping

In an FH/CDMA network, the rough coordination of the transmit times of the users and the existence of switching times will limit or eliminate the collisions among users and make multiuser processing unnecessary. In a completely asynchronous network, multiuser detection may be desirable, but it is much more challenging for frequency-hopping systems than for direct-sequence systems. An optimum multiuser detector requires that the receiver knows the hopping patterns and hop transition times of all users to be detected and can simultaneously demodulate the signals at all carrier frequencies. These requirements are completely unrealistic for any practical network of frequency-hopping systems. A much more practical multiuser detector exploits differences in the hop transition times of the users in an asynchronous frequency-hopping network [29]. These differences expose portions of the desired and interfering signals in a way that can be exploited by an iterative demodulator, channel estimator, and decoder. The receiver synchronizes with the frequency-hopping pattern of the desired signal and estimates the timing information of the interfering signals. An important part of the processing is the use of the expectation-maximization algorithm (Chap. 8) for channel estimation. For both nonfading and Rayleigh fading channels, this multiuser detector accommodates more strong interference signals than a conventional frequency-hopping receiver, but alternative and more robust frequency-hopping systems are possible (Chap. 8).

Problems

6.1. Using the method outlined in the text, derive (6.19).

6.2. A Gold sequence is constructed from a maximal sequence with characteristic polynomial $1 + x^2 + x^3$. The second sequence is obtained by decimation of the maximal sequence by $q = 3$. (a) Find one period of each of the two sequences. Is the second sequence maximal? (b) List the seven cross-correlation values of this pair of sequences. Show that they are a preferred pair.

6.3. The characteristic polynomials for generating Gold sequences of length 7 are: $f_1(x) = 1+x+x^3$ and $f_2(x) = 1+x^2+x^3$. (a) What is the generating function for the maximal Gold sequence generated by $f_1(x)$ and initial contents l00? (b) What is the generating function for the maximal Gold sequence generated by $f_2(x)$ and initial contents 100? (c) What is the general expression for the generating function of an arbitrary nonmaximal Gold sequence? (d) What is the generating function for the Gold sequence generated by adding the sequences in (a) and (b)? (e) What is the value at $k = 0$ of the periodic cross correlation between the sequences in (a) and (b)?

6.4. A small set of Kasami sequences is formed by starting with the maximal sequence generated by the characteristic polynomial $1 + x^2 + x^3 + x^4 + x^8$. After decimation by q, a second sequence with characteristic polynomial $1 + x + x^4$ is found. (a) What is the value of q? How many sequences are in the set? What is the period of each sequence? What is the peak magnitude of the periodic cross-correlation? Draw a block diagram of the generator of the small Kasami set. (b) Prove whether or not the second sequence is maximal.

6.5. The small set of the preceding problem is extended to a large set of Kasami sequences by a decimation of the original maximal sequence by q_1. A third sequence with characteristic polynomial $1 + x^2 + x^3 + x^4 + x^5 + x^7 + x^8$ is found. (a) What is the value of q_1? How many sequences are in the large set? What is the period of each sequence? What is the peak magnitude of the periodic cross-correlation? Draw a block diagram of the generator of the large Kasami set. (b) Prove whether or not the third sequence is maximal.

6.6. Show that (6.33) is equivalent to (6.19) when $d_{-1}^{(i)} = d_0^{(i)}$.

6.7. For the feedback shift register of Fig. 6.4 with initial contents of 002, list the successive contents during one period of the output sequence.

6.8. Apply Jensen's inequality to (2.130) with $X = \cos 2\phi$ and use the fact that $E[\cos 2\phi] = 0$ to obtain a lower bound identical to the right-hand side of (2.133). Thus, the *balanced QPSK* system, for which $d_1(t) = d_2(t)$, provides a lower symbol error probability against tone interference than the dual quaternary or QPSK system for which $d_1(t) \neq d_2(t)$. What is the lower bound on $\mathcal{E}_s$ that provides a sufficient convexity condition for all f_d?

6.9. Derive (6.71) for both rectangular and sinusoidal chip waveforms.

6.10. Use bounding and approximation methods to establish (6.96).

6.11. Derive (6.121) and (6.122). For the latter, start by observing that $var\ (I_{te}) = E_{\mathbf{K}}\{E[I_{te}^2\,|\mathbf{K}\,\}-(E_{\mathbf{K}}\{E[I_{te}\,|\mathbf{K}\,\})^2$, where $\mathbf{K}$ represents the set $\{K_i\}$.

6.12. Using the methods outlined in the text, derive (6.143) and then (6.144).

6.13. Using the methods outlined in the text, derive (6.146) and then (6.147).

6.14. Consider an FH/CDMA network with two mobiles that communicate with a base station. The modulation is ideal DPSK, the receiver uses EGC, and both the environmental noise and the spectral splatter are negligible. The propagation conditions are such that one signal arriving at the base station is 10 dB stronger than the other one during a time interval without power control. Use (5.133) and (5.176) with $L = 1$ and $L = 2$ to assess the relative merits for each user of introducing power control in the presence of Rayleigh fading. Assume that $M_1 = 10$, which reduces the channel-symbol error probability, and that an acceptable average channel-symbol error probability is 0.02.

6.15. Consider the maximum-likelihood detector when all the spreading sequences are mutually orthogonal. Use (6.200) to show that the detector decouples the data symbols in the sense that the decision for each data symbol is not influenced by the other data symbols.

6.16. A simpler derivation of the decorrelating detector is available if one starts with the assumption that the detector has the filter bank as its first stage. Starting with this assumption and (6.200), derive the decorrelating detector. Show that the multiple-access interference is completely decorrelated from the estimator $\widehat{\mathbf{d}}$.

6.17. Consider the decorrelating detector for two synchronous users. (a) Evaluate the two sampled correlator outputs when the received signal is (6.198). (b) Use the linear transformation matrix to construct a detailed block diagram of the receiver. Write equations for the symbol estimates. (c) Evaluate the noise covariance matrix at the input and at the output of the linear transformer.

6.18. Consider the conventional detector for two synchronous users. (a) Evaluate $P_s(0)$ as $N_0 \to 0$ for the three cases: $\rho C \leq 1$, $\rho C \geq 1$, and $\rho C = 1$. (b) For $\rho C \leq 1$, find the noise level that minimizes $P_s(0)$.

6.19. Consider the MMSE and decorrelating detectors for synchronous users with orthogonal spreading sequences. Show that the symbol error probability is identical for both detectors.

6.20. Consider the MMSE receiver for two synchronous users. (a) Evaluate the linear transformation matrix. (b) Construct a detailed block diagram of the receiver. (c) Write equations for the symbol estimates.

References

1. F. Adachi, M. Sawahashi, and K. Okawa, "Tree-structured Generation of Orthogonal Spreading Codes with Different Lengths for Forward Link of DS-CDMA Mobile Radio," *IEE Electronics Letters*, pp. 27-28, Jan. 1997.
2. D. S. Saini and M. Upadhyay, "Multiple Rake Combiners and Performance Improvement in 3G and Beyond WCDMA Systems," *IEEE Trans. Veh. Technol*., vol. 58, pp. 3361–3370, Sept. 2009.
3. D. V. Sarwate and M. B. Pursley, "Crosscorrelation Properties of Pseudorandom and Related Sequences," *Proc. IEEE*, vol. 68, pp. 593–619, May 1980.
4. M. B. Pursley, "Spread-Spectrum Multiple-Access Communications," in *Multi-User Communications Systems*, G. Longo, ed., New York: Springer-Verlag, 1981.
5. M. B. Pursley, D. V. Sarwate, and W. E. Stark, "Error Probability for Direct-Sequence Spread-Spectrum Multiple-Access Communications—Part 1: Upper and Lower Bounds," *IEEE Trans. Commun.*, vol. 30, pp. 975–984, May 1982.
6. A. R. Hammons and P. V. Kumar, "On a Recent 4-Phase Sequence Design for CDMA," *IEICE Trans. Commun.*, vol. E76-B, pp. 804–813, Aug. 1993.
7. T. G. Macdonald and M. B. Pursley, "The Performance of Direct-Sequence Spread Spectrum with Complex Processing and Quaternary Data Modulation," *IEEE J. Select. Areas Commun.*, vol. 18, pp. 1408–1417, Aug. 2000.
8. S. Xie and S. Rahardja, "Performance Evaluation for Quaternary DS-SSMA Communications with Complex Signature Sequences over Rayleigh-fading Channels," *IEEE Trans. Wireless Commun*., vol. 4, pp. 266–77, Jan. 2005.
9. D. Torrieri, "Performance of Direct-Sequence Systems with Long Pseudonoise Sequences," *IEEE J. Select. Areas Commun.*, vol. 10, pp. 770–781, May 1992.
10. G. Zang and C. Ling, "Performance Evaluation for Band-limited DS-CDMA Systems Based on Simplified Improved Gaussian Approximation," *IEEE Trans. Commun.*, vol. 51, pp. 1204–1213, July 2003.
11. D. Torrieri, "Instantaneous and Local-Mean Power Control for Direct-Sequence CDMA Cellular Networks," *IEEE Trans. Commun.*, vol. 50, pp. 1310–1315, Aug. 2002.
12. G. Stuber, *Principles of Mobile Communication, 2nd ed.* Boston: Kluwer Academic, 2001.
13. I. S. Gradsteyn and I. M. Ryzhik, *Tables of Integrals, Series, and Products, 6th ed.* San Diego: Academic Press, 2000.
14. M. Zorzi, "On the Analytical Computation of the Interference Statistics with Applications to the Performance Evaluation of Mobile Radio Systems," *IEEE Trans. Commun.*, vol. 45, pp. 103–109, Jan. 1997.
15. C. C. Lee and R. Steele, "Closed-loop Power Control in CDMA Systems," *IEE Proc.-Commun.*, vol. 143, pp. 231–239, Aug. 1996.
16. B. Levy, Principles of Signal Detection and Parameter Estimation. New York: Springer, 2008.
17. A. J. Viterbi, *CDMA Principles of Spread Spectrum Communication*. Reading, MA: Addison-Wesley, 1995.
18. C. Ding, Y. Yang, and X. Tang, "Optimal Sets of Frequency Hopping Sequences from Linear Cyclic Codes," *IEEE Trans. Inf. Theory, vol. 56,* pp. 3605–3612, July 2010.
19. D. Peng and P. Fan, "Lower bounds on the Hamming auto- and cross correlations of frequency-hopping sequences," *IEEE Trans. Inf.* Theory, vol. 50, pp. 2149–2154, Sept. 2004.
20. D. Torrieri, "Mobile Frequency-Hopping CDMA Systems," *IEEE Trans. Commun.*, vol. 48, pp. 1318–1327, Aug. 2000.
21. F. Adachi and J. D. Parsons, "Unified Analysis of Postdetection Diversity for Binary Digital FM Radio," *IEEE Trans. Veh. Technol*., vol. 37, pp. 189–198, Nov. 1988.
22. D. Torrieri, *Principles of Secure Communication Systems, 2nd ed.* Boston: Artech House, 1992.
23. J. G. Proakis and M. Salehi, *Digital Communications, 5th ed.* New York: McGraw-Hill, 2008.
24. S. Verdu, *Multiuser Detection*. New York: Cambridge University Press, 1998.

25. X. Wang and H. V. Poor, *Wireless Communication Systems*, Upper Saddle River, NJ: Prentice-Hall, 2004.
26. S. Haykin, *Adaptive Filter Theory, 4th ed.* Upper Saddle River, NJ: Prentice-Hall, 2002.
27. S. P. Weber, J. G. Andrews, X. Yang, and G. de Veciana, "Transmission Capacity of Wireless Ad Hoc Networks with Successive Interference Cancellation," *IEEE Trans. Inf. Theory, vol. 53,* pp. 2799–2812, Aug. 2007.
28. M. Sawahashi, K. Higuchi, H. Andoh, and F. Adachi, "Experiments on Pilot Symbol-Assisted Coherent Multistage Interference Canceller for DS-CDMA Mobile Radio," *IEEE J. Select. Areas Commun.*, vol. 20, pp. 433–449, Feb. 2002.
29. X. Tan and J. M. Shea, "An EM Approach to Multiple-Access interference Mitigation in Asynchronous Slow FHSS Systems," *IEEE Trans. Wireless Commun.*, vol. 7, pp. 2661-2670, July 2008.

Chapter 7
Detection of Spread-Spectrum Signals

The ability to detect the presence of spread-spectrum signals is often required by cognitive radio, ultra-wideband, and military systems. This chapter presents an analysis of the detection of spread-spectrum signals when the spreading sequence or the frequency-hopping pattern is unknown and cannot be accurately estimated by the detector. Thus, the detector cannot mimic the intended receiver, and alternative procedures are required. The goal is limited in that only detection is sought, not demodulation or decoding. Nevertheless, detection theory leads to impractical devices for the detection of spread-spectrum signals. An alternative procedure is to use a radiometer or energy detector, which relies solely on energy measurements to determine the presence of unknown signals. The radiometer has applications not only as a detector of spread-spectrum signals, but also as a sensing method in cognitive radio and ultra-wideband systems.

7.1 Detection of Direct-Sequence Signals

The results of Sect. 2.3 indicate that the maximum magnitude of the power spectral density of a direct-sequence signal with a random spreading sequence is $A^2T_c/4 = \mathcal{E}_s/2G$, where $\mathcal{E}_s$ is the symbol energy and G is the processing gain. A spectrum analyzer usually cannot detect a signal with a power spectral density below that of the background noise, which has spectral density $N_0/2$. Thus, a received $\mathcal{E}_s/N_0 > G$ is an approximate necessary, but not sufficient, condition for a spectrum analyzer to detect a direct-sequence signal. If $\mathcal{E}_s/N_0 < G$, detection may still be probable by other means. If not, the direct-sequence signal is said to have a *low probability of interception*.

Detection theory leads to various detection receivers depending on precisely what is assumed to be known about the signal to be detected. We make the idealized assumptions that the chip timing of the spreading waveform is known and that whenever the signal is present, it is present during the entire observation interval. The spreading sequence is modeled as a random binary sequence, which implies that

D. Torrieri, *Principles of Spread-Spectrum Communication Systems*,
DOI 10.1007/978-1-4419-9595-7_7, © Springer Science+Business Media, LLC 2011

a time shift of the sequence by a chip duration corresponds to the same stochastic process. Thus, to account for uncertainty in the chip timing, one might partition a chip interval of known duration among several parallel detectors each of which implements a different chip timing.

Consider the detection of a direct-sequence signal with PSK modulation:

$$s(t) = \sqrt{2S}p(t)\cos(2\pi f_c t + \theta), \quad 0 \le t \le T \tag{7.1}$$

where S is the average signal power, f_c is the known carrier frequency, and θ is the carrier phase assumed to be constant over the *observation interval* $0 \le t \le T$. The spreading waveform $p(t)$, which subsumes the random data modulation, is

$$p(t) = \sum_{i=-\infty}^{\infty} p_i \psi(t - iT_c) \tag{7.2}$$

where the $\{p_i\}$ are modeled as a random binary sequence, and $\psi(t)$ is the chip waveform. To determine whether a signal $s(t)$ is present based on the observation of the received signal, classical detection theory requires that one choose between the hypothesis H_1 that the signal is present and the hypothesis H_0 that the signal is absent. Over the observation interval, the received signal under the two hypotheses is

$$r(t) = \begin{cases} s(t) + n(t), & H_1 \\ n(t), & H_0 \end{cases} \tag{7.3}$$

where $n(t)$ is zero-mean, white Gaussian noise with two-sided power spectral density $N_0/2$.

Consider the vector space of continuous-time, finite-energy signals defined over the observation interval (Sect. 4.1). The coefficients of the observed waveform in terms of the N_s orthonormal basis functions may be used as the received vector $\mathbf{r} = [r_1\, r_2 \ldots r_{N_s}]$. Let $f(\mathbf{r}|H_1, \theta, \mathbf{p})$ denote the conditional density function of $\mathbf{r}$ given hypothesis H_1, the value of θ, and the random binary sequence $\{p_i\}$. Let $f(\mathbf{r}|H_0)$ denote the conditional density function of $\mathbf{r}$ given hypothesis H_0, The *average likelihood ratio* of the received signal $r(t)$ [1], which is compared with a threshold for a detection decision, is

$$\Lambda(r(t)) = \lim_{N_s \to \infty} \frac{E_{\theta,p}[f(\mathbf{r}|H_1, \theta, \mathbf{p})]}{f(\mathbf{r}|H_0)} \tag{7.4}$$

where $E_{\theta,p}$ is the expectation over θ and the random sequence $\{p_i\}$. The basis functions $\{\phi_i(t)\}$, $i = 1, 2, ..., N_s$ are orthonormal over the observation interval, which implies that

$$\int_0^T \phi_i(t)\phi_k(t)dt = \delta_{ik}, \quad i \ne k. \tag{7.5}$$

The waveforms $r(t)$, $s(t)$, and $n(t)$ have the expansions

$$r(t) = \lim_{N_s\to\infty} \sum_{i=1}^{N_s} r_i \phi_i(t), \quad s(t) = \lim_{N_s\to\infty} \sum_{i=1}^{N_s} s_i \phi_i(t), \quad n(t) = \lim_{N_s\to\infty} \sum_{i=1}^{N_s} n_i \phi_i(t). \tag{7.6}$$

The expansion coefficients r_i, s_i, and n_i are related by $r_i = s_i + n_i$ under hypothesis H_1 and $r_i = n_i$ under hypothesis H_0. Application of (7.5) and (7.6) yields

$$r_i = \int_0^T r(t)\phi_i(t)dt, \quad s_i = \int_0^T s(t)\phi_i(t)dt, \quad n_i = \int_0^T n(t)\phi_i(t)dt,$$
$$i = 0, 1, \ldots, N_s. \tag{7.7}$$

Since the noise is zero-mean, the expected values of r_i under the two hypotheses are

$$E[r_i \mid H_1] = s_i, \quad E[r_i \mid H_0] = 0. \tag{7.8}$$

The white Gaussian process $n(t)$ has autocorrelation (Appendix A)

$$R_n(\tau) = \frac{N_0}{2}\delta(\tau). \tag{7.9}$$

Using this equation, (7.7) and (7.5), we find that the Gaussian variables n_i and n_k, $i \neq k$, are uncorrelated, and hence statistically independent. The variance of r_i is the same under both hypotheses:

$$var[r_i \mid H_k] = E\left[n_i^2\right] = \frac{N_0}{2}, \quad k = 0, 1. \tag{7.10}$$

The independence of the $\{n_i\}$ implies the independence of the $\{r_i\}$. Since each coefficient is Gaussian with variance $N_0/2$,

$$f(\mathbf{r}|H_1, \theta, \mathbf{p}) = \prod_{i=1}^{N_s} \frac{1}{\sqrt{\pi N_0}} \exp\left[-\frac{(r_i - s_i)^2}{N_0}\right] \tag{7.11}$$

$$f(\mathbf{r}|H_0) = \prod_{i=1}^{N_s} \frac{1}{\sqrt{\pi N_0}} \exp\left(-\frac{r_i^2}{N_0}\right). \tag{7.12}$$

Substituting these equations into (7.4) and using the continuity of the exponential function, we obtain

$$\Lambda(\mathbf{r}) = E_{\theta,p}\left\{\exp\left[\frac{2}{N_0} \lim_{N_s\to\infty} \sum_{i=1}^{N_s} r_i s_i - \frac{1}{N_0} \lim_{N_s\to\infty} \sum_{i=1}^{N_s} s_i^2\right]\right\}. \tag{7.13}$$

By substituting the orthonormal expansions given by (7.6) into the integral, and using the orthonormality of the basis functions, we obtain

$$\int_0^T r(t)s(t)dt = \lim_{N_s\to\infty} \sum_{i=1}^{N_s} r_i s_i \tag{7.14}$$

$$\int_0^T s^2(t)dt = \lim_{N_s\to\infty} \sum_{i=1}^{N_s} s_i^2. \tag{7.15}$$

By substituting these equations into (7.13), the average likelihood ratio may be expressed in terms of the signal waveforms as

$$\Lambda[r(t)] = E_{\theta,p}\left\{\exp\left[\frac{2}{N_0}\int_0^T r(t)s(t)dt - \frac{\mathcal{E}}{N_0}\right]\right\} \tag{7.16}$$

where $\mathcal{E}$ is the energy in the signal waveform over the observation interval of duration T.

If N is the number of chips, each of duration T_c, received in the observation interval, then there are 2^N equally likely patterns of the spreading sequence. For *coherent detection*, we make the assumption that θ is somehow accurately estimated so that it can be removed from consideration. Mathematically, we set $\theta = 0$ in (7.1), substitute it and (7.2) into (7.16), and evaluate the expectations to obtain

$$\Lambda(r(t)) = \exp\left(-\frac{\mathcal{E}}{N_0}\right)\sum_{j=1}^{2^N}\exp\left[\frac{2\sqrt{2S}}{N_0}\sum_{i=0}^{N-1} p_i^{(j)} r_i'\right] \quad \text{(coherent)} \tag{7.17}$$

where $p_i^{(j)}$ is chip i of pattern j and

$$r_i' = \int_{iT_c}^{(i+1)T_c} r(t)\psi(t - iT_c)\cos(2\pi f_c t)\,dt. \tag{7.18}$$

These equations indicate how $\Lambda(r(t))$ is to be calculated by the ideal coherent detector. The factor $\exp(-\mathcal{E}/N_0)$ is irrelevant in the sense that it can be merged with the threshold level with which the average likelihood ratio is compared.

For the more realistic *noncoherent detection* of a direct-sequence signal, the received carrier phase is assumed to be uniformly distributed over $[0, 2\pi)$. Substituting (7.1) and (7.2) into (7.16), using a trigonometric expansion, dropping the irrelevant factor that can be merged with the threshold level, and then evaluating the expectation over the random binary sequence, we obtain the average likelihood ratio:

$$\Lambda(r(t)) = E_\theta\left\{\sum_{j=1}^{2^N}\exp\left[\frac{2\sqrt{2S}}{N_0}\sum_{i=0}^{N-1} p_i^{(j)}\left(r_{ic}\cos\theta - r_{is}\sin\theta\right)\right]\right\} \tag{7.19}$$

where

$$r_{ic} = \int_{iT_c}^{(i+1)T_c} r(t)\psi\,(t - iT_c)\cos(2\pi f_c t)\,dt \tag{7.20}$$

$$r_{is} = \int_{iT_c}^{(i+1)T_c} r(t)\psi\,(t - iT_c)\sin(2\pi f_c t)\,dt \tag{7.21}$$

and $E_\theta\{\,\}$ denotes the expectation with respect to θ.

Using (1.73) and the uniform distribution of θ, the average likelihood ratio becomes

$$\Lambda(r(t)) = \sum_{j=1}^{2^N} I_0\left(\frac{2\sqrt{2SR_j}}{N_0}\right) \quad \text{(noncoherent)} \tag{7.22}$$

where $I_0(\cdot)$ is the modified Bessel function of the first kind and order 0, and

$$R_j = \left[\sum_{i=0}^{N-1} p_i^{(j)} r_{ic}\right]^2 + \left[\sum_{i=0}^{N-1} p_i^{(j)} r_{is}\right]^2. \tag{7.23}$$

These equations define the optimum noncoherent detector for a direct-sequence signal. The presence of the desired signal is declared if (7.22) exceeds a threshold level.

The implementation of either the coherent or noncoherent optimum detector would be very complicated, and the complexity would grow exponentially with N, the number of chips in the observation interval. Calculations [2] indicate that the ideal coherent and noncoherent detectors typically provide 3 dB and 1.5 dB advantages, respectively, over the far more practical wideband radiometer, which is analyzed in the next section. The use of four or two wideband radiometers, respectively, can compensate for these advantages with less complexity than the optimum detectors. Furthermore, implementation losses and imperfections in the optimum detectors are likely to be significant.

7.2 Radiometer

A *radiometer* or *energy detector* is a device that uses energy measurements to determine the presence of unknown signals [3]. The radiometer is notable for its extreme simplicity and its meager requirement of virtually no information about a target signal other than its rough spectral location. The radiometer has applications not only as a detector of spread-spectrum signals, but also as a sensing method in cognitive radio systems and as a detector in ultra-wideband systems.

Suppose that the signal to be detected is approximated by a zero-mean, white Gaussian process. Consider two hypotheses that both assume the presence of a

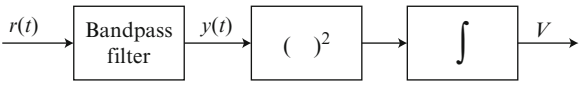

Fig. 7.1 Ideal radiometer

zero-mean, bandlimited white Gaussian process over an observation interval $0 \leq t \leq T$. Under H_0, only noise is present, and the two-sided power spectral density over the signal band is $N_0/2$, while under H_1, both signal and noise are present, and the power spectral density is $N_1/2$ over this band. Using orthonormal basis functions as in the derivation of (7.11) and (7.12), we find that the conditional densities are approximated by

$$f(\mathbf{r}|H_i) = \prod_{k=1}^{\infty} \frac{1}{\sqrt{\pi N_i}} \exp\left(-\frac{r_k^2}{N_i}\right), \qquad i = 0, 1. \tag{7.24}$$

Calculating the likelihood ratio, taking the logarithm, and merging constants with the threshold, we find that the decision rule is to compare

$$V = \sum_{k=1}^{\infty} r_k^2 \tag{7.25}$$

to a threshold. If we use the properties of orthonormal basis functions, then we find that the test statistic is

$$V = \int_0^T r^2(t)dt \tag{7.26}$$

where the assumption of bandlimited processes is necessary to ensure the finiteness of the statistic. A device that implements this test statistic is called an *energy detector* or *radiometer*. Although it was derived for a bandlimited white Gaussian signal, the radiometer is a reasonable configuration for determining the presence of unknown deterministic signals. Although a single radiometer is incapable of determining whether one or more than one signal has been detected, narrowband interference can be rejected by the methods of Sect. 2.7.

Theoretically superior devices require much more information about the target signals than does the radiometer and have other practical limitations. These devices have greatly increased computational complexity compared with the radiometer, and they provide an improved performance primarily when the noise-estimation errors of the radiometer are substantial. As discussed subsequently, appropriate methods will keep these errors and their impact small.

An ideal radiometer has the form shown in Fig. 7.1. The input signal $r(t)$ is filtered, squared, and integrated to produce an output that is compared to a threshold. The receiver decides that the target signal has been detected if and only if the threshold is exceeded. Since accurate analog integrators are difficult to implement and very power consuming, a much more practical radiometer uses bandpass sampling and has the form shown in Fig. 7.2. A practical radiometer with baseband

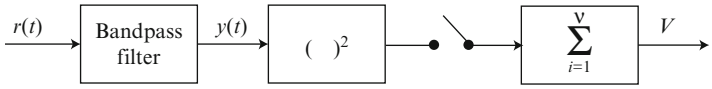

Fig. 7.2 Radiometer with bandpass sampling

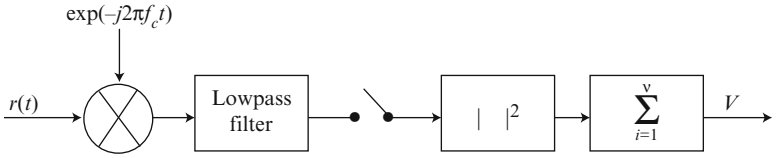

Fig. 7.3 Radiometer with baseband sampling

sampling is shown in Fig. 7.3. The mathematical analyses of all three forms of the radiometer lead to the same performance equations, but the analyses of the two practical radiometers entail significantly fewer approximations and, hence, provide more reliable results. The analysis of the radiometer with bandpass sampling, which is the most frequently implemented radiometer, is provided subsequently.

The bandpass filter in Fig. 7.2 is assumed to approximate an ideal rectangular filter that passes the target signal s(t) with negligible distortion while eliminating interference and limiting the noise. If the target signal has an unknown arrival time, the observation interval during which samples are taken is a sliding window with the oldest sample discarded as soon as a new sample is taken. The filter has center frequency f_c, bandwidth W, and produces the output

$$y(t) = s(t) + n(t) \tag{7.27}$$

where $n(t)$ is bandlimited white Gaussian noise with a two-sided power spectral density equal to $N_0/2$.

A bandlimited deterministic signal can be represented as (Appendix A.1)

$$s(t) = s_c(t)\cos 2\pi f_c t - s_s(t)\sin 2\pi f_c t. \tag{7.28}$$

Since the spectrum of $s(t)$ is confined within the filter passband, $s_c(t)$ and $s_s(t)$ have frequency components confined to the band $|f| \leq W/2$. The Gaussian noise emerging from the bandpass filter can be represented in terms of quadrature components as (Appendix A.2)

$$n(t) = n_c(t)\cos 2\pi f_c t - n_s(t)\sin 2\pi f_c t \tag{7.29}$$

where the power spectral densities of $n_c(t)$ and $n_s(t)$ are

$$S_c(f) = S_s(f) = \begin{cases} N_0\,, & |f| \leq W/2 \\ 0\,, & |f| > W/2 \end{cases}. \tag{7.30}$$

The associated autocorrelation functions are

$$R_c(\tau) = R_s(\tau) = \sigma^2 sinc(W\tau) \tag{7.31}$$

where $\sigma^2 = N_0 W$ is the noise power and $sinc(x) = sin(x)/x$.

Let v denote the number of samples collected by the radiometer of Fig. 7.2. At sampling rate W, the duration of the observation interval of the target signal is $T = \frac{v}{W}$. Substituting (7.28) and (7.29) into (7.27), squaring, and sampling at rate W, we obtain the output

$$\begin{aligned} V = & \frac{1}{2}\sum_{i=1}^{v}\left\{(s_c[i]+n_c[i])^2 + \left(s_s[i]+n_s[i]\right)^2\right\} \\ & + \frac{1}{2}\sum_{i=1}^{v}\left\{(s_c[i]+n_c[i])^2\, c[i] + (s_s[i]+n_s[i])^2\, s[i]\right\} \\ & - \sum_{i=1}^{v}\left\{(s_c[i]+n_c[i])\,(s_s[i]+n_s[i])\, s[i]\right\} \end{aligned} \tag{7.32}$$

where $s_c[i] = s_c(i/W)$, $n_c[i] = n_c(i/W)$, $s_s[i] = s_s(i/W)$, $n_s[i] = n_s(i/W)$, $c[i] = \cos(4\pi f_c i/W)$, and $s[i] = \sin(4\pi f_c i/W)$. This output provides a test statistic that is compared with a threshold.

If $v \gg 1$ and $f_c \gg W$, the fluctuations of $c[i]$ and $s[i]$ cause the final two summations in (7.32) to be negligible compared with the first summation. Equation (7.31) indicates that the zero-mean random variable $n_c(i/W)$ is statically independent of the zero-mean random variable $n_c(j/W)$ for all integers i and j such that $i \neq j$. Similarly, the zero-mean random variables $n_s(i/W)$ and $n_s(j/W)$ are statistically independent if $i \neq j$. Since $n(t)$ is a zero-mean Gaussian process and has a power spectral density that is symmetrical about f_c, $n_c(t)$ and $n_s(t)$ are zero-mean, independent Gaussian processes (Appendix A.2), and hence $n_c(i/W)$ is statically independent of $n_s(j/W)$. Therefore, for the AWGN channel in which $s_c[i]$ and $s_s[i]$ are deterministic, the test statistic may be expressed as

$$V = \frac{\sigma^2}{2}\sum_{i=1}^{v}(A_i^2 + B_i^2) \tag{7.33}$$

where the $\{A_i\}$ and the $\{B_i\}$ are statistically independent Gaussian random variables with unit variances and means

$$m_{1i} = E[A_i] = \frac{s_c[i]}{\sigma} \tag{7.34}$$

$$m_{2i} = E[B_i] = \frac{s_s[i]}{\sigma}. \tag{7.35}$$

The random variable $2V/\sigma^2$ has a *noncentral chi-squared (χ^2) distribution* (Appendix B.1) with $2v$ degrees of freedom and a noncentral parameter

$$\begin{aligned}\lambda &= \sum_{i=1}^{v}\left(m_{1i}^2 + m_{2i}^2\right) = \frac{1}{\sigma^2}\sum_{i=1}^{v}\left(s_c^2[i] + s_s^2[i]\right)\\ &\approx \frac{1}{N_0}\int_0^T \left[s_c^2(t) + s_s^2(t)\right]dt \approx \frac{2}{N_0}\int_0^T s^2(t)dt\\ &= \frac{2\mathcal{E}}{N_0}\end{aligned} \tag{7.36}$$

where $\mathcal{E}$ is the energy of the target signal, and the first approximation is obtained by dividing the integration interval into v parts, each of duration 1/W. Let γ denote the *energy-to-noise-density ratio* $\mathcal{E}/N_0$. From the noncentral χ^2 distribution, the probability density function of V is determined:

$$f_V(x) = \frac{1}{\sigma^2}\left(\frac{x}{\sigma^2\gamma}\right)^{(v-1)/2}\exp\left(-\frac{x}{\sigma^2} - \gamma\right)I_{v-1}\left(\frac{2\sqrt{x\gamma}}{\sigma}\right)u(x) \tag{7.37}$$

where $u(x) = 1, x \geq 0$, and $u(x) = 0, x < 0$, and $I_n(\cdot)$ is the modified Bessel function of the first kind and order n defined by

$$I_n(x) = \sum_{i=0}^{\infty}\frac{(x/2)^{n+2i}}{i!(n+i)!}. \tag{7.38}$$

Substituting (7.38) into (7.37) and setting $\gamma = 0$, we obtain the probability density function in the absence of a signal:

$$f_V(x) = \frac{1}{\sigma^2(v-1)!}\left(\frac{x}{\sigma^2}\right)^{v-1}\exp\left(-\frac{x}{\sigma^2}\right)u(x), \quad \gamma = 0. \tag{7.39}$$

Applying the statistics of Gaussian variables to (7.33), using the fact that a zero-mean Gaussian random variable x has $E[x^4] = 3E[x^2]$, and substituting (7.36) yields

$$E[V] = \sigma^2(v+\gamma) \tag{7.40}$$

$$var(V) = \sigma^4(v+2\gamma). \tag{7.41}$$

Let V_t denote the threshold such that if $V > V_t$, the receiver decides that the target signal is present. Therefore, a false alarm occurs if $V > V_t$ when the target signal is absent. The incomplete gamma function is defined as

$$\Gamma(a,x) = \int_x^{\infty} e^{-t}t^{a-1}dt, \quad Re\,(a) > 0 \tag{7.42}$$

and the gamma function $\Gamma(a) = \Gamma(a, 0)$ is defined as

$$\Gamma(a) = \int_0^\infty e^{-t} t^{a-1} dt, \quad Re\,(a) > 0. \tag{7.43}$$

When $a = n$ is a positive integer, the integration of $\Gamma(n, x)$ by parts $n - 1$ times yields

$$\Gamma(n, x) = (n-1)! e^{-x} \sum_{i=0}^{n-1} \frac{x^i}{i!} \tag{7.44}$$

and $\Gamma(n) = (n-1)!$. Integration of (7.39) over (V_t, ∞), a change of variables, and the application of (7.42) to (7.44) gives the false-alarm probability

$$P_F = \frac{\Gamma(v, V_t/\sigma^2)}{\Gamma(v)} = \exp\left(-\frac{V_t}{\sigma^2}\right) \sum_{i=0}^{v-1} \frac{1}{i!} \left(\frac{V_t}{\sigma^2}\right)^i. \tag{7.45}$$

The threshold V_t is usually set to a value that ensures a specified P_F. Thus, if the estimate of σ^2 is σ_e^2, then

$$V_t = \sigma_e^2 G_v^{-1}(P_F) \tag{7.46}$$

where $G_v^{-1}(\cdot)$ is the inverse function of $P_F(V_t/\sigma^2)$. Since the series in (7.45) is finite, this inverse can be numerically computed by applying Newton's method. If the exact value of the noise power is known, then $\sigma_e^2 = \sigma^2$ in (7.46).

The *generalized Marcum Q-function* is defined as

$$Q_m(\alpha, \beta) = \int_\beta^\infty x \left(\frac{x}{\alpha}\right)^{m-1} \exp\left(-\frac{x^2 + \alpha^2}{2}\right) I_{m-1}(\alpha x) dx \tag{7.47}$$

where m is a nonnegative integer, and α and β are nonnegative real numbers. The target signal is detected if $V > V_t$ when the target signal is present during the observation interval. The integration of (7.38) and a change of variables yields the detection probability

$$P_D = Q_v\left(\sqrt{2\gamma}, \sqrt{2V_t/\sigma^2}\right). \tag{7.48}$$

for the AWGN channel.

For $v > 100$, the generalized Marcum Q-function in (7.48) is difficult to compute and to invert. If $v \gg 1$, the central limit theorem for the sum of independent random variables with finite means and bounded variances indicates that the distribution of V is approximately Gaussian. Using (7.40) and (7.41) and the Gaussian distribution, we obtain

$$P_D \cong Q\left[\frac{V_t/\sigma^2 - v - \gamma}{\sqrt{v + 2\gamma}}\right], \quad v \gg 1 \tag{7.49}$$

where the *Q-function* is defined as

$$Q(x) = \frac{1}{\sqrt{2\pi}} \int_x^\infty \exp\left(-\frac{y^2}{2}\right) dy. \tag{7.50}$$

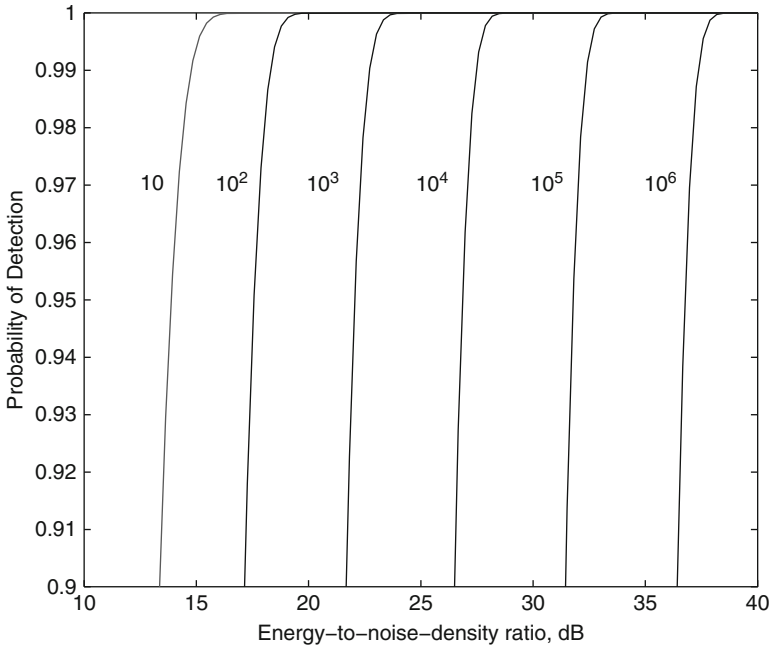

Fig. 7.4 Probability of detection for the AWGN channel, $\sigma_e^2 = \sigma^2$, and $P_F = 10^{-3}$. Plots are labeled with ν

Setting $\gamma = 0$ in (7.49) gives an approximate equation for P_F. Inverting this equation, we obtain an approximate equation for V_t in terms of P_F, σ^2, and ν. Accordingly, if the estimate of σ^2 is σ_e^2, then the threshold required for specified P_F is

$$V_t \cong \sigma_e^2[\sqrt{\nu}Q^{-1}(P_F) + \nu], \quad \nu \gg 1 \tag{7.51}$$

where $Q^{-1}(\cdot)$ denotes the inverse of the Q-function, and ideally $\sigma_e^2 = \sigma^2$. The approximations provided by (7.49) and (7.51) are very accurate if $\nu \geq 100$.

In most applications, there is a required false-alarm rate F, which is the expected number of false alarms per unit time. If successive observation intervals do not overlap each other except possibly at end points, then the required probability of false alarm is $P_F = FT$.

Figure 7.4 depicts P_D versus the energy-to-noise-density ratio γ for a radiometer operating over the AWGN channel with $\sigma_e^2 = \sigma^2$ and $P_F = 10^{-3}$. Equation (7.46) is used to calculate V_t. Equation (7.48) is used to calculate P_D for $\nu = 10$ and $\nu = 100$. For $\nu \geq 1{,}000$, (7.49) is used to calculate P_D. The figure illustrates that the signal energy required to achieve a desired P_D increases as ν increases because additional energy is needed to overcome the noise in each additional sample. However, since the average signal power is equal to $\gamma\sigma^2/\nu$, the average signal power required decreases as ν increases.

If the coherence time of Rayleigh fading exceeds the observation interval, then the energy of a target signal in Rayleigh fading is a random variable with an exponential distribution (Appendix B.4, B.5) and average value $E[\mathcal{E}] = \bar{\mathcal{E}}$. Thus, the average probability of detection is

$$\bar{P}_D = \int_0^\infty \frac{1}{\bar{\gamma}} \exp\left(-\frac{\gamma}{\bar{\gamma}}\right) P_D(\gamma) d\gamma \tag{7.52}$$

where $\bar{\gamma} = \bar{\mathcal{E}}/N_0$ and $P_D(\gamma)$ is given by (7.48). The substitution of (7.47) and (7.38) into (7.48), the interchange of the summation and integration, a change of variables, and the evaluation of the integral using (7.42) gives

$$P_D(\gamma) = \sum_{i=0}^{\infty} \frac{\Gamma(i+\nu, V_t/\sigma^2)\gamma^i e^{-\gamma}}{\Gamma(i+\nu)\Gamma(i+1)}. \tag{7.53}$$

The substitution of this series into (7.52), the interchange of the summation and integration, a change of variables, the evaluation of the integral using (7.43), and the substitution of (7.44) yields

$$\bar{P}_D = \sum_{i=0}^{\infty} \left(\frac{\bar{\gamma}}{\bar{\gamma}+1}\right)^i \sum_{k=0}^{\nu-1+i} \frac{\exp\left(-\frac{V_t}{\sigma^2}\right)}{(\bar{\gamma}+1)\, k!} \left(\frac{V_t}{\sigma^2}\right)^k. \tag{7.54}$$

Dividing the inner series into two series, using (7.45), evaluating one series, and rearranging the remaining two series, we obtain

$$\bar{P}_D = P_F + \sum_{k=\nu}^{\infty} \frac{\exp\left(-\frac{V_t}{\sigma^2}\right)}{(\bar{\gamma}+1)\, k!} \left(\frac{V_t}{\sigma^2}\right)^k \sum_{i=k-\nu+1}^{\infty} \left(\frac{\bar{\gamma}}{\bar{\gamma}+1}\right)^i. \tag{7.55}$$

Evaluation of the inner geometric series, use of the series for the exponential function to express the remaining infinite series for $\bar{P}_D$ as an exponential minus a finite series, and the application of (7.42) yields

$$\bar{P}_D = P_F + \left(\frac{\bar{\gamma}+1}{\bar{\gamma}}\right)^{\nu-1} \exp\left(-\frac{V_t/\sigma^2}{\bar{\gamma}+1}\right) \left[1 - \frac{\Gamma\left(\nu, \frac{\bar{\gamma} V_t/\sigma^2}{\bar{\gamma}+1}\right)}{\Gamma(\nu)}\right] \tag{7.56}$$

for $\bar{\gamma} > 0$. Equations for $\bar{P}_D$ in the presence of Nakagami-m and Ricean fading may be found in [4] and [5].

The outputs of L radiometers, each processing ν samples, can be combined to provide diversity reception for fading channels. In a selection-combining diversity scheme, the largest radiometer output is compared with the threshold V_t to

determine the presence of the target signal. Thus, if each radiometer processes independent noise, the probability of false alarm is

$$P_F = 1 - \prod_{i=1}^{L} [1 - P_{F0}(\sigma_i^2)] \tag{7.57}$$

where σ_i^2 is the noise power of radiometer i and $P_{F0}(\sigma_i^2)$ is given by the right-hand side of (7.45) with $\sigma^2 = \sigma_i^2$. Let σ_e^2 denote an estimated noise power that is known to exceed σ_i^2, $i = 1, 2, ..., L$, with high probability. Using this estimate for each σ_i^2 and solving (7.57) for V_t, we ensure that a specified P_F is almost always achieved. We obtain

$$V_t \cong \sigma_e^2 G_v^{-1} (1 - (1 - P_F)^{1/L}) \tag{7.58}$$

which indicates that V_t must be increased with increases in L, the amount of diversity, if a specified P_F is to be achieved. If each radiometer receives a target signal that experiences independent Rayleigh fading, then the average probability of detection is

$$\bar{P}_D = 1 - \prod_{i=1}^{L} [1 - \bar{P}_{D0}(\bar{\gamma}_i, \sigma_i^2)] \tag{7.59}$$

where $\bar{\gamma}_i$ is the expected value of γ in radiometer i and $\bar{P}_{D0}(\bar{\gamma}_i, \sigma_i^2)$ is given by the right-hand side of (7.54) with $\sigma^2 = \sigma_i^2$ and $\bar{\gamma} = \bar{\gamma}_i$. Equation (7.59) reduces to (7.56) when $L = 1$ and there is no selection diversity.

Figure 7.5 shows $\bar{P}_D$ versus the average energy-to-noise-density ratio $\bar{\gamma}$ for $\sigma_i^2 = \sigma_e^2 = \sigma^2$, $\bar{\gamma}_i = \bar{\gamma}$, $P_F = 10^{-3}$, and $L = 1$ and $L = 2$. A comparison of this figure with the preceding one indicates that the impact of the fading is pronounced at high values of $\bar{P}_D$. When $L = 1$, the required signal energy to achieve a specified $\bar{P}_D$ over the Rayleigh channel is increased by roughly 8 dB or more relative to the required signal energy over the AWGN channel. When selection diversity with $L = 2$ is used, this increase is reduced to roughly 3 dB or more. However, further increases in L produce only minor and diminishing gains. An alternative diversity scheme is square-law combining, which is analyzed in [5] and provides a performance similar to that of selection combining.

7.2.1 *Estimation of Noise Power*

The greatest obstacle to the implementation and efficient operation of the radiometer is its extreme sensitivity to imperfect knowledge of the noise power. The sensitivity is due to the typical extensive overlapping of the probability densities under the two hypotheses of presence or absence of the target signal. This overlap causes a small change in the threshold due to the imperfect estimation of the noise power to have a large impact on the probabilities of false alarm and detection.

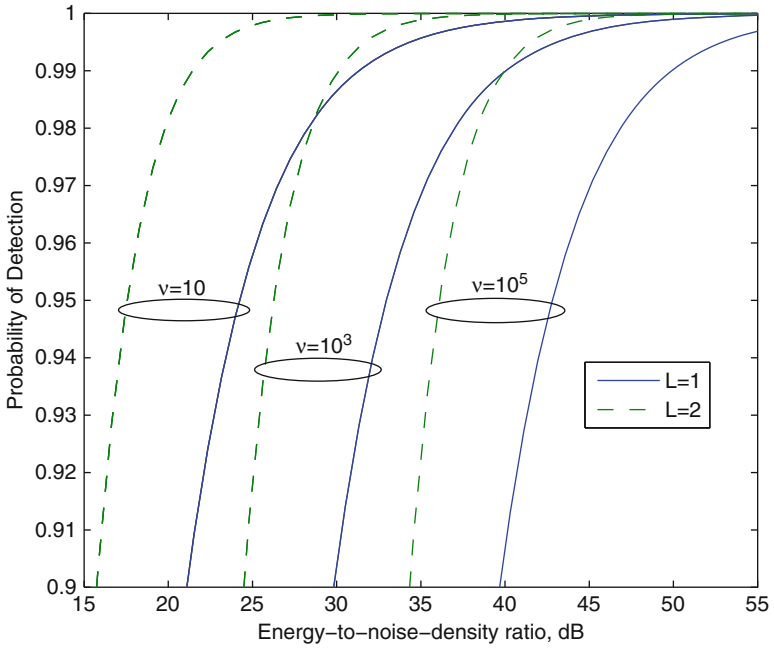

Fig. 7.5 Average probability of detection for Rayleigh fading, $\sigma_i^2 = \sigma_e^2 = \sigma^2$, $\bar{\gamma}_i = \bar{\gamma}$, $P_F = 10^{-3}$, and $L = 1$ and $L = 2$

To ensure that the threshold is large enough that the required P_F is achieved regardless of true value of noise power σ^2, the estimate of the power must be set to the upper end of the measurement uncertainty interval. If measurements indicate that the noise power is between a lower bound σ_l^2 and an upper bound σ_u^2, then the threshold should be calculated using σ_u^2 as the power estimate σ_e^2. It is important that the *error factor* $h = \sigma_e^2/\sigma^2$ is as close to unity as possible to avoid degrading P_D or $\bar{P}_D$, particularly when ν is large. In principle, one can estimate the noise power by measuring the output V of a radiometer over a sufficiently large observation interval when no target signals are received. The estimate of the noise power is V/ν, and (7.40) and (7.41) indicate that its mean is σ^2 and its standard deviation is $\sigma^2/\sqrt{\nu}$. Since Chebyshev's inequality (Sect. 4.2) implies that it is highly unlikely that the measurement error exceeds five standard deviations, the range of power estimates is highly likely to be between $\sigma_l^2 = \sigma^2(1 - 5/\sqrt{\nu})$ and $\sigma_u^2 = \sigma^2(1 + 5/\sqrt{\nu})$. Thus, setting $h = (1 + 5/\sqrt{\nu})$ makes it highly likely that the specified P_F is achieved, and the error factor h can be made arbitrarily small by using a sufficiently large observation interval. For example, if $W = 1$ MHz and $T = 1$ s, then $\nu = 10^6$ and $h = 1.005$.

The noise power is nonstationary primarily because of temperature variations, vibrations, aging, and nonstationary environmental noise. Laboratory measurements indicate that the noise power can change by 0.1% in a few minutes [6]. Thus, if

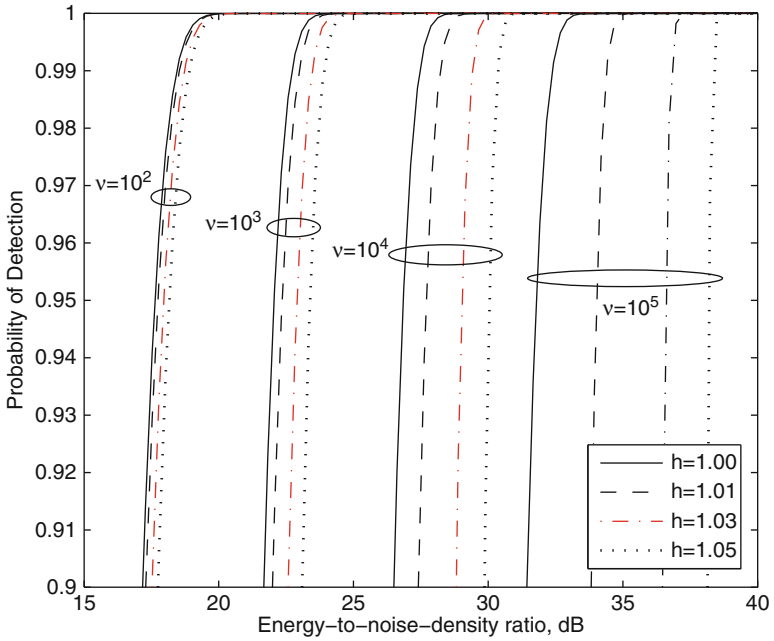

Fig. 7.6 Probability of detection for the AWGN channel, $P_F = 10^{-3}$, and various values of h

accurate measurements can be made shortly before the radiometer is used to detect a target signal, the estimated noise power is upper bounded by σ_u^2, and the noise power can change by no more than 0.1%, then using $\sigma_e^2 = 1.001\sigma_u^2$ to calculate the threshold will ensure a specified P_F with high probability and limit the degradation to P_D or $\bar{P}_D$ caused by the fact that $\sigma_e^2 > \sigma^2$.

An auxiliary radiometer operating over an adjacent spectral region potentially can be used to estimate the noise power in parallel with a radiometer detecting a target signal. An advantage of this method is that time-dependent fluctuations in the noise power are generally negligible over a practical observation interval. The main requirements are that there is negligible target-signal power in the auxiliary radiometer and that the ratio of the two noise powers is an approximately known constant during the observation interval.

The impact of the imperfect estimation of the noise power is illustrated in Figs. 7.6–7.8 for $P_F = 10^{-3}$ and various values of the error factor. Figure 7.6 depicts P_D versus γ for a radiometer and the AWGN channel. As observed in this figure, the required signal energy for a specified P_D and ν increases with h. If $\nu \leq 10^4$ and $h \leq 1.01$, the increase is less than 0.90 dB. The increase in required signal energy when $h > 1.0$ is partially offset by the decrease in the actual P_F below the specified P_F because the threshold is increased by approximately the factor h, as observed from (7.51). Figures 7.7 and 7.8 depict $\bar{P}_D$ versus $\bar{\gamma}$ for a radiometer and the Rayleigh fading channel. In Fig. 7.7, $L = 1$; in Fig. 7.8,

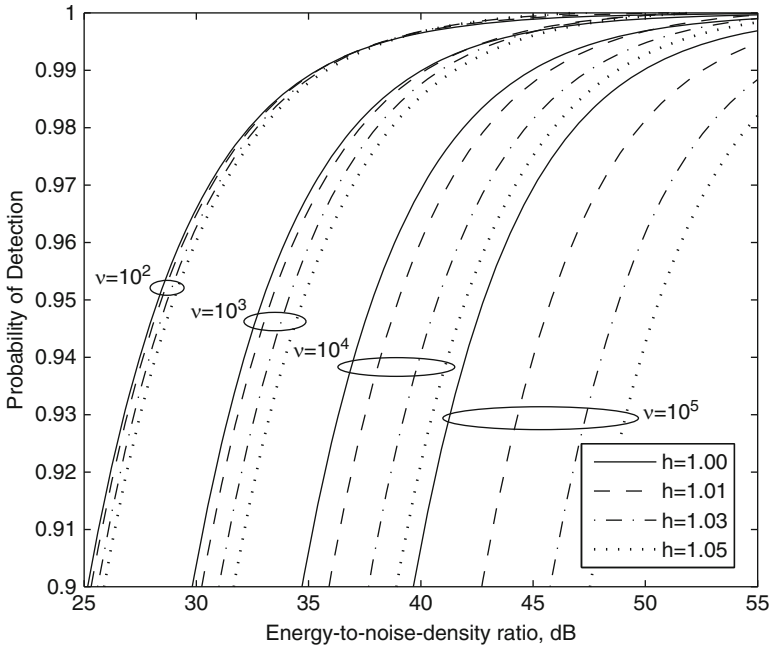

Fig. 7.7 Average probability of detection for Rayleigh fading, $P_F = 10^{-3}$, $L = 1$, and various values of h

$L = 2$, $\sigma_i^2 = \sigma_e^2 = h\sigma^2$, and $\bar{\gamma}_i = \bar{\gamma}$. The effects of h and ν are fairly similar in Figs. 7.6–7.8. As ν increases, the frequency and accuracy of the noise-power estimates must increase if the performance degradation is to be kept small.

7.2.2 Other Implementation Issues

To avoid processing noise outside the spectral region occupied by the target signal, the bandpass filter should have as small a bandwidth as possible. If it is known that a target signal occupies a small subband somewhere within the larger passband of the bandpass filter, then one can isolate the target signal in its subband by inserting a FFT after the sampler in Fig. 7.2. Parallel outputs of the transformer can be applied to separate radiometers, each one processing a distinct subband defined by the transformer. With this architecture, multiple signals can be simultaneously detected over a number of subbands.

Wideband signals, such as direct-sequence and ultra-wideband signals, can be detected by a radiometer, but both the sampling rate and the noise power increase with the bandwidth of the radiometer. The radiometer can serve as a basic component of a channelized radiometer for the detection of frequency-hopping signals (Sect. 7.4).

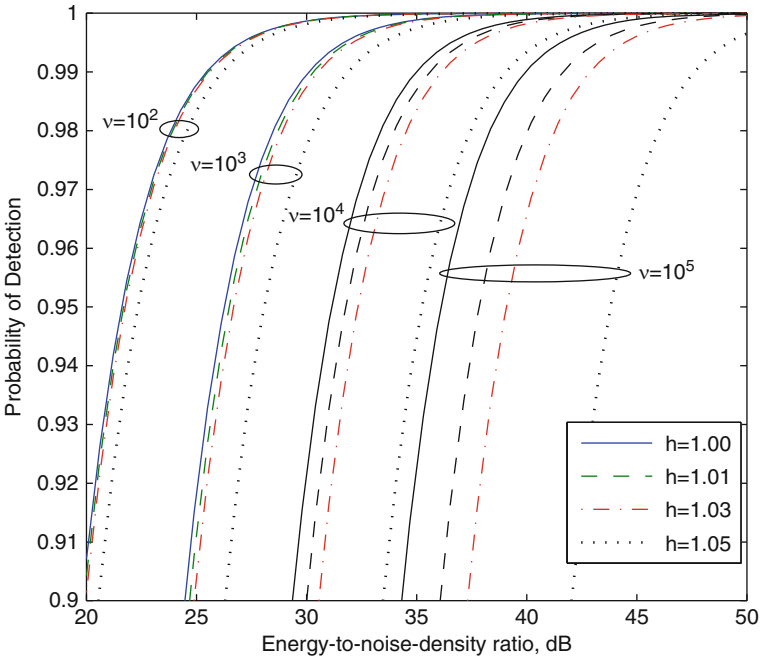

Fig. 7.8 Average probability of detection for Rayleigh fading, $P_F = 10^{-3}$, $L = 2$, and several values of h

It is desirable for the observation interval to be large enough to collect the energy of not only the main target signal but also its significant multipath components. Thus, the extent of the observation interval or, equivalently, the number of samples is largely determined by the delay power spectrum or intensity profile of the multipath to the degree that it is known. A sample at the end of the interval should only be added if the increase in processed signal energy is sufficient to compensate for the increase in noise variance in the radiometer output.

The required value of γ to achieve specified values of P_F and P_D over the AWGN channel may be obtained by inverting (7.48), which is computationally difficult but can be closely approximated by inverting (7.49) if $\nu \gg 1$. We assume that $V_t/\sigma^2 > \nu/2$, which is always satisfied in a practical system with $P_F \leq 0.5$. Using (7.49), we obtain the required value:

$$\gamma_r(\nu) = h\sqrt{\nu}\beta + (h-1)\nu + \psi(\beta, \xi, \nu, h), \quad \nu \gg 1 \tag{7.60}$$

where

$$\beta = Q^{-1}(P_F), \quad \xi = Q^{-1}(P_D), \quad h = \sigma_e^2/\sigma^2 \tag{7.61}$$

$$\psi(\beta, \xi, \nu, h) = \xi^2 - \xi\sqrt{\xi^2 + 2\beta h\sqrt{\nu} + (2h-1)\nu}. \tag{7.62}$$

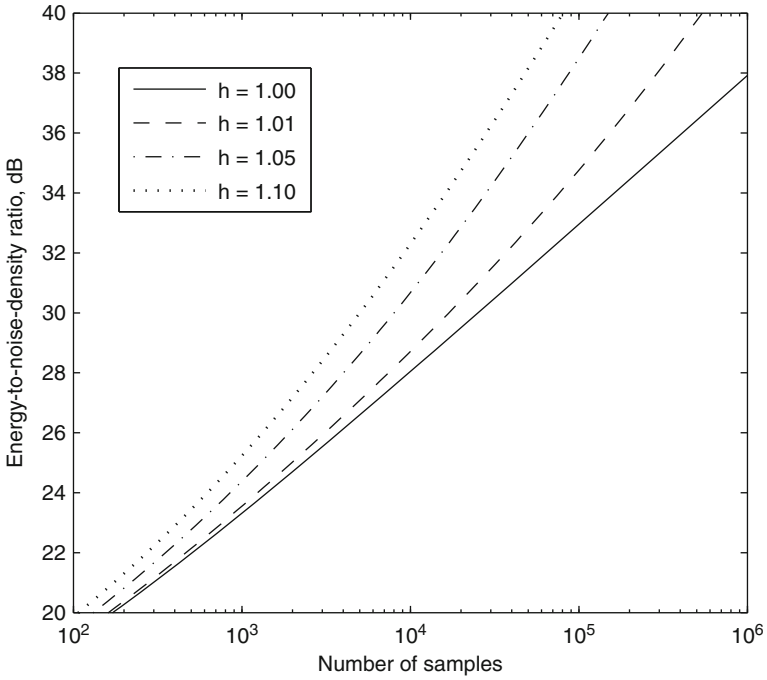

Fig. 7.9 Required energy-to-noise-density ratio for the AWGN channel, $P_D = 0.999$, $P_F = 10^{-3}$, and various values of h

As ν increases, the significance of the third term in (7.60) decreases, while that of the second term increases if $h > 1$. Figure 7.9 shows the *required energy-to-noise-density ratio* $\gamma_r(\nu)$ versus ν for $P_D = 0.999$, $P_F = 10^{-3}$, and various values of h.

To increase the probability of detection, it is desirable to continue collecting additional samples if the increase in $\gamma_r(\nu)$, which is proportional to the required signal energy, is less than the increase in $\gamma(\nu)$, which is proportional to the signal energy that is processed by the radiometer. If we approximate the integer ν by treating it as a continuous variable, then collecting additional samples beyond ν_0 samples already collected is potentially useful if

$$\frac{\partial \gamma_r(\nu_0)}{\partial \nu} < \frac{\partial \gamma(\nu_0)}{\partial \nu}. \tag{7.63}$$

The derivative $\partial \gamma_r(\nu_0)/\partial \nu$ can be determined from the curves of Fig. 7.9 or by using (7.60). The derivative $\partial \gamma(\nu_0)/\partial \nu$ can be calculated from knowledge of the waveform of the target signal or from the intensity profile of the target signal's multipath if the latter is known.

As an example, suppose that $P_D = 0.999$ and $P_F = 10^{-3}$ are required when the radiometer operates over the AWGN channel, $h = 1.05$, and $\nu_0 = 800$.

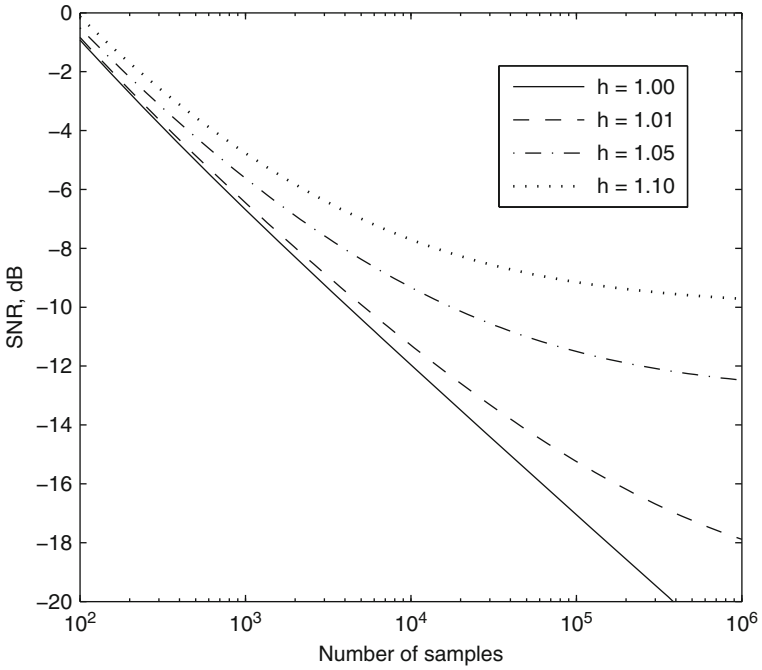

Fig. 7.10 Required SNR for the AWGN channel, $P_D = 0.999$, $P_F = 10^{-3}$, and various values of h

Then Fig. 7.9 indicates that $\gamma_r(\nu_0) \simeq 24\,\text{dB}$ and $\partial \log_{10} \gamma_r(\nu_0)/\partial \log_{10} \nu \approx 0.6$. Therefore, $\partial \gamma_r(\nu_0)/\partial \nu \approx 0.6\gamma_r(\nu_0)/\nu_0$. Suppose that the target signal has constant power over a time interval exceeding the observation interval of the radiometer so that $\partial \gamma(\nu_0)/\partial \nu \approx \gamma(\nu_0)/\nu_0$. Then collecting more samples is useful if $\gamma(\nu_0) > 0.6\gamma_r(\nu_0)$ or $\gamma(\nu_0) > 21.8\,\text{dB}$. If $\gamma(\nu_0) > 24\,\text{dB}$, then P_D already exceeds its required value if $P_F = 10^{-3}$, and collecting more samples increases P_D further. If $21.8\,\text{dB} < \gamma(\nu_0) < 24\,\text{dB}$, then collecting sufficiently more samples will potentially allow $P_D = 0.999$ and $P_F = 10^{-3}$ to be achieved.

A different perspective is gained by examining the required value of the SNR to achieve specified values of P_F and P_D over the AWGN channel. The *required SNR*, defined as

$$S_r(\nu) = \gamma_r(\nu)/\nu \tag{7.64}$$

may be computed using (7.60) and is shown in Fig. 7.10 for the AWGN channel, $P_D = 0.999, P_F = 10^{-3}$, and various values of h. It is observed that if $S_r \geq -14\,\text{dB}$ and $h \leq 1.01$, then the required number of samples increases by a factor of roughly 3 or less relative to the required number for $h = 1.0$.

Equations (7.64) and (7.60) indicates that

$$\lim_{\nu \to \infty} S_r(\nu) = h - 1. \tag{7.65}$$

The significance of this limit is that if the SNR of the target signal is below $h - 1$, then specified values of P_F and P_D cannot be achieved no matter how many samples are collected.

As an example, suppose that the SNR of the target signal is approximately -12 dB over a long observation interval when it is present, and that $P_D = 0.999$ and $P_F = 10^{-3}$ are desired when the radiometer operates over the AWGN channel. Figure 7.10 indicates that the desired P_D and P_F can not be achieved if $h \geq 1.10$. However, if the noise-power estimation is timely and accurate enough that $h \leq 1.05$, then the desired P_D and P_F can be achieved with the collection of $\nu \approx 3 \cdot 10^5$ or fewer samples; only $\nu \approx 2 \cdot 10^4$ or fewer are needed if $h \leq 1.01$.

Because of its large bandwidth and low power spectral density, a direct-sequence signal is difficult to detect by any device that cannot despread it. The effectiveness of a radiometer in detecting a direct-sequence signal depends on the collection of enough samples and sufficient received signal energy.

7.3 Detection of Frequency-Hopping Signals

An interception receiver intended for the detection of frequency-hopping signals may be designed according to the principles of classical detection theory or according to more intuitive ideas. The former approach is useful in setting limits on what is possible, but the latter approach is more practical and flexible and less dependent on knowledge of the characteristics of the frequency-hopping signals.

To enable a tractable analysis according to classical detection theory, the idealized assumptions are made that the hopset is known and that the hop epoch timing, which includes the hop-transition times is known. Consider slow frequency-hopping signals with CPM (FH/CPM) or continuous-phase FSK that have N_h hops. The signal over the ith hop interval is

$$s(t) = \sqrt{2S}\cos\left[2\pi f_j t + \phi(\mathbf{d}_n, t) + \phi_i\right], \ (i-1)T_h \leq t < iT_h \tag{7.66}$$

where S is the average signal power, f_j is the carrier frequency associated with the ith hop, $\phi(\mathbf{d}_n, t)$ is the CPM component that depends on the data sequence $\mathbf{d}_n$, and ϕ_i is the phase associated with the ith hop. Let $\{f_{ji}\}$ denote the sequence of the N_h carrier frequencies. Let the vector $\boldsymbol{\omega}$ denote the parameters $\{f_{ji}\}, \{\phi_i\}$, and the components of $\mathbf{d}_n$, which are modeled as random variables. A derivation similar to that of (7.16) yields

$$\Lambda[r(t)] = E_{\boldsymbol{\omega}}\left\{\exp\left[\frac{2}{N_0}\int_0^{N_h T_h} r(t)s(t)dt - \frac{N_h \mathcal{E}_h}{N_0}\right]\right\} \tag{7.67}$$

where $\mathcal{E}_h$ is the energy per hop.

The M carrier frequencies in the hopset are assumed to be equally likely over a given hop and statistically independent from hop to hop for N_h hops. Dividing the

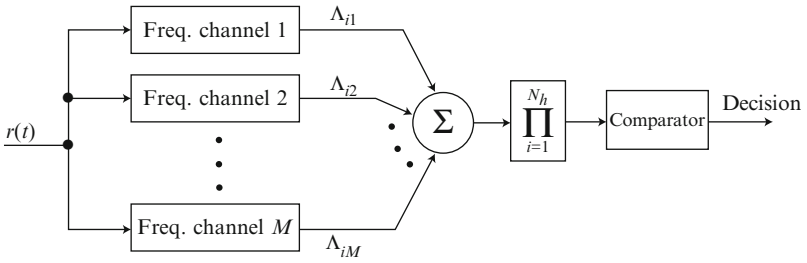

Fig. 7.11 General structure of optimum detector for frequency-hopping signal with N_h hops and M frequency channels

integration interval in (7.67) into N_h parts, averaging over the M frequencies, and dropping the irrelevant factor $1/M$, we obtain

$$\Lambda[r(t)] = \prod_{i=1}^{N_h} \sum_{j=1}^{M} \Lambda_{ij}[r(t)|f_j] \tag{7.68}$$

$$\Lambda_{ij}[r(t)|f_j] = E_{\boldsymbol{d}_n,\phi_i}\left\{\exp\left[\frac{2}{N_0}\int_{(i-1)T_h}^{iT_h} r(t)s(t)dt - \frac{\mathcal{E}_h}{N_0}\right]\right\} \tag{7.69}$$

where the argument of $\Lambda_{ij}[r(t)|f_j]$ indicates that the carrier frequency over the ith hop is f_j, and the expectation is over the remaining random parameters $\boldsymbol{d}_n$ and ϕ_i. The decomposition in (7.68) indicates that the general structure of the detector has the form illustrated in Fig. 7.11. The average likelihood ratio $\Lambda[r(t)]$ is compared with a threshold to determine whether a signal is present. The threshold may be set to ensure the tolerable false-alarm probability when the signal is absent. Assuming that $\mathcal{E}_h = ST_h$ is the same for every hop and carrier frequency, we may drop the irrelevant factor $\exp(-\mathcal{E}_h/N_0)$ in (7.69), which only affects the threshold level.

Each of the N_d data sequences that can occur during a hop is assumed to be equally likely. For *coherent detection* of FH/CPM [7], we assume that the $\{\phi_i\}$ are somehow accurately estimated. Thus, we set $\phi_i = 0$ in (7.66), substitute it into (7.69), and then evaluate the remaining expectation to obtain

$$\Lambda_{ij}[r(t)|f_j] = \sum_{n=1}^{N_d} \exp\left\{\frac{2\sqrt{2S}}{N_0}\int_{(i-1)T_h}^{iT_h} r(t)\cos\left[2\pi f_j t + \phi(\mathbf{d}_n, t)\right]\right\} \quad \text{(coherent)} \tag{7.70}$$

where irrelevant factors have been dropped. This equation indicates how Λ_{ij} in Fig. 7.11 is to be calculated for each hop i and each frequency channel j corresponding to carrier frequency f_j. Equations (7.68) and (7.70) define the optimum coherent detector for any slow frequency-hopping signal with CPM.

For noncoherent detection of FH/CPM [8], the received carrier phase ϕ_i is assumed to be uniformly distributed over $[0, 2\pi)$ during a given hop and statistically

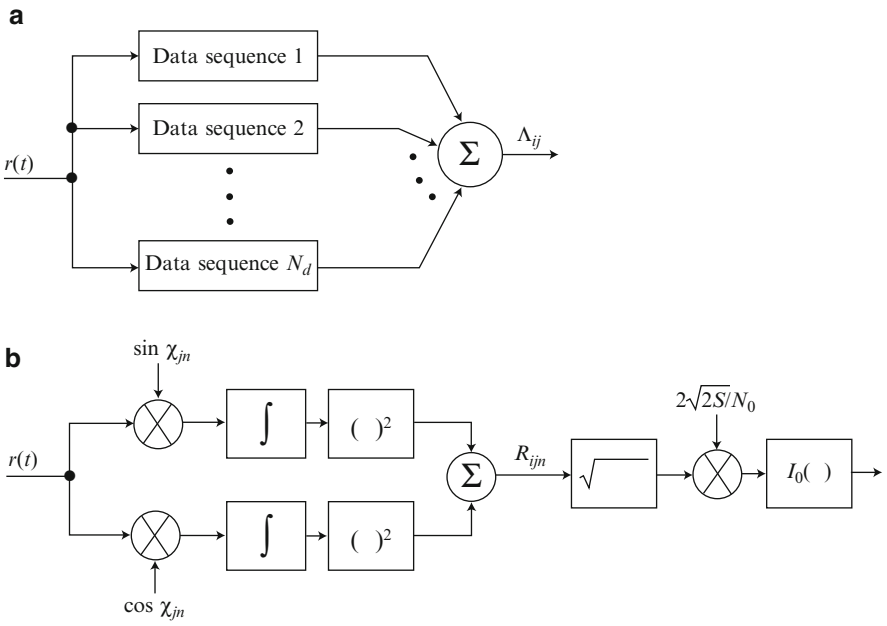

Fig. 7.12 Optimum noncoherent detector for slow frequency hopping with CPM: (**a**) basic structure of frequency channel j for hop i with parallel cells for N_d candidate data sequences, and (**b**) cell for data sequence n

independent from hop to hop. Substituting (7.66) into (7.69), averaging over the random phase in addition to the sequence statistics, and dropping irrelevant factors yields

$$\Lambda_{ij}[r(t)|f_j] = \sum_{n=1}^{N_d} I_0\left(\frac{2\sqrt{2SR_{ijn}}}{N_0}\right) \qquad \text{(noncoherent)} \tag{7.71}$$

where

$$R_{ijn} = \left\{\int_{(i-1)T_h}^{iT_h} r(t)\cos\left[\chi_{jn}(t)\right]dt\right\}^2 + \left\{\int_{(i-1)T_h}^{iT_h} r(t)\sin\left[\chi_{jn}(t)\right]dt\right\}^2 \tag{7.72}$$

and

$$\chi_{jn}(t) = 2\pi f_j t + \phi(\mathbf{d}_n, t) \tag{7.73}$$

Equations (7.68), (7.71), (7.72), and (7.73) define the optimum noncoherent detector for any slow frequency-hopping signal with CPM. The means of producing (7.71) is diagrammed in Fig. 7.12.

A major contributor to the huge computational complexity of the optimum detectors is the fact that with N_s data symbols per hop and an alphabet size q, there may be $N_d = q^{N_s}$ data sequences per hop. Consequently, the computational burden

grows exponentially with N_s. However, if it is known that the data modulation is CPFSK with a modulation index $h = 1/n$, where n is a positive integer, the computational burden has a linear dependence on N_s [8]. Even then, the optimum detectors are extremely complex when the number of frequency channels is large.

The preceding theory may be adapted to the detection of fast frequency-hopping signals with FSK as the data modulation. Since there is one hop per FSK channel symbol, the information is embedded in the sequence of carrier frequencies. Thus, we may set $N_d = 1$ and $\phi(\mathbf{d}_n, t) = 0$ in (7.70) and (7.71). For coherent detection, (7.70) reduces to

$$\Lambda_{ij}[r(t)|f_j] = \exp\left[\frac{2\sqrt{2S}}{N_0}\int_{(i-1)T_h}^{iT_h} r(t)\cos\left(2\pi f_j t\right)dt\right] \qquad \text{(coherent)}. \quad (7.74)$$

Equations (7.68) and (7.74) define the optimum coherent detector for a fast frequency-hopping signal with FSK. For noncoherent detection, (7.71), (7.72), and (7.73) reduce to

$$\Lambda_{ij}[r(t)|f_j] = I_0\left(\frac{2\sqrt{2SR_{ij}}}{N_0}\right) \qquad \text{(noncoherent)} \quad (7.75)$$

$$R_{ij} = \left[\int_{(i-1)T_h}^{iT_h} r(t)\cos(2\pi f_j t)dt\right]^2 + \left[\int_{(i-1)T_h}^{iT_h} r(t)\sin(2\pi f_j t)dt\right]^2. \quad (7.76)$$

Equations (7.68), (7.75), and (7.76) define the optimum noncoherent detector for a fast frequency-hopping signal with FSK. Performance analyses for the detectors of fast frequency-hopping signals are given in [7].

Instead of basing detector design on the average likelihood ratio, one might apply a composite hypothesis test in which the presence of the signal is detected while simultaneously one or more of the unknown parameters under hypothesis H_1 are estimated. To simultaneously detect the signal and determine the frequency-hopping pattern, (7.68) is replaced by the *generalized likelihood ratio*:

$$\Lambda\left[r(t)\right] = \prod_{i=1}^{N_h} \max_{i \le j \le M} \left\{\Lambda_{ij}\left[r(t)|f_j\right]\right\} \quad (7.77)$$

where the equations and subsystems for $\Lambda_{ij}[r(t)|f_j]$ remain the same. Equation (7.77) indicates that a maximum-likelihood estimate of f_j is made for each hop. Thus, an optimum test to determine the frequency channel occupied by the frequency-hopping signal is conducted during each hop. Although the detection performance is suboptimal when the generalized likelihood ratio is used to design a detector, this detector provides an important signal feature and is slightly easier to implement and analyze [7, 8].

7.4 Channelized Radiometer

Among the many alternatives to the optimum detector, two of the most useful are the *wideband radiometer* and the *channelized radiometer*. The wideband radiometer is notable in that it requires virtually no detailed information about the parameters of the frequency-hopping signals to be detected other than their rough spectral location. The price paid for this robustness is much worse performance than that of more sophisticated detectors that exploit additional information about the signal [8]. The channelized radiometer is designed to explicitly exploit the spectral characteristics of frequency-hopping signals. In its optimal form, the channelized radiometer gives a performance nearly as good as that of the ideal detector. In its suboptimal form, the channelized radiometer trades performance for practicality and the easing of the required *a priori* information about the signal to be detected.

A *channelized radiometer* comprises K parallel radiometers, each of which has the form of Fig. 7.1 and monitors a disjoint portion of the hopping band of a frequency-hopping signal, as depicted in Fig. 7.13. The largest of the sampled radiometer outputs is compared to a threshold V_t stored in a comparator. If the threshold is exceeded, the comparator sends a 1 to the summer; otherwise it sends a 0. If the hop dwell epochs are at least approximately known, the channelized radiometer may improve its detection reliability by adding the 1's produced by N consecutive comparator outputs corresponding to multiple frequency hops of the signal to be detected. A signal is declared to be present if the sum V equals or exceeds the integer r, which serves as a second threshold. The two thresholds V_t are r are jointly optimized for the best system performance.

Ideally, $K = M$, the number of frequency channels in a hopset, but many fewer radiometers may be a practical or economic necessity; if so, each radiometer may monitor M_r frequency channels, where $1 \leq M_r \leq M$. Because of insertion losses and the degradation caused by a power divider, it is unlikely that many more than 30 parallel radiometers are practical. An advantage of each radiometer covering many frequency channels is the reduced sensitivity to imprecise knowledge of the spectral boundaries of frequency channels. Since it is highly desirable to implement the parallel radiometers with similar circuitry, their bandwidths are assumed to be identical henceforth.

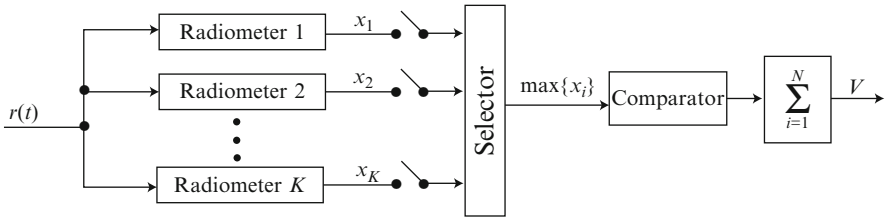

Fig. 7.13 Channelized radiometer

To prevent steady interference in a single radiometer from causing false alarms, the channelized radiometer must be able to recognize when one of its constituent radiometers produces an output above the threshold for too many consecutive samples. The channelized system may then delete that constituent radiometer's output from the detection algorithm or it may reassign the radiometer to another spectral location.

In the subsequent analysis of the channelized radiometer of Fig. 7.13, the observation interval of the parallel radiometers, which is equal to the sampling interval, is assumed to equal the hop duration T_h. The effective observation time of the channelized radiometer, $T = NT_h$, should be less than the minimum expected message duration to avoid processing extraneous noise. Let B denote the bandwidth of each of the M_r frequency channels encompassed by a radiometer passband. Let P_{F1} denote the probability that a particular radiometer output at the sampling time exceeds the comparator threshold V_t when no signal is present. It follows in analogy with (7.45) that

$$P_{F1} = \frac{\Gamma(\nu, V_t/\sigma^2)}{\Gamma(\nu)} = \exp\left(-\frac{V_t}{\sigma^2}\right) \sum_{i=0}^{\nu-1} \frac{1}{i!} \left(\frac{V_t}{\sigma^2}\right)^i \tag{7.78}$$

where the noise power is $\sigma^2 = N_0 M_r B$ and the number of samples per hop dwell time is $\nu = \lfloor T_h M_r B \rfloor$. Thus, if the estimate of σ^2 is σ_e^2,

$$\begin{aligned} V_t &= \sigma_e^2 G_\nu^{-1}(P_{F1}) \\ &\cong \sigma_e^2[\sqrt{\nu} Q^{-1}(P_F) + \nu], \quad \nu \gg 1 \end{aligned} \tag{7.79}$$

where $G_\nu^{-1}(\cdot)$ is the inverse function of $P_{F1}(V_t/\sigma^2)$ and the approximation is obtained in the same manner as (7.51). The probability that at least one of the K parallel radiometer outputs exceeds V_t is

$$P_{F2} = 1 - (1 - P_{F1})^K \tag{7.80}$$

assuming that the channel noises are statistically independent because the radiometer passbands are disjoint. The probability of a false alarm of the channelized radiometer is the probability that the output V equals or exceeds a threshold r:

$$P_F = \sum_{i=r}^{N} \binom{N}{i} P_{F2}^i (1 - P_{F2})^{N-i}. \tag{7.81}$$

To solve this equation for P_{F2} in terms of P_F, we observe that the *incomplete beta function* is defined as

$$B_x(a, b) = \int_0^x t^{a-1}(1-t)^{b-1} dt, \quad 0 \le x \le 1, a > 0, b > 0 \tag{7.82}$$

where $B_1(a,b)$ is the *beta function. Let* $F(x|a,b) = B_x(a,b)/B_1(a,b)$. Applying the binomial theorem to the integrand of (7.82) when a and b are integers, and then integrating term-by-term, we obtain the series expansion of the incomplete beta function. A comparison with (7.81) indicates that

$$P_F = F(P_{F2}|r, N-r+1). \tag{7.83}$$

The inverse of this function, which we denote by $F^{-1}(\cdot)$, may be easily computed by Newton's method or approximations [6]. Therefore, if $\nu \gg 1$, (7.79), (7.80), and (7.83) may be combined to determine the approximate threshold necessary to achieve a specified P_F:

$$V_t \cong \sigma_e^2 \left[\sqrt{\nu} Q^{-1} \left\{ 1 - \left[1 - F^{-1}(P_F|r, N-r+1) \right]^{1/K} \right\} + \nu \right], \quad \nu \gg 1 \tag{7.84}$$

where it is assumed that σ^2 does not vary across the hopping band, and hence there is one σ_e^2 and one V_t for all the parallel radiometers.

It is assumed that at most a single radiometer receives significant signal energy during each hop dwell time. Let P_{D1} denote the probability that a particular radiometer output exceeds the threshold when a signal is present in that radiometer. By analogy with (7.48) and (7.49),

$$\begin{aligned} P_{D1} &= Q_\nu \left(\sqrt{2\mathcal{E}_h/N_0}, \sqrt{2V_t/\sigma^2} \right) \\ &\cong Q\left[\frac{V_t/\sigma^2 - \nu - \mathcal{E}_h/N_0}{\sqrt{\nu + 2\mathcal{E}_h/N_0}} \right], \quad \nu \gg 1 \end{aligned} \tag{7.85}$$

where $\mathcal{E}_h$ is the energy per hop dwell time. Let P_{D2} denote the probability that the threshold is exceeded by the sampled maximum of the parallel radiometer outputs. It is assumed that when a signal is present it occupies any one of M frequency channels with equal probability, and that all radiometer passbands are within the hopping band. Consequently, the signal has probability M_r/M of being in the passband of a particular radiometer, and the *monitored fraction* $\mu = KM_r/M$ is the probability that the signal is in the passband of some radiometer. Since a detection may be declared in response to a radiometer that does not receive the signal,

$$P_{D2} = \mu \left[1 - (1 - P_{D1})(1 - P_{F1})^{K-1} \right] + (1-\mu) P_{F2} \tag{7.86}$$

where the second term vanishes if the radiometer passbands cover the hopping band so that $\mu = 1$.

The number of hop dwell times during which the signal is actually present is $N_1 \leq N$. The second threshold is exceeded if the comparator produces j 1's in response to these N_1 dwell times, $i - j$ 1's in response to the remaining $N - N_1$ dwell times that are observed, and $i \geq r$. Thus, the probability of detection when

the signal is actually present during $N_1 \leq N$ of the observed hop dwell times is

$$P_D = \sum_{i=r}^{N} \sum_{j=0}^{i} \binom{N_1}{j} \binom{N-N_1}{i-j} P_{D2}^{j} (1-P_{D2})^{N_1-j} P_{F2}^{i-j} (1-P_{F2})^{N-N_1-i+j} . \tag{7.87}$$

If at least the minimum duration of a frequency-hopping signal is known, the overestimation of N might be avoided so that $N_1 = N$. The detection probability then becomes

$$\begin{aligned} P_D &= \sum_{i=r}^{N} \binom{N}{i} P_{D2}^{i} (1-P_{D2})^{N-i} \\ &= F(P_{D2}|r, N-r+1) . \end{aligned} \tag{7.88}$$

A reasonably good, but not optimal, choice for the second threshold is $r = \lfloor N/2 \rfloor$ when the full hopping band is monitored by the channelized radiometer. In general, numerical results indicate that

$$r = \left\lfloor \mu \frac{N}{2} \right\rfloor \tag{7.89}$$

is a good choice for partial-band monitoring.

If detection decisions are made in terms of fixed observation intervals of duration $T = NT_h$, and successive intervals do not overlap except possibly at end points, then the false-alarm rate in units of false alarms per second is an appropriate design parameter. This type of detection is called *block detection,* and

$$P_F = FNT_h. \tag{7.90}$$

To prevent the risk of major misalignment of the observation interval with the time the signal is being transmitted, either block detection must be supplemented with hardware for arrival-time estimation or the duration of successive observation intervals should be less than roughly half the anticipated signal duration.

A different approach to mitigating the effect of a misalignment, called *binary moving-window detection*, is for the observation interval to be constructed by dropping the first hop dwell time of the preceding observation interval and adding a new hop dwell time. A false alarm is considered to be a new detection declaration at the end of the new observation interval when no signal is actually present. Thus, a false alarm occurs only if the comparator input for an added hop dwell time exceeds the threshold, the comparator input for the discarded hop dwell time did not, and the count for the intermediate hop dwell times was $r-1$. Therefore, the probability of a false alarm is

$$P_{F0} = C(0,1)C(r-1, N-1)C(1,1) \tag{7.91}$$

where

$$C(i,N) = \binom{N}{i} P_{F2}^{i} (1-P_{F2})^{N-i} , \quad i \leq N. \tag{7.92}$$

It follows that the false-alarm rate is

$$F_0 = \frac{P_{F0}}{T_h} = \frac{r}{NT_h}\binom{N}{r} P_{F2}^r \left(1 - P_{F2}\right)^{N+1-r}. \tag{7.93}$$

To compare the block and binary moving-window detectors, assume that P_{F2} is the same for both detectors. Since the right-hand side of (7.93) is proportional to the first term of the series in (7.81) and $F = P_F/NT_h$ for the block detector, the false-alarm rate F_0 of the binary moving-window detector has the upper bound given by

$$F_0 \le rF. \tag{7.94}$$

If $P_{F2} \ll 1/N$, the upper bound is tight, which implies that the false-alarm rate is nearly r times as large for moving-window detection as it is for block detection. Thus, moving-window detection usually requires a higher comparator threshold for the same false-alarm rate and, hence, more signal power to detect a frequency-hopping signal. However, moving-window detection with $N \approx N_1 \gg 1$ inherently limits the misalignment between the occurrence of the intercepted signal and some observation interval. If the signal occurs during two successive observation intervals, then for one of the observation intervals, the misalignment is not more than $T_h/2$.

As examples of the performance of the channelized radiometer, Figs. 7.14 and 7.15 plot P_D versus $\mathcal{E}_h/N_0$. It is assumed that there are $M = 2400$ frequency channels, block detection is used, $F = 10^{-5}/T_h$, $B = 250/T_h$, and $\nu = T_h\mu MB/K = 6 \cdot 10^5\mu/K \gg 1$. The signal duration is known and there is no misalignment so that $N_1 = N$. In Fig. 7.14, the full hopping band is monitored so that $\mu = 1$, $h = \sigma_e^2/\sigma^2 = 1$, and P_D is plotted for several values of K and N. The figure also shows the results for a wideband radiometer with $\nu = NT_hMB = 6 \cdot 10^5 \cdot N$, and $N = 150$ or 750. The substantial advantage of the channelized radiometer with $K = M$ and $M_r = 1$ is apparent. The channelized radiometer with $K = 30$ is much better than the wideband radiometer when $N = 150$, but $K = 150$ is needed for the advantage of the channelized radiometer to be preserved when $N = 750$. As N increases, the channelized radiometer can retain its advantage over the wideband radiometer by increasing K accordingly.

In Fig. 7.15, $N = 150$ and $K = 30$, but M_r and $h = \sigma_e^2/\sigma^2$ are variable. It is observed that when $h > 1$, the performance loss depends on the value of μ, which directly affects ν. The figure illustrates the trade-off when K and M are fixed and the monitored fraction μ decreases. Since $M_r = \mu M/K = 80\mu$ decreases, fewer frequency channels are monitored, ν decreases, the sensitivity to $h > 1$ decreases, and less noise enters a radiometer. The net result is beneficial when $\mu = 0.2$. However, the figure indicates that for $\mu = 0.1$ or 0.05, the hopping-band coverage becomes inadequate to enable a P_D greater than 0.998 and 0.968, respectively, regardless of $\mathcal{E}_h/N_0$. Thus, there is a minimum fraction $\mu_{\min}$ of the hopping band that must be monitored to ensure a specified P_D.

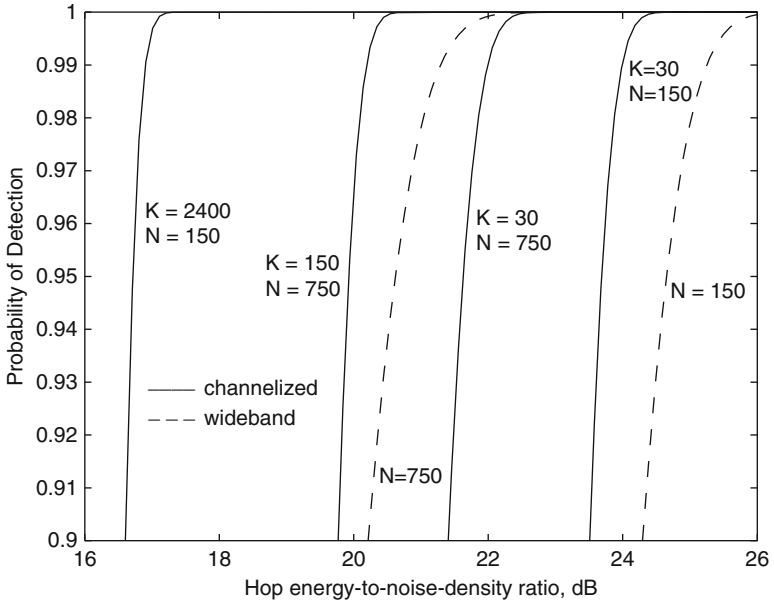

Fig. 7.14 Probability of detection versus $\mathcal{E}_h/N_0$ for channelized and wideband radiometers with full coverage, $N_1 = N$, $h = 1$, $M = 2400$, $F = 10^{-7}/T_h$, and $B = 250/T_h$

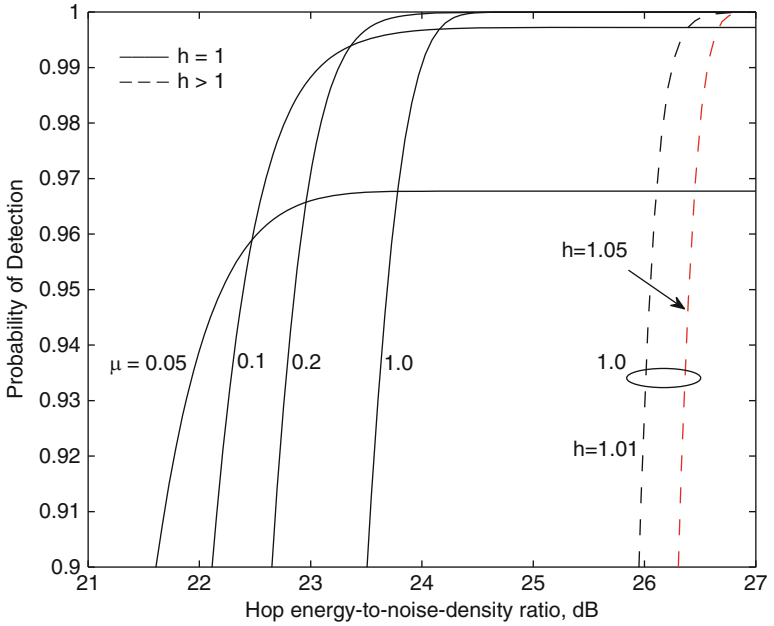

Fig. 7.15 Probability of detection for channelized radiometer with different monitored fractions, $N_1 = N = 150$, $K = 30$, $M = 2400$, $F = 10^{-7}/T_h$, $B = 250/T_h$, and $h = 1.0$, 1.01, and 1.05

As $\mathcal{E}_h/N_0 \to \infty$, (7.85) indicates that $P_{D1} \to 1$. Therefore, (7.86) implies that $P_{D2} \to \mu + (1-\mu)P_{F2}$. Suppose that $\mu = \mu_{\min}$ for a specified P_D. The threshold V_t is raised to a sufficiently high level that $P_{F2} \ll \mu_{\min}$ and, hence, $P_{D2} \approx \mu_{\min}$. If detection is to be accomplished for the minimum monitored fraction, then $r = 1$ is the best choice for the second threshold. For $r = 1$ and $N_1 = N$, (7.88) yields

$$P_D = 1 - (1 - P_{D2})^N. \tag{7.95}$$

Since $P_{D2} \approx \mu_{\min}$, (7.95) implies that even if $\mathcal{E}_h/N_0 \to \infty$, the realization of a specified P_D requires the minimum monitored fraction

$$\mu_{\min} \approx 1 - (1 - P_D)^{1/N}. \tag{7.96}$$

Thus, if $P_D = 0.99$ and $N = N_1 = 150$, then $\mu_{\min} \approx 0.03$. Many other aspects of the channelized radiometer, including the effects of timing misalignments, are examined in [9].

Problems

7.1. If the form and the parameters of a signal $s(t)$ to be detected are known, optimum detection in white Gaussian noise $n(t)$ can be accomplished by an ideal matched filter or correlator. Let $r(t)$ denote the received signal and T denote the observation interval. (a) Write an expression for the sampled output of an ideal matched filter. (b) This output r_1 is compared to a threshold V_t to determine whether the target signal is present. Suppose that it is present and coincides with an observation interval. Assuming that $n(t)$ is zero-mean and has two-sided power spectral density $N_0/2$ and that the signal energy is $\mathcal{E}$, what are the mean and the variance of r_1? (c) What is the probability of detection P_D? What is the probability of false alarm P_F? Express P_D in terms of P_F. (d) What is the value of $\mathcal{E}/N_0$ necessary to ensure specified values of P_F and P_D?

7.2. Derive (7.40) and (7.41). Use the fact that a zero-mean Gaussian random variable x has $E[x^4] = 3E[x^2]$.

7.3. The *receiver operating characteristic* (ROC) is a traditional plot depicting P_D versus P_F for various values of ν or $\mathcal{E}/N_0$. The ROC may be calculated from (7.49) and (7.45). Plot the ROC for the wideband radiometer with $\mathcal{E}/N_0 = 20\,\text{dB}$ and no noise-measurement error. Let $\nu = 10^4$ and 10^5.

7.4. Derive (7.53) and (7.56) using the methods described in the text.

7.5. Derive (7.60) using the method described in the text.

7.6. Find conditions under which (7.60) indicates that a negative energy is required. What is the physical implication of this result?

7.7. Consider a channelized radiometer that is to detect a frequency-hopping signal with $N = 1$ hop. (a) Find V_t in terms of P_F. (b) If $KM_r = M$, $h = 1$, $N_1 = N$, and $\mathcal{E}_h/N_0$ is small, derive the S/N_0 required for specified values of P_D and P_F.

References

1. B. Levy, *Principles of Signal Detection and Parameter Estimation*. New York: Springer, 2008.
2. A. Polydoros and C. L. Weber, "Detection Performance Considerations for Direct-Sequence and Time-Hopping LPI Waveforms," *IEEE J. Select. Areas Commun.*, vol. 3, pp. 727–744, Sept. 1985.
3. D. Torrieri, "The Radiometer and Its Practical Implementation," *Proc. IEEE Military Commun. Conf.*, Oct. 2010.
4. V. I. Kostylev, "Energy Detection of a Signal with Random Amplitude," *Proc. IEEE Int. Conf. Communications (ICC'02)*. New York: pp. 1606–1610, May 2002.
5. F. F. Digham, M. S. Alouini, and M. K. Simon, "On the Energy Detection of Unknown Signals over Fading Channels," *IEEE Trans. Commun.*, vol. 55, pp. 21–24, Jan. 2007.
6. D. A. Hill and E. B. Felstead, "Laboratory Performance of Spread Spectrum Detectors," *IEE Proc.-Commun.*, vol. 142, pp. 243–249, Aug. 1995.
7. N. C. Beaulieu, W. L. Hopkins, and P. J. McLane, "Interception of Frequency-Hopped Spread-Spectrum Signals," *IEEE. J. Select. Areas Commun.*, vol. 8, pp. 853–870, June 1990.
8. B. K. Levitt, U. Cheng, A. Polydoros, and M. K. Simon, "Optimum Detection of Slow Frequency-Hopped Signals," *IEEE Trans. Commun.*, vol. 42, pp. 1990–2000, Feb./March/April 1994.
9. L. E. Miller, J. S. Lee, and D. J. Torrieri, "Frequency-Hopping Signal Detection Using Partial Band Coverage," *IEEE Trans. Aerosp. Electron. Syst.*, vol. 29, pp. 540–553, April 1993.

Chapter 8
Systems with Iterative Channel Estimation

The estimation of channel parameters, such as the fading amplitude and the power spectral density of the interference plus noise, is essential to the effective use of soft-decision decoding. Channel estimation may be implemented by the transmission of pilot signals that are processed by the receiver, but pilot signals entail overhead costs, such as the loss of data throughput. Deriving maximum-likelihood channel estimates directly from the received data symbols is often prohibitively difficult. There is an effective alternative when turbo or low-density parity-check codes are used. The expectation-maximization algorithm provides an iterative approximate solution to the maximum-likelihood equations and is inherently compatible with iterative demodulation and decoding. Two examples of advanced spread-spectrum systems that apply the expectation-maximization algorithm for channel estimation are described and analyzed in this chapter. These systems provide good illustrations of the calculations required in the design of advanced systems.

8.1 Expectation-Maximization Algorithm

The expectation-maximization (EM) algorithm offers a low-complexity iterative approach to maximum-likelihood estimation [1]. A substantial body of literature exists on EM-based techniques for channel estimation, data detection, and multiuser detection.

Maximum-likelihood estimation of a nonrandom vector of m parameters $\boldsymbol{\theta}$ is obtained by maximizing the conditional probability density function $f(\mathbf{y}|\boldsymbol{\theta})$ of a random vector $\mathbf{Y} = [Y_1 \cdots Y_N]^T$ of the observations. Since the logarithm is a monotonic function of its argument, the maximum-likelihood estimate $\hat{\boldsymbol{\theta}}_{ml}$ of $\boldsymbol{\theta}$ may be expressed as

$$\hat{\boldsymbol{\theta}}_{ml} = \arg\max_{\theta} \ln f(\mathbf{y}|\boldsymbol{\theta}) \tag{8.1}$$

D. Torrieri, *Principles of Spread-Spectrum Communication Systems*,
DOI 10.1007/978-1-4419-9595-7_8, © Springer Science+Business Media, LLC 2011

where $\ln f(\mathbf{y}|\boldsymbol{\theta})$ is the *log-likelihood function*. When the likelihood function is differentiable, the maximum-likelihood estimate is the solution of the *likelihood equation*:

$$\nabla \ln f(\mathbf{y}|\boldsymbol{\theta})\big|_{\theta=\hat{\theta}_{ml}} = \mathbf{0} \tag{8.2}$$

where ∇ is the gradient vector, which is defined as

$$\nabla = \left[\frac{\partial}{\partial\theta_1} \cdots \frac{\partial}{\partial\theta_N}\right]^T. \tag{8.3}$$

When (8.2) cannot be solved in closed form, it can sometimes be solved iteratively by applying Newton's method or fixed-point methods. When an iterative maximum-likelihood solution is intractable, an alternative procedure is the EM algorithm, which has the major advantage that it requires no calculations of gradients or Hessians.

The EM algorithm is based on the postulate that the set of observations $\{Y_i\}$ forming the random data vector $\mathbf{Y}$ is a subset of or derived from a larger data set $\{Z_i\}$ forming a random data vector $\mathbf{Z}$ such that the maximization of the conditional density functions $f(\mathbf{z}|\boldsymbol{\theta})$ is mathematically tractable. The data vector $\mathbf{Y}$ is called the *incomplete* data vector, and the data vector $\mathbf{Z}$ is called the *complete* data vector. The complete data vector $\mathbf{Z}$ is related to each observation Y_k by a many-to-one transformation. Since this transformation is not invertible, there is no unique mapping from $\mathbf{Z}$ to $\mathbf{Y}$. The function $\ln f(\mathbf{z}|\boldsymbol{\theta})$ does not directly provide a useful estimate of $\boldsymbol{\theta}$ because $\mathbf{Z}$ is not observable, so the expectation of $\ln f(\mathbf{z}|\boldsymbol{\theta})$ given both $\mathbf{Y} = \mathbf{y}$ and an estimate of $\boldsymbol{\theta}$ is iteratively maximized by the EM algorithm.

Since $\mathbf{Y}$ is determined by $\mathbf{Z}$, $f(\mathbf{z}, \mathbf{y}|\boldsymbol{\theta}) = f(\mathbf{z}|\boldsymbol{\theta})$ and the definition of a conditional density implies that

$$f(\mathbf{z}|\mathbf{y}, \boldsymbol{\theta}) = \frac{f(\mathbf{z}|\boldsymbol{\theta})}{f(\mathbf{y}|\boldsymbol{\theta})}. \tag{8.4}$$

Therefore,

$$\ln f(\mathbf{y}|\boldsymbol{\theta}) = \ln f(\mathbf{z}|\boldsymbol{\theta}) - \ln f(\mathbf{z}|\mathbf{y}, \boldsymbol{\theta}). \tag{8.5}$$

Beginning with an assumed initial estimate $\hat{\boldsymbol{\theta}}_0$, the EM algorithm computes successive estimates $\hat{\boldsymbol{\theta}}_i$ that increase the value of $\ln f(\mathbf{y}|\hat{\boldsymbol{\theta}}_i)$. Let

$$E_{\mathbf{z}|\mathbf{y},\hat{\boldsymbol{\theta}}_i}[g(\mathbf{z})] = \int g(\mathbf{z}) f(\mathbf{z}|\mathbf{y}, \hat{\boldsymbol{\theta}}_i) d\mathbf{z} \tag{8.6}$$

denote the expectation of $g(\mathbf{Z})$ with respect to the density $f(\mathbf{z}|\mathbf{y}, \hat{\boldsymbol{\theta}}_i)$, where $g(\mathbf{Z})$ is some function of the random vector $\mathbf{Z}$. Integrating both sides of (8.5) over $f(\mathbf{z}|\mathbf{y}, \hat{\boldsymbol{\theta}}_i)$ yields

$$\ln f(\mathbf{y}|\boldsymbol{\theta}) = E_{\mathbf{z}|\mathbf{y},\hat{\boldsymbol{\theta}}_i}[\ln f(\mathbf{z}|\boldsymbol{\theta})] - E_{\mathbf{z}|\mathbf{y},\hat{\boldsymbol{\theta}}_i}[\ln f(\mathbf{z}|\mathbf{y}, \boldsymbol{\theta})]. \tag{8.7}$$

Lemma. *For any* $\hat{\boldsymbol{\theta}}_{i+1}$,

$$E_{\mathbf{z}|\mathbf{y},\hat{\boldsymbol{\theta}}_i}[\ln f(\mathbf{z}|\mathbf{y}, \hat{\boldsymbol{\theta}}_{i+1})] \le E_{\mathbf{z}|\mathbf{y},\hat{\boldsymbol{\theta}}_i}[\ln f(\mathbf{z}|\mathbf{y}, \hat{\boldsymbol{\theta}}_i)] \tag{8.8}$$

with equality if and only if $f(\mathbf{z}|\mathbf{y}, \hat{\boldsymbol{\theta}}_{i+1}) = f(\mathbf{z}|\mathbf{y}, \hat{\boldsymbol{\theta}}_i)$.

Proof. Since $\ln a - \ln b = \ln a/b$,

$$E_{\mathbf{z}|\mathbf{y},\hat{\boldsymbol{\theta}}_i}[\ln f(\mathbf{z}|\mathbf{y},\hat{\boldsymbol{\theta}}_{i+1}] - E_{\mathbf{z}|\mathbf{y},\hat{\boldsymbol{\theta}}_i}[\ln f(\mathbf{z}|\mathbf{y},\hat{\boldsymbol{\theta}}_i)] = E_{\mathbf{z}|\mathbf{y},\hat{\boldsymbol{\theta}}_i}\left[\ln \frac{f(\mathbf{z}|\mathbf{y},\hat{\boldsymbol{\theta}}_{i+1})}{f(\mathbf{z}|\mathbf{y},\hat{\boldsymbol{\theta}}_i)}\right].$$

Since $\ln x = x - 1$ when $x = 1$ and a double differentiation proves that $\ln x$ is a concave function of x for $x > 0$, $\ln x \leq x - 1$ for $x > 0$ with equality if and only if $x = 1$. Therefore,

$$E_{\mathbf{z}|\mathbf{y},\hat{\boldsymbol{\theta}}_i}\left[\ln \frac{f(\mathbf{z}|\mathbf{y},\hat{\boldsymbol{\theta}}_{i+1})}{f(\mathbf{z}|\mathbf{y},\hat{\boldsymbol{\theta}}_i)}\right] \leq \int \left[\frac{f(\mathbf{z}|\mathbf{y},\hat{\boldsymbol{\theta}}_{i+1})}{f(\mathbf{z}|\mathbf{y},\hat{\boldsymbol{\theta}}_i)} - 1\right] f(\mathbf{z}|\mathbf{y},\hat{\boldsymbol{\theta}}_i)\,d\mathbf{z}$$
$$= 0$$

which proves the inequality and the condition for equality. □

We define

$$\chi(\boldsymbol{\theta},\hat{\boldsymbol{\theta}}) = E_{\mathbf{z}|\mathbf{y},\hat{\boldsymbol{\theta}}}[\ln f(\mathbf{z}|\theta)]. \tag{8.9}$$

Theorem. *If successive estimates are computed as*

$$\hat{\theta}_{i+1} = \arg\max_{\boldsymbol{\theta}} \chi(\boldsymbol{\theta},\hat{\boldsymbol{\theta}}_i) \tag{8.10}$$

and $\ln f(\mathbf{y}|\boldsymbol{\theta})$ *has an upper bound, then the sequence* $\{\ln f(\mathbf{y}|\hat{\boldsymbol{\theta}}_i))\}$ *converges to a limit as* $i \to \infty$.

Proof. The hypothesis of the theorem implies that $\chi(\hat{\boldsymbol{\theta}}_{i+1},\hat{\boldsymbol{\theta}}_i) \geq \chi(\hat{\boldsymbol{\theta}}_i,\hat{\boldsymbol{\theta}}_i)$. This inequality, the lemma, (8.7), and (8.9) imply that

$$\ln f(\mathbf{y}|\hat{\theta}_{i+1}) \geq \ln f(\mathbf{y}|\hat{\boldsymbol{\theta}}_i)$$

with equality if and only if

$$\chi(\hat{\boldsymbol{\theta}}_{i+1},\hat{\boldsymbol{\theta}}_i) = \chi(\hat{\boldsymbol{\theta}}_i,\hat{\boldsymbol{\theta}}_i), \quad f(\mathbf{z}|\mathbf{y},\hat{\boldsymbol{\theta}}_{i+1}) = f(\mathbf{z}|\mathbf{y},\hat{\boldsymbol{\theta}}_i).$$

A bounded monotonically increasing sequence converges to a limit. Therefore, if $\ln f(\mathbf{y}|\hat{\boldsymbol{\theta}}_i)$ has an upper bound, then it converges to a limit as $i \to \infty$. □

This theorem leads directly to the algorithm, which has two primary computational steps: an expectation (*E-step*) and a maximization (*M-step*).

EM Algorithm.

1. Set $i = 0$ and select the initial estimate $\hat{\boldsymbol{\theta}}_0$.
2. E-step: Compute $\chi(\boldsymbol{\theta},\hat{\boldsymbol{\theta}}_i) = E_{\mathbf{z}|\mathbf{y},\hat{\boldsymbol{\theta}}_i}[\ln f(\mathbf{z}|\boldsymbol{\theta})]$.
3. M-step: Compute $\hat{\boldsymbol{\theta}}_{i+1} = \arg\max_{\boldsymbol{\theta}} \chi(\boldsymbol{\theta},\hat{\boldsymbol{\theta}}_i)$.

4. If i does not exceed some preset maximum and $\|\hat{\boldsymbol{\theta}}_{i+1} - \hat{\boldsymbol{\theta}}_i\| > \epsilon$, where ϵ is preset positive number, then return to the E-step. Otherwise, terminate the iterations. □

If $\ln f(\boldsymbol{y}|\boldsymbol{\theta})$ is not concave, the sequence $\{\ln f(\mathbf{y}|\hat{\boldsymbol{\theta}}_i)\}$ may converge to a local maximum rather than a global maximum of $\ln f(\boldsymbol{y}|\boldsymbol{\theta})$, and $\hat{\boldsymbol{\theta}}$ may not converge to $\hat{\boldsymbol{\theta}}_{ml}$. Furthermore, an iteration of the EM algorithm might produce a jump of $\hat{\boldsymbol{\theta}}_i$ from the vicinity of one local maximum to the vicinity of another local maximum of $\ln f(\mathbf{y}|\hat{\boldsymbol{\theta}}_i)$. Thus, it may be necessary to execute the EM algorithm with several different values of the initial vector $\hat{\boldsymbol{\theta}}_0$ to ensure that $\hat{\boldsymbol{\theta}}_i \rightarrow \hat{\boldsymbol{\theta}}_{ml}$ or a close approximation of it.

In many applications, $\mathbf{Y}$ is part of the complete data vector $\mathbf{Z} = [\mathbf{Y}\ \mathbf{X}]$, where $\mathbf{X}$ is called the *missing* data vector. In this case,

$$\ln f(\mathbf{z}|\boldsymbol{\theta}) = \ln f(\mathbf{y}|\mathbf{x}, \boldsymbol{\theta}) + \ln f(\mathbf{x}|\boldsymbol{\theta}). \tag{8.11}$$

Since $f(\mathbf{z}|\mathbf{y}, \hat{\boldsymbol{\theta}}_i) = f(\mathbf{x}, \mathbf{y}|\mathbf{y}, \hat{\boldsymbol{\theta}}_i) = f(\mathbf{x}|\mathbf{y}, \hat{\boldsymbol{\theta}}_i)$, $E_{\mathbf{z}|\mathbf{y},\hat{\boldsymbol{\theta}}_i}[\cdot] = E_{\mathbf{x}|\mathbf{y},\hat{\boldsymbol{\theta}}_i}[\cdot]$, and (8.9) becomes

$$\chi(\boldsymbol{\theta}, \hat{\boldsymbol{\theta}}_i) = E_{\mathbf{x}|\mathbf{y},\hat{\boldsymbol{\theta}}_i}[\ln f(\mathbf{z}|\boldsymbol{\theta})]. \tag{8.12}$$

Bayes' rule gives

$$f(\mathbf{x}|\mathbf{y}, \hat{\boldsymbol{\theta}}_i) = \frac{f(\mathbf{y}|\mathbf{x}, \hat{\boldsymbol{\theta}}_i) f(\mathbf{x}|\hat{\boldsymbol{\theta}}_i)}{f(\mathbf{y}|\hat{\boldsymbol{\theta}}_i)} \tag{8.13}$$

which is used in the evaluation of the expected value in (8.12).

Example. As a practical example, consider a random binary sequence X_i, $i = 1, \ldots, N$, transmitted over the AWGN channel. The received random vector $\mathbf{Y} = [Y_1 \ldots Y_N]^T$ is

$$\mathbf{Y} = A\mathbf{X} + \mathbf{n} \tag{8.14}$$

where A is a positive constant amplitude, $\mathbf{X} = [X_1 \ldots X_N]^T$ is the vector of bits, and $\mathbf{n} = [n_1 \ldots n_N]^T$ is the vector of noise samples, which are assumed to be independent, identically distributed, zero-mean, Gaussian random variables with variance v. The bits are assumed to be independent of each other and the parameters, and $X_i = 1$ with probability $1/2$ and $X_i = -1$ with probability $1/2$. Thus, density functions involving $\mathbf{X}$ are replaced by probability functions. It is desired to estimate the parameter vector $\boldsymbol{\theta} = [A\ \ v]^T$.

Equation (8.14) and the system model imply that

$$f(\mathbf{y}|\mathbf{x}, \boldsymbol{\theta}) = \prod_{i=1}^{N} \frac{1}{\sqrt{2\pi v}} \exp\left[-\frac{(y_i - Ax_i)^2}{2v} \right]. \tag{8.15}$$

By expanding the product and matching terms in the summation, we find that

$$\sum_{\mathbf{x}} f(\mathbf{y}|\mathbf{x}, \boldsymbol{\theta}) = \prod_{k=1}^{N} [f_1(y_k|\boldsymbol{\theta}) + f_2(y_k|\boldsymbol{\theta})] \tag{8.16}$$

where the summation is over all 2^N possible values of $\mathbf{x}$, $f_1(y_k|\boldsymbol{\theta})$ is Gaussian with mean A and variance v, and $f_2(y_k|\boldsymbol{\theta})$ is Gaussian with mean $-A$ and variance v. Since $\mathbf{X}$ is independent of $\boldsymbol{\theta}$, $Pr(\mathbf{x}|\boldsymbol{\theta}) = Pr(\mathbf{x}) = 2^{-N}$, and

$$f(\mathbf{y}|\boldsymbol{\theta}) = \sum_{\mathbf{x}} f(\mathbf{y}, \mathbf{x}|\boldsymbol{\theta}) = 2^{-N} \sum_{\mathbf{x}} f(\mathbf{y}|\mathbf{x}, \boldsymbol{\theta})$$

$$= 2^{-N} \prod_{k=1}^{N} [f_1(y_k|\boldsymbol{\theta}) + f_2(y_k|\boldsymbol{\theta})]. \tag{8.17}$$

Substitution of this equation into the likelihood equation (8.2) results in a mathematically intractable set of equations. Thus, we apply the EM algorithm to estimate $\boldsymbol{\theta}$.

We define the complete data vector as $\mathbf{Z} = [\mathbf{Y}\ \mathbf{X}]^T$. We have

$$\ln f(\mathbf{z}|\boldsymbol{\theta}) = \ln f(\mathbf{y}|\mathbf{x}, \boldsymbol{\theta}) - N \ln 2. \tag{8.18}$$

Substitution of (8.15) into (8.18) yields

$$\ln f(\mathbf{z}|\boldsymbol{\theta}) = C - \frac{N}{2} \ln v - \frac{1}{2v} \sum_{k=1}^{N} (y_k - Ax_k)^2 \tag{8.19}$$

where C is a constant that does not depend on the parameters A and v. Therefore, (8.12) and (8.13) give

$$\chi(\boldsymbol{\theta}, \hat{\boldsymbol{\theta}}_i) = C - \frac{N}{2} \ln v - \frac{1}{2v} \sum_{k=1}^{N} \sum_{\mathbf{x}} (y_k - Ax_k)^2 \Pr(\mathbf{x}|\mathbf{y}, \hat{\boldsymbol{\theta}}_i) \tag{8.20}$$

$$\Pr(\mathbf{x}|\mathbf{y}, \hat{\boldsymbol{\theta}}_i) = \frac{2^{-N} f(\mathbf{y}|\mathbf{x}, \hat{\boldsymbol{\theta}}_i)}{f(\mathbf{y}|\hat{\boldsymbol{\theta}}_i)} \tag{8.21}$$

where $\hat{\boldsymbol{\theta}}_i = [\hat{A}_i\ \hat{v}_i]^T$. Using (8.17), and (8.21), we obtain

$$\sum_{\mathbf{x}} (y_k - Ax_k)^2 \Pr(\mathbf{x}|\mathbf{y}, \hat{\boldsymbol{\theta}}_i)$$

$$= \frac{\sum_{\mathbf{x}/k} (y_k - A)^2 f(\mathbf{y}|\mathbf{x}/k, x_k = 1, \hat{\boldsymbol{\theta}}_i) + \sum_{\mathbf{x}/k} (y_k + A)^2 f(\mathbf{y}|\mathbf{x}/k, x_k = -1, \hat{\boldsymbol{\theta}}_i)}{\prod_{k'=1}^{N} [f_1(y_{k'}|\hat{\boldsymbol{\theta}}_i) + f_2(y_{k'}|\hat{\boldsymbol{\theta}}_i)]} \tag{8.22}$$

where $\mathbf{x}/k$ denotes the vector $\mathbf{x}$ excluding the component x_k. The substitution of equations similar to (8.16) into (8.22) yields

$$\sum_{\mathbf{x}} (y_k - Ax_k)^2 \Pr(\mathbf{x}|\mathbf{y}, \hat{\boldsymbol{\theta}}_i) = \frac{(y_k - A)^2 f_1(y_k|\hat{\boldsymbol{\theta}}_i) + (y_k + A)^2 f_2(y_k|\hat{\boldsymbol{\theta}}_i)}{f_1(y_k|\hat{\boldsymbol{\theta}}_i) + f_2(y_k|\hat{\boldsymbol{\theta}}_i)}$$

$$= A^2 + y_k^2 - 2Ay_k \tanh\left(\frac{\hat{A}_i y_k}{\hat{v}_i}\right). \tag{8.23}$$

The substitution of this equation into (8.20) gives

$$\chi(\boldsymbol{\theta}, \hat{\boldsymbol{\theta}}_i) = C - \frac{N}{2} \ln v - \frac{NA^2}{2v} - \frac{1}{2v} \sum_{k=1}^{N} \left[y_k^2 - 2Ay_k \tanh\left(\frac{\hat{A}_i y_k}{\hat{v}_i} \right) \right] \tag{8.24}$$

which completes the E-step.

The estimates that maximize $\chi(\boldsymbol{\theta}, \hat{\boldsymbol{\theta}}_i)$ are obtained by solving

$$\frac{\partial \chi(\boldsymbol{\theta}, \hat{\boldsymbol{\theta}}_i)}{\partial A}\Big|_{\boldsymbol{\theta}=\hat{\boldsymbol{\theta}}_{i+1}} = 0, \quad \frac{\partial \chi(\boldsymbol{\theta}, \hat{\boldsymbol{\theta}}_i)}{\partial v}\Big|_{\boldsymbol{\theta}=\hat{\boldsymbol{\theta}}_{i+1}} = 0. \tag{8.25}$$

Combining the solutions, we obtain the M-step:

$$\hat{A}_{i+1} = \frac{1}{N} \sum_{k=1}^{N} y_k \tanh\left(\frac{\hat{A}_i y_k}{\hat{v}_i} \right) \tag{8.26}$$

$$\hat{v}_{i+1} = \frac{1}{N} \sum_{k=1}^{N} y_k^2 - \hat{A}_{i+1}^2. \tag{8.27}$$

A suitable set of initial values are

$$\hat{A}_0 = \frac{1}{N} \sum_{k=1}^{N} |y_k|, \quad \hat{v}_0 = \frac{1}{N} \sum_{k=1}^{N} y_k^2 - \hat{A}_0^2. \tag{8.28}$$

which completes the algorithm specification. □

8.1.1 Fixed-Point Iteration

In the maximization step of the expectation-maximization method, derivatives are calculated and set equal to zero. After algebraic transformations, we can often obtain one or more equations of the form $f(x) = 0$ that must be solved. The solution is the value x_s, such that $f(x_s) = 0$ when $x = x_s$. If $f(x)$ is a polynomial of degree 3 or higher or if $f(x)$ includes transcendental functions, then a closed-form solution or formula for x_s may not exist, and an approximation method may be necessary.

The *fixed-point iteration method* [2] is a method that does not require the calculation of the derivative of $f(x)$, which may be difficult. To use the method, $f(x) = 0$ is algebraically transformed into an equation of the form

$$x = g(x). \tag{8.29}$$

Then the solution x_s such that

$$x_s = g(x_s) \tag{8.30}$$

which implies that $f(x_s) = 0$, is computed iteratively. After an initial estimate x_0 of the solution, the *fixed-point iteration* is

$$x_{n-1} = g(x_n) \quad n = 0, \ 1, \ \ldots \tag{8.31}$$

which converges to the solution x_s under certain conditions. This solution is called the *fixed point* of $g(x)$ because $g(x_s) = x_s$.

Sufficient convergence conditions for the fixed-point iteration are established by the following theorem. Let $g'(x)$ denote the derivative of $g(x)$ with respect to x.

Theorem. *Suppose that $g(x)$ has a continuous derivative such that $|g'(x)| \leq K < 1$ in an interval I_0. If $x_s \epsilon I_0$ and $x_s = g(x_s)$, then the fixed-point iteration converges so that $x_n \to x_s$ as $n \to \infty$ for any $x_0 \epsilon I_0$.*

Proof. According to the mean-value theorem of calculus, there is a number $u \epsilon (x_s, x_n)$ such that

$$g(x_n) - g(x_s) = g'(u)(x_n - x_s). \tag{8.32}$$

Since by hypothesis $|g'(x)| \leq K$ for $(x_s, x_n) \epsilon I_0$,

$$|g(x_n) - g(x_s)| \leq K|x_n - x_s|. \tag{8.33}$$

Equations (8.30), (8.31), and (8.33) yield

$$|x_n - x_s| = |g(x_{n-1}) - g(x_s)| \leq K|x_{n-1} - x_s|. \tag{8.34}$$

Repeated application of this inequality implies that

$$|x_n - x_s| \leq K^n |x_0 - x_s|. \tag{8.35}$$

Since $K < 1$, $K^n \to 0$ and $|x_n - x_s| \to 0$ as $n \to \infty$. Therefore, $x_n \to x_s$ as $n \to \infty$. □

The algebraic transformation from the equation $f(x) = 0$ to the equation $x = g(x)$ can usually be performed in more than one way. The value of K that $|g'(x)| < K$ for $x \epsilon I_0$ is generally different for each transformation. Among those transformations for which $K<1$, thereby ensuring convergence of the fixed-point iteration, choosing the specific transformation with the smallest value of K maximizes the speed of convergence.

For example, suppose that $f(x) = x^2 + ax + b = 0$ where $x \neq 0, a \neq 0$. Then one algebraic transformation gives $x = -(x^2 + b)/a$. For this transformation, $g'(x) = -2x/a$ and convergence occurs if $|x| < |a|/2$. A second algebraic transformation gives $x = -a - bx^{-1}$. Then $g'(x) = b/x^2$ and convergence occurs if $|x| > \sqrt{|b|}$. The two intervals in which convergence of the fixed-point iteration is ensured do not intersect if $a^2 < 4|b|$.

8.2 Direct-Sequence Systems

Since the wireless channel and possibly multiple-access or other interference cause random amplitude and phase variations in the received data, the accuracy of channel state information (CSI) at the receiver is critical for coherent demodulation and efficient soft-decision decoding. Current and next-generation cellular protocols such as W-CDMA (Wideband Code-Division Multiple Access) and 3GPP LTE (Third-Generation Partnership Project Long-Term Evolution) specify the use of pilot-assisted channel estimation (PACE) [3]. *Pilot symbols* or reference signals are known symbols either multiplexed with or superimposed onto the transmitted data in the time or frequency domain, with the associated disadvantages of a loss in spectral or power efficiency and an unsuitability for fast-fading channels with a coherence time shorter than the pilot-symbol transmission rate. Although the primary role of pilot symbols in most cellular standards is channel estimation, pilot symbols often play a secondary role in cell, frame, or symbol synchronization, but alternative methods of synchronization may be used when pilot symbols are unavailable [4, 5]. *Blind channel-estimation methods,* which typically use second-order statistics of the received symbols for channel estimation, avoid the implementation cost of pilot symbols, but have performance losses [6]. Improved performance is achieved by using channel estimation based on the EM algorithm [7]. In this section, a direct-sequence system featuring both iterative EM channel estimation and iterative detection and decoding without *any* pilot symbols is described [8]. The channel estimation includes an estimation of the received *interference-power spectral density*, which is due to both the thermal noise and the time-varying interference. An accurate estimate enables improved interference suppression by the decoder.

Figure 8.1 shows the block diagram of a dual quaternary DS/CDMA transmitter (Sect. 2.4) comprising a channel encoder, QPSK modulator, and a direct-sequence spreading generator that multiplies orthogonal chip sequences with the in-phase and quadrature modulator inputs. The input to the encoder in the figure is modeled as a random binary sequence of length K, which is denoted by $\mathbf{m} = [m(1), \ldots, m(K)]$, $m(i_{bit}) \in [1, 0]$.

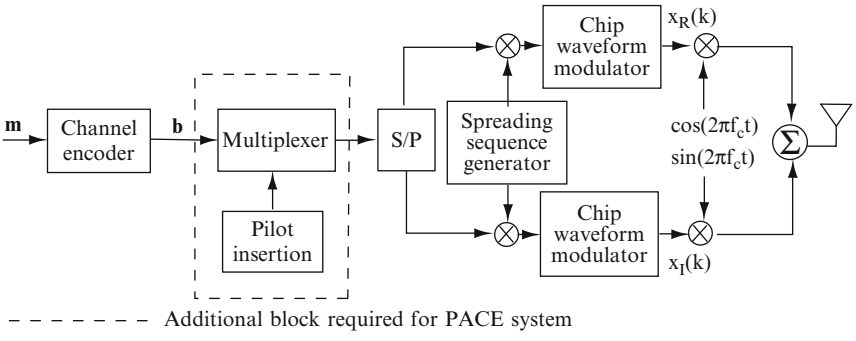

Fig. 8.1 DS/CDMA transmitter with QPSK modulation

8.2.1 Encoding, Modulation, and Channel Estimation

Each $1 \times K$ message vector $\mathbf{m}$ is encoded into a $1 \times N$ codeword $\mathbf{b} = [b(1), \ldots, b(N)]$ using a systematic, extended, irregular repeat-accumulate (IRA) code (Sect. 1.6). IRA codes offer a combination of the linear complexity of turbo encoding and the lower complexity of LDPC decoding without compromising on performance. The (N, K) rate-$1/2$ IRA code is constructed using density evolution [9] with maximum node degrees $d_v = 8$ and $d_c = 7$ in (1.190) and (1.191). We obtain a strong IRA code with degree distributions

$$\begin{aligned} v(x) &= 0.00008 + 0.31522x + 0.34085x^2 + 0.0.06126x^6 + 0.28258x^7 \\ \chi(x) &= 0.62302x^5 + 0.37698x^6. \end{aligned} \tag{8.36}$$

The $(N - K) \times N$ IRA systematic parity-check matrix and the generator matrix are defined by (1.192) and (1.194), respectively.

Gray-labeled QPSK (Sect. 1.7) is used with 2 encoded bits mapped into a modulation symbol $x(k) \in \{\pm 1, \pm j\}$, $k = 1, \ldots, N/2$, $j = \sqrt{-1}$. Although QPSK is assumed, the subsequent analysis and simulation is easily extended to q-ary QAM. Parallel streams of code bits are each spread using a Gold sequence with spreading factor G chips/code bit before rectangular pulse-shaping that produces the real and imaginary components of $x(k)$, i.e., $x_R(k) = \mathrm{Re}\,(x\,(k))$ and $x_I\,(k) = \mathrm{Im}\,(x\,(k))$. In practice, an IF would be used before the carrier frequency upconversion, but the upconversion from baseband to the IF is omitted for clarity in Fig. 8.1.

No channel interleaving is applied to the IRA code due to the inherent interleaving characteristics of the IRA encoder, which can be alternatively represented as a repetition code concatenated with an interleaver and an accumulator. The interleaver is essentially embedded within the matrix $\mathbf{H}_1$ that is part of the generator matrix defined by (1.194).

Each codeword or frame comprises $N/2$ QPSK code symbols and $NG/2$ spreading-sequence chips for each QPSK component. Each of these frames comprises two different types of subframes or blocks. A *fading block* has N_b code bits over which the fading amplitude is assumed to be constant. An *interference block* has N_{ib} code bits over which the interference level is assumed to be constant. The complex fading amplitude associated with both spreading sequences during a fading block is

$$B = \sqrt{\mathcal{E}_s}\alpha e^{j\theta} \tag{8.37}$$

where $\mathcal{E}_s$ is the average energy per QPSK symbol, α is the magnitude of the fading amplitude with $E\left[\alpha^2\right] = 1$, and θ is the unknown fading-induced channel phase.

8.2.2 Iterative Receiver Structure

Figure 8.2 shows a block diagram of the dual-quaternary iterative receiver. The received signal is downconverted, passed through chip-matched filters, and despread

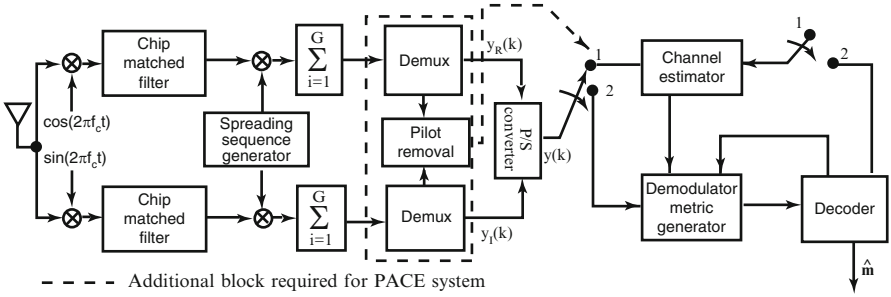

Fig. 8.2 Iterative DS/CDMA receiver with channel estimator

by a synchronized spreading sequence in each branch, with the downconverter and synchronization devices omitted in the figure for clarity. Accurate synchronization in the receiver is assumed to prevent self-interference between the two spreading sequences of the desired user. Let $N_0/2$ denote the two-sided power spectral density of the Gaussian noise. For the flat-fading scenario and a particular fading block, the complex envelope of the received signal at the kth symbol time with active multiple-access interference, which appears at the output of the parallel-to-serial (P/S) converter, may be expressed as

$$\begin{aligned} y(k) &= y_R(k) + jy_I(k) \\ &= Bx(k) + J(k) + n(k), \ 1 \le k \le \frac{N}{2} \end{aligned} \tag{8.38}$$

where $x(k)$ is the complex transmitted code symbol of the desired user, $n(k)$ is a complex zero-mean, circularly symmetric, Gaussian noise sample with $E\left[|n_k|^2\right] = N_0$, and $J(k)$ is the interference at the demodulator (Sect. 1.1). If pilot symbols are received, they are removed by each demultiplexer (Demux) and applied to the channel estimator.

The time-varying multiple-access interference is assumed to be generated by interfering users with a structure identical to the desired user, albeit the spreading sequences differ and the complex fading amplitudes are independent. The great benefit of the direct-sequence spread spectrum is that the despreading in the receiver tends to whiten the interference-power spectral density over the code-symbol passband, and the subsequent filtering tends to produce a residual interference with an approximate Gaussian distribution. Thus, the combined interference and thermal noise is modeled as additive Gaussian noise with a two-sided power spectral density $A/2$ that is constant over each block of N_{ib} code bits but varies from block-to-block. This model enables the derivation of an EM estimator for A that is used in the demodulator metric and leads to the suppression of the interference.

A *receiver iteration* is defined as a decoder iteration followed by internal EM iterations in the channel estimator of Fig. 8.2, and then a single demodulator metric

generation. Let r denote the index for the internal EM iteration, $r = 1, \ldots, r_{max}$; let l denote the index for the closed-loop receiver iteration, $l = 1, \ldots, l_{max}$.

Let $\hat{\theta}_{(r)}^{(l)} = \left(\widehat{B}_{(r)}^{(l)}, \widehat{A}_{(r)}^{(l)}\right)$ represent the estimates of the complex fading amplitude and interference-power spectral density parameters at the rth EM iteration during the lth overall receiver iteration. EM iterations commence after the initial channel estimation and decoding, which is obtained while the switch in Fig. 8.2 is set to position 1. The subsequent receiver iterations are performed while the switch is set to position 2 in order to refine the initial channel estimate with the aid of soft feedback from the channel decoder.

8.2.3 EM Algorithm

The direct calculation of the maximum-likelihood channel estimator $\hat{\theta}$ from a received data vector $\mathbf{y} = [y(1), \ldots, y(N_d)]$ of N_d code symbols is not feasible because the computational complexity increases exponentially with N_d. Instead, the EM algorithm is used with the *complete received data vector* defined as $\mathbf{z} = (\mathbf{x}, \mathbf{y})$, where the missing data vector $\mathbf{x}$ is the transmitted signal vector.

Since $\mathbf{x}$ is independent of the parameter θ, (8.11) becomes

$$\ln f(\mathbf{z}|\boldsymbol{\theta}) = \ln f(\mathbf{y}|\mathbf{x}, \boldsymbol{\theta}) + \ln f(\mathbf{x}). \tag{8.39}$$

Assuming independent symbols and zero-mean, circularly symmetric, Gaussian noise and interference, we obtain

$$f(\mathbf{y}|\mathbf{x}, \boldsymbol{\theta}) = \frac{1}{(\pi A)^{N_d}} \exp\left(-\sum_{k=1}^{N_d} \frac{\left(|y(k) - Bx(k)|^2\right)}{A}\right). \tag{8.40}$$

Therefore, since $|x(k)|^2 = 1 \quad \forall k$,

$$\ln f(\mathbf{y}|\mathbf{x}, \boldsymbol{\theta}) = -N_d \cdot \ln(A) - \frac{1}{A} \sum_{k=1}^{N_d} \left[|y(k)|^2 + |B|^2 - 2\mathrm{Re}\left(y^*(k) B x(k)\right)\right] \tag{8.41}$$

where an irrelevant constant has been dropped.

E-step: The E-step requires the calculation of the conditional expectation of the conditional log-likelihood of $\mathbf{z} = (\mathbf{y}, \mathbf{x})$:

$$\chi\left(\boldsymbol{\theta}, \hat{\boldsymbol{\theta}}_{(r)}^{(l)}\right) = E_{\mathbf{z}|\mathbf{y}, \hat{\boldsymbol{\theta}}_{(r)}^{(l)}} \left[\ln f(\mathbf{z}|\boldsymbol{\theta})\right] \tag{8.42}$$

where $\hat{\boldsymbol{\theta}}_{(r)}^{(l)}$ is the previous estimate. Using (8.39) and (8.41) and observing that $\ln f(\mathbf{x})$ in (8.39) is independent of θ, and hence irrelevant to the subsequent maximization, we obtain

$$\chi\left(\theta, \hat{\theta}_{(r)}^{(l)}\right) = -N_d \cdot \ln(A) - \frac{1}{A}\sum_{k=1}^{N_d}\left[|y(k)|^2 + |B|^2 - 2\mathrm{Re}\left(y^*(k)B\bar{x}_{(r)}^{(l)}(k)\right)\right] \tag{8.43}$$

where $\bar{x}_{(r)}^{(l)}(k) = E_{\mathbf{z}|\mathbf{y},\hat{\theta}_{(r)}^{(l)}}[x(k)] = E_{\mathbf{x}|\mathbf{y},\hat{\theta}_{(r)}^{(l)}}[x(k)]$. Assuming the independence of each transmitted symbol $x(k)$ and the independence of $x(k)$ and $\hat{\theta}_{(r)}^{(l)}$, and using Bayes' law and the fact that (8.40) can be expressed as a product of N_d factors, we obtain

$$\bar{x}_{(r)}^{(l)}(k) = E_{x(k)|y(k),\hat{\theta}_{(r)}^{(l)}}[x(k)] \tag{8.44}$$

where

$$f\left(x(k)|y(k), \hat{\boldsymbol{\theta}}_{(r)}^{(l)}\right) = \frac{f\left(y(k) \mid x(k), \hat{\boldsymbol{\theta}}_{(r)}^{(l)}\right)}{f\left(y(k) \mid \hat{\boldsymbol{\theta}}_{(r)}^{(l)}\right)}\Pr(x(k)) \tag{8.45}$$

and

$$f\left(y(k)|x(k), \hat{\boldsymbol{\theta}}_{(r)}^{(l)}\right) = \frac{1}{\pi \widehat{A}_{(r)}^{(l)}}\exp\left(-\frac{|y(k) - \widehat{B}_{(r)}^{(l)}x(k)|^2}{\widehat{A}_{(r)}^{(l)}}\right). \tag{8.46}$$

M-step: Taking the derivative of (8.43) with respect to the real and imaginary parts of the complex-valued B, and then setting the results equal to zero, we obtain the estimate of the complex fading amplitude at iteration $r+1$ as

$$\mathrm{Re}\left(\widehat{B}_{(r+1)}^{(l)}\right) = \frac{1}{N_d}\sum_{k=1}^{N_d}\mathrm{Re}\left(y^*(k)\,\bar{x}_{(r)}^{(l)}(k)\right) \tag{8.47}$$

$$\mathrm{Im}\left(\widehat{B}_{(r+1)}^{(l)}\right) = -\frac{1}{N_d}\sum_{k=1}^{N_d}\mathrm{Im}\left(y^*(k)\,\bar{x}_{(r)}^{(l)}(k)\right). \tag{8.48}$$

Similarly, maximizing (8.43) with respect to A leads to

$$\widehat{A}_{(r+1)}^{(l)} = \frac{1}{N_d}\sum_{k=1}^{N_d}\left|y(k) - \widehat{B}_{(r+1)}^{(l)}\bar{x}_{(r)}^{(l)}(k)\right|^2. \tag{8.49}$$

The fading phase and amplitude can be explicitly estimated from (8.47) and (8.48), but that is unnecessary.

Let $s_1 = \Pr(x(k) = +1)$, $s_2 = \Pr(x(k) = +j)$, $s_3 = \Pr(x(k) = -1)$, $s_4 = \Pr(x(k) = -j)$, and let $s_\beta^{(l)}$, $\beta = 1, 2, 3, 4$, denote the code-symbol probabilities obtained from the soft outputs of the channel decoder. To calculate $\bar{x}_{(r)}^{(l)}(k)$,

the approximation $s_\beta = s_\beta^{(l)}$, $\beta = 1, 2, 3, 4$ is used. Using the approximation and (8.46) to calculate the denominator of (8.45), and then substituting (8.45) into (8.44), the expectation of $x(k)$ at the rth EM and lth receiver iteration is calculated as

$$\bar{x}_{(r)}^{(l)}(k) = \frac{s_1^{(l)} R_{1,(r)}^{(l)} + j s_2^{(l)} R_{2,(r)}^{(l)} - s_3^{(l)} R_{3,(r)}^{(l)} - j s_4^{(l)} R_{4,(r)}^{(l)}}{\sum_{\beta=1}^{4} s_\beta^{(l)} R_{\beta,(r)}^{(l)}} \tag{8.50}$$

where likelihood-ratio $R_{\beta,(i)}^{(l)}$ depends on the current channel estimates as

$$R_{1,(r)}^{(l)} = \exp\left[\frac{2}{\widehat{A}_{(r)}^{(l)}} \mathrm{Re}(\widehat{B}_{(r)}^{(l)} y(k))\right], \quad R_{2,(r)}^{(l)} = \exp\left[\frac{2}{\widehat{A}_{(r)}^{(l)}} \mathrm{Im}(\widehat{B}_{(r)}^{(l)} y(k))\right]$$
$$R_{3,(i)}^{(l)} = \exp\left[-\frac{2}{\widehat{A}_{(r)}^{(l)}} \mathrm{Re}(\widehat{B}_{(r)}^{(l)} y(k))\right], \quad R_{4,(r)}^{(l)} = \exp\left[-\frac{2}{\widehat{A}_{(r)}^{(l)}} \mathrm{Im}(\widehat{B}_{(r)}^{(l)} y(k))\right] \tag{8.51}$$

and

$$\widehat{B}_{(0)}^{(l)} = \widehat{B}_{(r_{\max})}^{(l-1)}, \quad 1 \le l \le l_{\max}. \tag{8.52}$$

Methods for obtaining the initial estimates $\left(\widehat{B}_{(r_{max})}^{(0)}, \widehat{A}_{(r_{\max})}^{(0)}\right)$ of each fading block are described subsequently.

Therefore, for a given receiver iteration, $\bar{x}_{(r)}^{(l)}(k)$ and $R_{\beta,(r)}^{(l)}$ are updated r_{max} number of times using decoder feedback $s_\beta^{(l)}$. In the next receiver iteration, after channel re-estimation, the fading-amplitude and interference-power spectral density estimates are updated, and then used by the demodulator and channel decoder to recompute $\bar{x}_{(r)}^{(l+1)}(k)$ and $R_{\beta,(r)}^{(l+1)}$. This process is repeated again for r_{max} EM iterations, and the aforementioned cycles continue similarly for subsequent receiver iterations.

In estimating the fading parameters, we set $N_d = N_b/2$; in estimating A, we choose $N_{ib} \le N_b$ and set $N_d = N_{ib}/2$. The EM estimator first finds the value of $\widehat{B}_{(r)}^{(l)}$ for a fading block of size N_b. Then it finds the value of $\widehat{A}_{(r)}^{(l)}$ for each smaller or equal interference block of size N_{ib} using the value of $\widehat{B}_{(r)}^{(l)}$ found for the larger or equal fading block. When pilot symbols are used, we set $\bar{x}_{(r)}^{(l)}(k) = x(k)$ for each known pilot bit, and there are no EM iterations if only known pilot bits are processed in calculating the channel estimates.

The constellation labeling (Sect. 1.7) of each QPSK symbol by two bits is the following. The symbol $x(k) = +1$ is labeled 00; the symbol $x(k) = +j$ is labeled 01; the symbol $x(k) = -1$ is labeled 11; the symbol $x(k) = -j$ is labeled 10. Let b_1, b_2 denote the two successive bits of a QPSK symbol, and v_1, v_2 denote the corresponding log-likelihood ratios that are fed back by the channel decoder.

Consider bit $b_1(k)$ of symbol $x(k)$ after receiver iteration l. Substituting (8.46) into (1.205), we obtain the *extrinsic log-likelihood ratio* for $b_1(k)$:

$$z_1^{(l)}(k) = \log\left[\frac{\sum\limits_{x(k):b_1(k)=1} \exp\left\{\frac{2}{\widehat{A}_{(r_{\max})}^{(l)}}\mathrm{Re}\left[\widehat{B}_{(r_{\max})}^{(l)} y^*(k)x(k)\right] + b_2(k)\,v_2\right\}}{\sum\limits_{x(k):b_1(k)=0} \exp\left\{\frac{2}{\widehat{A}_{(r_{\max})}^{(l)}}\mathrm{Re}\left[\widehat{B}_{(r_{\max})}^{(l)} y^*(k)x(k)\right] + b_2(k)\,v_2\right\}}\right] \tag{8.53}$$

where both sums are over two symbols.

In the sum in the numerator, $b_1(k)=1$ if $x(k)=-j$ or -1. If $x(k)=-j$, then $2\mathrm{Re}\left[\widehat{B}_{(r_{\max})}^{(l)} y^*(k)x(k)\right]/\widehat{A}_{(r)}^{(l)} + b_2(k)\,v_2 = 2\mathrm{Im}\left[\widehat{B}_{(r_{\max})}^{(l)} y^*(k)\right]/\widehat{A}_{(r)}^{(l)}$; if $x(k)=-1$, then $2\mathrm{Re}\left[\widehat{B}_{(r_{\max})}^{(l)} y^*(k)x(k)\right]/\widehat{A}_{(r)}^{(l)} + b_2(k)\,v_2 = -2\mathrm{Re}\left[\widehat{B}_{(r_{\max})}^{(l)} y^*(k)\right]/\widehat{A}_{(r)}^{(l)} + v_2$. The sum in the denominator is evaluated similarly. Further similar calculations provide the extrinsic log-likelihood ratio for $b_2(k)$. Therefore, the demodulation metrics (extrinsic log-likelihood ratios) $z_\nu^{(l)}(k)$, $\nu = 1, 2$, for bits 1, 2 of symbol k that are applied to the channel decoder are

$$z_1^{(l)}(k) = \log\left\{\frac{\exp\left[G^{(l)}(k)\right] + \exp\left[-F^{(l)}(k)+v_2\right]}{\exp\left[F^{(l)}(k)\right] + \exp\left[-G^{(l)}(k)+v_2\right]}\right\} \tag{8.54}$$

$$z_2^{(l)}(k) = \log\left\{\frac{\exp\left[-G^{(l)}(k)\right] + \exp\left[-F^{(l)}(k)+v_1\right]}{\exp\left[F^{(l)}(k)\right] + \exp\left[G^{(l)}(k)+v_1\right]}\right\} \tag{8.55}$$

where

$$F^{(l)}(k) = \frac{2}{\widehat{A}_{(r_{\max})}^{(l)}}\mathrm{Re}\left[\widehat{B}_{(r_{\max})}^{(l)} y^*(k)\right],\ G^{(l)}(k) = \frac{2}{\widehat{A}_{(r_{\max})}^{(l)}}\mathrm{Im}\left[\widehat{B}_{(r_{\max})}^{(l)} y^*(k)\right]. \tag{8.56}$$

The number of EM iterations and the receiver latency are reduced by applying a *stopping criterion*. Iterations stop once $\widehat{B}_{(r)}^{(l)}$ is within a specified fraction of its value at the end of the previous iteration or a specified maximum number is reached. The fraction should be sufficiently small (perhaps 10%) that the performance loss will be insignificant.

8.2.4 Perfect Phase Information at Receiver

The carrier synchronization provided by a phase-locked loop in several second and third-generation cellular standards such as IS-95 and CDMA2000 can be exploited to obviate the need to estimate the channel phase. Assuming perfect phase information at the receiver, the fading amplitude is real-valued and

nonnegative, and (8.48) does not have to be computed. The EM algorithm generates updated channel estimates as shown in (8.47)–(8.49) *after* the initial coherent demodulation and decoding that precedes the first receiver iteration. Blind initial estimates $\left(\widehat{B}^{(0)}_{(r_{max})}, \widehat{A}^{(0)}_{(r_{\max})}\right)$ for each fading block can be obtained from the received symbols as

$$\widehat{B}^{(0)}_{(r_{max})} = \frac{2}{N_b} \sum_{k=1}^{N_b/2} |y(k)| \tag{8.57}$$

$$\widehat{A}^{(0)}_{(r_{\max})} = \max\left[D - \left(\widehat{B}^{(0)}_{(r_{max})}\right)^2, h \cdot \left(\widehat{B}^{(0)}_{(r_{max})}\right)^2\right] \tag{8.58}$$

where

$$D = \frac{2}{N_b} \sum_{k=1}^{N_b/2} |y(k)|^2 \tag{8.59}$$

represents the average power of the received symbols, and $D - \left(\widehat{B}^{(0)}_{(r_{max})}\right)^2$ is the difference between that power and the average power of a desired symbol. Equation (8.57) would provide a perfect estimate in the absence of noise and interference. The parameter $h > 0$ is chosen such that $\left(\widehat{B}^{(0)}_{(r_{max})}\right)^2 / \widehat{A}^{(0)}_{(r_{\max})}$ does not exceed some maximum value. Ideally, h is a function of $\mathcal{E}_s/N_0$, but here a constant $h = 0.1$ is always used for simplicity. This approach for the initial channel estimates is called *blind method I* in the sequel.

Although the EM estimation is a relatively low-complexity iterative approach to maximum-likelihood estimation, it consumes a much larger number of floating-point operations than pilot-assisted schemes do. To evaluate the complexity of the EM estimator in terms of required real additions and multiplications per block of N_d code symbols, each complex addition is equated to two real additions, each complex multiplication is equated to four real multiplications, and divisions are equated with multiplications. Equations (8.47)–(8.49) require $6N_d + 4$ real additions and $12N_d + 4$ real multiplications per EM iteration. Equations (8.54) and (8.55) require 6 real additions, 30 real multiplications, and the computation of 4 exponentials per EM iteration. Each of these calculations is repeated for each of $l_{\max} r_{\max}$ total EM iterations. The initial estimates calculated using (8.57)–(8.59), which only need to be computed once prior to the first EM iterations, require $2N_d$ real additions, $8N_d + 7$ real multiplications, and the computation of the maximum of two real numbers. A PACE receiver that uses only pilot symbols for channel estimation requires $6N_d + 4$ real multiplications and $12N_d + 4$ real multiplications to compute (8.47)–(8.49) once and does not need to compute the other equations. Thus, EM estimation increases the amount of computation for channel estimation by a factor of more than $l_{\max} r_{\max}$ relative to PACE.

8.2.5 No Phase Information at Receiver

The initial channel estimates in (8.57) and (8.58) for blind method I are expected to be degraded significantly when the phase information is also unknown, since an arbitrary initial phase value (e.g., 0 radians) must be assumed. To circumvent this problem, the initial receiver iteration consists of hard-decision demodulation and channel decoding, after which each decoded bit is used as $\bar{x}^{(0)}_{(r_{max})}(k)$ in (8.47)–(8.49). This step is followed by the regular EM estimation process in subsequent receiver iterations. This approach for the initial channel estimates, which is referred to as *blind method II* in the sequel, results in increased receiver latency relative to the previous method when phase information is available.

8.2.6 Blind-PACE Estimation Trade-Offs

Assuming an identical transmit-power constraint and information bit-rate in both cases, the elimination of pilots creates the following possibilities for methods I and II:

- (Case A) An increase in the number of transmitted information symbols.
- (Case B) An increase in transmitted information-symbol duration.
- (Case C) An increase in the number of transmitted parity bits (lowered IRA code rate).

The modifications listed above offset the loss in system performance due to the degraded channel estimation obtained from blind methods I and II with respect to PACE. Assuming that the no-pilot cases A, B, and C have the same transmitted frame duration as the frame with pilot symbols, cases A, B, and C provide the most favorable throughput, spectral efficiency, and bit error rate, respectively.

8.2.7 Simulation Results

In all the simulations, the block sizes are equal, and the information-bit rate is 100 kb/s. Increasing the block sizes increases the accuracy of the EM estimators, but decreasing the block sizes allows closer tracking of the channel parameters and includes more diversity in the receiver computations. In most of the simulations, except where stated, $N_{ib} = N_b = 40$ and spreading factor is $G = 31$. The number of closed-loop receiver iterations is set to $l_{max} = 9$, as there is insignificant performance improvement for $l_{max} > 9$. The number of internal EM iterations is $r_{\max} = 10$. A rate-$1/2$ IRA code (data block size $K = 1{,}000$) with sum-product algorithm decoding (Sect. 1.6) is used without channel interleaving. The iterative PACE receiver considered for comparison contains 9.1% pilot-symbol overhead,

which has been shown to have a decoding performance close to the conventional 3GPP LTE receiver. For each of the representative scenarios tested, 5,000 Monte Carlo simulation trials were conducted.

Correlated fading of the desired signal and a mobile velocity of 120 km hr^{-1} are assumed. Flat fading is assumed in most of the simulations, whereas a frequency-selective channel is examined in the final simulation. The correlated fading model uses the autocorrelation of the channel response for two-dimensional isotropic scattering given by (5.39). The complex fading amplitude during block n, which is denoted by B_n, is computed as

$$B_n = \sqrt{J_0(2\pi f_d\, T_f)}B_{n-1} + \sqrt{1 - J_0(2\pi f_d\, T_f)}B_{dn}, \quad B_1 = B_{d1} \tag{8.60}$$

where f_d is the Doppler shift, T_f is the duration of a block, and B_{dn} is a complex fading amplitude selected for block n from the complex zero-mean, circularly symmetric, Gaussian distribution. For this distribution, the magnitude of the amplitude has a Rayleigh distribution and the phase has a uniform distribution.

The bit error rate (BER), which is equal to the information-bit error probability (Sect. 1.1), is calculated as a function of the energy-to-noise-density ratio $\mathcal{E}_b/N_0$, where $\mathcal{E}_b = (N/2K)\mathcal{E}_s$ is the energy per bit. The *information throughput* is a vital performance criterion in addition to the BER. One of the primary motivations in removing pilot symbols is the expectation of achieving greater information throughput, even though the BER may be degraded marginally. The information throughput is defined as

$$\mathcal{T} = \frac{\text{information bits in a codeword}}{\text{codeword duration}} \times (1 - BER) \quad \text{bits/s.} \tag{8.61}$$

8.2.7.1 Single-User Environment, Perfect Phase Knowledge

Figures 8.3 and 8.4 illustrate the performance when there is a single-user with perfect phase knowledge at the receiver. Figure 8.3 displays the BER versus $\mathcal{E}_b/N_0$ for an IRA-coded iterative receiver operating with perfect CSI, PACE, blind method I with cases A, B, and C, and blind method II with cases A and C, respectively. The key observation is that blind method II is worse than method I by 2 dB at $BER = 10^{-3}$ for both case A and case C, which illustrates the well-known sensitivity of the EM algorithm to the accuracy of the initial estimates.

The addition of extra parity bits to blind method I (case C, rate-1,000/2,200) offers the greatest improvement in BER, surpassing even the rate-1/2 code with perfect CSI at high E_b/N_0. The increase in number of information symbols (case A) results in the worst BER performance with a separation of 1 dB and 0.5 dB from PACE and case B at $BER = 10^{-3}$, respectively. The various scenarios featured in the figure were also tested under a slow-fading channel with mobile velocity of 10 km hr^{-1}. It was observed that all the BER curves were shifted towards the right

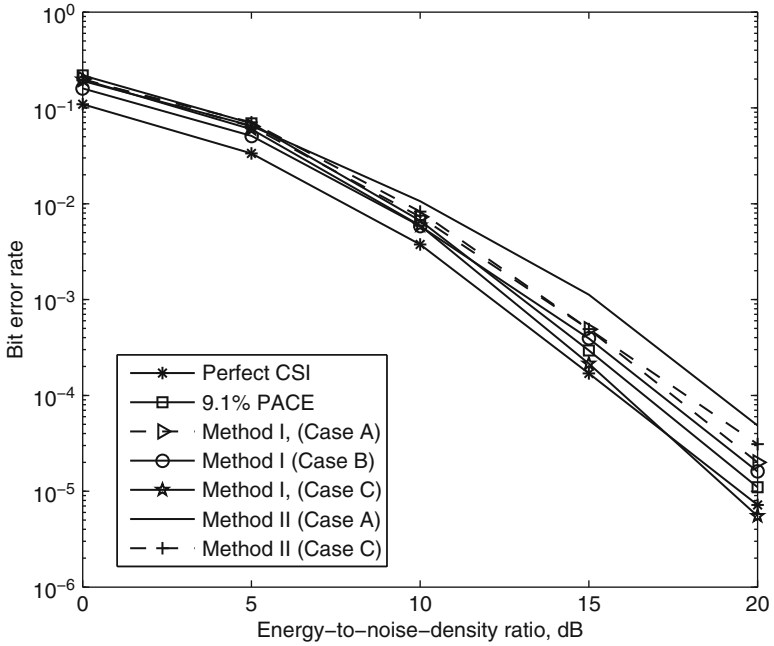

Fig. 8.3 BER versus $\mathcal{E}_b/N_0$ for IRA-coded iterative receiver in single-user environment with a perfectly estimated phase

by as much as 7 dB at $BER = 10^{-3}$ due to the loss of diversity, but the overall trends among the different cases remained the same.

Figure 8.4 exhibits information throughput $\mathcal{T}$ versus E_b/N_0 for the IRA-coded iterative receiver with the scenarios of Fig. 8.3. The throughput advantage of case A is achieved even though no pilot symbols are used at all; i.e., the initial estimation is totally blind. It is evident that increasing the symbol duration or adding additional parity information does not give the blind methods any significant advantage in throughput over PACE. Both blind methods with cases B, C and PACE provide about 20% less throughput than the receiver with perfect CSI.

8.2.7.2 Multiuser Environment, Unknown Phase

A 4-user interference environment with equal mean bit energies for all users at the receiver, $\mathcal{E}_b/N_0 = 20$ dB, and no phase information at the receiver is examined next. It is assumed that both the interference levels and the unknown phase are constant during each subframe. Each interference signal experiences independent correlated fading and uses independent data and Gold sequences with respect to the desired signal. The simulation uses chip-synchronous interference signals, which is a worst-case assumption (Sect. 6.2). Two variations of channel estimation

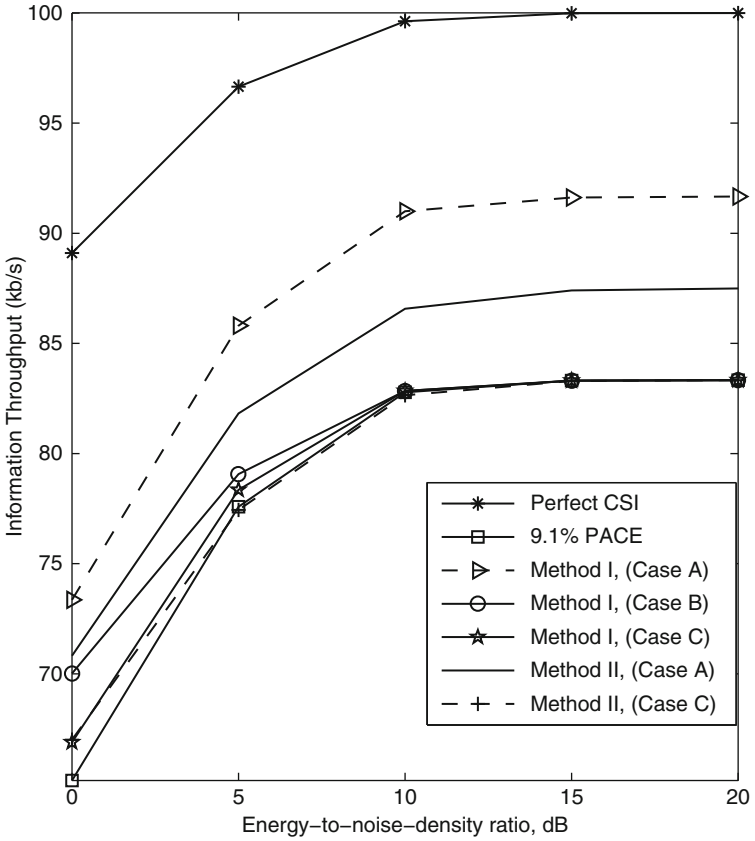

Fig. 8.4 Information throughput versus $\mathcal{E}_b/N_0$ for IRA-coded iterative receiver in single-user environment with a perfectly estimated phase

are examined here: *partially adaptive* with only complex fading amplitude $\widehat{B}_{(i)}^{(l)}$ estimated using (8.47), (8.48), and $\widehat{A}_{(r)}^{(l)}$ set equal to N_0 for all subframes; and *fully adaptive* estimation of both $\widehat{B}_{(r)}^{(l)}$ and $\widehat{A}_{(r)}^{(l)}$ using (8.47), (8.48), and (8.49).

Figure 8.5 displays IRA-coded BER versus E_b/N_0 for partially and fully adaptive channel estimation per fading block and case C for both blind methods. The mismatch of $\widehat{A}$ and the true value of A at the demodulator and decoder results in a high error floor for the partially adaptive cases. The intuition behind the error floor is that the partially adaptive estimator overestimates the true SINR by disregarding the multiple-access interference, with the degree of overestimation increasing with SINR. The fully adaptive estimation offers a more accurate SINR estimate and, hence, suppresses interference and reduces the error floor significantly. This interference suppression is achieved without using the far more elaborate multiuser and signal cancellation methods that could be implemented in a DS/CDMA receiver. For both partially and fully adaptive estimation, it is observed that blind method

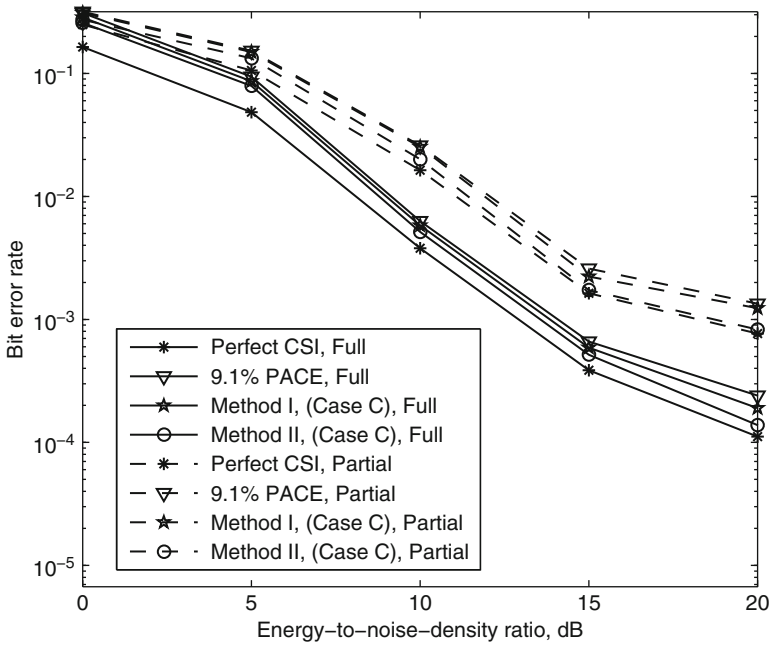

Fig. 8.5 BER versus $\mathcal{E}_b/N_0$ for IRA-coded iterative receiver affected by multiple-access interference from four users, fully and partially adaptive estimation, and unknown phase

II now outperforms method I due to better phase estimation, whereas both blind methods outperform PACE at $BER = 10^{-3}$ due to the added parity information.

Figure 8.6 demonstrates the IRA-coded receiver throughput offered by the blind methods with case A compared to PACE under multiple-access interference. The blind methods always provide a better throughput compared to PACE; for example, method I with case A is superior by 9% to both PACE scenarios when $\mathcal{E}_b/N_0 > 5$ dB. It is observed that both partial and fully-adaptive estimation methods offer a similar asymptotic throughput, which indicates that partial channel estimation may be sufficient for applications with a non-stringent BER criterion. On the other hand, error-critical applications requiring less than $BER = 10^{-3}$ must use the fully adaptive channel estimation, as seen from Fig. 8.5.

8.2.7.3 Varying Fading-Block Size, Unknown Phase

In urban mobile environments, the phase can be expected to change significantly after approximately $0.01/f_d$ s to $0.04/f_d$ s, where f_d is the maximum Doppler shift. For the assumed mobile velocity of 120 km hr^{-1}, this time range corresponds to roughly 10 to 40 code bits at 100 kb s^{-1}. The fading and interference block sizes

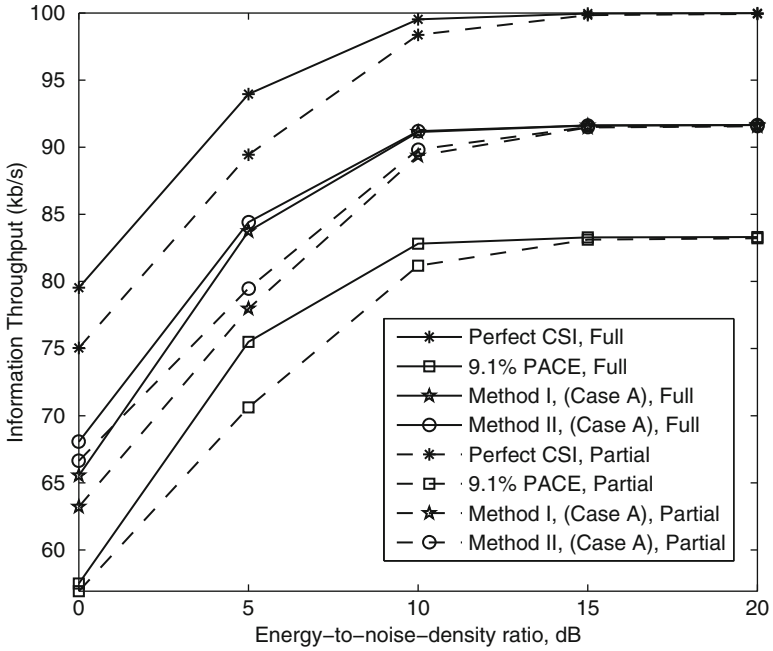

Fig. 8.6 Information throughput versus $\mathcal{E}_b/N_0$ for IRA-coded iterative receiver affected by multiple-access interference from four users, fully and partially adaptive estimation, and unknown phase

$N_b = N_{ib}$ are therefore varied accordingly, and *no* phase information is assumed to be available at the receiver for the next set of results.

Figure 8.7 displays fully adaptive IRA-coded BER versus E_b/N_0 for blind methods I and II with case C, 9.1% PACE, and perfect CSI decoding for $N_b = 10$ and 40 in a single-user environment. An improvement of 1 to 2 dB was observed for all methods for the smaller fading-block size of $N_b = 10$ due to the increased fading diversity. The throughput with case A is shown in Fig. 8.8. It is observed that the throughput gains of the blind methods over PACE (roughly 9% at intermediate to high E_b/N_0) are preserved even when the phase is initially unknown at the receiver.

8.2.7.4 Varying Multiple-Access Interference, Unknown Phase

Figure 8.9 displays IRA-coded iterative receiver performance for blind method II, case C with 3 and 6 multiple-access interference signals and equal mean bit energies for all users. The partially adaptive estimation is unable to cope with the interference caused by six multiple-access interference signals regardless of the spreading factor, whereas the fully adaptive estimation offers a substantial improvement in BER. The benefit of an increased spreading factor ($G = 127$ versus $G = 31$) is more apparent

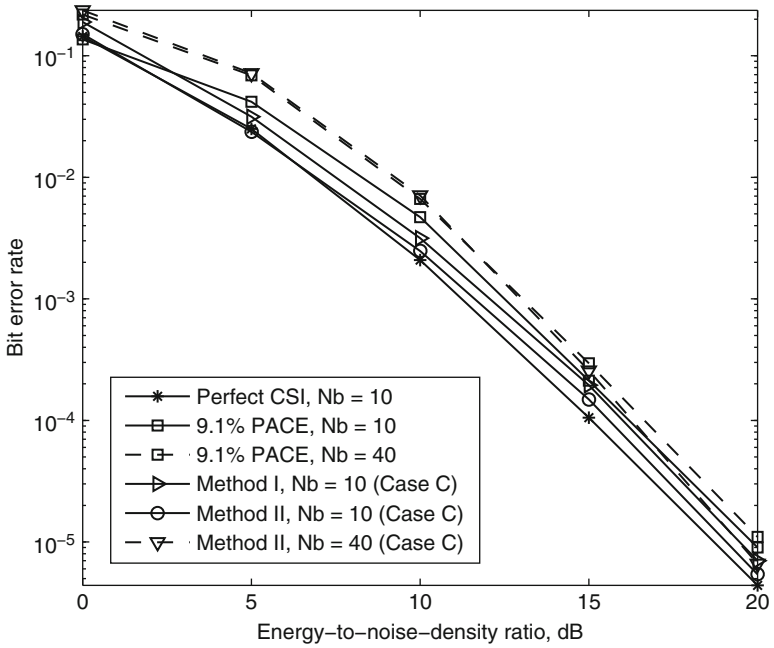

Fig. 8.7 BER versus $\mathcal{E}_b/N_0$ for IRA-coded iterative receiver in single-user environment, varying N_b, unknown phase

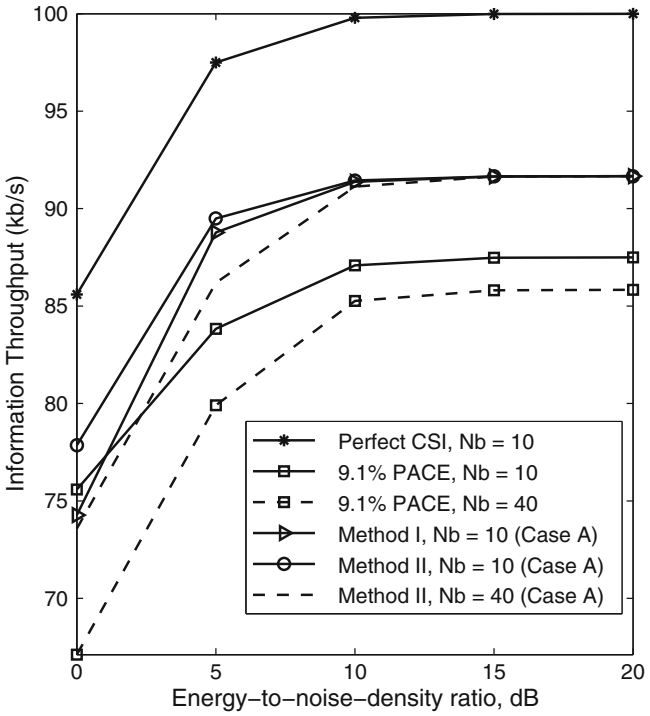

Fig. 8.8 Information throughput versus $\mathcal{E}_b/N_0$ for IRA-coded iterative receiver in single-user environment, varying N_b, unknown phase

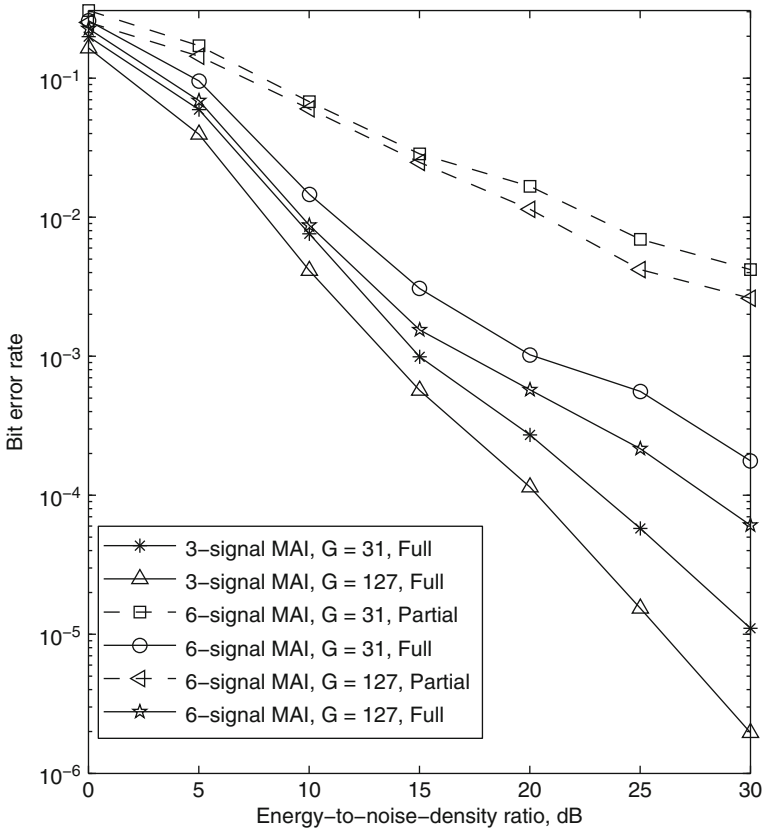

Fig. 8.9 BER versus $\mathcal{E}_b/N_0$ for IRA-coded iterative receiver affected by an unknown phase and various spreading factors, number of multiple-access interference (MAI) signals, and degrees of adaptation

at low bit error rates for fully adaptive estimation. For example, the fully adaptive estimation with three multiple-access interference signals improves by a factor of approximately 5 dB at $BER = 10^{-5}$, despite nonorthogonal spreading sequences and imperfect CSI.

8.2.7.5 Multipath Channel

A DS/CDMA system can exploit a frequency-selective fading channel by using a rake demodulator (Sect. 5.6). As an example, we assume a channel with three resolvable multipath components (with known delays) of the desired signal and a rake combiner with three corresponding fingers. The multipath components undergo independent fading across the fingers, but follow the correlated fading assumption

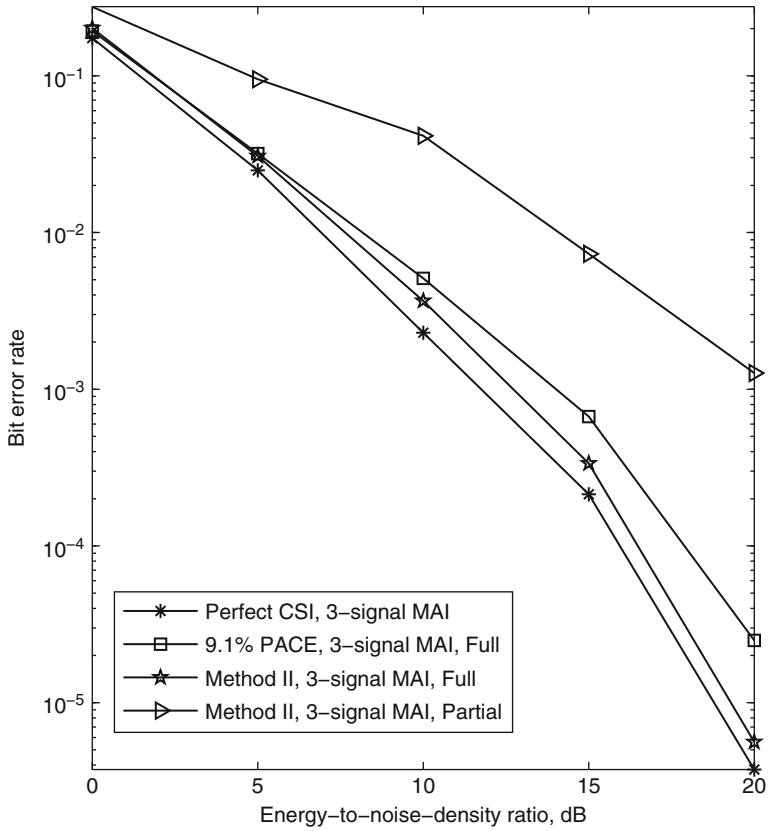

Fig. 8.10 BER versus $\mathcal{E}_b/N_0$ for IRA-coded iterative rake receiver with three resolvable multipaths, three fingers, and three multiple-access interference (MAI) signals

over time. The magnitudes of the fading amplitudes of the components follow an exponentially decaying power profile across the fingers:

$$E\left[\alpha_l^2\right] = e^{-(l-1)}, \quad l = 1, 2, 3. \tag{8.62}$$

Each interference signal has the same power level in each finger and undergoes independent correlated fading. Because of the independent multipath fading amplitudes for the desired signal, the EM-based channel estimation is performed separately in each finger. The rake demodulator performs MRC of the received symbol copies based on channel estimates computed at all fingers. The decision statistic obtained from the rake demodulator is then passed to the QPSK demodulator metric generator, which generates soft inputs for the common decoder. The soft outputs of the decoder are fed back to the three channel estimator blocks, which then recompute updated fading amplitudes.

Figure 8.10 displays the rake demodulator performance for three multiple-access interference signals with Method II under case C, where all users have length-127

Gold sequences. It is observed that the additional diversity due to rake combining improves performance as expected, but the performance disparity between partially and fully adaptive estimation remains large.

The simulation results indicate that pilot symbols are not essential to the effectiveness of DS/CDMA receivers with coding, coherent detection, and channel estimation. If the pilot symbols are replaced by information symbols, the throughput increases relative to PACE whether or not interference is present. If the BER is the primary performance criterion, then replacing the pilot symbols by parity symbols gives a lower BER than PACE. If the spectral efficiency is of primary importance, then extending the symbol duration after the removal of the pilot symbols offers an improvement relative to PACE, albeit at the cost of a slight increase in the BER.

The simulation results indicate that the despreading and the subsequent estimation of the interference-power spectral density enables the significant suppression of interference. This suppression is achieved without using the far more elaborate multiuser and signal cancellation methods that could be implemented in a DS/CDMA receiver.

8.3 Guidance from Information Theory

Information theory is renowned for establishing fundamental limits on what can be achieved by a communication system. The theory also provides insight into favorable choices of code rates and signal characteristics. The guidance provided by information theory is used in the next section to design robust frequency-hopping systems.

Let $\mathbf{X}$ and $\mathbf{Y}$ denote continuously distributed random vectors, which are vectors with components that are continuously distributed random variables. Let $f(\mathbf{x}, \mathbf{y})$ denote the joint probability density function of $\mathbf{X}$ and $\mathbf{Y}$, and let $f(\mathbf{x})$ and $f(\mathbf{y})$ denote the associated marginal probability density functions. The *average mutual information* between $\mathbf{X}$ and $\mathbf{Y}$, in bits per channel use, is defined as [4, 10]

$$I(\mathbf{X}, \mathbf{Y}) = \int_{\mathsf{R}(\mathbf{y})} \int_{\mathsf{R}(\mathbf{x})} f(\mathbf{x}, \mathbf{y}) \log_2 \frac{f(\mathbf{x}, \mathbf{y})}{f(\mathbf{x}) f(\mathbf{y})} d\mathbf{x} d\mathbf{y} \tag{8.63}$$

where $\mathsf{R}(\mathbf{y})$ and $\mathsf{R}(\mathbf{x})$ are the domains or regions of integration for $\mathbf{y}$ and $\mathbf{x}$, respectively. The *channel capacity* is defined as the maximum value of $I(\mathbf{X}, \mathbf{Y})$ over all possible choices of the density $f(\mathbf{x})$. Consider the two-dimensional AWGN channel for which the complex-valued input and output symbols are continuously distributed. A fundamental result of information theory is that the channel capacity is

$$\mathsf{C} = \log_2 \left(1 + \frac{\mathcal{E}_s}{N_0} \right) \tag{8.64}$$

where $\mathcal{E}_s$ is the energy per symbol or two-dimensional complex input, and $N_0/2$ is the two-sided noise-power spectral density. For the Gaussian channel with a power

constraint and a code-rate R, there exists a sequence of codes such that the maximal probability of error tends to zero if $R \leq C$.

Digital communication systems transmit discrete-valued symbols and receive continuous-valued outputs. Let X denote a discrete random variable that is drawn from an input alphabet of q symbols and is applied to the input of a modulator. Let the continuously distributed random vector $\mathbf{Y}$ denote the channel outputs or matched-filter outputs. The *average mutual information between* X *and* $\mathbf{Y}$ is defined as

$$I(X, \mathbf{Y}) = \sum_{i=1}^{q} P[x_i] \int_{\mathsf{R}(\mathbf{y})} f(\mathbf{y}\,|x_i) \log_2 \frac{f(\mathbf{y}\,|x_i)}{f(\mathbf{y})} d\mathbf{y} \tag{8.65}$$

where $P[x_i]$ is the probability that $X = x_i$, $i = 1, 2, \ldots, q$, and $f(\mathbf{y}\,|x_i)$ is the conditional probability density function of $\mathbf{Y}$ given that $X = x_i$. This equation can be obtained from (8.63) by making the replacements $f(\mathbf{x}) \to P[x_i]$ and $f(\mathbf{x}, \mathbf{y}) \to f(\mathbf{y}\,|x_i)P[x_i]$ and replacing one of the integrals by a summation. The density $f(\mathbf{y})$ may be expressed as

$$f(\mathbf{y}) = \sum_{i=1}^{q} P[x_i]\, f(\mathbf{y}\,|x_i). \tag{8.66}$$

If (8.65) is maximized with respect to $P[x_i]$, the average mutual information is called the *channel capacity of the discrete-input, continuous-output channel*.

Suppose that the channel inputs are selected to have equal probability so that $P[x_i] = 1/q$, $i = 1, 2, \ldots, q$, in (8.65) and (8.66). Then the *constrained channel capacity* under the uniform inputs constraint is

$$C = \log_2 q + \frac{1}{q} \sum_{i=1}^{q} \int_{\mathsf{R}(\mathbf{y})} f(\mathbf{y}\,|x_i) \log_2 \frac{f(\mathbf{y}\,|x_i)}{\sum_{i=1}^{q} f(\mathbf{y}\,|x_i)} d\mathbf{y}. \tag{8.67}$$

Consider a flat-fading channel and a receiver that has perfect channel state information about the complex fading amplitude $\mathcal{A}$ during each symbol interval. For communications over many symbol intervals, the *constrained channel capacity* is

$$C = \log_2 q + \frac{1}{q} \sum_{i=1}^{q} \int_{\mathsf{R}(a)} \int_{\mathsf{R}(\mathbf{y})} f(a) f(\mathbf{y}\,|x_i, a) \log_2 \frac{f(\mathbf{y}\,|x_i, a)}{\sum_{i=1}^{q} f(\mathbf{y}\,|x_i, a)} d\mathbf{y} da \tag{8.68}$$

where $f(a)$ is the two-dimensional probability density function of the real and imaginary components of the complex fading amplitude, $\mathsf{R}(a)$ is the region of integration of the complex amplitude, and $f(\mathbf{y}\,|x_i, a)$ is the conditional probability density function of $\mathbf{Y}$ given that $X = x_i$ and the complex amplitude is $\mathcal{A} = a$. For a Gaussian $f(\mathbf{y}\,|x_i, a)$ with a power constraint and a code-rate R, there exists a sequence of codes such that the maximal probability of error tends to zero if $R \leq C$.

8.4 Robust Frequency-Hopping Systems

This section describes and analyzes a robust frequency-hopping system with noncoherent detection, iterative turbo decoding and demodulation, and channel estimation [11]. The system is designed to be effective not only when operating over the AWGN and fading channels but also in environments with multiple-access interference and multitone jamming.

Noncoherent or differentially coherent demodulation has practical advantages and is often necessary because of the difficulty of phase estimation after every frequency hop. A common choice of modulation is orthogonal frequency-shift keying (FSK). With orthogonal FSK, the energy efficiency can be improved by increasing the alphabet size q, which is equal to the number of possible transmit frequencies in the signal set during each hop dwell interval. The problem is that a large bandwidth B_u of each frequency channel, although necessary to support a large number of transmit frequencies, reduces the number of frequency channels available when the hopping is over a spectral region with fixed bandwidth W. This reduction makes the system more vulnerable to both multiple-access frequency-hopping signals and multitone jamming (Sect. 3.2). A reduction in B_u is obtained by using nonorthogonal continuous-phase frequency-shift keying (CPFSK). As an example of the importance of B_u, consider multitone jamming of a frequency-hopping system with q-ary CPFSK in which the thermal noise is absent and each jamming tone has its carrier frequency within a distinct frequency channel. The uncoded symbol-error probability is given by (3.58), which explicitly indicates the significant benefit of a small bandwidth in reducing the effect of multitone jamming.

Robust system performance is provided by using nonorthogonal CPFSK, a turbo code, BICM, iterative decoding and demodulation, and channel estimation. The bandwidth of q-ary CPFSK decreases with reductions in the modulation index h. Although the lack of orthogonality when $h < 1$ will cause a performance loss for the AWGN and fading channels, the turbo decoder makes this loss minor compared with the gain against multiple-access interference and multitone jamming.

The system with noncoherent, nonorthogonal CPFSK has the following primary advantages relative to other systems with differential detection, coherent detection, or orthogonal modulation:

1. No extra reference symbol and no estimation of the phase offset in each dwell interval are required.
2. It is not necessary to assume that the phase offset is constant throughout a dwell interval.
3. The channel estimators are much more accurate and can estimate an arbitrary number of interference and noise spectral-density levels.
4. The compact spectrum during each dwell interval allows more frequency channels and, hence, enhances performance against multiple-access interference and multitone jamming.

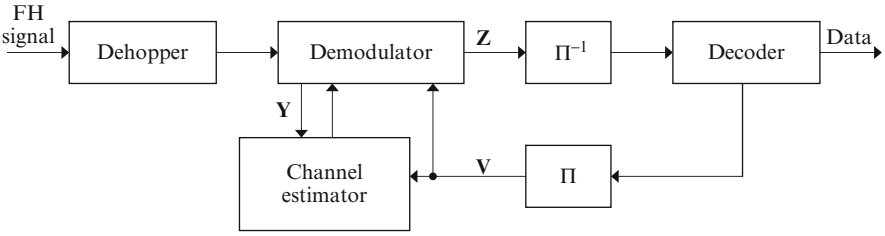

Fig. 8.11 Architecture of receiver for frequency-hopping system with turbo code. Π = interleaver; Π^{-1} = deinterleaver

5. Because noncoherent detection is used, system complexity is independent of the choice of h, and thus there is much more design flexibility than is possible in coherent CPFSK systems.

8.4.1 System Model

In the transmitter of the system, which uses BICM (Sect. 1.7), encoded message bits are interleaved and then placed into a length-N_d vector $\mathbf{d}$ with elements $d_i \in \{1, 2, ..., q\}$, each of which represents $m = \log_2 q$ bits. The vector $\mathbf{d}$ generates the sequence of tones that are frequency-translated by the carrier frequency of the frequency-hopping waveform during a signaling interval. After the modulated signal passes through an AWGN or fading channel with partial-band or multiple-access interference, the receiver front-end dehops the signal, as shown in Fig. 8.11. The dehopped signal passes through a bank of q matched filters, each of which is implemented as a quadrature pair. The output of each matched filter is sampled at the symbol rate to produce a sequence of complex numbers. Assuming that symbol synchronization exists, the complex samples are then placed into an $q \times N_d$ matrix $\mathbf{Y}$ whose ith column represents the outputs of the matched filters corresponding to the ith received symbol. The matrix $\mathbf{Y}$ is applied to the channel estimator and is used to produce an $m \times N_d$ matrix $\mathbf{Z}$ of demodulator bit metrics.

The demodulator exchanges information with both the turbo decoder and the channel estimators. After deinterleaving, the demodulator bit metrics are applied to the decoder. The decoder feeds a priori information (in the form of an $m \times N_d$ matrix $\mathbf{V}$ of decoder bit metrics) back to the demodulator and channel estimator, in accordance with the turbo principle. Frequency-selective fading changes the fading amplitude from hop to hop, and the partial-band and multiple-access interference change the interference and noise during some hop dwell intervals. Consequently, estimates of the fading amplitude and the spectral density of the interference and noise are computed for a block size N_b that is smaller than or equal to the number

of symbols in the hop dwell interval. If there are N_b symbols per block, then there are $\lceil N_d/N_b \rceil$ blocks per codeword.

8.4.2 Demodulator Metrics

The complex envelope of a unit-energy q-ary CPFSK symbol waveform with zero initial phase offset is

$$s_l(t) = \frac{1}{\sqrt{T_s}} e^{j2\pi lht/T_s}, \quad 0 \le t \le T_s, \quad l = 1, 2, \ldots, q \tag{8.69}$$

where T_s is the symbol duration and h is the modulation index. Because of the continuous-phase constraint, the initial phase of CPFSK symbol i is $\phi_i = \phi_{i-1} + 2\pi lh$. The phase continuity ensures the compact spectrum of the CPFSK waveform. Suppose that symbol i of a codeword uses unit-energy waveform $s_{d_i}(t)$, where the integer d_i is a function of the codeword. If this codeword is transmitted over a channel with fading and additive Gaussian noise, the received signal for symbol i can be expressed in complex notation as

$$r_i(t) = \text{Re}\left[\alpha_i \sqrt{2\mathcal{E}_s} s_{d_i}(t) e^{j2\pi f_c t + \theta_i}\right] + n_i(t), \quad 0 \le t \le T_s$$
$$i = 1, 2, \ldots, N_d \tag{8.70}$$

where $n_i(t)$ is independent, zero-mean, white Gaussian noise with two-sided power spectral density $N_{0i}/2$, f_c is the carrier frequency, $\mathcal{E}_s$ is the signal energy, and α_i is the magnitude of the complex fading amplitude. Without loss of generality, we assume $E[\alpha_i^2] = 1$ so that the average received symbol energy is $\mathcal{E}_s$. The phase θ_i is the phase due to the contributions of the CPFSK constraint, the fading, and the frequency offset of the receiver. One might consider exploiting the inherent memory in the CPFSK when computing the metric transferred from the demodulator to a decoder, but phase stability over several symbols is necessary, and the demodulator functions as a rate-one inner decoder. Furthermore, a trellis demodulator requires a rational h and the number of states depends on the denominator of h. More design flexibility exists if the demodulator metrics are computed on a symbol-by-symbol basis, and the memory in the turbo code is exploited rather than the memory in the modulation.

Matched-filter k, which is matched to $s_k(t)$, produces the output samples

$$y_{k,i} = \sqrt{2} \int_0^{T_s} r_i(t) e^{-j2\pi f_c t} s_k^*(t) dt$$
$$i = 1, 2, \ldots, N_d, \quad k = 1, 2, \ldots, q. \tag{8.71}$$

The substitution of (8.70) into (8.71) and the approximation that each of the $\{s_k(t)\}$ has a spectrum confined to $|f| < f_c$ yields

$$y_{k,i} = \alpha_i \sqrt{\mathcal{E}_s} e^{j\theta_i} \rho_{d_i - k} + n_{k,i} \tag{8.72}$$

where

$$n_{k,i} = \sqrt{2} \int_0^{T_s} n_i(t) e^{-j2\pi f_c t} s_k^*(t) dt \tag{8.73}$$

and

$$\rho_l = \frac{\sin(\pi h l)}{\pi h l} e^{j\pi h l}. \tag{8.74}$$

Since $n_i(t)$ is zero-mean and white and the spectra of the $\{s_k(t)\}$ are confined, it follows that each $n_{k,i}$ is zero-mean,

$$E[n_{k,i} n_{l,i}^*] = N_{0i} \rho_{l-k} \tag{8.75}$$

and the $\{n_{k,i}\}$ have circular symmetry:

$$E[n_{k,i} n_{l,i}] = 0. \tag{8.76}$$

Since $n_i(t)$ is a Gaussian process, the real and imaginary components of $n_{k,i}$ are jointly Gaussian, and the set $\{n_{k,i}\}$ comprises *complex-valued jointly Gaussian random variables.*

Let $\mathbf{y}_i = [y_{1,i} \ldots y_{q,i}]^T$ denote the column vector of the matched-filter outputs corresponding to symbol i, and let $\mathbf{n} = [n_{1,i} \ldots n_{q,i}]^T$. Then given that the transmitted symbol is d_i, the symbol energy is $\mathcal{E}_s$, the fading amplitude is a_i, the noise-power spectral density is $N_{0i}/2$, and the phase is θ_i, $\mathbf{y}_i = \overline{\mathbf{y}}_i + \mathbf{n}$, where $\overline{\mathbf{y}}_i = E[\mathbf{y}_i | d_i, \mathcal{E}_s, \alpha_i, N_{0i}, \theta_i]$. Equation (8.72) indicates that the kth component of $\overline{\mathbf{y}}_i$ is

$$\overline{y}_{k,i} = \alpha_i \sqrt{\mathcal{E}_s} e^{j\theta_i} \rho_{d_i - k}. \tag{8.77}$$

The covariance matrix of $\mathbf{y}_i$ is

$$\begin{aligned} \mathbf{R}_i &= E[(\mathbf{y}_i - \overline{\mathbf{y}}_i)(\mathbf{y}_i - \overline{\mathbf{y}}_i)^H \mid d_i, \alpha_i \sqrt{\mathcal{E}_s}, N_{0i}, \theta_i] \\ &= E[\mathbf{n}\mathbf{n}^H] \end{aligned} \tag{8.78}$$

and its elements are given by (8.75). It is convenient to define the matrix $\mathbf{K} = \mathbf{R}_i / N_{0i}$ with components

$$K_{kl} = \rho_{l-k}. \tag{8.79}$$

We can represent the conditional probability density function of $\mathbf{y}_i$ given that the transmitted symbol is d_i, the symbol energy is $\mathcal{E}_s$, the fading amplitude is α_i, the noise-power spectral density is $N_{0i}/2$, and the phase is θ_i as

$$f(\mathbf{y}_i|d_i, \alpha_i\sqrt{\mathcal{E}_s}, N_{0i}, \theta_i) = \frac{1}{\pi^q N_{0i}^q \det \mathbf{K}} \exp\left[-\frac{1}{N_{0i}}(\mathbf{y}_i - \overline{\mathbf{y}}_i)^H \mathbf{K}^{-1}(\mathbf{y}_i - \overline{\mathbf{y}}_i)\right] \tag{8.80}$$

where $\mathbf{K}$ is independent of $(d_i, \mathcal{E}_s, \alpha_i, N_{0i}, \theta_i)$.

An expansion of the quadratic in (8.80) yields

$$\begin{aligned} Q_i &= (\mathbf{y}_i - \overline{\mathbf{y}}_i)^H \mathbf{K}^{-1}(\mathbf{y}_i - \overline{\mathbf{y}}_i) \\ &= \mathbf{y}_i{}^H \mathbf{K}^{-1}\mathbf{y}_i + \overline{\mathbf{y}}_i{}^H \mathbf{K}^{-1}\overline{\mathbf{y}}_i - 2\mathrm{Re}(\mathbf{y}_i{}^H \mathbf{K}^{-1}\overline{\mathbf{y}}_i). \end{aligned} \tag{8.81}$$

Equations (8.77) and (8.79) indicate that $\overline{\mathbf{y}}_i$ is proportional to the $d_i th$ column of $\mathbf{K}$:

$$\overline{\mathbf{y}}_i = \alpha_i\sqrt{\mathcal{E}_s} e^{j\theta_i} \mathbf{K}_{:,d_i}. \tag{8.82}$$

Since $\mathbf{K}^{-1}\mathbf{K} = \mathbf{I}$, only the $d_i th$ component of the column vector $\mathbf{K}^{-1}\overline{\mathbf{y}}_i$ is nonzero, and

$$Q_i = \mathbf{y}_i{}^H \mathbf{K}^{-1}\mathbf{y}_i + \alpha_i^2 \mathcal{E}_s - 2\alpha_i\sqrt{\mathcal{E}_s}\mathrm{Re}(y_{d_i,i} e^{-j\theta_i}). \tag{8.83}$$

For *noncoherent* signals, it is assumed that each θ_i is uniformly distributed over $[0, 2\pi)$. Substituting (8.83) into (8.80), expressing $y_{d_i,i}$ in polar form, and using (1.73) to integrate over θ_i, we obtain the probability density function

$$f(\mathbf{y}_i|d_i, \alpha_i\sqrt{\mathcal{E}_s}, N_{0i}) = \frac{\exp\left(-\frac{\mathbf{y}_i{}^H \mathbf{K}^{-1}\mathbf{y}_i + \alpha_i^2\mathcal{E}_s}{N_{0i}}\right)}{\pi^q N_{0i}^q \det \mathbf{K}} I_0\left(\frac{2\alpha_i\sqrt{\mathcal{E}_s}\,|y_{d_i,i}|}{N_{0i}}\right) \tag{8.84}$$

where $I_0(\,)$ is the modified Bessel function of the first kind and order zero. Since the white noise $n_i(t)$ is independent from symbol to symbol, $\mathbf{y}_i$ with the density given by (8.84) is independent of $\mathbf{y}_l$, $i \neq l$.

Let $\widehat{A}$ and $\widehat{B}$ denote the estimates of $A = N_0$ and $B = 2\alpha\sqrt{\mathcal{E}_s}$, respectively, for a dwell interval of N_b symbols during which $\alpha_i = \alpha$ and $N_{0i} = N_0$ are constants. Let $b_{k,i}$ denote bit k of symbol i. Let $\mathbf{Z}$ denote the $m \times N_d$ matrix whose element $z_{k,i}$ is the log-likelihood ratio for $b_{k,i}$ computed by the demodulator. The matrix $\mathbf{Z}$ is reshaped into a row vector and deinterleaved, and the resulting vector $\mathbf{z}'$ is fed

into the turbo decoder. The extrinsic information $\mathbf{v}'$ at the output of the decoder is interleaved and reshaped into a $m \times N_d$ matrix $\mathbf{V}$ containing the a priori information:

$$v_{k,i} = \log \frac{p(b_{k,i} = 1|\mathbf{Z}\backslash z_{k,i})}{p(b_{k,i} = 0|\mathbf{Z}\backslash z_{k,i})} \tag{8.85}$$

where conditioning on $\mathbf{Z}\backslash z_{k,i}$ means that the extrinsic information for bit $b_{k,i}$ is produced without using $z_{k,i}$. Since $\mathbf{V}$ is fed back to the demodulator,

$$z_{k,i} = \log \frac{p(b_{k,i} = 1|\mathbf{y}_i, \gamma'_{\lceil i/N_b \rceil}, \mathbf{v}_i\backslash v_{k,i})}{p(b_{k,i} = 0|\mathbf{y}_i, \gamma'_{\lceil i/N_b \rceil}, \mathbf{v}_i\backslash v_{k,i})} \tag{8.86}$$

where $\gamma' = \{\hat{A}, \hat{B}\}$. Partition the set of symbols $\mathcal{D} = \{1, ..., q\}$ into two disjoint sets $\mathcal{D}_k^{(1)}$ and $\mathcal{D}_k^{(0)}$, where $\mathcal{D}_k^{(b)}$ contains all symbols labelled with $b_k = b$. As indicated by (1.205), the extrinsic information can then be expressed as

$$z_{k,i} = \log \frac{\sum_{d \in \mathcal{D}_k^{(1)}} f(\mathbf{y}_i|d, \gamma'_{\lceil i/N_b \rceil}) \prod_{\substack{l=1 \\ l \neq k}}^{m} \exp(b_l(d) v_{l,i})}{\sum_{d \in \mathcal{D}_k^{(0)}} f(\mathbf{y}_i|d, \gamma'_{\lceil i/N_b \rceil}) \prod_{\substack{l=1 \\ l \neq k}}^{m} \exp(b_l(d) v_{l,i})} \tag{8.87}$$

where $b_l(d)$ is the value of the lth bit in the labelling of symbol d. Substituting (8.84) into (8.87) and cancelling common factors, we obtain

$$z_{k,i} = \log \frac{\sum_{d \in \mathcal{D}_k^{(1)}} I_0\left(\gamma_{\lceil i/N_b \rceil}|y_{d_i,i}|\right) \prod_{\substack{l=1 \\ l \neq k}}^{m} \exp(b_l(d) v_{l,i})}{\sum_{d \in \mathcal{D}_k^{(0)}} I_0\left(\gamma_{\lceil i/N_b \rceil}|y_{d_i,i}|\right) \prod_{\substack{l=1 \\ l \neq k}}^{m} \exp(b_l(d) v_{l,i})} \tag{8.88}$$

where only the ratio $\gamma = \hat{B}/\hat{A}$ is needed rather than the individual estimates. Since the preceding and subsequent equations in this section refer to a specific receiver iteration, the superscript denoting the receiver-iteration number is omitted to simplify the notation.

8.4.3 Channel Estimators

Since under block fading and time-varying interference, A and B can change on a block-by-block basis, each block is processed separately and in an identical fashion. To maintain robustness, the estimators make no assumptions regarding the distribution of the quantities to be estimated, nor do they make any assumptions regarding the correlation from block to block. The estimators directly use the channel observation for a single block while the observations of the other blocks are used indirectly through feedback of extrinsic information from the decoder.

Thus in this section, Y is a generic $q \times N_b$ received block, $d = [d_1, ..., d_{N_b}]$ is the corresponding set of transmitted symbols, and $\{\hat{A}, \hat{B}\}$ is the corresponding set of channel estimators.

Rather than attempting to directly evaluate the maximum-likelihood estimates, the EM algorithm can be used as an iterative approach to estimation. Let $\{\mathbf{Y}, \mathbf{d}\}$ denote the *complete* data set. Since $\log f(\mathbf{d})$ is independent of A and B and, hence, does not affect the maximization, the log-likelihood of the complete data set is $L(A, B) = \log f(\mathbf{Y}, \mathbf{d}|A, B) = \log f(\mathbf{Y}|\mathbf{d}, A, B) + \log f(\mathbf{d}) \sim \log f(\mathbf{Y}|\mathbf{d}, A, B)$.

Since $\mathbf{y}_i$ and $\mathbf{y}_l$ are independent for $i \neq l$, (8.84) implies that

$$f(\mathbf{Y}|\mathbf{d}, A, B) = \frac{\exp\left[-\frac{D}{A} - \frac{N_b B^2}{4A} + \sum_{i=1}^{N_b} \log I_0\left(\frac{B|y_{d_i,i}|}{A}\right)\right]}{(\pi^q A^q \det \mathbf{K})^{N_b}} \tag{8.89}$$

where

$$D = \sum_{i=1}^{N_b} \mathbf{y}_i{}^H \mathbf{K}^{-1} \mathbf{y}_i . \tag{8.90}$$

After dropping irrelevant constants, we obtain

$$L(A, B) \sim -qN_b \log A - \frac{D}{A} - \frac{N_b B^2}{4A} + \sum_{i=1}^{N_b} \log I_0\left(\frac{B\,|y_{d_i,i}|}{A}\right). \tag{8.91}$$

The form of this equation indicates that the parameters A and B must both be estimated rather than just the ratio B/A.

Let r denote the EM iteration number, and $\hat{A}^{(r)}$, $\hat{B}^{(r)}$ the estimates of A, B during the r^{th} iteration. The *expectation* step (E-step) requires the calculation of

$$Q(A, B) = E_{\mathbf{d}|\mathbf{Y}, \hat{A}^{(r-1)}, \hat{B}^{(r-1)}}\left[L(A, B)\right] \tag{8.92}$$

where the expectation is taken with respect to the unknown symbols $\mathbf{d}$ conditioned on $\mathbf{Y}$ and the estimates $\hat{A}^{(r-1)}$, $\hat{B}^{(r-1)}$ from the previous EM iteration. Substituting (8.91) into (8.92), it is found that

$$\begin{aligned} Q(A, B) = &-qN_b \log A - \frac{D}{A} - \frac{N_b B^2}{4A} \\ &+ \sum_{i=0}^{N_b-1} \sum_{k=1}^{q} p_{k,i}^{(r-1)} \log I_0\left(\frac{B\,|y_{k,i}|}{A}\right) \end{aligned} \tag{8.93}$$

where

$$p_{k,i}^{(r-1)} = p(d_i = k|\mathbf{y}_i, \hat{A}^{(r-1)}, \hat{B}^{(r-1)}) = \frac{f(\mathbf{y}_i|d_i = k, \hat{A}^{(r-1)}, \hat{B}^{(r-1)})p(d_i = k)}{f(\mathbf{y}_i|\hat{A}^{(r-1)}, \hat{B}^{(r-1)})}. \tag{8.94}$$

The last step uses the fact that d_i is independent of $\hat{A}^{(r-1)}$ and $\hat{B}^{(r-1)}$. Applying (8.84), we obtain

$$p_{k,i}^{(r-1)} = \alpha_i^{(r-1)} I_0\left(\frac{\hat{B}^{(r-1)}|y_{k,i}|}{\hat{A}^{(r-1)}}\right) p(d_i = k) \tag{8.95}$$

where $\alpha_i^{(r-1)}$ is the normalization factor forcing $\sum_{k=1}^{q} p_{k,i}^{(r-1)} = 1$, i.e.,

$$\alpha_i^{(r-1)} = \frac{1}{\sum_{k=1}^{q} I_0\left(\frac{\hat{B}^{(r-1)}|y_{k,i}|}{\hat{A}^{(r-1)}}\right) p(d_i = k)} \tag{8.96}$$

and $p(d_i = k)$ is the probability that $d_i = k$, which is estimated by the decoder.

The *maximization* step (M-step) is

$$\hat{A}^{(r)}, \hat{B}^{(r)} = \arg\max_{A,B} Q(A, B) \tag{8.97}$$

which can be found by setting the derivatives of the function $Q(A, B)$ with respect to A and B to zero. The solution to the corresponding system of equations is

$$\hat{A}^{(r)} = \frac{1}{qN_b}\left(D - \frac{N_b(\hat{B}^{(r)})^2}{4}\right) \tag{8.98}$$

$$\hat{B}^{(r)} = \frac{2}{N_b}\sum_{i=1}^{N_b}\sum_{k=1}^{q} p_{k,i}^{(r-1)}\,|y_{k,i}|\,F\left(\frac{4qN_b\hat{B}^{(r)}|y_{k,i}|}{4D - N_b(\hat{B}^{(r)})^2}\right) \tag{8.99}$$

where $F(x) = I_1(x)/I_0(x)$, and $I_1(x)$ is the modified Bessel function of the first kind and order one defined by (7.38).

While a closed form solution to (8.99) is difficult to obtain, it can be found recursively by using the fixed-point iteration method of Sect. 8.1. The recursion involves initially replacing $\hat{B}^{(r)}$ on the right-hand side of (8.99) with $\hat{B}^{(r-1)}$ from the previous EM iteration. To select an initial estimate for B, consider what happens in the absence of noise. Without noise, (8.72) implies that either $|y_{k,i}| = a\sqrt{\mathcal{E}_s}$ (when $k = d_i$) or $|y_{k,i}| = 0$ (otherwise). Thus, an estimate for $a\sqrt{\mathcal{E}_s} = B/2$ can be achieved by taking the maximum $|y_{k,i}|$ over any column of $\mathbf{Y}$. To account for

the possibility of noise, the average can be taken across all columns in the block, resulting in

$$\hat{B}^{(0)} = \frac{2}{N_b} \sum_{i=1}^{N_b} \max_k |y_{k,i}| . \tag{8.100}$$

The initial estimate of A is found from $\hat{B}^{(0)}$ by evaluating (8.98) for $r = 0$. After the initial values $\hat{A}^{(0)}$ and $\hat{B}^{(0)}$ are calculated, the initial probabilities $\{p_{k,i}^{(0)}\}$ are calculated from (8.95) and (8.96). The EM algorithm terminates when $\hat{B}^{(r)}$ converges to some fixed value, typically in fewer than 10 EM iterations.

The complexity of the channel estimation for each receiver iteration is as follows. The initial estimate of $\hat{B}$ calculated using (8.100) requires N_b maximizations over q values, $N_b - 1$ additions, and a single multiplication by $2/N_b$. The calculation of D in (8.90), which only needs to be computed once prior to the first EM iteration, requires $N_b q(q + 1)$ multiplications and $N_b q^2 - 1$ additions. For each EM iteration, the calculation $\hat{A}^{(r)}$ using (8.98) requires only two multiplications and an addition. Calculating $p_{k,i}^{(r-1)}$ using (8.95) and (8.96) requires $3N_b q + 1$ multiplications, $N_b(q - 1)$ additions, and $N_b q$ lookups of the $I_0(\cdot)$ function. Calculation of $\hat{B}^{(r)}$ by solving (8.99) is recursive, and complexity depends on the number of recursions for each value of r. Suppose that there are ξ recursions, then the calculation will require $N_b q + \xi(2N_b q + 4)$ multiplications, $\xi N_b q$ additions, and $\xi N_b q$ lookups of the $F(\cdot)$ function. A stopping criterion is used for the calculation of $\hat{B}$ such that the recursions stop once $\hat{B}$ is within 10% of its value during the previous recursion or a maximum number of 10 recursions is reached. With such a stopping criterion, an average of only two or three recursions are required.

8.4.4 Selection of Modulation Index

Let B_{max} denote the maximum bandwidth of the CPFSK modulation such that the hopping band accommodates enough frequency channels to ensure adequate performance against multiple-access interference and multitone jamming. We seek to determine the values of h, q, and code-rate R of the turbo code that provide a good performance over the fading and AWGN channels in the presence of partial-band interference. For specific values of the modulation parameters h and q, the code rate is limited by the bandwidth requirement. Let $B_u T_b$ denote the normalized, 99-percent power bandwidth of the uncoded CPFSK modulation. This value can be found for nonorthogonal CPFSK by numerically integrating the power-spectrum equations of Sect. 3.2. When a code of rate R is used, the bandwidth becomes $B_c = B_u/R$. Since $B_c \leq B_{max}$ is required, the minimum code rate that achieves the bandwidth constraint is $R_{min} = B_u/B_{max}$.

Guidance in the selection of the best values of h, q, and $R \geq R_{\min}$ is provided by information theory. For specific values of h and q, we evaluate the capacity $C(\gamma)$ as a function of $\gamma = \mathcal{E}_s/N_0$ under a bandwidth constraint for both the Rayleigh

and AWGN channels. Since the noncoherent demodulator will include channel estimation, perfect channel state information is assumed. Symbols are drawn from the signal set with equal probability. With these assumptions, a change of variables with $\mathbf{u} = \mathbf{y}_i/\sqrt{\mathcal{E}_s}$, (8.84), and (8.68), the capacity for the fading channel may be expressed as

$$C(\gamma) = \log_2 q - \frac{1}{q}\sum_{\nu=1}^{q}\int\int f(\alpha) f(\mathbf{u}|\nu,\alpha) \times \log_2 \frac{\sum_{k=1}^{q} I_0\left(2\alpha\gamma\,|u_k|\right)}{I_0\left(2\alpha\gamma\,|u_\nu|\right)} d\mathbf{u}d\alpha \tag{8.101}$$

where $f(\alpha)$ is the density of the magnitude of the fading amplitude, the $(2q+1)$-fold integration is over all values of α and the $2q$ real and imaginary components of $\mathbf{u}$, and

$$f(\mathbf{u}|\nu,\alpha) = \frac{\gamma^q \exp[-\gamma(\mathbf{u}^H\mathbf{K}^{-1}\mathbf{u}+\alpha^2)]}{\pi^q \det\mathbf{K}} I_0\left(2\alpha\gamma\,|u_\nu|\right). \tag{8.102}$$

Equation (8.101) is numerically integrated by the Monte Carlo method. To determine the minimum $\mathcal{E}_b/N_0$ necessary to maintain $C(\gamma)$ above the code-rate R, we use the relationship $\mathcal{E}_s = R\mathcal{E}_b \log_2 q$ and solve the equation

$$R = C(R\mathcal{E}_b \log_2 q/N_0) \tag{8.103}$$

for all code rates such that $R_{min} \le R \le 1$. For noncoherent systems under severe bandwidth constraints, the R that minimizes $\mathcal{E}_b/N_0$ will typically be $R = R_{\min}$, but under loose bandwidth constraints the R that minimizes $\mathcal{E}_b/N_0$ could possibly be larger than R_{min} (in which case the actual bandwidth is less than B_{max}).

Figures 8.12 and 8.13 show plots of the minimum $\mathcal{E}_b/N_0$ versus h for $2 \le q \le 32$, $B_{\max}T_b = 2$, and $B_{\max}T_b = \infty$. Figure 8.12 is for the AWGN channel, and Fig. 8.13 is for the Rayleigh fading channel. When $B_{\max}T_b = 2$, the curves are truncated because there is a maximum value of h beyond which no code exists that satisfies the bandwidth constraint. For each value of q, in each figure there is an optimal value of h that gives the smallest value of the minimum $\mathcal{E}_b/N_0$. This smallest value decreases with q, but there are diminishing returns and the implementation complexity increases rapidly for $q > 8$. Let f_e denote the offset in the estimated carrier frequency at the receiver due to the Doppler shift and the frequency-synthesizer inaccuracy. The separation between adjacent frequencies in a CPFSK symbol is $hf_b/R\log_2 q$, where f_b denotes the information-bit rate. Since this separation must be much larger than f_e if the latter is to be negligible as assumed in (8.71),

$$f_e \ll \frac{hf_b}{R\log_2 q} \tag{8.104}$$

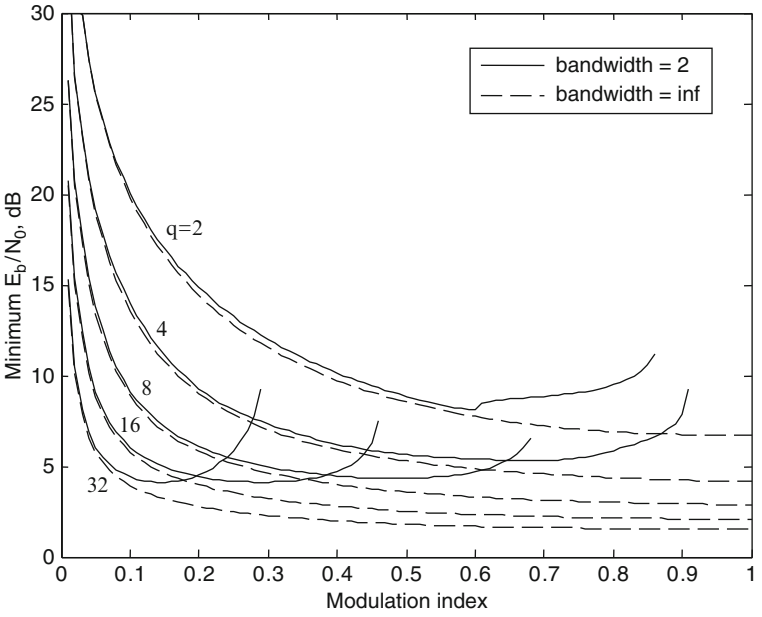

Fig. 8.12 Minimum $\mathcal{E}_b/N_0$ versus h for the AWGN channel, $2 \leq q \leq 32$, $B_{\max}T_b = 2$, and $B_{\max}T_b = \infty$

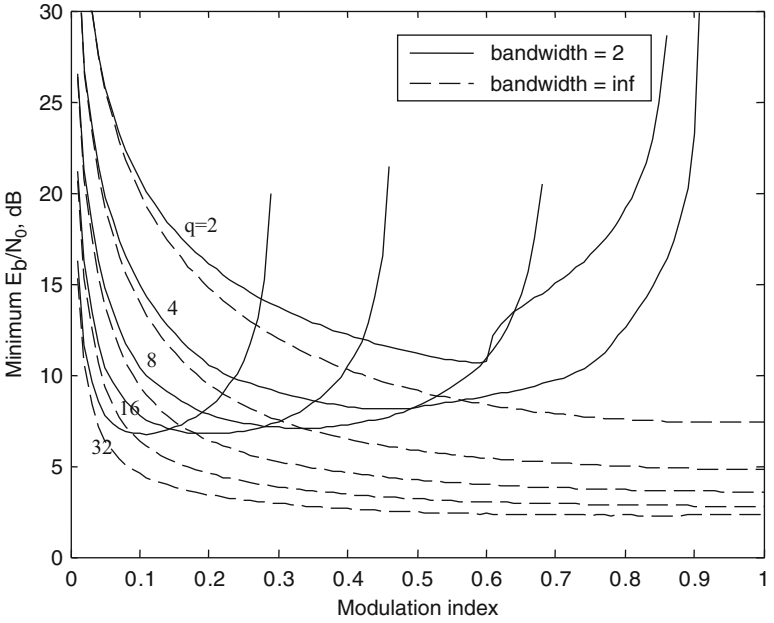

Fig. 8.13 Minimum $\mathcal{E}_b/N_0$ versus h for the Rayleigh channel, $2 \leq q \leq 32$, $B_{\max}T_b = 2$, and $B_{\max}T_b = \infty$

is required. Since the optimal h decreases while $R \log_2 q$ increases with q, (8.104) is another reason to choose $q \leq 8$. For $q = 4$ in Fig. 8.13, $h = 0.46$ is the approximate optimal value when $B_{\max} T_b = 2$, and the corresponding code rate is approximately $R = 16/27$. For $q = 8$, $h = 0.32$ is the approximate optimal value when $B_{\max} T_b = 2$, and the corresponding code rate is approximately $R = 8/15$. For both $q = 8$ and $q = 4$, (8.104) is satisfied if $f_e \ll 0.2 f_b$. At the optimal values of h, the plots indicate that the loss is less than 1 dB for the AWGN channel and less than 2 dB for the Rayleigh channel relative to what could be attained with the same value of q, $h = 1$ (orthogonal CPFSK), and an unlimited bandwidth.

8.4.5 *Performance in Partial-Band Interference*

Simulation experiments were conducted to assess the benefits and trade-offs of using the nonorthogonal CPFSK coded modulation and accompanying channel estimator in a frequency-hopping system that suppresses partial-band interference. Interference is modeled as additional Gaussian noise within a fraction μ of the hopping band. The density of the interference (i.e., additional noise) is I_{t0}/μ, where I_{t0} is the spectral density when $\mu = 1$ and the total interference power is conserved as μ varies. The parameter A represents the spectral density due to the noise and the interference during a dwell interval. The bandwidth is assumed to be sufficiently small that the fading is flat within each frequency channel, and hence the symbols of a dwell interval undergo the same fading amplitude. The fading amplitudes are independent from hop to hop, which models the frequency-selective fading that varies after each hop. A block coincides with a dwell interval, and hence is suitable for the estimation of a single fading amplitude. Three alphabet sizes are considered: binary ($q = 2$), quaternary ($q = 4$), and octal ($q = 8$).

The simulated system uses the widely deployed turbo code from the UMTS specification [3], which has a constraint length of 4, a specified code-rate matching algorithm, and an optimized variable-length interleaver that is set to 2,048. Simulation experiments with both turbo and convolutional codes of various constraint lengths indicate that the selected code provides close to the best performance in Rayleigh fading, although a constraint-length 3 is actually slightly better than the constraint-length 4 turbo code. However, in interference the performance difference is negligible. Since there is no standardized turbo code of constraint-length 3 with an optimized interleaver, the standardized UMTS code was selected for the simulated system in this section. If the dwell time is fixed but the codeword length is extended beyond the specified 2,048 bits, then the number of hops per codeword will increase. As a result, the diversity order will increase, but the benefit of increased diversity order obeys a law of diminishing returns, and the benefit is minor at the bit error rates of interest (approximately 10^{-3}). The values of modulation index h and code rate R are selected to be close to the information-theoretic optimal values given previously for Rayleigh fading under the bandwidth constraint $B_{\max} T_b = 2$. In particular, a system with $q = 2$ uses $h = 0.6$ and $R = 2,048/3,200$, one with

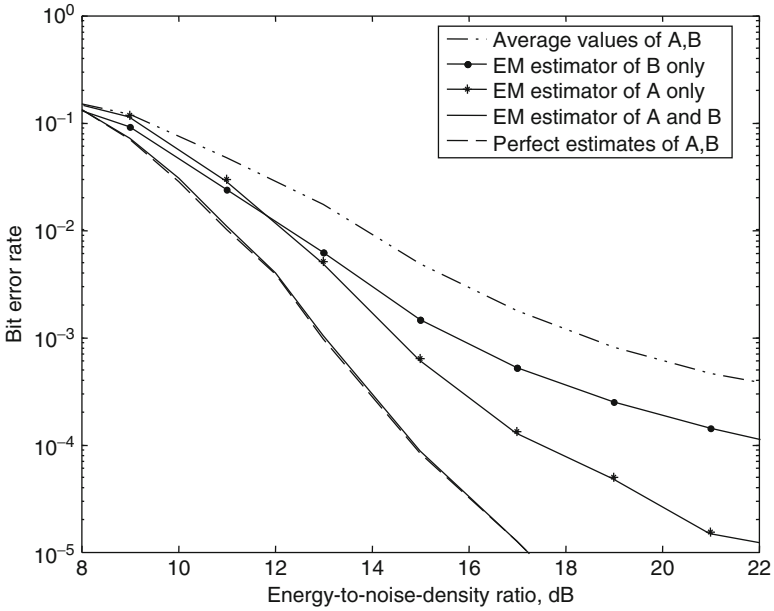

Fig. 8.14 Bit error rates of systems with various estimators in Rayleigh block fading with partial-band interference, $\mu = 0.6$, $\mathcal{E}_b/I_{t0} = 13\,\text{dB}$, turbo-coded octal CPFSK, $h = 0.32$, code rate 2,048/3,840, and 32 hops per codeword

$q = 4$ uses $h = 0.46$ and $R = 2,048/3,456$, and one with $q = 8$ uses $h = 0.32$ and $R = 2,048/3,840$. A receiver iteration comprises the steps of channel estimation, demapping, and one full turbo-decoding iteration. Up to 20 receiver iterations are executed. An early halting routine stops the iterations once the data is correctly decoded (which can be determined, for instance, by using the cyclic redundancy check specified in the UMTS standard). The number of hops per codeword may vary, and results below show the impact of changing this value.

Figure 8.14 illustrates the influence of channel estimation on the bit error rate (BER) of the system. For this figure, $\mu = 0.6$, $\mathcal{E}_b/I_{t0} = 13\,\text{dB}$, the channel undergoes block-by-block Rayleigh fading, and octal CPFSK is used with 32 hops per codeword. The uppermost curve in the figure shows the performance of a simple system that does not attempt to estimate A or B. Instead, the system sets these values to their statistical averages: $A = N_0 + I_{t0}$, and $B = 2E[\alpha]\sqrt{\mathcal{E}_s} = \sqrt{\pi\mathcal{E}_s}$, as implied by (B.37) of Appendix B. It can be seen that the performance of such a system is rather poor, as it has no knowledge of which hops have experienced interference and which have not. The system can be improved by estimating A and/or B on a block-by-block basis using the EM estimator. The second curve from the top shows the performance when only B is estimated on a block-by-block basis (and $A = N_0 + I_{t0}$), while the next curve down shows the performance when only A is estimated on a block-by-block basis (and $B = \sqrt{\pi\mathcal{E}_s}$). The second lowest curve

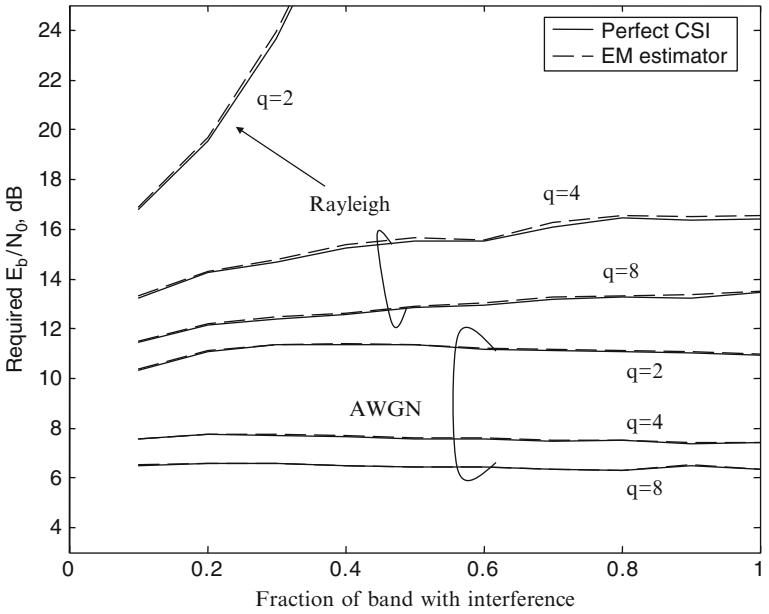

Fig. 8.15 Required $\mathcal{E}_b/N_0$ to achieve $BER = 10^{-3}$ as a function of μ for binary, quaternary, and octal turbo-coded CPFSK in both AWGN and Rayleigh fading channels with $\mathcal{E}_b/I_{t0} = 13$ dB and $B_{\max}T_b = 2$

shows the performance when both A and B are estimated on a block-by-block basis with the EM estimator, while the lowest curve shows the performance with perfect CSI, i.e., when A and B are known perfectly. As can be seen, there is a large gap between perfect CSI and simply using the average values of A and B. This gap can be partially closed by estimating either A and B independently on a block-by-block basis, and the gap closes almost completely by estimating them jointly.

Figure 8.15 illustrates the robustness of the estimator as a function of the alphabet size, channel type, and fraction of partial-band interference μ. The figure shows the value of $\mathcal{E}_b/N_0$ required to achieve a BER of 10^{-3} as a function of μ for several systems with $\mathcal{E}_b/I_{t0} = 13$ dB. For each of the three alphabet sizes, both AWGN and block Rayleigh fading (again, 32 hops per codeword) are considered. For each of these six cases, the performance using perfect CSI and the performance with the EM estimator are shown. Across the entire range of tested parameters, the estimator's performance nearly matches that of perfect CSI. The benefit of increasing the alphabet size is apparent. For instance, in AWGN, increasing q from 2 to 4 improves performance by about 4 dB while increasing it again from 4 to 8 yields another 1.2 dB gain. The gains in Rayleigh fading are even more dramatic. Although the performance in AWGN is relatively insensitive to the value of μ, the performance in Rayleigh fading degrades as μ increases, and when $q = 2$, this degradation is quite severe.

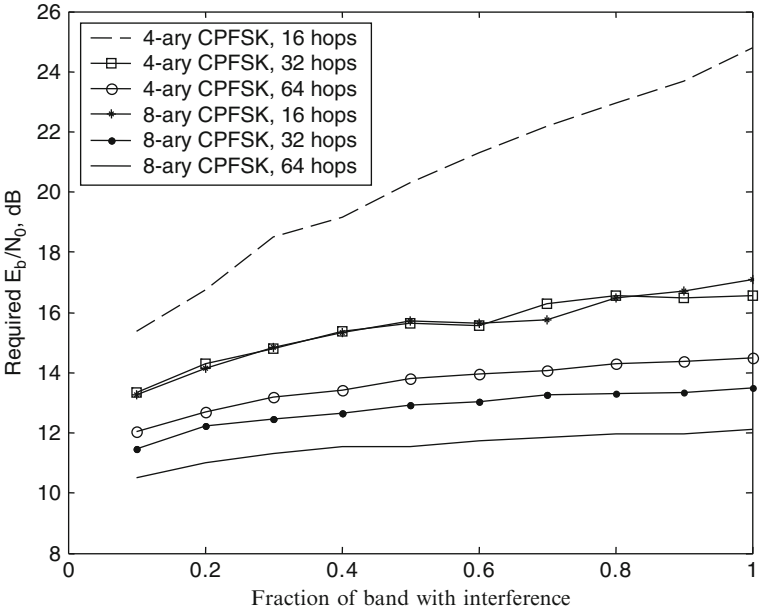

Fig. 8.16 Required $\mathcal{E}_b/N_0$ to achieve $BER = 10^{-3}$ as a function of μ for quaternary and octal CPFSK in Rayleigh block fading with partial-band interference, EM estimation, $\mathcal{E}_b/I_{t0} = 13$ dB, and various hops per codeword

If the hop rate increases, the increase in the number of independently fading dwell intervals per codeword implies that more diversity is available in the processing of a codeword. However, the shortening of the dwell interval makes the channel estimation less reliable by providing the estimator with fewer samples. The influence of the number of hops per codeword is shown in Fig. 8.16 as a function of μ for quaternary and octal CPFSK using the EM estimator, Rayleigh block fading, and partial-band interference with $\mathcal{E}_b/I_{t0} = 13$ dB. Since the codeword length is fixed for each q, increasing the number of hops per codeword results in shorter blocks. For $q = 4$, there are 108, 54, or 27 symbols per hop when there are 16, 32, or 64 hops per codeword, respectively. For $q = 8$, there are 80, 40, or 20 symbols per hop when there are 16, 32, or 64 hops per codeword, respectively. Despite the slow decline in the accuracy of the EM channel estimates, the diversity improvement is sufficient to produce an improved performance as the number of code symbols per hop decreases. However, decreasing to fewer than 20 code symbols per hop will begin to broaden the spectrum significantly, as indicated in Sect. 3.2, unless the parameter values are changed.

Existing fielded frequency-hopping systems, such as GSM, Bluetooth, and combat net radios, use binary MSK with h = 0.5 or binary Gaussian FSK, and do not have fading-amplitude estimators. Figures 8.15 and 8.14 illustrate the substantial performance penalties resulting from the use of a binary modulation

and the absence of fading-amplitude estimation, respectively. The cost of the superior performance of the robust system is primarily the increased computational requirements. Other proposed nonbinary frequency-hopping systems use channel estimators to achieve an excellent performance against partial-band interference and AWGN. However, they are not resistant to multiple-access interference because the transmitted symbols are not spectrally compact, and the channel estimators are not designed to estimate multiple interference and noise spectral-density levels. As described subsequently, the robust system accommodates substantial multiple-access interference.

8.4.6 Asynchronous Multiple-Access Interference

Multiple-access interference may occur when two or more frequency-hopping signals share the same physical medium or network, but the hopping patterns are not coordinated. A collision occurs when two or more signals using the same frequency channel are received simultaneously. Since the probability of a collision in a network is decreased by increasing the number of frequency channels in the hopset, a spectrally compact modulation is highly desirable when the hopping band is fixed.

Simulation experiments were conducted to compare the effect of the number of users of an ad hoc network on systems with different values of q and h. All network users have asynchronous, statistically independent, randomly generated hopping patterns. Let T_i denote the random variable representing the relative transition time of frequency-hopping interference signal i or the start of its new dwell interval relative to that of the desired signal. The ratio T_i/T_s is uniformly distributed over the integers in $[0, N_h - 1]$, where N_h is the number of symbols per dwell interval, and it is assumed that the switching time between dwell intervals is negligible. Let M denote the number of frequency channels in the hopset shared by all users. Since two carrier frequencies are randomly generated by each interference signal during the dwell interval of the desired signal, the probability is $1/M$ that the interference signal collides with the desired signal *before* T_i, and the probability is $1/M$ that the interference signal collides with the desired signal *after* T_i. Each interference signal transmits a particular symbol with probability $1/q$ (common values of q and h are used throughout the network). The response of each matched filter to an interference symbol is given by the same equations used for the desired signal. The soft-decision metrics sent to the decoder are generated in the usual manner but are degraded by the multiple-access interference.

The transmitted powers of the interference and the desired signals are the same. All the interference sources are randomly located at a distance from the receiver within four times the distance of the desired-signal source. All signals experience a path loss with an attenuation power law equal to 4 and independent Rayleigh fading. The interference signals also experience independent shadowing (Sect. 5.1) with a shadow factor equal to 8 dB.

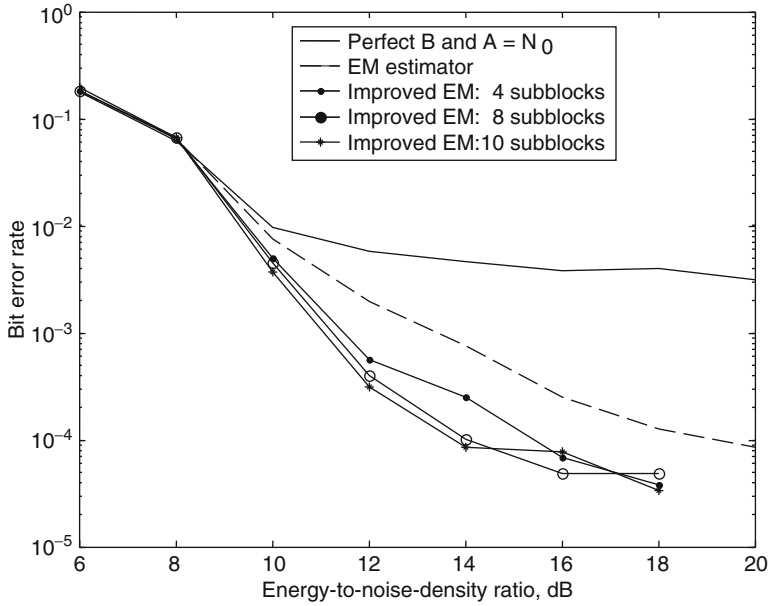

Fig. 8.17 Bit error rates of systems with various estimators in Rayleigh block fading with multiple-access interference created by 30 users. Turbo-coded octal CPFSK is used with $h = 0.32$, code rate 2,048/3,840, and 32 hops per codeword

The simulations consider CPFSK alphabet sizes from the set $q = \{2, 4, 8\}$. The hopping band has the normalized bandwidth $WT_b = 2{,}000$. Both orthogonal and nonorthogonal modulation are considered. For the orthogonal case, the code rate is chosen to be 2,048/6,144, which is close to the information-theoretic optimal value in Rayleigh fading when $h = 1$. Taking into account the 99% power bandwidth of the resulting signal, there are $M = 312, 315$, and 244 frequency channels for binary, quaternary, and octal orthogonal CPFSK, respectively. For the nonorthogonal case, a bandwidth constraint $B_{\max} T_b = 2$ is assumed so that there are $M = 1{,}000$ frequency channels. As in the previous examples, values of h and R that are close to the information-theoretic optimal values for this bandwidth constraint are selected (i.e. $h = 0.6$ and $R = 2{,}048/3{,}200$ for $q = 2$, $h = 0.46$ and $R = 2{,}048/3{,}456$ for $q = 4$, and $h = 0.32$ and $R = 2{,}048/3{,}840$ for $q = 8$). In all cases, there are 32 hops per codeword.

In the presence of multiple-access interference, it is important to accurately estimate the values of A and B. The impact of the channel estimation technique is illustrated in Fig. 8.17 for a system with 30 users all transmitting nonorthogonal octal CPFSK. The uppermost curve shows what happens when the receiver ignores the presence of interference. In this case, B is set to its actual value (perfect CSI for B), while A is set to N_0, its value without interference. Performance can be

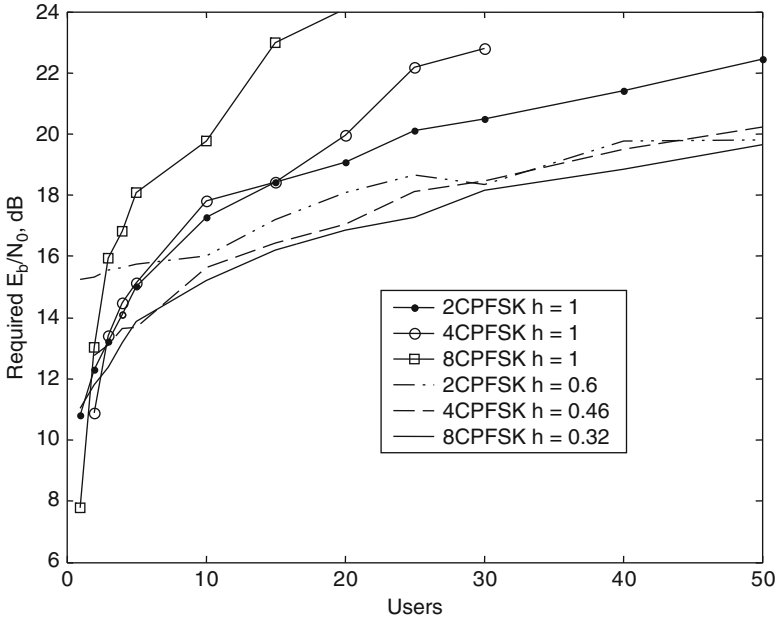

Fig. 8.18 Required $\mathcal{E}_b/N_0$ to achieve $BER = 10^{-4}$ as a function of the number of users for turbo-coded CPFSK in Rayleigh block fading. $B_{\max}T_b = 2$ for nonorthogonal signaling

improved by using the EM-based estimators for jointly estimating A and B on a block-by-block basis, as illustrated by the second curve from the top.

Unlike the partial-band interference case, where the value of A is constant for the entire duration of the hop, the value of A in the presence of multiple-access interference will not generally be constant due to the asynchronous hopping. This fact suggests that performance can be improved by partitioning the block into multiple sub-blocks, and obtaining a separate estimate of A for each sub-block. Such estimates can be found from a simple modification of the EM-based estimator. The estimator first finds the value of B for the entire block from (8.99) as before. Next, it finds the value of A for each sub-block from (8.98) using the value of B found for the entire block and the value of D for just that sub-block (with N_b set to the size of the sub-block). The bottom three curves in Fig. 8.17 show the performance when 4, 8, or 10 sub-blocks are used to estimate A. While it is beneficial to use more sub-blocks at low $\mathcal{E}_b/N_0$, at higher $\mathcal{E}_b/N_0$ even using only four sub-blocks is sufficient to give significantly improved performance. This method of sub-block estimation entails essentially no additional complexity.

Figures 8.18 and 8.19 show the energy efficiency as a function of the number of users. In Fig. 8.18, the performance using the block EM estimator (no sub-block estimation) is shown. In particular, the minimum required value of $\mathcal{E}_b/N_0$ to achieve a bit error rate equal to 10^{-4} is given as a function of the number of users. The performance is shown for both orthogonal and nonorthogonal modulation and the

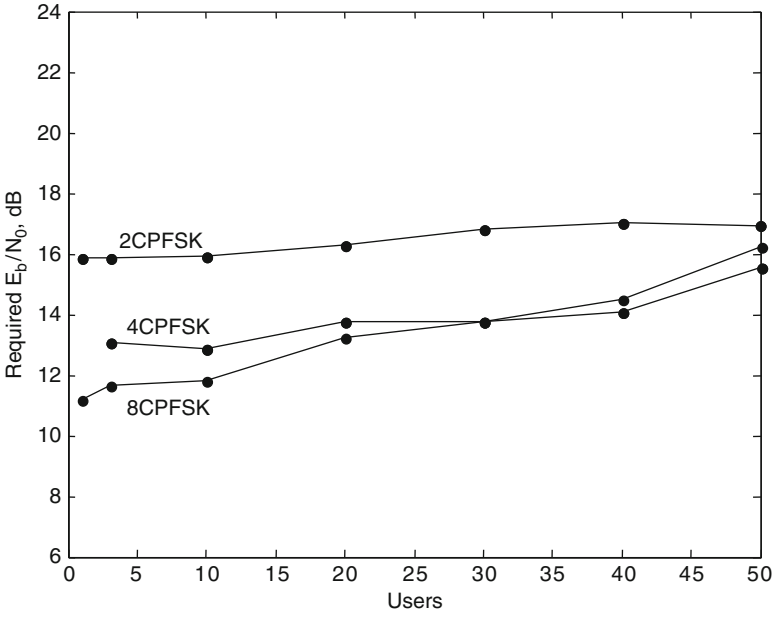

Fig. 8.19 Required $\mathcal{E}_b/N_o$ to achieve $BER = 10^{-4}$ as a function of the number of users for improved EM estimation and nonorthogonal binary, quaternary, and octal turbo-coded CPFSK in the presence of Rayleigh block fading

three values of q. For a lightly loaded system (less than five users), the orthogonal systems outperform the nonorthogonal ones because orthogonal modulation is more energy efficient in the absence of interference. However, as the number of users increases beyond about five, the nonorthogonal systems offer superior performance. The reason is that the improved spectral efficiency of a nonorthogonal modulation allows more frequency channels, thereby decreasing the probability of a collision. With orthogonal modulation, performance as a function of the number of users degrades more rapidly as q increases because larger values of q require larger bandwidths. In contrast, with nonorthogonal modulation, the best performance is achieved with the largest value of q, although performance with $q = 2$ or $q = 4$ is only about $1-2$ dB worse than with $q = 8$. When there are 50 users, nonorthogonal CPFSK with $q = 8$ is about 3 dB more energy efficient than the more conventional orthogonal CPFSK with $q = 2$.

Figure 8.19 shows the performance with nonorthogonal CPFSK when sub-block estimation is used instead of block estimation, but the system parameters remain the same. For $q = 8$ there are 10 sub-blocks of $40/10 = 4$ symbols, for $q = 4$ there are nine sub-blocks of $54/9 = 6$ symbols, and for $q = 2$ there are 10 sub-blocks of $100/10 = 10$ symbols. A comparison with Fig. 8.18 indicates that for $q = 8$ and 50 users, there is a 4 dB gain in energy efficiency relative to the block estimator. It is also observed that when using the sub-block estimator, the performance is less

sensitive to the number of users, and that in a very lightly loaded system, the block estimator offers better performance (since then A is likely to be constant for the entire hop).

The noncoherent frequency-hopping system with nonorthogonal CPFSK is highly robust in environments including frequency-selective fading, partial-band interference, multitone jamming, and multiple-access interference. The robustness is due to the iterative turbo decoding and demodulation, the channel estimator based on the EM algorithm, and the spectrally compact modulation.

Problems

8.1. Let X_{1i} and X_{2i} denote independent, zero-mean, Gaussian random variables with variances V_1 and V_2, respectively, for $i = 1, \ldots, N$. The received random vector is $\mathbf{Y} = [Y_1 \ldots Y_N]^T$, where $Y_i = aX_{1i} + b\ X_{2i}$, and a and b are known constants. It is desired to derive maximum-likelihood estimates $\widehat{V}_1$ and $\widehat{V}_2$ of the variances. (a) Evaluate the likelihood equations and show that they provide a single equation that does not have a unique solution even when $N \to \infty$. Interpret this result in terms of the variance of Y_i, $i = 1, \ldots, N$. (b) Define a complete data vector. Apply the EM algorithm and use (8.4) to obtain estimates of the variances. If the EM algorithm converges, the estimates provided may converge to none or any of the possible maximum-likelihood estimates, depending on the initial estimates.

8.2. (a) Consider the equation $f(x) = x^2 - 3x + 1 = 0$. Find two different representations of this equation that have the form $x = g(x)$, and find sufficient conditions for convergence of the fixed-point iteration for both representations. Show that the initial value $x_0 = 2$ does not satisfy one of these conditions for an interval that includes it. Show by numerical computation that convergence to the smaller solution of $f(x) = 0$ occurs nevertheless. (b) Consider the equation $f(x) = x^3 + x - 1 = 0$, which has a solution near $x = 0.68$. Find a representation of this equation having the form $x = g(x)$ and satisfying the sufficient condition for convergence of the fixed-point iteration for any initial x_0. Show that $x = 1 - x^3$ is not the required representation.

8.3. Derive (8.47) to (8.49) from (8.43).

8.4. Using the method outlined in the text, derive (8.50) from (8.44), (8.45), and (8.46).

8.5. Use calculations similar to those in the text to complete the derivation of (8.54) and (8.55).

8.6. Show how the spectrum confinement leads to (8.72).

8.7. Derive (8.98) and (8.99) from (8.93).

References

1. B. Levy, *Principles of Signal Detection and Parameter Estimation*. New York: Springer, 2008.
2. E. Kreyszig, *Advanced Engineering Mathematics, 10th ed.* Hoboken, NJ: Wiley, 2011.
3. *Third Generation Partnership Project (3GPP)*; Technical Specification Group Radio Access Network; Evolved Universal Terrestrial Radio Access (E-UTRA); *Physical Channels and Modulation*, (Release 9), http://www.3gpp.org/ftp/Specs/archive/36_series/36.211/, 2010.
4. J. G. Proakis and M. Salehi, *Digital Communications, 5th ed.* New York: McGraw-Hill, 2008.
5. I. N. Psaromiligkos, S. N. Batalama, and M. J. Medley, "Rapid Combined Synchronization/Demodulation Structures for DS-CDMA Systems - Part I: Algorithmic Developments," *IEEE Trans. Commun*., vol. 51, pp. 983 - 994, June 2003.
6. X. Wang and H. V. Poor, *Wireless Communication Systems*, Upper Saddle River, NJ: Prentice-Hall, 2004.
7. J. Choi, *Adaptive and Iterative Signal Processing in Communications, Cambridge Univ. Press*, 2006.
8. D. Torrieri, A. Mukherjee, and H. M. Kwon, "Coded DS-CDMA systems with Iterative Channel Estimation and No Pilot Symbols," *IEEE Trans. Wireless Commun.*, vol. 9, pp. 2012-2021, June 2010.
9. W. E. Ryan and S. Lin, *Channel Codes: Classical and Modern*. Cambridge, UK: Cambridge University Press, 2009.
10. T. M. Cover and J. M. Thomas, *Elements of Information Theory, 2nd ed*. Hoboken, NJ: Wiley, 2006.
11. D. Torrieri, S. Cheng, and M. C. Valenti, "Robust Frequency Hopping for Interference and Fading Channels," IEEE Trans. Communications, vol. 56, pp. 1343-1351, Aug. 2008.

Appendix A
Signal Characteristics

A.1 Bandpass Signals

A *bandpass signal* has its power spectrum in a spectral band surrounding a carrier frequency, which is usually at the center of the band. The *Hilbert transform* provides the basis for signal representations that facilitate the analysis of bandpass signals and systems. The Hilbert transform of a real-valued function $g(t)$ is

$$H[g(t)] = \hat{g}(t) = \frac{1}{\pi}\int_{-\infty}^{\infty}\frac{g(u)}{t-u}\,du. \tag{A.1}$$

Since its integrand has a singularity, the integral is defined as its Cauchy principal value:

$$\int_{-\infty}^{\infty}\frac{g(u)}{t-u}\,du = \lim_{\epsilon\to 0}\left[\int_{-\infty}^{t-\epsilon}\frac{g(u)}{t-u}\,du + \int_{t+\epsilon}^{\infty}\frac{g(u)}{t-u}\,du\right] \tag{A.2}$$

provided that the limit exists. Since (A.1) has the form of the convolution of $g(t)$ with $1/\pi t$, $\hat{g}(t)$ results from passing $g(t)$ through a linear filter with an impulse response equal to $1/\pi t$. The transfer function of the filter is given by the Fourier transform

$$\mathcal{F}\left\{\frac{1}{\pi t}\right\} = \int_{-\infty}^{\infty}\frac{\exp(-j2\pi ft)}{\pi t}\,dt \tag{A.3}$$

where $j = \sqrt{-1}$. This integral can be rigorously evaluated by using contour integration. Alternatively, we observe that since $1/t$ is an odd function,

$$\begin{aligned}\mathcal{F}\left\{\frac{1}{\pi t}\right\} &= -2j\int_{0}^{\infty}\frac{\sin 2\pi ft}{\pi t}\,dt\\ &= -j\ \mathrm{sgn}(f)\end{aligned} \tag{A.4}$$

D. Torrieri, *Principles of Spread-Spectrum Communication Systems*,
DOI 10.1007/978-1-4419-9595-7, © Springer Science+Business Media, LLC 2011

where $\text{sgn}(f)$ is the *signum function* defined by

$$\text{sgn}(f) = \begin{cases} 1, & f > 0 \\ 0, & f = 0 \\ -1, & f < 0. \end{cases} \tag{A.5}$$

Let $G(f) = \mathcal{F}\{g(t)\}$, and let $\hat{G}(f) = \mathcal{F}\{\hat{g}(t)\}$. Equations (A.1) and (A.4) and the convolution theorem imply that

$$\hat{G}(f) = -j\ \text{sgn}(f)G(f). \tag{A.6}$$

Because $H[\hat{g}(t)]$ results from passing $g(t)$ through two successive filters, each with transfer function $-j\ \text{sgn}(f)$,

$$H[\hat{g}(t)] = -g(t) \tag{A.7}$$

provided that $G(0) = 0$.

Equation (A.6) indicates that taking the Hilbert transform corresponds to introducing a phase sift of $-\pi$ radians for all positive frequencies and $+\pi$ radians for all negative frequencies. Consequently,

$$H[\cos 2\pi f_c t] = \sin 2\pi f_c t \tag{A.8}$$

$$H[\sin 2\pi f_c t] = -\cos 2\pi f_c t. \tag{A.9}$$

These relations can be formally verified by taking the Fourier transform of the left-hand side of (A.8) or (A.9), applying (A.6), and then taking the inverse Fourier transform of the result. If $G(f) = 0$ for $|f| > W$ and $f_c > W$, the same method yields

$$H[g(t)\cos 2\pi f_c t] = g(t)\sin 2\pi f_c t \tag{A.10}$$

$$H[g(t)\sin 2\pi f_c t] = -g(t)\cos 2\pi f_c t. \tag{A.11}$$

A *bandpass signal* is one with a Fourier transform that is negligible except for $f_c - W/2 \le |f| \le f_c + W/2$, where $0 \le W < 2f_c$ and f_c is the center frequency. If $W \ll f_c$, the bandpass signal is often called a *narrowband signal*. A complex-valued signal with a Fourier transform that is nonzero only for $f > 0$ is called an *analytic signal*.

Consider a bandpass signal $g(t)$ with Fourier transform $G(f)$. The analytic signal $g_a(t)$ associated with $g(t)$ is defined to be the signal with Fourier transform

$$G_a(f) = [1 + \text{sgn}(f)]G(f) \tag{A.12}$$

which is zero for $f \le 0$ and is confined to the band $|f - f_c| \le W/2$ when $f > 0$. The inverse Fourier transform of (A.12) and (A.6) imply that

$$g_a(t) = g(t) + j\hat{g}(t). \tag{A.13}$$

The *complex envelope* of $g(t)$ is defined by

$$g_l(t) = g_a(t) \exp[-j2\pi f_c t] \tag{A.14}$$

where f_c is the center frequency if $g(t)$ is a bandpass signal. Since the Fourier transform of $g_l(t)$ is $G_a(f + f_c)$, which occupies the band $|f| \leq W/2$, the complex envelope is a baseband signal that may be regarded as an *equivalent lowpass representation* of $g(t)$. Equations (A.13) and (A.14) imply that $g(t)$ may be expressed in terms of its complex envelope as

$$g(t) = \text{Re}[g_l(t) \exp(j2\pi f_c t)]. \tag{A.15}$$

The complex envelope can be decomposed as

$$g_l(t) = g_c(t) + jg_s(t) \tag{A.16}$$

where $g_c(t)$ and $g_s(t)$ are real-valued functions. Therefore, (A.15) yields

$$g(t) = g_c(t) \cos(2\pi f_c t) - g_s(t) \sin(2\pi f_c t). \tag{A.17}$$

Since the two sinusoidal carriers are in phase quadrature, $g_c(t)$ and $g_s(t)$ are called the *in-phase* and *quadrature* components of $g(t)$, respectively. These components are lowpass signals confined to $|f| \leq W/2$.

Applying Parseval's identity from Fourier analysis and then (A.6), we obtain

$$\int_{-\infty}^{\infty} \hat{g}^2(t)\, dt = \int_{-\infty}^{\infty} |\hat{G}(f)|^2\, df = \int_{-\infty}^{\infty} |G(f)|^2\, df = \int_{-\infty}^{\infty} g^2(t)\, dt. \tag{A.18}$$

Therefore,

$$\begin{aligned} \int_{-\infty}^{\infty} |g_l(t)|^2\, dt &= \int_{-\infty}^{\infty} |g_a(t)|^2\, dt = \int_{-\infty}^{\infty} g^2(t)\, dt + \int_{-\infty}^{\infty} \hat{g}^2(t)\, dt \\ &= 2\int_{-\infty}^{\infty} g^2(t)\, dt = 2\mathcal{E} \end{aligned} \tag{A.19}$$

where $\mathcal{E}$ denotes the energy of the bandpass signal $g(t)$.

A.2 Stationary Stochastic Processes

Consider a stochastic process $n(t)$ that is a zero-mean, wide-sense stationary process with autocorrelation

$$R_n(\tau) = E[n(t)n(t + \tau)] \tag{A.20}$$

where $E[x]$ denotes the expected value of x. The Hilbert transform of this process is the stochastic process defined by

$$\hat{n}(t) = \frac{1}{\pi} \int_{-\infty}^{\infty} \frac{n(u)}{t-u} du \tag{A.21}$$

where it is assumed that the Cauchy principal value of the integral exists for almost every sample function of $n(t)$. This equation indicates that $\hat{n}(t)$ is a zero-mean stochastic process. The zero-mean processes $n(t)$ and $\hat{n}(t)$ are *jointly wide-sense stationary* if their correlation and cross-correlation functions are not functions of t. A straightforward calculation using (A.21) and (A.20) gives the cross-correlation

$$R_{n\hat{n}}(\tau) = E[n(t)\hat{n}(t+\tau)] = \frac{1}{\pi} \int_{-\infty}^{\infty} \frac{R_n(u)}{\tau - u} du = \hat{R}_n(\tau). \tag{A.22}$$

A similar derivation using (A.7) yields the autocorrelation

$$R_{\hat{n}}(\tau) = E[\hat{n}(t)\hat{n}(t+\tau)] = R_n(\tau). \tag{A.23}$$

Equations (A.20), (A.22), and (A.23) indicate that $n(t)$ and $\hat{n}(t)$ are jointly wide-sense stationary.

The *analytic signal* associated with $n(t)$ is the zero-mean process defined by

$$n_a(t) = n(t) + j\hat{n}(t). \tag{A.24}$$

The autocorrelation of the analytic signal is defined as

$$R_a(\tau) = E[n_a^*(t)n_a(t+\tau)] \tag{A.25}$$

where the asterisk denotes the complex conjugate. Using (A.20) and (A.22) to (A.25), we obtain

$$R_a(\tau) = 2R_n(\tau) + 2j\hat{R}_n(\tau) \tag{A.26}$$

which establishes the wide-sense stationarity of the analytic signal.

Since (A.20) indicates that $R_n(\tau)$ is an even function, (A.22) yields

$$R_{n\hat{n}}(0) = \hat{R}_n(0) = 0 \tag{A.27}$$

which indicates that $n(t)$ and $\hat{n}(t)$ are uncorrelated. Equations (A.23), (A.26), and (A.27) yield

$$R_{\hat{n}}(0) = R_n(0) = 1/2R_a(0). \tag{A.28}$$

The *complex envelope* of $n(t)$ or the *equivalent lowpass representation* of $n(t)$ is the zero-mean stochastic process defined by

$$n_l(t) = n_a(t)\exp(-j2\pi f_c t) \tag{A.29}$$

where f_c is an arbitrary frequency usually chosen as the center or carrier frequency of $n(t)$. The complex envelope can be decomposed as

$$n_l(t) = n_c(t) + jn_s(t) \tag{A.30}$$

where $n_c(t)$ and $n_s(t)$ are real-valued, zero-mean stochastic processes.

Equations (A.29) and (A.30) imply that

$$\begin{aligned} n(t) &= Re[n_l(t)\exp(j2\pi f_c t)] \\ &= n_c(t)\cos(2\pi f_c t) - n_s(t)\sin(2\pi f_c t). \end{aligned} \tag{A.31}$$

Substituting (A.24) and (A.30) into (A.29) we find that

$$n_c(t) = n(t)\cos(2\pi f_c t) + \hat{n}(t)\sin(2\pi f_c t) \tag{A.32}$$

$$n_s(t) = \hat{n}(t)\cos(2\pi f_c t) - n(t)\sin(2\pi f_c t). \tag{A.33}$$

The *autocorrelations* of $n_c(t)$ and $n_s(t)$ are defined by

$$R_c(\tau) = E[n_c(t)n_c(t+\tau)] \tag{A.34}$$

and

$$R_s(\tau) = E[n_s(t)n_s(t+\tau)]. \tag{A.35}$$

Using (A.32) and (A.33) and then (A.20), (A.22), and (A.23) and trigonometric identities, we obtain

$$R_c(\tau) = R_s(\tau) = R_n(\tau)\cos(2\pi f_c\tau) + \hat{R}_n(\tau)\sin(2\pi f_c\tau) \tag{A.36}$$

which shows explicitly that if $n(t)$ is wide-sense stationary, then $n_c(t)$ and $n_s(t)$ are wide-sense stationary with the same autocorrelation function. The variances of $n(t)$, $n_c(t)$, and $n_s(t)$ are all equal because

$$R_c(0) = R_s(0) = R_n(0). \tag{A.37}$$

A derivation similar to that of (A.36) gives the cross-correlation

$$R_{cs}(\tau) = E[n_c(t)n_s(t+\tau)] = \hat{R}_n(\tau)\cos(2\pi f_c\tau) - R_n(\tau)\sin(2\pi f_c\tau). \tag{A.38}$$

Equations (A.36) and (A.38) indicate that $n_c(t)$ and $n_s(t)$ are jointly wide-sense stationary, which then implies that

$$R_{sc}(\tau) = E[n_s(t)n_c(t+\tau)] = R_{cs}(-\tau). \tag{A.39}$$

Equations (A.27) and (A.38) give

$$R_{cs}(0) = 0 \tag{A.40}$$

which implies that $n_c(t)$ and $n_s(t)$ are uncorrelated.

Since $n(t)$ is wide-sense stationary, $R_n(-\tau) = R_n(\tau)$. It then follows from (A.17) and a change of the integration variable that $\widehat{R}_n(-\tau) = -\widehat{R}_n(\tau)$. Combining these equations with (A.38) yields $R_{cs}(-\tau) = -R_{cs}(\tau)$. This equation and (A.39) indicate that

$$R_{cs}(\tau) = -R_{sc}(\tau). \tag{A.41}$$

Equations (A.30), (A.37), and (A.41) imply that

$$E[n_I(t)n_I(t+\tau)] = 0. \tag{A.42}$$

A complex-valued, zero-mean stochastic process that satisfies this equation is called a *circularly symmetric* process. Thus, the complex envelope of a zero-mean, wide-sense stationary process is a circularly symmetric process.

Equation (A.21) indicates that $\hat{n}(t)$ is generated by a linear operation on $n(t)$. Therefore, if $n(t)$ is a zero-mean Gaussian process, $\hat{n}(t)$ and $n(t)$ are zero-mean jointly Gaussian processes. Equations (A.32) and (A.33) then imply that $n_c(t)$ and $n_s(t)$ are zero-mean jointly Gaussian processes. Since they are uncorrelated, $n_c(t)$ and $n_s(t)$ are statistically independent, zero-mean Gaussian processes.

The *power spectral density* of a signal is the Fourier transform of its autocorrelation. Let $S(f)$, $S_c(f)$, and $S_s(f)$ denote the power spectral densities of $n(t)$, $n_c(t)$, and $n_s(t)$, respectively. We assume that $S_n(f)$ occupies the band $f_c - W/2 \le |f| \le f_c + W/2$ and that $f_c > W/2 \ge 0$. Taking the Fourier transform of (A.36), using (A.6), and simplifying, we obtain

$$S_c(f) = S_s(f) = \begin{cases} S_n(f - f_c) + S_n(f + f_c), & |f| \le W/2 \\ 0, & |f| > W/2. \end{cases} \tag{A.43}$$

Thus, if $n(t)$ is a passband process with bandwidth W of the positive frequencies, then $n_c(t)$ and $n_s(t)$ are baseband processes with bandwidths $W/2$. This property and the statistical independence of $n_c(t)$ and $n_s(t)$ when $n(t)$ is Gaussian make (A.31) a very useful representation of $n(t)$.

Similarly, the cross-spectral density of $n_c(t)$ and $n_s(t)$ can be derived by taking the Fourier transform of (A.38) and using (A.6). After simplification, the result is

$$S_{cs}(f) = \begin{cases} j[S_n(f - f_c) - S_n(f + f_c)], & |f| \le W/2 \\ 0, & |f| > W/2. \end{cases} \tag{A.44}$$

If $S_n(f)$ is locally symmetric about f_c, then

$$S_n(f_c + f) = S_n(f_c - f), \quad |f| \le W/2. \tag{A.45}$$

Since a power spectral density is a real-valued, even function, $S_n(f_c - f) = S_n(f - f_c)$. Equation (A.45) then yields $S_n(f + f_c) = S_n(f - f_c)$ for $|f| \leq W/2$. Therefore, (A.44) gives $S_{cs}(f) = 0$, which implies that

$$R_{cs}(\tau) = 0 \tag{A.46}$$

for all τ. Thus, $n_c(t)$ and $n_s(t + \tau)$ are uncorrelated for all τ, and if $n(t)$ is a zero-mean Gaussian process, then $n_c(t)$ and $n_s(t + \tau)$ are statistically independent for all τ.

The autocorrelation of the complex envelope is defined by

$$R_l(\tau) = E[n_l^*(t)n_l(t + \tau)]. \tag{A.47}$$

Equations (A.29) and (A.26) imply that the complex envelope of a zero-mean, wide-sense stationary process is wide-sense stationary. Equations (A.28) and (A.29) yield

$$R_l(0) = 2R_n(0). \tag{A.48}$$

Substituting (A.30) into (A.47) and using (A.36) and (A.38), we obtain

$$R_l(\tau) = 2R_c(\tau) + j2R_{cs}(\tau). \tag{A.49}$$

The power spectral density of $n_l(t)$, which we denote by $S_l(f)$, can be derived from (A.49), (A.44), and (A.43). If $S_n(f)$ occupies the band $f_c - W/2 \leq |f| \leq f_c + W/2$ and $f_c > W/2 \geq 0$, then

$$S_l(f) = \begin{cases} 4S_n(f + f_c), & |f| \leq W/2 \\ 0, & |f| > W/2. \end{cases} \tag{A.50}$$

Equations (A.36) and (A.38) yield

$$R_n(\tau) = 2R_c(\tau)\cos(2\pi f_c\tau) - 2R_{cs}(\tau)\sin(2\pi f_c\tau). \tag{A.51}$$

Equations (A.51) and (A.49) imply that

$$R_n(\tau) = Re\left[R_l(\tau)\exp(j2\pi f_c\tau)\right]. \tag{A.52}$$

We expand the right-hand side of this equation by using the fact that $Re[z] = (z + z^*)/2$. Taking the Fourier transform and observing that $S_l(f)$ is a real-valued function, we obtain

$$S_n(f) = \frac{1}{4}S_l(f - f_c) + \frac{1}{4}S_l(-f - f_c). \tag{A.53}$$

If $S_n(f)$ is locally symmetric about f_c, then (A.50) and (A.45) imply that $S_l(-f) = S_l(f)$, and (A.53) becomes

$$S_n(f) = \frac{1}{4}S_l(f - f_c) + \frac{1}{4}S_l(f + f_c). \tag{A.54}$$

Many communication signals are modeled as bandpass signals having the form

$$s(t) = A\,\mathrm{Re}\,[s_l\,(t)\exp\,(j2\pi f_c t + \theta)] \tag{A.55}$$

where A is the amplitude and θ is an independent random variable that is uniformly distributed over $0 \leq \theta < 2\pi$. Equation (A.15) indicates that the complex envelope of $s(t)$ is $As_l\,(t)\exp\,(j\theta)$. The power spectral density of the complex envelope is equal to $AS_l(f)$, where $S_l(f)$ is the power spectral density of $s_l\,(t)$. The power spectral density of $s(t)$ is calculated by applying (A.54) or (A.53).

A.3 Direct-Conversion Receiver

Receivers often extract the complex envelope of the desired signal before applying it to a matched filter. The main components in a *direct-conversion* receiver are shown in Fig. A.1a. The spectra of the received signal $g(t)$, the input to the baseband filter $g'(t) = g(t)\exp(-j2\pi f_c t)$, and the complex envelope $g_l(t)$ are depicted in Fig. A.1b. Let $2h(t)$ denote the impulse response of the filter. The output of the filter is

$$y(t) = \int_{-\infty}^{\infty} 2\,g(\tau)\exp(-j2\pi f_c\tau)h(t-\tau)\,d\tau. \tag{A.56}$$

Using (A.15) and the fact that $\mathrm{Re}(x) = (x + x^*)/2$, where x^* denotes the complex conjugate of x, we obtain

$$y(t) = \int_{-\infty}^{\infty} g_l(\tau)h(t-\tau)\,d\tau + \int_{-\infty}^{\infty} g_l(\tau)h(t-\tau)\exp(-j4\pi f_c\tau)\,d\tau. \tag{A.57}$$

The second term is the Fourier transform of $g_l(\tau)h(t-\tau)$ evaluated at frequency $-2f_c$. Assuming that $g_l(\tau)$ and $h(t-\tau)$ have transforms confined to $|f| < f_c$, their product has a transform confined to $|f| < 2f_c$, and the second term in (A.57) vanishes. If the Fourier transform of $h(t)$ is a constant over the passband of $g_l(t)$, then (A.57) implies that $y(t)$ is proportional to $g_l(t)$, as desired. Figure A.1c shows the direct-conversion receiver for real-valued signals.

The direct-conversion receiver alters the character of the noise $n(t)$ entering it. Suppose that $n(t)$ is a zero-mean, white Gaussian noise process with autocorrelation

$$R_n(\tau) = E[n(t)n(t+\tau)] = \frac{N_0}{2}\delta(\tau) \tag{A.58}$$

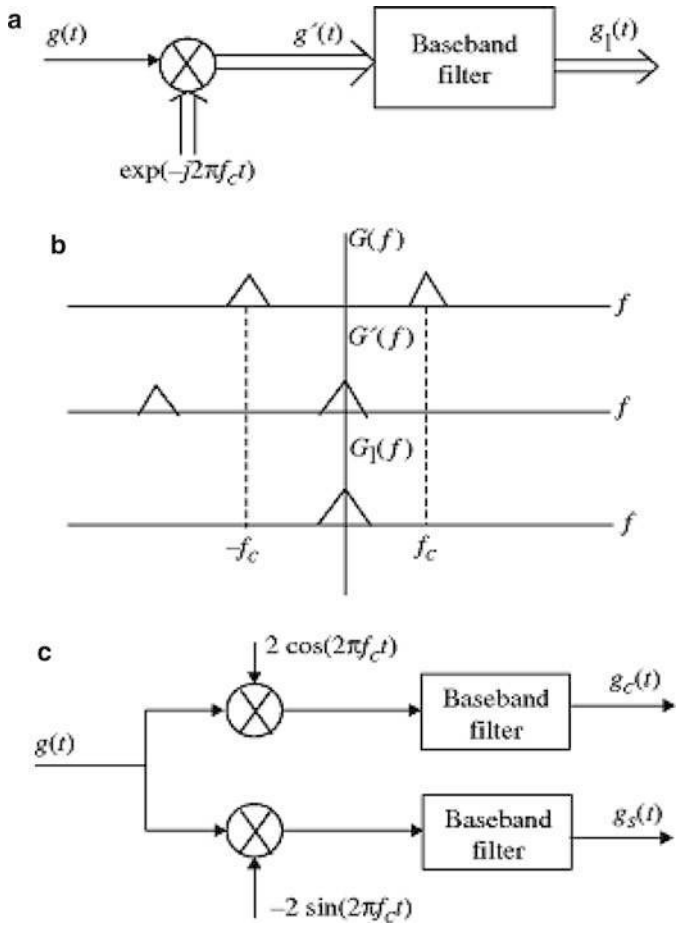

Fig. A.1 Envelope extraction: (**a**) direct-conversion receiver, (**b**) associated spectra, and (**c**) implementation with real-valued signals

where $\delta(\tau)$ denotes the Dirac delta function, and $N_0/2$ is the two-sided noise-power spectral density. The complex-valued noise at the output of Fig. A.1a is

$$z(t) = \int_{-\infty}^{\infty} 2n(u)e^{-j2\pi f_c u}h(t-u)du \tag{A.59}$$

Since it is a linear function of $n(t)$, $z(t)$ is zero-mean and its real and imaginary parts are jointly Gaussian. The autocorrelation of a wide-sense stationary, complex-valued process $z(t)$ is defined as

$$R_z(\tau) = \frac{1}{2}E[z^*(t)z(t+\tau)]. \tag{A.60}$$

Substituting (A.59), interchanging the expectation and integration operations, using (A.58) to evaluate one of the integrals, and then changing variables, we obtain

$$R_z(\tau) = N_0 \int_{-\infty}^{\infty} h(u)h^*(u+\tau)du. \tag{A.61}$$

If the filter is an ideal bandpass filter with Fourier transform

$$H(f) = \begin{cases} 1, & |f| \le W \\ 0, & otherwise \end{cases} \tag{A.62}$$

then evaluating the Fourier transform of both sides of (A.61) gives the power spectral density

$$S_z(f) = \begin{cases} N_0, & |f| \le W \\ 0, & otherwise. \end{cases} \tag{A.63}$$

Thus, if the subsequent filters have narrower bandwidths than W or if W$\rightarrow \infty$, then the autocorrelation of z(t) may be approximated by

$$R_z(\tau) = N_0\delta(\tau). \tag{A.64}$$

This approximation permits major analytical simplifications. Equations (A.59) and (A.58) imply that

$$E[z(t)z(t+\tau)] = 2N_0 e^{-j4\pi f_c t} \int_{-\infty}^{\infty} e^{j4\pi f_c u} h(u+\tau)h(u)\,du. \tag{A.65}$$

If $W < f_c$, then reasoning similar to that following (A.57) leads to

$$E[z(t)z(t+\tau)] = 0 \tag{A.66}$$

which indicates that the complex-valued stochastic process $z(t)$ is a *circularly symmetric* process. Let $z^R(t)$ and $z^I(t)$ denote the real and imaginary parts of $z(t)$, respectively. Since $z(t)$ is zero-mean, $z^R(t)$ and $z^I(t)$ are zero-mean. Setting $\tau = 0$ in (A.66) and (A.60), and then using (A.61), Parseval's identity, and (A.62), we obtain

$$E[(z^R(t))^2] = E[(z^I(t))^2] = 2N_0W \tag{A.67}$$

$$E[(z^R(t)z^I(t))] = 0. \tag{A.68}$$

Thus, $z^R(t)$ and $z^I(t)$ are zero-mean, independent Gaussian processes with the same variance.

Appendix B
Probability Distributions

B.1 Chi-Square Distribution

Consider the random variable

$$Z = \sum_{i=1}^{N} A_i^2 \tag{B.1}$$

where the $\{A_i\}$ are independent Gaussian random variables with means $\{m_i\}$ and common variance σ^2. The random variable Z is said to have a *noncentral chi-square (χ^2) distribution* with N degrees of freedom and a *noncentral parameter*

$$\lambda = \sum_{i=1}^{N} m_i^2. \tag{B.2}$$

To derive the probability density function of Z, we first note that each A_i has the density function

$$f_{A_i}(x) = \frac{1}{\sqrt{2\pi}\sigma} \exp\left[-\frac{(x-m_i)^2}{2\sigma^2}\right]. \tag{B.3}$$

From elementary probability, the density of $Y_i = A_i^2$ is

$$f_{Y_i}(x) = \frac{1}{2\sqrt{x}}[f_{A_i}(\sqrt{x}) + f_{A_i}(-\sqrt{x})]\, u(x) \tag{B.4}$$

where $u(x) = 1, x \geq 0$, and $u(x) = 0, x < 0$. Substituting (B.3) into (B.4), expanding the exponentials, and simplifying, we obtain the density

$$f_{Y_i}(x) = \frac{1}{\sqrt{2\pi x}\sigma} \exp\left(-\frac{x+m_i^2}{2\sigma^2}\right) \cosh\left(\frac{m_i\sqrt{x}}{\sigma^2}\right) u(x). \tag{B.5}$$

The characteristic function of a random variable X is defined as

$$C_X(j\nu) = E[e^{j\nu X}] = \int_{-\infty}^{\infty} f_X(x) \exp(j\nu x)\, dx \tag{B.6}$$

where $j = \sqrt{-1}$, and $f_X(x)$ is the density of X. Since $C_X(j\nu)$ is the conjugate Fourier transform of $f_X(x)$,

$$f_X(x) = \frac{1}{2\pi} \int_{-\infty}^{\infty} C_X(j\nu) \exp(-j\nu x)\, d\nu \tag{B.7}$$

From Laplace or Fourier transform tables, it is found that the characteristic function of $f_{Y_i}(x)$ is

$$C_{Y_i}(j\nu) = \frac{\exp[jm_i^2\nu/(1 - j2\sigma^2\nu)]}{(1 - j\sigma^2\nu)^{1/2}}. \tag{B.8}$$

The characteristic function of a sum of independent random variables is equal to the product of the individual characteristic functions. Because Z is the sum of the Y_i, the characteristic function of Z is

$$C_Z(j\nu) = \frac{\exp[j\lambda\nu/(1 - j2\sigma^2\nu)]}{(1 - j\sigma^2\nu)^{N/2}} \tag{B.9}$$

where we have used (B.2). From (B.9), (B.7), and Laplace or Fourier transform tables, we obtain the probability density function of *noncentral* χ^2 *random variable* with N degrees of freedom and a noncentral parameter λ:

$$f_Z(x) = \frac{1}{2\sigma^2} \left(\frac{x}{\lambda}\right)^{(N-2)/4} \exp\left[-\frac{x + \lambda}{2\sigma^2}\right] I_{N/2-1}\left(\frac{\sqrt{x\lambda}}{\sigma^2}\right) u(x) \tag{B.10}$$

where $I_n(\ )$ is the modified Bessel function of the first kind and order n. This function may be represented by

$$I_n(x) = \sum_{i=0}^{\infty} \frac{(x/2)^{n+2i}}{i!\,\Gamma(n + i + 1)} \tag{B.11}$$

where the gamma function is defined as

$$\Gamma(x) = \int_0^{\infty} y^{x-1} \exp(-y) dy\ , \quad \mathrm{Re}(x) > 0. \tag{B.12}$$

The probability distribution function of a noncentral χ^2 random variable is

$$F_Z(x) = \int_0^x \frac{1}{2\sigma^2} \left(\frac{y}{\lambda}\right)^{(N-2)/4} \exp\left(-\frac{y + \lambda}{2\sigma^2}\right) I_{N/2-1}\left(\frac{\sqrt{y\lambda}}{\sigma^2}\right) dy, \quad x \geq 0. \tag{B.13}$$

If N is even so that $N/2$ is an integer, then $F_Z(\infty) = 1$ and a change of variables in (B.13) yield

$$F_Z(x) = 1 - Q_{N/2}\left(\frac{\sqrt{\lambda}}{\sigma}, \frac{\sqrt{x}}{\sigma}\right), \quad x \geq 0 \tag{B.14}$$

where the *generalized Marcum Q-function* is defined as

$$Q_m(\alpha, \beta) = \int_{\beta}^{\infty} x \left(\frac{x}{\alpha}\right)^{m-1} \exp\left(-\frac{x^2 + \alpha^2}{2}\right) I_{m-1}(\alpha x)\, dx \tag{B.15}$$

and m is an integer. Since $Q_m(\alpha, 0) = 1$, it follows that $1 - Q_m(\alpha, \beta)$ is an integral with finite limits that can be numerically integrated. The mean, variance, and moments of Z can be easily obtained by using (B.1) and the properties of independent Gaussian random variables. The mean and variance of Z are

$$E[Z] = N\sigma^2 + \lambda \tag{B.16}$$

$$\sigma_z^2 = 2N\sigma^4 + 4\lambda\sigma^2 \tag{B.17}$$

where σ^2 is the common variance of the $\{A_i\}$.

From (B.9), it follows that the sum of two independent noncentral χ^2 random variables with N_1 and N_2 degrees of freedom, noncentral parameters λ_1 and λ_2, respectively, and the same parameter σ^2 is a noncentral χ^2 random variable with $N_1 + N_2$ degrees of freedom and noncentral parameter $\lambda_1 + \lambda_2$.

B.2 Central Chi-Square Distribution

To determine the probability density function of Z when the $\{A_i\}$ have zero means, we substitute (B.11) into (B.10) and then take the limit as $\lambda \to 0$. We obtain

$$f_Z(x) = \frac{1}{(2\sigma^2)^{N/2}\Gamma(N/2)} x^{N/2-1} \exp\left(-\frac{x}{2\sigma^2}\right) u(x). \tag{B.18}$$

Alternatively, this equation results if we substitute $\lambda = 0$ into the characteristic function (B.9) and then use (B.7). Equation (B.18) is the probability density function of a *central* χ^2 *random variable* with N degrees of freedom. The probability distribution function is

$$F_Z(x) = \int_0^x \frac{1}{(2\sigma^2)^{N/2}\Gamma(N/2)} y^{N/2-1} \exp\left(-\frac{y}{2\sigma^2}\right) dy, \quad x \geq 0. \tag{B.19}$$

If N is even so that $N/2$ is an integer, then integrating this equation by parts $N/2-1$ times yields

$$F_Z(x) = 1 - \exp\left(-\frac{x}{2\sigma^2}\right) \sum_{i=0}^{N/2-1} \frac{1}{i!} \left(\frac{x}{2\sigma^2}\right)^i, \quad x \geq 0. \tag{B.20}$$

By direct integration using (B.18) and (B.12) or from (B.16) and (B.17), it is found that the mean and variance of Z are

$$E[Z] = N\sigma^2 \tag{B.21}$$

$$\sigma_z^2 = 2N\sigma^4. \tag{B.22}$$

B.3 Rice Distribution

Consider the random variable

$$R = \sqrt{A_1^2 + A_2^2} \tag{B.23}$$

where A_1 and A_2 are independent Gaussian random variables with means m_1 and m_2, respectively, and a common variance σ^2. The probability distribution function of R must satisfy $F_R(r) = F_Z(r^2)$, where $Z = A_1^2 + A_2^2$ is a χ^2 random variable with two degrees of freedom. Therefore, (B.14) with $N = 2$ implies that

$$F_R(r) = 1 - Q_1\left(\frac{\sqrt{\lambda}}{\sigma}, \frac{r}{\sigma}\right), \quad r \geq 0 \tag{B.24}$$

where $\lambda = m_1^2 + m_2^2$. This function is called the *Rice probability distribution function*. The *Rice probability density function*, which may be obtained by differentiation of (B.24), is

$$f_R(r) = \frac{r}{\sigma^2} \exp\left(-\frac{r^2 + \lambda}{2\sigma^2}\right) I_0\left(\frac{r\sqrt{\lambda}}{\sigma^2}\right) u(r). \tag{B.25}$$

The moments of even order can be derived from (B.23) and the moments of the independent Gaussian random variables. The second moment is

$$E[R^2] = 2\sigma^2 + \lambda. \tag{B.26}$$

In general, moments of the Rice distribution are given by an integration over the density in (B.25). Substituting (B.11) into the integrand, interchanging the summation and integration, changing the integration variable, and using (B.12), we obtain a series that is recognized as a special case of the confluent hypergeometric function. Thus,

$$E[R^n] = (2\sigma^2)^{n/2} \exp\left(-\frac{\lambda}{2\sigma^2}\right) \Gamma\left(1 + \frac{n}{2}\right) {}_1F_1\left(1 + \frac{n}{2}, 1; \frac{\lambda}{2\sigma^2}\right), \quad n \geq 0 \tag{B.27}$$

where the *confluent hypergeometric function* is defined as

$$ {}_1F_1(\alpha, \beta; x) = \sum_{i=0}^{\infty} \frac{\Gamma(\alpha + i)\Gamma(\beta) x^i}{\Gamma(\alpha)\Gamma(\beta + i) i!}, \quad \beta \neq 0, -1, -2, \ldots. \tag{B.28} $$

The Rice density function often arises in the context of a transformation of variables. Let A_1 and A_2 represent independent Gaussian random variables with common variance σ^2 and means λ and zero, respectively. Let R and Θ be implicitly defined by $A_1 = R\cos\Theta$ and $A_2 = R\sin\Theta$. Then (B.23) and $\Theta = \tan^{-1}(A_2/A_2)$ describes a transformation of variables. A straightforward calculation yields the joint density function of R and Θ:

$$ f_{R,\Theta}(r, \theta) = \frac{r}{2\pi\sigma^2} \exp\left(-\frac{r^2 - 2r\lambda\cos\theta + \lambda^2}{2\sigma^2} \right), \quad r \geq 0, \quad |\theta| \leq \pi. \tag{B.29} $$

The density function of the envelope R is obtained by integration over Θ. Since the *modified Bessel function of the first kind and order zero* satisfies

$$ I_0(x) = \frac{1}{2\pi} \int_0^{2\pi} \exp(x\cos u)\, du \tag{B.30} $$

this density function reduces to the Rice density function (B.25). The density function of the angle Θ is obtained by integrating (B.29) over r. Completing the square of the argument in (B.29), changing variables, and defining the Q-function

$$ Q(x) = \frac{1}{\sqrt{2\pi}} \int_{-x}^{\infty} \exp\left(-\frac{y^2}{2} \right) dy = \frac{1}{2} \operatorname{erfc}\left(\frac{x}{\sqrt{2}} \right) \tag{B.31} $$

where erfc( ) is the complementary error function, we obtain

$$ f_\Theta(\Theta) = \frac{1}{2\pi} \exp\left(-\frac{\lambda^2}{2\sigma^2} \right) + \frac{\lambda\cos\Theta}{\sqrt{2\pi}\sigma} \exp\left(-\frac{\lambda^2 \sin^2\theta}{2\sigma^2} \right) \left[1 - Q\left(\frac{\lambda\cos\theta}{\sigma} \right) \right], $$

$$ |\Theta| \leq \pi. \tag{B.32} $$

Since (B.29) cannot be written as the product of (B.25) and (B.32), the random variables R and Θ are not independent.

Since the density function of (B.25) must integrate to unity, we find that

$$ \int_0^{\infty} r\, \exp\left(-\frac{r^2}{2b} \right) I_0\left(\frac{r\sqrt{\lambda}}{b} \right) dr = b \exp\left(\frac{\lambda}{2b} \right) \tag{B.33} $$

where λ and b are positive constants. This equation is useful in calculations involving the Rice density function.

B.4 Rayleigh Distribution

A Rayleigh-distributed random variable is defined by (B.23) when A_1 and A_2 are independent Gaussian random variables with zero means and a common variance σ^2. Since $F_R(r) = F_Z(r^2)$, where Z is a central χ^2 random variable with two degrees of freedom, (B.20) with $N = 2$ implies that the *Rayleigh probability distribution function* is

$$F_R(r) = 1 - \exp\left(-\frac{r^2}{2\sigma^2}\right), \quad r \geq 0. \tag{B.34}$$

The *Rayleigh probability density function*, which may be obtained by differentiation of (B.34), is

$$f_R(r) = \frac{r}{\sigma^2} \exp\left(-\frac{r^2}{2\sigma^2}\right) u(r). \tag{B.35}$$

By a change of variables in the defining integral, any moment of R can be expressed in terms of the gamma function defined in (B.12). Therefore,

$$E[R^n] = (2\sigma^2)^{n/2} \Gamma\left(1 + \frac{n}{2}\right). \tag{B.36}$$

Certain properties of the gamma function are needed to simplify (B.36). An integration by parts of (B.12) indicates that $\Gamma(1+x) = x\Gamma(x)$. A direct integration yields $\Gamma(1) = 1$. Therefore, when n is an integer, $\Gamma(n) = (n-1)!$. Changing the integration variable by substituting $y = z^2$ in (B.12), it is found that $\Gamma(1/2) = \sqrt{\pi}$.

Using these properties of the gamma function, we obtain the mean and the variance of a Rayleigh-distributed random variable:

$$E[R] = \sqrt{\frac{\pi}{2}}\sigma \tag{B.37}$$

$$\sigma_R^2 = \left(2 - \frac{\pi}{2}\right)\sigma^2. \tag{B.38}$$

Since A_1 and A_2 have zero means, the joint probability density function of the random variables $R = \sqrt{A_1^2 + A_2^2}$ and $\Theta = \tan^{-1}(A_2/A_1)$ is given by (B.29) with $\lambda = 0$. Therefore,

$$f_{R,\Theta}(r, \Theta) = \frac{r}{2\pi\sigma^2} \exp\left(-\frac{r^2}{2\sigma^2}\right), \quad r \geq 0, \quad |\Theta| \leq \pi. \tag{B.39}$$

Integration over Θ yields (A.35), and integration over r yields the uniform probability density function:

$$f_\Theta(\theta) = \frac{1}{2\pi}, \quad |\theta| \leq \pi. \tag{B.40}$$

Since (B.39) equals the product of (B.35) and (B.40), the random variables R and Θ are independent. In terms of these random variables, $A_1 = R\cos\Theta$ and $A_2 = R\sin\Theta$. A straightforward calculation using the independence and densities of R and Θ verifies that A_1 and A_2 are zero-mean, independent, Gaussian random variables with common variance σ^2. Since the square of a Rayleigh-distributed random variable may be expressed as $R^2 = A_1^2 + A_2^2$, where A_1 and A_2 are zero-mean, independent, Gaussian random variables with common variance σ^2, R^2 has the distribution of a central chi-square random variable with two degrees of freedom. Therefore, (B.18) with $N = 2$ indicates that the square of a Rayleigh-distributed random variable has an exponential probability density function with mean $2\sigma^2$.

B.5 Exponentially Distributed Random Variables

Both the square of a Rayleigh-distributed random variable and a central chi-square random variable with two degrees of freedom have exponential probability distribution and density functions. Consider the random variable

$$Z = \sum_{i=1}^{N} Y_i \tag{B.41}$$

where the $\{Y_i\}$ are independent, exponentially distributed random variables with unequal positive means $\{m_i\}$. The exponential probability density function of Y_i is

$$f_{Y_i}(x) = \frac{1}{m_i}\exp\left(-\frac{x}{m_i}\right)u(x). \tag{B.42}$$

A straightforward calculation yields the characteristic function

$$C_{Y_i}(j\nu) = \frac{1}{1 - j\nu m_i}. \tag{B.43}$$

Since Z is the sum of independent random variables, (B.43) implies that its characteristic function is

$$C_Z(j\nu) = \prod_{i=1}^{N} \frac{1}{1 - j\nu m_i}. \tag{B.44}$$

To derive the probability density function of Z, (B.7) is applied after first expanding the right-hand side of (B.44) in a partial-fraction expansion. The result is

$$f_Z(x) = \sum_{i=1}^{N} \frac{B_i}{m_i}\exp\left(-\frac{x}{m_i}\right)u(x) \tag{B.45}$$

where

$$B_i = \begin{cases} \prod_{\substack{k=1 \\ k \neq i}}^{N} \dfrac{m_i}{m_i - m_k}, & N \geq 2 \\ 1, & N = 1 \end{cases} \tag{B.46}$$

and $m_i \neq m_k$, $i \neq k$. A direct integration and algebra yields the probability distribution function

$$F_Z(x) = 1 - \sum_{i=1}^{N} B_i \exp\left(-\frac{x}{m_i}\right), \quad x \geq 0. \tag{B.47}$$

Equations (B.45) and (B.12) give

$$E[Z^n] = \Gamma(1+n) \sum_{i=1}^{N} B_i m_i^n, \quad n \geq 0. \tag{B.48}$$

When the $\{m_i\}$ are equal so that $m_i = m$, $1 \leq i \leq N$, then $C_Z(j\nu) = (1 - j\nu m)^{-N}$. Therefore, the probability density function of Z is

$$f_Z(x) = \frac{1}{(N-1)!m^N} x^{N-1} \exp\left(-\frac{x}{m}\right) u(x) \tag{B.49}$$

which is a special case of the *gamma density function*. Successive integration by parts yields the probability distribution function

$$F_Z(x) = 1 - \exp\left(-\frac{x}{m}\right) \sum_{i=0}^{N-1} \frac{1}{i!} \left(\frac{x}{m}\right)^i. \tag{B.50}$$

From (B.49) and (B.12), the mean and variance of Z are found to be

$$E[Z] = Nm \tag{B.51}$$

$$\sigma_Z^2 = Nm^2. \tag{B.52}$$

Appendix C
Convergence of Adaptive Algorithms

C.1 LMS Algorithm

C.1.1 Convergence of the Mean

The least-mean-square (LMS) algorithm computes the $N \times 1$ weight vector at iteration n as (Sects. 2.7 and 6.5)

$$\mathbf{W}(n+1) = \mathbf{W}(n) + 2\mu\epsilon^{*}(n)\,\mathbf{x}(n), \quad n = 0, 1, \ldots \tag{C.1}$$

where $\mathbf{x}(n)$ is a zero-mean $N \times 1$ input vector,

$$\epsilon(n) = d(n) - y(n) = d(n) - \mathbf{W}^{H}(n)\mathbf{x}(n) \tag{C.2}$$

is the estimation error, $d(n)$ is the desired response, and

$$y(n) = \mathbf{W}^{H}(n)\mathbf{x}(n) \tag{C.3}$$

is the filter output. The *adaptation constant* μ controls the rate of convergence of the algorithm. We prove convergence of the mean weight vector under the assumption that the input vectors $\{\mathbf{x}(n)\}$ are statistically independent, stationary random vectors. The assumption is valid at least when the sampling times of the components of $\mathbf{x}(n+1)$ are separated in time from those of $\mathbf{x}(n)$ by intervals that are large compared to the correlation time of the input process. The *Wiener–Hopf equation* for the optimal weight vector, which minimizes the mean-square estimation error, is

$$\mathbf{W}_0 = \mathbf{R}_{xx}^{-1}\mathbf{R}_{xd} \tag{C.4}$$

where

$$\mathbf{R}_{xx} = E\left[\mathbf{x}(n)\mathbf{x}^{H}(n)\right] \tag{C.5}$$

is the $N \times N$ Hermitian *correlation matrix* of $\mathbf{x}(n)$ and

$$\mathbf{R}_{xd} = E\left[\mathbf{x}(n)d^*(n)\right] \tag{C.6}$$

is the $N \times 1$ *cross-correlation* vector. If we assume that $E[|y(n)|^2] \neq 0$ when $\mathbf{W}(n) \neq \mathbf{0}$, then $\mathbf{R}_{xx}$ must be positive definite. If $\mathbf{W}(n) = \mathbf{W}_0$, then (C.2) indicates that the minimum mean-square estimation error is

$$\epsilon_m^2 = E[|d(n)|^2] - \mathbf{R}_{xd}^H \mathbf{R}_{xx}^{-1} \mathbf{R}_{xd}. \tag{C.7}$$

If $\mathbf{x}(n+1)$ is independent of $\mathbf{x}(k)$ and $d(k)$, $k \leq n$, (C.1) implies that $\mathbf{W}(n)$ is independent of $\mathbf{x}(n)$. Thus, the expected value of the weight vector satisfies

$$E[\mathbf{W}(n+1)] = (1 - 2\mu\mathbf{R}_{xx})E[\mathbf{W}(n)] + 2\mu\mathbf{R}_{xd}. \tag{C.8}$$

This discrete-time equation is linear and time invariant. Its equilibrium point is easily calculated to be $\mathbf{W}_0$. From (C.4) and (C.8), it follows that

$$E[\mathbf{W}(n+1)] - \mathbf{W}_0 = (\mathbf{I} - 2\mu\mathbf{R}_{xx})\{E[\mathbf{W}(n)] - \mathbf{W}_0\}. \tag{C.9}$$

With an initial weight vector $\mathbf{W}(0)$, this equation implies that

$$E[\mathbf{W}(n+1)] - \mathbf{W}_0 = (\mathbf{I} - 2\mu\mathbf{R}_{xx})^{n+1}[\mathbf{W}(0) - \mathbf{W}_0] \tag{C.10}$$

where $\mathbf{W}(0)$ might be the identity matrix or an estimate of $\mathbf{W}_0$. Since $\mathbf{R}_{xx}$ is Hermitian and positive definite, it can be represented as

$$\mathbf{R}_{xx} = \mathbf{Q}\mathbf{\Lambda}\mathbf{Q}^{-1} = \mathbf{Q}\mathbf{\Lambda}\mathbf{Q}^H \tag{C.11}$$

where $\mathbf{Q}$ is the unitary modal matrix of $\mathbf{R}_{xx}$ with eigenvectors as its columns, and $\mathbf{\Lambda}$ is the diagonal matrix of eigenvalues of $\mathbf{R}_{xx}$. Therefore, (C.10) can be expressed as

$$\begin{aligned} E[\mathbf{W}(k+1)] - \mathbf{W}_0 &= [\mathbf{I} - 2\mu\boldsymbol{Q}\mathbf{\Lambda}\boldsymbol{Q}^{-1}]^{n+1}[\mathbf{W}(0) - \mathbf{W}_0] \\ &= \mathbf{Q}[\mathbf{I} - 2\mu\mathbf{\Lambda}]^{n+1}\mathbf{Q}^{-1}[\mathbf{W}(0) - \mathbf{W}_0]. \end{aligned} \tag{C.12}$$

This equation indicates that

$$\lim_{n\to\infty}[\mathbf{I} - 2\mu\mathbf{\Lambda}] = \mathbf{0} \tag{C.13}$$

is necessary and sufficient for the weight vector to converge to its optimal value:

$$\lim_{n\to\infty} E[\mathbf{W}(n)] = \mathbf{W}_0 = \mathbf{R}_{xx}^{-1}\mathbf{R}_{xd}. \tag{C.14}$$

A necessary and sufficient condition for (C.13), and hence (C.14), is that the diagonal elements of the diagonal matrix $[\mathbf{I} - 2\mu\mathbf{\Lambda}]$ have magnitudes less than unity. Since $\mathbf{R}_{xx}$ is Hermitian and positive definite, its eigenvalues, $\lambda_1, \lambda_2, ..., \lambda_n$, are positive. Therefore, the diagonal elements of $\mathbf{I} - 2\mu\mathbf{\Lambda}$, which are $1 - 2\mu\lambda_1$, $1 - 2\mu\lambda_2, ..., 1 - 2\mu\lambda_N$, have magnitudes less than unity if and only if

$$|1 - 2\mu\lambda_{\max}| < 1 \tag{C.15}$$

where $\lambda_{\max}$ is the maximum eigenvalue of $\mathbf{R}_{xx}$. This equation yields the necessary and sufficient convergence condition:

$$0 < \mu < \frac{1}{\lambda_{\max}}. \tag{C.16}$$

Although stronger convergence results can be proved if the inputs are stationary processes and μ is allowed to decrease with the iteration number, making μ constant gives the adaptive system flexibility in processing nonstationary inputs.

The matrix multiplications in (C.12) indicate that during adaptation the weights undergo transients that vary as sums of terms of the form $(1 - 2\mu\lambda_i)^k$. These transients determine the rate of convergence of the mean vector. The *time constants* of the convergence are defined so that

$$|1 - 2\mu\lambda_i|^n = \exp\left(-\frac{n}{\tau_i}\right), \quad i = 1, 2, ..., N \tag{C.17}$$

which yields

$$\tau_i = -\frac{1}{ln(|1 - 2\mu\lambda_i|)}, \quad i = 1, 2, ..., N. \tag{C.18}$$

As explained subsequently, the convergence of the weight covariances and the mean-square error require, under reasonable assumptions, that $\mu < 1/2\lambda_{\max}$. With this restriction, it follows from (C.18) that the maximum time constant is

$$\tau_{\max} = -\frac{1}{ln(1 - 2\mu\lambda_{\min})}, \quad 0 < \mu < \frac{1}{2\lambda_{\max}} \tag{C.19}$$

where $\lambda_{\min}$ is the smallest eigenvalue of $\mathbf{R}_{xx}$. If μ is close to the upper bound in (C.19), then $\tau_{\max}$ is largely determined by the *eigenvalue spread* defined as $\lambda_{\max}/\lambda_{\min}$.

C.1.2 Misadjustment

If the random vectors $\mathbf{W}(n)$ and $\mathbf{x}(n)$ are independent, then (C.2), (C.4), and (C.7) imply that

$$E[|\epsilon(n)|^2] = \epsilon_m^2 + E[\mathbf{V}^H(n)\mathbf{R}_{xx}\mathbf{V}(n)] \tag{C.20}$$

where

$$\mathbf{V}(n) = \mathbf{W}(n) - \mathbf{W}_0. \tag{C.21}$$

Even if $E[\mathbf{W}(n)] \rightarrow \mathbf{W}_0$, it does not follow that $E[|\epsilon|^2] \rightarrow \epsilon_m^2$. A measure of the extent to which the LMS algorithm fails to provide the ideal performance is the excess mean-square error, $E[[\epsilon|^2]-\epsilon_m^2$. A dimensionless measure of the performance loss, called the *misadjustment*, is defined as

$$M = \frac{\lim_{k\rightarrow\infty} E[|\epsilon(n)|^2] - \epsilon_m^2}{\epsilon_m^2}. \tag{C.22}$$

To derive an expression for the misadjustment, we make the following four assumptions:

1. The jointly stationary processes $\mathbf{x}(n+1)$ and $d(n+1)$ are independent of $\mathbf{x}(k)$ and $d(k)$, $k \leq n$. It then follows from (C.1) that $\mathbf{W}(n)$ is independent of $\mathbf{x}(n)$ and $d(n)$.
2. The adaptation constant satisfies

$$0 < \mu < \frac{1}{tr(\mathbf{R}_{xx})}. \tag{C.23}$$

3. $E[\| \mathbf{V}(n) \|^2]$ converges as $n \rightarrow \infty$.
4. As $n \rightarrow \infty$, $|\epsilon(n)|^2$ and $\| \mathbf{x}(n) \|^2$ become uncorrelated so that

$$\lim_{k\rightarrow\infty} E[|\epsilon(n)|^2 \| \mathbf{x}(n) \|^2] = tr(\mathbf{R}_{xx}) \left\{ \lim_{n\rightarrow\infty} E[|\epsilon(n)|^2] \right\}. \tag{C.24}$$

Assumptions 1 and *2* imply convergence of the mean weight vector, which requires (C.16), because the sum of the eigenvalues of a square matrix is equal to its trace, and hence

$$\lambda_{\max} < \sum_{i=1}^{N} \lambda_i = tr(\mathbf{R}_{xx}). \tag{C.25}$$

The total input power is $E\left[\| \mathbf{x}(n) \|^2\right] = tr(\mathbf{R}_{xx})$. For *Assumption 3* to be true, a tighter restriction on μ than *Assumption 2* may be necessary. *Assumption 4* is physically plausible, but it is an approximation.

Equations (C.1) and (C.21) imply that

$$\mathbf{V}(n+1) = \mathbf{V}(n) + 2\mu\epsilon^*(n)\,\mathbf{x}(n). \tag{C.26}$$

It follows that

$$\begin{aligned} E[\| \mathbf{V}(n+1) \|^2] = {} & E[\| \mathbf{V}(n) \|^2] + 4\mu Re\{E[\epsilon^*(n)\,\mathbf{V}^H(n)\mathbf{x}(n)]\} \\ & + 4\mu^2 E[|\epsilon(n)|^2 \| \mathbf{x}(n) \|^2]. \end{aligned} \tag{C.27}$$

Assumption 1 and (C.2), (C.5), and (C.6) yield

$$E[\epsilon^*(n)\,\mathbf{V}^H(n)\mathbf{x}(n)] = E[\,\mathbf{V}^H(n)\mathbf{R}_{xd}] - E[\mathbf{V}^H(n)\mathbf{R}_{xx}\mathbf{W}(n)]. \tag{C.28}$$

Substitution of (C.21), (C.4), and (C.20) gives

$$E[\epsilon^*(n)\,\mathbf{V}^H(n)\mathbf{x}(n)] = \epsilon_m^2 - E[|\epsilon(n)|^2]. \tag{C.29}$$

Substituting (C.29) into (C.27), taking the limit as $n \to \infty$, and using *Assumptions 3* and *4*, we obtain

$$\lim_{k\to\infty} E[|\epsilon(n)|^2] = \frac{\epsilon_m^2}{1-\mu tr(\mathbf{R}_{xx})}. \tag{C.30}$$

Assumption 2 ensures that the right-hand side of this equation is positive and finite, which could not be guaranteed if the less restrictive (C.16) were assumed instead. Substituting (C.30) into (C.22), we obtain

$$M = \frac{\mu tr(\mathbf{R}_{xx})}{1-\mu tr(\mathbf{R}_{xx})}. \tag{C.31}$$

This result applies to both the real and complex discrete-time LMS algorithms. According to (C.31), increasing μ to improve the convergence rate has the side effect of increasing the misadjustment. For fixed μ, the misadjustment increases with the total input power.

C.2 Frost Algorithm

C.2.1 Convergence of the Mean

The Frost or linearly constrained minimum-variance algorithm computes the $N \times 1$ weight vector as (Sect. 6.5)

$$\mathbf{W}(0) = \frac{1}{G}\mathbf{p}_k \tag{C.32}$$

$$\mathbf{W}(n+1) = \left(\mathbf{I} - \frac{1}{G}\mathbf{p}_k\mathbf{p}_k^T\right)\left[\mathbf{W}(n) - 2\mu\mathbf{y}(n)\,\overline{d}_k^*(n)\right] + \frac{1}{G}\mathbf{p}_k \tag{C.33}$$

where $\mathbf{p}_k$ is the $N \times 1$ vector of the spreading sequence of user k, $\mathbf{y}(n)$ is the $N \times 1$ input vector comprising output samples of a chip-matched filter, and

$$\overline{d}_k(n) = \mathbf{W}^H(n)\,\mathbf{y}(n) \tag{C.34}$$

is the $N \times 1$ filter output vector. The optimal weight vector is

$$\mathbf{W}_0 = \frac{\mathbf{R}_y^{-1}\mathbf{p}_k}{\mathbf{p}_k^T\mathbf{R}_y^{-1}\mathbf{p}_k} \tag{C.35}$$

where

$$\mathbf{R}_y = E\left[\mathbf{y}(n)\,\mathbf{y}^H(n)\right] \tag{C.36}$$

is the $N \times N$ Hermitian *correlation matrix* of $\mathbf{y}(n)$. The spreading sequence is normalized so that

$$\mathbf{p}_k^T\mathbf{p}_k = G \tag{C.37}$$

If $\mathbf{y}(n+1)$ is independent of $\mathbf{y}(k)$, $k \le n$, then $\mathbf{W}(n)$ and $\mathbf{y}(n)$ are independent and (C.33) implies that

$$E[\mathbf{W}(n+1)] = \mathbf{A}[\mathbf{I} - 2\mu\mathbf{R}_y]E[\mathbf{W}(n)] + \frac{1}{G}\mathbf{p}_k, \quad n \ge 0 \tag{C.38}$$

where

$$\mathbf{A} = \left(\mathbf{I} - \frac{1}{G}\mathbf{p}_k\mathbf{p}_k^T\right). \tag{C.39}$$

Equations (C.38), (C.39), (C.21), (C.35), and (C.37) yield

$$\mathbf{V}(n+1) = \mathbf{A}\mathbf{V}(n) - 2\mu\mathbf{A}\mathbf{R}_y\mathbf{V}(n), \quad n \ge 0. \tag{C.40}$$

Direct multiplication verifies that $\mathbf{A}^2 = \mathbf{A}$. It then follows from (C.40) that $\mathbf{A}\mathbf{V}(n) = \mathbf{V}(n)$, $n \ge 1$. It is easily verified that $\mathbf{A}\mathbf{V}(0) = \mathbf{V}(0)$. Consequently,

$$\begin{aligned}\mathbf{V}(n+1) &= [\mathbf{I} - 2\mu\mathbf{A}\mathbf{R}_y\mathbf{A}]\mathbf{V}(n) \\ &= [\mathbf{I} - 2\mu\mathbf{A}\mathbf{R}_\mathbf{y}\mathbf{A}]^{n+1}\mathbf{V}(0), \quad n \ge 0.\end{aligned} \tag{C.41}$$

A straightforward calculation verifies that the matrix $\mathbf{A}\mathbf{R}_y\mathbf{A}$ is Hermitian, and hence it has a complete set of orthonormal eigenvectors. Direct calculation proves that

$$\mathbf{A}\mathbf{R}_\mathbf{y}\mathbf{A}\mathbf{p}_k = \mathbf{0} \tag{C.42}$$

which indicates that $\mathbf{p}_k$ is an eigenvector of $\mathbf{A}\mathbf{R}_\mathbf{y}\mathbf{A}$ with eigenvalue equal to zero. Let $\mathbf{e}_i$, $i = 1, 2, \ldots, N-1$, denote the $N-1$ remaining orthonormal eigenvectors. Because the $\mathbf{e}_i$ must be orthogonal to $\mathbf{p}_k$,

$$\mathbf{p}_k^T\mathbf{e}_i = \mathbf{0}, \quad i = 1, 2, \ldots, N-1. \tag{C.43}$$

From this equation and (C.39), it follows that

$$\mathbf{A}\mathbf{e}_i = \mathbf{e}_i, \quad i = 1, 2, \ldots, N-1. \tag{C.44}$$

Let σ_i denote the eigenvalue of $\mathbf{AR_yA}$ associated with the unit eigenvector $\mathbf{e}_i$. Using (C.44), we obtain

$$\sigma_i = \mathbf{e}_i^H \mathbf{AR_yA}\mathbf{e}_i = \mathbf{e}_i^H \mathbf{R_y}\mathbf{e}_i, \quad i = 1, 2, ..., N-1. \tag{C.45}$$

Since $\mathbf{e}_i$ is a unit vector, the Rayleigh quotient of (5.86) implies that

$$\lambda_{\min} \leq \mathbf{e}_i^H \mathbf{R}_y \mathbf{e}_i \leq \lambda_{\max} \tag{C.46}$$

where $\lambda_{\min}$ and $\lambda_{\max}$ are the smallest and largest eigenvalues, respectively, of the Hermitian matrix $\mathbf{R}_y$. If we assume that $\mathbf{R_y}$ is a positive definite, then $\lambda_{\min} > 0$, and hence $\sigma_i > 0, i = 1, 2, ..., N-1$. We conclude that the $\{\mathbf{e}_i\}$ correspond to nonzero eigenvalues.

Equations (C.21), (C.32), (C.35), and (C.37) indicate that $\mathbf{p}_k^T \mathbf{V}(0) = \mathbf{0}$. Therefore, $\mathbf{V}(0)$ is equal to a linear combination of the $\mathbf{e}_i$, $i = 1, 2, ..., N-1$, which are the eigenvectors of $\mathbf{AR}_{xx}\mathbf{A}$ corresponding to the nonzero eigenvalues. If $\mathbf{V}(0)$ is equal to the eigenvector $\mathbf{e}_l$ with eigenvalue σ_l, then (C.41) indicates that

$$\mathbf{V}(n+1) = (1 - 2\mu\sigma_l)^{n+1} \mathbf{e}_l, \quad n \geq 0. \tag{C.47}$$

Therefore, a necessary and sufficient condition for the convergence of the mean weight vector is that $|1 - 2\mu\sigma_i| < 1$ for $i = 1, 2, ..., N-1$. Since $\sigma_i > 0$, the necessary and sufficient condition for convergence is

$$0 < \mu < \frac{1}{\sigma_{\max}}. \tag{C.48}$$

Analogously to (C.18), the convergence of the mean weight vector of the Frost algorithm has transients that can be characterized by the time constants

$$\tau_i = -\frac{1}{\ln(|1 - 2\mu\sigma_i|)}, \quad i = 1, 2, ..., N-1. \tag{C.49}$$

If $0 < \mu < 1/2\sigma_{\max}$, the largest time constant is

$$\tau_{\max} = -\frac{1}{\ln(1 - 2\mu\sigma_{\min})}, \quad 0 < \mu < \frac{1}{2\sigma_{\max}} \tag{C.50}$$

where $\sigma_{\min}$ is the smallest nonzero eigenvalue of $\mathbf{AR_yA}$. If μ is close to the upper bound in (C.50), then $\tau_{\max}$ is largely determined by the *eigenvalue spread* defined as $\sigma_{\max}/\sigma_{\min}$.

Index